# ALLOYS FOR THE EIGHTIES

*General Chairman:*
H. N. Lander

*Editor:*
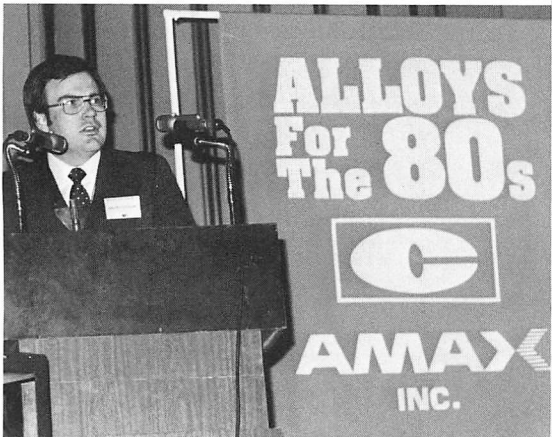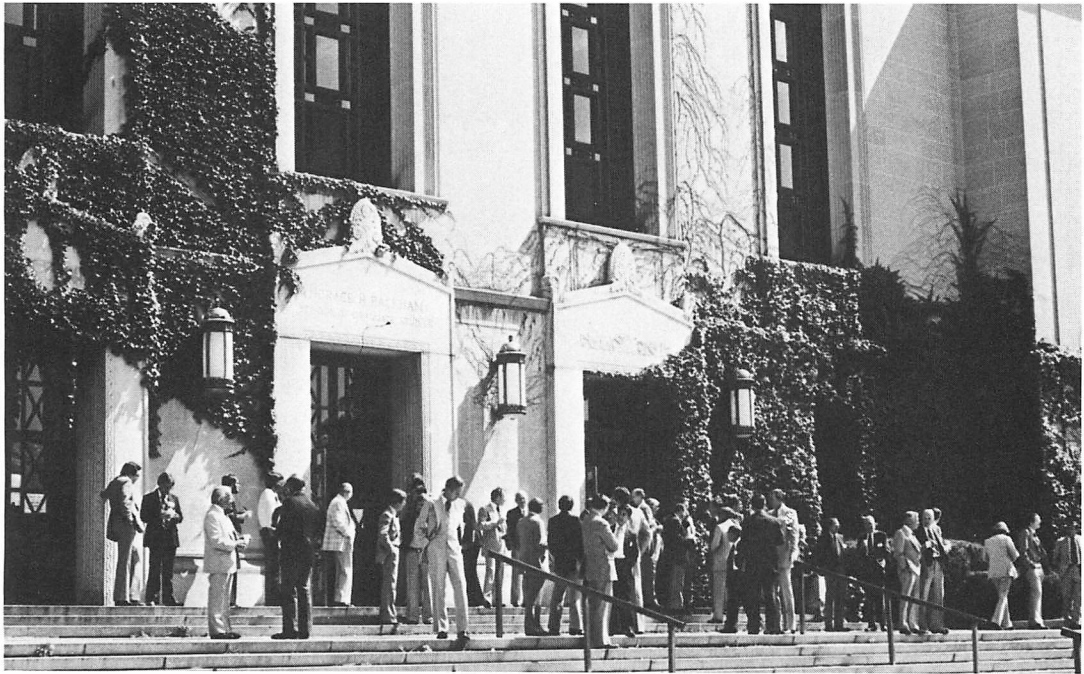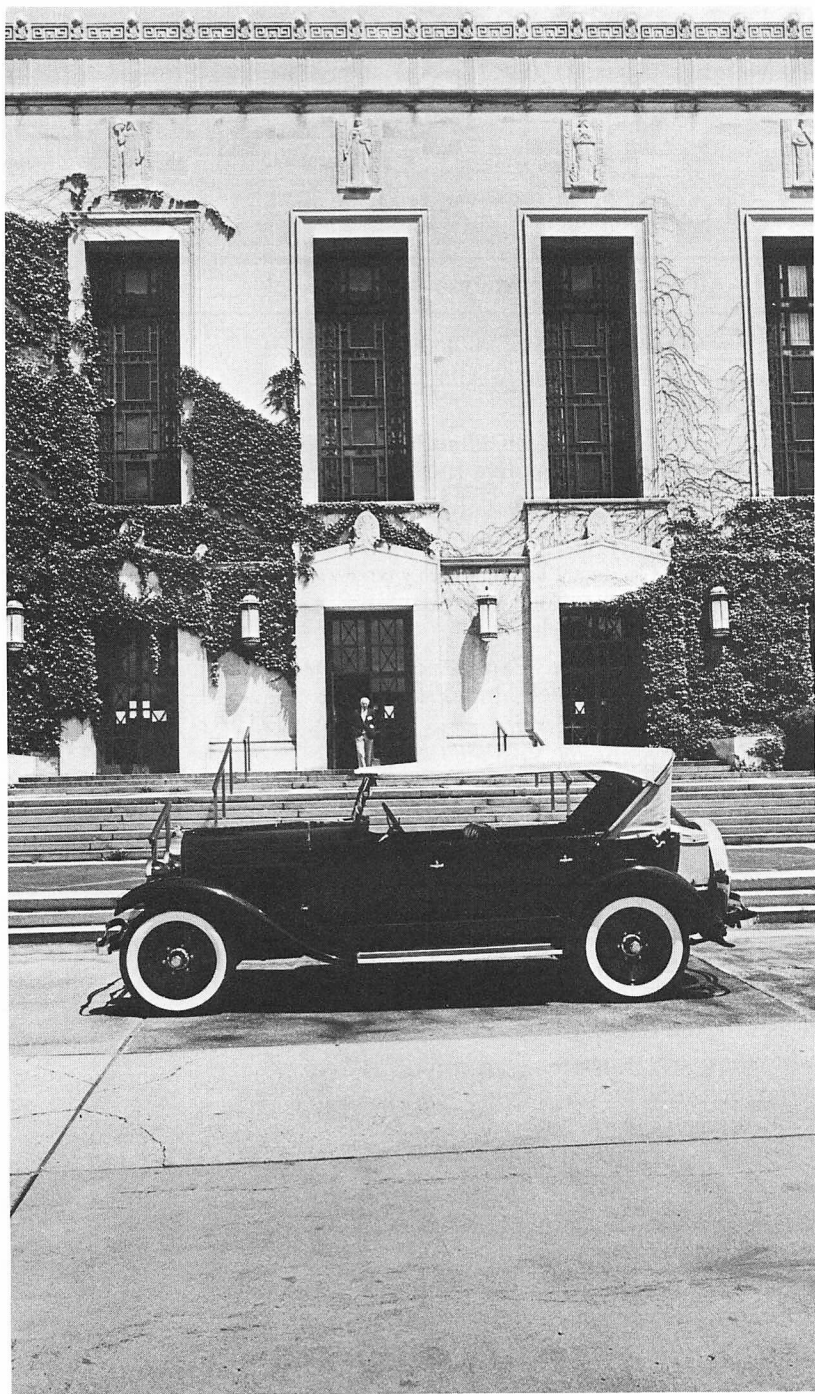Robert Q. Barr

**CLIMAX MOLYBDENUM COMPANY**
ONE GREENWICH PLAZA, GREENWICH, CONNECTICUT 06830

**ALLOYS** FOR THE EIGHTIES

# ALLOYS FOR THE EIGHTIES

## Table of Contents

# The Future of Alloy Steels in the Automobile

by G. H. Robinson
General Motors Research Laboratories

Alloy steels and the automobile are intimately related. Most of the modern low alloy, heat treated engineering steels were developed (or conceived) in response to the needs of the industry for materials which would survive under extreme conditions of shock and repeated loading. Even in the early days of the industry, performance and economy requirements demanded light weight, and thus highly stressed, mechanisms. Nickel alloy steels were used in axles as early as 1900; by 1912 the Society of Automotive Engineers had established the SAE numbering system for alloy steels and the ASTM had published standard specifications for automotive alloy steels which included nickel, nickel-vanadium, nickel-chromium and nickel-chromium-vanadium alloys.[1] Chromium-molybdenum steel saw application in the 1912 Wills Sainte Claire automobile, and the carbon-manganese grade was introduced by Buick in 1915.[2]

Today the technology of heat treated alloy steels would appear to have reached maturity, with present work concentrated on accurate prediction of hardenability, microstructure and properties from chemical composition and cooling rate and the balancing of composition to minimize cost.

Predictions of the future of alloy steels in the automobile could, therefore, involve merely a simple extrapolation of current trends in alloy usage, taking cognizance of the forces, technical or economic, responsible for the trends.

A review of past efforts at predicting the future, however, makes one uneasy with such a quantitative approach. In 1956, A. L. Boegehold[3] predicted that "the future car [by 1980] will use no nickel in shafts or gears," a straightforward extrapolation, based on the then current economic forces—the cost and availability of nickel in the 1950s. The complete elimination of nickel has not occurred and does not even appear likely today. He also predicted that, by 1980, average engine compression ratios would be greater than 11:1, using 120 octane gasoline (Figure 1). Again, a reasonable prediction based on the technical forces for improved fuel economy. Actual compression ratios of current spark ignition engines average 8.2:1 and use fuel of about 90 octane, a consequence of the then unforeseen impact of severe restric-

tions, by government regulation, on vehicle emissions. The regulations led to catalytic treatment of the engine exhaust, and the catalyst was poisoned or inactivated by the lead additive used to provide high octane number. Elimination of the additive, and the resultant lower octane rating, required a reduction in engine compression ratio to avoid severe spark knock. The emissions regulations thus imposed new technical forces which invalidated the extrapolation.

Since any attempt at a quantitative update predicting alloy steel applications would probably involve similar uncertainties, we have chosen to approach the question of the future of alloy steels in the automobile qualitatively, by tracing the major threads of the evolution of these materials and then identifying some present or potential substitutes for the traditional alloy steel applications. From this background, we will define what we
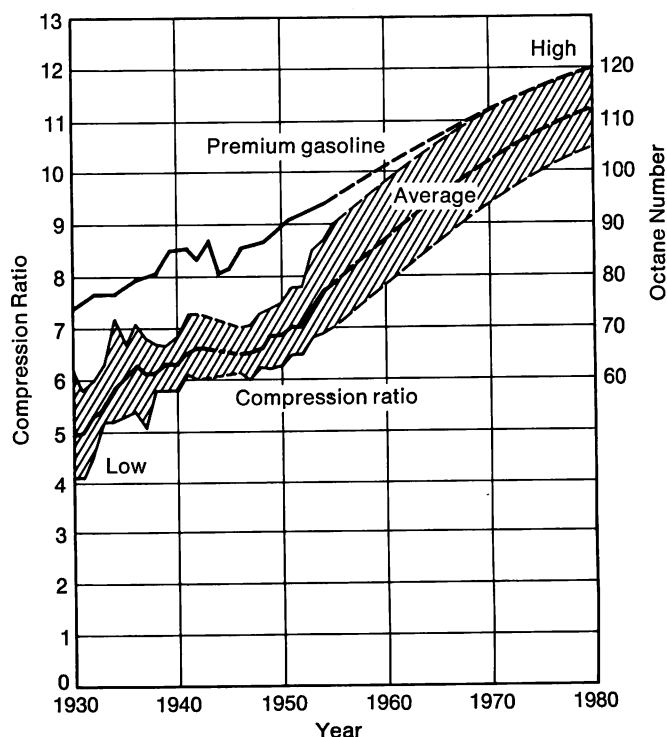


FIGURE 1—*Trends in compression ratio and octane rating as predicted by Boegehold in 1956.*

perceive as the major development challenges for automotive alloy steels of the future.

## The Past

The history of automotive alloy steels begins with nickel, and the early days of the industry saw extensive application of nickel steels. The preeminent position of this class of alloy steels is reflected today in the SAE numbering system, which assigned the 2000 series to straight nickel steels (the 1000 series being carbon steels). Since that time, automotive metallurgists have worked to reduce nickel content and, thus, alloy cost, with notable success. The 2000 series is now obsolete. In the process, a multitude of different compositions was developed for automotive and other machine components. The proliferation of alloy steels in the early 1900s corresponding to the early growth of the industry is illustrated in Figure 2. The activity in the automotive industry of this period is typified by a paper appearing in the 1921 Transactions of the American Society for Steel Treating[4] discussing the development of molybdenum steels. The author states: "at this time the Ford car was built for the most part of steel which was ordered to conform to the analysis, 0.23-0.28% carbon, 1% chromium, 0.18% vanadium and 0.70-0.90% manganese. This analysis was so written that the steelmaker would average 7% of his heats on the low side and 15% on the high side (of the carbon range). The low carbon heats were used for case hardened parts and the high carbon ones for oil quench-

ing (sic) parts. Thus, one specification covers all parts of the car except specialties such as ball bearings and magnet steels for the magneto. On account of the monopoly on vanadium and the royalty on its use, a search was made for a steel which would replace the chrome vanadium for universal use in an automobile." The author went on to describe a "systematic and logical search of the periodic system" to find a new alloy, which culminated in a series of chromium-molybdenum steels.

Advantages of the new steels were reported to include ready availability of chromium and molybdenum, ease of production in the steel mill, improved tensile properties and toughness, lack of sensitivity to forging and hardening temperatures, and improved machinability—all attributed to the presence of molybdenum.

Alloy development in the early days was characterized almost entirely by this "mystique" of alloys, where individual alloying elements or combinations of elements were considered uniquely responsible for steel properties. The mystique tended to be perpetuated by the common practice of steel producers and alloy suppliers to publish "physical property charts," such as that reproduced in Figure 3. The charts plotted the effect of tempering temperature after austenitizing and quenching on tensile strength, ductility and hardness. Since the data were generated from tensile specimens cut from one-inch diameter (25 mm) heat treated bars, steels that would not completely harden in this section size compared poorly with the higher alloy steels which did through harden. The charts thus tended to reinforce the supposi-
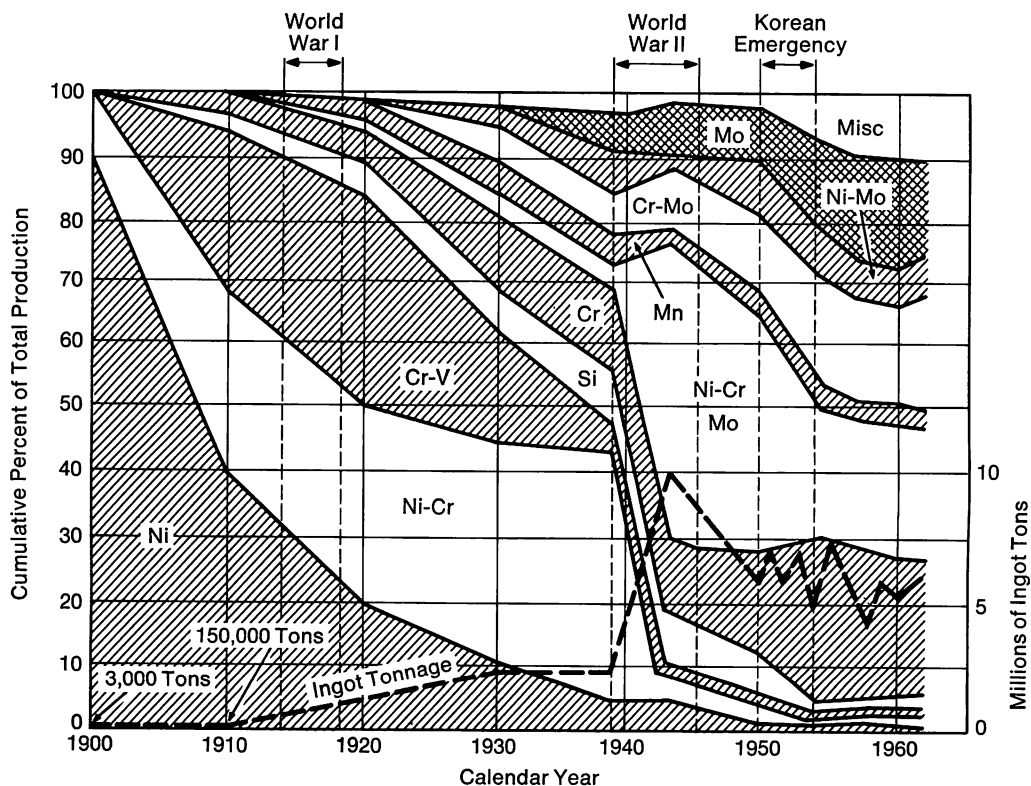


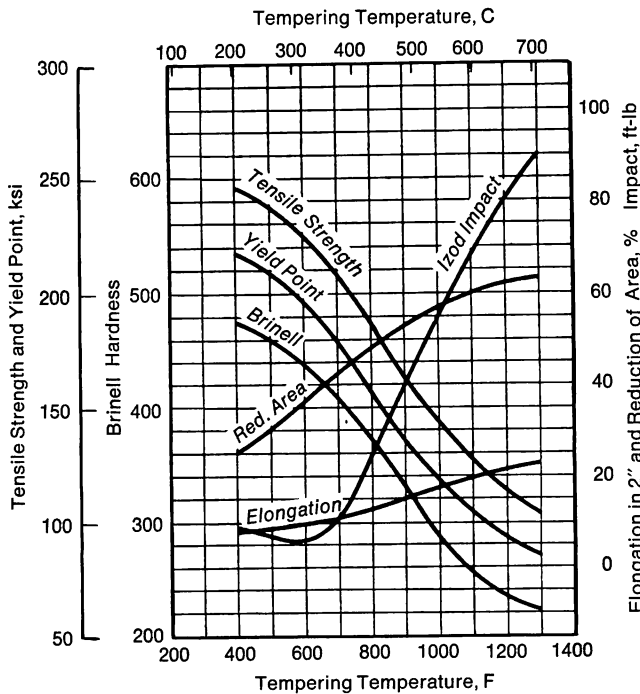FIGURE 2—Cumulative percent of alloy steel type produced by year.

Tempering Temperature, C



FIGURE 3—Typical "physical property" chart for a nickel-chromium alloy steel.

Selection of materials for automotive components involves much more than alloy cost for equivalent hardenability. Other considerations include the characteristics already noted in the development of the early chromium-molybdenum steels such as annealing characteristics, machinability, reproducibility of heat treatment response and ability to meet varied and complex engineering functions.

This complexity of demands, coupled with perceived (or preconceived) differences in the characteristics of "equivalent" steels in meeting the demands, have resulted in the establishment of an increasing number of alloy combinations. In 1940, the SAE listed 65 standard grades of low alloy steels; today there are 90, not counting the "H band" series, plus many so-called "modified" steels specified by individual manufacturers. During the same period, 88 obsolete grades—no longer in major commercial use—have been deleted. This continuing activity suggests that the technology of alloy steels is actually still a long way from maturity.

Furthermore, the continuing search for new and better materials for automotive components is extending beyond the traditional wrought alloy steels, and the competition is increasing.

## The Competition—Alternates to Alloy Steels

The strongest present competitor to alloy steel in the automobile is cast iron. Probably the first substitution occurred in the engine valve train, where hardened steel camshafts and lifters were replaced by alloyed gray iron. Although the final economics were probably favorable, the major force in the substitution was technical. The heterogeneous microstructure of the hardened alloy iron, consisting of graphite and massive carbides in a martensite matrix, provided a surface which resisted seizure under boundary lubrication conditions much more effectively than the hardened steel it replaced.

Beginning in the 1950s, another inroad into the alloy steel area occurred in the crankshaft. In early engines, crankshaft fatigue was a common problem, requiring high quality tempered martensite structures plus, in some models, induction hardened fillets or nitrided cases to prevent failure. Reason: The early in-line long-stroke engines required long and spindly crankshafts with resultant high bending stresses. As engines became more compact, the cranks became stockier, and the design limitation became deflection rather than fatigue strength. This change in the technical forces prompted a strong move from steel to pearlitic malleable and pearlitic nodular cast irons. A similar shift is apparent in connecting rods, and additional substitutions of alloy steels by nodular irons are occurring at an accelerating pace.

One of the most recent is the successful application of an austempered nodular iron for rear axle ring and

tion that each alloy steel had a combination of properties peculiar to itself and different from other steels.

By the late thirties, however, observations such as those by Janetsky and Baeyerts[5] that a close correlation existed between hardness and tensile strength of steels regardless of alloy composition, and the concepts of hardenability generated by Bain,[6] Grossman,[7] Boegehold[8] and others started to bring a high degree of order out of this chaos.

The order was based on some specific simplifying assumptions, namely, (a) all tempered martensites of the same carbon content and hardness are equal, and (b) the sole effect of alloying elements is to permit the attainment of a fully martensitic structure on quenching.

In more recent years, the research community, for the most part, has shifted its concentration increasingly toward the microscopic level in studies of transformation kinetics and mechanisms, the detailed morphology and crystallography of microconstituents, and strengthening mechanisms.

At the same time, the hardenability concept of alloying is being made more quantitative by development of reasonably accurate methods to predict structure and tensile properties from composition and cooling rates.[9-11] Practicing metallurgists in the plants, however, although accepting the basic assumptions of the hardenability concept, have continued to maintain some of the old alloy "mystique." Some of the unique effects of specific elements, such as the influence of molybdenum in reducing susceptibility to temper embrittlement, are well established. Others are less well defined.

drive pinion gears, components traditionally made from carburized alloy steel[12] (Figure 4). The nodular iron offers improved function in noise damping and resistance to scoring, in addition to greatly improved machinability, and the lower density compared to steel results in a weight reduction of nearly 1 kg (2.2 lb) for a 220 mm (8¾ in.) gear set.

Another viable alternate to wrought alloy steel is high density sintered iron powder. A 1976 GM intermediate size vehicle with automatic transmission and power steering contained about 3.5 kg (7.7 lb) of sintered iron, including oil pump gears, rocker arm balls and clutch pressure plates (Figure 5).[13] Many of the past applications have been relatively low density materials, substituting principally for gray cast iron. Hot forming to theoretical density can, however, provide properties approaching those of medium hardness heat treated alloy steels. Differential side pinions (Figure 6) have been successfully produced by hot forming, and a transmission rotor clutch (Figure 7) has been in high volume production with hot formed sintered iron for several years. Principal deterrent to further expansion of PM into the traditional alloy steel applications is powder cleanliness. Present day commercial atomized iron and iron alloy powder contains inclusions of slag, refractory or deoxidation products which affect machinability and, more importantly, seriously reduce fatigue durability. Correction of this situation, however, appears to be entirely feasible even with current technology, and expanded application is almost certain.



FIGURE 4—Nodular iron rear axle ring gear and drive pinion.



| | | kg | lb |
|---|---|---|---|
| A) | Shock Absorbers | 0.16 | 0.342 |
| B) | Brakes | 0.16 | 0.347 |
| C) | Ignition System | 0.06 | 0.122 |
| D) | Engine | 0.56 | 1.242 |
| E) | Automatic Transmission | 1.93 | 4.254 |
| F) | Steering System | 0.62 | 1.376 |
| | Total | 3.49 | 7.683 |
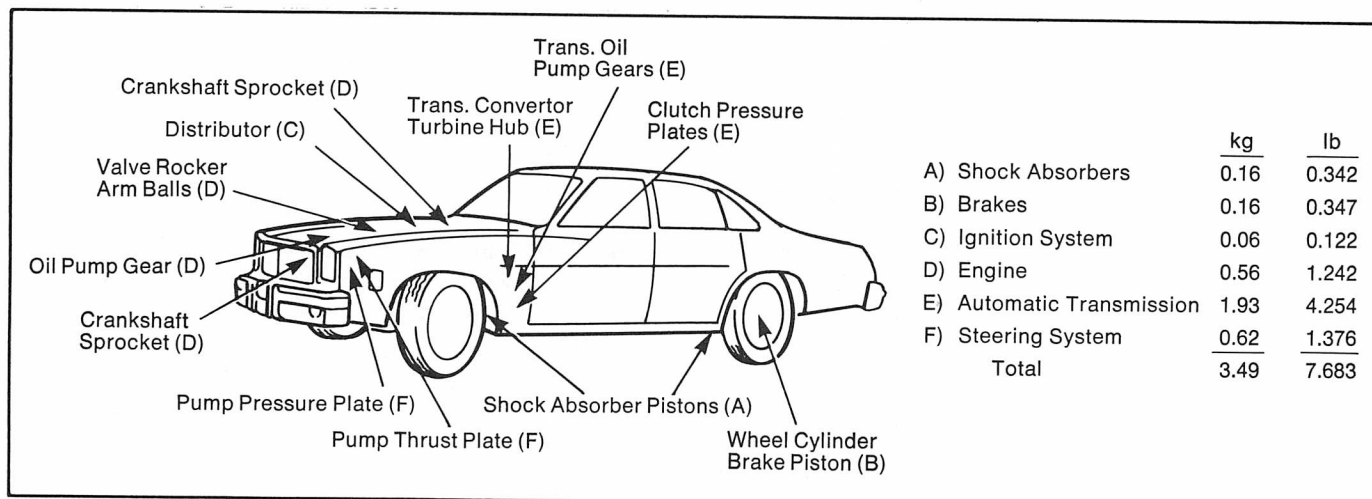
FIGURE 5—Sintered iron components in a 1976 intermediate size car.
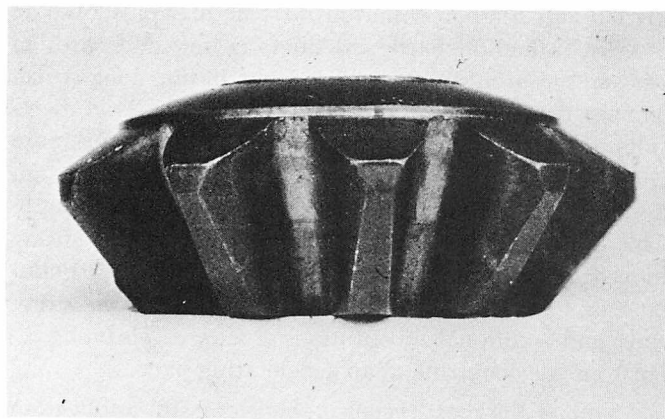


FIGURE 6—Sintered and hot formed differential side pinion.

Farther in the future, other competitors may see practical implementation as alternates to hardened steel. One possibility is ceramic materials for parts currently made of hardened alloys, primarily to resist wear. Another is represented by fiber-reinforced composites, which may find application in components of simple geometry and loading, such as torsion members and leaf springs.

In general, the continuing technical and economic forces of emissions, weight reduction and conservation of material and energy will act to decrease the usage of our conventional heat treated steels.
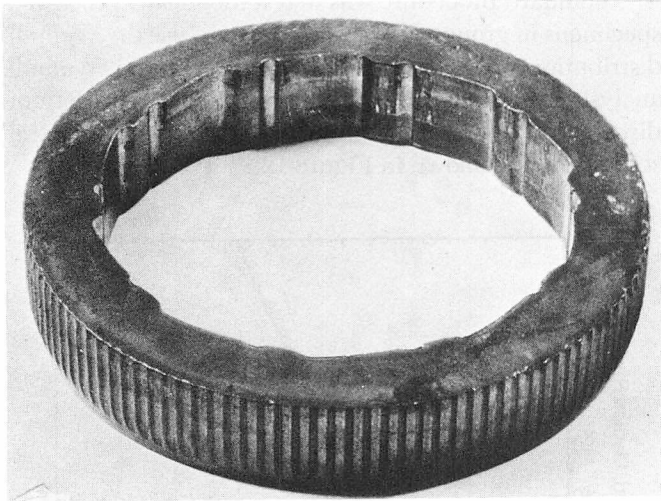
FIGURE 7—Sintered and hot formed transmission rotor clutch.



FIGURE 8—Endurance limit-hardness relationship for medium carbon alloy steels.

The area of applications which appears most immune to substitution is the most highly stressed components, such as power transmission gears and shafting, ball and roller bearings and spring members. These components, which may be through hardened, case hardened by induction heating, or case carburized, are characterized by high hardness, HRC 50 and above. Coincidentally, the technology of high hardness steels is the least understood aspect of heat treated steels, and parameters such as surface hardness, case depth, core properties and even alloy composition are defined entirely on the basis of past experience and component testing.

The uncertainty involved in quantifying fatigue properties of hardened steel is typified by the work of Garwood,[14] some of whose findings are shown in Figure 8. His results confirmed what everyone had realized; namely, that fatigue predictability and thus component reliability, decreased rapidly as hardness increased above some maximum which appeared to depend on carbon content and, possibly, alloy composition.

Garwood's data for SAE 4140, quenched and then tempered to various hardness levels (Figure 9) typify this behavior. Note that no fatigue endurance limit is indicated for the HRC 46 tests, and at HRC 50 no attempt is made to even indicate an average stress-life relationship.

A similar situation is shown in Figure 10, taken from the work of Fisher and Sheehan,[15] except that here the authors have attempted to fit an S-N curve to the data. This is a dangerous practice because there is a tendency for the S-N curve, sans data points, to find its way into handbooks used by design engineers who proceed to use the curve in calculations as if it were an analytical relationship.

The fact that high hardness steels are extensively
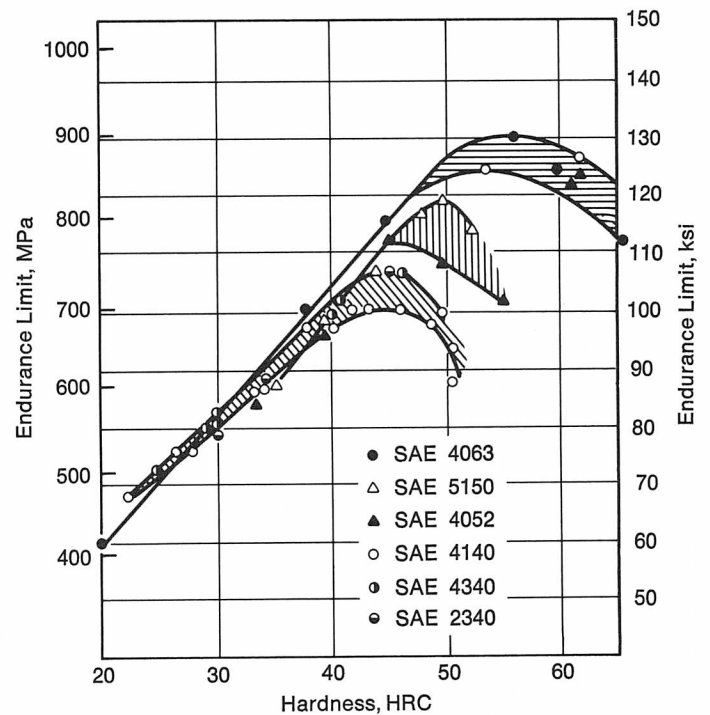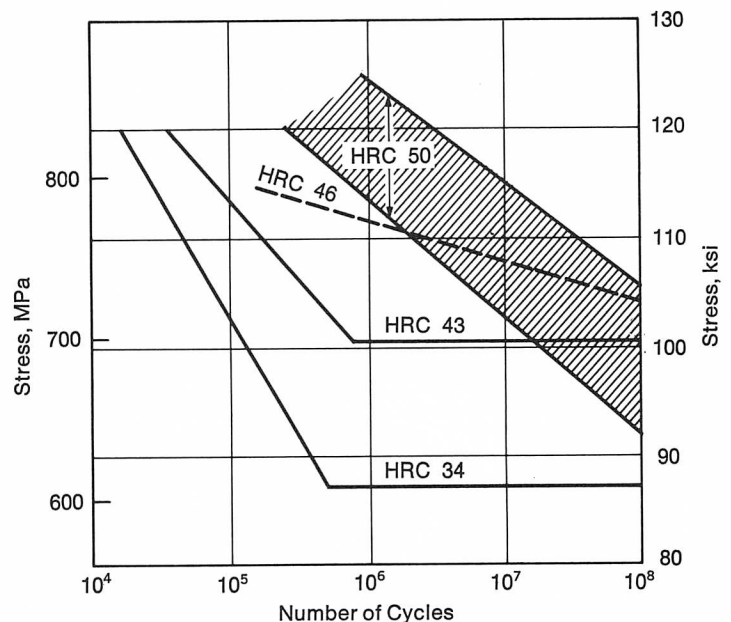


FIGURE 9—S-N curves (reversed bending) for SAE 4140 steel.

and successfully applied in components subject to fatigue merely indicates that the components are designed to accommodate the lower side of the band. Herein lies a major challenge to the more effective use of alloy steels.
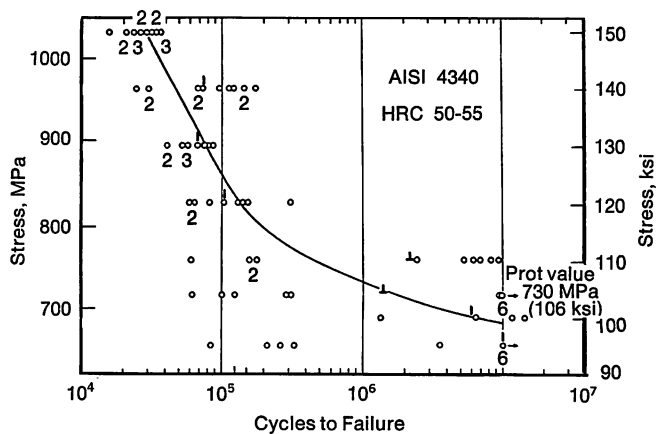
FIGURE 10—Rotating beam fatigue data.

## The Challenges

General Motors Research Laboratories made several attempts in the late fifties and early sixties to clarify the fatigue behavior of high hardness steels, with a notable lack of success.[16,17] A review of some of the findings and the questions they raised may serve to stimulate further activity in this important but difficult area of research.

The test material in the GMR work was SAE 52100 steel, hardened and tempered to HRC 61-63. This alloy, a 1% carbon, 1½% chromium grade, was selected because the retained austenite level could be easily varied by adjusting the austenitizing temperature. The starting structure was spheroidized carbides in ferrite; as the austenitizing temperature was raised, increasing solution of carbide produced a higher carbon matrix and, hence, higher austenite content after heat treatment.

All tests were run at a single stress level because of the difficulty of defining an endurance limit in material of this high a hardness. The specimens, of rectangular cross section, were loaded in unidirectional bending; the mode of stressing is shown schematically in Figure 11.
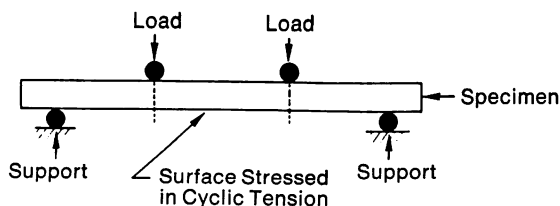


FIGURE 11—Loading method for unidirectional fatigue tests.

The symmetrical loading produced a uniform bending moment over the central 50 mm (2 in.) portion of the specimen. This loading was chosen so that a substantial sample of material was subjected to the maximum stress, a situation more conducive to revealing the average properties of the material than the traditional R. R. Moore specimen where only a small region at the location of minimum diameter experiences the maximum stress.

Standard procedure was to test identically processed specimens in groups of at least ten and to use the Weibull distribution function[18] to estimate median life. Weibull analysis is convenient in that it can handle a variety of distributions on a common set of coordinates. A typical set of results is shown in Figure 12.
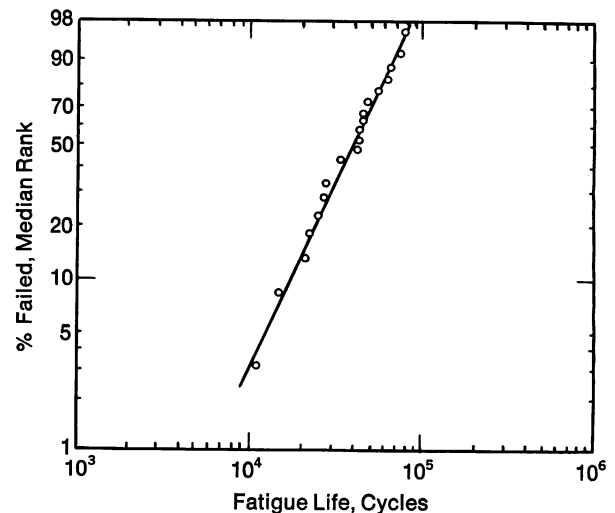


FIGURE 12—Weibull plot of fatigue data.
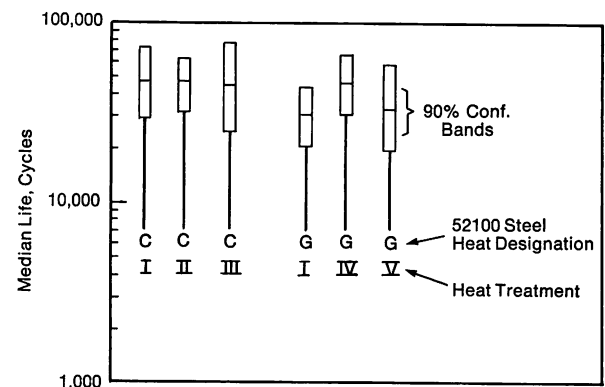


FIGURE 13—Effect of heat treatment variations on fatigue life of hardened SAE 52100 steel.

We initially envisioned several factors which we felt would influence the fatigue behavior of a hardened steel such as grain size and retained austenite level. Figure 13 shows the results obtained with a number of different austenitizing treatments which produced quite obvious differences in microstructure. The center of each bar in the plot represents the median life of the group. Surprisingly, considering the width of the confidence bands, no really significant differences are evident.
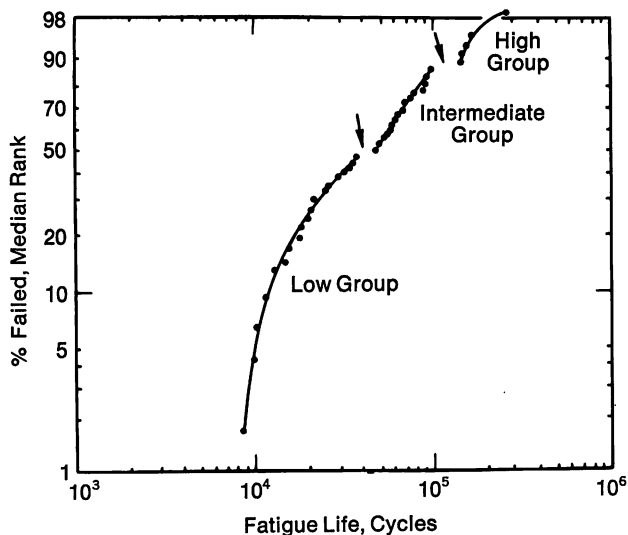
FIGURE 14—Weibull plot of fatigue data for 40 specimens of hardened SAE 52100 steel.

A further disturbing observation, made when the lot size was increased to improve the statistical confidence, was that the plotted results showed a "fine structure" in the life distribution. One such plot is shown in Figure 14. Lives of the 40 "identical" specimens fell into three distinct populations, a low group, a high group and a group intermediate between the two.

Replotting the data as separate populations (Figure 15) gave straight lines, each having a slope characteristic of a normal distribution. Close examination of samples from each group revealed no apparent differences.

Examination of fatigue data generated by other investigators on hardened alloy steels shows similar multiple life distributions, indicating that this phenomenon is

not associated with a particular material or test technique. Figure 16, plotting data reported by Frith,[19] is typical of the observed behavior.
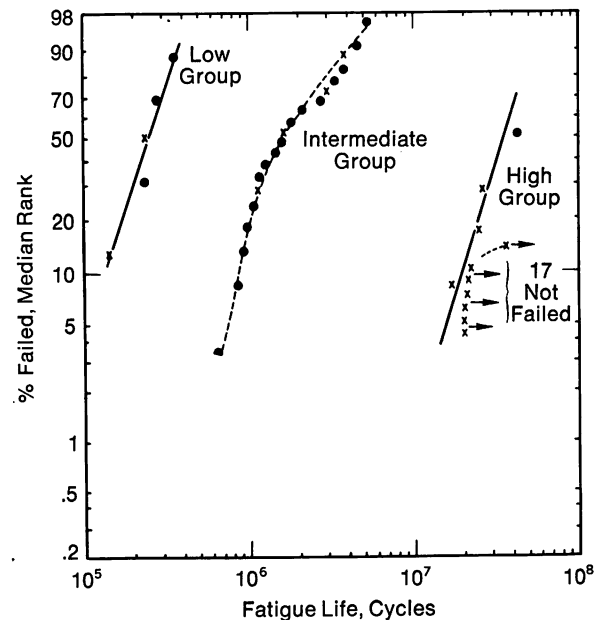


FIGURE 16—Weibull plot of reverse bending tests of EN31 (C-Cr) steels at HRC 62.

Component design must obviously be limited by the performance of the weakest link—the lowest group.

If the causes for the low and intermediate life groups could be identified and eliminated, the effective performance and reliability of hardened steel components would be significantly improved. To date, however, no satisfactory explanation for the multiple distribution has been reported.

Another, more general challenge to alloy steel technology is the alloy "mystique" mentioned earlier. Certain alloying elements do have unique effects on properties. The influence of others is doubtful. What is required is a concerted application of modern techniques to define effects, and the associated mechanisms, of alloying in medium and high carbon steels. With such knowledge, alloys can be optimized for specific applications, and truly equivalent grades can be identified to conserve critical alloying elements.



FIGURE 15—Data from Figure 14 plotted as separate groups.

## Summary

Trends in the technology of the automobile indicate an increasing replacement of low and medium hardness alloy steels by other materials, notably cast irons and powder metal products. The principal role of high hardness steels will continue to be in highly stressed applications requiring maximum resistance to fatigue, and a major challenge to the technology of alloy steels is the

understanding and control of fatigue behavior. Finally, the utility of alloy steels will be greatly enhanced by an increased understanding of the specific effects of the various alloying elements, individually and in combination, on material properties and service performance.

# References

1. *The Sorby Centennial Symposium on the History of Alloy Steels*, C. S. Smith, Ed., Gordon and Breach Science Publishers, New York, 1965, 473.

2. Anon., *Automotive Industries, 155* (1), July 1976, 36.

3. A. L. Boegehold, *Metal Progress, 70*, Sept. 1956, 103.

4. C. McKnight, *Transactions of American Society for Steel Treating, 1* (6), 1921, 288.

5. *ASM Metals Handbook*, 1948 Ed., 456.

6. E. C. Bain, *Trans. AIME, 100*, 1932, 13.

7. M. A. Grossman, *Trans. AIME, 150*, 1942, 227.

8. A. L. Boegehold, *Trans. SAE, 49*, 1941, 266.

9. *Hardenability Concepts with Applications to Steel*, D. Doane and J. Kirkaldy, Ed., TMS-AIME, 1978, 518.

10. Ibid., 493.

11. Ibid., 546.

12. Central Foundry Division, GMC (brochures).

13. P. Vernia, *Proceedings, Powder Metal Technical Conference*, Hoeganaes Corp., 1978.

14. *Interpretation of Tests and Correlation with Service*, ASM, 1951, 1.

15. J. I. Fisher and J. P. Sheehan, *WADC Technical Report 58-289*, Feb. 1959, 3.

16. R. F. Thomson, *ASM Transactions Quarterly, 56* (4), 1963, 802.

17. E. R. Mantel and G. H. Robinson, *Metal Progress, 92* (5), Nov. 1967, 65.

18. L. G. Johnson, *Industrial Mathematics, 2*, 1951, 1.

19. P. H. Frith, *Journal of the Iron and Steel Institute, 180* (II), 1955, 26.

# Discussion

H. TAMEHIRO, *Nippon Steel Corporation.* I would like to ask about the future of boron-containing steels inasmuch as boron has a pronounced effect on hardenability and is also very cost-effective.

G. H. ROBINSON. I think the future of boron steels is very strong and that we are going to see increasing applications of boron steels. I think it's limited only by a couple of things: one is the experience in the early fifties with boron steels which were highly variable. (As soon as people could get alloy, they went back to alloy steels which the mills seemed to handle more effectively) and the other is understanding and controlling of the effect of boron. We use a lot of it now in the industry, and I think the use is going to grow because it certainly is a cost-effective material as far as hardenability is concerned.

J. DODD, *Climax Molybdenum Company.* You did mention a very important development, that being the introduction of nodular irons for applications which have hitherto been the sole field for steel forgings and castings. The examples you've quoted are unalloyed irons. Do you visualize the growth of a new family of alloyed nodular irons comparable to the alloyed steels?

G. H. ROBINSON. Yes, I think that's a definite possibility.

I think there are still applications to be made with the conventional unalloyed nodular iron, but as you get into heat treated structures and specific requirements and certainly the more we learn about the actual effects of alloys the better we'll be able to use them in these materials. There are some other restrictions in nodular irons because you're trying to deal with two equilibrium systems, the graphite and the carbide systems, and so you are not as free as with steels in alloying.

L. M. PETRICK, *Ebasco Services.* I've looked at martensite primarily in weld heat affected zones, and I consider it to be caused by two different mechanisms. One is the interstitial type, carbon or carbon primarily, and the other one is the alloy or substitutional type caused by alloy additions at very low carbon contents. The reason that I bring this up is that I find the substitutional type martensite tougher than the interstitial type. But again, I'm looking at steels and wrought materials as opposed to the high carbon materials that you're looking at, so perhaps there is a difference there.

G. H. ROBINSON. Certainly if you're comparing plate and lath martensites, you will see quite a difference, and this is related to carbon content. I think this reflects one of the challenges I gave this group, that being that we really have a lot to learn about the effects of alloying elements in steels beyond the simple hardenability effects.

# Some Facts and Considerations of Trends in Gear Steels for the Automotive Industry

by C. Razim
Daimler-Benz AG

When selecting material for highly stressed transmission components, three basic economic factors must be taken into account. These are:

1. service characteristics,
2. processing properties, and
3. material costs.

They must be in a well-balanced relationship as indicated in Figure 1.

Each component produced in a series must, on principle, be conceded a failure rate during operation, however small it may be. This rate is marked by the distance AS in Figure 1. A certain expenditure for the manufacture of the component (distance BS) and costs determined by the type of material specified (distance CS) are allocated to this failure rate. In the processing industry, the material expenditure amounts to roughly 50% of the total. Material selection is, therefore, extremely significant.

Consequently the question arises for high performance transmissions as to the optimum case hardening steel and its processing.

## Stressing High Performance Gears

The various types of stresses to which gears can be subjected are best explained by typical forms of damage, the most important of which are shown in Figure 2.

Figure 2a shows "case crushing," in which cracks spread below the surface finally leading to a shell-type breaking out of the tooth flanks.

Contrary to this, the pitting damages on the tooth flank in Figure 2b are often of a smaller type and need not directly lead to a function loss. They are mostly restricted to areas below the pitch circle and are not very deep.

Pure surface damage is shown in Figure 2c. Erosion wear—as *one* possible occurrence of wear—led to a local attrition of the tooth flank. Wear by "fretting" (adhesive wear) and "abrasion" (abrasive wear), which are also known as tooth flank damage, may also be cited in this context.

Figure 2d gives an example of gear damage caused by an impact load. Whole areas of the tooth area break out and lead to an immediate function failure.

Finally, Figure 2e shows fatigue fractures with small residual fractures caused by repeated overloading, simi-



FIGURE 1—*Principles of material selection.*
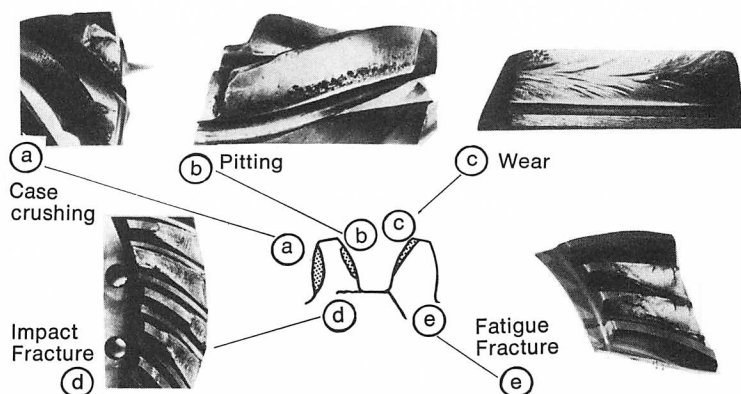


FIGURE 2—*Types of gear failures.*

**a** (top-left chart)

Bending Stress or Strength

Material bending strength

Applied bending stress

Depth Below Surface

a

**b** (top-right chart)

In case of higher friction

Shear Stress or Strength

Material shear strength

Applied shear stress

Depth Below Surface

b

**c** (bottom-left chart)

Material shear strength

Shear Stress or Strength

Applied shear stress

Depth Below Surface

c

**d** (bottom-right chart)

Wear Resistance or Load

Wear resistance

Wear load

Depth Below Surface

d

*FIGURE 3—Stress-strength ratio in case hardened steels.*

larly resulting in component failure. Further theoretical stress analysis of these damages results in the material mechanics relationships included in Figure 3:

Tooth shape and kinematics determine the type of stress; in the case of Figures 2d and 2e, these can mainly be considered as bending stresses. The load distribution allocated to it is shown in Figure 3a. The maximum stress is at the surface, thus determining the point of maximum strain. If the pertinent bending strength of the material is exceeded, impact, endurance or fatigue fractures are incurred in the area of the tooth base. Here it must

always be distinguished between a predominantly sudden load and a load of rather a smooth nature.

Of a completely different type, is the stress leading to pitting (cavities) according to Figure 2b. A maximum shear stress acting under the surface in the case of pure rolling stress is shifted through a superimposed friction force near the surface or directly to the surface. Corresponding to Figures 2b and 3b, these damages occur in areas close to the surface. Neglecting some exceptional cases, the crack source is always located at the surface of the tooth flank in the area of negative sliding.[3] Damage

of this type occurs if the ratio of shear stress to shear strength repeatedly exceeds a critical quantity (so far not accurately known).

The ratio of shear stress to shear strength is also decisive for damage produced by case crushing. However, not the case but the transition zone (Figure 3c) from the carburized case material to the core material is important in this instance. Here too a critical quantity may not be exceeded. R. Pedersen and S. L. Rice give a value of approximately 0.6 for this quantity.[4]

The wear resistance of case hardened components is described to a first approximation by the surface hardness. If a direct material contact is made between the tooth flanks as a result of poor lubrication conditions, considerable wear must be expected (Figure 3d). This wear will be greater the lower the surface hardness.

The most important types of damage which can occur on gears are listed in Table I. Allocated to these are the material properties which essentially determine the development of these types of damages. These again are compared with the quantities (e.g. alloy or type of structure) which finally determine material properties. The factors influencing the microstructure are listed. These change during the course of the production process and have a decisive effect on component behavior. The most important factors are surface oxidation (SO), residual austenite content (RA), surface carbon content (SC), low temperature cooling (SR) and rolling work hardening (WH). These factors exclusively influence the surface zones of a case hardened component; i.e. those areas, which, in conformity with Figure 3, are subjected to the maximum stress. Seen under this aspect, all those metallurgical measures are of paramount importance which can have an effect in the surface zones.

## The Significance of Carbon and Chromium

As shown by H. U. Meyer,[5] the steel composition is very important from the standpoint of carburizing behavior.

It is well known that, dependent on the carbon potential with given carburizing conditions, a typical alloy surface carbon content is obtained (Figure 4). The carbon level is due to the carbon activity of the steel, which again directly depends on the solute alloying element content.[6] Chromium is an important element in that it causes a very strong shift of the equilibrium between solute and supersaturated carbon toward smaller carbon contents.[7] This in turn is equivalent to the well-known tendency toward supercarburization, corresponding to the result shown in Figure 4 as a consequence of carburizing with a high carbon potential atmosphere.

Apart from this, the carburizing equilibrium obtained for a given alloy after a sufficiently long time is temperature dependent in the sense that carbon solubility increases with rising temperature. Since it should be endeavored to select the carburizing temperature as high as possible even taking into account optimum energy utilization (Figure 5), a consideration of the effect of the alloying elements in case hardening steel is also necessary.

The following quantitative relationship between residual austenite after continuous quenching and heat treatment of specially melted case hardening steels was provided by W. J. Harris and M. Cohen[8] and by G. Bierwirth:[9]

**Table I**—Factors Affecting Failures of Case Hardened Gears

| Failure Type | Required Properties | Desired Structure | Critical Factors | Composition Effects |
|---|---|---|---|---|
| High Cycle Fatigue | Strength ($\sigma_{el}$) | Surface: Martensite Core: Martensite (+ Bainite) | RA $\downarrow$, SO$\downarrow$, SR$\downarrow$, SC$\updownarrow$, WH$\uparrow$ | |
| Impact Fatigue | Strength ($\sigma_{el}$) Deformability ($\epsilon_{pl}$) | " | RA $\downarrow$, SO? , SR$\downarrow$, SC$\downarrow$, WH? | Cr$\downarrow$, C $\downarrow$ Core |
| Bending Strength (Impact) | Strength ($\sigma_{el}$) Deformability ($\epsilon_{pl}$) | " | Brugger $\ominus$  ?  $\downarrow$  $\ominus$<br>RA $\downarrow$, SO $\downarrow$, SR $\downarrow$, SC $\uparrow$, WH $\uparrow$<br>ICS$\downarrow$ | Ni $\uparrow$ |
| Surface Fatigue | Strength ($\sigma_{el}$) | " | RA $\uparrow$, SO$\ominus$, SR? , SC$\updownarrow$, WH$\uparrow$ | |
| Wear | Hardness (HV) | " | RA $\downarrow$, SO$\uparrow$, SR$\uparrow$, SC$\updownarrow$, WH$\uparrow$ | |

$\sigma_{el}$ = Elastic Limit  
$\epsilon_{pl}$ = Elongation after Fracture  
HV = Vickers Hardness

RA = Retained Austenite  
SO = Surface Oxidation  
SR = Subzero Refrigeration  
SC = Surface Carbon Content  
WH = Work Hardening  
ICS = Initial Crack Stress

Distance from Surface, in.

| Steel | C | Mn | Cr | Ni | Mo |
|-------|------|------|------|------|------|
| 20 MnCr 5 | 0.20 | 1.28 | 1.17 | — | — |
| 5120 | 0.17 | 0.81 | 0.72 | — | — |
| 6120 | 0.20 | 0.83 | 0.70 | V = 0.13 | |
| 3310 | 0.13 | 0.54 | 1.56 | 3.52 | — |
| 16 MnCr 5 | 0.16 | 1.11 | 1.00 | — | — |
| 3114 B | 0.16 | 0.87 | 0.60 | — | 0.31 |
| 8620 | 0.19 | 0.75 | 0.56 | 0.60 | 0.21 |
| 3114 A | 0.17 | 0.87 | 0.29 | — | 0.30 |
| 4317 | 0.19 | 0.58 | 0.48 | 1.82 | 0.25 |
| 1018 | 0.17 | 0.72 | 0.01 | — | — |
| 3128 | 0.17 | 0.47 | 0.09 | 0.16 | 0.54 |
| 4028 | 0.25 | 0.73 | 0.14 | 0.14 | 0.22 |
| 3131 | 0.19 | 0.50 | 0.10 | 0.17 | 0.40 |
| 4620 | 0.19 | 0.56 | 0.21 | 1.72 | 0.23 |
| 4817 | 0.18 | 0.51 | — | 3.47 | 0.25 |

Distance from Surface, mm

*FIGURE 4—Carbon content in surface zones of carburized steels.*

$$V\gamma = \exp^{-K(M_s - T_q)}$$

where $V\gamma$ = Residual austenite in % by volume

$M_s$ = Martensite temperature (start)

$T_q$ = Lowest temperature reached after quenching

$K$ = Constant ($\sim 1.4 \times 10^{-2}$).

This shows the importance of the $M_s$ temperature in the practical performance of the heat treatment of case hardening steels. With adequate cooling rate for a given temperature of the quenching bath, it clearly determines the microstructure in the surface zone of a case hardened component.

It is well known that of all alloying elements which are commonly used, carbon has the greatest influence on the position of the $M_s$ temperature,[10] a severe drop of the $M_s$ temperature being found with increasing carbon content. The difference ($M_s$-$T_q$) in the formula consequently becomes continually smaller and, because of the prevailing relationship, the RA content increasingly greater. Figure 6 explains the relationships described thus far. With low carburizing temperatures, the carbon pickup is limited. Corresponding to the prevailing carbon potential, this leads to minor supersaturation only with higher alloying contents (e.g., Cr), this being the reason that only little residual austenite prevails after the martensite formation. An increase in the carburizing
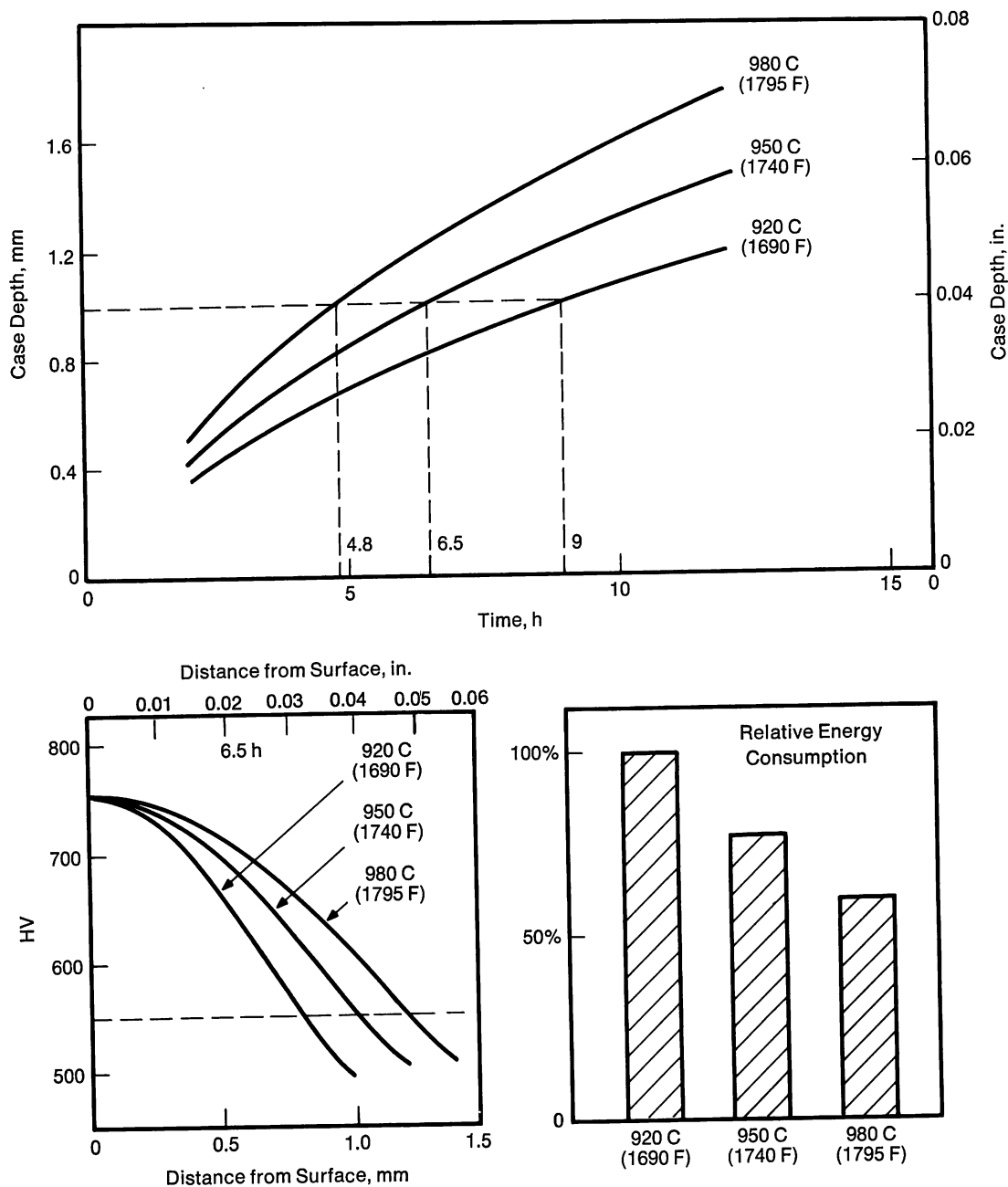
FIGURE 5—Energy consumption as a function of carburizing temperature.

temperature increases the carbon pickup, thus resulting in a drop in the $M_s$ temperature and an increase in residual austenite.

In addition to this, existing alloying elements increasingly form a solid solution resulting in an indirect carbon supersaturation with simultaneous shifting of the $M_s$ point to lower temperatures. In conformity with Figure 4, there is a strong effect of chromium which promotes residual austenite formation, masking the effects of all remaining alloying elements. A change in the $M_s$ temperature and shifting of the equilibrium lines in the iron-carbon diagram result in a gradual increase of the RA content with increasing chromium.

A further effect of alloying is the high affinity of chromium and oxygen. Corresponding to its thermo-dynamical potential, stable chromium oxides are formed by contact with oxygen. Consequently an increased tendency for surface oxidation is obtained in interaction with silicon and aluminum.

## Mechanical Properties of Case Hardened Components

### Fatigue Strength Behavior

The negative effect of residual austenite on the rotating bending strength of a notched sample ($\alpha_K = 1.86$) is shown by the example of a case hardened Cr-Ni steel in Figure 7. As carbon was raised from 0.65 to 1.2% (corresponding to a residual austenite of about 80%), the
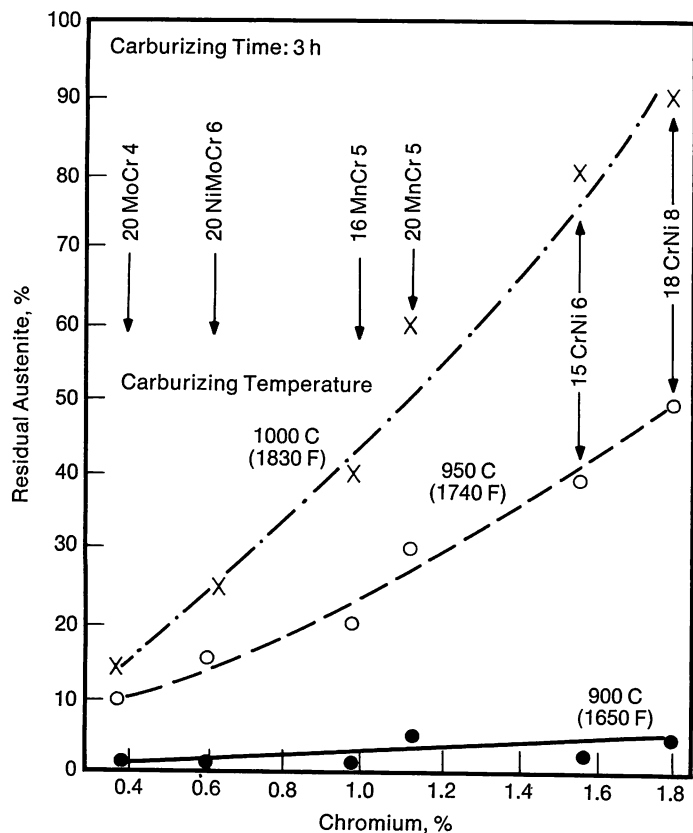
FIGURE 6—Residual austenite vs. chromium content.

fatigue strength dropped from 700 to 540 MPa (102 to 78 ksi). This was also discovered on other steels, test pieces and components.[11,12] It confirms the well-known experience that fatigue strength is reduced by increased residual austenite.

Figure 7 also explains that elimination or reduction of residual austenite by an additional low temperature treatment leads to a further deterioration. This is the result of unfavorable residual stresses from the secondary martensite formation.[12,13]

If case hardening steels are carburized in gas at 930 C (1705 F), the formation of a light surface oxidation is technically almost unavoidable. It is known that this also reduces fatigue strength (approximately 20%, Figure 8). Since the removal of the impaired skin layer by means of electrolytic polishing is very difficult to accomplish in production, the only possibility of improvement is a final shot peening treatment. However, the positive effect is limited to the fatigue strength only (Figure 9).

## Impact Fatigue Strength

R. A. DePaul investigated the impact fatigue strength of case hardened steels.[14] He arrived at the conclusion that this property is improved with increasing nickel content. A more comprehensive evaluation of the test results included in this work provides the additional
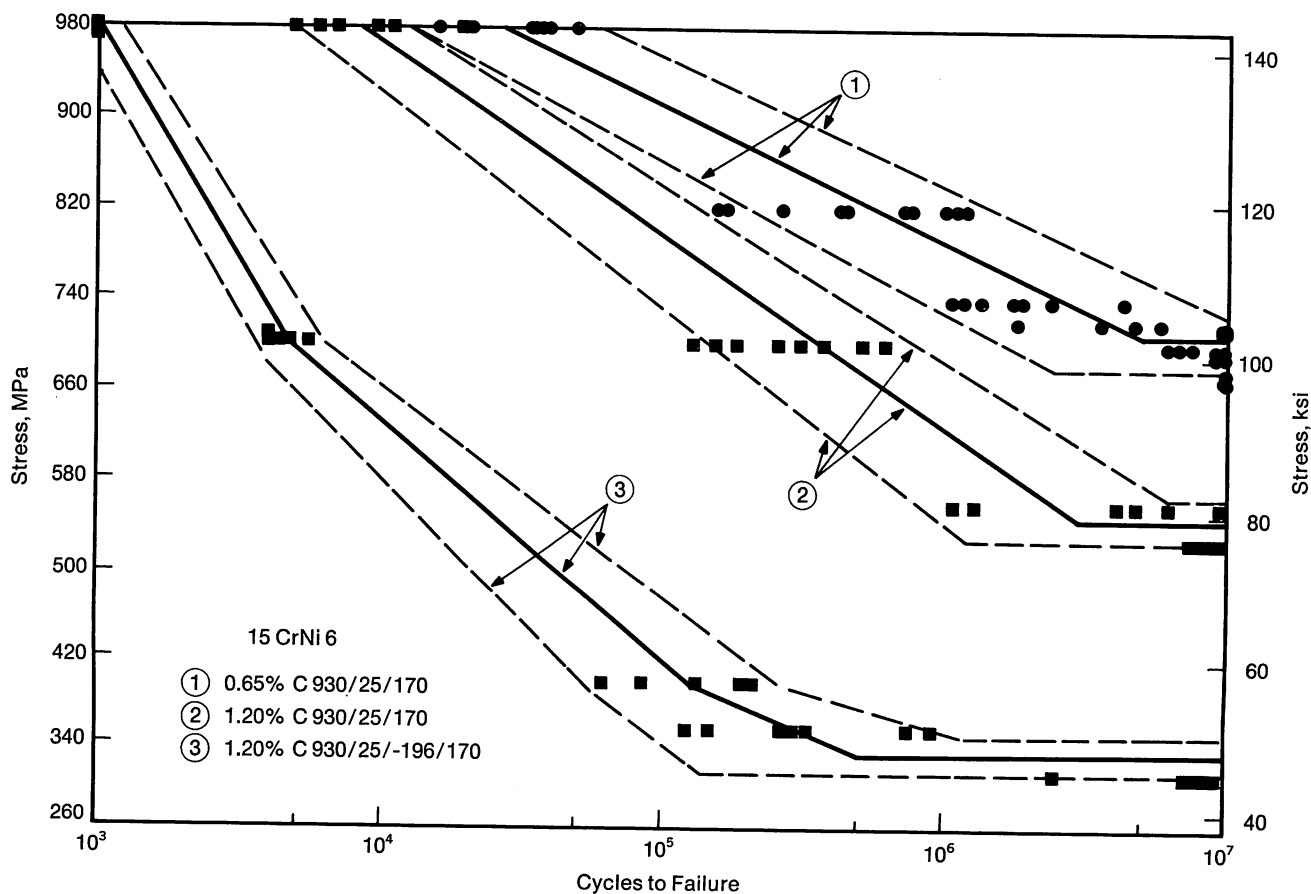


FIGURE 7—Effect of subzero refrigeration on fatigue life of case hardened steels.

conclusion shown in Figure 10. According to this, impact strength is closely related to the chromium content of the alloys, and deviations from the curve are associated with carbon content.

With roughly similar chromium contents, the impact fatigue limit is essentially a linear function of carbon con-

tent (Figure 11), not of the nickel or molybdenum contents. The results show that service life under repeated impact stresses is not so much determined by the mechanical properties (e.g., hardness, core strength, yield point), but by the alloy and particularly by the carbon content.

This leads to the conclusion that service life is mainly
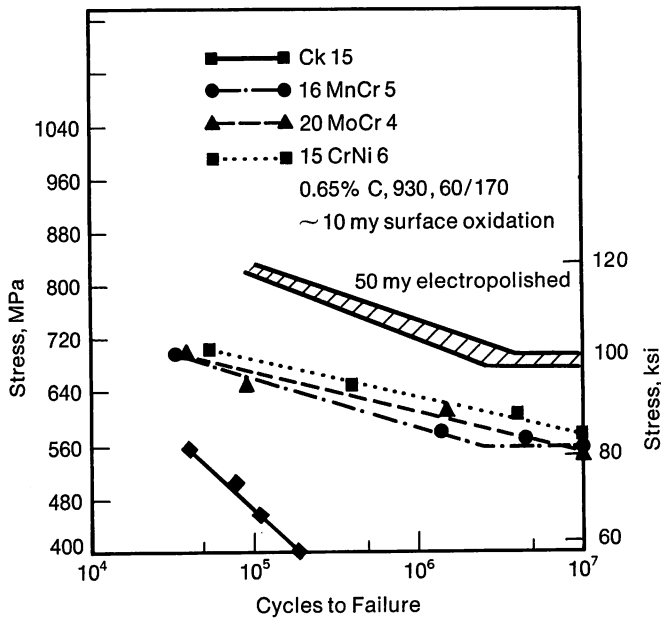
FIGURE 8—Martensitic structure as optimum for high fatigue strength.
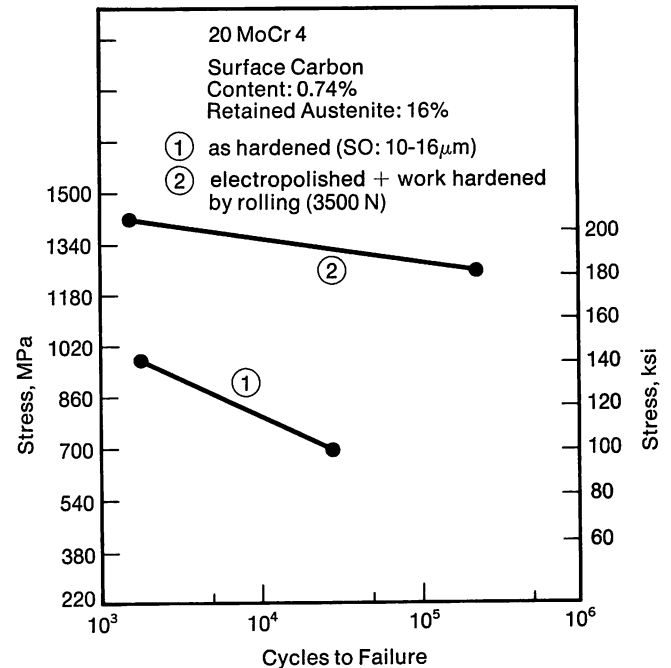
FIGURE 9—Effect of surface oxidation on fatigue behavior.
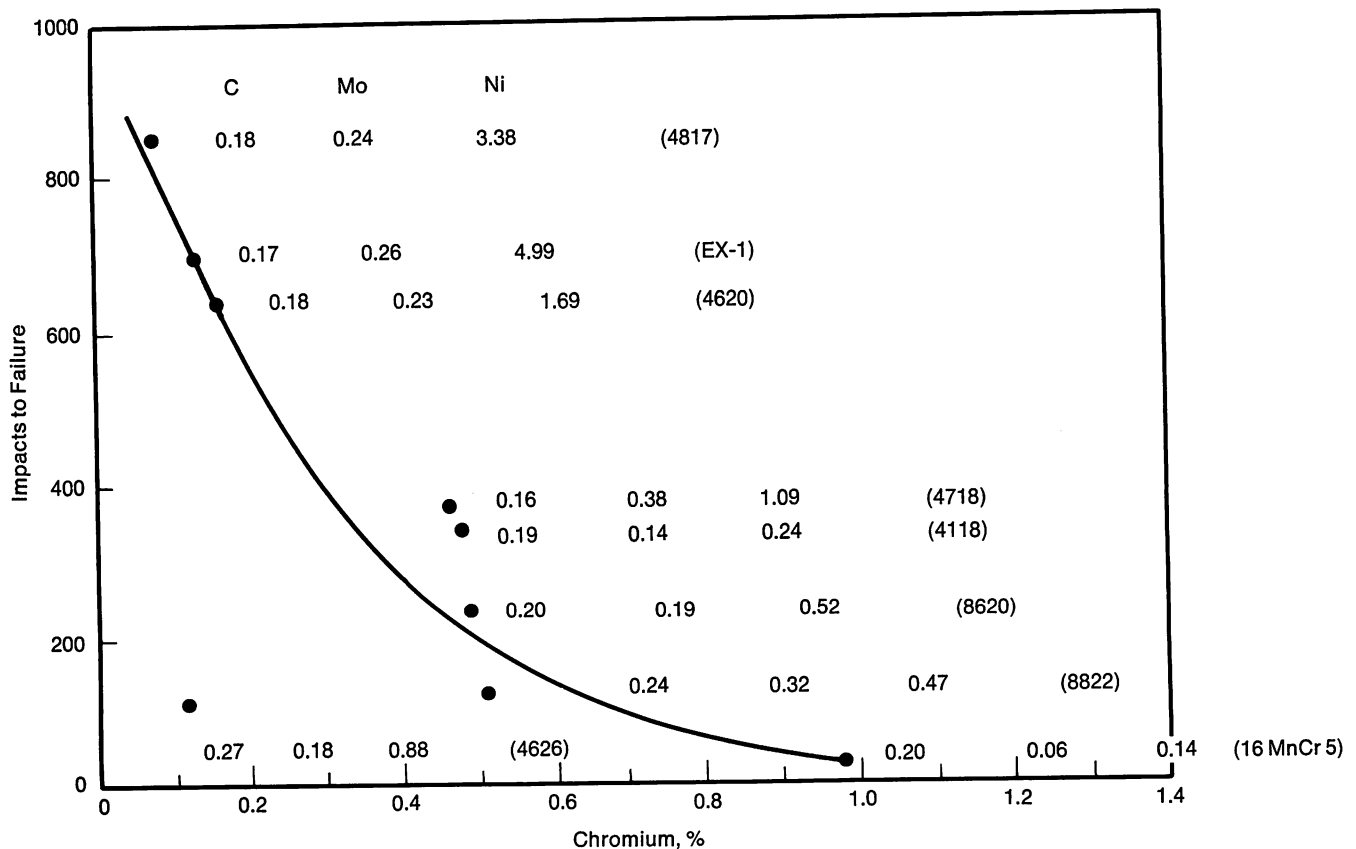
FIGURE 10—Impact fatigue vs. chromium content.

a function of the "crack propagation speed" in the base material. The case hardened layer is brittle thus aggravating the test.[15] The dependence of "toughness" on the carbon content of the base material was previously described by E. Theis[16] and B. Prenosil.[17]

## Impact Bending Strength

Various authors investigated "toughness" using the impact test.[12, 18, 19] The results are somewhat conflicting but contain the concurrent information given in schematic form in Figure 12. The "Brugger sample" was used as the test piece in most cases.[19]

In the hardened condition, the maximum impact force is determined by the core strength, but these results are subject to severe scattering.

In the case hardened condition, no better differenciation of the types of steel occurs at low case hardening depths (< 1.4 mm, 0.055 in.). However, the scattering is reduced. The values in this area are independent of the surface carbon content. Now, as before, they describe mainly the properties of the core material.

With greater case hardening depths (> 1.4 mm, 0.055 in.), the impact forces drop severely and differenciate less clearly between different types of steels. An additional influence of carbon can be seen at greater case hardening depths. The maximum values are achieved by steels with low case carbons, and the lowest values are associated with steels with high surface carbon contents. With low surface carbon and great case hardening depths, the relationship between chromium content and impact strength again becomes apparent as shown in Figure 10. With increasing chromium content (above 0.17%), a very drastic drop in the values occurs at first, with a value of approximately 1.5% seemingly representing a minimum limit.

The influence of surface oxidation or a subsequent shot peening treatment on the results of the impact tests cannot be established.[12] Residual austenite contents or carbides do not appear to be important.

With low case hardening depths, an evaluation of the toughness of the hardened layer by means of the impact test does not appear to be possible. Tests conducted with the "Brugger sample" mainly describe the properties of the base material.

## Initial Crack Strength of Notched Samples

The ability of the carburized and hardened surface zone to sustain plastic deformation without initial cracks



FIGURE 11—Impact fatigue vs. carbon content.
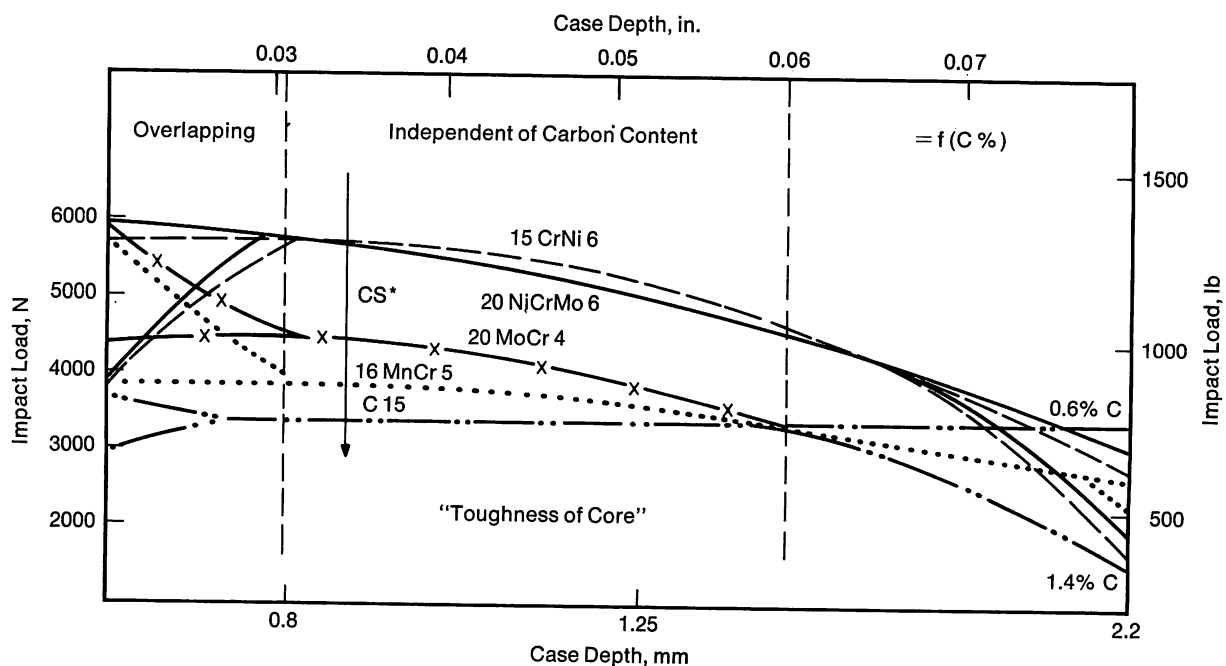


FIGURE 12—Impact load factors.
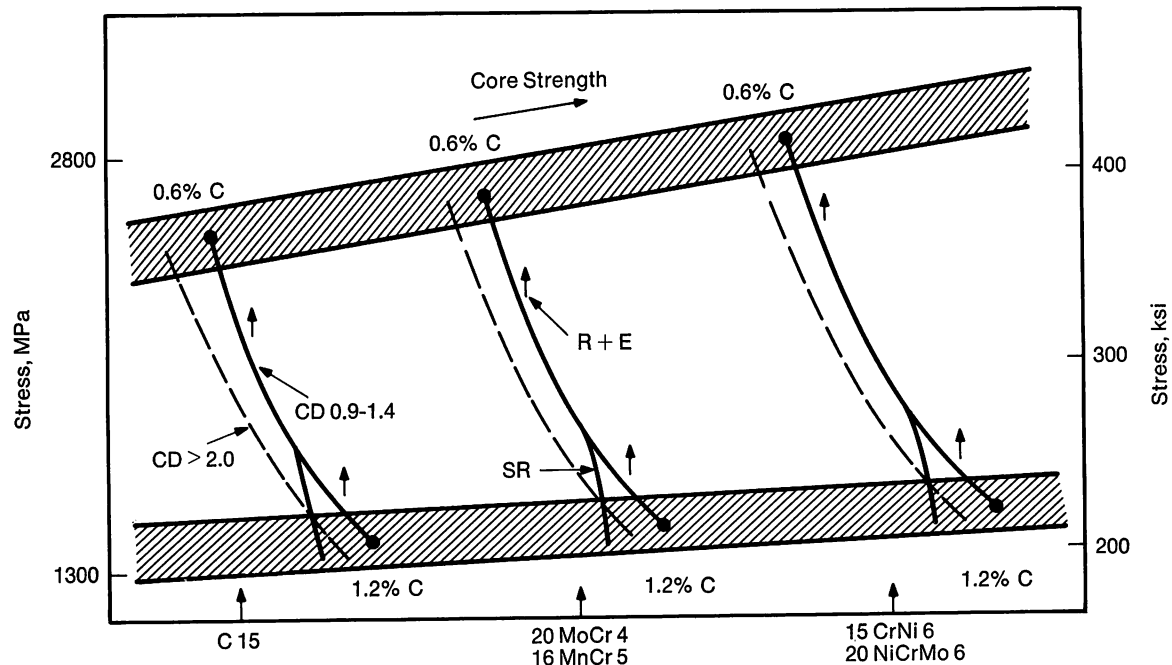
FIGURE 13—Initial crack strength.

is frequently valued as a criterion of "toughness." The static bend test is useful in determining this property. A suitable measuring quantity can then be the initial crack strength. If this is attained, the initial crack is formed in the carburized and hardened surface zone. A summary of the results obtained to date is shown in Figure 13. This relationship was worked out from the measurement of W. Beumelburg.[12]

With low surface carbon contents (~ 0.6%), the initial crack strength rises with increasing core strength. The core strength of the selected samples is dependent on the alloy content, gradually rising through C 15, 20 MoCr 4 and 16 MnCr 5, 20 NiMoCr 6 and 15 CrNi 6.

With high surface carbon contents, the initial crack strength becomes less dependent on the core strength (i.e. hardenability), however, it drops to a considerably lower level. A low temperature stress relief treatment results in a deterioration of these values. Increasing the case depth to more than 1.4 mm (0.055 in.) also results in a reduction of the initial crack strength. Electrolytic polishing and rolling to eliminate the negative effect of surface oxidation shift the initial crack strength toward greater values.

The effect of a high surface carbon content, resulting in considerable residual austenite, is evident in Figure 14. The dependence on the core strength (e.g. hardenability) is still noticeable, even if an additional factor appears to be effective which obviously influences the initial crack strength, but which to date has not yet been clearly established.

## Resistance to Surface Fatigue

The behavior of case hardened gears and laboratory
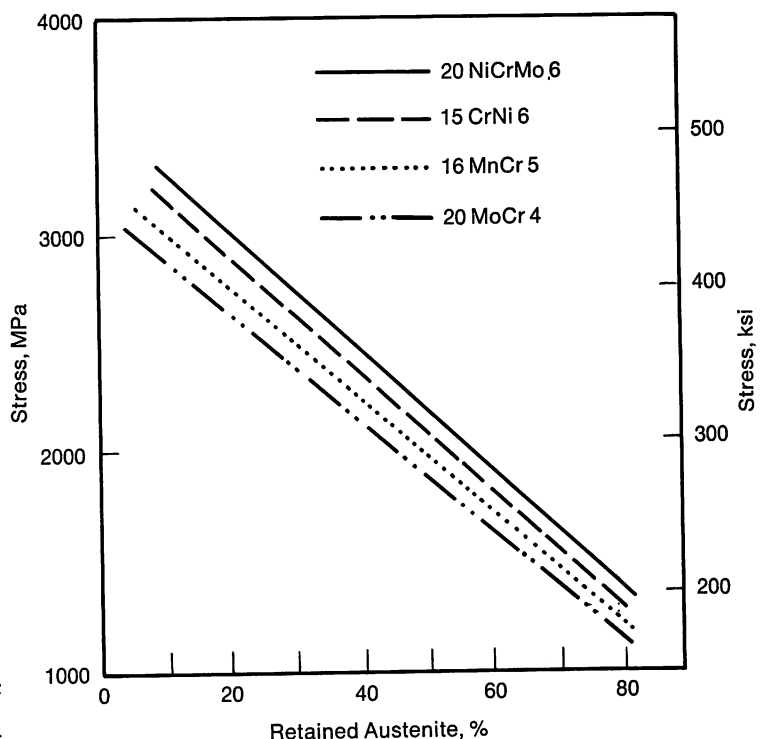


FIGURE 14—Initial crack strength vs. retained austenite.

samples was established in extensive tests.[20-24] The most important result of this work is that not so much the composition of the steel but rather the existing structure determines the resistance to pitting.

A martensitic case with limited quantities of residual austenite must be achieved to keep abrasive wear low. High residual austenite contents lead to high surface fatigue strength as a result of work hardening occurring

on load application; there is, however, the risk of increased wear or fretting.

Detrimental and definitely to be avoided are structures containing pearlite or bainite.

### Sliding Wear

Surface hardness is a measure of sliding wear as a first approximation. A fully martensitic surface zone offers the greatest resistance to wear, while the presence of pearlite, bainite or residual austenite is detrimental.

Quantitative statements regarding the dependence of wear resistance on the residual austenite content have been reported.[25] Wear behavior as function of hardness was also described.[26]

## Structure and/or Alloy-Dependent Properties of Case Hardening Steels

Evaluating the service properties of case hardened components with regard to their dependence on the type of steels used, it is evident that it is necessary to differentiate between service properties dependent on the metallurgical condition of the surface zone and service properties which are also (or exclusively) determined by the core material.

Part of the former are the fatigue strength, the pitting resistance on tooth flanks (rolling + sliding) and the resistance to wear. Part of the latter are the pitting resistance on antifriction bearings (pure rolling), the resistance to case crushing and crack propagation under impact stress where the surface cracks early.

"Toughness" is still not clearly defined. If it is understood as the ability of "removing load peaks through plastic deformation," properties of the surface zone are primarily concerned. Questions of this type then belong to the group of problems of "development of cracks."

If it is understood as the ability "to prevent cracks developed in the case hardened layer on overloading from propagating into the core material," the core properties are concerned in this case. The analysis and interpretation then concern the problem of "crack propagation."

Available results indicate that the fatigue strength of case hardened components is determined by the structure. A fully martensitic case produces the optimum fatigue strength regardless of the alloy type. This is also true to a certain extent for the resistance to surface fatigue, the work hardening which takes place during the load application leading to structures of high (martensite) hardness even with samples originally containing residual austenite.

Pitting and case crushing under the surface are closely connected with the type of structure prevailing at points of overload. The type of structure in turn is

directly dependent on hardenability and thus on the alloy composition. Consequently strength and type of alloy are more closely related in areas below the surface than on the surface. Here the martensite formation is achieved in any case with correctly conducted carburization and adequate cooling. However, a suitable chemical composition must prevail in the core.

These relationships explain the functions shown in Figures 12 to 14 when the core strength (or the hardenability with identical sample shape and treatment) is considered as the determining factor. However, the assumption fails for the interpretation of Figures 10 and 11 where an alloy influence is unmistakable.

The possible effect of chromium must be pointed out once again in this connection. All corresponding results obtained during investigations of "toughness" give reason to assumptions that a special significance is attached to this element that is not yet clearly comprehensible, therefore requiring further investigation.

Experience has shown that there are alloying elements which may become effective in increasing hardenability and/or changing toughness. It is known that, in addition to carbon, boron belongs to this list. Obviously chromium also increases the hardenability as well as "brittleness" at the same time, at least accelerating "crack propagation," as shown in Figure 10.

## Heat Treatability of Case Hardening Steels

Taking into account all of the data and facts previously stated, the following practical conclusions are justified. The principle zone of stress of gears is in the surface. The first incipient cracks and defects occur here.[27] The heat treatment must therefore produce an optimum structure in this area. This is characterized by as fully a martensitic structure as possible and the absence of all nonmartensitic constituents. Regarding the direct hardening which must be employed for reasons of energy and cost, this requirement makes special demands on the furnace process since only a relatively small range of surface carbon contents leads to the maximum hardness resulting from martensite formation. This in turn is a precondition for maximum wear resistance.

If the heat treatment response of various steels is examined under this aspect, the relationships shown in Figure 15 are obtained. The maximum hardness of approximately HV 880 is achieved by steel 20 MoCr 4. Among the steels examined, this is the alloy with the lowest hardenability. With increasing hardenability, the attainable maximum hardness drops to approximately HV 800. At the same time, the specific maximum hardness shifts toward lower carbon contents of about 0.75% for the Mo-Cr steel and about 0.6% for the Cr-Ni steel.

Of special importance to the practical heat treatment is the carbon range, $\Delta C$, which can be utilized for
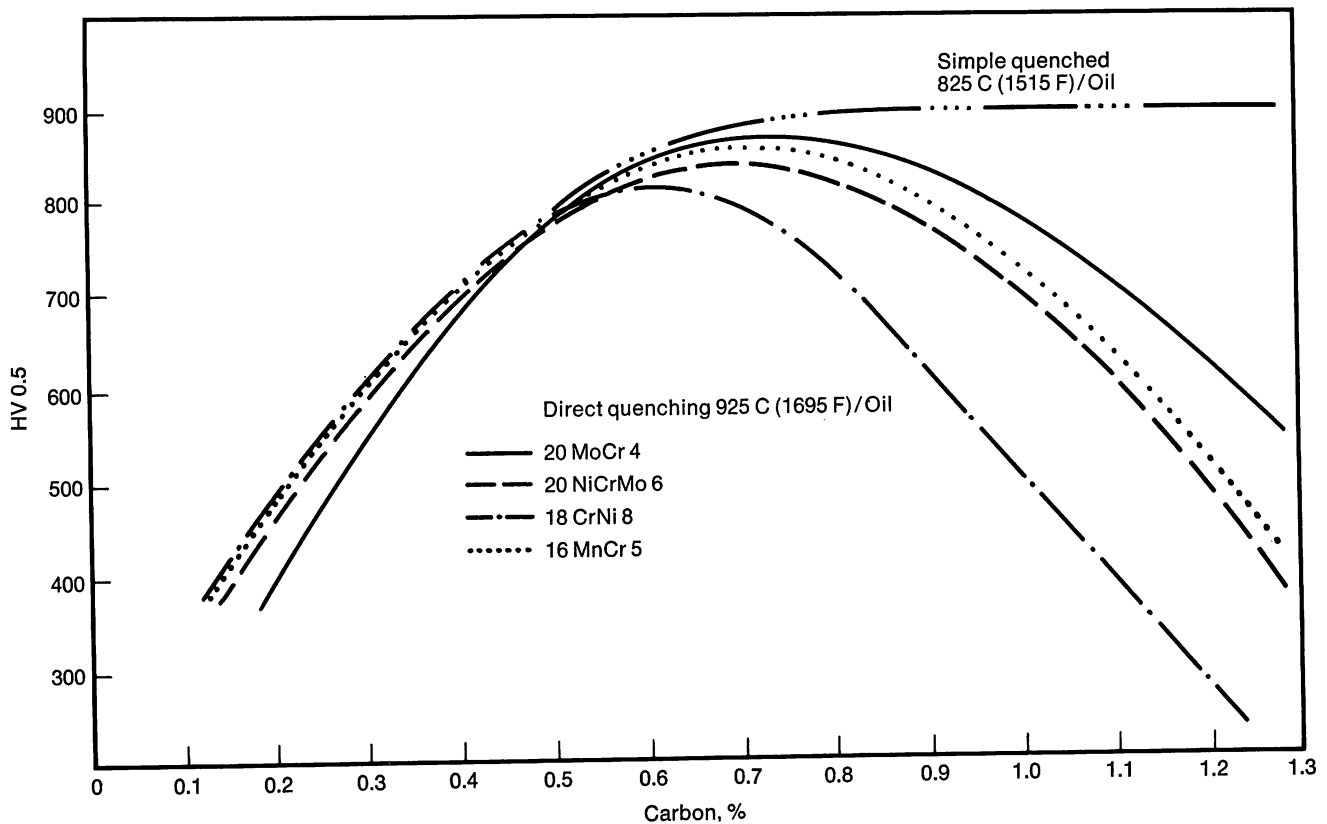
FIGURE 15—Hardness vs. carbon content.

the achievement of a minimum hardness value of, for example, HV 800. The values for the individual steels are:

|  | $\Delta C$ |
|---|---|
| Cr-Ni steel | 0.15 |
| Ni-Mo-Cr steel | 0.34 |
| Mn-Cr steel | 0.38 |
| Mo-Cr steel | 0.44 |

In other words, the optimum alloy from a heat treatment point of view is characterized by a relatively low hardenability. It is attained by alloying contents of approximately 0.5% Mo and 0.5% Cr. This steel was developed for the introduction of direct hardening and, because of its ease of heat treatment, is a standard steel today despite unfavorable pricing.

If higher core strengths are required to support the case hardened layer or to prevent case crushing, further alloying additions are required. However, probably the most inexpensive element, chromium, cannot be recommended without reservation since the impact fatigue limit is negatively influenced by chromium (Figure 10). When considering whether impact strength is important for the application—as may be the case for highly stressed commercial vehicle transmissions—one is faced with the alternative of using either less chromium or more nickel. Using less chromium seems to be on the safer side according to Figure 10.

Nickel or molybdenum are recommended as alloying additives to ensure adequate hardenability. It is then a question of economy if nickel or molybdenum should be given preference. The ratio of the effects on hardenability must be taken into account here, approximately 3.5 times the quantity of nickel being required as molybdenum.[28] In addition, the mechanical processing (extruding, machining, etc.) must be taken into account. High nickel contents can complicate processing so that expensive preliminary treatments are required.

## Trends and Possible Future Developments

It is generally known that the strength of case hardened components can be improved by shot peening. This applies especially to high cycle fatigue and, to a lesser degree, to low cycle fatigue.

Strength in both fatigue ranges[29] and in bending[12] can be increased considerably through work hardening by rolling. Increases in the fatigue strength of over 100% through high pressure work hardening are quite possible (Figure 16). Despite sharp notches ($\alpha_K \sim 2$), the fracture does not occur in the area of the greatest tension but in the considerably thicker cross section of the sample (Figure 17). A further development of this method with the aim of work hardening tooth base radii will have far-reaching consequences. Maximum bending stresses of case hardened gears can be increased considerably.
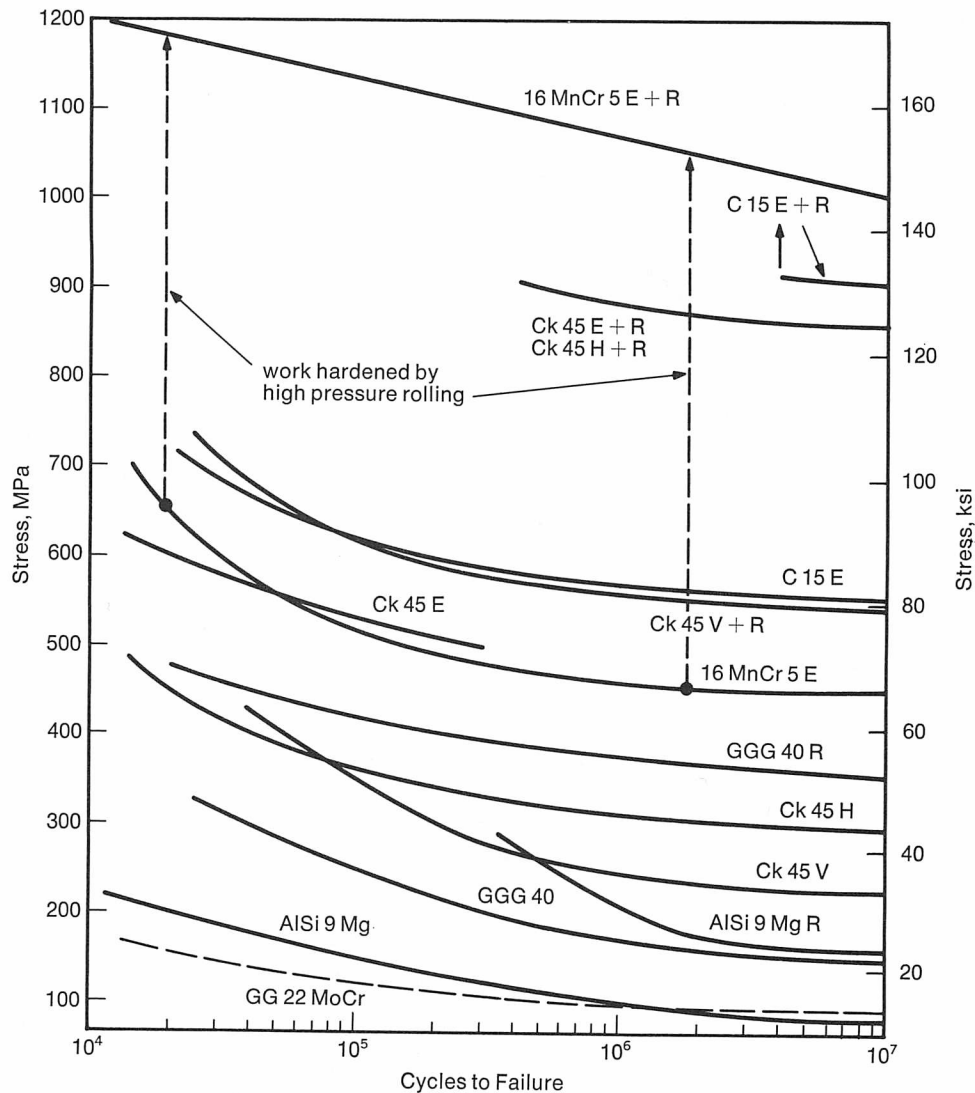
FIGURE 16—*Increase of bending fatigue by rolling process.*



As Hardened



Work Hardened by Rolling
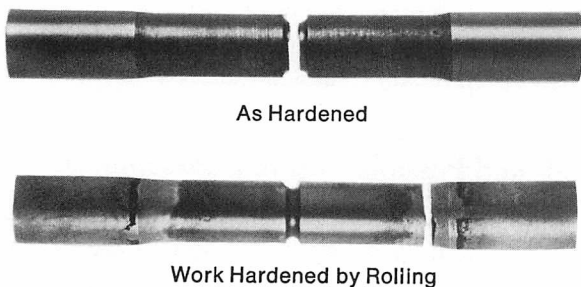
FIGURE 17—*Notched bending fatigue sample Ck 45 (SAE 1045) case hardened.*

Favorable materials with respect to cost, for instance spheroidal graphite cast iron, could be upgraded to a strength level roughly corresponding to the steels which are used today (Figure 18).

A summary of the available fatigue data is schematically shown in Figure 19.

Assuming that a component with a fully martensitic surface according to Figure 8 reaches a fatigue strength of 700 MPa (100 ksi), damage by surface oxidation re-

sults in a drop. This drop is higher the greater the residual austenite content in the surface zone, reaching a final value of 400 MPa (58 ksi).

Starting from the value of 700 MPa (100 ksi), considered as optimum, surface work hardening by high-pressure rolling increases the strength to approximately 1000 MPa (145 ksi) (Figure 16). The possible range between maximum and minimum values is ± 350 MPa (50 ksi). With respect to a bar of identical strength, this means that the cross section and thus the weight can be reduced considerably if it is possible to avoid faulty heat treatments and to work harden the surface zone.

The tendency toward surface oxidation is reduced with the reduction of elements with an affinity for oxygen. The tendency to supercarburize and thus form residual austenite is smallest with low chromium steels. The attainable maximum surface hardness drops with increasing hardenability, e.g. by the addition of nickel according to Figure 15. These facts would clearly speak in favor of using molybdenum as an alloying element if economic aspects could be neglected. Since this is not
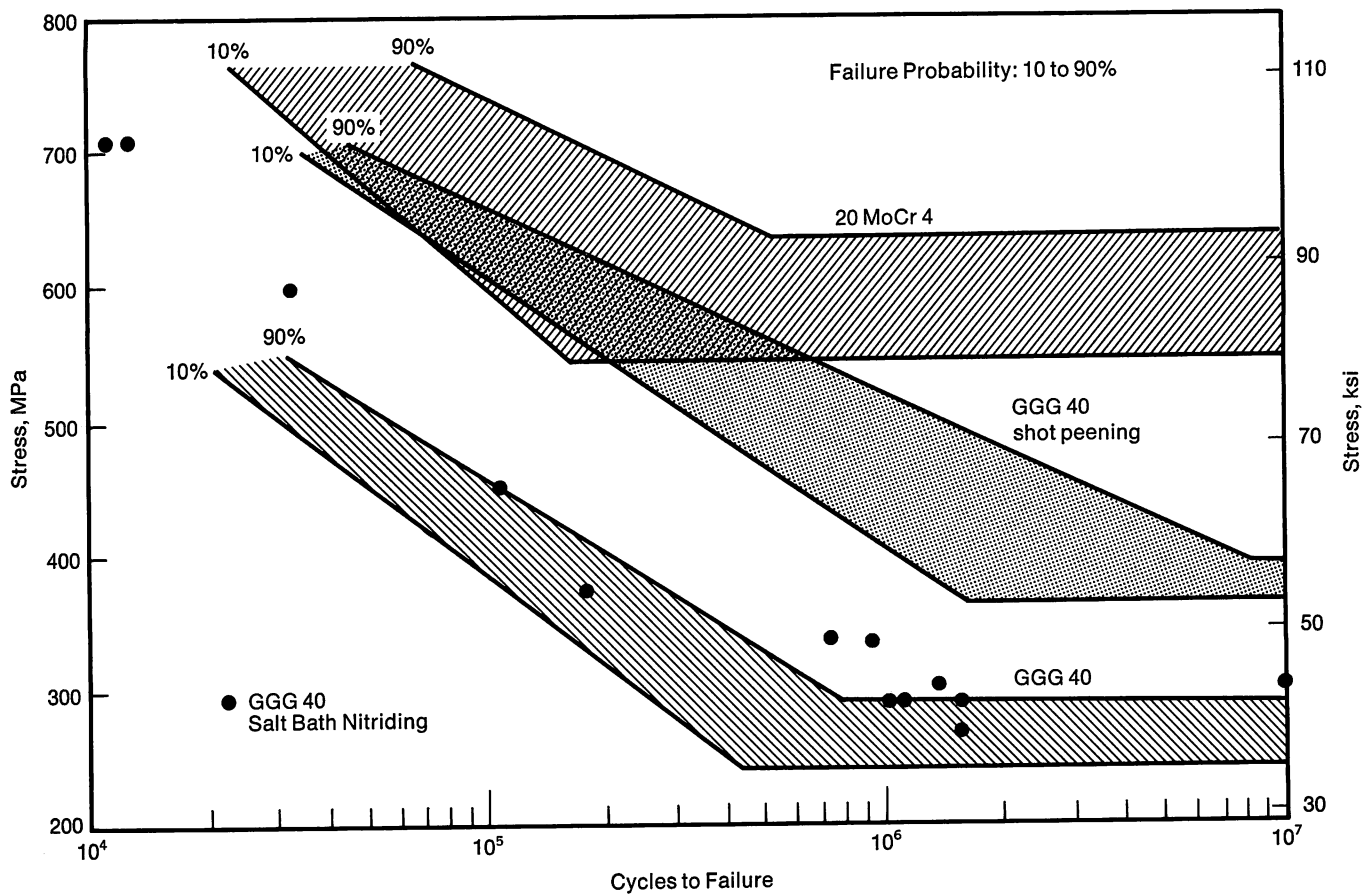
*FIGURE 18—S-N curves for gear materials.*
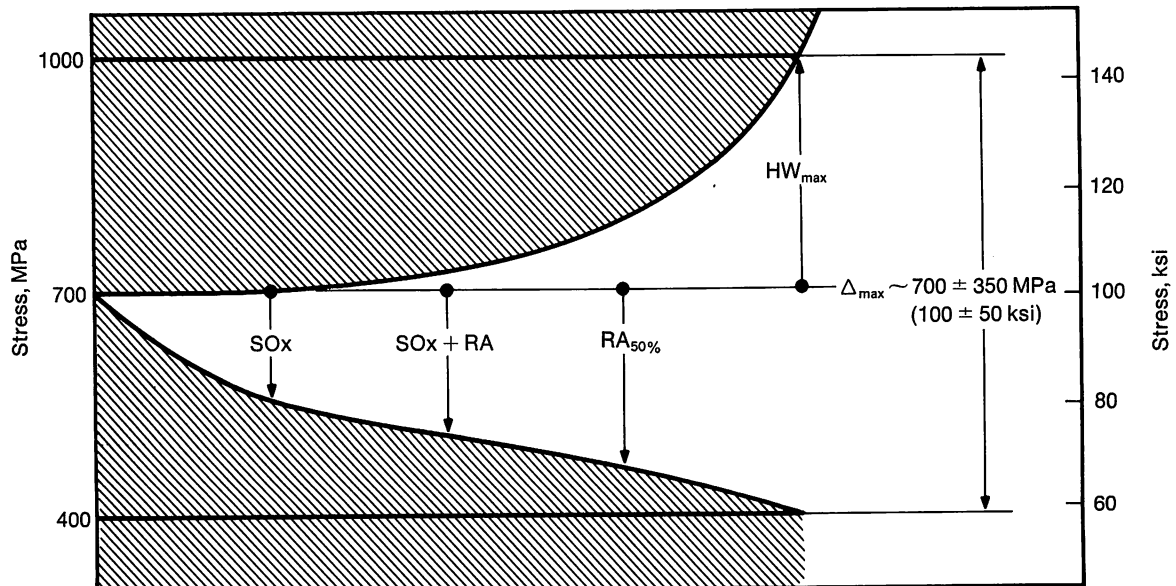


*FIGURE 19—Endurance limit of case hardened steels depending on surface condition.*

the case, the future will be characterized by the fact that through improvement of steel production metallurgy, the furnace process for the heat treatment, and through the application of suitable surface work hardening methods, more cost-effective case hardening steels will be developed and used.

Two development tendencies deserve special mention:

1. Further development of Cr-Mn steels with the objective of an improved grain size stability by adding niobium, and improvement in the warping behavior of these steels by adding boron in the range from 0.001 to 0.003%.

2. Optimization of temperature control and more accurate adjustment of the carburizing atmosphere, the latter by using oxygen probes for indirect control of the carbon potential in narrow ranges.

# References

1. C. Razim, VDI-Z, 119 (11), 1977, 539.

2. V. K. Sharma, G. H. Walter and D. H. Breen, Product Engineering, 50 (6), 1979, 49.

3. C. Razim, Doctoral Dissertation, Technische Hochschule Stuttgart, 1967.

4. R. Pedersen and S. L. Rice, Trans. SAE, 69, 1961, 370.

5. H. U. Meyer, Berg- und Hüttenmännische Monatshefte, 105, 1960, 292.

6. H. Brandis, Unpublished results, 1980.

7. K. Bungardt, E. Kunze and H. Brandis, DEW-Technische Berichte, 5 (1), 1965, 1.

8. W. J. Harris and M. Cohen, Trans. AIME, 180, 1949, 447.

9. G. Bierwirth, Schweiz. Arch., 30 (4), 1964, 104.

10. L. D. Jaffe and J. H. Hollomon, Trans. AIME, 167, 1946, 617.

11. C. Razim, Osterr. Ingenieur Zeitschr., 20 (4), 1977, 124.

12. W. Beumelburg, Doctoral Dissertation, Universität Karlsruhe, 1974.

13. V. R. Hartmann, Doctoral Dissertation, Universität Karlsruhe, 1974.

14. R. A. DePaul, SAE Paper No. 710277, 1971, 6.

15. L. J. Ebert, F. T. Krotine and A. R. Troiano, Härterei-Techn. Mitt., 24 (1), 1969, 38.

16. E. Theis, Archiv Eisenhüttenwes., 32 (9), 1961, 633.

17. B. Prenosil, Härterei-Techn. Mitt., 21 (3), 1966, 199.

18. A. Randak, H. H. Domalski and H. Jesper, Schweiz. Arch., 30 (4), 1964, 113.

19. H. Brugger and G. Kraus, Archiv Eisenhüttenwes., 32 (8), 1961, 529.

20. M. A. H. Howes and J. P. Sheehan, SAE Paper No. 740222, 1974.

21. J. P. Sheehan and M. A. H. Howes, SAE Paper No. 720268, 1972.

22. J. P. Sheehan and M A. H. Howes, SAE Paper No. 730580, 1973.

23. C. Razim, Härterei-Techn. Mitt., 22 (4), 1967, 317.

24. J. S. Learman and G. T. Eldis, SAE Paper No. 760665, 1976.

25. Anon., Nickel Alloy Steels Data Book, The International Nickel Company, New York, 1975.

26. H. W. Shidemantle and R. B. Bicknell, SAE Special Technical Publication No. 228, 1962.

27. H. Streng, VDI-Berichte, 268, 1976, 207.

28. A. F. de Retana and D. V. Doane, Met. Progress, 100 (3), 1971, 65.

29. C. Razim, Härterei-Techn. Mitt., 23 (1), 1968, 1.

# Discussion

G. KRAUSS, Colorado School of Mines. Martensite is, of course, very hard, and there is a tendency toward brittleness, but I think that it often gets blamed for poor performance that is caused by other microstructural components. For example, inclusions, undissolved carbide particles, residual elements and trace elements such as phosphorus. Very often we try to develop a good microstructure of quenched-and-tempered martensite, but when things go wrong it's the result of these other interactions. The slide on the effect of chromium (Figure 10) is possibly an indication of this sort of interaction, possibly a carbide formation.

C. RAZIM. I agree, but I do not currently have any further information on these effects. We know that there is a strong dependence on alloying of the type of martensite, the structure changing from acicular to lath martensite.

D. E. DIESBURG, Climax Molybdenum Company, I'd like to have your comment on what you think the role of adding boron to the manganese-chrome steel is. The boron is added in an unprotected condition so it's not adding to hardenability. Is that correct?

C. RAZIM. The effect of boron is to increase both hardenability and ductility, but I believe the previous author mentioned the related problems. Some years ago we emphasized boron to reduce the cost of the steels, but it was necessary to go back to conventional alloys. One problem is consistency of properties which can mean tolerances of 0.001 to 0.003%

boron. At one time, we worked with steels with higher boron contents, but this was not successful.

G. H. WALTER, International Harvester Company. I would just like to comment that we really must get at this business of explaining individual alloy effects. It is difficult to rationalize slides that show impact fatigue decreasing linearly with chromium, or increasing linearly with nickel when there are many other effects besides alloying effects such as the nature of the intergranular oxide at the surface, the residual stress levels and the retained austenite levels. Generally, in the experiments that I've seen to date, these things have not been controlled, and I think it is dangerous to construct plots of alloy versus impact fatigue.

M. G. H. WELLS, Colt Industries. I would like to ask whether the authors looked at the origin of failure of fatigue specimens. We frequently find that nonmetallic inclusions are very important in fatigue failures. Professor Krauss mentioned this briefly, so I would like to ask whether the effects of different fatigue levels could be attributed to the cleanliness level of the steels and whether you see what your needs are for cleanliness levels for steels in the future, whether any improved steelmaking methods, such as electroslag remelting or even vacuum arc remelt grades might ever get into automobiles. These are in the aircraft industry and are obviously more expensive, but the fatigue life does improve greatly with improved cleanliness.

C. Razim. Electron microscopy enables us to recognize that every crack starts at an inclusion.

G. H. Robinson, *General Motors Research Laboratories.* We certainly look at fatigue origins too, but not in every one could we find an inclusion. Now, if you want to polish through the fracture, you'll usually find one; however, if you look at the other end of the specimen you will find them there too. So I have never been really satisfied that one could always unambiguously pin down that origin to an inclusion. I do not think that we are that certain.

I certainly think that as special melting techniques become economical and in the areas where they do have the biggest advantages, they will help. You may recall the work some years ago that showed that contact fatigue in ball bearings improved as the sulfur content increased. It looked like the presence of a sulfide layer and the refractory inclusion made things better. These are the combinations that you must treat with care. I am in favor of getting rid of the nonmetallic inclusions if it can be done at a price.

Y. E. Smith, *Climax Molybdenum Company.* I would like to respond to Mr. Walter's comment with partial agreement and partial disagreement. I think we are all in favor of separating the variables as much as we can and studying their effects individually, and I think it's also true that this is a very difficult thing to do. It is extremely difficult to do in a complex composite such as in a carburized case with retained austenite and carbides and varying compositions. So occasionally there are places where we have to look at the situation with more than one variable, and carburizing steels is certainly one of those situations. For practical applications, it is important to do the heat treating and study the variables under conditions that conform to the practical situation that you must have commercially. We have followed this procedure in our studies at Climax in showing some of the effects that have been referred to. You could possibly look at a 1% chromium case without any carbides but that would require extreme processing that wouldn't make sense for practical applications. So, for the point of showing the effects that can expect to get in various alloy steels under practical conditions, one must accept some of these interferences and also accept some of the undesirable properties that result from undesirable alloying, for example, high chromium and the resulting carbides that will always be present under practical conditions.

# Automotive Sheet Steels for the 1980s

by C. L. Magee and R. G. Davies
Ford Motor Company

This paper considers the recent past and future potential for high strength sheet steel applications in motor vehicles. The much-discussed materials substitution that is taking place in the automotive industry to reduce weight and thereby decrease fuel consumption is most notably confirmed by the rapid application of the emerging classes of high strength sheet steels. Trade-offs among design needs, fabrication constraints and steel production economics are gradually evolving new and useful HSS grades. A summary of current views of the desirability of various material properties will be given.

The metallurgy of the various types of high strength steels that are available in sheet form is briefly reviewed. The current understanding of the underlying microstructure/production practice/property interrelationships is also discussed. Topics of importance include monotonic and fatigue strength, energy absorption, reproducibility and some key aspects of weldability and formability. Particular attention is given to ductility (work hardening) and the very important new classes of dual phase steels.

An assessment of the evolving alloy needs is also given. Although the general needs and general trends are becoming reasonably clear, it is extremely difficult to project specific alloys because of limitations of current knowledge concerning production, application and detailed economic competitiveness of the various steel production approaches.

## Historical Perspective

The use of high strength steels (HSS) for stamped automotive products is less than 10 years old, although high strength quenched-and-tempered steels have been in automotive use for over 50 years. In this brief review of HSS, we shall be solely concerned with the hot-rolled and cold-rolled sheet steels. Up until the early 1960s, such HSS that were available in hot-rolled gauges had carbon levels that made them difficult to form and weld; these steels relied on a mixture of ferrite and pearlite for strength.

In the middle 1960s, research at Jones and Laughlin Steel Company showed that, by careful control of the final finishing temperature at the hot-rolling mill and by spray cooling the hot band on the run-out table, a dramatic increase in strength could be obtained in the HSS.[1] The strengthening was the result of both grain refinement and the precipitation of carbides and/or carbonitrides. Thus, to obtain a given strength level, the carbon content could be reduced which improved weldability, while the finer grain size led to better toughness. All major U.S. steel companies now produce HSS containing V, Nb or Ti for grain refinement and precipitation hardening; the choice of alloying addition appears to be partly historical and partly dependent upon melting and rolling practice. Indeed, it can vary among mills within a given steel company. A further improvement in formability and toughness, especially in the transverse direction, was obtained when the HSS were treated with rare earth metals to produce globular sulfides instead of the usual MnS stringers.[2,3] Thus, by the early 1970s, there was a family of formable, weldable hot-rolled HSS with yield strengths between 345 MPa (50 ksi) and 552 MPa (80 ksi)—the SAE 950 to 980 grades; these steels are now referred to as conventional HSS.

The development of cold-rolled (< 1.8 mm, 0.07 in. thickness) HSS sheets started with the Inland Steel production of a fully martensitic steel by very rapidly quenching a low carbon steel (~ SAE 1010) as it exited a continuous annealing line; by varying the subsequent tempering temperature, a family of fully martensitic steels are produced with tensile strengths ranging from 827 MPa (120 ksi) to 1380 MPa (200 ksi).[4] These martensitic steels unfortunately have very limited ductilities (< 6% total elongation) and therefore cannot be stamped into complex shapes although they are successfully roll-formed. The production of cold-rolled (or thin gauge) steels with yield strengths of 345 MPa (50 ksi) and above did not start until the 1970s. It was found that yield strengths of about 345 MPa (50 ksi) can be obtained mainly by grain size control and a minor amount of precipitation. Unfortunately during the batch annealing to produce a recrystallized structure, most of the carbide/carbonitride precipitates coalesce and so are much less effective in strengthening the steels. Higher strength steels therefore require additional strengthening from

residual cold work and/or a precipitate; TiC is fairly resistant to gross overaging. This has led to the development of the plain carbon recovery-annealed steels with strengths up to 483 MPa (70 ksi) but with limited ductilities, and the partially recrystallized Ti-containing steels with strengths up to 965 MPa (140 ksi).[5]

Commencing in the middle 1960s, Japanese steelmakers began to develop so-called dual phase steels (ferrite plus martensite mixtures) concurrently with the conventional HSS; one of the first reports of this work was given in 1975.[6] In the U.S., dual phase steel development began several years later as an outgrowth of the study of the properties of conventional HSS.[7] The attraction of dual phase steels is that, for a given tensile strength, these steels have the greatest total elongation (best formability) of any HSS.[8, 9] These dual phase steels are now emerging into wide commercial availability, and because of the better formability that they exhibit, the use of such steels is expected to expand rapidly in the coming years.

## Types and Availability of HSS

From the above introduction, it is clear that there are three basic types of HSS:

### Conventional

These steels, available with yield strengths from 345 MPa (50 ksi) to 552 MPa (80 ksi), are strengthened by a combination of grain refinement, solid solution additions (P, Si and Mn) and V, Nb or Ti carbide (or carbonitride) precipitation hardening.[10] The higher the strength, the more precipitate is required, while, at the lowest strengths, solution hardening by phosphorus is sometimes sufficient. These steels are available over the full strength range in hot-rolled gauges, but there is only limited availability at the highest strength level in cold-rolled gauges.

### Recovery Annealed

These steels, which rely on retained cold work for some of their strengthening, are produced by a controlled recovery-anneal treatment of a heavily cold-rolled low carbon or low alloy steel.[5] Due mainly to rolling mill load limitations, these steels are only available over a restricted gauge range of about 1.0-1.7 mm (0.04-0.065 in.). The martensitic quenched-and-tempered low carbon steels which are strengthened by the transformation dislocation substructure, can also be put into this category of HSS.

### Dual Phase

Dual phase steels consist essentially of a dispersion of high carbon martensite in a fine grained (< 5 μm) ferrite matrix. This structure is produced by intercritically annealing in the $\alpha + \gamma$ region and cooling at such a rate as to transform most of the austenite to martensite. It has been found that, to a good first approximation, the strength of dual phase steels is linearly proportional to the percentage of martensite in the structure.[11] Thus, the only fundamental limitation on obtainable strength is the upper limit of weldable, 100% low carbon martensite (~ 1240 MPa, 180 ksi). Since the dual phase structure is obtained as a final heat treatment step, usually on a continuous annealing line, these steels can be obtained in all thicknesses. For such materials, hardenability (of the small austenite patches) becomes an important feature, and thus alloy additions such as Mo, Cr, etc. have been investigated.[12-15]

If the tensile strength, which is approximately proportional to both the fatigue[16] and crush resistance,[17] is plotted as a function of total elongation, which has been found in practice to be a reasonable measure of formability, then the above HSS can be represented by three distinct curves, Figure 1. The most important point to note is that at all strength levels, dual phase steels have the highest elongation (formability).

## Physical Metallurgy

It is the combination of strength and ductility that is of the utmost importance when considering HSS for stamped automotive components. The strength of the steel is a primary determinant of the thickness (or weight) required for the part to carry out its function, i.e. dent resistance, durability (fatigue), crush resistance, etc., while the ease of making the part is controlled, to a large extent, by the ductility of the steel. The strengthening mechanisms operative in HSS have been outlined in the above sections. However, little can be said concerning the ductility of HSS except that inclusion content should be as low as possible and the grain size as fine as possible. For dual phase steels, a fine grained, clean (precipitate and interstitial free), substitutionally strengthened ferrite provides the best ductility;[8] adequate hardenability is necessary to obtain martensite.

It should be emphasized that for *all HSS* we are concerned with strength/ductility trade-offs. Either property reported alone as a function of microstructure or alloying is relatively meaningless from a practical and from a fundamental viewpoint. Indeed, it is important to realize that a concern for ductility at a fixed strength revolves about work hardening behavior.[18] Considere's well known finding is that uniform elongation is a balance between geometric softening and work hardening.[19] The instability criterion is simply that stress equals work hardening rate at instability.

Superior strength/ductility combinations thus imply superior work hardening at strains near instability
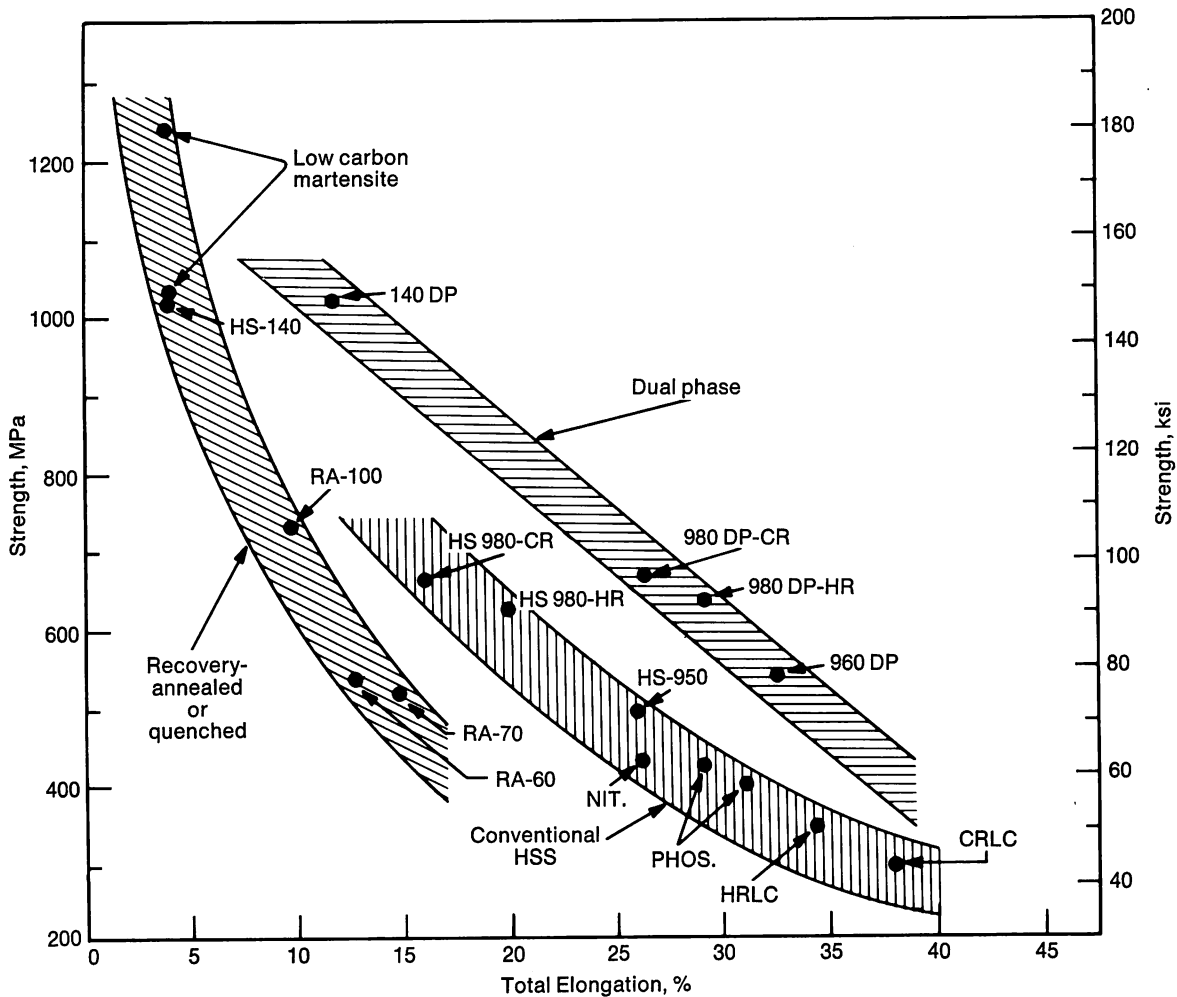
*FIGURE 1—Total elongation as a function of ultimate tensile strength for some of the commercially available high strength steels.*

$(\epsilon \sim 0.2)$. Figure 2 shows the work hardening rate plotted as a function of strain for several conventional and dual phase steels.[18] The main point to note is that the dual phase steels show higher work hardening rates at all strains (approximately a factor of two) than the conventional steels. Figure 3 shows several stress/strain curves drawn on the same work hardening/strain plot. The intersection points $(\sigma = d\sigma/d\epsilon)$ are the uniform strains for each steel (indicated by the circles). The $\sigma$-$\epsilon$ curves for conventional steels intersect their work hardening rate curves at lower strength/ductility values. This result demonstrates that the strength/ductility enhancement directly results from increased work hardening behavior. Thus fundamental research should be aimed at understanding and, if possible, increasing the work hardening rate of steels, especially dual phase steels.

## Work Hardening of Dual Phase Steels

From the above discussion, it is clear that to optimize the mechanical properties of dual phase steels, it is necessary to have a knowledge of the factors that control the work hardening rate. Since the dual phase steels in
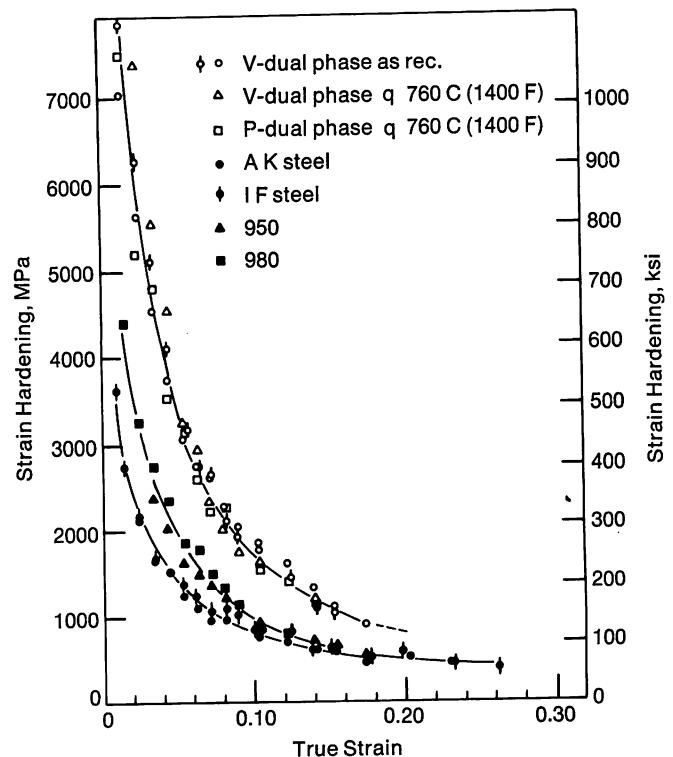


*FIGURE 2—Strain hardening as a function of strain for dual phase, conventional high strength and low carbon steels.*
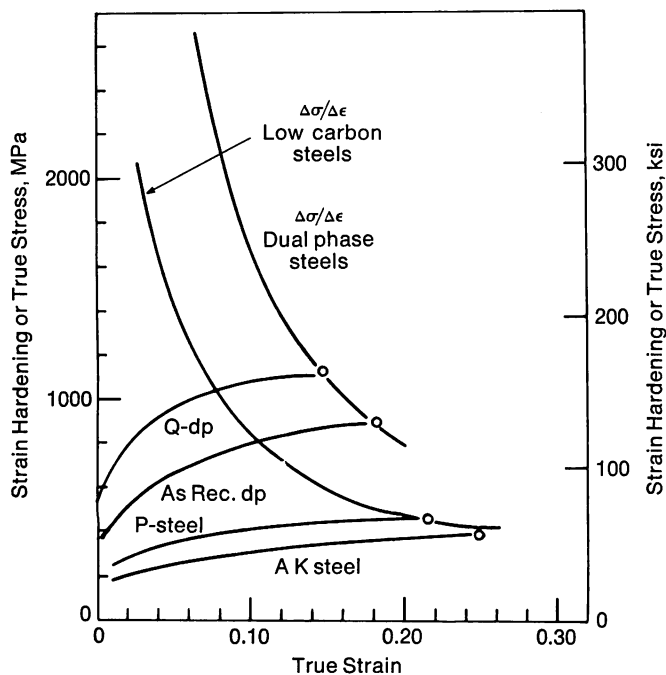
FIGURE 3—Strain hardening and true stress as a function of strain for both dual phase and low carbon steels; the strain hardening lines are taken from Figure 2. The circles indicate the extent of uniform elongation.



FIGURE 4—Work or strain hardening as a function of strain for iron and several alloys; the standard dual phase steel line is from Figure 2. a) Iron-silicon alloys and a "dual phase ferrite"; b) Iron-phosphorus alloys.

common use consists of at least 80% ferrite, it is to be expected that the properties of this ferrite will have a major influence on the work hardening of the steel; the other 20% or less of the structure is a high carbon ($\sim$ 0.6% C) martensite which may contain a small amount of retained austenite.[14, 20] The ferrite in these dual phase steels is usually fine grained ($<$ 5 $\mu$m), relatively free of interstitial elements and precipitates, and often strengthened by the addition of substitutional alloying elements such as Si and/or P.[8]

The influence of Si and P on the work hardening of fine grained ($\sim$ 10 $\mu$m) pure iron alloys is shown in Figure 4. It can be seen that the higher the alloy addition, the greater the work hardening at all strain levels. In Figure 4a, it can also be seen that the Fe-1.5 Mn-0.55 Si-0.1 V alloy (the approximate composition of the ferrite in the most common dual phase steel) behaves similarly to the Fe-2% Si alloy especially at high strains. Thus it is concluded that the 1.5 Mn and 0.1 V are having beneficial effects, similar to an extra 1.5 Si, on work hardening. Grain size changes over the range from 10 to 30 $\mu$m in this synthetic dual phase ferrite had no influence on the work hardening rate.

The influence of varying the martensite content and the carbon content of the martensite on the work hardening of dual phase steels was also investigated. Although increasing the martensite content from approximately 7 to 18% increased the work hardening rate at low strains (Figure 5), there is essentially no change in the work hardening rate at strains above 0.12. Similarly, the higher carbon martensites initially work harden more rapidly,

Figure 6, but, at the highest strains, the curves for the two alloys become identical.

From these results, it appears that the properties of the ferrite are of primary importance in determining the work hardening rate of dual phase steels. This is demonstrated in Figure 7 where the addition of 2% Si or 1.5% Si —0.1% P to a dual phase steel leads to an increase in the work hardening rate over that observed in the usual dual phase steels containing only about 0.5% Si or 0.07% P. However, the presence of the martensite islands does lead to an additional increment in work hardening rate,

Figure 4. It is still to be determined whether the size and distribution of the martensite islands influence the work hardening rate. It is also unclear to what extent the retained austenite present in some martensite islands[14, 20] contributes to the higher work hardening rates by a TRIP[21] mechanism.

## Perspectives on Vehicle Application

The high strength sheet steels discussed here have
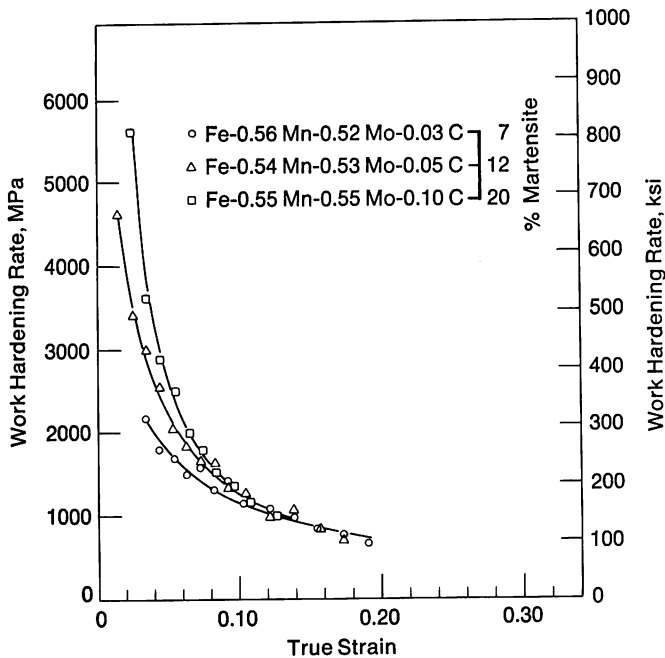


FIGURE 5—*Work hardening as a function of strain for dual phase steels containing various amounts of martensite.*

been undergoing extensive development during the past ten years. During this same period, their role in private transportation vehicles has grown from first tentative applications to more widescale utilization. In this section, we will give a broad overview of this trend.

The application of the HSS materials in U.S. vehicles began in about 1972 in a few engine mounts, with the first major use of the materials occurring in 1974 for bumper reinforcements. Table I gives some of the estimated dates and kinds of applications in U.S. vehicles. Figure 8 shows the overall usage of these high strength sheet steels in Ford vehicles.[22] This graph also compares the HSS application rate with that for plastics in U.S. vehicles. It is seen that the extremely rapid increase in weight of HSS justifies our calling it the quiet materials revolution. The increases in plastics usage have been much more widely publicized.

The HSS materials first became commercially available in the U.S. in the early 1970s, and their use in private transportation vehicles has also occurred first here. Currently, worldwide application of these materials in private transportation vehicles is occurring. It would appear that the use of HSS in foreign automotive industries is lagging that in the U.S. by anywhere from 3 to 8 years. In light of this history, it will be interesting to see whether the earlier emergence of dual phase steels in Japan[6] leads to earlier extensive application of these materials in Japanese vehicles.

The rapid materials substitution of high strength sheet steel for mild steel has resulted from the relative effectiveness of the change in terms of cost/weight trade-offs, and from the relatively minor impact of HSS on the manufacturing methods and facilities used in the auto-



FIGURE 6—*Work hardening as a function of strain for two dual phase steels containing about 15% martensite but with martensites of different carbon contents.*



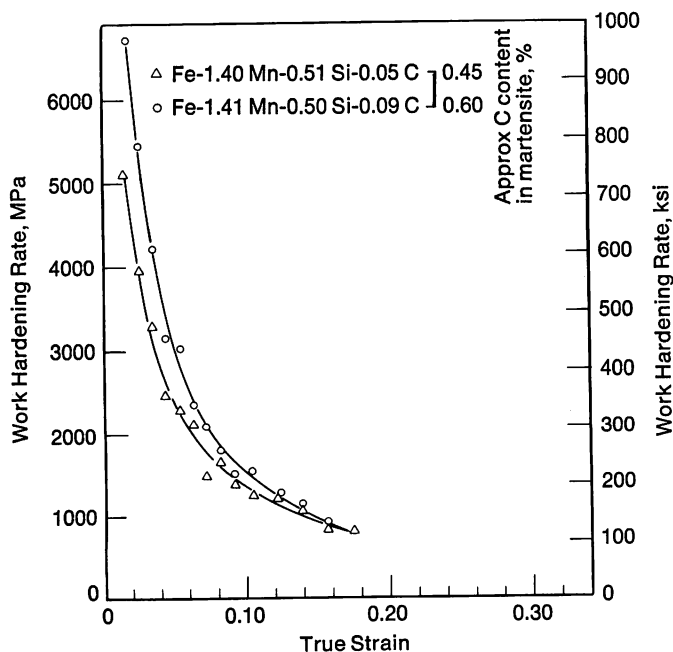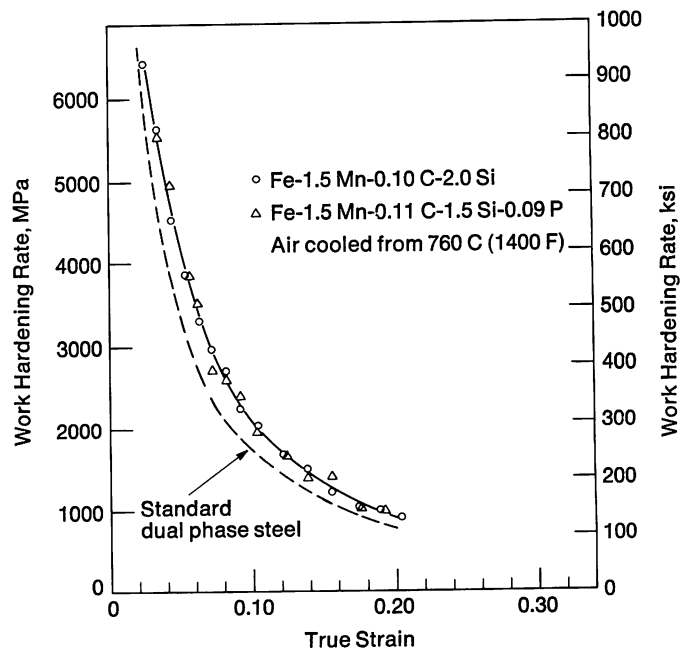FIGURE 7—*Work hardening as a function of strain for high silicon and silicon plus phosphorus dual phase steels showing enhanced work hardening over the standard dual phase steel.*

**Table I**—HSS Application Timing

| 1972 | Engine Mounts |
|------|---------------|
| 1974 | Bumper Reinforcements (345 MPa, 50 ksi)<br>Side Door Beams |
| 1976 | Bumper Facebars (345 MPa, 50 ksi)<br>Side Door Beams (965 MPa, 140 ksi)<br>Exterior Panels (275 MPa, 40 ksi) |
| 1978 | Body Structural Parts (275 MPa, 40 ksi)<br>Wheels, Suspension Arms (550 MPa, 80 ksi)<br>Frame Members (345 MPa, 50 ksi) |
| 1980 | Redesigned Structural (550 MPa, 80 ksi) |
| 1984 | Vehicle-Wide Application<br>(415 to 965 MPa, 60 to 140 ksi) |
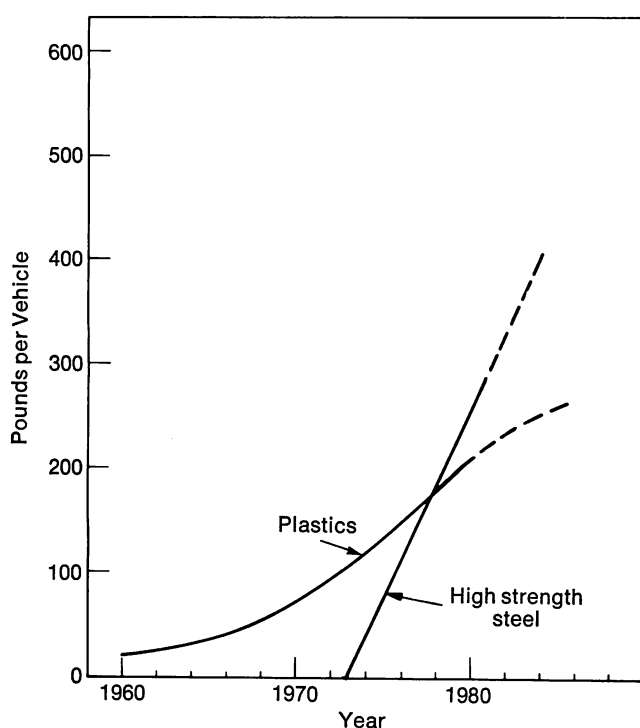


FIGURE 8—*Overall rate of application of HSS and plastics in automobiles.*

motive industry.* Of course, the change is not simply achieved because proper utilization of HSS requires improved design methodology, improved stamping and assembly techniques, and significant increases in material and process/quality control in steel and automotive plants.

## Application Issues

The HSS usage achieved already has not occurred

---

* Although retooling and extensive stamping process modification is required, the needed investment is still small compared to plastics which usually require wholly new fabrication and assembly facilities.

without many difficult technical issues being raised and either fully or partially solved. Future applications will, of course, occur beyond those already in place but not without continuous technical development of the materials and an increase in our knowledge of where HSS is most effective. In this section, some of these important issues will be reviewed to indicate the kinds of material properties that are important in application studies. In a broad sense, these revolve around materials, design and fabrication and have been discussed in more detail in the literature.[22] The major design and fabrication issues will be highlighted in this section.

In the design area, the key question is the amount of weight reduction that can be achieved in various specific components using each of the varieties of HSS. This overall problem revolves around consideration of crash or energy absorption, fatigue or durability, rigidity or ride quality, corrosion and some other related issues. The major structural design constraints on the vehicle are in the area of energy absorption, durability and rigidity. The reader is referred to Reference 22 for a discussion of the redesign methods available in the area of rigidity.

The energy absorption properties of a structure are determined both by structural and material parameters. Recent investigations[17, 23, 24] have established the role that materials and structures have in the load deflection
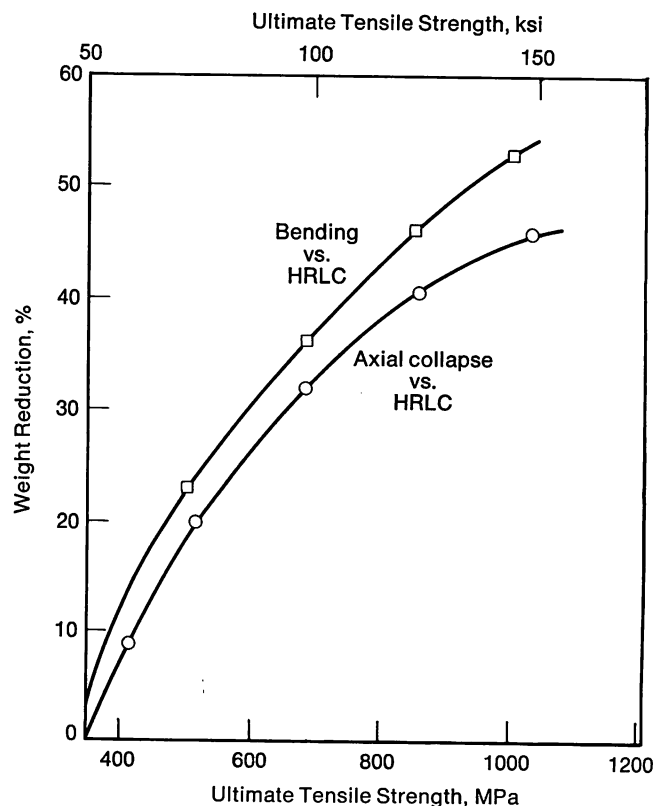


FIGURE 9—*The effect of ultimate tensile strength on weight reduction for axial collapse and 3-point bending of square beams. Weight reduction is calculated relative to HRLC as the baseline material.*
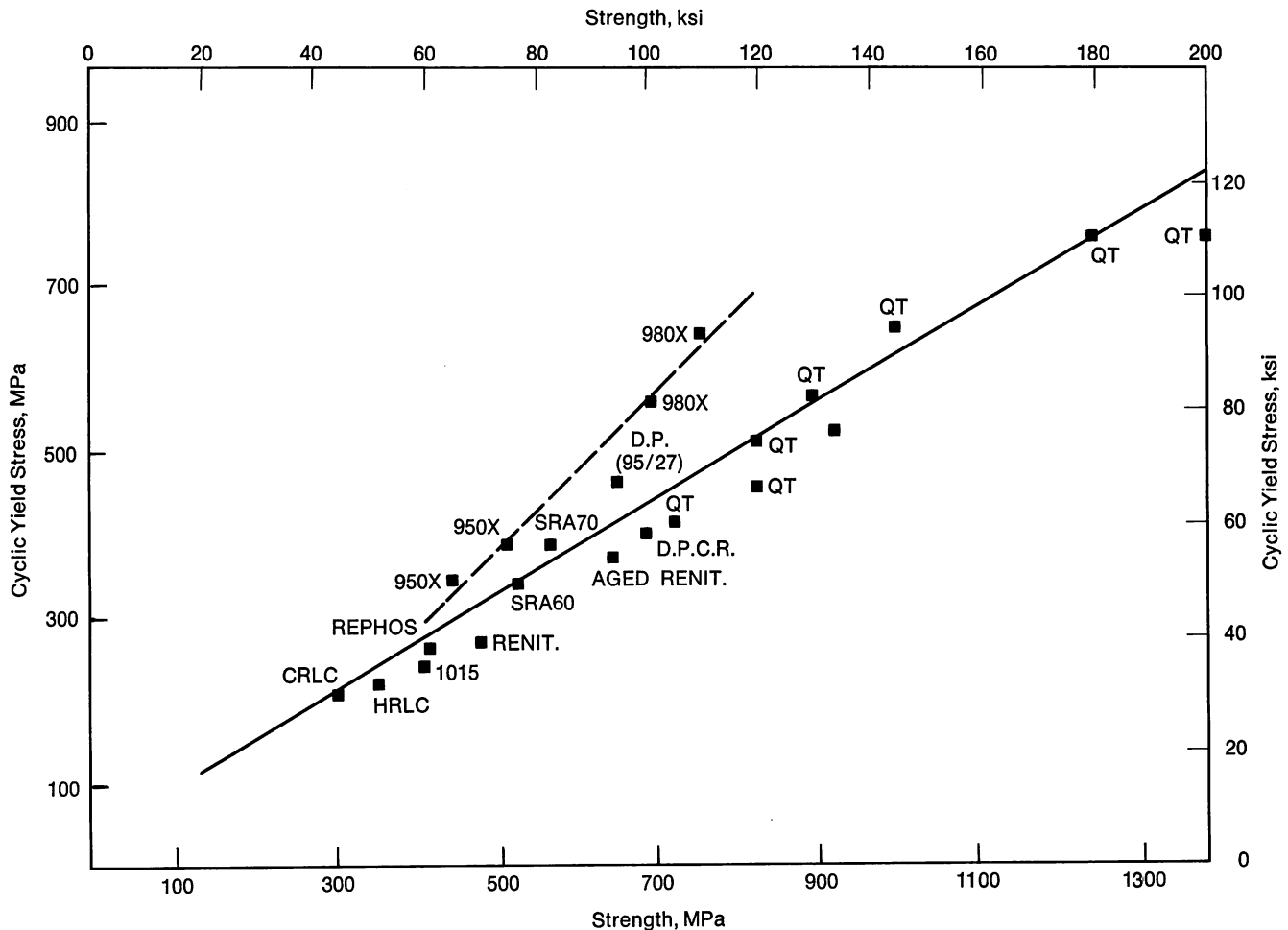
FIGURE 10—*The interrelation of cyclic yield strength for a variety of steels on the ultimate tensile strength.*

characteristics of simple structures. This work has covered a variety of material, structural and loading mode variations. Based on this work, one can calculate or estimate the weight reductions possible with various strength materials. Figure 9 shows the plot of the weight reduction percentage against material strength for two simple loading modes. The major effect noted is that the loads in axial collapse are directly proportional to the ultimate tensile strength (and not the yield strength of the material).[23,24] Thus, the use of higher strength steels allows for reduced weight in components that are primarily used in energy absorbing applications. An example of this is the widespread use of HSS side door beams with a large weight reduction over original mild steel versions. The achieved weight reductions have been close to those predicted by the work reviewed here. In parts where rigidity requirements are also met, lower weight reductions will be obtained.[17,22]

A second key problem area in structural vehicle design is the attainment of adequate durability or fatigue life. For this design constraint, material properties again play a complex and interactive role. The weight reduction for individual HSS grades used in specific durability-related components will depend on the state of loading,

the details of the load deflection history and relative notch severity. Thus, as in the case for crush controlled components, percent weight reduction will be component-sensitive. Nonetheless, a most important material property, the cyclic yield strength, generally increases as the tensile strength of the material increases (see Figure 10).[16] Similar correlations with yield strength[22] are not as strong. Higher cyclic stress/strain curves minimize the local plastic strain under given imposed loads or deflections. This leads to higher design loads at all fatigue lives. A second material property, the damage accumulated in any imposed local cyclic strain, is only improved for HSS in the long life fatigue range. The overall conclusion (as has been known with heat treated steels used in springs and other suspension components for a long time) is that lighter weight components can be fabricated from HSS for durability-controlled components. Table II gives an estimate of these weight reductions for different materials considered in this report.

A last design-related issue that should be considered briefly is corrosion. As discussed in Reference 22, general application of HSS and its accompanying downgauging should entail more effective coatings and protection. Such effects are simultaneously occurring and represent

*Spot Welding*

Material Weldability: *Acceptable* Welds Over *Specified* Range of Welding Parameters
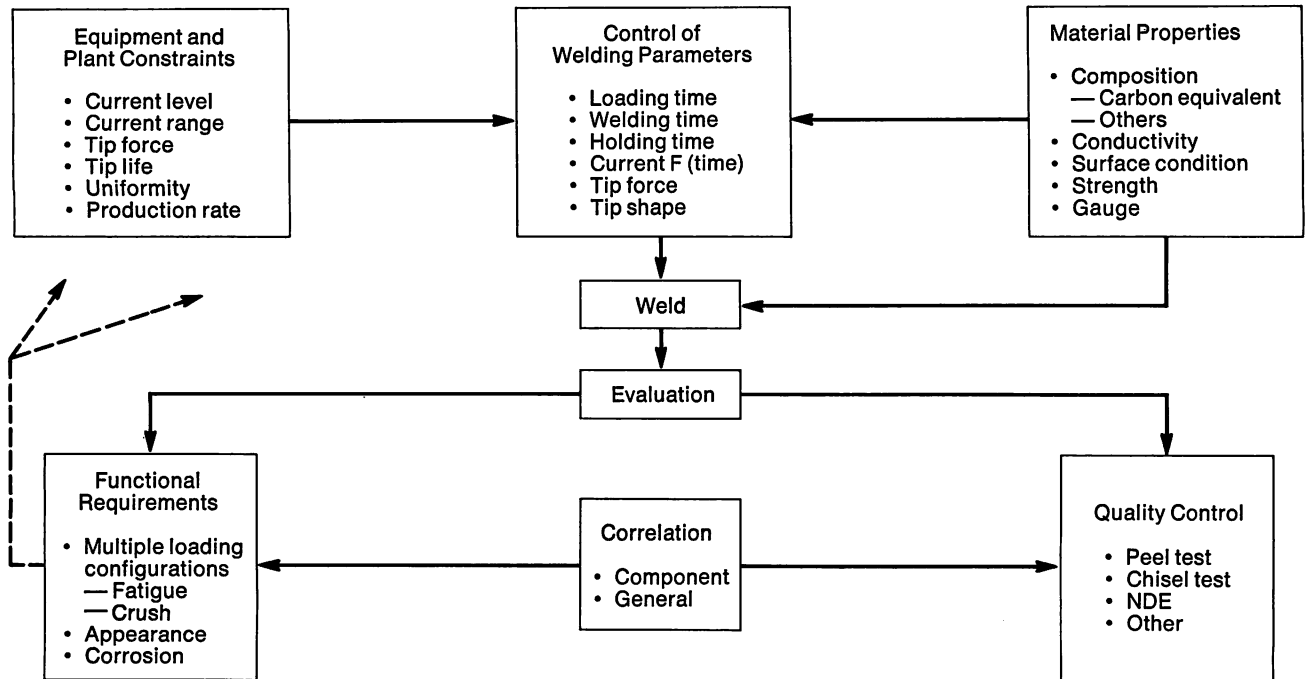


*FIGURE 11—Schematic flow chart of factors involved in weldability of HSS.*

**Table II**—Percentage Weight Reduction for Durability

| Material | Replacing CRLC | Replacing HRLC |
|---|---|---|
| 150/6* | 45 | 42 |
| 150/12 | 45 | 42 |
| 110/12 | 40 | 35 |
| 90/18 | 36 | 32 |
| 90/27 | 36 | 22 |
| 75/33 | 22 | 16 |
| 65/27 | 18 | 12 |
| 60/29 | 7 | 0 |

* Tensile strength (ksi)/total elongation designation for HSS.

another cost penalty (probably small) associated with HSS applications. However, the net effect of downgauging and more protection will be better corrosion resistant vehicles since a small amount of protection is more beneficial than the thickness of material given up on downgauging.

Other issues that are of significance in the substitution of the new HSS for mild steel involve fabrication of components from the material. In the fabrication of sheet metal components, two major processes must be considered. These are the sheet metal forming and the spot welding of the materials. (Coating, painting, finishing and other attaching processes are often more difficult in HSS, but the problems to be resolved are minor compared to those encountered in welding and forming.)

In spot welding, a large number of variables are in-
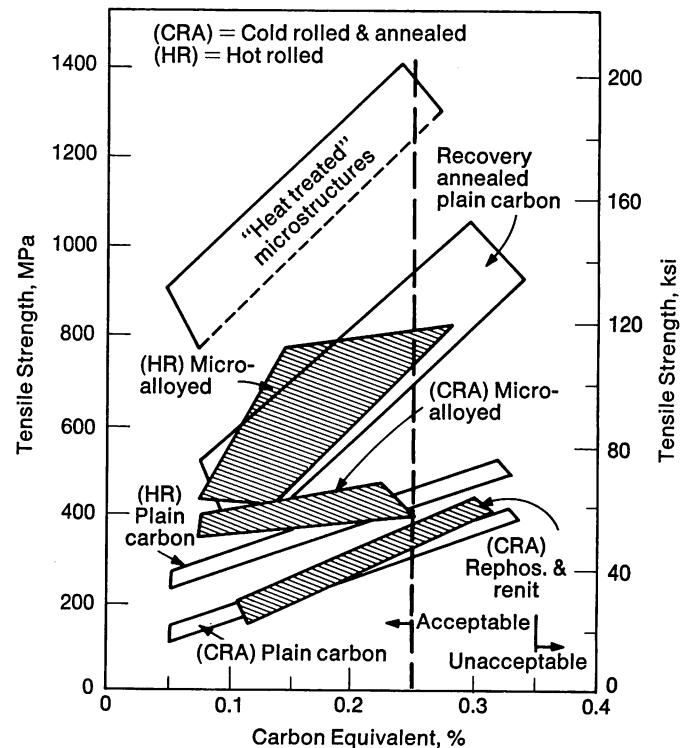


*FIGURE 12—The relation between strengthening mechanisms in steels and carbon equivalent indicating the range for acceptable materials from a welding viewpoint.*

volved in making reliable and effective spot welds (see Figure 11).[25] Figure 12 shows the material characteristics that are generally felt to accompany the attainment of a good weld. Basically, one wants to achieve low carbon

"equivalence" at high strengths, and this favors heat treated, precipitation hardened and fine grained steels. The relative fatigue life and crash resistance of spot welded HSS structures is also an issue, but, in all cases studied thus far, design solutions (e.g. more spot welds) have been available.

The most difficult and all-encompassing technical issues in the application of HSS to vehicles involve sheet metal forming. A full discussion of this problem would in itself be sufficient to cover an entire book and so will only be briefly considered here. The overall formability of a steel *cannot* be assessed in a simple quantitative way because of the different complex variables which constitute the fabrication process for any given component. From an overall materials assessment viewpoint, probably the best rating for formability is the total elongation to failure measured in a tensile test. This measure of ductility for a range of HSS is shown in Figure 1. Such a simple ranking does not take into account the specifics of any given component forming operation, and the details of the process can promote formability of a given type and thus effect the ranking. For example, the failure strain in a stretch forming operation is a function of the biaxial strain state. Thus, failure limit diagrams rather than tensile results are needed for materials, and these have been determined for selected high strength steels.[7, 26, 27]

In stretch forming, the ability of a material to distribute strain is also important in achieving overall shape changes. In general, the substitution of higher strength materials results in lower work hardening and hence reduced strain distribution capability (see section on work hardening of dual phase steels). On the other hand, the deep drawing ability of sheet material is essentially independent of tensile ductility and is normally defined in terms of limiting draw ratio which is only affected by the plastic anisotropy of the material. The r values are generally not much different between conventional mild steels and high strength steels (Table III).[7, 27] A further failure mechanism of interest in sheet metal forming is local fracture which can occur in sharp bend radii or along edges of sheared parts. In general, the higher the strength the greater the sensitivity to local failure, and subtle changes in the processing operation may be necessary to overcome such problems. In this case, tensile elongation is not a good measure of formability, but rather a local fracture measurement is superior. Control

of sulfur content and sulfide shape seems to play a key role in developing improved materials for local fracture resistance.[2] The last problem area in sheet metal forming that will be discussed is that of shape control or part springback. In general, higher strength materials at reduced gauge will show greater springback for a given part.[18, 28] The tendency for high strength materials to show greater variability in springback because of the greater absolute magnitude is a problem that is not easily overcome by die changes. Thus, tighter quality control and material specifications must evolve. These specifications will not rely on typical properties, but will be carefully designed for the minimum and maximum properties seen in incoming sheet material.

As a summary of the application issues, a variety of complex and interrelated problems arises in trying to use high strength steels in vehicles. In light of the problems, it might be surprising to see the already extensive utilization of these materials (Figure 8). This would not have occurred without technological developments and improved understanding of the materials and the issues discussed above. Continued progress, particularly in sheet metal forming technology, will pace the continued application of these high strength sheet steels.

## Application Projections and Alloy Implications

In this section, an attempt will be made to project the potential long term applicability of high strength sheet steels in private transportation vehicles. Such projections are obviously uncertain in light of the technical problems and still developing material technology described in the preceeding sections. Nonetheless, the application research studies and the trend depicted in Figure 8 give a strong basis for the premise that use of these materials will continue to rise.

Although the total weight of steel in future vehicles is somewhat uncertain, it is possible to project that sheet steel stampings will make up about 40% of future vehicle weights. The overall penetration of high strength steel among the sheet steels is now about 20% in Ford vehicles; the authors speculate that this penetration will reach 30 to 50% of the total automotive sheet steel by the end of the decade; 60 to 80% of these materials will be in gauges below 1.8 mm (.072 in.) and thus will be in the nominally cold-rolled gauges. These estimates, though rough, are still far less speculative than any estimates one can make of specific material types that will be used.

To consider the problem of material types, one has to first break the application spectrum into the cold-rolled and hot-rolled varieties. It is our opinion that for the cold-rolled category, materials based on solution hardening and/or minor alloy additions will constitute almost one-half the high strength steels used. The supe-

**Table III**—Typical Values of n and r for HSS

| Steel | n | r |
|---|---|---|
| 45/35* | 0.22 | 0.85 |
| 65/27 | 0.16 | 1.10 |
| 65/35 | 0.26 | 1.12 |
| 90/18 | 0.13 | 0.95 |
| 90/27 | 0.22 | 0.98 |

* Tensile strength (ksi)/total elongation designation for HSS.

rior formability at a given strength level indicates that dual phase steels may well make up much of the remainder of these materials. The relative advantages of continuous annealing lines in economically producing consistent higher strength products will probably dictate that almost all cold-rolled HSS (conventional and dual phase) will be made on such facilities.

In the hot-rolled category, the dual phase materials will not probably be as significant a fraction of the total high strength steel application. There are two reasons behind this conclusion. The first is that the addition of continuous annealing to a hot-rolled product will always entail an extra process and therefore cost. The second reason is that stretch forming in thicker parts is less significant, so the superior work hardening of the dual phase steels is of reduced importance. Thus, we anticipate that somewhat less than half of the hot-rolled materials utilized will end up being dual phase products; the remainder being conventional precipitation hardened, fine grained materials.

The projection of potential alloy uses is even more problematical than the projection of the potential material types. The specific alloying elements that will be added will of course include columbium, vanadium, titanium and molybdenum, but, at this point, no reliable means for deciding among these is apparent. In addition to the problem of determining what material types will prove the most economical, the utilization of alloying elements will be dependent on the types of processing that the steel companies find most economical for producing such materials. In particular, the quenching facilities on continuous annealing lines used for the production of the cold-rolled steels are critical. In the final analysis, we anticipate the total addition of the above alloying elements to be less than one pound per vehicle. Thus, we would expect the additional alloying elements added to HSS sheet steels to be less than those found now in the heat treated steels used in suspension springs, spindles, connecting rods, etc.

In summary, we speculatively project the application of high strength sheet steels per vehicle to approach the 135 to 270 kg (300 to 600 lb) range by the end of the decade. It is expected by this period that the worldwide automotive industry will utilize such materials so a total market larger than 10 million tons per year is possible for these high strength sheet steels. The materials will have a predominant component of continuously annealed products; solution hardened, microalloyed and heat treated materials will be among those utilized. The alloying

elements listed above, though small in quantity, will be key features in obtaining higher strength economically thus achieving very significant worldwide fuel savings.

# References

1. E. R. Morgan, T. E. Dancy and M. Korchynsky, *J. Metals, 17* (8), 1965, 829.
2. L. Luyckx, J. R. Bell, A. McLean and M. Korchynsky, *Met. Trans., 1,* 1970, 3341.
3. R. D. Engquist, *Metal Progress, 77* (5), 1960, 180.
4. W. H. McFarland and H. L. Taylor, *Metal Progress, 96* (2), 1969, 73.
5. P. B. Lake and J. J. Grenawalt, SAE Preprint 770163, Feb. 1977.
6. S. Hayami and T. Furukawa, Proc. *Microalloying Conf.,* Washington, D.C., 1975, 311.
7. M. S. Rashid, SAE Preprint 760206, Feb. 1976.
8. R. G. Davies, Proc. of Symposium, *Formable HSLA and Dual-Phase Steels,* AIME, 1979, 25.
9. J. H. Bucher and E. G. Hamburg, SAE Preprint 770164, Feb. 1977.
10. M. Korchynsky and H. Stuart, Symposium, *Low Alloy High Strength Steels,* Ges. Electromet mbH, Düsseldorf, Germany, 1970, 17.
11. R. G. Davies, *Met. Trans. A, 9A,* 1978, 671.
12. J. Morrow and G. Tither, *J. Metals, 30* (3), 1978, 16.
13. D. Aichbhaumik and R. R. Goodhart, SAE Preprint 790010, Feb. 1979.
14. J. M. Rigsbee and P. J. Vander Arend, Proceedings of Symposium, *Formable HSLA and Dual-Phase Steels,* AIME, 1979, 56.
15. R. G. Davies and C. L. Magee, Proc. of Vanitec Seminar, *Vanadium Cold Pressing and Dual-Phase Steels,* Oct. 1978, W. Berlin, Germany, 25.
16. R. W. Landgraf, ASTM STP 467, American Society for Testing and Materials, Philadelphia, 1970.
17. C. L. Magee and P. H. Thornton, SAE Preprint 780434, Feb. 1978.
18. R. G. Davies and C. L. Magee, *J. Metals, 31* (11), 1979, 17.
19. M. Considere, *Ann. Ponts Chaussees, 9* (6), 1885, 574.
20. J. Y. Koo and G. Thomas, *Mat. Sci. and Eng., 24,* 1976, 187.
21. V. F. Zackay, E. R. Parker, D. Fahr and R. Busch, *Trans. ASM, 60,* 1967, 252.
22. C. L. Magee, R. G. Davies and P. Beardmore, *J. Metals,* (to be published).
23. P. H. Thornton and C. L. Magee, *Trans. ASME, 99,* 1977, 114.
24. P. H. Thornton, *J. Metals* (to be published).
25. B. Pollard and R. H. Goodenow, SAE Preprint 790006, Feb. 1979.
26. M. S. Rashid, SAE Preprint 770211, Feb. 1977.
27. W. G. Brazier and R. Stevenson, SAE Preprint 780137, Feb. 1978.
28. R. G. Davies, Ford Motor Company, Unpublished results.

# Discussion

W. E. LITTMANN, *Dresser Industries*. Could the author comment on the fatigue properties of the heat affected zone in dual phase steel welds under ordinary and stress corrosion conditions or under corrosion fatigue conditions?

C. L. MAGEE. I would like to answer this question by explaining what we know about spot welds in mild steel, and that is very little. We are doing a lot of spot weld fatigue work and we are learning a lot about mild steel spot welds and about other materials as well. There is no particular problem; in fact we have had rather good success with dual phase spot welds and for reasons we do not entirely understand. As to corrosion, we have only begun to look at the corrosion fatigue of spot welds. There is very little information on this subject.

# Alloying and Transformation Control in Mn-Si-Cr-Mo As-Rolled Dual Phase Steels

by G. T. Eldis, A. P. Coldren and F. B. Fletcher
Climax Molybdenum Company

Approximately five years have elapsed since the rather unique mechanical properties of ferrite plus martensite mixtures, or "dual phase" steels, were first introduced in the high strength low alloy (HSLA) steel literature.[1] Their low initial yield strength (275-410 MPa, 39.9-59.5 ksi), high work hardening rate at low strains (275 to 340 MPa, 39.9 to 49.3 ksi strength increase after 3-5% tensile strain), high tensile strength and large uniform elongation made them the first truly highly formable HSLA steels. As such they were greeted with enthusiasm by a large segment of the automotive industry. At the present time, dual phase steel technology is at the stage of learning how to best take advantage of the materials' forming characteristics, for which components these steels are cost-effective, and how the new combination of mechanical properties and the new steel compositions may effect other properties such as fatigue strength and weldability. Interest remains high, and dual phase steels will no doubt find their way into a large number of automotive components during the next few years, components such as wheels, control arms, bumpers and others where good formability and high strength in the finished product are required.

The term "dual phase" was coined to describe the microstructure of this new class of steels which is now recognized to consist of relatively hard islands of martensite plus retained austenite ("MA constituent") dispersed in a matrix of soft and highly ductile ferrite. It is the matrix which provides the excellent ductility of the material, while the MA constituent imparts the high tensile strength. The high residual stresses and/or high initial mobile dislocation density associated with the MA constituent promote the low initial yield strength and high initial work hardening rate.[2] Dual phase steel was first produced by heat treatment, and most of the literature to date deals with heat treated material.[3, 4] The heat treatment concept is easy to grasp from basic metallurgical principles. The steel with an initial ferrite plus carbide structure is heated into the intercritical temperature region where the carbides dissolve, leaving a mixture of ferrite plus carbon-rich austenite. On subsequent cooling at relatively moderate rates, depending on the steel alloy content, the carbon-rich austenite has sufficient hardenability to transform to martensite.

The idea of obtaining a dual phase microstructure without heat treatment, that is, obtaining ferrite plus MA in the as hot-rolled strip, is an attractive one because of the potential savings of heat treatment costs. It was first conceived at the Climax laboratory[5] and was sparked by the observation that the Climax-developed acicular ferrite linepipe steels sometimes contain several percent MA constituent in the as-rolled condition.[6] It had been noted that higher chromium, manganese, molybdenum and silicon contents seemed to promote the formation of MA, and work was undertaken on a fairly extensive matrix of steels to determine the compositions that would minimize the amount of acicular ferrite, pearlite and bainite in these steels in the as-rolled condition after processing in a fairly typical manner for hot-rolled strip. This preliminary work led to the selection of a steel containing nominally 0.06% C, 1.2% Mn, 0.9% Si, 0.6% Cr and 0.4% Mo for use in a commercial mill trial, and that first trial met with very encouraging success.[7] Subsequent refinements of composition and additional mill trials ultimately resulted in a steel of nominal composition 0.06% C, 0.90% Mn, 1.35% Si, 0.45% Cr and 0.35% Mo. This steel has been used to successfully produce as-rolled dual phase steel strip on a large number of hot strip mills in both North America and Europe under a fairly wide range of finish rolling and coiling temperatures.[8]

Throughout the rather hectic period of development of the as-rolled dual phase (ARDP) chemistry, little work was undertaken to quantitatively define the effects of the various alloying elements on the transformation kinetics of deformed (hot-rolled) austenite. There were two principal reasons for this. First, the above described "empirical" program was proceeding so rapidly and so well that there seemed to be little time—or need—for such a quantitative study. Second, it is well known, qualitatively, that austenite deformation accelerates the transformation kinetics. This effect has been quantitatively studied to a limited degree.[9] But the transformation kinetics of austenite in the present study could be thoroughly studied

**Table I**—Steel Compositions

| Steel No. | Element, % | | | | | | | | |
|---|---|---|---|---|---|---|---|---|---|
| | C | Mn | Si | Mo | Cr | Al | N | P | S |
| Cr Series | | | | | | | | | |
| 1 | 0.050 | 0.90 | 1.19 | 0.38 | —[a] | 0.05 | 0.005 | 0.011 | 0.006 |
| 2 | 0.049 | 0.90 | (1.19)[b] | (0.38) | 0.16 | (0.05) | (0.005) | (0.011) | (0.006) |
| 3 | 0.048 | 0.90 | (1.19) | (0.38) | 0.30 | (0.05) | (0.005) | (0.011) | (0.006) |
| 4 | 0.048 | 0.89 | (1.19) | (0.38) | 0.48 | (0.05) | (0.005) | (0.011) | (0.006) |
| Mo Series | | | | | | | | | |
| 5 | 0.049 | 0.91 | 1.21 | — | 0.50 | 0.04 | 0.006 | 0.010 | 0.007 |
| 6 | 0.049 | 0.92 | (1.21) | 0.15 | (0.50) | (0.04) | (0.006) | (0.010) | (0.007) |
| 7 | 0.049 | 0.92 | (1.21) | 0.30 | (0.50) | (0.04) | (0.006) | (0.010) | (0.007) |
| 8 | 0.048 | 0.91 | (1.21) | 0.50 | (0.50) | (0.04) | (0.006) | (0.010) | (0.007) |
| Si Series | | | | | | | | | |
| 9 | 0.070 | 0.93 | 0.99 | 0.27 | 0.32 | 0.04 | 0.005 | 0.011 | 0.007 |
| 10 | 0.070 | 0.92 | 1.50 | (0.27) | (0.32) | (0.04) | (0.005) | (0.011) | (0.007) |
| 11 | 0.070 | 0.93 | 2.00 | (0.27) | (0.32) | (0.04) | (0.005) | (0.011) | (0.007) |

[a] None added and not analyzed.

[b] Values in parentheses are assumed on the basis of analysis of the first ingot in each series.

only with the austenite in the undeformed condition, while, commercially, the ARDP steel results from transformation of deformed austenite, the degree of deformation being unknown and difficult to quantify.

As the pace of the empirical program slowed with the occurrence of successful mill trials, it became apparent that a better quantitative understanding of the effects of the individual alloying elements on control of the austenite transformation kinetics was needed, even if only undeformed austenite could be studied. There was considerable debate regarding why the particular combination of elements worked as well as it did in promoting a dual phase microstructure in the as-rolled condition. Furthermore, the relatively high alloy content, notably the silicon and molybdenum contents, was causing concern among some steel producers, and a study of transformation behavior would perhaps indicate ways of reducing the amount of alloy used.

This study was therefore undertaken to determine, by means of dilatometry, the effects of alloying on the control of austenite transformation in Mn-Si-Cr-Mo ARDP steels under conditions of continuous cooling. Three alloy variables, silicon, chromium and molybdenum, were selected for study. Manganese was held constant here, since its level (nominally 0.9%) seemed to cause no concern among steel producers, and all prior work with higher manganese contents indicated deleterious effects.[7,8] Carbon was also held constant since, in a manner analogous to heat treated dual phase steels,[10] the most effective role of carbon appeared to be that of controlling the relative amount of ferrite and MA and hence the strength of the final product.

## Experimental Procedure

### Materials

The materials for this study were prepared in the laboratory as aluminum-killed induction heats melted and cast under an argon atmosphere. In all, three 34 kg (75 lb) heats were melted, and each was poured into several copper chilled steel molds, adding alloy to the melt between ingot pours to obtain the compositions desired. The composition of each ingot was determined by chemical analysis of a 25 mm (1 in.) diameter button specimen cast as an integral part of the ingot. These analyses are presented in Table I. The 89 mm (3.5 in.) diameter by 114 mm (4.5 in.) long ingots were soaked at 1260 C (2300 F) and press forged to 25 mm (1 in.) thick plates. Test specimens as described below were prepared from these plates.

### Austenite Transformation Studies

A Formastor-F quench dilatometer was used to study austenite transformation kinetics. This instrument employs induction heating of the test specimens in vacuo and allows cooling at a wide range of controlled rates. The test specimen has cylindrical geometry, 3 mm (0.12 in.) diameter by 10 mm (0.39 in.) length. A 2 mm (0.08 in.) diameter hole is bored axially into one end to accommodate a Pt/Pt-Rh thermocouple which is percussion welded to the bottom of the hole for temperature measurement and control.

During heating and cooling of the specimens, output from the thermocouple and from a length-sensing differ-

**Table II**—Range of Cooling Rates Used in Determining CCT Diagrams

| Cooling Cycle[a] | Mode of Cooling[b] | Rate of Cooling,[c] C/s (F/s) | | Time to Cool from 800 to 500 C (1470 to 930 F), s |
|---|---|---|---|---|
| 1 | HeQ-H | 137 | (247) | 2.2 |
| 2 | HeQ-M | 94.3 | (170) | 3.2 |
| 3 | HeQ-L | 19.1 | (34) | 15.7 |
| 4 | Nat. | 5.23 | (9.4) | 57.4 |
| 5 | PPD | 3.65 | (6.6) | 82.2 |
| 6 | PPD | 1.24 | (2.2) | 242 |
| 7 | PPD | 0.50 | (0.9) | 600 |
| 8 | PPD | 0.19 | (0.3) | 1,580 |
| 9 | PPD | 0.040 | (0.07) | 7,500 |
| 10 | PPD | 0.0087 | (0.016) | 34,500 |

[a] See numbers near top of each cooling curve in CCT diagrams.
[b] HeQ = Helium Gas Quench; H, M, L = high, medium and low He flow rates, respectively.
Nat. = Radiation Cooling in Vacuum.
PPD = Programmed Power Decrease.
[c] Tangent at 700 C (1290 F).

ential transformer is simultaneously recorded with an X-Y recorder to obtain plots of specimen length vs. temperature. Transformation temperatures and an estimate of the volume fraction transformed determined from these data are used to construct continuous cooling transformation (CCT) diagrams. The procedure is described in detail elsewhere.[11]

In the present investigation, the critical temperatures $Ac_1$ and $Ac_3$ were first determined for each composition by heating a specimen of each in the dilatometer at 2 C/min (3.6 F/min) over the range 650 to 1250 C (1200 to 2280 F). Samples of each steel were then austenitized in the dilatometer for 20 minutes at a temperature of about 30 C (55 F) above the $Ac_3$ and cooled at various controlled rates. Ten different cooling programs were employed for each steel. Table II gives details of the range of approximate cooling rates used in constructing the CCT diagrams.

**Metallography**

After cooling in the dilatometer, each specimen was cold-mounted in an epoxy resin compound and prepared for metallography by normal mechanical polishing techniques. The specimens were etched in 2% nital for optical examination. For examination in the scanning electron microscope, the specimens were etched in a mixture of 4 g picric acid + 1 ml nitric acid in 100 ml of ethanol. This was followed by vapor deposition of a thin Au-Pd film on the specimens to eliminate charging in the electron beam.

**Table III**—Austenitizing Temperatures, Austenite Grain Sizes and Critical Temperatures of the Steels Investigated

| Steel No. | Critical Temperatures, C (F) | | Austenitizing Temperature, C (F) | ASTM Grain Size No. |
|---|---|---|---|---|
| | $Ac_1$ | $Ac_3$ | | |
| Cr Series | | | | |
| 1 | 710 (1310) | 995 (1825) | 1010 (1850) | 5-6 |
| 2 | 720 (1330) | 970 (1780) | 1000 (1830) | 5-6 |
| 3 | 712 (1315) | 968 (1775) | 1000 (1830) | 5-6 |
| 4 | 735 (1355) | 985 (1805) | 1015 (1860) | 4-5 |
| Mo Series | | | | |
| 5 | 745 (1375) | 990 (1815) | 1025 (1875) | (a) |
| 6 | 730 (1345) | 965 (1770) | 995 (1825) | (a) |
| 7 | 730 (1345) | 975 (1785) | 1010 (1850) | 6 |
| 8 | 725 (1335) | 985 (1805) | 1020 (1870) | 6 |
| Si Series | | | | |
| 9 | 720 (1330) | 940 (1725) | 970 (1780) | 7-8 |
| 10 | 735 (1355) | 990 (1815) | 1020 (1870) | 4-5 |
| 11 | 740 (1365) | 1060 (1940) | 1095 (2005) | 5-6 |

(a) All dilatometer specimens contained sufficient polygonal ferrite to obscure the prior austenite grain structure so determination was not possible.

Quantitative metallography was performed for a limited number of specimens by point counting to check the accuracy of the dilatometric estimates of volume fraction transformed. The prior austenite grain size was determined by the comparison method on dilatometer specimens that had transformed to a predominantly bainitic microstructure (the bainitic transformation most clearly delineates the prior austenite grain boundaries in these steels). The hardness (HV10) of each dilatometer specimen was determined.

## Results and Discussion

Three series of steels were prepared for this study (Table I): a chromium series (0-0.5%) at constant silicon (1.2%) and molybdenum (0.4%) contents; a molybdenum series (0-0.50%) at constant chromium (0.5%) and silicon (1.2%) contents; and a silicon series (1-2%) at constant chromium (0.3%) and molybdenum (0.3%) contents. Table III shows the critical temperatures, the austenitizing temperatures used in the dilatometric studies and the prior austenite grain sizes of the steels.

The austenite transformation behavior of the eleven steels is shown in the CCT diagrams of Figures 1-11. Each diagram shows the ten cooling cycles employed, numbered 1-10 (see Table II). The hardness of each transformed dilatometer specimen is given in a circle at the

bottom of each respective cooling curve. Along each cooling curve, the temperatures at which austenite transformation occurs and the type of transformation product are indicated. Dashed lines through the regions of austenite transformation are isotransformation contours that give the dilatometric estimate of the volume percent of austenite that has transformed on cooling to a given temperature. The results of quantitative metallography performed to verify the accuracy of these estimates are given in Table IV.

**Table IV**—Polygonal Ferrite Content Determined by Quantitative Metallography on Selected Dilatometer Specimens

| Steel | Cooling Cycle | Polygonal Ferrite, Vol.-% |
|---|---|---|
| 3 | 6 | 74 |
| | 7 | 76 |
| | 8 | 78 |
| 4 | 6 | 82 |
| | 7 | 81 |
| | 8 | 83 |
| 7 | 6 | 78 |
| | 7 | 84 |
| 8 | 7 | 81 |
| | 8 | 82 |
| | 9 | 83 |



FIGURE 1—CCT diagram for Steel no. 1 (0.05% C, 0.90% Mn, 1.20% Si, 0.40% Mo).

FIGURE 2—CCT diagram for Steel no. 2 (0.05% C, 0.90% Mn, 1.20% Si, 0.15% Cr, 0.40% Mo).
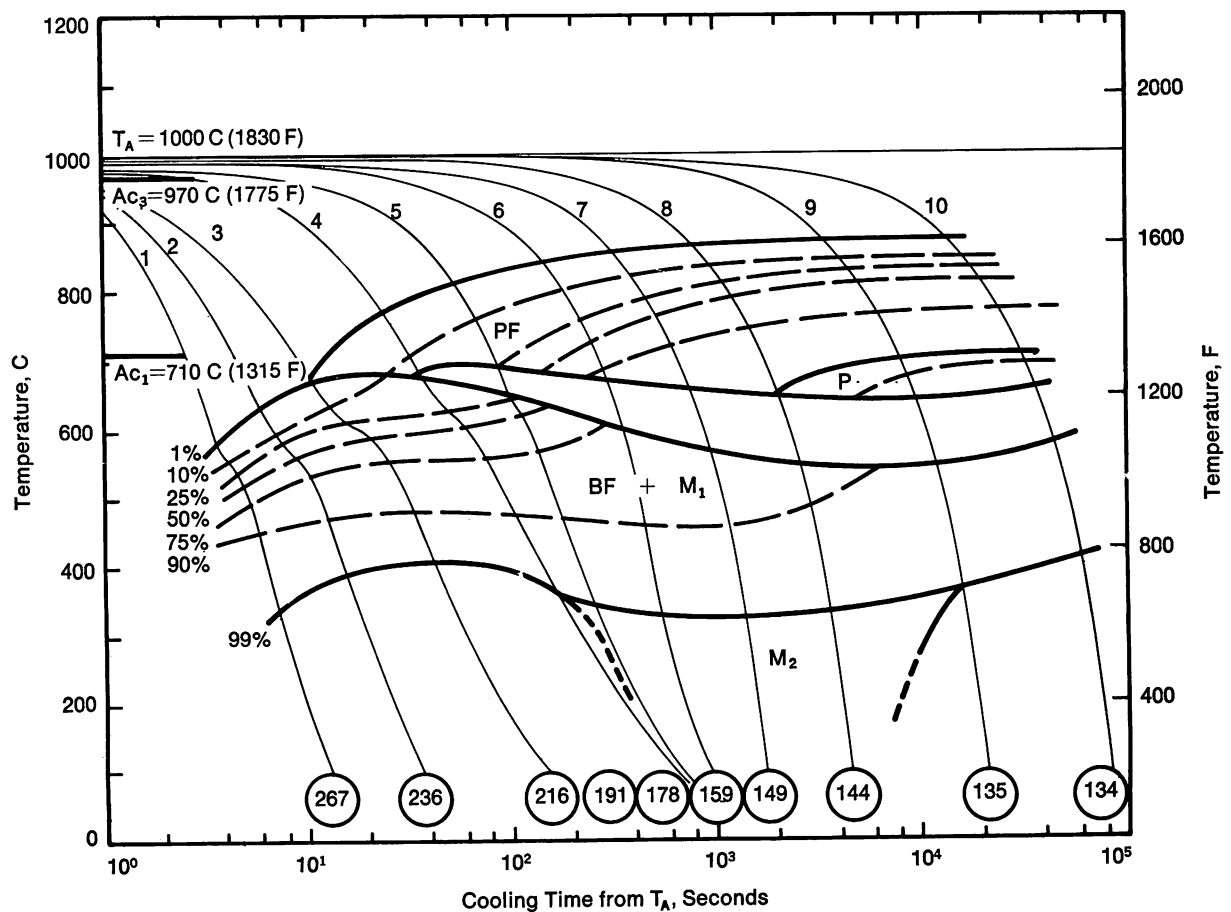
FIGURE 3—CCT diagram for Steel no. 3 (0.05% C, 0.90% Mn, 1.20% Si, 0.30% Cr, 0.40% Mo).
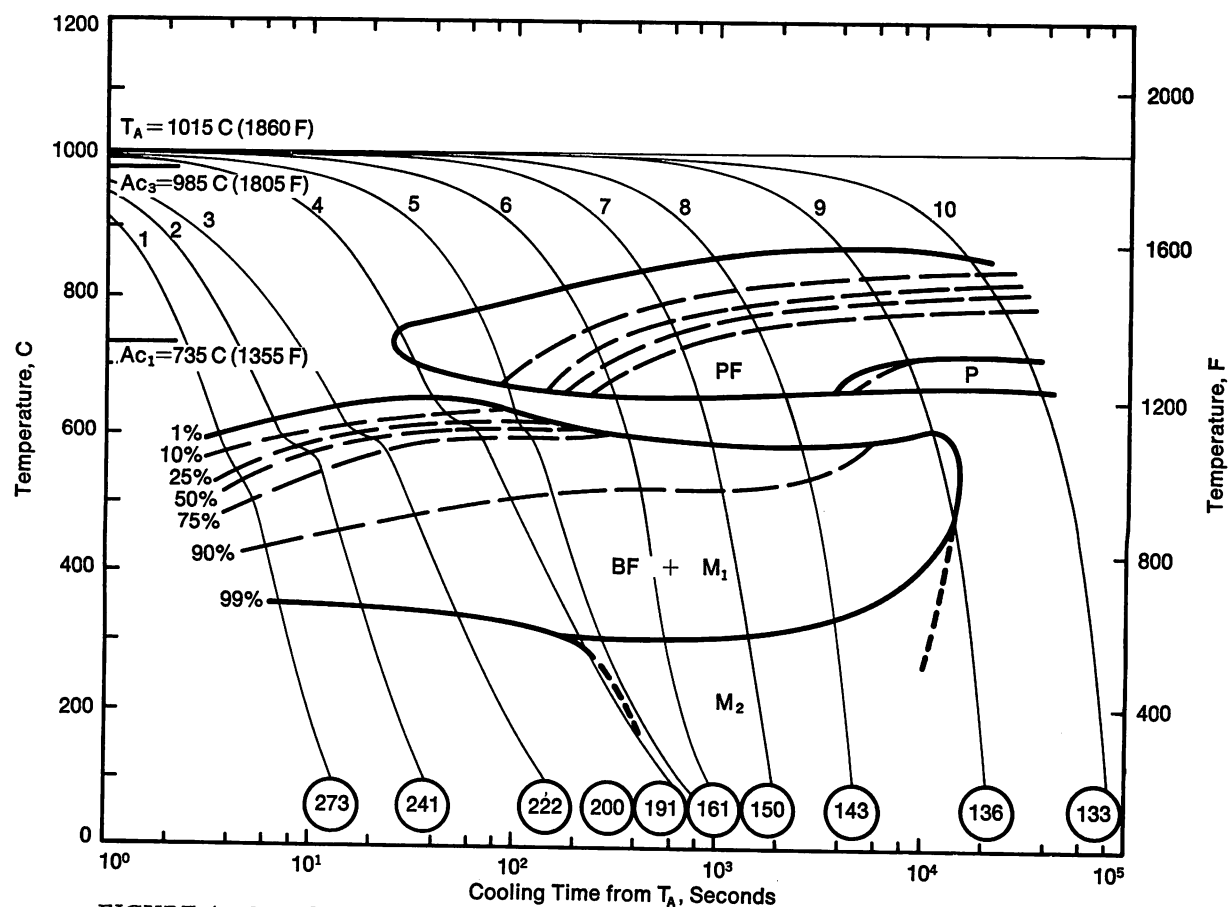
FIGURE 4—CCT diagram for Steel no. 4 (0.05% C, 0.90% Mn, 1.20% Si, 0.50% Cr, 0.40% Mo).
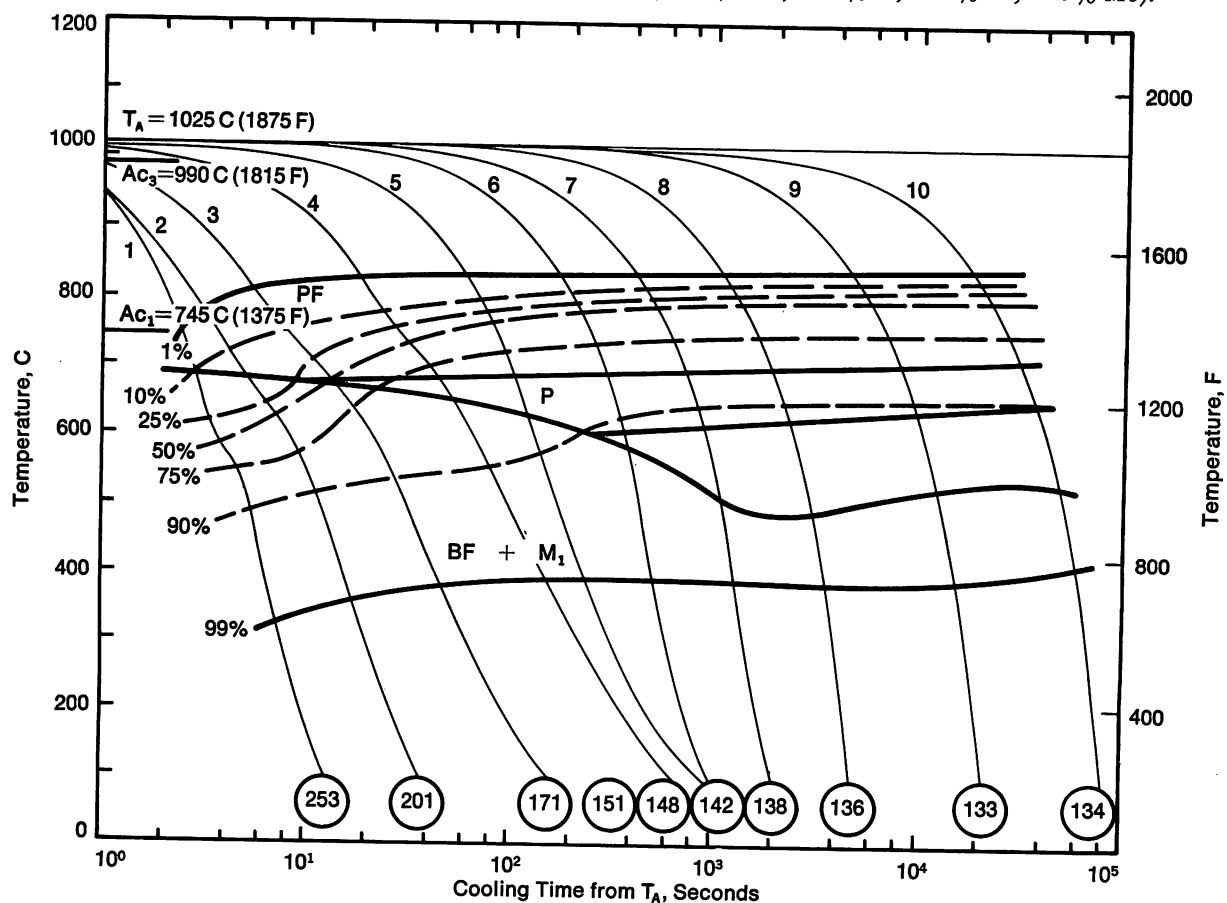


FIGURE 5—CCT diagram for Steel no. 5 (0.05% C, 0.90% Mn, 1.20% Si, 0.50% Cr).
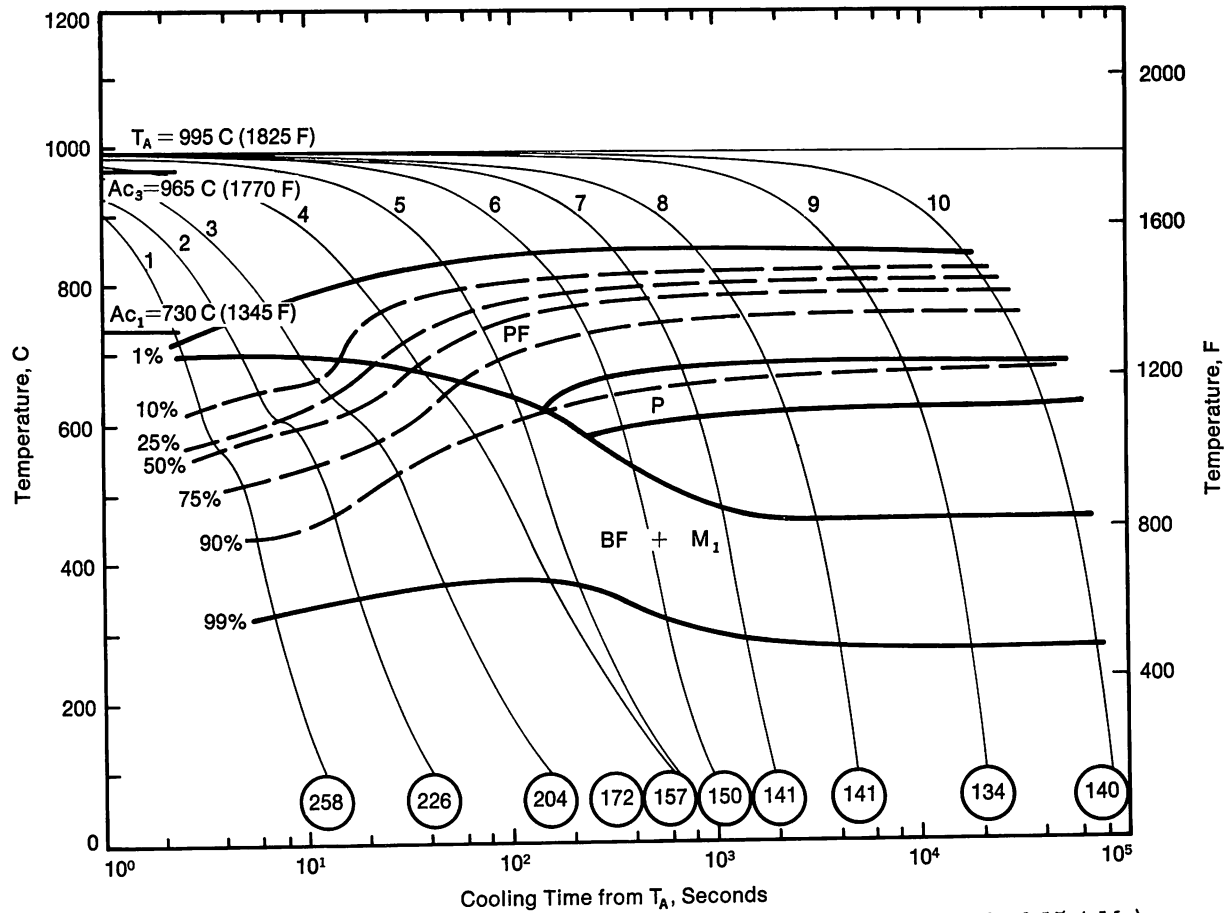
*FIGURE 6—CCT diagram for Steel no. 6 (0.05% C, 0.90% Mn, 1.20% Si, 0.50% Cr, 0.15% Mo).*
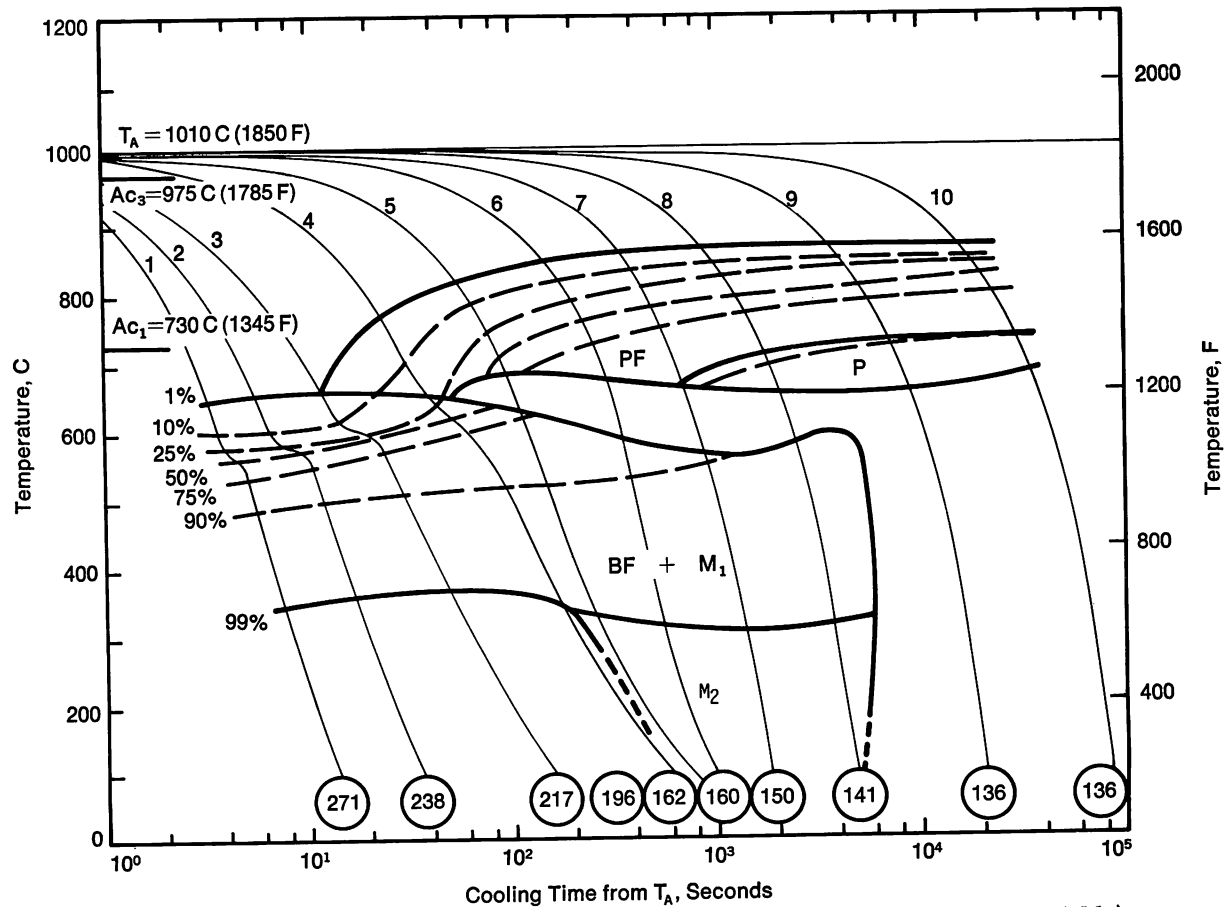


*FIGURE 7—CCT diagram for Steel no. 7 (0.05% C, 0.90% Mn, 1.20% Si, 0.50% Cr, 0.30% Mo).*
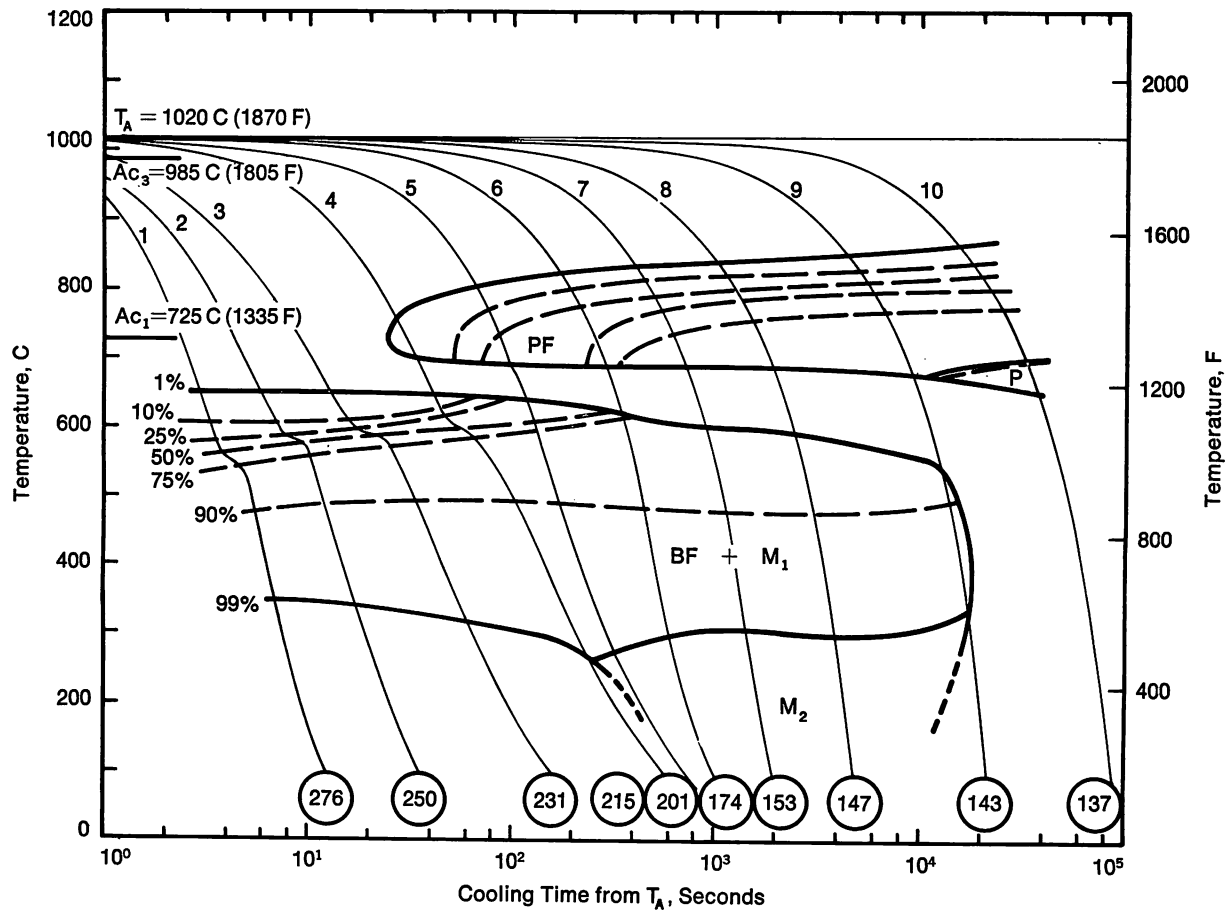
*FIGURE 8—CCT diagram for Steel no. 8 (0.05% C, 0.90% Mn, 1.20% Si, 0.50% Cr, 0.50% Mo).*
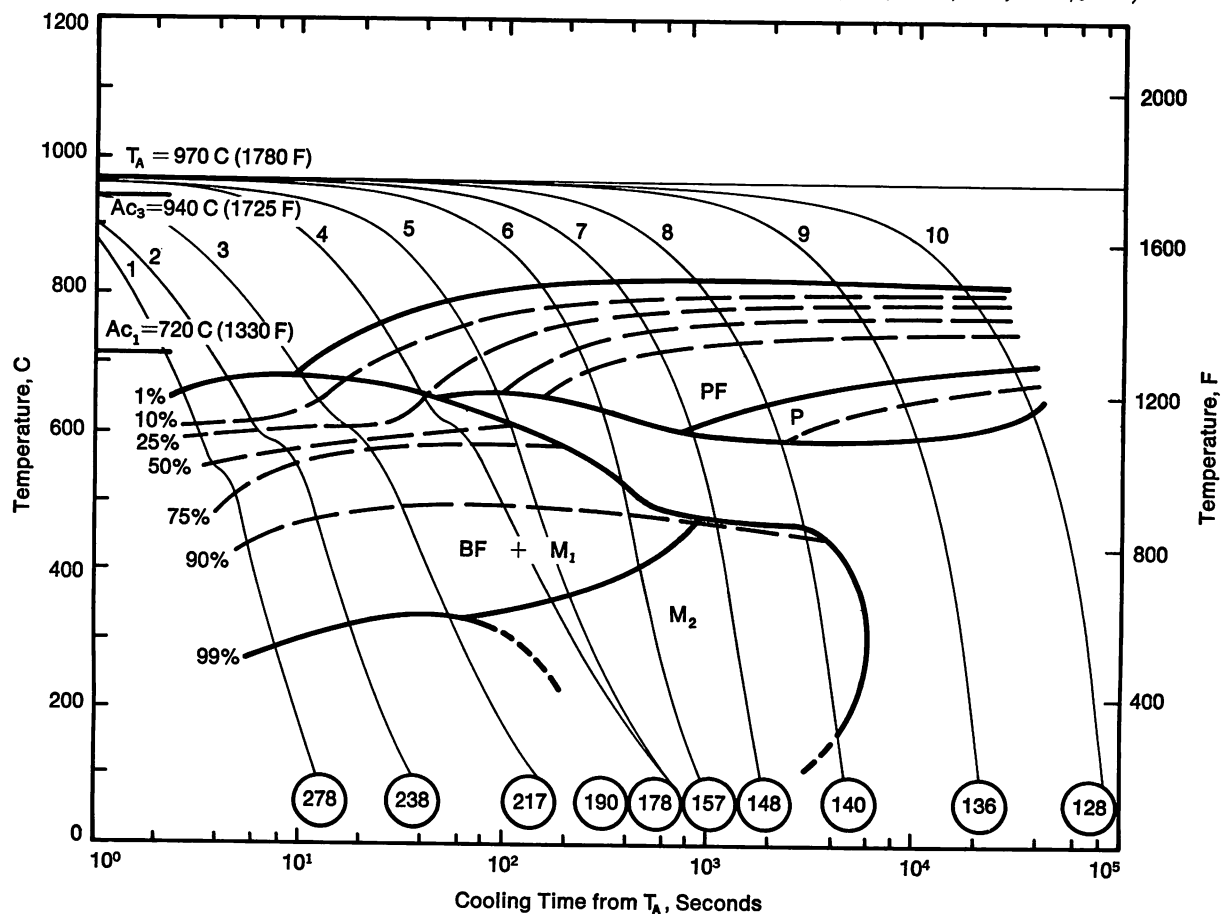


*FIGURE 9—CCT diagram for Steel no. 9 (0.07% C, 0.90% Mn, 1.00% Si, 0.30% Cr, 0.30% Mo).*
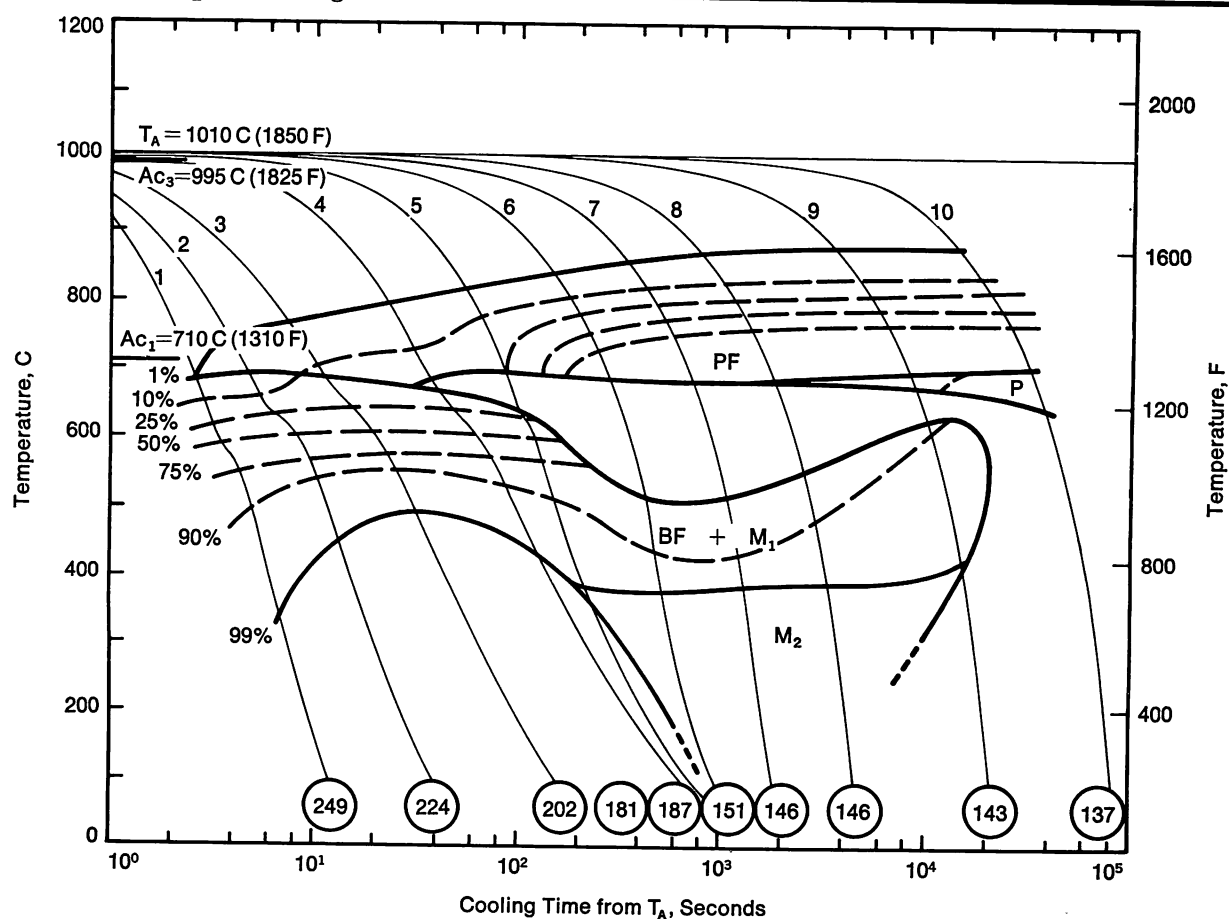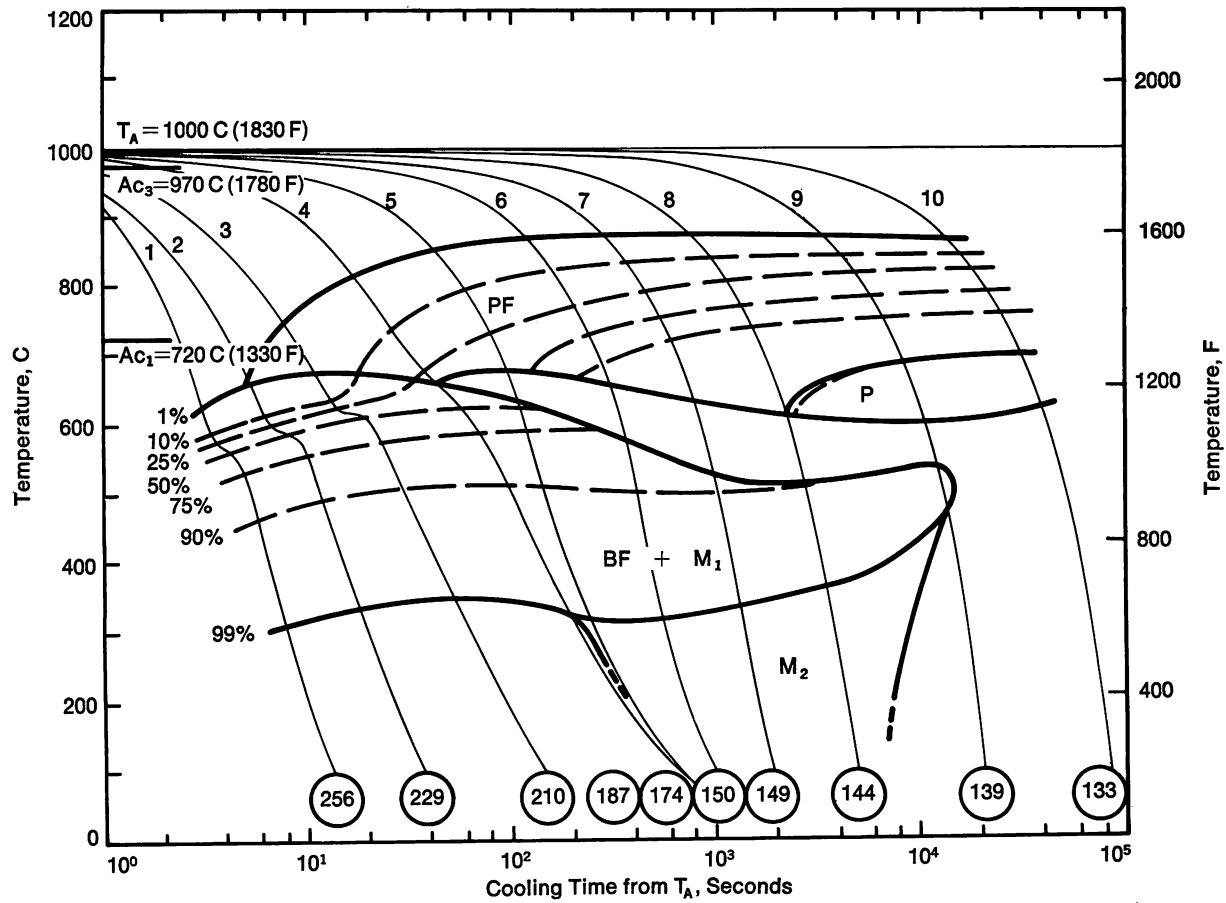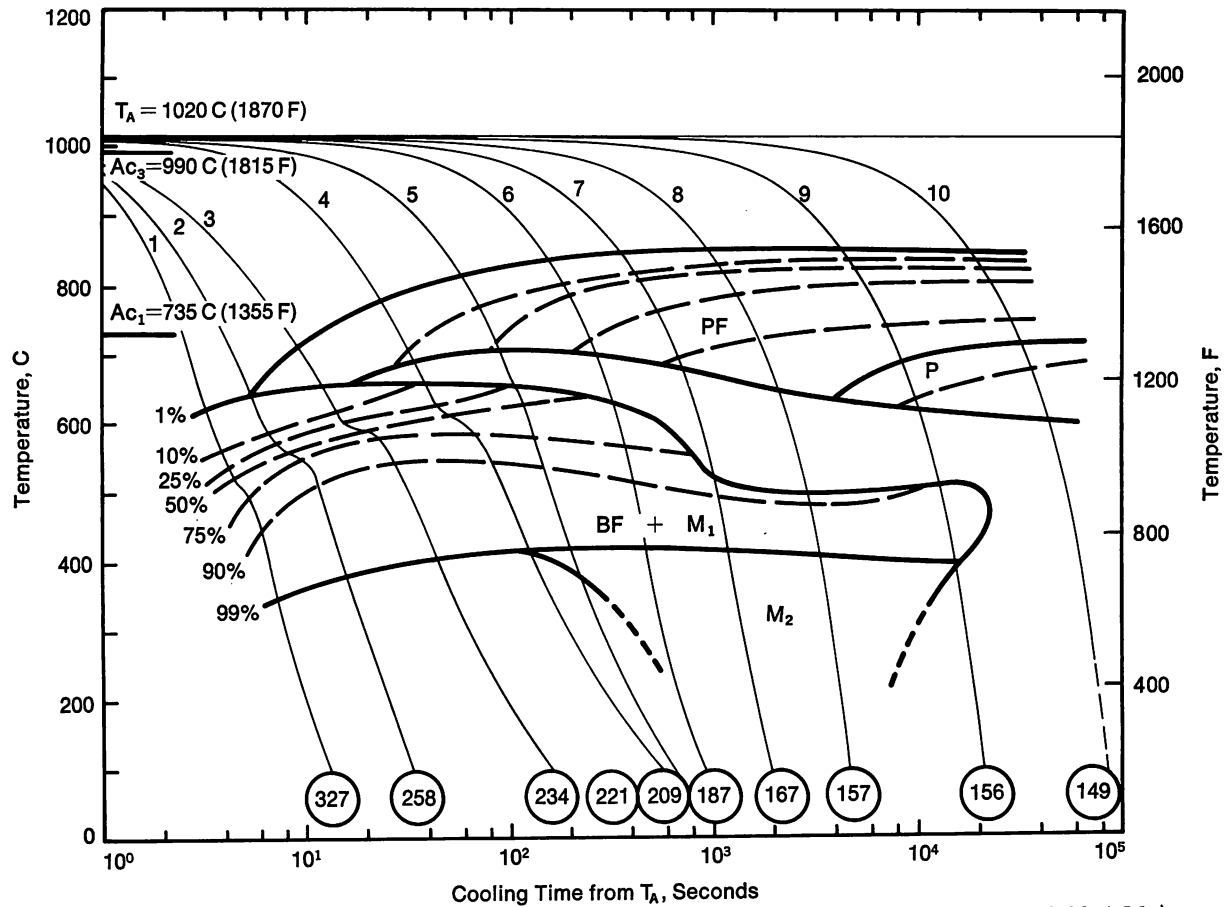
FIGURE 10—CCT diagram for Steel no. 10 (0.07% C, 0.90% Mn, 1.50% Si, 0.30% Cr, 0.30% Mo).
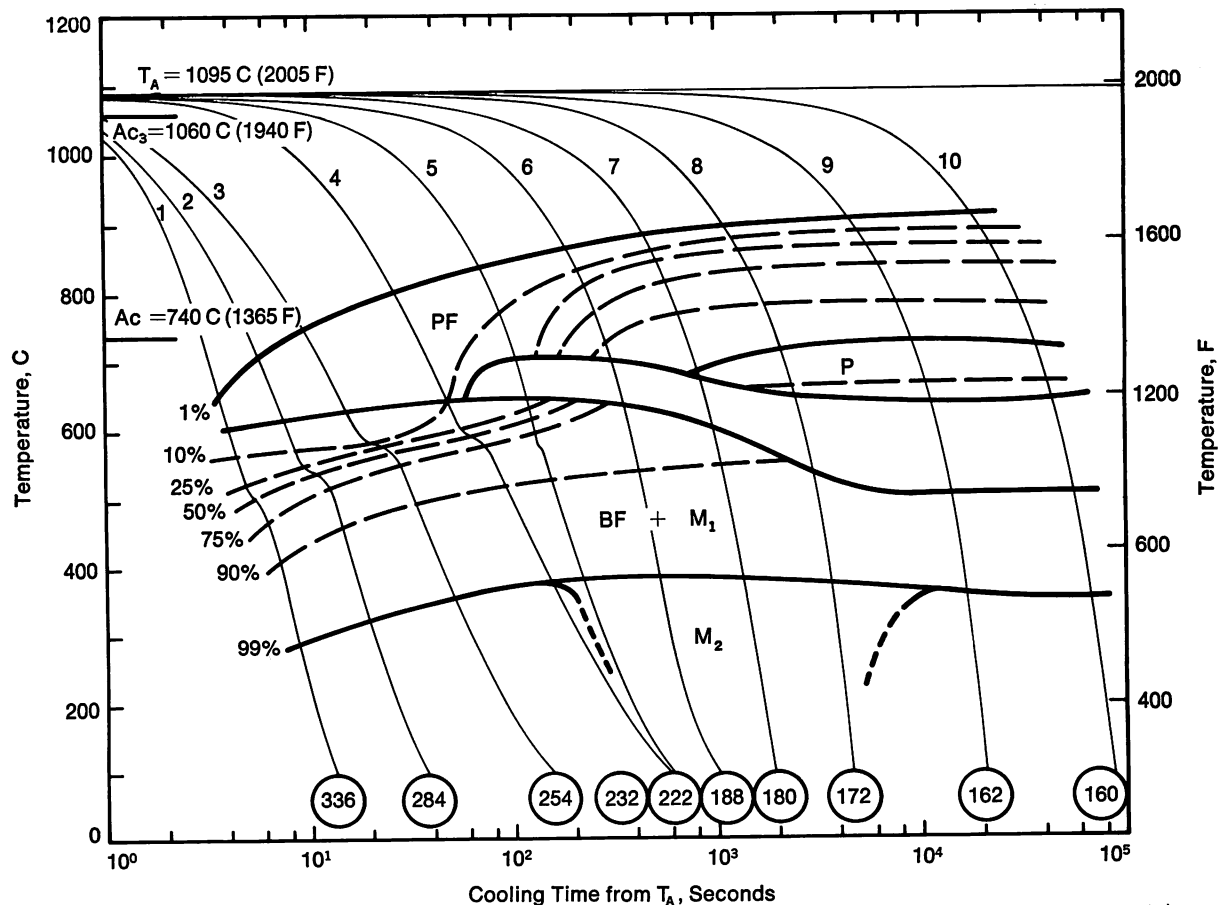


FIGURE 11—CCT diagram for Steel no. 11 (0.07% C, 0.90% Mn, 2.00% Si, 0.30% Cr, 0.30% Mo).

The basic features of the diagrams are the same for all eleven steels. Four different transformation products were observed, depending on cooling rate: polygonal ferrite (PF); pearlite (P); a bainitic transformation product (designated BF + $M_1$ and described further below); and a high carbon martensitic transformation product ($M_2$). $M_2$ was observed to form at low temperatures (typically less than 400 C, 750 F) and at intermediate cooling rates, that is, at cooling rates where transformation to 25% or more PF at higher temperatures had occurred and resulted in significant carbon enrichment of the remaining austenite. At these cooling rates, the dilatometric data indicated incomplete transformation of the austenite on reaching room temperature, and this is so indicated on the CCT diagrams by the absence of a completion (99%) line at those cooling rates. It should be noted here



(100 X)

a
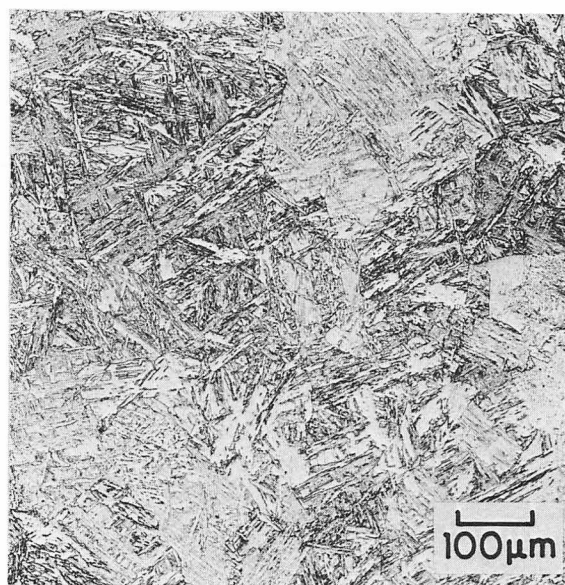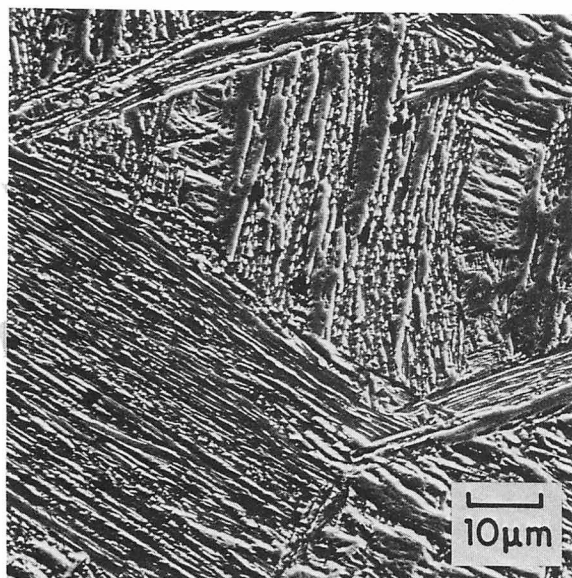


(1000 X)

b



(10,000 X)

c

FIGURE 12—Optical (a) and scanning electron micrographs (b, c) of microstructures in Steel 4 produced by cooling cycle no. 1 (Figure 4).

BF = Bainitic Ferrite
$M_1$ = Lower Carbon Martensite

that the boundary between the BF + $M_1$ and $M_2$ transformation regions was not always well defined on the dilatometer records, and the line shown represents the authors' best estimate of its location.

Figures 12-15 are representative micrographs of the transformation products observed. The bainitic transformation product formed at two different cooling rates is shown in Figures 12 and 13. The morphology of the bainite that forms in these steels differs from that usually associated with an upper bainite transformation. Instead of carbides between the ferrite laths, a martensitic constituent is observed. This morphology has been observed



(100 X)

a
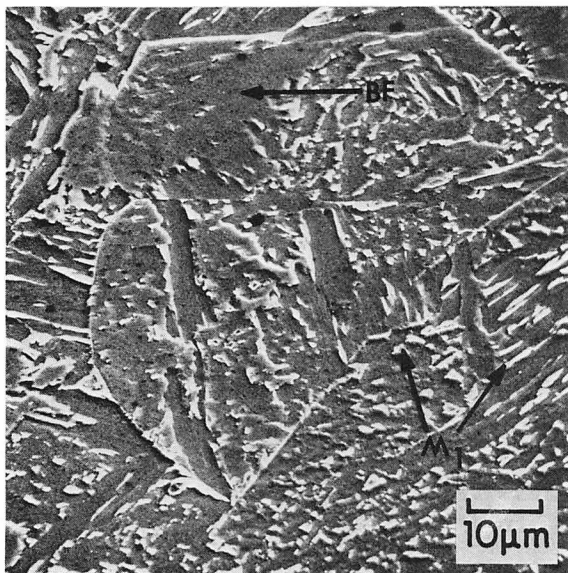


(1000 X)

b
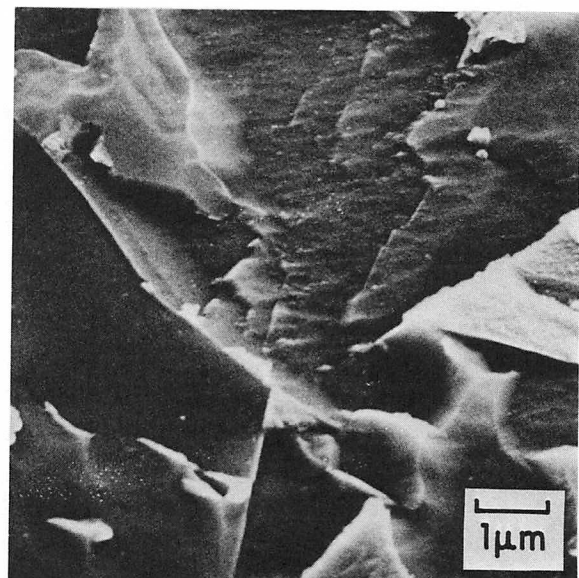


(10,000 X)

c

FIGURE 13—*Optical (a) and scanning electron (b, c) micrographs of microstructures in Steel 4 produced by cooling cycle no. 3 (Figure 4).*

BF = Bainitic Ferrite
$M_1$ = Lower Carbon Martensite

previously.[12] In the authors' experience, low carbon contents and high alloy contents, particularly Si + Cr + Mo, promote this inter-lath martensite in preference to inter-lath carbides during bainitic decomposition of the austenite. The different appearance of the bainitic transformation product in Figures 12 and 13, specifically the different length-to-width ratio of the ferrite laths, apparently results from the difference in average transformation temperature—and hence growth rate—imposed by the different cooling rates employed. In keeping with convention at the Climax laboratory, this bainitic transformation product is here referred to as "bainitic
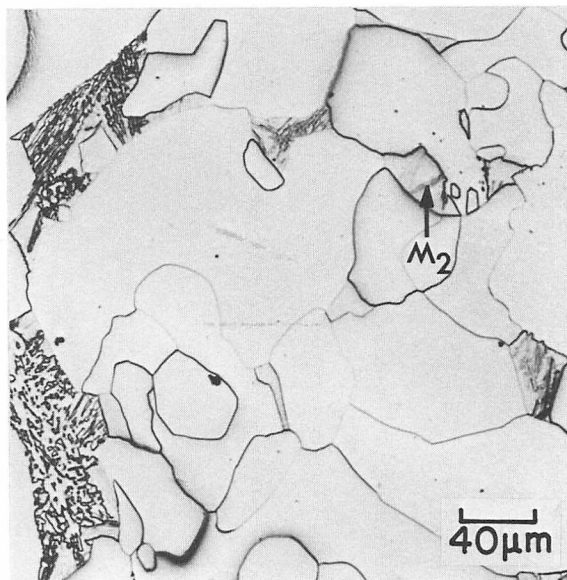


(250 X)

a
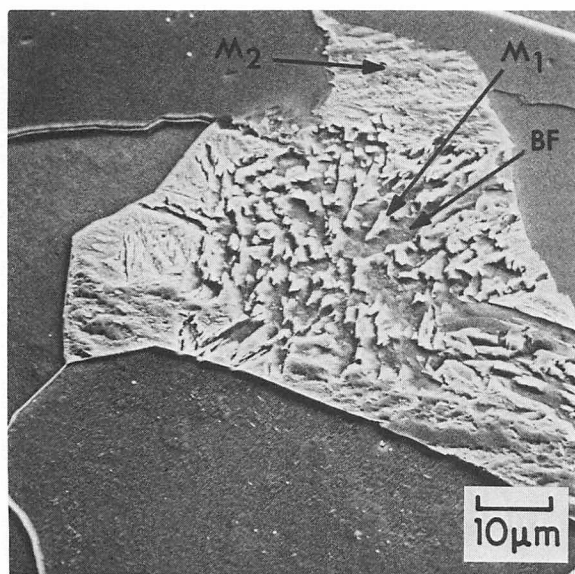


(1000 X)

b
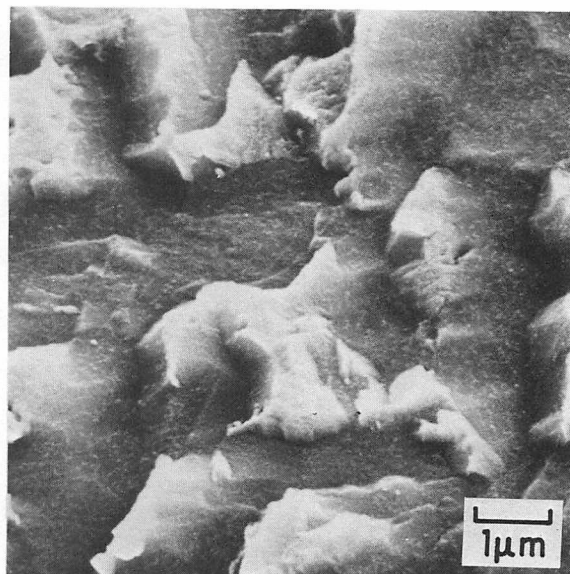


(10,000 X)

c

FIGURE 14—Optical (a) and scanning electron (b, c) micrographs of microstructures in Steel 4 produced by cooling cycle no. 7 (Figure 4).

BF = Bainitic Ferrite
M₁ = Lower Carbon Martensite
M₂ = Higher Carbon Martensite

ferrite + martensite," BF + M$_1$. The subscript "1" is used to distinguish the relatively low carbon inter-lath martensite from higher carbon martensite, M$_2$, discussed below.

Figure 14 shows the combination of transformation products resulting from cooling at intermediate rates.

For the cooling rate in question, the final microstructure consists of about 80 vol.-% PF, 15 vol.-% BF + M$_1$ and 5 vol.-% M$_2$ plus retained austenite. In Figures 14a and 14b, the morphological differences between M$_1$ ("blocky" appearance) and M$_2$ (tendency toward lenticular plates with some definition of midribs) is illustrated. Figure 14a



(100 X)

a
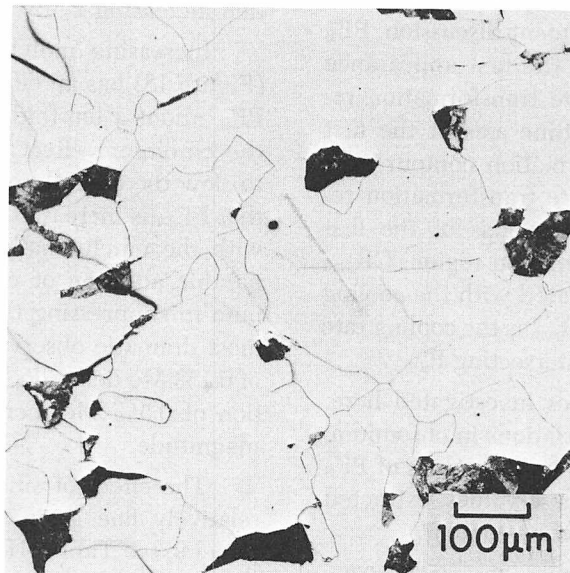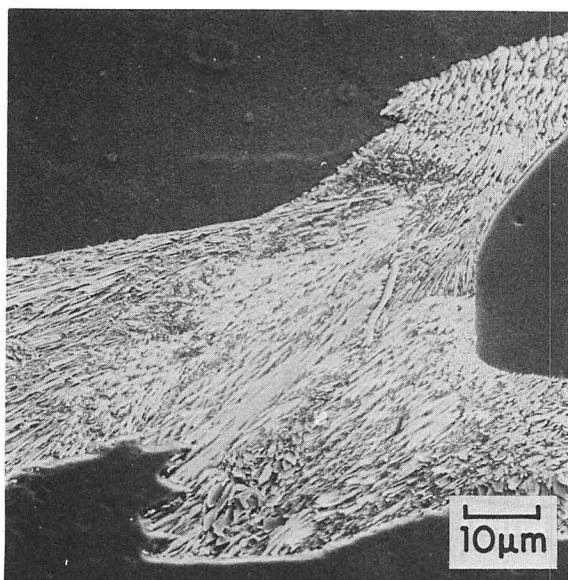


(1000 X)

b
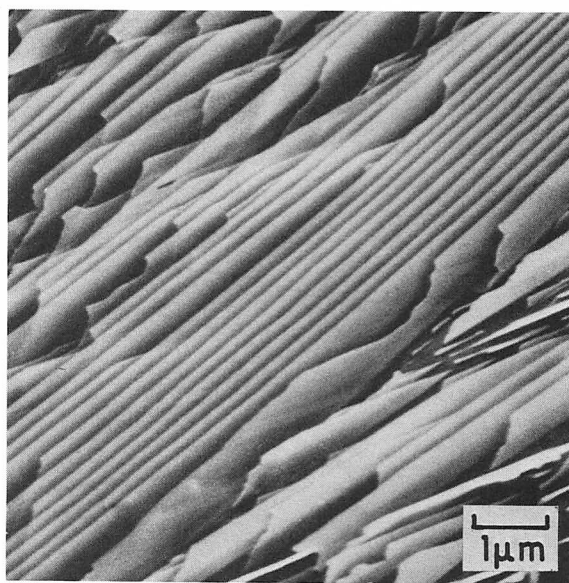


(10,000 X)

c

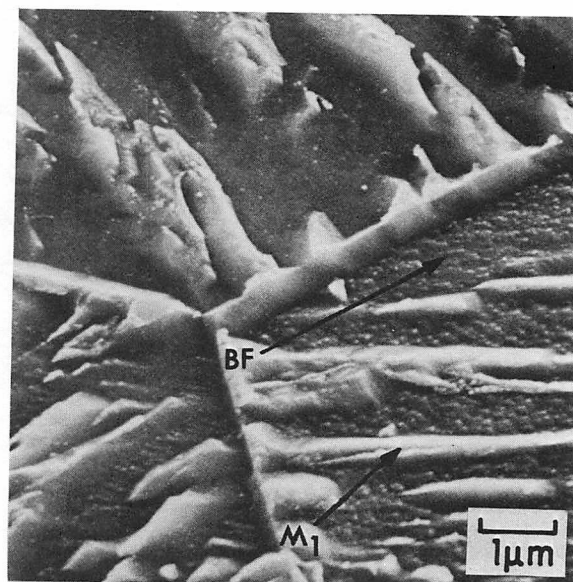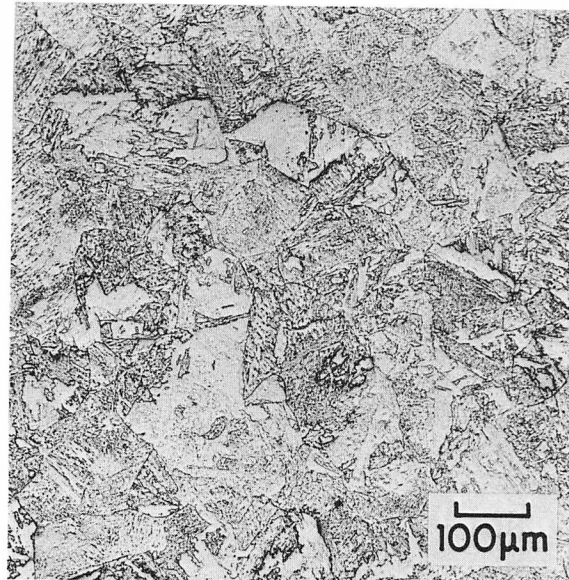FIGURE 15—*Optical (a) and scanning electron (b, c) micrographs of microstructures in Steel 4 produced by cooling cycle no. 10 (Figure 4).*

*Dark phase in (a) is pearlite.*
*White phase in (a) is polygonal ferrite.*

also shows areas which are apparently largely austenitic with a few M₂ plates crossng them. Apparently M₂ has a higher carbon content than M₁.

Figure 15 illustrates the polygonal ferrite and pearlite transformation products resulting from the slowest cooling rates.

Figure 16 is a schematic CCT diagram which serves to define some terms used in subsequent discussion. $PF_S$ is the location on the time axis of the first appearance (the "nose") of the polygonal ferrite transformation region. $PF_{75}$ is the location on the time axis of the first appearance of the 75% isotransformation contour as it passes through the polygonal ferrite transformation region. $P_S$ is the location on the time axis of the first appearance of the pearlite transformation region. $CR_{max}$ is defined as the cooling rate associated with the cooling curve which intersects $PF_{75}$, and $CR_{min}$ is the cooling rate associated with the cooling curve intersecting $P_S$.

Over the range of cooling rates investigated here, the most significant effect of the variations in chromium, molybdenum and silicon contents is on the values of $PF_S$ $PF_{75}$ and $P_S$. Figures 17-19 show these values, extracted from Figures 1-11, as a function of alloy content.

Increasing chromium content from 0 to 0.5% (Figure 17) has a substantial effect on $PF_S$, delaying the start of the polygonal ferrite reaction by about one order of magnitude in time. Once the PF reaction starts, however, it appears to progress relatively rapidly regardless of the chromium content, so that a 0.5% Cr addition delays $PF_{75}$ by only a factor of about 1.5 compared with the chromium-free steel. The effect of chromium on the pearlite reaction is also relatively modest, a 0.5% addition increasing $P_S$ by about a factor of two.

Increasing molybdenum content from 0 to 0.5% (Figure 18) has an effect similar to that of chromium on $PF_S$, about a ten-fold increase. However, in contrast to the chromium effect, the molybdenum addition seems to slow the overall polygonal ferrite reaction kinetics so that $PF_{75}$ is increased by about a factor of 20, compared with the much smaller increase resulting from a comparable addition of chromium. The effect of molybdenum in suppressing the pearlite reaction is perhaps the most dramatic observation of this study: Each addition of 0.1% Mo delays $P_S$ by about a factor of four. The addition of 0.5% Mo increases $P_S$ by some three orders of magnitude.

The effect of silicon is obscured somewhat by the relatively fine grain size obtained in the 1% Si steel (Steel 9, see Table III). The arrows on the data points in Figure 19 indicate the expected direction of change in the data if a grain size correction were applied. Unfortu-
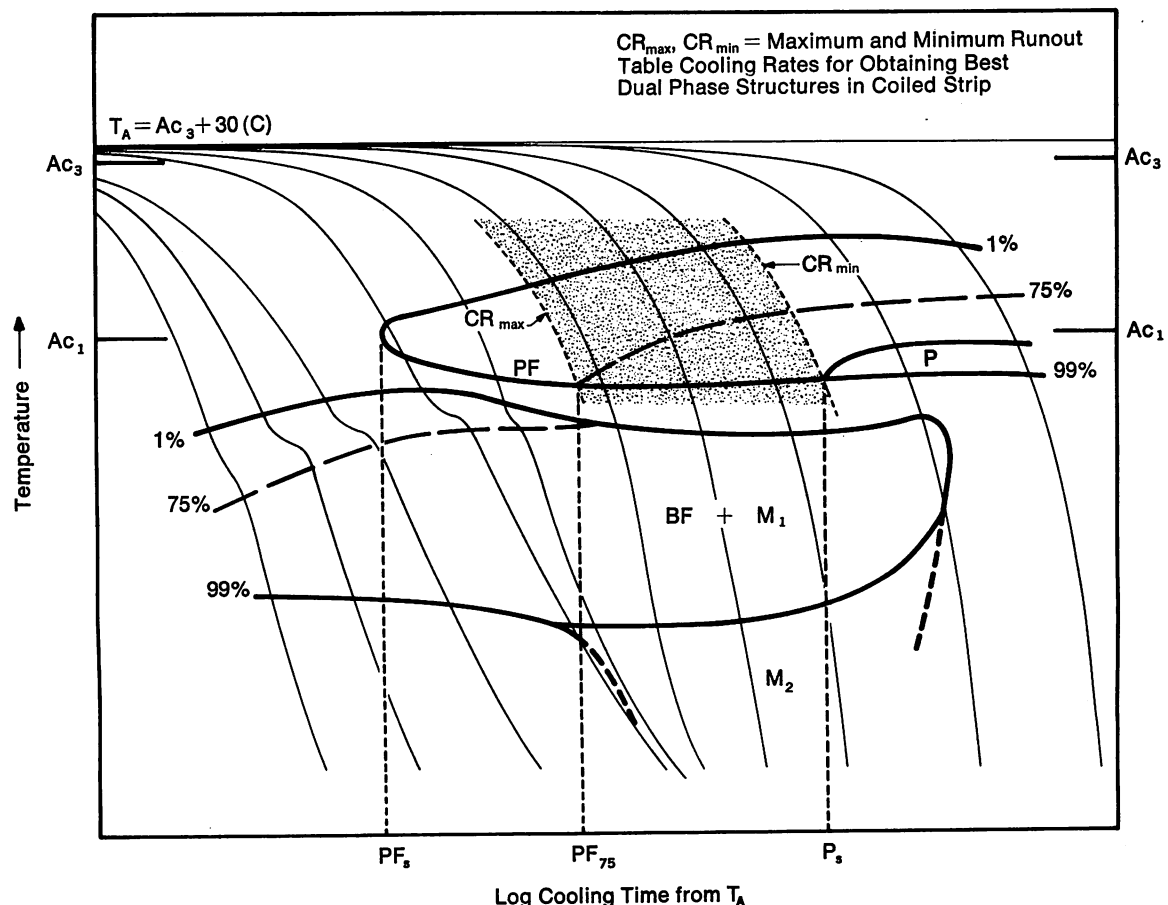


*FIGURE 16—Schematic CCT diagram illustrating definitions of $T_A$, $CR_{max}$, $CR_{min}$, $PF_S$, $PF_{75}$, and $P_S$.*
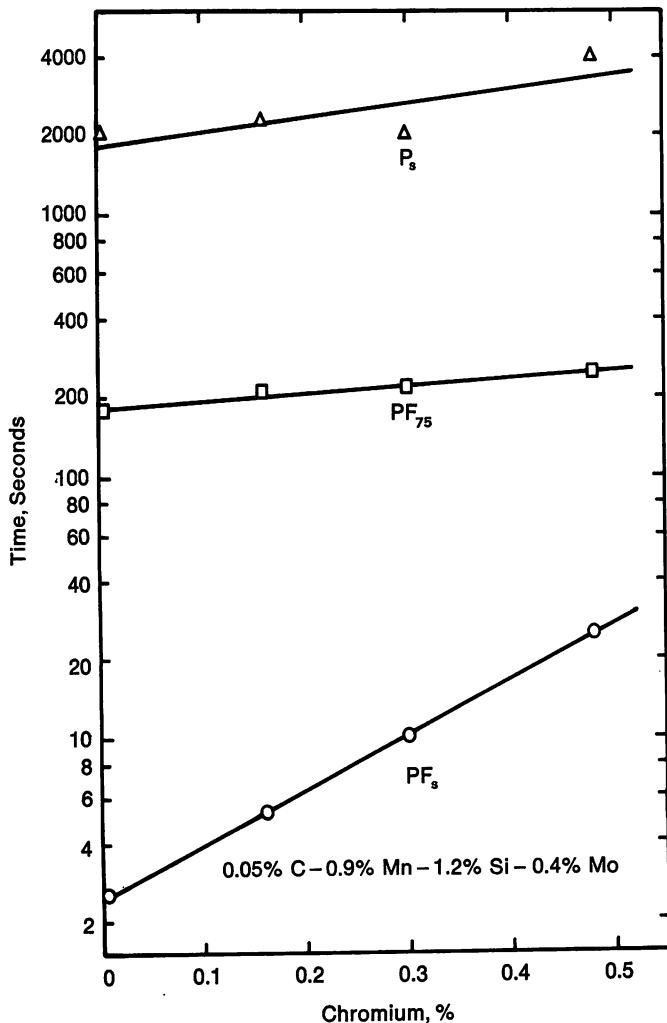
FIGURE 17—Effect of chromium on the location of $PF_S$, $PF_{75}$ and $P_S$ (see Figure 16).



FIGURE 18—Effect of molybdenum on the location of $PF_S$, $PF_{75}$ and $P_S$. (see Figure 16).

nately, the magnitude of this change with grain size has not been quantitatively defined for CCT diagrams. In prior work,[7] a CCT diagram for a 0.9% Si ARDP steel was determined. That steel had the same austenite grain size as the 1.5 and 2% Si steels of this study but also had higher manganese (1.2%), chromium (0.6%) and molybdenum (0.4%) contents. Approximate correction factors for the higher chromium and molybdenum contents can be found in Figures 17 and 18: A 0.1% change in chromium content changes $PF_S$, $PF_{75}$ and $P_S$ by factors of about 1.8, 1.1 and 1.2, respectively; a 0.1% change in molybdenum content changes $PF_S$, $PF_{75}$ and $P_S$ by factors of about 1.8, 1.8, and 3.1, respectively. Applying these approximate corrections to the CCT data from Reference 7, and ignoring (of necessity) the contribution of manganese, produces the data for 0.9% Si shown in Figure 19. Although this data manipulation is approximate and less than satisfying, it does lead to a result which is in keeping with empirical observations made during the early commercial mill trials mentioned in the introduction to this paper: An increase in silicon content resulted in an increase in the amount of polygonal ferrite formed

during hot strip mill processing. This is in agreement with the decrease in $PF_S$ and $PF_{75}$ with increasing silicon content shown in Figure 19.

## General Discussion

In commercial production of hot-rolled carbon steel strip of, say, 2.5 mm (0.1 in.) thickness, the slab of 20-30 mm (0.78-1.2 in) thickness passes through a finish rolling train of several rolling stands in tandem, exiting the last stand at the desired strip gauge and at a strip temperature typically in the range of 850 to 950 C (1560 to 1740 F). The strip then passes through a water cooling section where it is rapidly cooled (30 to 50 C/second, 55 to 90 F/second) to 550 to 650 C (1020 to 1200 F) before entering the coiler. The coil cools to room temperature at a rate of about 25 to 30 C/hour (45 to 55 F/hour).

To successfully produce dual phase steel on a hot strip mill, one must select an alloy which results in a

FIGURE 19—*Effect of silicon on the location of $PF_s$, $PF_{75}$ and $P_s$ (see Figure 16). Data for 0.9% Si from Reference 7.*

terminology are maintained here. Near the nose of the PF transformation region are arrows that indicate the shifts in the location of the PF region that would generally be expected under normal processing conditions such as heat-to-heat variations in composition and coil-to-coil variations in the amount of austenite deformation (arising principally from variations in finish rolling temperature). Also indicated is the fact that, under normal conditions, variations in run-out table cooling rate are to be expected. The strength and ductility of dual phase steel are sensitive to the relative amounts of polygonal ferrite and martensite present.[10] Thus, to produce steel of consistent mechanical properties under normal processing conditions, it is clear that the steel must exhibit at the outset little variation in the amount of polygonal ferrite that forms under the variable processing conditions. This means that the CCT diagram must exhibit a range of cooling rates over which the pearlite reaction is avoided *and* the variation in PF content is small. The greater this range, bound by $PF_x$ and $P_s$ in the schematic diagram, the less sensitive the steel will be to processing variations and hence the easier to produce.

In addition, there is a minimum amount, x, of polygonal ferrite that must form over this range of cooling rates. The ferrite growth enriches the remaining austenite carbon content. As discussed below, this carbon enrichment contributes significantly to the stability of the austenite during cooling of the coiled strip, ensuring that martensite rather than bainite will form. Experience from mill trials has shown that, for steels containing 0.04 to 0.07% carbon, the formation of 85 to 90 vol.-% polygonal ferrite is required to ensure adequate austenite stability. That ensures that less than 5% bainitic ferrite will form during cooling of the coil, and that small amount does not appear to impair mechanical properties.

In these terms, one can determine a measure of the "processability" of the eleven steels investigated here by examining the $P_s/PF_{75}$ ratio, which is a measure of the width of the shaded area in Figure 16. This ratio is plotted in Figure 21 as a function of alloy content.

In a steel containing 1.2% Si and 0.4% Mo, the effect of chromium on the $P_s/PF_{75}$ ratio is quite small. One is tempted to conclude at this point that chromium could be eliminated from the Mo-Si steel chemistry with no detrimental effects. However, as discussed below, the effect of chromium on austenite stability during coil cooling has not yet been defined and must be considered.

In a steel containing 1.2% Si and 0.5% Cr, the effect of molybdenum is very strong. At 0% Mo, the $P_s/PF_{75}$ ratio is less than one, indicating that, by conventional processing, it would be virtually impossible to obtain a reasonable amount of polygonal ferrite and still avoid the formation of pearlite in a molybdenum-free steel (see also Figure 5). Between 0 and 0.2% Mo, the $P_s/PF_{75}$ rises relatively slowly to a value of about seven, and thereafter rises sharply to a value of about 35 at 0.5% Mo.

microstructure of polygonal ferrite plus MA constituent after processing under the typical hot mill conditions described above. Specifically, the polygonal ferrite must not begin to form until rolling is complete since deformed ferrite is detrimental to the ductility of dual phase steel. Nearly all the desired ferrite must form before the steel reaches the coiling temperature because the ferrite growth rates at the coiling temperature and below become vanishingly small. The pearlite reaction must be avoided because, to the extent that pearlite forms, the dual phase properties (low yield strength, no yield point elongation, high work hardening rate) are impaired. And the austenite that does not transform to polygonal ferrite must have sufficient stability to avoid the bainite reaction and transform instead to martensite during cooling of the coil because bainitic transformation products are nearly as detrimental to mechanical properties as pearlitic constituents.

Figure 20 shows schematically how a steel with the proper CCT characteristics would interact with the hot mill processing. Previously introduced abbreviations and

FIGURE 20—Schematic illustration of interaction between hot strip mill processing and austenite transformation behavior required to produce ARDP steel.
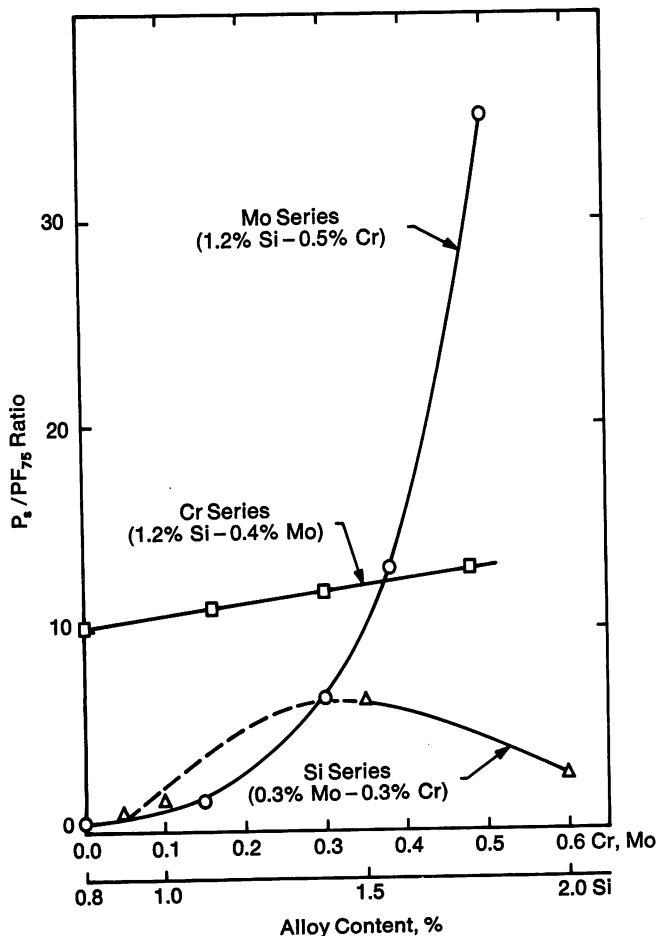


FIGURE 21—Effect of Cr, Mo and Si contents in the processability of ARDP steel.

In a steel containing nominally 0.3% Cr and 0.3% Mo, the silicon effect at first glance appears to be minimal. But closer consideration of the data indicates that silicon is very essential for obtaining adequate processability. At silicon contents below 1%, $P_s/PF_{75}$ is less than unity, an unacceptably low value for commercial production because it precludes obtaining an adequate amount of polygonal ferrite while still avoiding the pearlite reaction. The ratio increases fairly rapidly with silicon content, reaching a maximum value of about 6.5 at about 1.5% Si, then dropping again to unacceptably low values as silicon content is further increased.

In general, the greater the $P_s/PF_{75}$ ratio, the easier the processing should be because of the greater variability in manufacturing conditions that can be tolerated while still obtaining product of consistent microstructure and properties. The lower limit of acceptability of the $P_s/PF_{75}$ ratio will depend on the specific steel mill in question and the degree of control that can be exercised over the inherent production variables (composition, finish rolling temperature and run-out table cooling rate variations). The tighter this control, the lower the allowable $P_s/PF_{75}$ ratio. Steels with a $P_s/PF_{75}$ ratio in the range of 10 to 15 have been successfully processed on a number of North American and European hot strip mills. On this basis, a steel containing 1.2/1.5% Si, 0.4/0.5% Cr and 0.33/0.38% Mo would be recommended by the authors. Leaner molybdenum and chromium contents may be acceptable, but additional mill trials are needed to determine this.

The upper limit of acceptable $P_S/PF_{75}$ ratio will in general be determined by the desire to minimize alloy cost. It is conceivable that a given mill may have sufficient lack of control to require a very high $P_S/PF_{75}$ ratio, as high as 35, perhaps, attainable by alloying with about 0.5% Mo. If that much molybdenum is required, the possibility exists that, relative to the average run-out table cooling rate for that mill, $PF_{75}$ will be too large. (In terms of Figure 10, $PF_X$ would lie to the right of the illustrated run-out table cooling curve.) Insufficient PF would be obtained in spite of an adequate $P_S/PF_{75}$ ratio. The situation could be corrected by decreasing the chromium and manganese contents, to center the "cooling rate window" over the average mill cooling rate, while still maintaining a large $P_S/PF_{75}$ ratio.

In the above discussion, the need for stability of the untransformed austenite during cooling of the coil, so that martensite rather than bainite will form as the transformation product, has been noted. Figure 20 illustrates the required transformation behavior schematically. Figures 1-11 imply that none of the steels investigated here has the required austenite stability; that is, all steels form some bainitic transformation product at all cooling rates except perhaps the very slowest, where the austenite transforms completely to ferrite plus pearlite. Yet steels of composition similar to Steels 3, 4, 7 and 8 of this study have been successfully processed to dual phase microstructures in commercial mill trials, indicating that they do indeed have the required austenite stability under typical mill conditions.

The reason for the apparent difference in austenite stability, at coiling temperatures and below, between the commercial mill trials and the laboratory CCT studies must be related to the hot deformation of the austenite during commercial processing. It is well known that deformation of austenite accelerates the polygonal ferrite reaction. In the present laboratory studies of undeformed austenite, it was found that the maximum amount of polygonal ferrite formed at any cooling rate that avoided the pearlite reaction was about 75 to 80 vol.-% (see Figures 1-11 and Table IV). But in commercial mill trials, the dual phase microstructure has typically exhibited 90 vol.-% ferrite or more. Thus, deformation has accelerated the ferrite reaction so that more ferrite can form before the temperature becomes too low for ferrite growth. Assuming near zero solubility of carbon in ferrite for both cases, a simple mass balance shows that the austenite carbon content on reaching the coiling temperature during commercial processing must be about twice that of the laboratory processed (undeformed) material on reaching the same temperature. Apparently, this extra carbon content is responsible for the greater stability of the austenite during coil cooling exhibited in the commercial trials.

This study of transformation behavior has served to demonstrate how the elements silicon, chromium and molybdenum work to control the high temperature transformation kinetics (ferrite and pearlite reactions), leading to a workable "cooling rate window" that will allow the steel to transform to a consistent amount of polygonal ferrite under an acceptable range of variables inherent in the overall steel production process (composition, strip finish rolling temperature and run-out table cooling rate and coiling temperature). But the effects of the composition variables on the stability of untransformed austenite during cooling of the coil were not well defined. Thus, although the data in Figure 21 ($P_S/PF_{75}$ ratio) indicate, for example, that a chromium-free steel would result in a dual phase microstructure during hot strip mill processing, the authors would not recommend such a composition at the present time until the austenite stability question can be answered.

Based on the CCT data presented here and on the results of successful mill trials to date which indicate that a $P_S/PF_{75}$ ratio of 10 is adequate, and mindful of the as yet unanswered question of the stability of the carbon-enriched austenite at the coiling temperature and below, the authors would recommend the following composition for ARDP steel of 620 to 690 MPa (89.9 to 100 ksi) tensile strength on conventional hot strip mills: 0.04/0.07% C, 0.8/1.0% Mn, 1.2/1.5% Si, 0.4/0.5% Cr, 0.33/0.38% Mo. The steel should be aluminum-killed. Phosphorus and sulfur should be kept as low as possible with rare earth or zirconium additions for inclusion shape control in accord with good HSLA steelmaking practice. Recommended hot mill processing is quite conventional: slab reheat—1150/1315 C (2100/2400 F); finish rolling— 870/925 C (1600/1700 F); coiling—455/635 C (850/ 1175 F).

## Summary and Conclusions

A study of transformation behavior under continuous cooling conditions was conducted to determine the individual effects of chromium, molybdenum and silicon in a Mn-Si-Cr-Mo as-rolled dual phase (ARDP) steel. This steel was developed earlier through an alloy development program involving laboratory steels as well as steels produced in commercial mill trials and metallographically analyzed in the laboratory. Experience from the previous mill trials has shown that the key to successful production of ARDP steel is the avoidance of pearlite and of excessive (greater than 5%) amounts of bainitic ferrite. In steels containing 0.04/0.07% C, bainite is avoided by ensuring transformation to at least 85% polygonal ferrite on the run-out table. The resulting carbon enrichment of the remaining austenite islands provides sufficient hardenability to suppress the bainitic transformation.

The purpose of the present study was to determine the effects of chromium, molybdenum and silicon on the

continuous cooling transformation characteristics and thereby find the best combination for ensuring 85% polygonal ferrite formation and avoiding pearlite completely over a wide range of cooling rates. The numerical measure employed to express the size of this cooling rate window is the ratio $P_S/PF_{75}$, where $P_S$ is the time to first appearance of pearlite on cooling and $PF_{75}$ is the time to first appearance of 75% polygonal ferrite.

The following conclusions are drawn in part from the present study and in part from earlier mill trial experience:

- The influence of chromium in the range from 0 to 0.5% in a steel containing 0.05% C, 0.9% Mn, 1.2% Si and 0.4% Mo is to increase the $P_S/PF_{75}$ ratio slightly, from 10 to 11.5.

- The effect of molybdenum in the range from 0 to 0.5% in a steel containing 0.05% C, 0.9% Mn, 1.2% Si and 0.5% Cr is to increase the $P_S/PF_{75}$ ratio markedly, from 0.5 to 35.0, well above the estimated minimum value of 10 required for reproducible production on commercial mills. This remarkable effect derives from molybdenum's unusual differential effect of delaying $P_S$ (from 10 to 10,000 seconds) much more than it delays $PF_{75}$ (from 25 to 350 seconds).

- Silicon's influence in the range from 1 to 2% in a steel containing 0.07% C, 0.9% Mn, 0.3% Cr and 0.3% Mo is to increase $P_S/PF_{75}$ from approximately 1.0 at 1% Si to 6.5 at 1.5% Si, and then to decrease the ratio to 2.6 at 2% Si. Over the range from 1 to 1.5% Si, $PF_{75}$ decreases by nearly an order of magnitude while $P_S$ remains nearly constant.

- The currently recommended composition range for obtaining reproducible properties in commercial production of ARDP steel is 0.04/0.07% C, 1.2/1.5% Si, 0.8/1.0% Mn, 0.4/0.5% Cr, 0.33/0.38% Mo. It may be possible to process steels of leaner chromium and molybdenum contents, but further trials are needed on individual mills to determine empirically each mill's control over processing variables and hence the minimum requisite $P_S/PF_{75}$ ratio.

# References

1. S. Hayami and T. Furukawa, Proceedings Microalloying '75, Washington, D. C., 1976, 311.

2. R. G. Davies, Met. Trans. A, 9A, (1) 1978, 41.

3. A. T. Davenport, Ed., Proceedings of Symposium Formable HSLA and Dual-Phase Steels, TMS/AIME, Warrendale, Pa., 1979.

4. R. A. Kot and J. W. Morris, Jr., Eds., Proceedings of Symposium Structure and Properties of Dual-Phase Steels, TMS/AIME, Warrendale, Pa., 1979.

5. A. P. Coldren, G. Tither and D. V. Doane, U. S. Patent No. 4,072,543, February 7, 1978.

6. V. Biss and R. L. Cryderman, Met. Trans., 2, August 1971, 2267.

7. A. P. Coldren and G. Tither, Journal of Metals, 30, April 1978, 6.

8. A. P. Coldren and G. T. Eldis, Journal of Metals, 31, March 1980, 37.

9. Y. E. Smith and C. A. Siebert, Met. Trans., 2, June 1971, 1711.

10. G. T. Eldis, Proceedings of Symposium Structure and Properties of Dual-Phase Steels, TMS/AIME, Warrendale, Pa., 1979.

11. G. T. Eldis, Proceedings of Symposium Hardenability Concepts with Applications to Steel, TMS/AIME, Warrendale, Pa., 1978.

12. L. J. Habraken and M. Economopoulos, Proceedings of Symposium Transformation and Hardenability in Steels, Climax Molybdenum Company, 1967, 69.

# Discussion

R. STEVENSON, General Motors Corporation. What is the effect of retained austenite on the properties of dual phase steels?

G. T. ELDIS. Retained austenite is always present, as we now know. I have yet to see any conclusive evidence that the amount is sufficient to significantly effect any part of the stress/strain curve. As far as I know, it is rather innocuous. It is probably transforming after a few percent strain, and we just do not see an effect.

A. B. ROTHWELL, Foothills Pipe Lines (Yukon) Ltd. This discussion describes some results, obtained in the course of a study on transformation behavior of dual phase steels carried out at the Noranda Research Centre, which are complementary to the work reported by Eldis et al. In particular, the effects of austenite deformation on subsequent transformation, referred to by the authors, are confirmed and quantified.

Initial dilatometric studies, similar to those described by the authors, had shown that, even in steels which had been successfully processed in industrial hot strip mills, dual phase structures could not be reproduced in the laboratory at cooling rates typical of the strip mill run-out table (typically 10-25 C/s, 18-45 F/s). In particular, insufficient ferrite was formed

in the upper transformation range, so that large quantities of undesirable bainite were formed on subsequent cooling.

Accordingly, an investigation was undertaken, in conjunction with McGill University, of the effect of austenite deformation on the transformation behavior of a typical dual phase steel. The chemical composition was: 0.07% C, 1.03% Mn, 1.11% Si, 0.42% Mo, 0.54% Cr. $Ac_1$ and $Ac_3$ temperatures were 707 and 970 C (1305 and 1780 F), respectively. Continuous cooling transformation characteristics were determined dilatometrically, as before. The effect of deformation was studied using the computer-controlled hot torsion machine at McGill University. Testpieces were austenitized at 1100 C (2010 F) for 5 minutes (an adequate treatment for a material containing no microalloying additions). They were then deformed by a total of 70% (equivalent surface shear strain) and allowed to recrystallize. This was intended to simulate the grain refining effect of the roughing deformation in the hot strip mill. Testpieces were then cooled at a rate of 1 C/s (1.8 F/s) to either 980 or 920 C (1795 or 1690 F) (respectively 10 C, 18 F above and 50 C, 90 F below $Ac_3$) and deformed a further 70%, simulating the deformation imparted in the finishing train. They were finally gas cooled at 10 C/s (18 F/s) to a temperature in the range 650-810 C (1200-1490 F), and immediately water quenched to room temperature. The gas cool-

ing was intended to simulate water cooling on the run-out table; while, for reasons connected with temperature control, the cooling rate is a little slow, it is not believed that this has any fundamental effect on the nature of the observations. Figure 1 is a schematic representation of the time-temperature-deformation cycles employed.

Testpieces were sectioned longitudinally and examined metallographically. The portion of the cross section which had been untransformed at the quench temperature appeared as dark etching bainite or martensite. By quenching from successively lower temperatures, it was possible to follow the progress of the ferrite transformation. A quantitative determination of the ferrite volume fraction was carried out by point counting on the layers adjacent to the testpiece surface.

Figure 2 shows the variation of ferrite volume fraction with quench temperature for the two deformation temperatures. About 50% ferrite had formed by 650 C (1200 F) in the case of the 980 C (1795 F) deformation temperature; with a deformation temperature of 920 C (1690 F), on the other hand, the corresponding figure was over 80%. Figure 3 shows the CCT diagram determined by dilatometry, without deformation; the cooling curve experienced by the hot torsion testpieces, from the deformation temperature, is superim-



FIGURE 1—Schematic time-temperature-deformation profile for hot torsion testpieces.
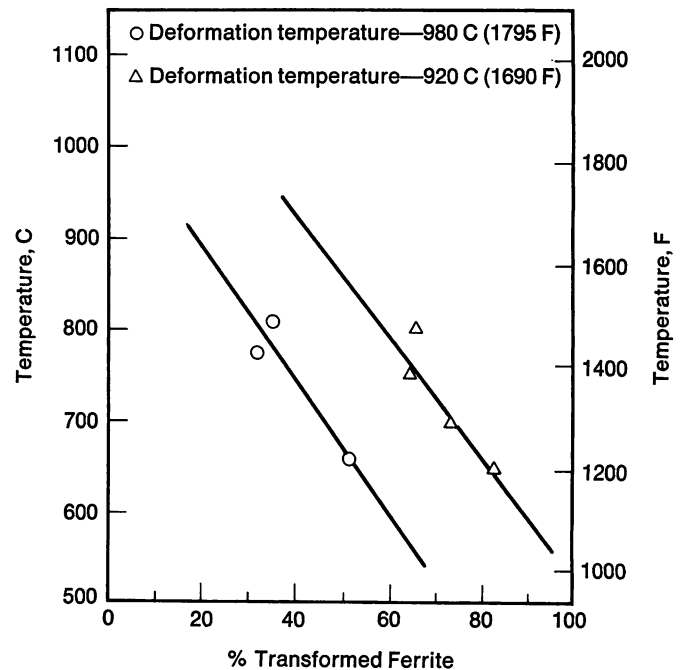


FIGURE 2—Effect of deformation temperature on rate of polygonal ferrite transformation.
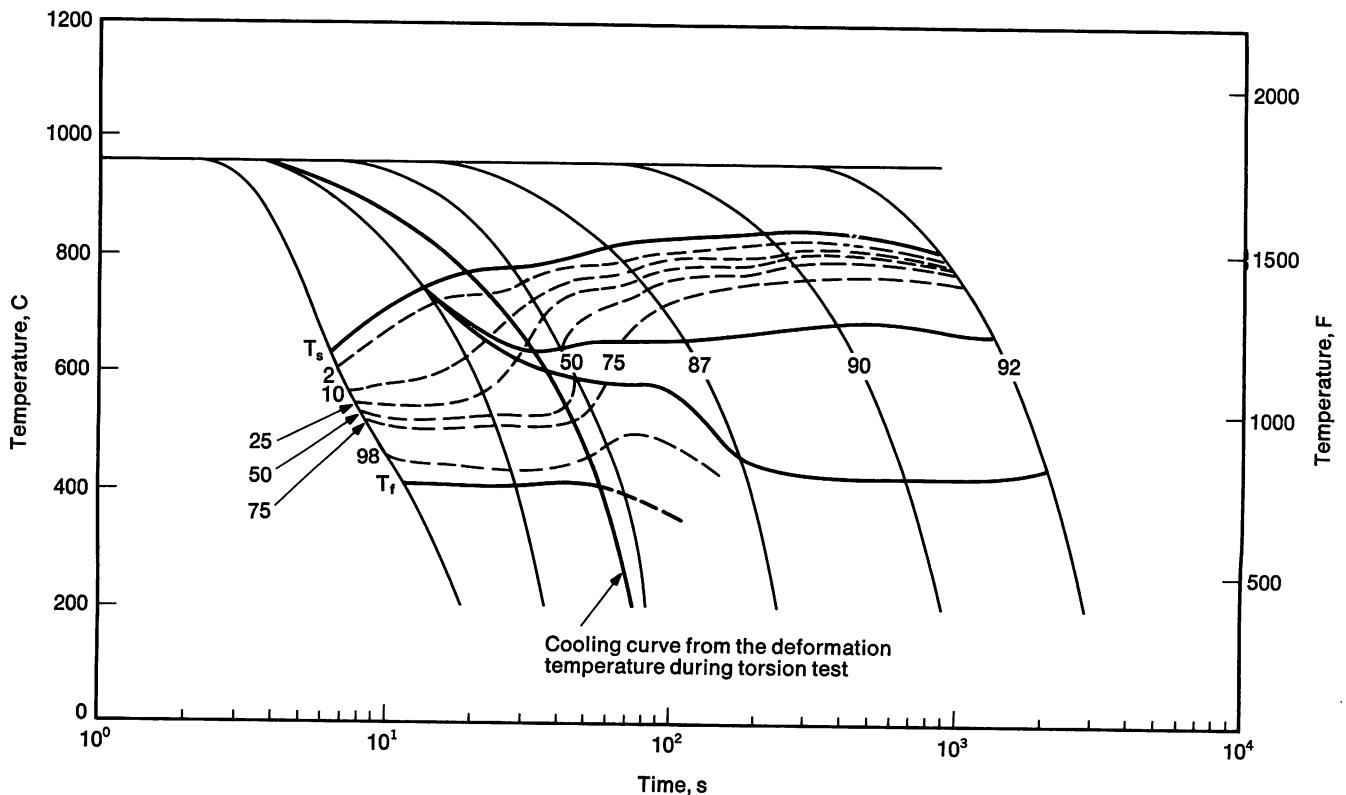


FIGURE 3—CCT curve determined by dilatometry with superimposed cooling curve for hot torsion testing.

posed. It is clear that no more than 25% ferrite would be expected in the absence of deformation.

On the basis of the present results, it is impossible to determine whether this strong effect of deformation, and of deformation temperature, is the result of the deformation *per se*, of grain size and substructural effects, or of a combination of both. Certainly, earlier dilatometric work had indicated substantial differences in ferrite kinetics between steels which remained fine grained at the austenitization temperature and those which did not. On the other hand, the strong effect of the lower deformation temperature indicates that deformation below the $Ac_3$ may be important; one of the main practical roles of silicon would thus be to elevate the $Ac_3$ to a value significantly above the typical hot mill finishing range. Further work at McGill will aim to clarify these questions.

The authors rightly emphasize the importance of forming a sufficient quantity of polygonal ferrite over a range of cooling rates; however, diagrams such as that shown in Figure 20 (first put forward in Reference 7) can be misleading.

The lower transformation curve in a conventional CCT diagram represents the behavior of a series of austenites whose carbon contents increase with decreasing cooling rates; this arises from the rejection of a progressively greater amount of carbon as an increasing volume fraction of ferrite is formed. The lower transformation product formed by interrupted cooling of the type shown in Figure 20, however, is determined by the carbon content typical of the austenite remaining after cooling through the upper range (at the higher rate), regardless of where the slower rate intersects the lower transformation curve (which refers to cooling at a constant rate and thus, at long times, to an austenite highly enriched in carbon). It is this factor which explains the presence of coarse bainite whenever insufficient ferrite is formed in the upper transformation range; the simple superimposition of the interrupted cooling curve, as in Figure 20, would indicate that no coarse bainite can form when cooling at slow rates through the lower transformation range.

# Experience with the Production and Application of As-Rolled Dual Phase Steel

by E.-J. Drewes, Estel Hoesch Hüttenwerke AG and D. Daub,
Estel Hoesch Hohenlimburg-Schwerte AG

Far-reaching steps have been decided upon in the USA to save energy. As far as the motor car industry is concerned, there arose from this the need to save weight, and this has led to a number of interesting developments. In competition with other materials, this led, in the case of steel, to the development of high strength materials with good cold forming properties and to the dual phase steels.

Because of the policy of building unit cars (self-supporting coach work), and the manufacture of predominantly small and mid weight cars, the average weight in the European car industry is lower than in the USA. Furthermore, for some years, the European car manufacturers have been using high strength, microalloyed fine grained constructional steels (HSLA), particularly in the inside of cars. Savings in weight here are harder to achieve. Despite this, a further reduction in the weight of cars is being called for in Europe, and this does not apply only to export models. It was therefore obvious to look at the possibilities of dual phase steel.

The Estel company does not possess the continuous annealing line necessary for the production of cold-rolled dual phase steel, and the conversion of a galvanizing line for the production of intercritically annealed dual phase steel could not be considered for the moment. It was decided to use the Climax concept, that is, a dual phase steel produced as-hot-rolled.

Several papers have already reported on the development of this steel,[1-3] and the metallurgical aspects of this steel have also been referred to in the preceding lecture; it is therefore not necessary to elaborate on them. The subject of this paper is the production of dual phase steel in the as-rolled condition in available conventional plants. The individual properties will be described, and some instances of use which demonstrate the advantages and possibilities of this steel will be mentioned.

## Production of Experimental Material

Two melts were first made at the Hoesch Hüttenwerke in Dortmund in a 1.5 ton induction furnace, and a third melt was made in a 50 ton electric arc furnace. The aim analysis (Table I) agreed with the Climax Molybdenum Company composition on the basis of latest results obtained there.

Table I also summarizes the check analyses obtained from the rolled strip from the above heats. In the two 1.5 ton melts, the carbon content was unintentionally high at 0.09%. However, as will be seen later, the desired dual phase structure was obtained, and therefore the same carbon content was specified for the 50 ton melt. The value obtained was 0.10% C.

Si, Mn, P, S, Cr, Mo and Ce were very close to the specified analysis. In the electric arc furnace melts, the nitrogen content showed characteristically high values. The high aluminum content in melt number 100,826 was the result of an alloying fault.

**Table I**—Analyses of Dual Phase Steels

| | Element, % | | | | | | | | | |
|---|---|---|---|---|---|---|---|---|---|---|
| | C | Si | Mn | P | S | Mo | Cr | Al | Ce | N |
| Aim | 0.06 max | 1.20 | 0.90 | 0.010 max | 0.005 max | 0.35-0.40 | 0.35-0.40 | 0.04-0.06 | 1.5 x S | — |
| No. 100,825[a] | 0.09 | 1.11 | 0.89 | 0.012 | 0.007 | 0.38 | 0.39 | 0.080 | 0.010 | 0.010 |
| No. 100,826[a] | 0.09 | 1.32 | 1.00 | 0.013 | 0.008 | 0.41 | 0.45 | 0.135 | 0.008 | 0.012 |
| No. 812,849[b] | 0.10 | 1.22 | 1.02 | 0.012 | 0.005 | 0.36 | 0.39 | 0.067 | 0.010 | 0.011 |

[a] — 1.5 ton furnace.
[b] — 50 ton furnace.

The ingots from the 1.5 ton melts were rolled into slabs of 440 by 100 mm (17 by 4 in.) and rolled to different final thicknesses on the continuous medium-width strip mill of the Hoesch Werke Hohenlimburg-Schwerte AG. Of the electric furnace 50 ton melt, some was converted into slabs for Hohenlimburg (360 to 440 by 100 mm, 14 to 17 by 4 in.) and some into slabs for the hot wide strip mill in the Hoesch Hüttenwerke in Dortmund (760 by 230 mm, 30 by 9 in.), and then rolled further into other sizes. The rolling conditions are summarized in Table II.

**Table II**—Rolling Data

|  | Medium Strip (HWHS) | Wide Strip (HHW) |
|---|---|---|
| Average Finishing Temperature, C (F) | 870 (1600) | 860 (1580) |
| Average Coiling Temperature, C (F) | 580 (1075) | 580 (1075) |
| Run-Out Table Cooling | Laminar | Spray |
| Average Cooling Rate, C/sec (F/sec) | 25-40 (45-72) | 25 (45) |

## Test Results

The dual phase structure with 15 to 20% martensite can, with the above analyses, be obtained within the following temperature ranges:

> Finishing   840-900 C (1545-1650 F)
> Coiling     550-620 C (1020-1150 F)

Thus there are sufficiently wide temperature ranges for commercial production. However, combinations of extreme values were not evaluated for all thicknesses of strip. The rate of cooling is in accordance with the recommendations of Climax (theoretical 28 C/second, 50 F/second); this is also compatible with commercial mill practice.

Typical dual phase microstructures are shown in Figure 1 representing medium strip from melt 100,826. The fine martensite formation is evident from the photomicrographs.



20μm                    (1000 X)
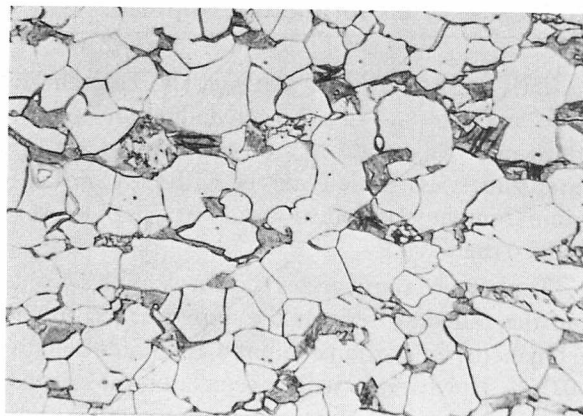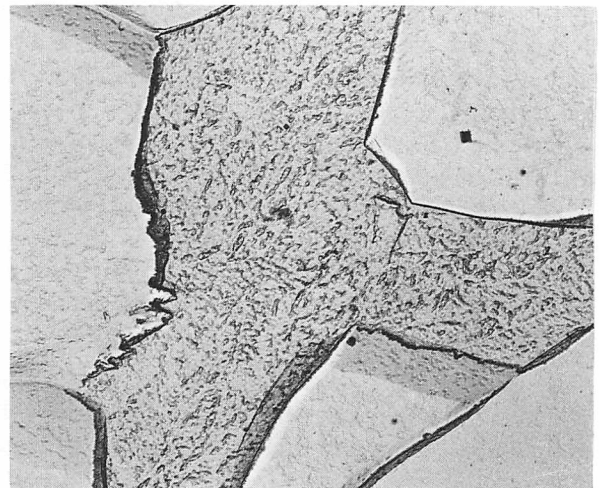


1μm                     (19,000 X)



2μm                     (11,000 X)

Ferrite and 15-20% Martensite

Grain size: 13 ASTM (C 89-52)

FIGURE 1—*Typical microstructure of dual phase steel.*

When the rate of cooling is too high or the coiling temperature too low, increasing amounts of bainite are observed, and when the coiling temperature is too high, some fine lamellar pearlite is formed. In the wide strip, there was a somewhat smaller amount of martensite. This is possibly the result of a lower cooling rate.

The mechanical properties of longitudinal specimens from all strips are given in Figure 2. Average values for strip ranging in thickness from 2.5 to 5 mm (0.1 to 0.2 in.) were as follows:

| | Medium Strip | Wide Strip |
|---|---|---|
| 0.2% Offset Yield Strength, MPa (ksi) | 450 (65.3) | 385 (55.8) |
| Tensile Strength, MPa (ksi) | 675 (97.9) | 690 (100.1) |
| Elongation, % | 28.5 | 29.5 |

Characteristic of a predominating amount of dual phase structure is the absence of yield point elongation in the tensile test.

The low yield strength of the wide strip is remarkable and probably due to the slower cooling in the mill. The comparatively high yield strength values of the 2 mm (0.08 in.) medium strip confirm this supposition. In the case of thin strip, the rate of cooling was quite high. Thus the values for the 2.0 mm (0.08 in.) strip were
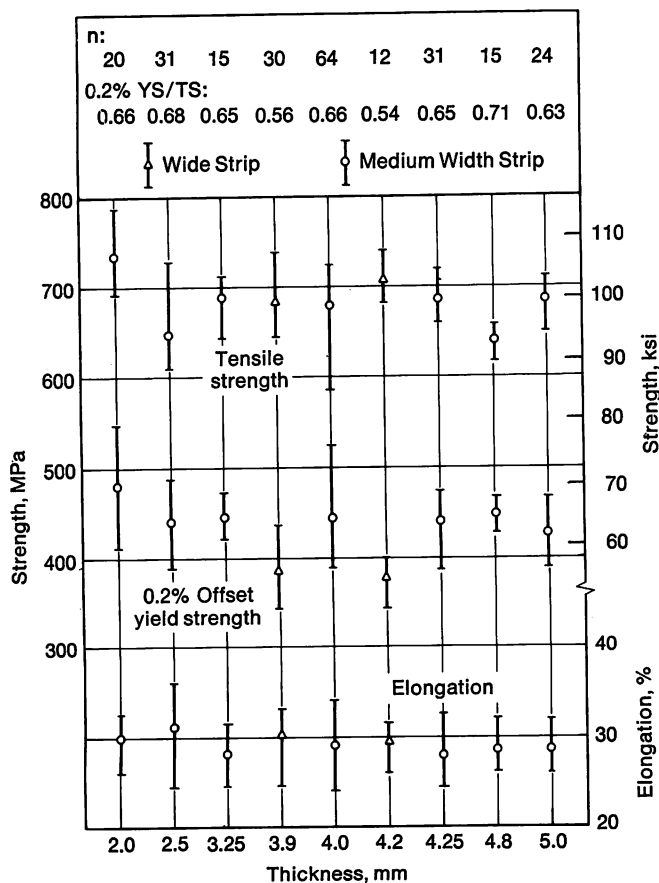
not considered in the average values. All material exhibited predominantly continuous yielding, high elongation at high tensile strength and low yield/tensile ratio.

The r and n values further characterize cold formability. As regards plastic anisotropy, r for the dual phase steel is of a somewhat higher mean value, and there is a lower planar anisotropy than in the case of HSLA steel of comparable yield strength. The r value distribution resembles more closely the more isotropic behavior of the unalloyed mild steels (Figure 3). Compared with the conventional HSLA steels, the dual phase steel shows considerably higher n values at comparable yield strengths, especially at low deformation. Values similar to mild steel ($\sim$ 0.2) are attained particularly for the hot wide strip. Somewhat lower n values were obtained for the medium width strip.

By the cold-rolling tests, the work hardening behavior of the dual phase steel can be demonstrated (Figure 4). The work hardening curve of the microalloyed steel QStE 420 TM is (compared to the mild steel St W 24) in principle pushed parallel to higher values. On the other hand, the work hardening curve of the dual phase steel shows, in the region of small deformation, a much steeper rise so that, in the case of initial yield strengths similar to HSLA steel, a very much higher final value is attained.

Erichsen cupping values were also determined for the various strip thicknesses. Despite the high strength of the dual phase material, cupping values were similar to those given for deep drawing grades in German standards (DIN). In some cases, the values correspond to a special deep drawing grade.



FIGURE 2—Tensile properties (parallel to rolling direction) of hot-rolled dual phase steel (average and scatter band over the length and width of the strips).
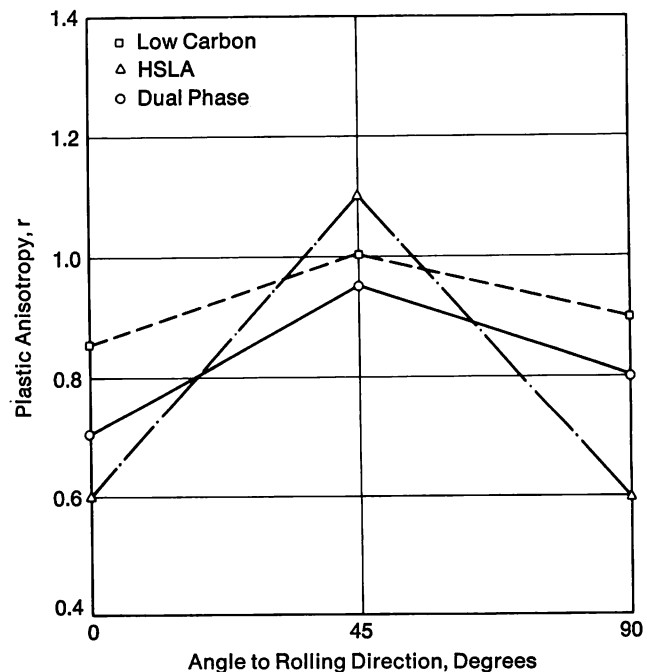


FIGURE 3—Values of r for hot-rolled dual phase steel, low carbon steels and HSLA steels.

Figure 5 shows a diagram of strength at elevated temperatures for 4 mm (0.16 in.) thick strip from melt 812,849. For purposes of comparison, the values for an unalloyed structural steel, St 52-3, as well as for an HSLA steel, QStE 460 TM (niobium alloyed), are given on the right side of the figure. In addition, the minimum values for 13 CrMo 4 4 are included. In the case of the dual phase steel, the increase in strength at 300 to 400 C (570 to 750 F) is interesting. Note that there is also a maximum in the elongation curve at the same temperature. This behavior differs markedly from that of the comparative steels. Further research is necessary to fully explain this behavior.

In the same way, the strength behavior at high temperatures was also investigated on strip 2 mm (0.08 in.) thick including samples which had been 5 or 10% cold rolled (Figure 6). The curve for the hot strength in the as-rolled condition corresponds to the curve shown in Figure 5. Because of the additional cold rolling, the curves have been moved to higher values. Hot strengths of $\geq$ 900 MPa (130 ksi) were obtained for the cold-rolled samples at 300 to 350 C (570 to 660 F).

FIGURE 4—Work hardening behavior of hot-rolled dual phase steel and other hot-rolled grades. ——>
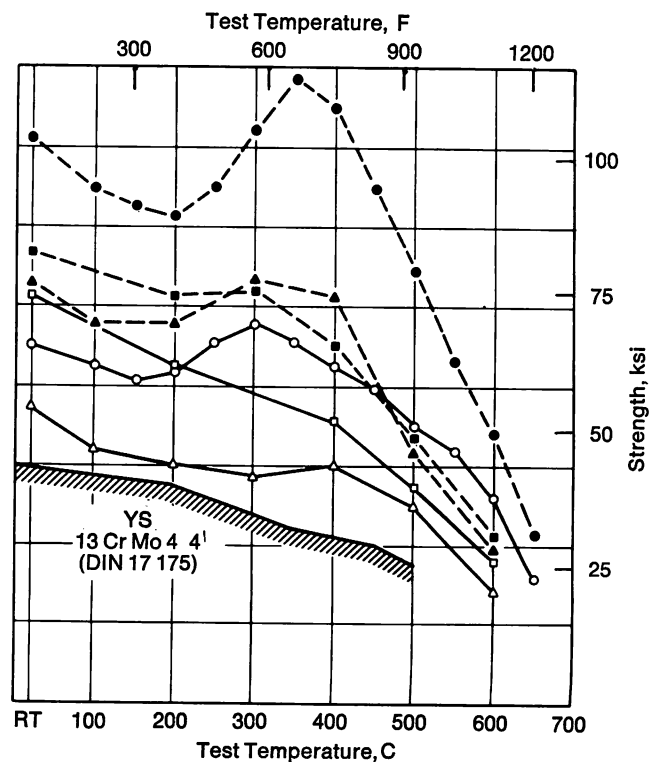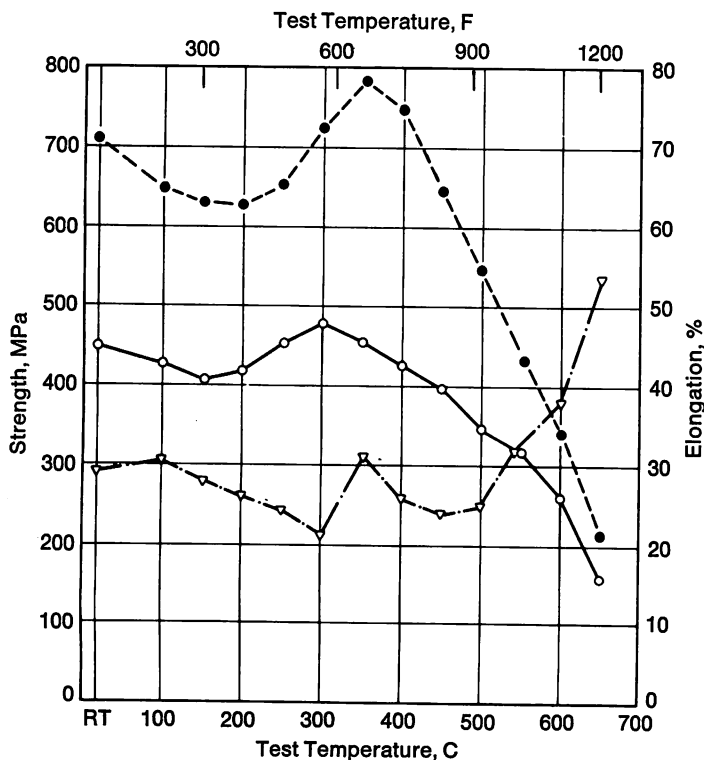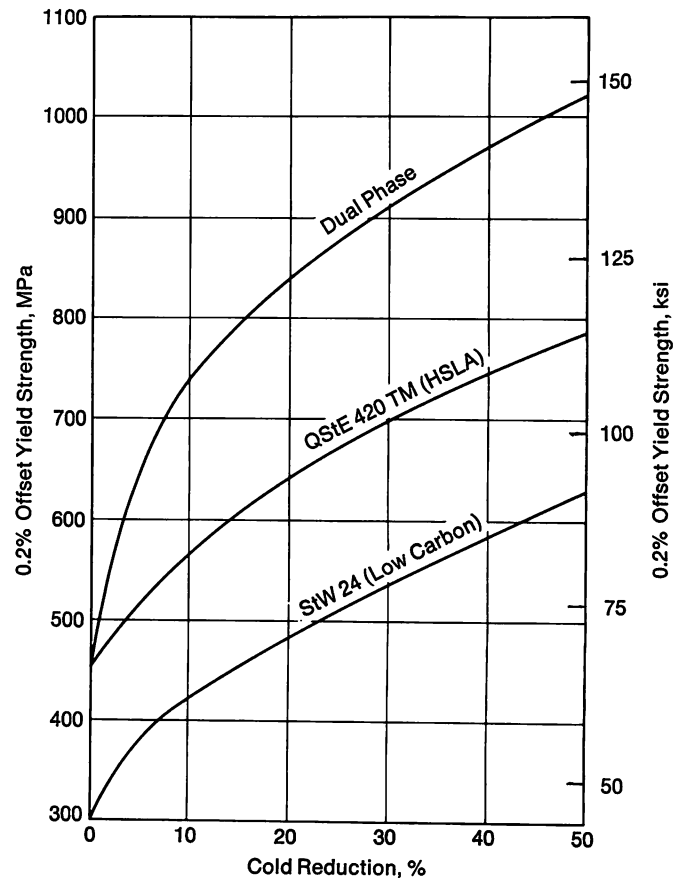
| | Check Analysis, % | | | | | | EL | TS | YS | Grade |
|---|---|---|---|---|---|---|---|---|---|---|
| C | Si | Mn | Nb | Ti | Cr | Mo | | | | |
| 0.10 | 1.20 | 1.00 | — | — | 0.39 | 0.36 | ▽ | ● | ○ | Dual Phase, Heat No. 812,849 |
| 0.10 | 0.02 | 0.55 | 0.04 | — | — | — | ■ | □ | Q St E 460 TM (HSLA Nb) |
| 0.19 | 0.27 | 0.97 | — | — | — | — | ▲ | △ | St 52-3 |

FIGURE 5—Strength at elevated temperatures (dual phase steel compared with conventional steel grades).
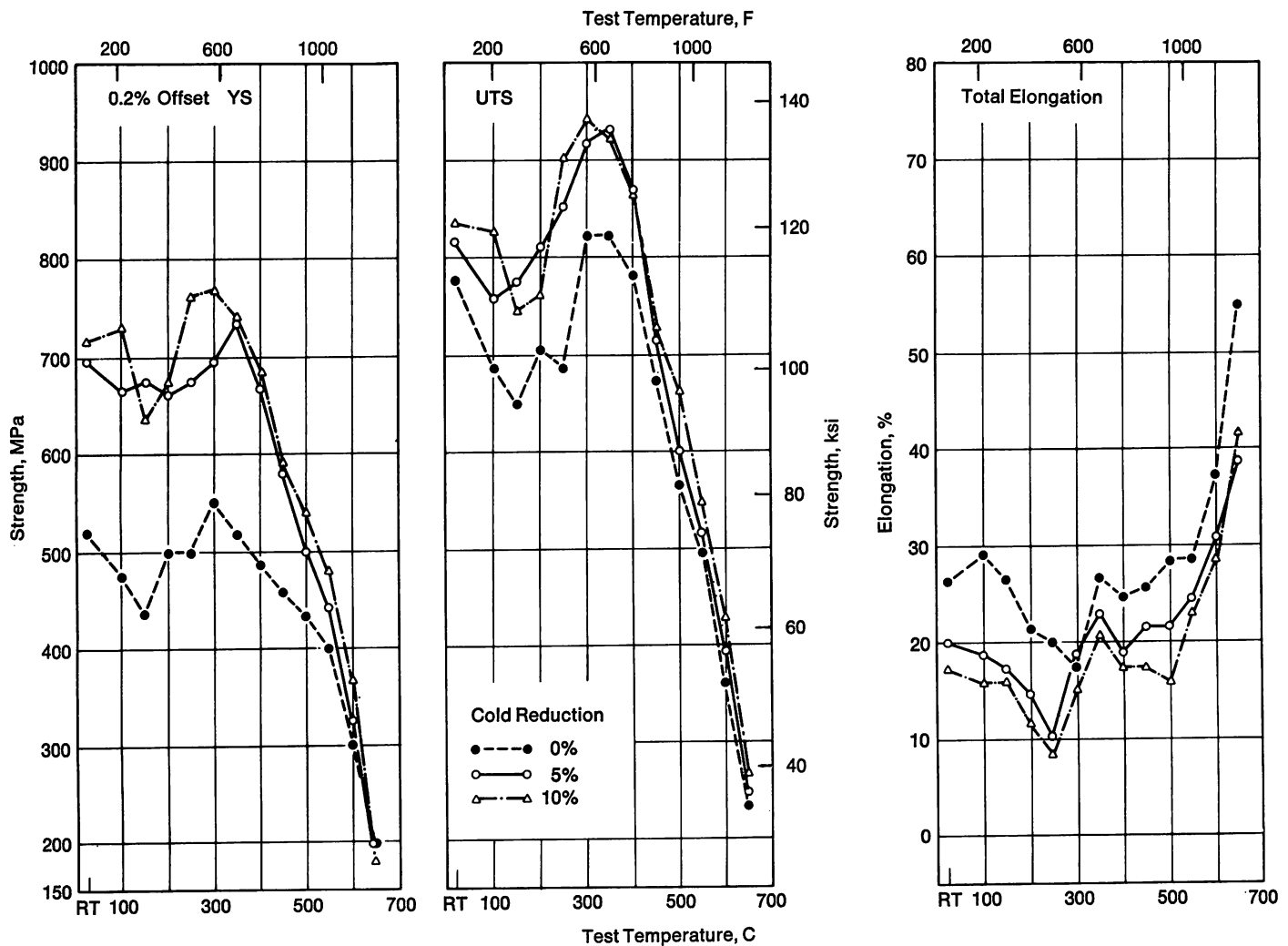
FIGURE 6—*Strength at elevated temperatures after cold reduction (heat no. 812,849; 2 mm, 0.08 in. thickness).*

The tempering behavior of the hot-rolled dual phase steel is described in Figure 7 on a hot strip 4 mm (0.16 in.) thick from melt 812,849. Up to annealing temperatures of about 150 C (300 F), there is practically no change in the values. In the range between 200 and 700 C (390 and 1290 F), higher yield point values were measured. The tensile strength values initially increase slightly than decrease. The elongation values remain almost unchanged. Above 700 C (1290 F), there is an increase in the tensile strength and a drop in yield strength below the initial values. The high yield strength (thus high yield-tensile strength ratio and discontinuous yielding) following annealing in the 200 to 700 C (390 to 1290 F) range is probably the result of precipitation effects. Above the latter temperature, there is a return to expected dual phase behavior.

Experiments with 2 mm (0.08 in.) thick hot strip showed similar behavior. With additional cold reduction before tempering, there was a parallel displacement for the range up to an annealing temperature of 600 C (1110 F), while above that temperature, as was to be expected, no further effect of cold reduction was observed.
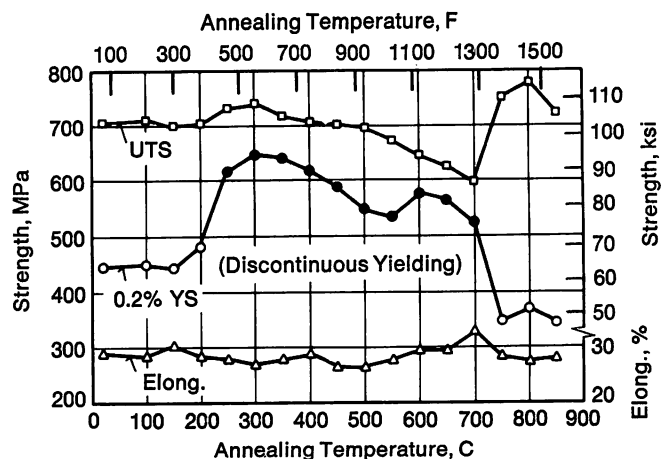


FIGURE 7—*Tensile properties of hot-rolled dual phase steel after tempering.*

Fatigue experiments on dual phase steel, on HSLA steel and a structural steel with a tensile strength of 460 MPa (67 ksi) were carried out (Figure 8). The endurance strength (low cycle range) of the dual phase steel is slightly above that of the HSLA steel and significantly
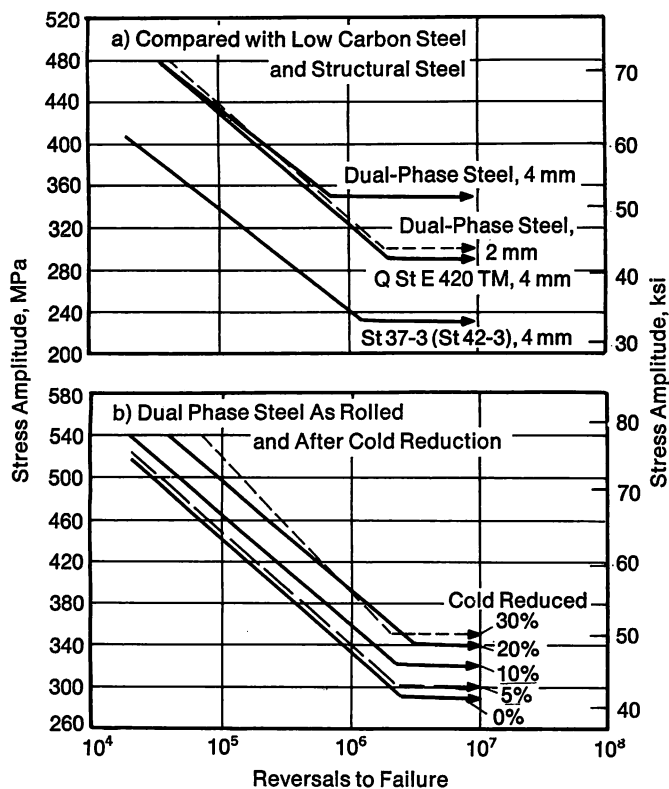
FIGURE 8—Fatigue properties of indicated hot-rolled steels.

above that of the structural steel. The differences are greater when the comparison is based on fatigue limit. The same holds for the effect of strip thickness of the dual phase steel specimens.

Increasing the amount of cold reduction increased both the low cycle endurance strength and the fatigue limit.

Further investigations are proceeding toward an explanation of the positive effect of tempering at 350 C (660 F) on fatigue properties.

With reference to planned applications, the shield arc and spot welding behavior of dual phase steel was compared with that of low carbon steels. The welds had sufficient toughness and tensile strength. In Figure 9a, the hardening behavior is shown in comparison to two deep drawing steels and the weldable structural steel St 52-3. As expected, the maximum hardness of the dual phase steel is above those of the mild steels, but with values of about HV3 270, it is not critical and does not reach the peaks of the St 52-3.

Results of the spot welding tests are reproduced in Figure 9b to show a comparison with a mild steel (St W 24). To optimize the welding schedules, only small changes in the welding current and in the electrode force were required. In the three criteria given here, the dual phase steel attains greater tensile values than the other



FIGURE 9—Weldability of hot-rolled dual phase steel.

steels used in comparison while still exhibiting ductile fracture behavior in the welds.

## Examples of Application

With reference to a reduction in vehicle weight, automotive wheels are of interest for two reasons. First, the five wheels provided with each car constitute a signifi-



Wheel Disc No.

1    5

4.8 mm (0.19 in.)
Initial Thickness

4.8 mm (0.19 in.)

2    6

4.25 mm (0.17 in.)

4.25 mm (0.17 in.)

3    7

3.90 mm (0.15 in.)

4.0 mm (0.16 in.)

4

3.90 mm (0.15 in.)

FIGURE 10—Sections of different wheel discs produced from hot-rolled dual phase steel.

cant part of the total weight. Second, through a reduction of the thickness, and thereby of the weight of the wheels, the unsprung weight is reduced, making possible savings in wheel suspensions, the chassis, etc. Figure 10 shows the sections of seven different types of wheel discs for which the hot-rolled dual phase steel has been substituted for mild steels.

With the exception of wheel disc No. 4, which presents pressing problems even when using mild, unalloyed grades, all the types shown can be made from hot-rolled dual phase steel without special problems. Wheel disc No. 4 could only be made by lowering the pressing speed, but deviations in shape still remained.

In Figure 11, the different process stages for disc No. 2, are demonstrated. Essential drawing operations are finished in the first three stages, if one disregards the hole expansion later on. Using the scribed circle test, the strains which occur in the most strongly deformed regions are measured. In Figure 12, the strain distributions for the dual phase steel and for the comparative material St 37-3 are given. Despite the much greater initial strength, similar or slightly higher strains were found in the dual phase steel.

In the upper part of Figure 13, the changes in thickness measured across the section and related to the original thickness are given for disc 3. The lower parts of the figure show the hardening of the material after deformation by hardness values in the center of the thickness of the sheet. A comparison with production material (R St 37-3) is given. There is no important difference between the two materials with respect to the variation in thickness. Because of the higher initial value, the hardness in the dual phase steel is definitely greater in the whole profile section. The increase in hardness (increase in strength) is rather greater in the dual phase steel than
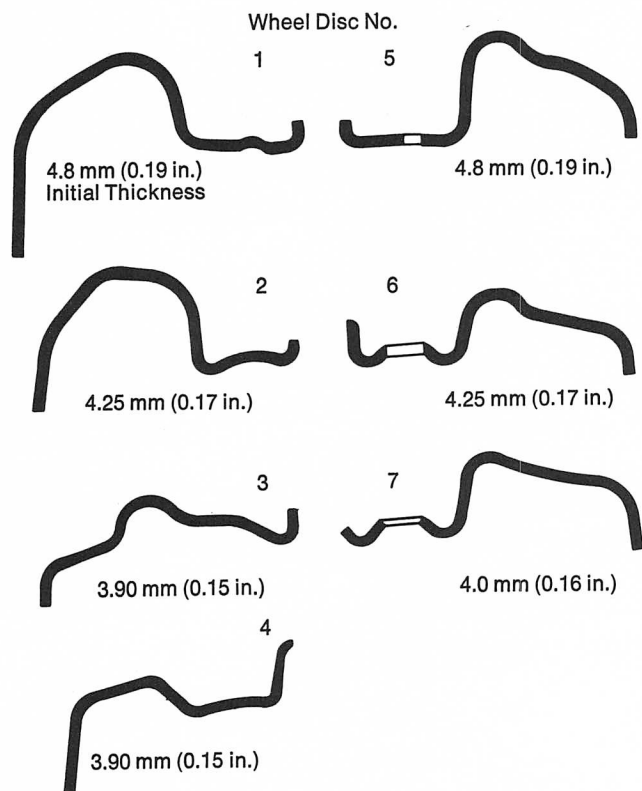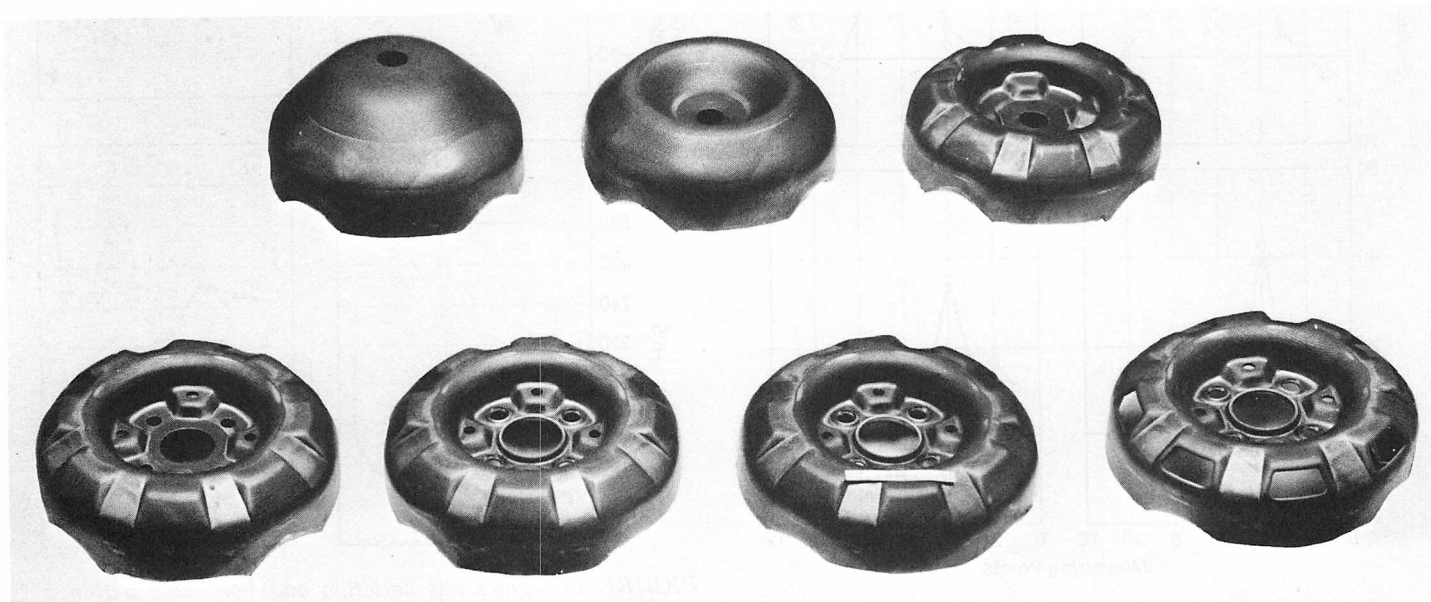


FIGURE 11—Process stages for wheel disc No. 2, "Golf-Passat" (VW) (heat 100,826; 4.25 mm, 0.17 in. thickness).

in the steel used for comparison, but there are no extreme hardness peaks.

The wheel discs of dual phase steel can easily be welded to the normal production rims from mild steel. The rim roll test confirmed the integrity of the welds.

The numbers of cycles to failure in bending fatigue are reported in Figure 14 in relation to the tensile strength. In the appended table, the steels used in the press shop for production, as well as some HSLA steels used experimentally, are included.

It is evident that the tensile strength of the material is related to the number of cycles obtained. Furthermore, the large differences from one wheel disc to another are to be regarded as an indication that the geometry of the wheel and other factors are important.

In some cases, attempts have been made to use dual phase material of reduced thickness without changing the production tools. These experiments were not successful [use of 4 mm (0.16 in.) thick strip against a production strip of 4.8 mm (0.19 in.)]. It is quite evident that the tools must be adapted exactly to the strip thickness used.

Figure 15 shows an example of use as a plate brake backing (Girling) with various heavily deformed areas. Considerable cold reduction in this part was possible using the dual phase steel. Cracks in the region of the central hole arose because a smaller hole punched out at an intermediate stage was considerably expanded. In this case, the punching caused hardening at the sheared edges, with the result that further expansion of the hole was not possible. This example clearly shows that manufacturing conditions must be adapted to the special properties of the material.

## Summary

The Climax alloying concept based on the elements Mn, Si, Cr and Mo has been adopted for the production of hot-rolled dual phase steel. Melts from a 1.5 ton induction furnace and a 50 ton electric arc furnace were hot-rolled on conventional mills.

Typical dual phase properties were achieved with sufficient uniformity over the length and the width of the
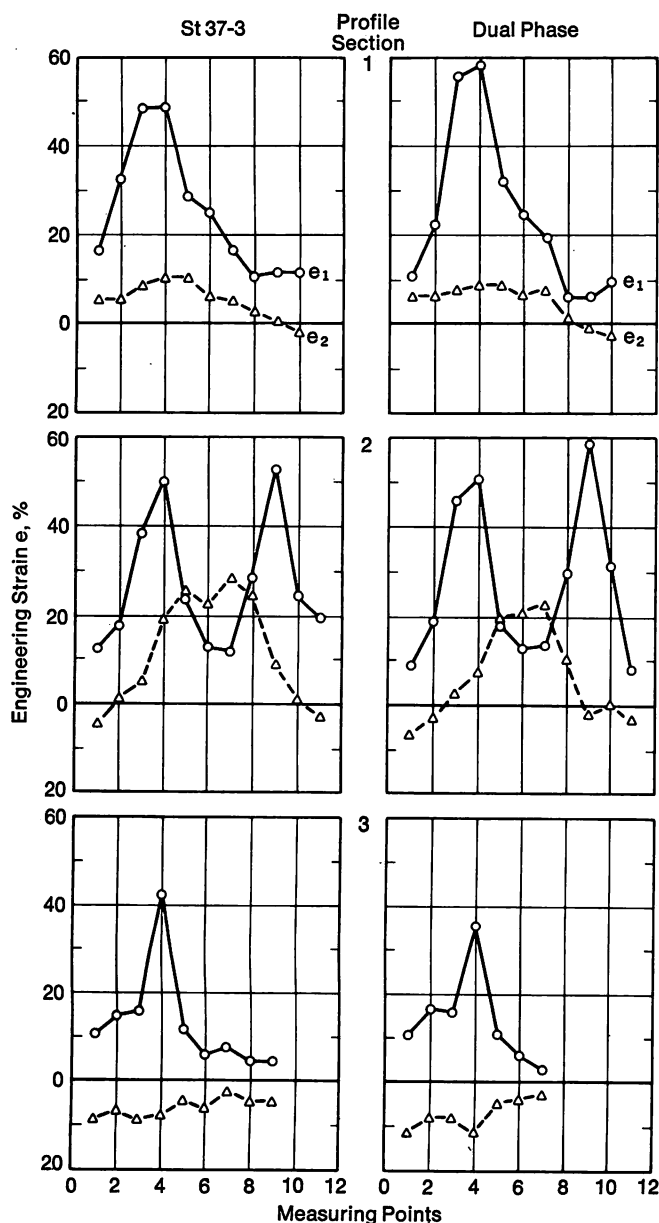


FIGURE 12—Strain distribution of dual phase steel and mild steel within different profile sections of wheel disc No. 2.
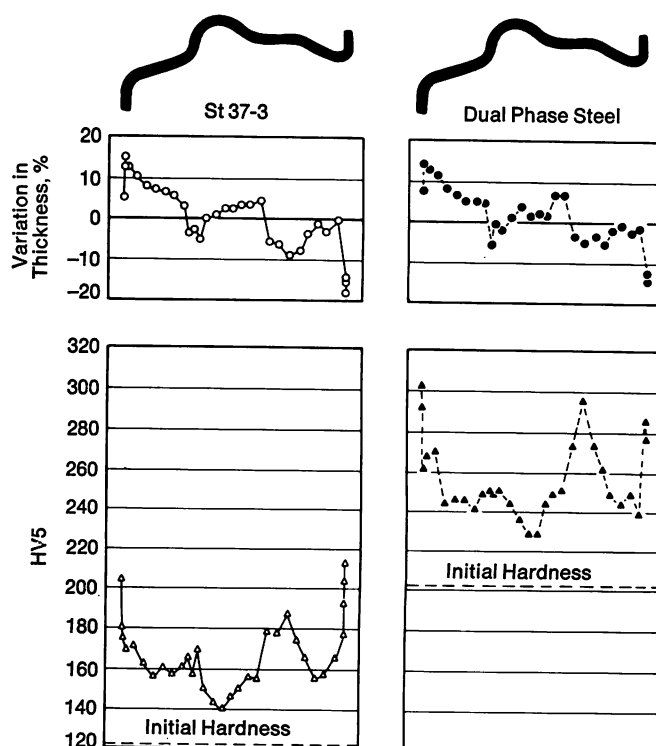


FIGURE 13—Thickness variation and hardening within a profile section of wheel disc No. 3 for a hot-rolled dual phase steel and a plain carbon steel.
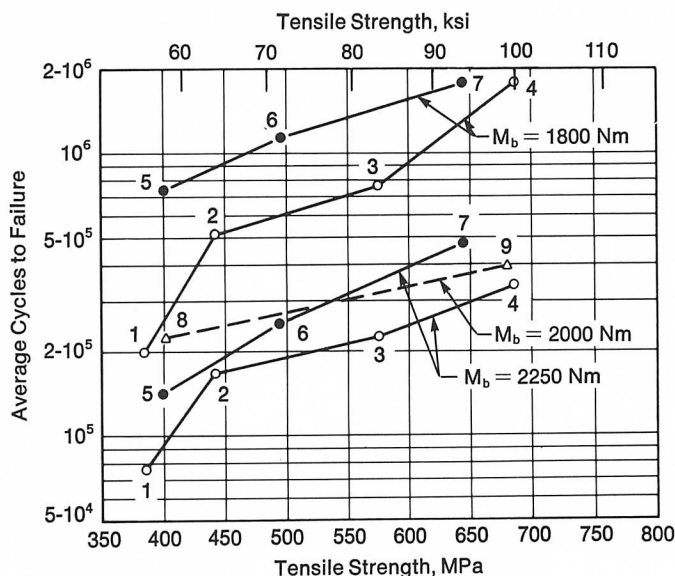
FIGURE 14—Bending fatigue test data for dual phase, low carbon and HSLA steels. Wheel discs 1, 2 and 3.

| Point | Grade | Thickness, mm | (in.) | 0.2% Yield Strength, MPa | (ksi) | Tensile Strength, MPa | (ksi) | Total Elongation, % |
|-------|-------|---------------|-------|--------------------------|-------|-----------------------|-------|---------------------|
| 1 | St 37-3 | 4.25-4.30 | (0.17) | 275 | (39.9) | 383 | (55.5) | 42.5 |
| 2 | St 42-3 | 4.25-4.30 | (0.17) | 300 | (43.5) | 440 | (63.8) | 41.0 |
| 3 | QStE 420 TM | 4.25-4.30 | (0.17) | 475 | (68.9) | 569 | (82.5) | 27.0 |
| 4 | Dual Phase | 4.25-4.30 | (0.17) | 444 | (64.4) | 687 | (99.6) | 28.0 |
| 5 | St 37-3 | 4.80 | (0.19) | 300 | (43.5) | 400 | (58.0) | 41.5 |
| 6 | QStE 380 TM | 4.80 | (0.19) | 405 | (58.7) | 492 | (71.4) | 30.0 |
| 7 | Dual Phase | 4.80 | (0.19) | 450 | (65.3) | 645 | (93.5) | 38.5 |
| 8 | R St 37-3 | 3.90 | (0.15) | 296 | (42.9) | 402 | (58.3) | 41.5 |
| 9 | Dual Phase | 3.90 | (0.15) | 390 | (56.6) | 708 | (102.7) | 29.5 |
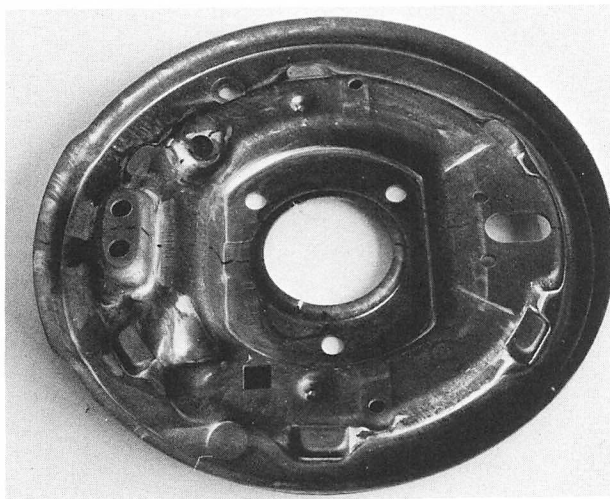


FIGURE 15—Plate brake backing made with 2.5 mm (0.1 in.) dual phase steel, heat 812,849.

strips. This was obtained for medium width hot-rolled strips (320-500 mm, 12.5-19.7 in.) as well as for hot-rolled wide strip (744 mm, 29 in.) which were produced on different rolling mills.

Good manufacturing properties such as formability and weldability were demonstrated by several examples.

A considerable improvement in fatigue properties was obtained compared with conventional grades used for cold forming operations. This improvement provides the basis for reduction in thickness and thereby a decrease in weight.

High strength values at elevated temperatures and a hardening effect after tempering could be interesting for special applications.

## References

1. A. P. Coldren and G. Tither, *J. Metals, 30* (4), April 1978, 6.

2. A. P. Coldren, A. Cornford, J. R. Hiam and G. Tither, Unpublished data, Climax Molybdenum Co., 1978.

3. G. Tither, A. P. Coldren and J. W. Morrow, *Iron and Steelmaker, 6* (8), August 1979, 16.

# Superalloys for Gas Turbines — Another 20 Years?

by F. L. VerSnyder and E. R. Thompson
United Technologies Research Center

The performance and efficiency of the aircraft gas turbine engine, like all thermal engines, is a direct function of the maximum cycle temperature. This was the prime motivation behind the continuous search for turbine materials capable of operating at increasingly higher temperatures in the high pressure turbine section of the aircraft gas turbine engine. During the last 30 years, the turbine inlet temperature of the gas turbine engine has been increased by 530 C (950 F), that is from 815 to 1345C (1500 to 2450 F).

In the late 1940s and throughout most of the 1950s, high temperature materials research and alloy development related to gas turbine operations covered a very broad spectrum of materials from stainless steels to refractory alloys to cermets.[1] During the mid 1950s, vacuum metallurgy emerged as the optimum melting technique for the production of superalloys. Concurrently, a better understanding of the metallurgy and therefore the potential of nickel-base superalloys was evolving. In the late 1950s and early 1960s, the need to employ precision castings to meet ever increasing turbine temperatures became evident. It is important to note that, through the mid 1960s, alloy designers were focussed on increasing $\gamma'$ ($Ni_3Al$) volume fraction for increased high temperature strength. Gamma prime volume fractions of 60% are now common.[2] Unfortunately, increasing $\gamma'$ volume fraction generally brought with it the difficulty of increased macrosegregation in large ingot castings. In the extreme, this made advanced superalloys, otherwise attractive as new turbine disk materials, virtually unforgeable. By the mid 1960s, the rapid development of increasingly sophisticated air cooling designs to combat high turbine temperatures put nickel- and cobalt-base superalloys at the forefront in aircraft gas turbine applications with nickel-base alloys, the decided leader, being 40% of engine weight.[3] During this same period, a decided shift in emphasis between processing and alloy development was occurring. Processing started to lead the way; the process was chosen first, and the alloys were tailored to the process. Throughout the 1960s, both the military and commercial engine fields were expanding vigorously with commercial engines evolving from military engine predecessors. By the beginning of the 1970s, the climate for gas turbine engine development and the related materials and processing research and development had begun a major change from the preceding decades. Engine design objectives became much more mission specific with commercial engines emphasizing increasingly better specific fuel consumption and durability. The military continued to pursue ever increasing thrust-to-weight ratios. Couple these factors with increased design sophistication and an emphasis on cost consciousness, and it becomes clear that material development has become much more complex with the emphasis on close coordination between engine design, process metallurgy and alloy design. Also, during the 1970s, world turmoil resulted in a dislocation in the world metal market making elements such as cobalt very expensive and politically insecure. Consequently, the emphasis in this discourse on present day and future opportunities will focus on politically secure resources, i.e. nickel-base superalloys. Two processes which have evolved to assume major importance during the last decade are directional solidification (an evolution of precision casting) and superalloy powder metallurgy processing, both of which are presently in use in aircraft gas turbines. A rapidly emerging field is that of directed energy processing which should hold great promise for the future.

The value of rapid cooling as a means for preventing or reducing segregation of alloy phases has become well recognized. However, to carry out processes that include rapid cooling efficiently requires precise energy control. Lasers afford such control. This represents perhaps the most important reason for present use of lasers in material research and for the present and future use of lasers as processing tools. The laser provides a clean, remote source of thermal energy that can be used effectively in air, vacuum and almost any gas atmosphere. Furthermore, the use and transfer of laser energy is highly adaptable to automation.

These three areas of superalloy processing will be considered in turn.

# Directional Solidification and Single Crystal Casting Technology
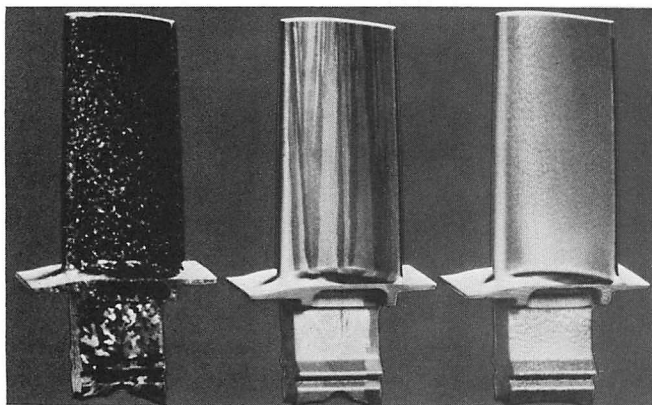


FIGURE 1—*The evolution of cast turbine blades.*

Improvements in superalloys for turbine airfoil applications have been accomplished through investment vacuum casting (Figure 1). By manipulation of the investment vacuum casting process, a columnar grain[4] or single crystal[5] structure can be produced in superalloys by unidirectional solidification. Two conditions must be simultaneously satisfied to produce the desired grain structure. The first is that the heat is removed from the casting in a unidirectional manner, and the second that a positive temperature gradient be maintained ahead of the solidifying interface to prevent extraneous nucleation. These conditions can be achieved by pouring superheated metal against a chilled surface while concurrently establishing a suitable temperature gradient along the axial length of the mold by the use of induction heating methods.[6] The current process[7] relies on a mold translation technique to enhance heat transfer (Figure 2). An investment casting mold attached to a water cooled copper chill is placed within the confines of an induction heated cylindrical graphite susceptor. Once the proper axial temperature profile is established on the mold surface, the superheated alloy is poured. A holding period of a few minutes is allowed for the purpose of thermal stabilization and to permit some growth of solid to be initiated off the chill surface. To enhance the heat transfer and temperature gradient, the mold is withdrawn from the single zone induction coil at a predetermined rate past a radiation baffle placed at the base of the susceptor. During withdrawal, the solidification zone is kept near the line of the baffle for maximum effectiveness. This can be readily achieved over a range of translation rates. Single crystals can also be grown in the same equipment with the same solidification techniques; the major difference in the casting procedure is the use of a multiple-turn constriction adjacent to the chill plate which permits only one grain to enter the airfoil portion of the mold (Figure 3). As one considers this process, it becomes clear that the major solidification parameters, the thermal



Columnar grain casting process



Single crystal casting process
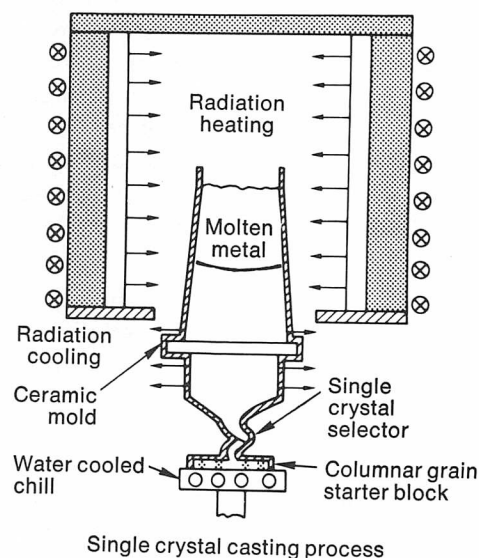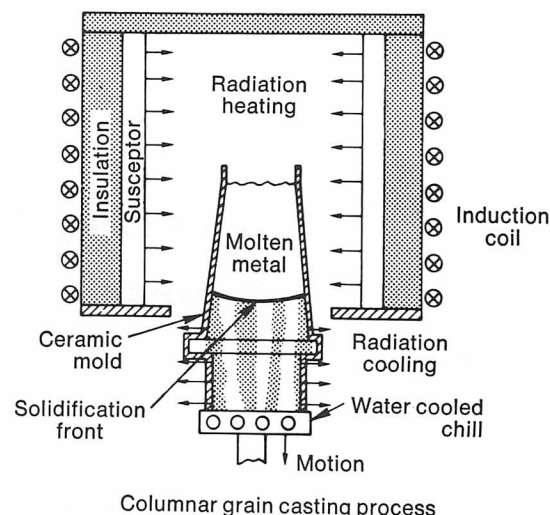
FIGURE 2—*Directional solidification and single crystal casting.*

gradient (G) at the liquid/solid interface and the growth rate (R) or rate at which the liquid/solid interface moves, are key to the success of the process. Considerable work has gone into the formulation and understanding of the relationship between G, R and structure. A schematic (Figure 4) of rate and gradient effects on grain shape defines our present understanding. In the unidirectional solidification of high temperature alloys, the type of ceramic mold and core material utilized are also critical because of their extended exposure to elevated temperatures. Changes in ceramic compositions and mold design can improve product quality when properly applied. Occasionally grain boundary cracking has been observed in columnar grain castings. This condition can often be corrected through manipulation of the casting parameters. In many instances, cracking of hollow airfoils is associated with thin walls in the casting. This source of difficulty can be eliminated by proper positioning of the core in the mold and close matching of the core and wax tooling. The addition of hafnium to columnar grain
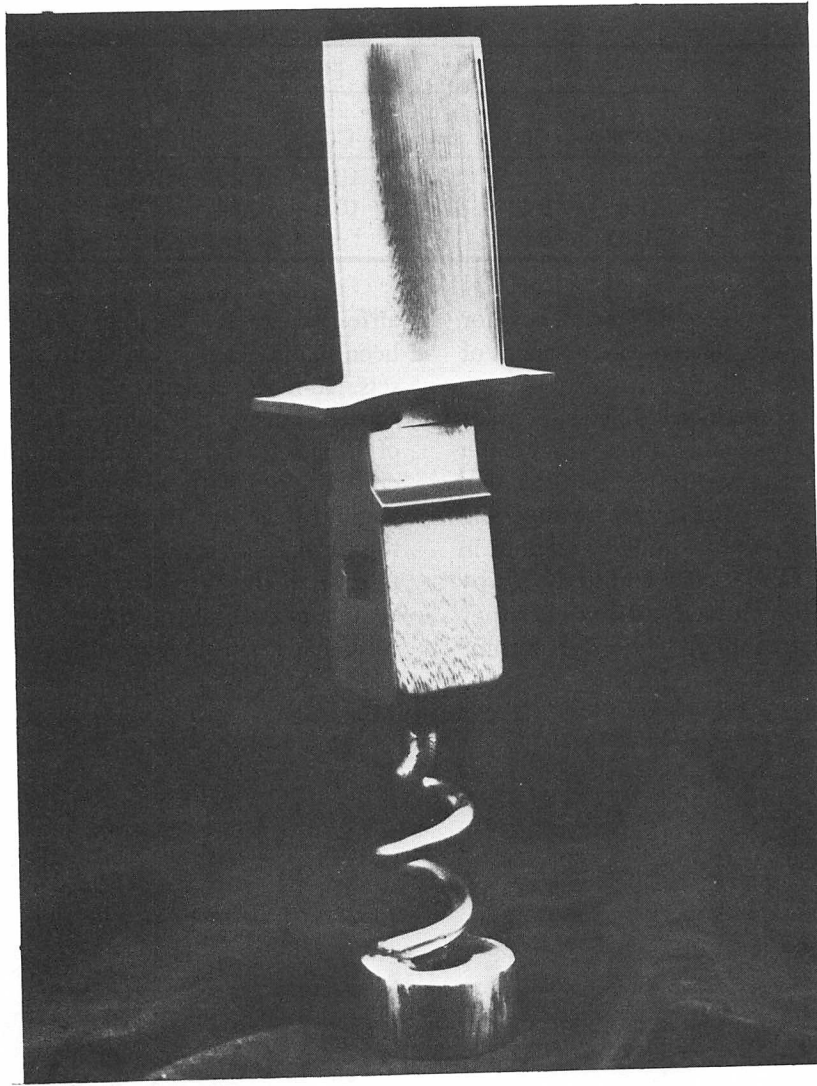
FIGURE 3—*Cast single crystal turbine blade with multiple-turn constriction still attached.*
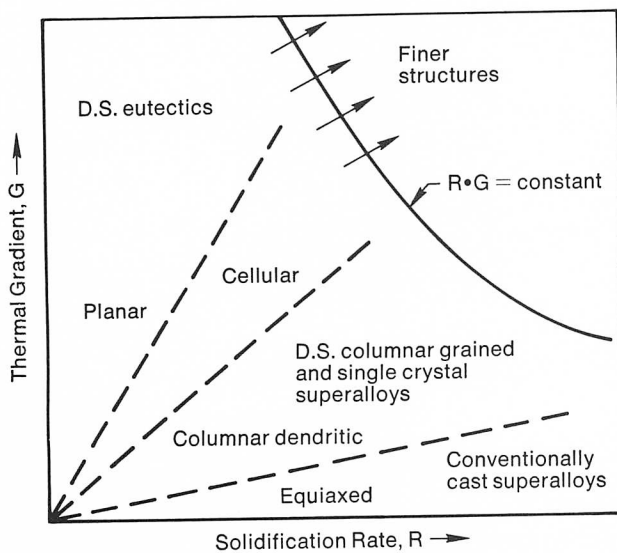


FIGURE 4—*Schematic of rate gradient effect on grain shape and the refining of microstructures by high cooling rates.*
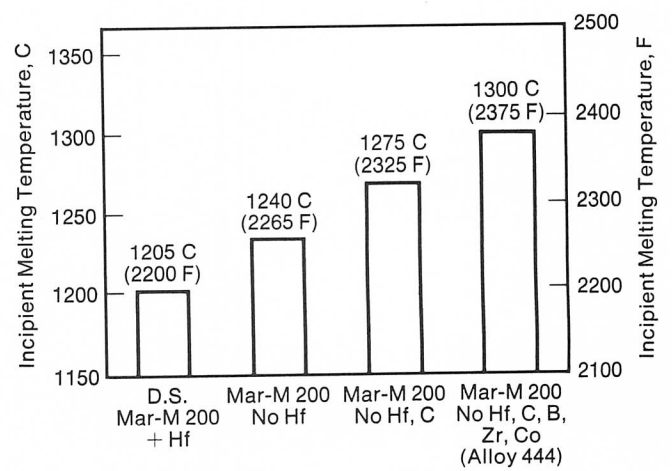


FIGURE 5—*Variation of incipient melting temperature with variation in alloy chemistry.*

**Table I**—Cast Alloys

| | Element, % | | | | | | | | | | | |
| | Al | Ti | Nb | Cr | W | Co | C | B | Zr | Hf | Nb+Ta | Ni |
|---|---|---|---|---|---|---|---|---|---|---|---|---|
| MAR-M200 | 5.0 | 2.0 | — | 9.0 | 12.0 | 10.0 | 0.15 | 0.015 | 0.05 | — | 1.0 | Bal |
| D.S. MAR-M200 + Hf | 5.0 | 2.0 | 1.0 | 9.0 | 12.5 | 10.0 | 0.14 | 0.015 | 0.05 | 2.0 | — | Bal |
| S.C. Alloy 444 | 5.1 | 1.98 | 0.91 | 8.6 | 11.1 | — | — | — | — | — | — | Bal |

nickel-base superalloys also reduces the tendency for grain boundary cracking because of the enhancement of transverse ductility.

The advantages of directionally solidified superalloy turbine airfoils over conventional castings are greater thermal fatigue life (8X), greater rupture life (2X), and greater rupture ductility (4X). The first use of directionally solidified turbine airfoils was in military engines in the mid 1960s followed in the late 60s and early 70s by application to commercial engines. Pratt and Whitney Aircraft has extensive directionally solidified turbine airfoil experience. Over 900,000 production castings have been made. This is the equivalent of over 4000 engine sets. In-flight service experience to date has demonstrated the superior properties. There have been a total of 3,250,000 total service hours in Pratt and Whitney Aircraft engines with almost 2,000,000 hours in the JT9D engine. Excellent durability has been demonstrated in the turbine hot section. An example is that the overhaul interval of the JT9D-59A/-70A/-7Q engines is now over 8000 hours. All of this experience to date has been with columnar grain directionally solidified superalloys.[8]
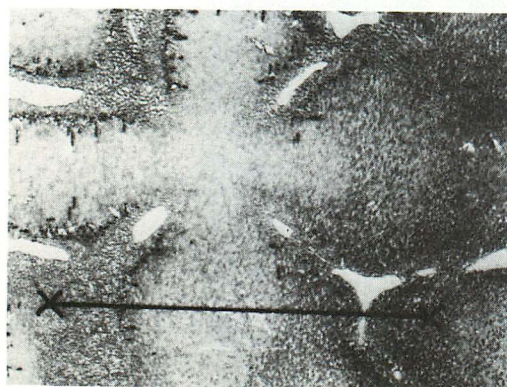


4 hours at 1205 C (2200 F)
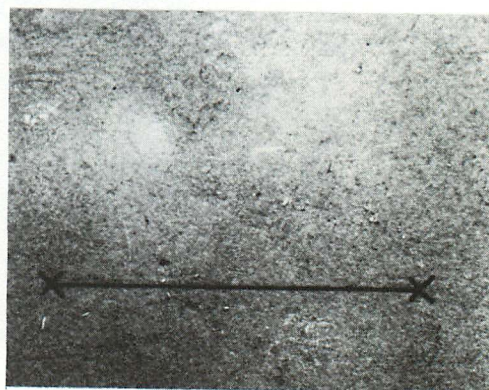
4 hours at 1300 C (2375 F)
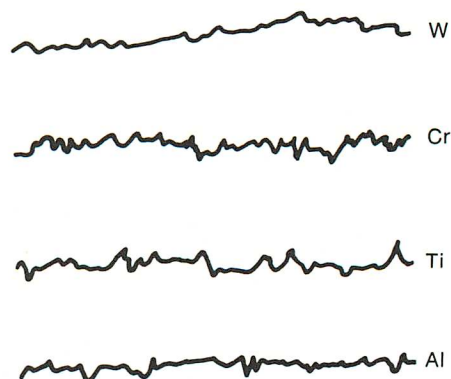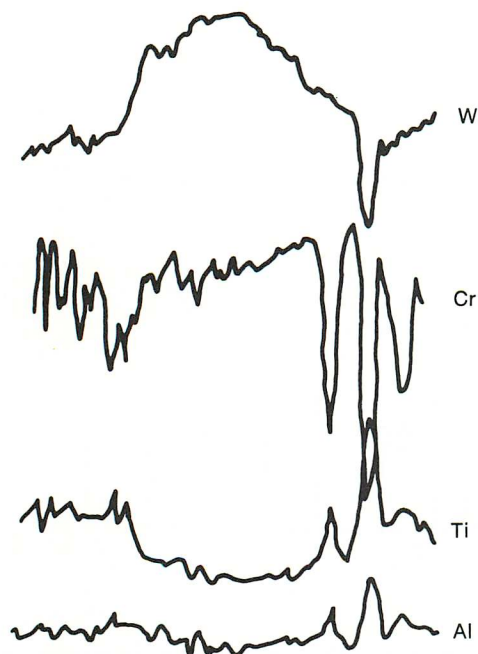
FIGURE 6—*Microstructure and microprobe analysis for specimens of two different solution heat treatments of Alloy 444.*
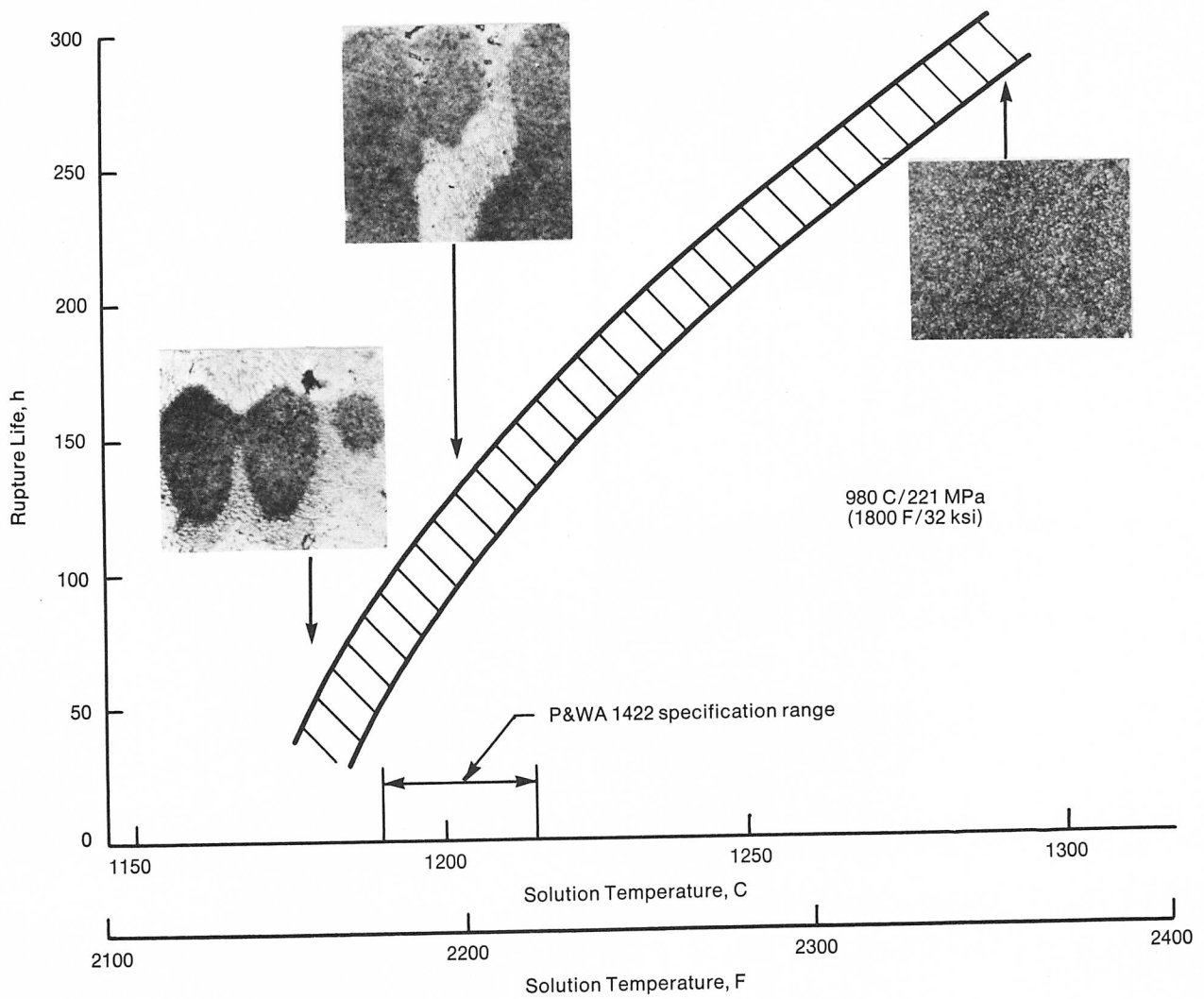
FIGURE 7—*Variation of rupture life with solution heat treating temperature of MAR-M200 + Hf (PWA 1422) and Alloy 444.*
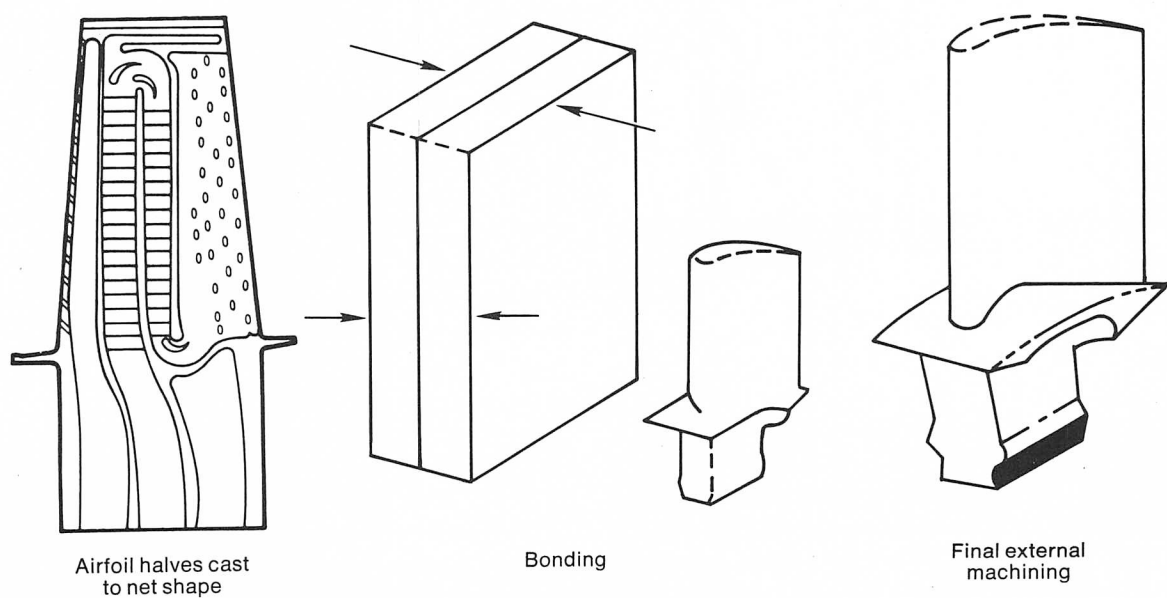


FIGURE 8—*Two-piece turbine blade assembly.*
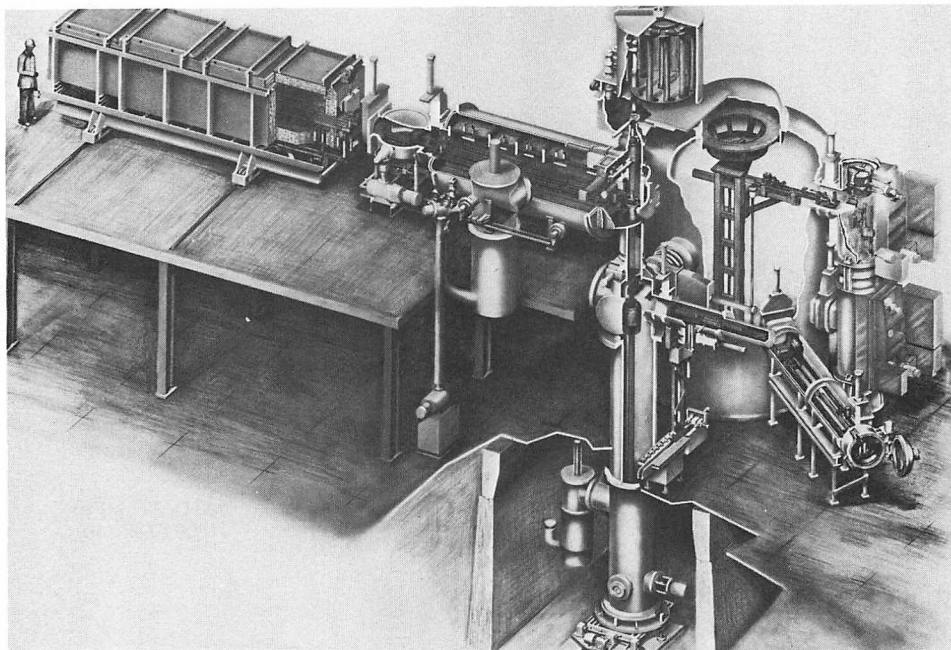
FIGURE 9—Casting unit of Pratt and Whitney Aircraft automated casting facility. It consists of an air electric preheat furnace followed by a vacuum preheat furnace where individual molds are preheated prior to entering the alloy melt chamber. After the molten alloy has been poured into the mold, it is passed by an elevator and a manipulator into the solidification chamber. Following solidification, the mold is transferred to a cooling chamber.
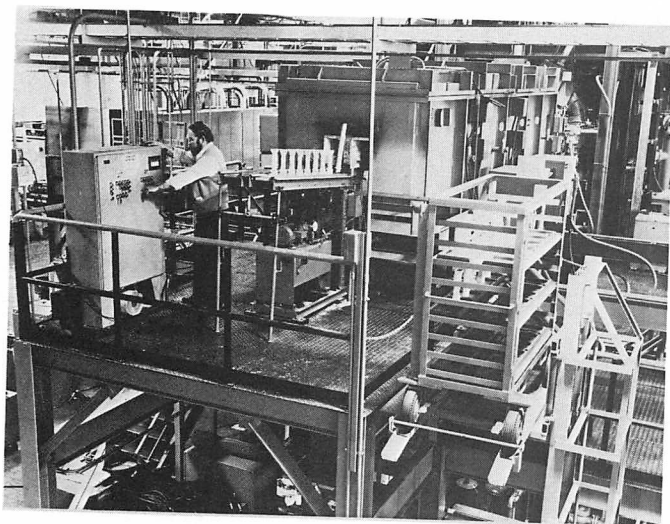


FIGURE 10—Ceramic investment molds entering the first preheat chamber.

Further advances can be achieved in increased strength and temperature capability through the use of single crystal superalloys. Since there are no grain boundaries in single crystal turbine parts, the alloying elements usually included as grain boundary strengtheners can be eliminated. This allows the omission of elements such as carbon, boron, zirconium and hafnium from the alloys (Table I). This in turn permits a new approach to alloy design. Alloys under present development have higher incipient melting temperatures (Figure 5). One can therefore increase the solution temperature to provide more homogeneous castings (Figure 6). The improved homogeneity provides a more uniform gamma prime distribution which leads to an increase in alloy strength for a particular alloy (Figure 7). The ability to make single crystal turbine airfoils gives engine designers new options such as higher turbine operating temperatures (which increase engine fuel efficiency) and turbine components with greater durability and life at current operating temperatures. Pratt and Whitney Aircraft has developed a single crystal alloy designated PWA 1480 which the commercial engine designers have chosen to use to lower the thrust/ fuel consumption of the JT9D-7R4 series and so increase fuel efficiency. Alloy design for single crystal technology is still in its infancy, and it is expected that further advances will be made leading to what we choose to call super single crystals of the future.

The description of directional solidification technology would not be complete without taking a look at future manufacturing technology. A highly automated computer-controlled production casting facility now in an advanced stage of development at Pratt and Whitney Aircraft may make it economical within two years to manufacture advanced directionally solidified or single crystal turbine blades that have improved internal air cooling features. Such efficient cooling of turbine blades provides an increase in engine performance. The two-

*FIGURE 11—A mold being transferred by the manipulator from the pouring station to the solidification chamber.*

piece blade design concept[9] is one approach to achieving this increased air cooling efficiency (Figure 8). This bonded blade approach has been developed concurrently with the development of the automated casting facility.

The casting unit of Pratt and Whitney Aircraft's automated casting facility is shown in a simplified artists rendering in Figure 9. The casting unit operates under the direct control of a dedicated process control computer. All operations past the first mold preheat occur under vacuum (Figure 10). The ceramic turbine blade molds move from a preheat zone through a lock where they are then mated with a copper chill plate. An elevator at the end of the furnace then lifts the mold up to receive the charge of molten superalloy. Superalloy melting is done by electron beam. The electron beam melting furnace delivers a precise amount of molten alloy to the waiting mold. Once the mold is filled, it is moved by a manipulator (Figure 11) to a solidification chamber where controlled solidification of the molten alloy into a directionally solidified or single crystal casting occurs. Both lower cost and better quality are the aims of this new production technology.

## Powder Metallurgy Processing

Although gas turbine engineers and metallurgists have not sought alternative materials to superalloys for high temperature turbine disks, particularly for the hottest turbine stages, they have sought to optimize the performance of superalloys to meet the demands of higher thrust-to-weight ratio engines. As mentioned earlier, advanced superalloys are prone to severe macro-segregation which inhibits successful ingot breakdown. Conceptually, powder metallurgy offers a method for overcoming this problem. Since the material is divided into small droplets while it is a homogeneous liquid, the maximum segregation distance is restricted to the size of the solidified droplet (assuming that the individual particles have the correct compositions). Early efforts using then conventional powder metallurgy techniques to process superalloys were frustrated by the oxidation of powders during processing which led to poor tensile and rupture ductility. The breakthrough came with inert powder processing.[10] In this process, the powder production, collection and densification were carried out in an inert atmosphere. Pratt and Whitney Aircraft, in cooperation with Universal Cyclops, who possessed a facility for processing in a high purity argon atmosphere, made the first attempt at inert powder processing. This early work, carried out on the alloy called Astroloy (see Table II), yielded remarkable results. Gas analysis of this first powder showed less than 100 ppm oxygen. In early superalloy vacuum metallurgy work, it had been shown that alloys containing less than 100 ppm oxygen had satisfactory tensile and creep rupture ductilities. Both microstructural studies and forging studies showed that macrosegregation had indeed been eliminated and the alloy was forgeable. This early work was the foundation stone for advanced superalloy powder metallurgy. The necessity of producing prealloyed powders of ever increasing purity brought about the development of a number of atomization processes which operate in an inert gas atmosphere or in vacuum. Three atomization techniques are in commercial use today: (a) argon gas atomization, (b) the rotating electrode process, and (c) the soluble gas process. Since several good reviews[11,12] are

**Table II**—Wrought Alloys

| | Element, % | | | | | | | | | | |
|---|---|---|---|---|---|---|---|---|---|---|---|
| | Cr | Co | C | Ti | Al | Mo | Nb | V | Zr | B | Hf | Ni |
| Astroloy | 15.0 | 17.0 | 0.06 | 3.5 | 4.0 | 5.0 | — | — | — | 0.03 | — | Bal |
| Astroloy (HIP + F) | 15.0 | 17.0 | 0.04 | 3.5 | 4.0 | 5.0 | — | — | — | 0.025 | — | Bal |
| Astroloy (HIP) | 15.0 | 17.0 | 0.03 | 3.5 | 4.0 | 5.0 | — | — | 0.045 | 0.02 | — | Bal |
| IN 100 (Mod.) | 12.4 | 18.5 | 0.07 | 4.3 | 5.0 | 3.2 | — | 0.8 | 0.06 | 0.02 | — | Bal |
| MERL 76 | 12.5 | 18.5 | 0.025 | 4.4 | 5.0 | 3.2 | 1.35 | — | 0.05 | 0.02 | 0.4 | Bal |

available concerning the details of the processes, it will suffice here to give a brief description of each.

### Inert Gas Atomization

Using vacuum metallurgy technique, a melt of the starting material poured through an opening of a refractory orifice is atomized into particles by an impinging high pressure gas stream, usually argon. The apparatus consists of the melt chamber connected to a long cooling tower through a nozzle at the upper end in which a high pressure gas breaks up the stream of molten metal. The lower end of the long cooling tower is usually water cooled and connected to a transport tube leading to a collection device.

### Rotating Electrode Process

This technique is akin to vacuum arc melting wherein a consumable rotating electrode of the desired alloy composition is melted by an arc from a directly opposed, nonrotating tungsten electrode. As an electrode

made up of the desired alloy rotates, centrifugal force causes the molten metal to shear off in the form of fine spherical droplets which freeze in flight and drop to the floor of the chamber. The chamber interior is evacuated and backfilled with helium or argon prior to making the powder. The bottom of the chamber is so constructed to provide a collection station.

### Soluble Gas Process

Vacuum induction metallurgy is used in a conventional crucible to melt the desired alloy. This melt chamber is positioned directly below an upper expansion chamber which is maintained under a vacuum of less than 10 torr. During vacuum melting, the melt is superheated and the chamber is pressurized with hydrogen gas. When the melt is ready, a valving mechanism is actuated to allow the expansion of the gas-saturated molten metal to transfer to the expansion chamber through a ceramic tube. The metal leaves the tube orifice as a fine spray of molten droplets formed by the sudden
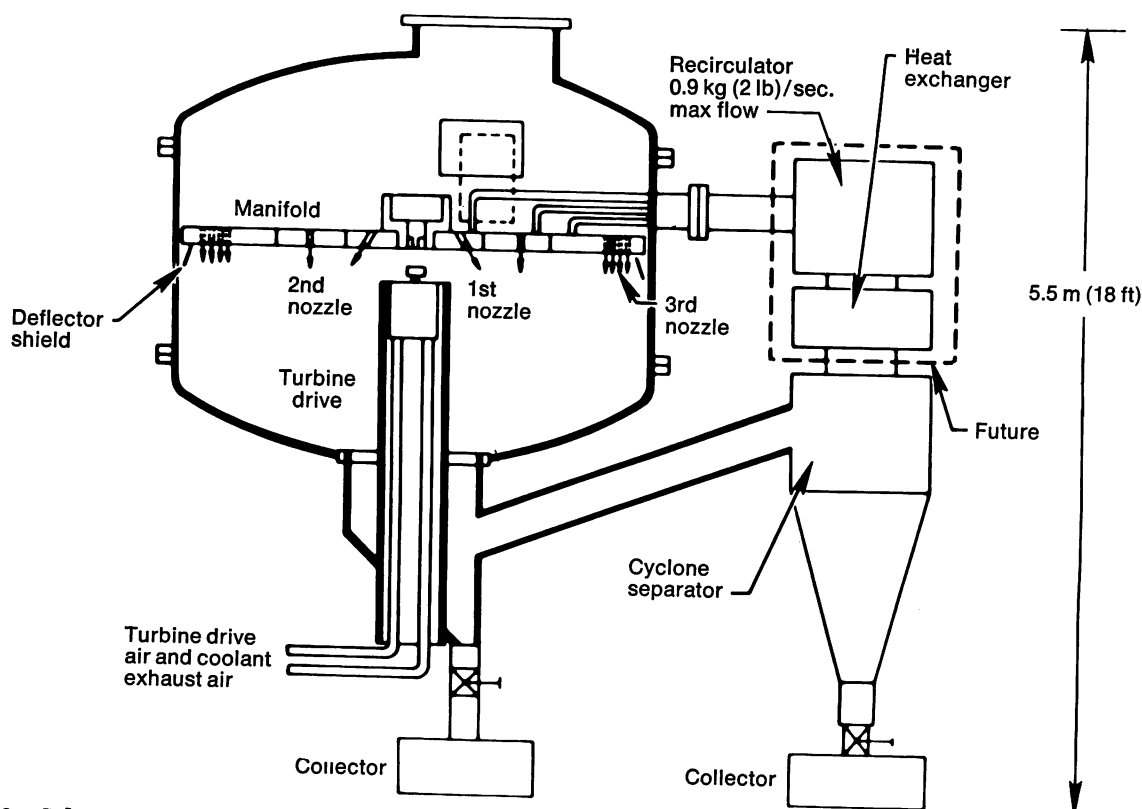


FIGURE 12—Schematic of centrifugal atomizer showing the arrangement for high mass flow gas quenching—RSR process.
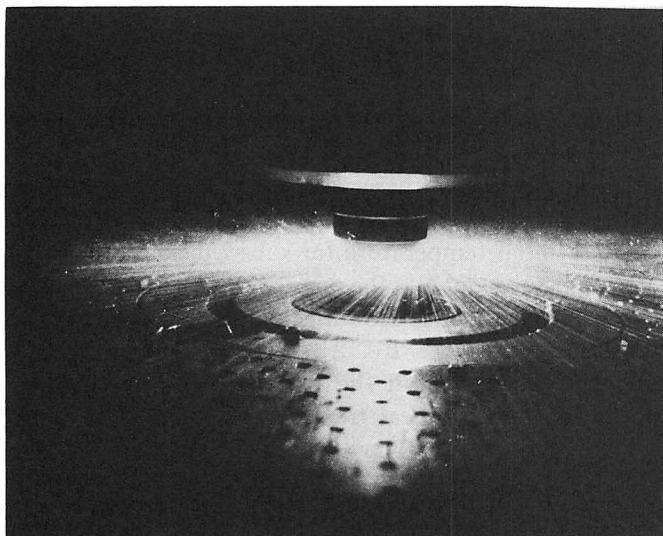
FIGURE 13—Molten metal flying from the spinning disk at 24,000 rpm during RSR process.



FIGURE 15—IN-100 turbine disk forging on bottom die of Gatorizing forging press.

release of the soluble gas. The cooled powder is subsequently drained from the expansion tank under vacuum into a tank which is then sealed off and backfilled with a nonreactive gas.

The foregoing powder processes are well established and form the basis for today's powder manufacture.

### RSR Process

Meanwhile a new powder process has arrived on the development scene. Rapid solidification rate (RSR)[13] powder process metallurgy is a new and exciting technology. It is based on rotary atomization. A schematic of the apparatus is shown in Figure 12. A vacuum induction heated superalloy charge is melted in the crucible at the top of the apparatus. The liquid metal is then poured into a transfer system which supplies a stable, continuous flow of molten metal to an atomizer whose central feature is a disk spinning at approximately 24,000 rpm (Figure 13). Molten metal centrifuged into particles ranging from 10 to 100 microns is subsequently solidified by an array of helium gas quenching jets. The cooling



FIGURE 14—Schematic of Gatorizing forging apparatus.

rate achieved during the helium gas quenching is on the order of a 1,000,000 C (1,800,000 F) per second. In view of the high cooling rate, it should be possible to produce new novel alloys and microstructures.[14] The alloy powders produced by this process typically have a higher incipient melting point than their more slowly solidified counterparts. Increases on the order of 43 C (77 F) to 82 C (148 F) in incipient melting point has been observed. This increase in incipient melting temperature permits higher solution temperatures of the consolidated material and therefore greater homogeneity and strength.

### Consolidation and Thermomechanical Working

Although numerous methods can be used to consolidate and subsequently process powdered alloys, the two that have received the most attention for advanced superalloys are extrusion followed by superplastic forming (Gatorizing*)[15] and direct hot isostatic pressing (HIP). Both operations are followed by a minimum amount of machining which accounts in part for their relative attractiveness. Stable ultrafine grain sizes can be developed in powder-processed advanced superalloys which permit these materials to be deformed superplastically. To prepare for Gatorizing, an advanced superalloy powder (e.g. IN 100) is compacted by extrusion just below the $\gamma'$ solvus. Adiabatic heating during extrusion leads to mo-

---

* Trademark of Pratt and Whitney Aircraft.

mentary solutioning of the $\gamma'$ followed by recrystallization and rapid reprecipitation of $\gamma'$ to stabilize the fine superplastic grain structure. Subsequent hot die forging (Figures 14 and 15) under controlled conditions of temperature and strain rate (Gatorizing) can produce complex, close tolerance shapes at low forming pressures. Powder metallurgy processing by this technique produced the first powder metallurgy compressor and turbine disks ever operated in a jet engine.[16] Since the process produces a part close to "net shape," not only is the amount of machining reduced but there is also a 2:1 reduction in the required input weight of starting material compared to more conventional processing.

Hot isostatic pressing (HIP) (Figure 16) is also a near net shape process.[17] In outline, the process is simple (Figure 17). Once powders have been classified, blended and finally out-gassed, they are encapsulated in a container having the desired shape of the final part (Figure 18). Several of these containers are mounted on a pallet and transferred to a preheat furnace where the desired initial temperature for subsequent processing is attained. Subsequently the parts are transferred to a HIP autoclave where they are subjected to pressure at a high temperature (Figure 19). After consolidation, the container is removed and the part proceeds through the normal inspection, heat treating and machining proce-
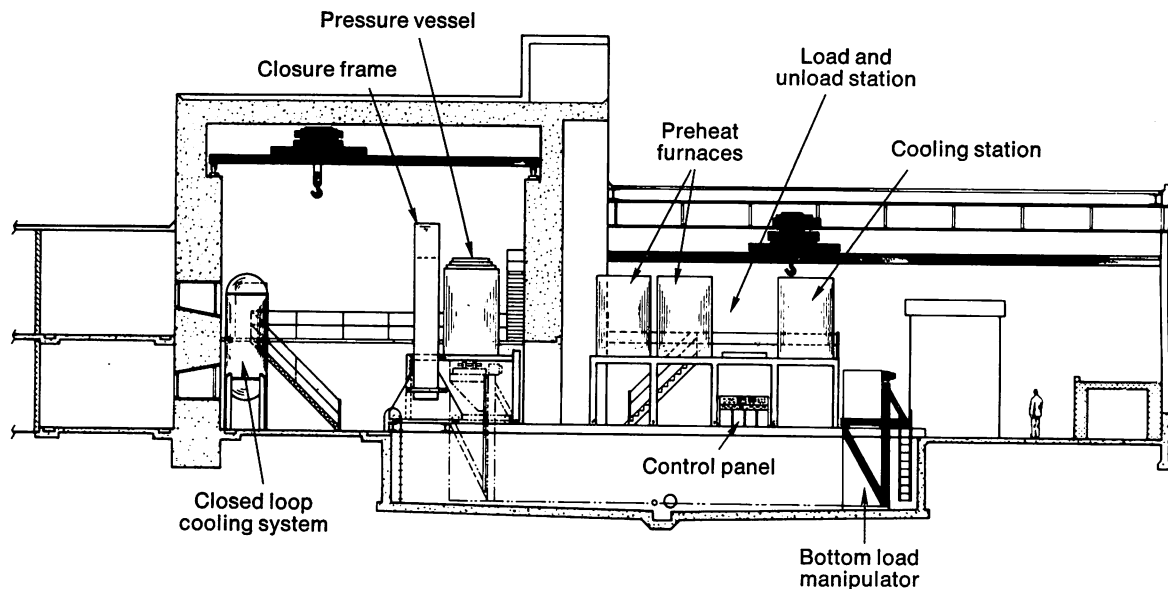


FIGURE 16—Schematic of Pratt and Whitney Aircraft hot isostatic press (HIP) facility.
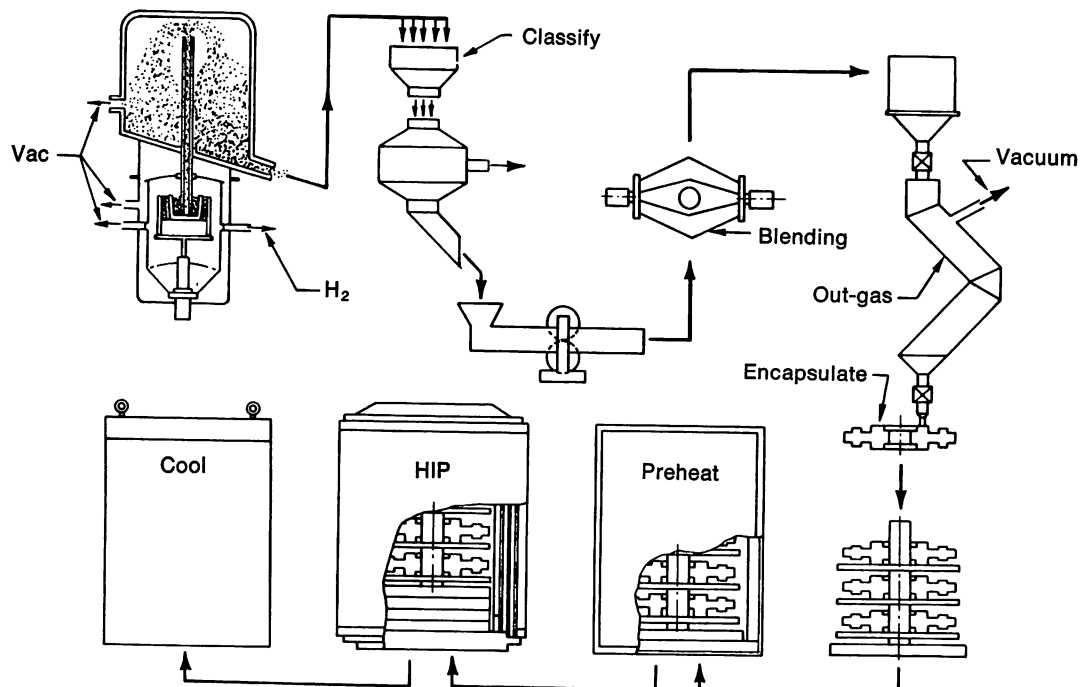


FIGURE 17—Flow diagram for hot isostatic pressing.
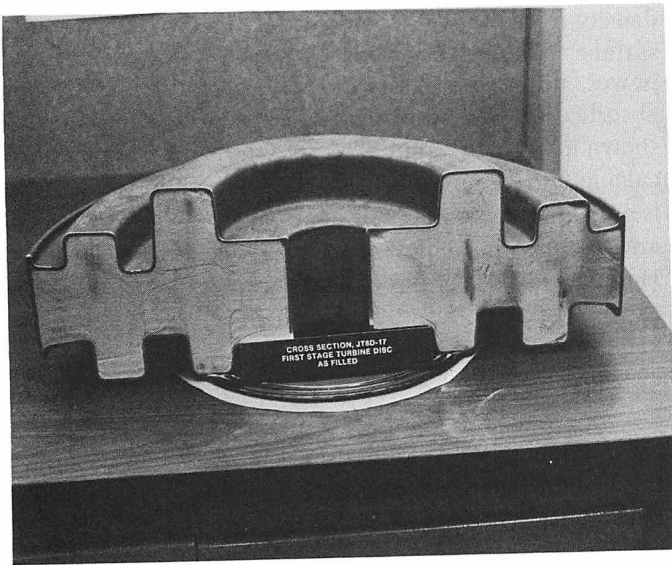
FIGURE 18—Photograph of a cross section of a filled container.
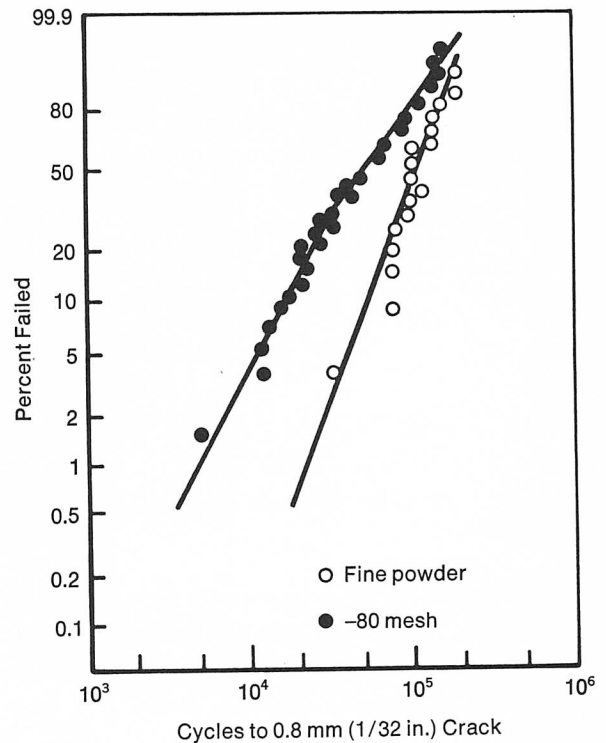


FIGURE 20—Coarse and fine powder low cycle fatigue results for hot isostatically pressed Astroloy.
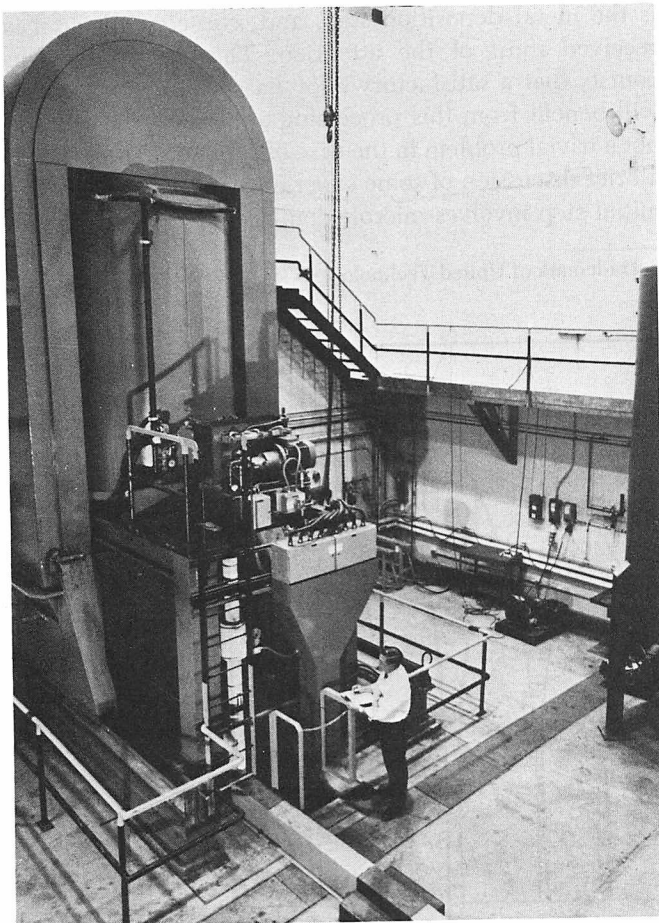


FIGURE 19—Closure frame for the cylindrical pressure vessel. The frame weighs 109,000 kg (120 tons) and stands 7.3 m (24 ft) high.

dures. In practice, each step of the process must be monitored very carefully to insure proper process control. Present day technology relies principally on metal containers, although work has also been done with both glass and ceramic containers.

Early concerns about the existence of prior powder particle boundaries in direct HIP products have largely been overcome. Process control and modification, detailed understanding of heat treatment and, importantly, compositional modification (Table II) have resulted in a mature, useful HIP technology.

Since the principal applications to date of advanced superalloy powder metallurgy has been to gas turbine disks, a word about low cycle fatigue (LCF) and powder cleanliness is in order. There are numerous ways in which inclusions can contaminate a powder metallurgy product. One type of inclusion which has been recognized and analyzed is the ceramic inclusions resulting from the melting operations or from atomization nozzles. To insure satisfactory LCF life for disks, it is necessary to reduce the size and number of these inclusions to a level at which they would be benign. One approach to achieving this goal is the use of fine powders to limit the maximum size of the inclusions. Figure 20 shows that fine powders, on the order of −200 mesh, fall on a separate and more beneficial Weibull line than the coarser −80 mesh powders. This, of course, is not the final answer to the cleanliness problem but only one approach. Complete cleanliness during melting (electron beam melting, for
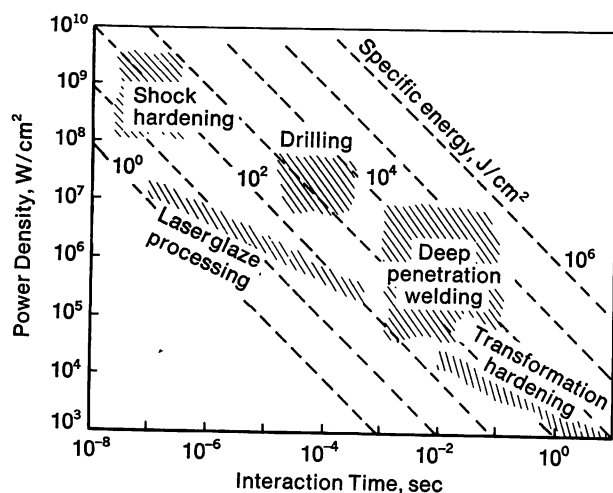
FIGURE 21—Operational regimes for laser material processing techniques.

example) and during subsequent handling must continue to be goals for advanced superalloy powder metallurgy of the future.

## Directed Energy Processing

Rapid surface-localized melting of metals including superalloys has been achieved by intense energy sources, especially focussed laser beam heating, which in turn can produce high cooling rates of the liquid by substrate self quenching. For the laser case, the results of material/beam interaction are depicted in Figures 21 through 23.[18] In Figure 21, the operational regimes for material processing are shown as a function of applied power density and beam interaction time; the band of specific interest is that labeled Laserglaze* where a beam with a power

density in the range of $10^4$-$10^7$ W/cm$^2$ rapidly scans the surface. The relationships between absorbed specific power, interaction time and melt depth and between absorbed specific power, melt depth and cooling rate are shown in Figures 22 and 23. From these plots which were calculated for pure nickel, one can see that cooling rate is a strong function of melt depth and power. Thin layers are required to achieve rapid solidification processing. Homogeneity and reduced segregation which were found to result from rapidly solidified powders are also achieved.

The extension of rapid solidification processing to near net shape fabrication, coupled with thermomechanical treatment and continuous inspection are embodied in the generic Directed Energy Processing concept under development at United Technologies. This bold step to advanced superalloy as well as other metal alloy fabrication is schematically illustrated in Figure 24. The concept has been derived from research on laser processing of materials.[19] Although the energy source in the illustration is a continuous, focussed laser beam, other high specific energy sources such as electron beam or plasma arc would be applicable. There are certain advantages to a laser source, however, and its use has been emphasized.

The most important element of the entire procedure is the metal deposition step, and, consequently, it has received most of the attention. This presupposes, of course, that a satisfactory alloy has been defined which will benefit from this processing approach. Since this is not a trivial problem in the case of superalloy processing, a brief discussion of some experience is appropriate. The initial step involves microfusion; the alloy should there-

---

* Trademark of United Technologies Corp.
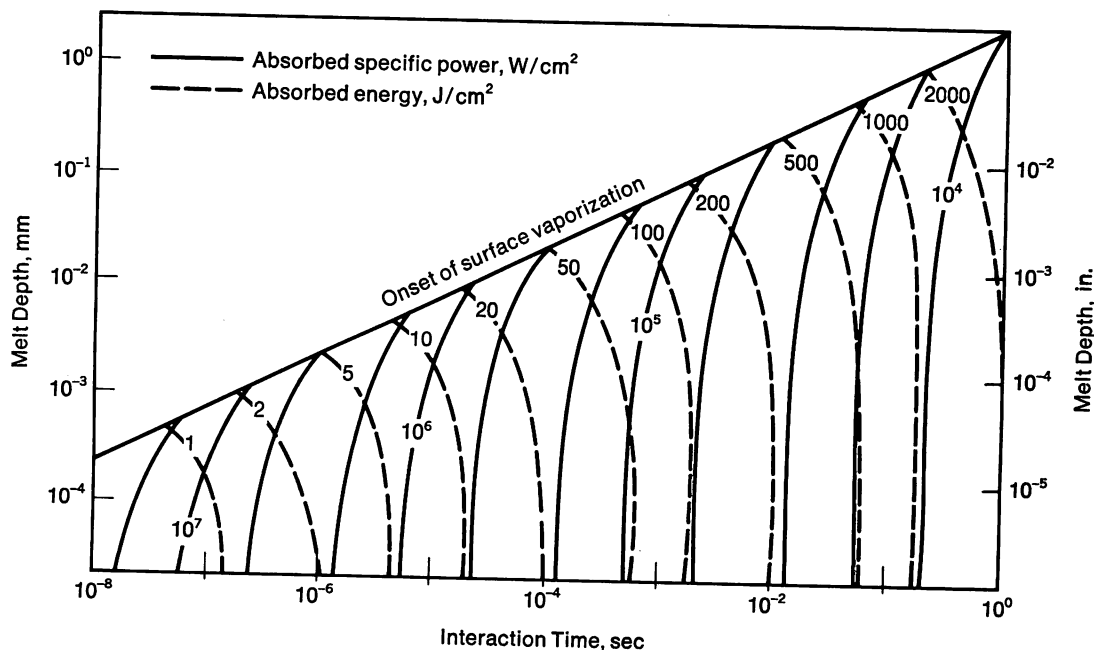


FIGURE 22—Surface melting characteristics of nickel.
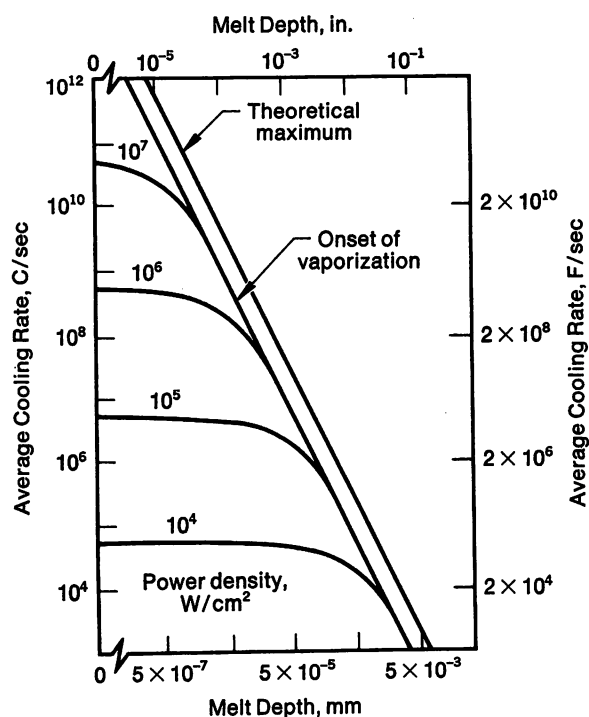
FIGURE 23—Effect of power density and melt depth on the cooling rate of nickel.
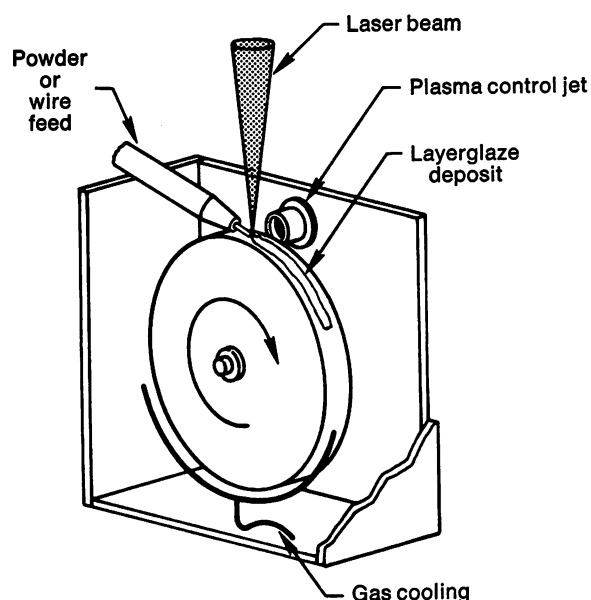


- Material deposited in thickness characteristic of laser glazing

- Rapid quenching produces characteristic structure / properties of laser glazed alloys

- Process ideal for rotating parts with cylindrical symmetry

FIGURE 25—Schematic of the Layerglaze process.



Station I — Structural deposition

Station II — Continuous inspections

Station III — Continuous mechanical treatment

Station IV — Continuous thermal treatment
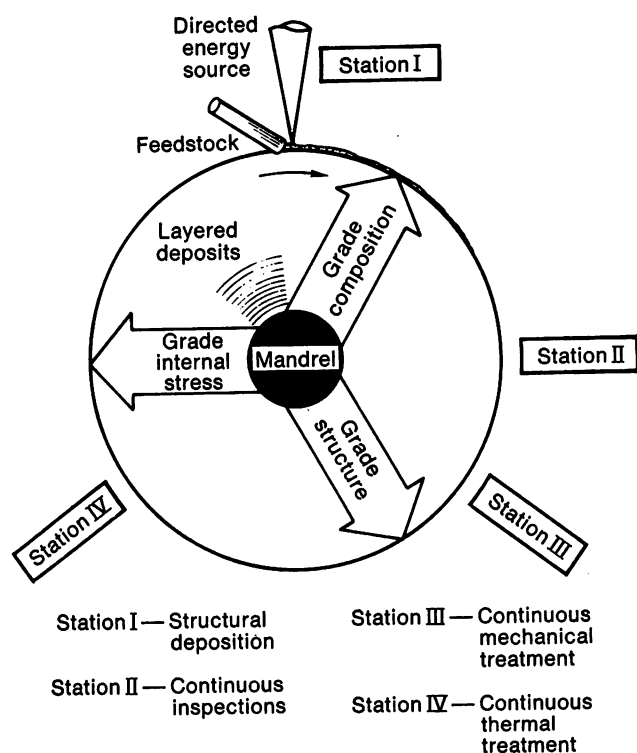
FIGURE 24—Schematic of directed energy in-situ processing.

fore possess the properties that permit its fusion and constrained resolidification without cracking. This renders unsatisfactory many of the high gamma prime superalloys. Alloys which are not so limited have been identified and have been successfully deposited. The deposition

buildup procedure depicted in Figure 25 and termed the Layerglaze process enables repetitive layers, which are fused together as a consequence of the intentional, slight remelting of the previous layer, to produce a fully dense and sound body. A bimetal, disk-shaped object which has been so produced from an experimental nickel-base alloy containing 8 a/o Al, 12 a/o Mo and 3 a/o Ta and IN-718 is pictured in Figure 26. In this case, the layer thicknesses are on the order of $125\mu m$.[20]

A wire feed has been used as a means for delivering the alloy for the deposition step, but the use of prealloyed or mixed elemental powders is favored because it provides a number of advantages. These advantages include, among others, the cost of the feed alloy and the relative ease with which compositions can be graded, should this be of interest.

The thin melt layers are rapidly solidified at rates in the range of $10^3$ to $10^5$ C/sec ($1.8 \times 10^3$ to $1.8 \times 10^5$ F/sec) by substrate self quenching. This rapid solidification produces a solid with improved homogeneity in comparison to normal castings and very much smaller segregation distances. These short distances allow compositional homogenization to occur after short exposures to high temperature.

The layer-by-layer deposition favors epitaxy, and large columnar grains form in the normal consequence of the Layerglaze process. As alluded to earlier, thermal

Partially etched

Final diameter: 132 mm (5.2 in.)    As machined

FIGURE 26—*Disk-shaped piece obtained by the* Layerglaze *process.*

stresses, which arise during the solidification and solid state cooling of a layer on an essentially cold and massive substrate, may produce substantial plastic deformation. Therefore, subsequent thermal treatments may be used not only to homogenize but also to recrystallize and provide a fine grained, equiaxed microstructure. Such a body should behave more isotropically than one with large columnar grains.

The second step of the Directed Energy Processing sequence may also be used to contribute deformation to the material. Although the step is principally intended to effect the residual stress state, its use coupled with thermal treatment may aid in the production of a recrystallized microstructure. By avoiding recrystallization, the advantages of a highly worked structure may, of course, be retained which may be advantageously employed in

certain applications.

The last step in the process is that of continuous non-destructive evaluation. Optical, acoustic and electromagnetic monitors are envisioned as possible techniques for in-line control. When a defect is discovered, repair might be effected by reglazing or, in more severe cases, by machining after which the process would be continued. Salvaging otherwise defective parts made possible by an active quality assurance procedure coupled with an *in situ* repair capability is a unique feature of Directed Energy Processing. Another unique aspect of the process is the ability to achieve compositional gradients which may be useful, for example, in optimizing wear, hardness and corrosion properties and to vary the grain structure of the deposit.

Although substantial development is required, prospects for the evolution of Directed Energy Processing as a future manufacturing tool are encouraging.

## Summary

Superalloys have another 20 years and more in critical gas turbine applications. No doubt some ground will be lost to composites and ceramics as the technology evolves. Nevertheless, it is quite likely that superalloys will remain 30 to 40% of engine weight much as they are today. What gives us confidence that this prediction can come true is, in a word, processing. The superalloy processes which we have discussed have evolved during the last decade and are still relatively new. Alloy design for single crystal technology has really just begun, and one can anticipate significant developments in the future leading to what we have called super single crystals. RSR powder technology, a recent innovation, can be expected to develop through advances in both processing and alloy design. Material processing by laser, a real newcomer on the scene, is so new that future applications are largely speculative at this point. Enough solid progress has been made to suggest that this kind of processing will result in a completely new approach to the manufacture of gas turbine components.

Superalloy metallurgy practitioners will, of course, continue to gain additional understanding in the area of strengthening mechanisms, oxidation/corrosion behavior and alloy consolidation. Cost, energy and resource efficiency as embodied in the net shape philosophy will continue to be a focus in the decade ahead. As has been said before, this will be the age of "tailored" superalloys.

One can conclude that superalloys and their processing are worthy of the attention of young, creative metallurgists looking to the future.

## Acknowledgments

sources, and we wish to thank them all. First, our colleagues in Materials Technology at United Technologies Research Center and our colleagues at Pratt and Whitney Aircraft, H. A. Hauser and his staff, J. B. Moore and his staff, and F. Fennessy and his staff.

The work reviewed in this paper covers a span of a decade or more and involves the efforts of many scientists, engineers and technologists. Many of those to whom credit is due are listed in the references that accompany this paper either as authors of technical publications or inventors to whom patents have been issued.

# References

1. R. F. Heheman and G. Mervin Ault (editors), *High Temperature Materials*, John Wiley & Sons, New York, 1959, 11.

2. R. F. Decker in P. R. Sahm and M. O. Speidel (editors), *High-Temperature Materials in Gas Turbines*, Elsevier Scientific Publishing, New York, 1974, 49.

3. F. L. VerSnyder and M. Gell in R. I. Jaffee and B. A. Wilcox (editors), *Fundamental Aspects of Structural Alloy Design*, Plenum Publishing, New York, 1977, 209.

4. *U. S. Patent 3,260,505*, 1966.

5. *U. S. Patent 3,494,709*, 1970.

6. F. L. VerSnyder and M. E. Shank, *Materials Science and Engineering, 6*, 1970, 213.

7. J. S. Erickson, et al. in P. R. Sahm and M. O. Speidel (editors), *High-Temperature Materials in Gas Turbines*, Elsevier Scientific Publishing, New York, 1974, 315.

8. B. N. Torell, *The Significance of Propulsion in Commercial Aircraft Productivity*, 17th Sir Charles Kingsfoot-Smith Memorial Lecture, Royal Aeronautical Society (Sydney Branch), 1975.

9. R. R. Sellers, et al., *AIAA/SAE Paper #77-948*, 1977, 1.

10. M. M. Allen, et al., *Metals Engineering Quarterly, 10*, 1970, 20.

11. G. H. Gessinger and M. J. Bomford, *International Metallurgical Review, 19*, 1974, 51.

12. A. Lawley, *The International Journal of Powder Metallurgy and Powder Technology, 13* (3), 1977, 169.

13. A. R. Cox, et al. in B. Kear, D. Muzyka, J. Tien and S. Wlodek (editors), *Superalloys: Metallurgy and Manufacture*, Claitor's Publishing, Baton Rouge, 1976, 45.

14. B. H. Kear, et al., *Met. Trans. A, 10A*, 1979, 191.

15. *U. S. Patent 3,519,503*, 1970.

16. R. L. Athey and J. B. Moore, *Society of Automotive Engineers*, Paper #751047, 1975.

17. M. J. Blackburn and R. A. Sprague, *Metals Technology, 4* (8), 1977, 388.

18. E. M. Breinan, et al., *Physics Today, 29* (11), 1976, 44.

19. E. M. Breinan and B. H. Kear in R. Mehrabian, B. Kear and M. Cohen (editors), *Rapid Solidification Processing*, Claitor's Publishing, Baton Rouge, 1978, 87.

20. E. M. Breinan, C. O. Brown and D. B. Snow, *Program to Investigate Advanced Laser Processing of Materials*, DARPA, 1st Annual Report, 1979, R79-914346-4.

# Discussion

E. H. KOTTCAMP, *Bethlehem Steel Corporation*. In the last illustration where you showed the build up of a composite disc, I assume you started with a laser deposit. How long does it take to form a part of that size by the process you use?

F. L. VERSNYDER. I just happened to have come prepared to answer that question. That took, at the rate of one centimeter per minute, seven hours to complete. Now, we're still in the laboratory, and we do not have an optimum system. But we think that it is possible to achieve an economic production rate. Our goal is a disc having a yield strength of 1725 MPa (250 ksi), and the gain from having the weight saving in an engine is so great that I think one could probably pay a little something extra in the cost of the disc.

E. EPREMIAN, *National Academy of Science*. Would you offer some speculation on what performance you see in terms of materials in the gas turbine, let's say at the end of the 80s in terms of operating life and operating temperatures, and what sort of materials and fabrication processes you think will evolve in that time.

F. L. VERSNYDER. You would have to address the question in two spheres. One would be the military where the objective is thrust-to-weight ratio. The other would be the commercial where the interest is fuel consumption. I think the goals in the commercial field will be much better fuel consumption and increased durability. I don't think there will be much push to go to higher temperatures; we are at 1340 C (2450 F) turbine gas inlet temperature now. I do think there will be considerable effort put into obtaining good fuel consumption. Another effort will be to get some of the critical elements such as chromium and cobalt out of the alloys that we are using now. In the military field, we will continue to pursue higher thrusts, and that will mean continuing emphasis on increased turbine temperatures. The ideal of course is optimum stoichiometric combustion, or 1650 C (3000 F). Whether we can get there with metals or not, I don't know. I don't anticipate as great a series of changes in alloys in the next decade as in the past because we cannot afford to do it anymore. Turbine technology, particularly in the commercial area, is getting to be relatively mature.

# High Strength Steels for Rail Transport

by D. H. Stone and W. J. Harris, Jr.
Association of American Railroads

Over the past twenty years, there has been an unbroken upward trend in the capacity, and thus gross vehicle weight, of railway freight cars in North America. In 1978, the average capacity of new freight cars was 77 tons, compared with a 64-ton average for cars retired from service.[1] This increase in load combined with increasing train speeds and lengths has placed new and severe demands on existing rail steels and cast steel components used in the car coupling system.

## Rail Steels

The ability of the rail to resist both wear and fracture depends on its mechanical properties, and it has become the lot of the metallurgist to attempt to provide a steel of satisfactory strength and toughness at a price which the user is willing to pay and the producer finds compensatory. Because of the sometimes conflicting demands for fracture resistance versus wear resistance, the first problem often can be to define what mechanical properties or characteristics shall be considered in the effort to optimize serviceability.

The standard rail steel in use today is a 0.69 to 0.82% C, 0.70 to 1.00% Mn steel with a fully pearlitic microstructure. The pearlite has a relatively coarse spacing of approximately 175 nm. This produces a steel with a typical yield strength of 480 MPa (70 ksi), tensile strength of 935 MPa (135 ksi), and fracture toughness of 40 MPa $\sqrt{m}$ (36 ksi $\sqrt{in}$.). This steel has served well for the past 80 years, and, in fact, still holds the ASTM specification A1 designation. However, the use of rails of this steel in modern service conditions has created problems with accelerated wear and crack initiation.

Two classes of improved rail steels have been developed to meet the need of these increasingly demanding service conditions. The first class is heat treated rails which are reaustenitized and quenched in air or oil to produce a fine pearlitic microstructure. Hyzak and Bernstein[2] have shown that heat treating has the advantage of increasing both strength and toughness. This is due to the fact that strength is dependent on pearlite interlamellar spacing, and toughness is a function of prior austenite

grain size. It has been found that heat treating rails to a yield strength of 870 MPa (125 ksi) and a tensile strength of 1200 MPa (175 ksi) increases the wear life by at least a factor of three.[3, 4]

The second class of improved rail steels is strengthened by alloying. Rails alloyed with 1% Cr, as well as rails with higher than standard silicon and manganese contents were introduced a number of years ago. Their development was based on somewhat empirical considerations, and these rails, under North American service conditions, did not perform as well as the heat treated rails. However, in 1976, workers at BHP in Australia[5] and Climax Molybdenum Company in the United States[6] reported the development of a series of chromium-molybdenum and chromium-molybdenum-vanadium steels which would harden during simulated mill cooling to strength levels at least equal to those of heat treated rails.

In the study at Climax Molybdenum, a series of steels was prepared in the laboratory, processed to simulate rail cooling, and evaluated for mechanical properties.[6] Yield strengths of up to 1117 MPa (162 ksi) were obtained in the investigation which included both pearlitic and bainitic steels. By way of example, a 0.73% C, 0.83% Mn, 0.16% Si, 0.75% Cr, 0.21% Mo steel, with a fine pearlitic microstructure, exhibited a 689 MPa (100 ksi) yield strength. The fine pearlite structure necessary to develop the strength was obtained by shifting the initial pearlite transition time from 100 seconds at 680 C (in conventional rail steels) to 1000 seconds at 650 C, as shown in Figure 1.

Two 100-ton commercial heats made of this approximate composition were processed into 65.5 kg/m (132 lb/yd) rail. The yield strengths ranged from 750 to 860 MPa (109 to 125 ksi), and the fracture toughness ($K_{Ic}$ value) ranged from 40 to 48 MPa $\sqrt{m}$ (36 to 44 ksi $\sqrt{in}$.). The microstructure of this product was predominantly fine pearlite, Figure 2, with small amounts of bainite in the web and flange. An accelerated (high load) rolling contact fatigue test showed no significant deterioration after five million cycles.

Test welds of the first-generation commercial chromium-molybdenum rail were made by both flash-butt
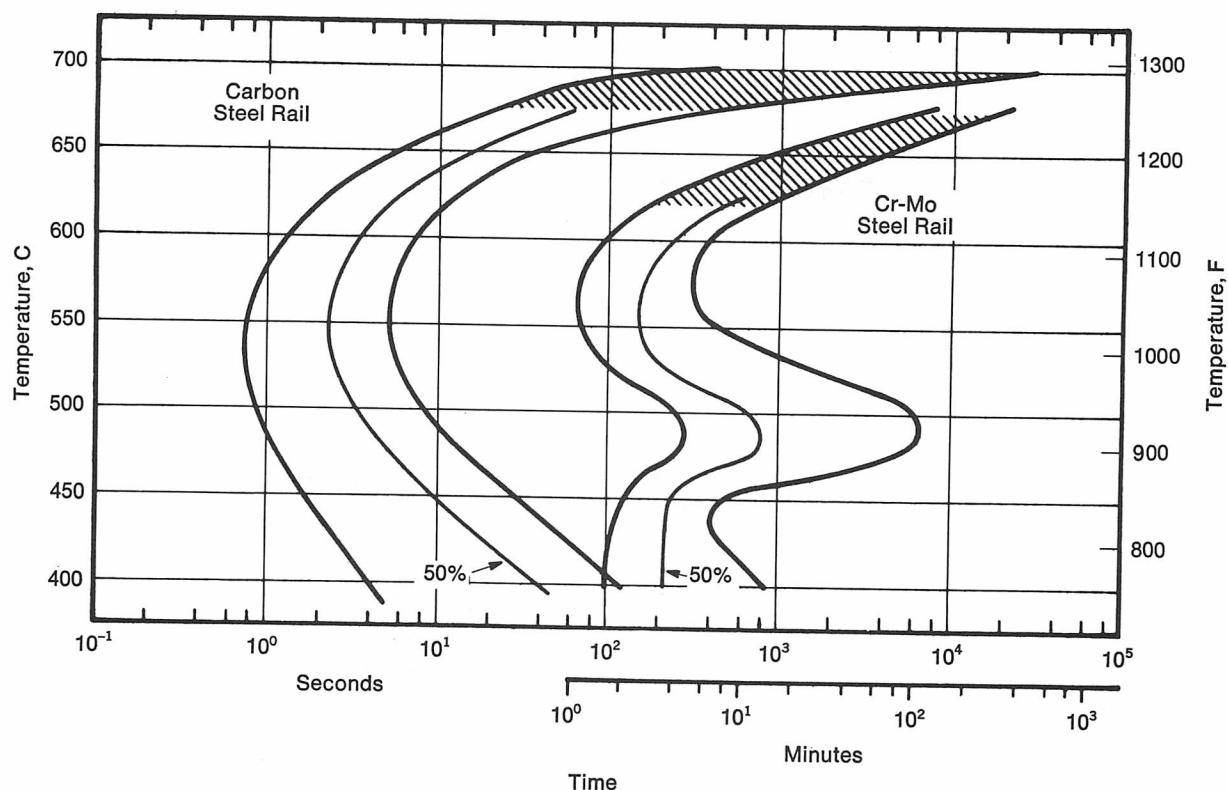
FIGURE 1—Isothermal transformation diagrams for standard carbon and first-generation Cr-Mo rail steels. Crosshatched areas represent the areas of transformation on cooling from rolling.
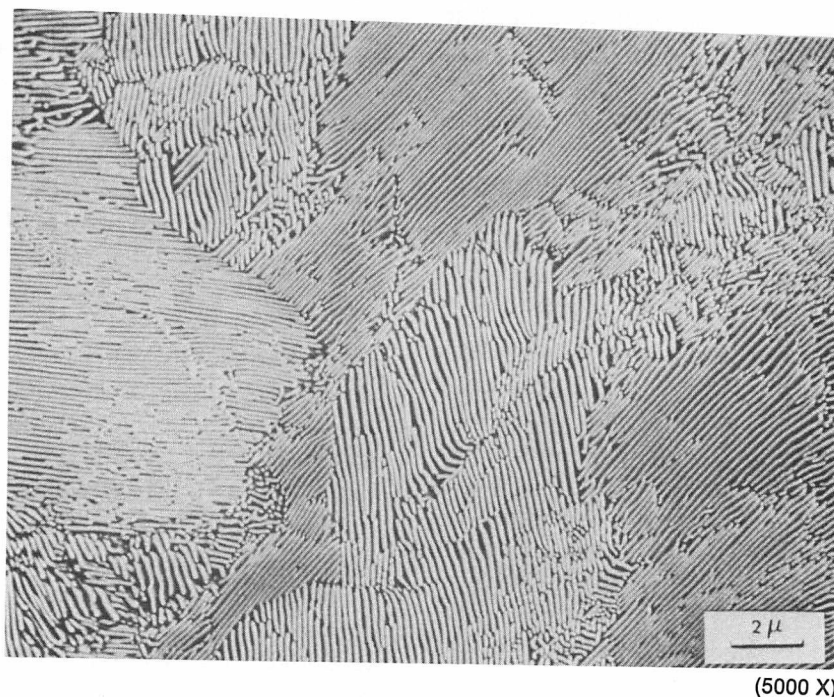


(5000 X)

FIGURE 2—Scanning electron micrograph of a Cr-Mo rail steel showing fine pearlite microstructure.

welding and thermite welding processes. Conventional flash-butt welding produced weld hardness peaks of about HRC 10 above the HRC 35 rail head hardness, and martensite bands were observed near the weld line. Somewhat lower hardness peaks resulted from welding by the Boutet thermite process, and the fusion zone was relatively soft.

Flash-butt welds in heavy duty rails should contain a minimum of martensite. However, because the HAZ cools at a faster rate than as-rolled rail, and because the chromium-molybdenum rail had high hardenability, bainite formed in the HAZ rather than fine pearlite. Since the bainite reaction in the chromium-molybdenum rail steel proceeded slowly, significant quantities of austenite

(5000 X)
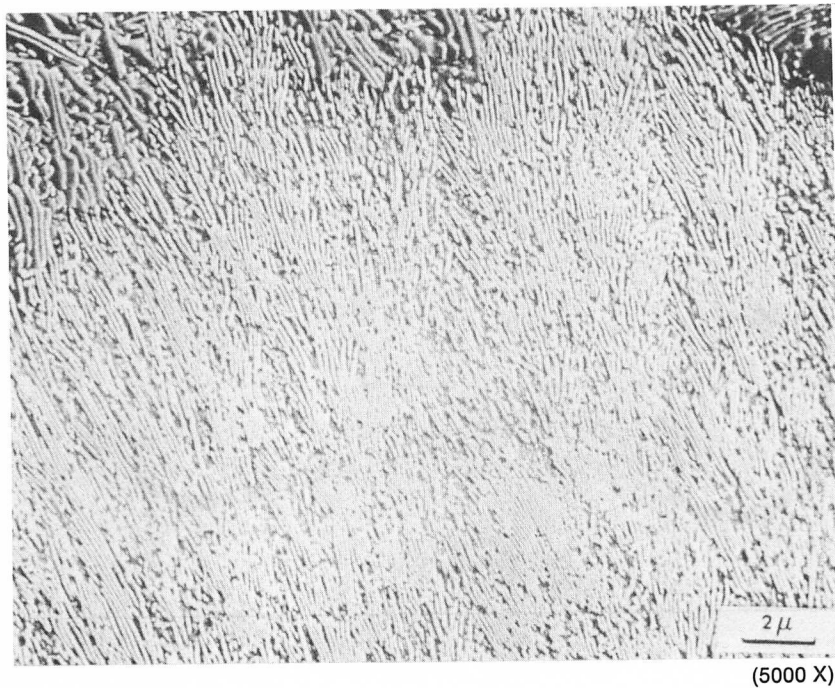
*FIGURE 3—Scanning electron micrograph of a Cr-Mo-V rail steel showing transitional pearlite microstructure.*

did not transform until the temperature of the HAZ dropped below the $M_s$ temperature, after which the remaining austenite transformed to martensite. The resulting weld HAZ microstructure was a mixture of bainite and martensite. Thus, when the conventional welding cycle for standard carbon steel rails was applied to the chromium-molybdenum rail steel, approximately 15% martensite formed, and the simulated weld region was HB 87 harder than the unaffected base metal. Subsequent laboratory simulations and actual rail welding trials demonstrated that postweld heat treatments could eliminate these problems.

Since the modification of conventional rail welding processes was not an ideal solution, however, attention was turned to modification of the steel itself. Laboratory work demonstrated that decreasing the manganese and chromium contents virtually eliminated martensite from the weld region of the chromium-molybdenum rail steel and reduced the hardness difference between the weld and unaffected base metal by 50%. Hence, a modified chromium-molybdenum rail steel with a composition range of 0.70 to 0.81% C, 0.50 to 0.70% Mn, 0.50 to 0.70% Cr and 0.18 to 0.23% Mo was identified. Such a steel exhibited the same as-rolled strength properties as unmodified chromium-molybdenum steel rails while containing less than 2% martensite in a simulated weld region cooled at the rate resulting from a conventional carbon steel flash-butt welding cycle. Clearly, the modified chromium-molybdenum rail steel offers an attractive alternative to unmodified chromium-molybdenum rail steel in terms of welding efficiency.[7]

More recently, a series of chromium-molybdenum-vanadium steels has been developed which extends the strength of the pearlite steels to near the ultimate obtainable.[8] One steel in the series which has extra high strength properties has a nominal composition of 0.70 to 0.80% C, 0.50 to 0.70% Mn, 0.50 to 0.70% Cr, 0.21 to 0.26% Mo and 0.08 to 0.12% V. This steel has a yield strength of 830 MPa (120 ksi), tensile strength of 1250 MPa (180 ksi) and hardness of HB 350-400 in the as-rolled condition.

It is apparent that vanadium has a pronounced effect on the properties of the chromium-molybdenum rail steels. In the above case, 0.1% V caused an increase in the yield strength of 120 to 176 MPa (17 to 25 ksi), an increase in the tensile strength of 120 to 180 MPa (17 to 26 ksi) and an increase in the hardness of about HB 36. When the microstructure is lamellar pearlite, as in chromium-molybdenum steels, vanadium improves the tensile ductility as well; however, there is some loss of ductility when the microstructure is transitional pearlite, Figure 3.

Full-scale wear tests of alloy steel rails have accompanied the development of new compositions. First-generation chromium-molybdenum rails were installed in the Facility for Accelerated Service Testing (FAST), a 7.7 km (4.8 mile) loop on which a train of 100-ton cars operates for 16 hours per day; a diagram of the loop is shown in Figure 4. FAST is a cooperative research program of the Federal Railroad Administration, the Association of American Railroads and the Railway Progress Institute. Part of the FAST experiment has been the evaluation of wear of different rail metallurgies. Table I shows that in this test, the chromium-molybdenum rails had wear rates which were either the lowest or next to the lowest.[9] It should be noted that the < 45 MGT data are for unlubricated conditions and the >45 MGT data
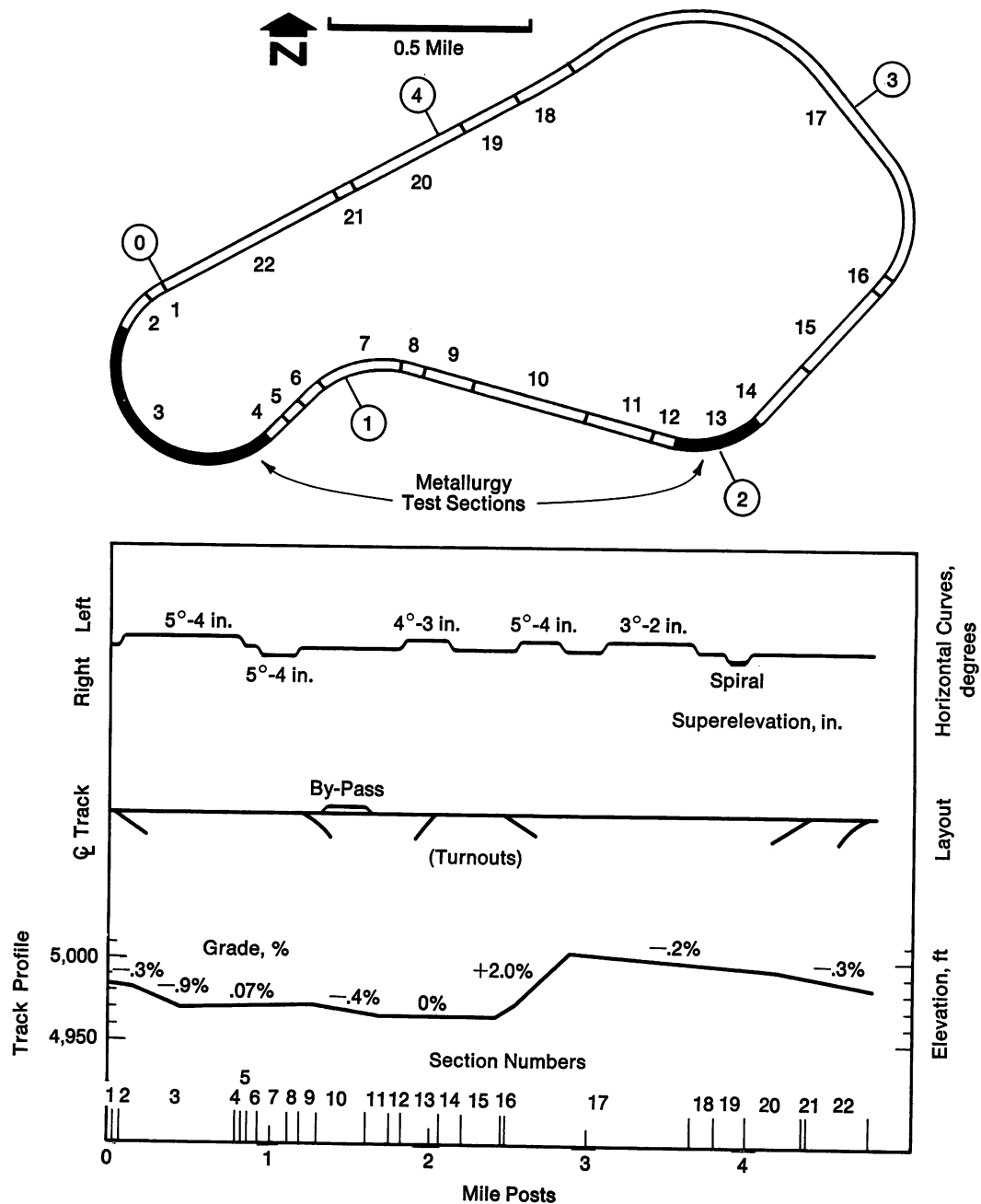
FIGURE 4—Diagram of the fast track.

Table I—Wear Rates Above and Below the Lubrication Transition for Different Tie Plate Cants

| | Head Area Loss, in./MGT | | | | | |
| | Tie Plate Cant | | | | | |
| Rail Metallurgy | 1 in 40 | | 1 in 14 | | 1 in 30 | |
| | <45 MGT | >45 MGT | <45 MGT | >45 MGT | <45 MGT | >45 MGT |
|---|---|---|---|---|---|---|
| Head Hardened | 0.00496 | 0.00046 | 0.00514 | 0.00092 | 0.00424 | 0.00097 |
| High Silicon | 0.00812 | 0.00110 | 0.00907 | 0.00119 | 0.00708 | 0.00154 |
| Fully Heat Treated | 0.00704 | 0.00046 | 0.00667 | 0.00149 | 0.00627 | 0.00183 |
| Chromium-Molybdenum | 0.00449 | 0.00092 | 0.00423 | 0.00107 | 0.00482 | 0.00085 |
| Standard Carbon | 0.01287 | 0.00167 | 0.01245 | 0.00127 | 0.01229 | 0.00156 |

are for well lubricated conditions.

Rails from the first two commercial heats of the first-generation composition were placed in curved sections of the Mt. Newman Railway in Australia. This is an iron ore railway which uses 100-ton cars. Figures 5 and 6 show that chromium-molybdenum rails had approximately double the wear life of standard carbon rails. Of the experimental rails included in the study summarized by Figure 6, the chromium-molybdenum rail was the best alloy rail and performed almost as well as a commer-

cially available head hardened rail.[10] Subsequent wear tests of chromium-molybdenum-vanadium rails in Australia[11] indicated that this steel should perform better than either chromium-molybdenum or head hardened rails.

## Cast Steels

The U.S. railroad industry is the nation's largest user of steel castings. A large percentage of these castings is used in the freight car coupling system, which experiences brittle fractures in service. To help alleviate this problem, a survey of fracture properties of commercially produced AAR cast steels was conducted as part of the Railroad Coupler Safety Research and Test Project (RPI-AAR Program).

It is essential as the railroad industry enters the eighties to review and, where necessary, rewrite material specifications based on the use of fracture mechanics principles for fracture properties characterization coupled with conventional metallurgical factors. To do otherwise is to neglect modern technological practices now widely used in the general engineering field, and thus it is to be expected that fracture mechanics will be applied to all fracture-related engineering problems in the railroad industry. Because of pending revisions of the AAR specifications for cast steel components, these
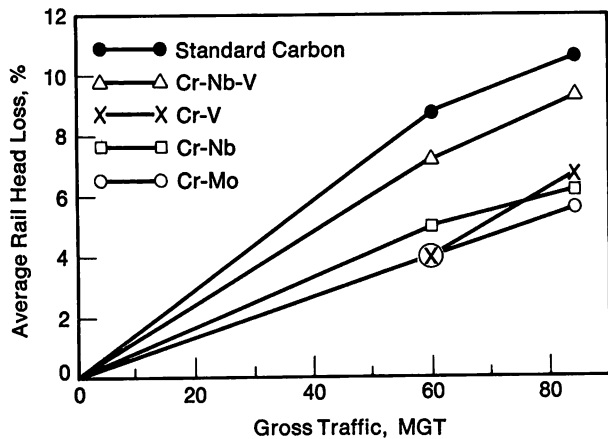


FIGURE 5—*Wear rates of standard carbon and alloy steel rails on a three-degree (582 m radius) curve on the Mt. Newman Railway.*
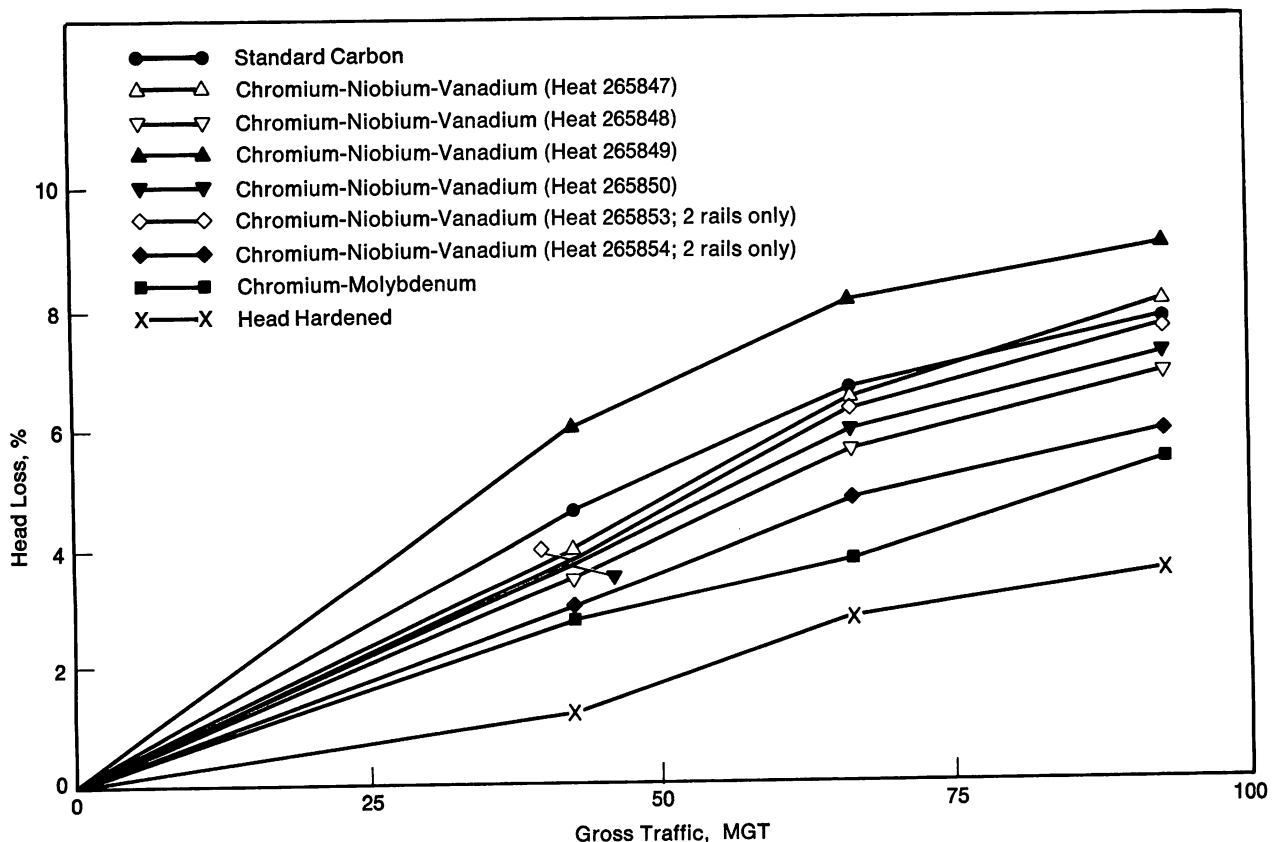


FIGURE 6—*Wear rates of indicated rails on a two-degree (873 m radius) curve on the Mt. Newman Railway.*

analyses are also of value in establishing appropriate fracture toughness specification requirements.

AAR use of fracture mechanics principles is not new. For example, in a report developed for the Railroad Tank Car Safety Research and Test Project, the TC-128 tank car steels were characterized and analyzed statistically in fracture mechanics terms.[12] Predictions of service performance, in the case of railroad accidents, were fully validated. Rail steels are another example of the use of modern fracture mechanics principles for characterization and analysis of properties.

The fracture behavior of steels changes over a range of temperatures, with the critical transition points being definable as the temperatures corresponding to the plane strain limit (L) and the yield criterion (YC). It is possible to relate the nominal stress levels which are required to propagate flaws in standard specimens (or in service) to the general forms of energy transition curves, Figure 7. The idealized fracture analysis type diagram at the top of Figure 7 indicates the changes in fracture behavior of a single specimen geometry with increasing nominal stress in a fracture toughness test. The top of Figure 7 also illustrates the simplified engineering method of plotting the L to YC temperature range as a straight line. Because of possibilities for impact overloads in railroad service, it is judged that fracture-prone components such as couplers should, at the lowest service temperature to be encountered, have fracture properties at least equal to the range of 0.5 YC (halfway between L and YC) to YC (high elastic-plastic). Preferably, the high end of the range (close to YC) should be used as the basis for the minimum fracture toughness acceptable for the lowest service temperature of interest.

In the survey of fracture properties of cast steels alluded to above, fracture tests were performed on two pearlitic steels, AAR Grades B and C (N & T), and two martensitic steels, AAR Grades C (Q & T) and E, at Case Western Reserve University.[13] Since a primary objective of the study was to permit characterization of the fracture behavior by fracture mechanics methods, the dynamic tear (DT) test using an ASTM-defined specimen[14] was employed to delineate the L to YC temperature range. Briefly, the DT test involves a notched, beam-type specimen that is impact loaded in three-point bending such that the total energy loss during separation is recorded. A schematic DT test curve is shown at the bottom of Figure 7 as is the method of indexing L and YC temperatures to the experimental curve. For the fracture analysis reported herein, the indexing procedure consisted of: (a) averaging the known nil-ductility transition (NDT) temperature and the temperature of the initial rise of the DT curve to obtain L, (b) averaging the (50%) midenergy and 50% shear fracture temperatures to obtain YC (both are reliable and conservative indications that YC properties are attained), and (c) using a straight line reference for the L to YC transition temperature range. A detailed examination of the effects of metallurgical variables on the fracture properties was also performed.

The composition and properties of the cast steels which were surveyed are given in Table II, with the steel source coded alphabetically. The values of L and YC were determined as noted above and are encompassed in the bands of Figure 8. By defining the L to YC transition temperature range, the steel fracture behavior is defined with respect to service temperatures. The correspondence to performance in service is direct. For a given steel, service temperatures below the value of L signify that brittle fractures can develop; service temperatures above YC signify that only ductile fracture (by overload) can develop. For most structures, a fracture value of 0.5 YC is generally sufficient to prevent fracture. This is due to the fact that most structures are designed to nominal stresses less than $0.5\,\sigma_{ys}$.

The Grade B and Grade C (N & T) steels can be accounted for by a single band of fracture behavior, as can the Grade C (Q & T) and Grade E steels, with the exception of the three steels indicated at the bottom of Figure 8. An important feature of the common band for quenched and tempered grades is the indication of approximately equal potential for the development of good low temperature fracture properties. Conversely, the susceptibility to brittle fracture of Grades B and C (N & T) experimental specimens at high temperatures is less than known field experience, so that the estimated upper limit
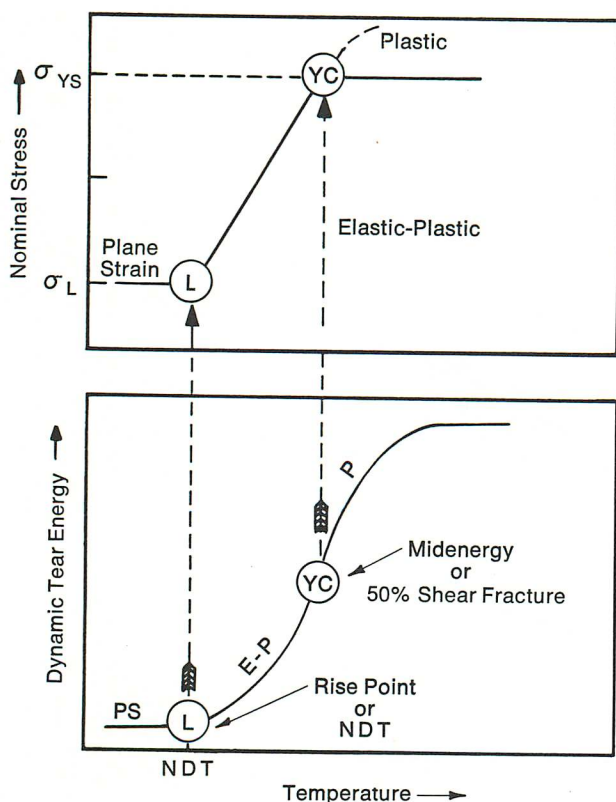


FIGURE 7—Indexing of idealized L-YC transition curve to DT test curves and to NDT.

**Table II**—Composition and Properties of AAR Cast Steels Evaluated in Case Western Reserve University Study

| Source | Element, % | | | | | | Tempering Temperature, Time, | | | Yield Strength, | | Critical Temperatures L | | YC | |
|---|---|---|---|---|---|---|---|---|---|---|---|---|---|---|---|
| | C | Mn | Ni | Cr | Mo | V | C | (F) | h | MPa | (ksi) | C | (F) | C | (F) |
| | | | Grade B (Normalized) | | | | | | | | | | | | |
| A | 0.30 | 0.75 | 0.08 | 0.14 | 0.03 | 0.01 | — none — | | | 330 | (48) | -15 | (5) | 21 | (70) |
| B | 0.27 | 0.76 | 0.06 | 0.09 | 0.03 | — | — none — | | | 315 | (46) | -12 | (10) | 27 | (80) |
| C | 0.27 | 0.72 | 0.10 | 0.12 | 0.08 | 0.01 | — none — | | | 315 | (46) | -15 | (5) | 24 | (75) |
| D | 0.21 | 0.66 | 0.15 | 0.18 | 0.09 | — | — none — | | | 290 | (42) | -32 | (-25) | 21 | (70) |
| AT | 0.29 | 0.71 | 0.20 | 0.28 | 0.03 | 0.04 | — none — | | | 345 | (50) | -7 | (20) | 46 | (115) |
| E | a | a | a | a | a | a | — none — | | | 330 | (48) | -9 | (15) | 27 | (80) |
| | | | Grade C (Normalized & Tempered) | | | | | | | | | | | | |
| A | 0.28 | 1.62 | 0.10 | 0.10 | 0.03 | — | 550 | (1020) | 2 | 455 | (66) | -7 | (20) | 41 | (105) |
| C | 0.29 | 1.46 | 0.10 | 0.11 | 0.13 | — | 660 | (1220) | 4 | 420 | (61) | 4 | (40) | 46 | (115) |
| D | 0.29 | 1.30 | 0.26 | 0.22 | 0.22 | — | 620 | (1150) | 3 | 450 | (65) | -34 | (-30) | 16 | (60) |
| E | 0.29 | 1.34 | 0.09 | 0.12 | 0.02 | — | 480 | (900) | 2 | 425 | (62) | -12 | (10) | 35 | (95) |
| F | 0.27 | 1.04 | 0.72 | 0.52 | 0.17 | — | 650 | (1200) | 2.5 | 440 | (64) | -18 | (0) | 35 | (95) |
| | | | Grade C (Quench & Tempered) | | | | | | | | | | | | |
| B | 0.27 | 0.76 | 0.06 | 0.09 | 0.03 | — | 550 | (1020) | 3 | 455 | (66) | -18 | (0) | 10 | (50) |
| A (C) | 0.33 | 1.65 | 0.08 | 0.10 | 0.04 | — | 665 | (1225) | 2 | 565 | (82) | -71 | (-95) | -29 | (-20) |
| E | 0.24 | 1.24 | 0.10 | 0.11 | 0.03 | — | 595 | (1100) | 2 | 560 | (81) | -37 | (-35) | 7 | (45) |
| C | 0.29 | 1.46 | 0.10 | 0.11 | 0.13 | 0.07 | 705 | (1300) | 4.5 | 455 | (66) | -71 | (-95) | -40 | (-40) |
| A (Q) | 0.28 | 1.37 | 0.08 | 0.34 | 0.17 | — | 705 | (1300) | 2 | 575 | (83) | -71 | (-95) | -37 | (-35) |
| D | 0.29 | 1.30 | 0.26 | 0.22 | 0.22 | — | 650 | (1200) | 3 | 595 | (86) | -71 | (-95) | -23 | (-10) |
| F | 0.22 | 1.28 | 0.90 | 0.51 | 0.28 | — | 675 | (1250) | 4.5 | 490 | (71) | -79 | (-110) | -37 | (-35) |
| | | | Grade E (Quench & Tempered) | | | | | | | | | | | | |
| A | 0.28 | 1.38 | 0.06 | 0.28 | 0.17 | — | 560 | (1040) | 2 | 875 | (127) | -55 | (-70) | -9 | (15) |
| C | 0.32 | 1.47 | 0.12 | 0.16 | 0.24 | 0.02 | 595 | (1100) | 4.5 | 840 | (122) | -60 | (-75) | -21 | (-5) |
| D | 0.25 | 1.25 | 0.19 | 0.30 | 0.27 | — | 650 | (1200) | 3 | 725 | (105) | -50 | (-55) | -23 | (-10) |
| E | 0.29 | 1.50 | 0.12 | 0.45 | 0.23 | — | 595 | (1100) | 2 | 885 | (128) | -70 | (-95) | -37 | (-35) |
| EL | 0.22 | 1.22 | 0.16 | 0.40 | 0.20 | — | 595 | (1100) | 2 | 765 | (111) | -20 | (-5) | 11 | (52) |
| EH | 0.30 | 1.46 | 0.19 | 0.52 | 0.30 | — | 650 | (1200) | 2 | 795 | (115) | -90 | (-135) | -68 | (-90) |
| F | 0.22 | 1.28 | 0.90 | 0.51 | 0.28 | — | 550 | (1025) | 3.5 | 795 | (115) | -70 | (-95) | -40 | (-40) |

a — not available.

for the behavior of these grades has been designated as shown. The bold arrow of Figure 8 simply represents the likely gap between the performance of the various grades of steel castings thus graphically indicating the superiority of the quenched-and-tempered grades to the normalized-and-tempered grades.

Figure 9 presents statistical expectancy bands based on adjusted Figure 8 bands. The high ends of these bands are used to designate a tentative specification limit (TSL) for the steels. If the TSL line is used for specification purposes, then YC properties no better than −18 C (0 F) could be guaranteed statistically for the Q & T steels. Similarly, YC properties no better than 50 C (120 F) could be guaranteed for the N & T steels.

There is no way the pearlitic steels can be improved to the extent of having fracture properties equivalent to the Q & T bainitic/martensitic steels. The gap between the two could possibly be closed, since a downward shift of the band by approximately 17 C (30 F) has been demonstrated for pearlitic rolled plate steels. However, such

attainment required exacting adjustments of metallurgical factors, which would not be economical for castings.

Because of the superior fracture properties of the quenched-and-tempered grades, the following discussion will emphasize metallurgical factors which are primarily germane to the steels with bainitic/martensitic microstructures. Inherent to the analysis of the role of metallurgical factors is the understanding that all producers (sources) of castings used fine grain deoxidation practice and austenitization temperatures of 900-925 C (1650-1700 F). However, there is inadequate *direct* information to compare the effectiveness of their quenching facilities.

Figures 10 and 11 show the L-YC curves for the individual castings of Grade C (Q & T) and Grade E, respectively. The curves are coded to Table II by source [capital letter(s)], relative alloy content (*H*igh, *M*edium, *L*ow), tempering temperature, (tempering time) and yield strength. The variations in alloy content and yield strength which are represented are substantial.

The Grade C (Q & T) steels with good fracture prop-

Temperature, F
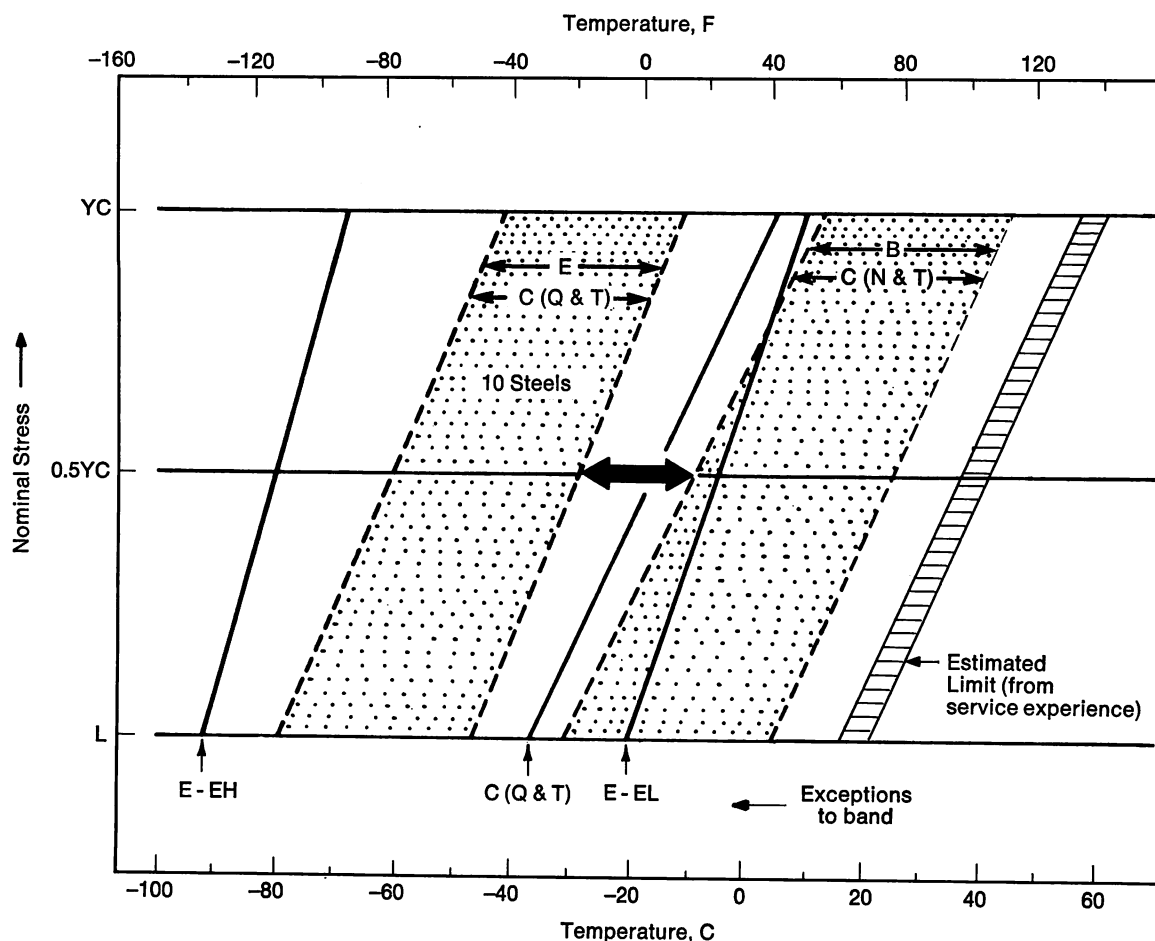


FIGURE 8—Summary of fracture behavior for cast steels.

erties, i.e., those to the left of TSL, were all tempered at 650 C (1200 F) or above. Such a treatment provides good fracture toughness for a range of carbon contents, as long as there is adequate hardenability available through alloying for the section sizes of interest. In fact, it appears that the carbon content could be kept on the low side for improved weldability and still meet the yield strength specification of 415 MPa (60 ksi) for this grade.

For the Grade E steels, Figure 11, the general tendency is for the fracture properties to improve with combined increases of alloy content and tempering temperature, indicating again the key role of hardenability. It appears that this combination plus low carbon would provide tough, weldable components with yield strengths safely above the specified value of 690 MPa (100 ksi).

The castings used for the fracture test samples had a simple geometry which provided for fast cooling rates in quenching. More complicated casting shapes may be expected to develop slower quench-cooling rates. Thus, mixed structures are more likely for the low alloy compositions (low hardenability), and poor fracture properties may result. The answer is to use sufficient alloy to insure good quenching response, that is, to eliminate mixed microstructures in production castings.

Returning to Figure 9, with microstructure as the

subject for attention, the high temperature location of the L-YC band for the B and C (N & T) steels is in line with expectations for the pearlitic microstructures which were observed in all cases. The steels which fell in the Q & T band, on the other hand, had martensitic/bainitic microstructures. The only three Q & T steels which fell outside the band on the high temperature side, i.e., to the right of TSL, were samples with pearlitic or partially pearlitic structures. This supports the well established fact that the development of pearlite as part of a quenched-and-tempered microstructure is highly detrimental to fracture properties, i.e., a relatively small percent of pearlite (say 10-15%) is highly detrimental in microstructures that otherwise are of the martensitic/bainitic type. These mixed microstructures must be avoided if meeting of TSL fracture quality is to be expected for the Q & T steels.

At the onset of the RPI-AAR program, the single most important practical question was whether fracture-safe castings could be guaranteed at railroad service temperatures. The results indicate that such castings can be produced economically with the following advantages:

1. elimination of brittle fracture problems at the minimum service temperatures for Q & T steels,
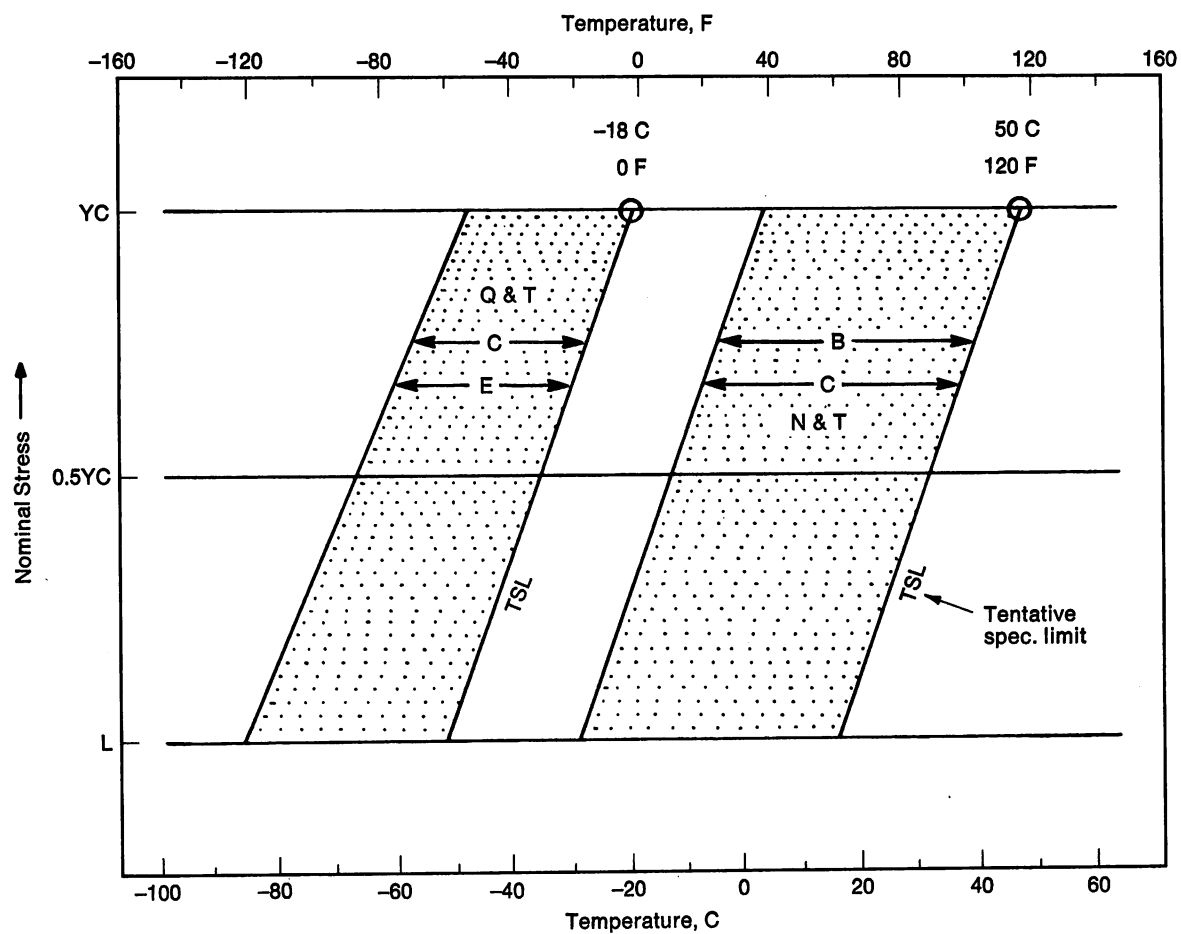
FIGURE 9—*Location of tentative specification limit (TSL) lines for steel grades.*
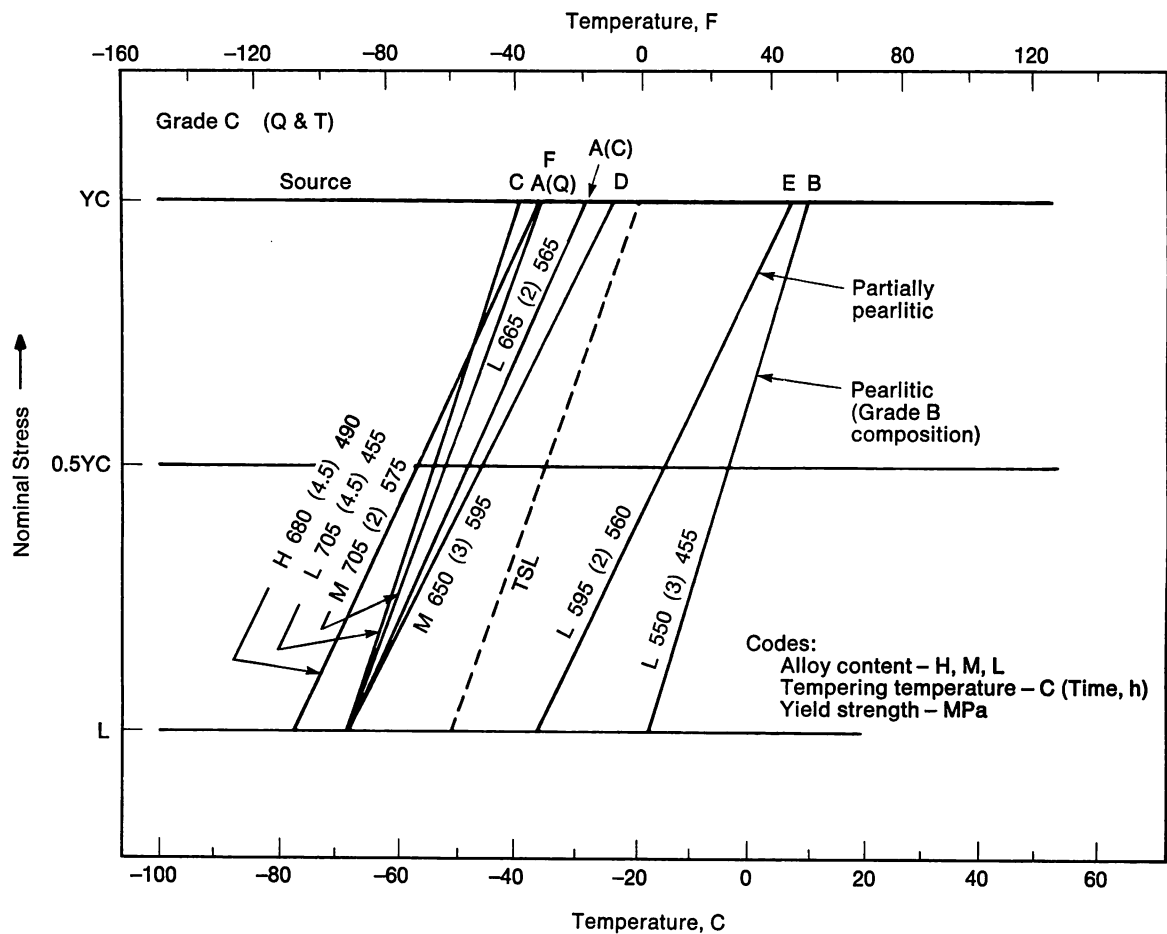
*FIGURE 10—Summary of grade C (Q&T) steels, referenced to metallurgical factors.*
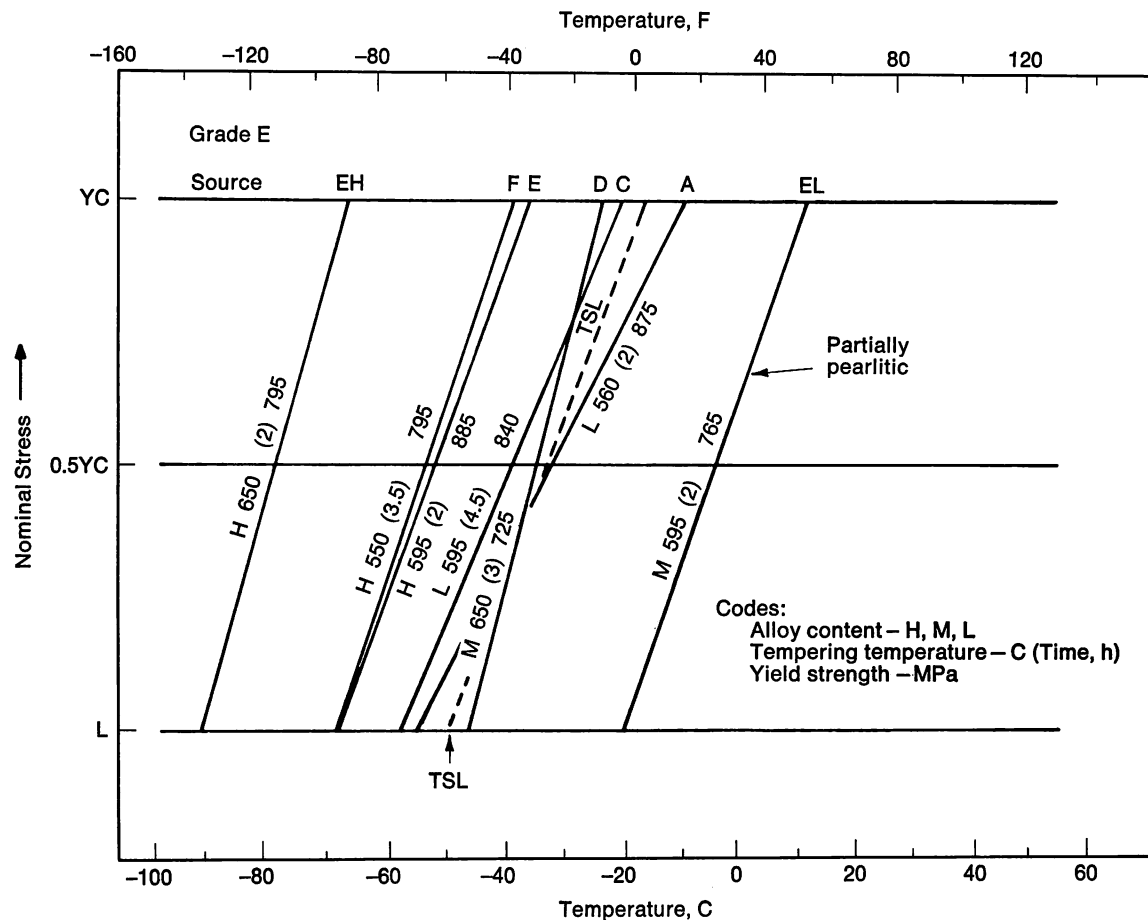
FIGURE 11—Summary of grade E steels, referenced to metallurgical factors.

2. high reproducibility of fracture properties in production parts,

3. specification of fracture properties in modern engineering terms,

4. improved weldability for repairs, and

5. guaranteed casting and test block properties.

# References

1. *Yearbook of Railroad Facts,* 1979 Edition, Association of American Railroads, Washington.

2. J. M. Hyzak and I. M. Bernstein, *Met. Trans. A,* 7A (8), August 1976, 1217.

3. L. DeLucca Silva and M. Lebre Nobrega, "A Research Trip for the Study of Axle Load," *Heavy Haul Railways Conference Proceedings,* Perth, Australia, September 1978, Session 312.

4. S. Bramwell and T. F. McElroy, "25 Years of Heavy Axle Load Unit Train Operation on the Quebec, North Shore and Labrador Railway," *Heavy Haul Railways Conference Proceedings,* Ibid., Session 107.

5. S. Marich and P. Curcio, "Development of High-Strength Alloyed Rail Steels Suitable for Heavy Duty Applications," *Rail Steels—Processing, Developments and Use,* ASTM STP 644, American Society for Testing and Materials, Philadelphia, 1978, 67.

6. Y. E. Smith, J. M. Sawhill, Jr., W. W. Cias and G. T. Eldis, "High-Strength Chromium-Molybdenum Rail Steels," *American Railway Engineering Association—Bulletin,* 77, June-July 1976, 621.

7. F. B. Fletcher and Y. E. Smith, "Development of High Strength Chromium-Molybdenum Rail Steel With Improved Weldability," *Heavy Haul Railways Conference Proceedings,* Ibid., Session 213.

8. F. B. Fletcher, Y. E. Smith and V. A. Biss, "Fast Welding Chromium-Molybdenum-Vanadium Extra-High-Strength Rail Steels," *Vanadium in Rail Steels,* Vanitec, Chicago, November 1979, Paper D.

9. R. K. Steele, "Some Results from the First FAST Metallurgy Experiment," *American Railway Engineering Association—Bulletin,* June-July 1979, 493.

10. P. Curcio, S. Marich and G. Nisich, "Performance of High Strength Rails in Track," *Heavy Haul Railways Conference Proceedings,* Ibid., Session 313.

11. S. Marich, "Development of Improved Rail and Wheel Materials," *Vanadium in Rail Steels,* Vanitec, Chicago, November 1979, Paper C.

12. P. C. Sigala and J. F. Wallace, "Evaluation of the Toughness Properties of Various Cast Steels," Case Western Reserve University, June 1977.

13. W. S. Pellini, R. J. Eiber and L. L. Olson, "Fracture Properties of Tank Car Steels—Characterization and Analysis," AAR Report R-192, August 1975.

14. "Dynamic Tear Energy of Metallic Materials," E-604-77, *ASTM Standards,* Part 10, 1979, 645.

# Materials for the LMFBR

by J. Archer, Ph. Berge and M. Weisz
Novatome, EDF and C.E.A.-CEN/SACLAY

## Materials for Sodium-Cooled Reactors

The metallurgical problems raised by materials in-
tended for use in a sodium-cooled fast neutron nuclear
power station are extremely varied. Problems of sodium
compatibility imply the generalized use of stainless
steels, usually austenitic. The use of sodium as coolant
has the effect that pressures are low (apart from the
water/steam circuit), but, owing to good heat transfer
properties, the power variations cause heat fluctuations
leading to thermal fatigue.

The temperature range within which the compo-
nents have to work is fairly wide (350 to 650 C, 660 to
1200 F). It covers a low temperature region where de-
formations and fractures may be taken to exclude time-
dependent phenomena and a high temperature region
where creep phenomena must be acounted for. The so-
called cold components can undergo incidental transients
in the creep region, which their constituent materials
must be able to withstand. The distinction between the
two regions is not clearly defined. In a conventional and
highly simplified way, the ASME Code proposes a single
temperature limit of 425 C (800 F). In France, it was
decided that a limit dependent on both time and tem-
perature should be set for each material, and an example
is given (Figure 1) for a 316L steel. Below this limit, the
low temperature rules may be applied, for example the
ASME Code of Section III. This limiting curve is a char-
acteristic of a material and should be determined in each
case.

A sodium-cooled nuclear power station uses a wide
variety of steel products for vessels, circuits, core-sup-
porting structures, baffles, outer structures of intermedi-
ate exchangers and steam generators. Austenitic steels
derived from grade 316 are used for the hot parts of
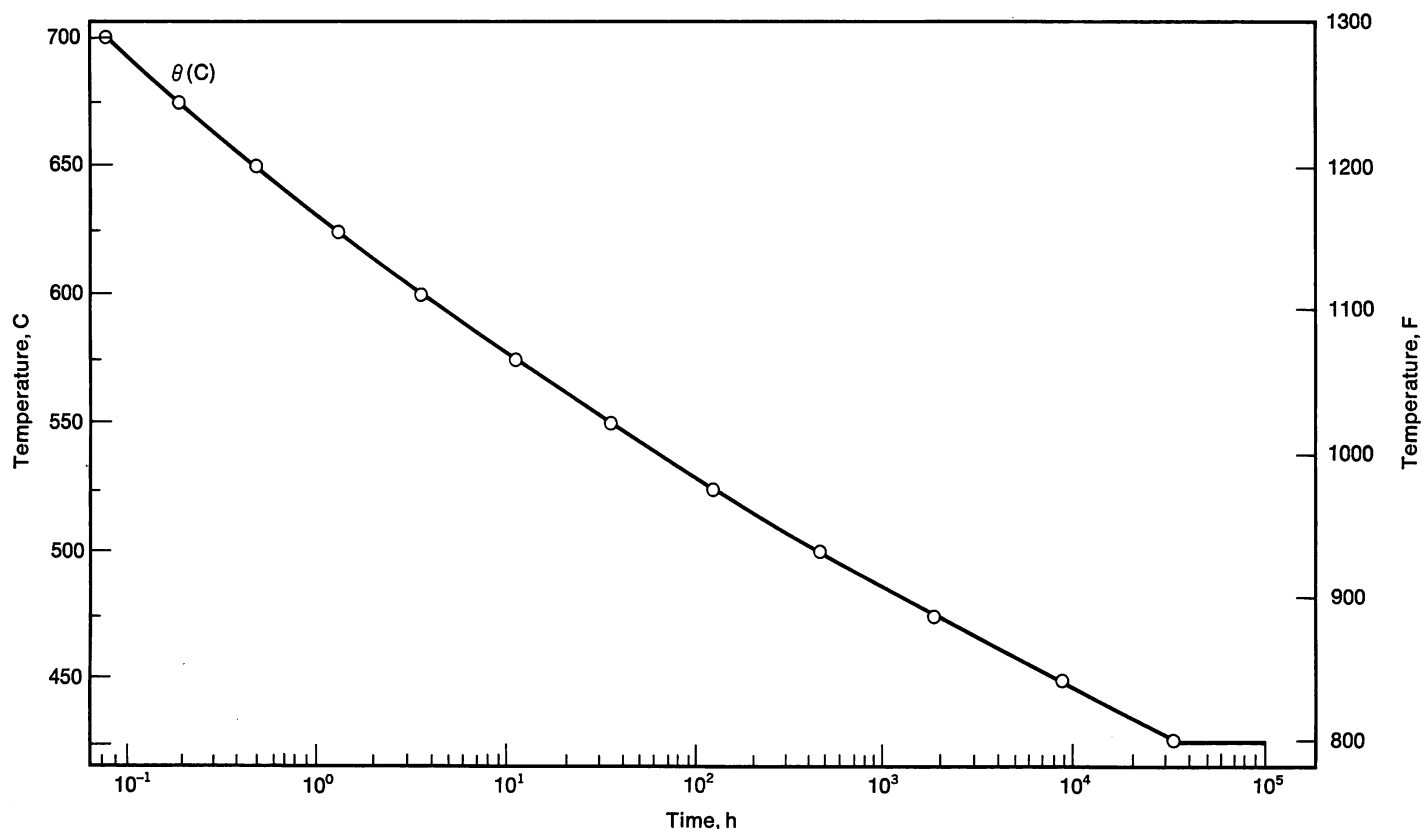


FIGURE 1—Relationship between temperature and time for negligible creep effects.

these circuits. The cold parts are made from a low carbon version of Type 304.

Forged plates for intermediate heat exchanger heads show mechanical property variations difficult to explain by chemical composition differences alone. The elastic limit at 550 C (1020 F) is strongly influenced by the forging method, while the composition range of basic 316 steel may be adjusted to obtain the mechanical characteristics needed.

As in the case of sheet steel, the problem of inclusion content in connection with fabrication techniques must be followed attentively.

Type 316L steel tubes for intermediate heat exchangers are representative of a thin-walled product which has an important role as primary circuit barrier.

Problems specific to CF-3 and CF-3M castings are:

1. The difficulty of obtaining representative samples in the laboratory.

2. Embrittlement at 475 C (885 F) owing to the rather high ferrite contents necessary (10 to 15%); effect of molybdenum on embrittlement kinetics; evaluation of the consequences arising from the low toughness obtained after long-term aging.

3. The fact that, while in principle these components are cold, it is necessary to estimate the effects of thermal transients which require knowledge of creep characterization up to 1000 hours at 400 to 500 C (750 to 930 F), and the definition of a temperature/time range where creep is insignificant.

Special austenitic steels are used for pump shafts, nuts and bolts and steam generator tubes. This case is one of the most complex and will be discussed in more detail below.

For Phenix and Super Phenix, the base plate of the main vessel top is a fairly complex cold structure (< 100 C, < 210 F) made with carbon steel where, because of the welded assembly design, the risk of lamellar tearing had to be accounted for. Certain precautions had to be taken with regard to the quality of the sheet (high short transverse properties, low sulfur content, etc.). The problem was complicated by the difficulty in finding a filler metal with a yield strength lower than the UTS of the base metal (about 480 MPa, 70 ksi). Another difficulty was the large-scale achievement of a heterogenous joint with the austenitic steel vessel.

The definition and characterization, especially by long term creep tests, of filler metals for welding or repairing the above-mentioned elements raises specific problems in view of their special metallurgical properties.

Austenitic steel assemblies (Type 316) for components working at high temperature require filler deposit compositions giving a minimum amount of ferrite to avoid high temperature cracking and a maximum to avoid embrittlement during high temperature service.

A 3 to 7% ferrite level seems a reasonable and industrially feasible compromise.

The mechanical properties of the weld deposits are somewhat different (Figure 2) from those of the base metal with higher yield stress, lower fracture elongation and work hardening coefficient. The creep behavior is also different (Figure 3). The creep rates are lower and the rupture stresses much closer to $\sigma$ 1% total than in the base metal. These properties of the welds are due to the high dislocation density brought about by welding stresses. At the maximum temperatures anticipated, this structure is not stable, which means that changes in the mechanical properties are to be expected during operation.

## Vessels and Hot Circuits

As already mentioned, the question of high temperature mechanical strength has led to the choice of Type 316 molybdenum austenitic steels. The final definition of the composition specifications was based on examination within the Super Phenix project of the following criteria:

1. Structural changes at high temperature and effects on toughness and sensitization to intercrystalline corrosion.
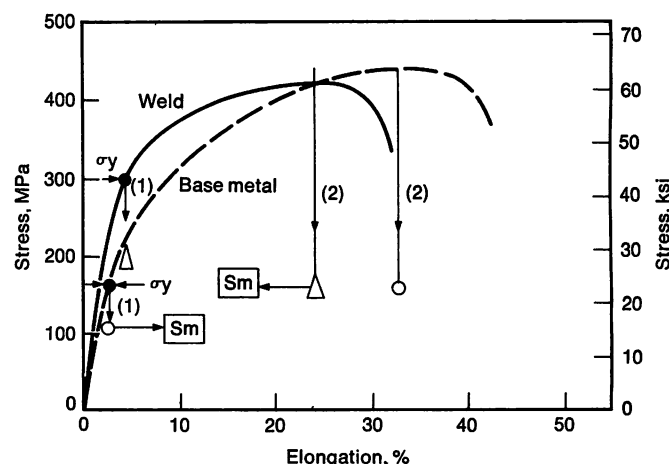


FIGURE 2—High temperature tensile behavior of typical weld metal.
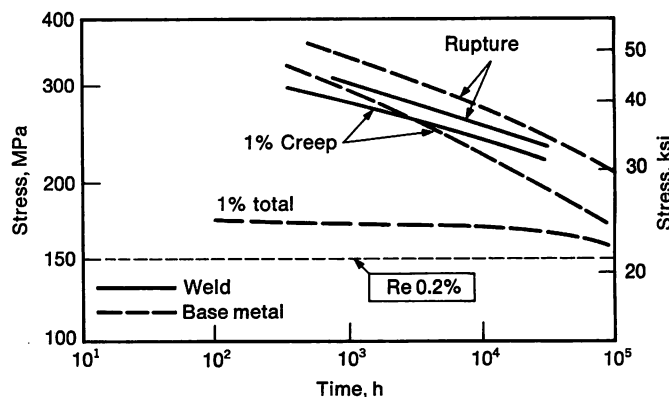


FIGURE 3—High temperature creep behavior of typical weld metal.

2. Adequate high temperature mechanical resistance.

3. Weldability, including absence of cracking at high temperature in the HAZ (limitation of the boron content for instance), compatability of the mechancial properties of filler metal and base metal.

4. Industrial experience.

Once the steel had been chosen according to these contradictory criteria, it was necessary to determine the allowable stresses ($S_{mt}$), creep equations, resistance to low cycle fatigue, effect of hold time, rules of accumulation of creep and fatigue and monotonic strain damage, crack propagation in fatigue, creep, etc.

It is not possible to deal with all of these points in detail, but two examples of problems treated will be developed which are more metallurgical in nature.

**Structural changes.** Complex precipitation sequences take place in austenitic steels over long periods at temperatures above 500 C (930 F). This leads to a degradation in the low temperature toughness measured by the fracture energy of U-notched bars. A large number of test results obtained after holding periods up to 50,000 hours are given in Figure 4.[1] In general, it was found that chromium equivalent should be limited to reduce embrittlement.

Moreover intergranular precipitation of $M_{23}C_6$ is responsible for sensitization to the intercrystalline corrosion likely to occur after long periods at 500 to 550 C (930 to 1020 F). This effect can be lessened by restricting the carbon content to 300 ppm, raising the chromium content and reducing the nickel content, but this upsets the balance of alpha/gamma elements needed to keep a certain low temperature toughness, hence the need to compromise.

Finally to maintain a high temperature strength equal to that of Type 316 steel in spite of the very low carbon concentration, some nitrogen is needed as well as a balance of alpha/gamma elements, here again not in favor of good toughness.

Table I shows the compromise we chose from these contradictory requirements (referred to as 316L SPH). The chemical composition ranges chosen were narrow but were satisfied without difficulty by the three European steelworks who supplied the plate for Super Phenix. A set of the compositional parameters is shown on a Pryce and Andrews diagram on which 0 and 1% ferrite are plotted (Figure 5). All the steelworks have tried to center their heats below the 0 ferrite line to reduce the problem of embrittlement.

It will be observed that the rectangle corresponding to the SPH specification lies inside a larger rectangle representing the steel used for the French PWR program and consequently cast in many heats, this experience having guided us in the definition of the closer SPH limits.

This choice of narrow specification ranges seems to have improved the scattering which, for tensile properties, is about half that of a Type 316 steel according to ASTM specification.

**Stress relief cracking.** This has been investigated extensively in the case of Nb austenitic steel (Type 347) because of incidents arising in operation of power plants in this country. Three factors are involved. They are presence of residual welding stresses, geometrical defects, and dissolution of MC type carbide in the HAZ during



$$P = \frac{-Q}{RT} + \log t$$

*FIGURE 4—Room temperature Charpy value for 316L.*

**Table I**—Specifications for 316L SPH Steel

**Chemical Composition, %**

| | | | |
|---|---|---|---|
| C | $\leq$ 0.030 | Mo | = 2.3/2.7 |
| Si | $\leq$ 0.50 | S | $\leq$ 0.025 |
| Mn | = 1.6/2.0 | P | $\leq$ 0.035 |
| Ni | = 12.0/12.5 | B | < 0.002 |
| Cr | = 17.0/18.0 | $N_2$ | = 0.06/0.08 |
| Co | $\leq$ 0.25 | Cu | $\leq$ 1.00 |
| Ta | $\leq$ 0.15 | | |

**Ferrite = 1%**

**Room Temperature Mechanical Properties**

| | |
|---|---|
| $Re_{0.2\%}$ | $\geq$ 220 MPa (32 ksi) |
| Rm | $\geq$ 525 MPa (76 ksi) |
| Elongation | $\geq$ 45% |
| KCU as-rolled $\begin{cases} e = 25 \text{ mm} \\ e = 25 \text{ mm} \end{cases}$ | $\geq$ 140 J/cm² (103 ft-lb/cm²)<br>$\geq$ 120 J/cm²  (88 ft-lb/cm²) |
| KCU 100 h—750 C (1380 F) | $\geq$ 100 J/cm²  (74 ft-lb/cm²) |

**Elevated Temperature Tensile Properties**

| | |
|---|---|
| at 450 C  (840 F), $Re_{0.2\%}$ | $\geq$ 120 MPa (17 ksi) |
| at 550 C (1020 F), $Re_{0.2\%}$ | $\geq$ 110 MPa (16 ksi) |
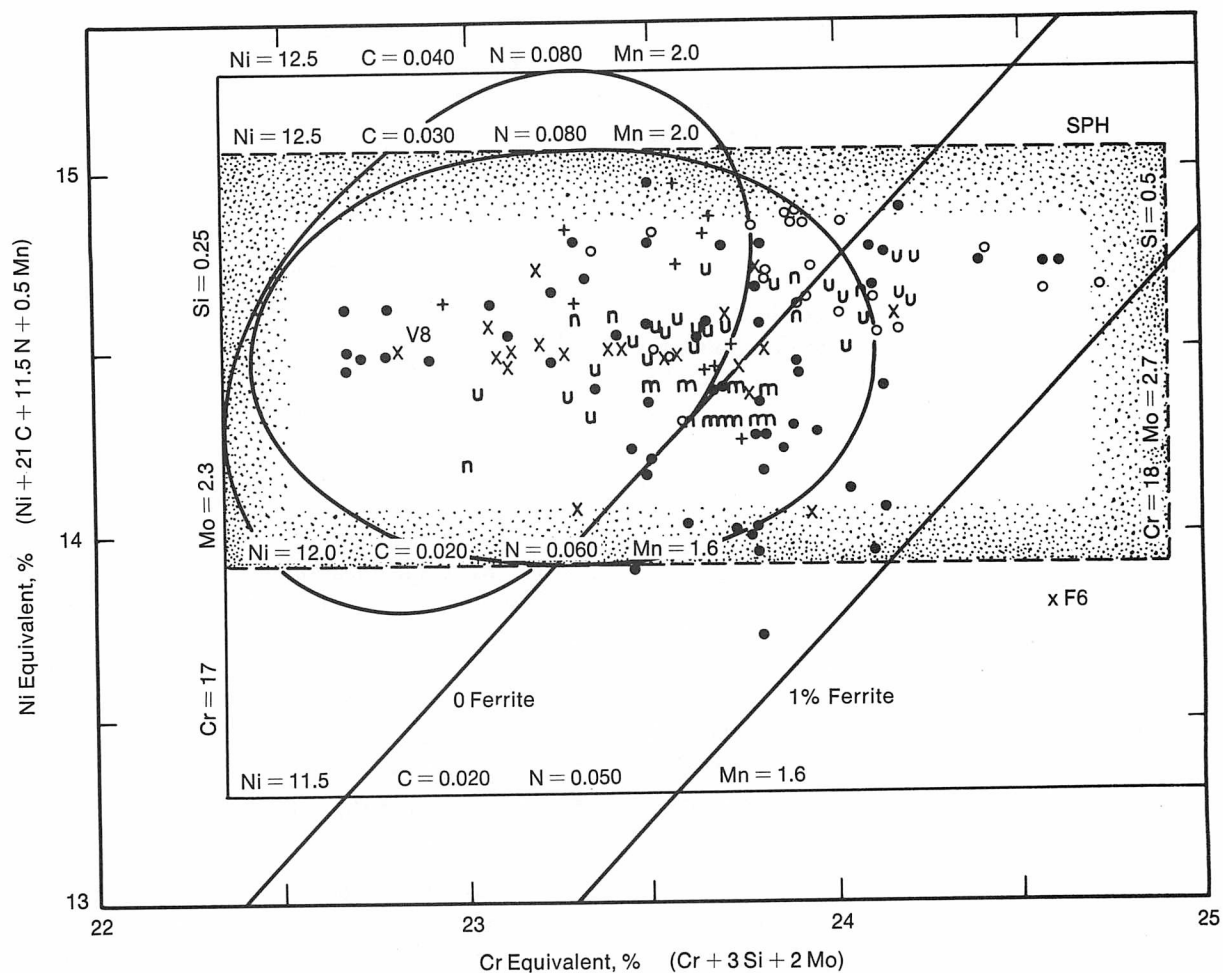
FIGURE 5—*Pryce and Andrews diagram for 316L SPH.*
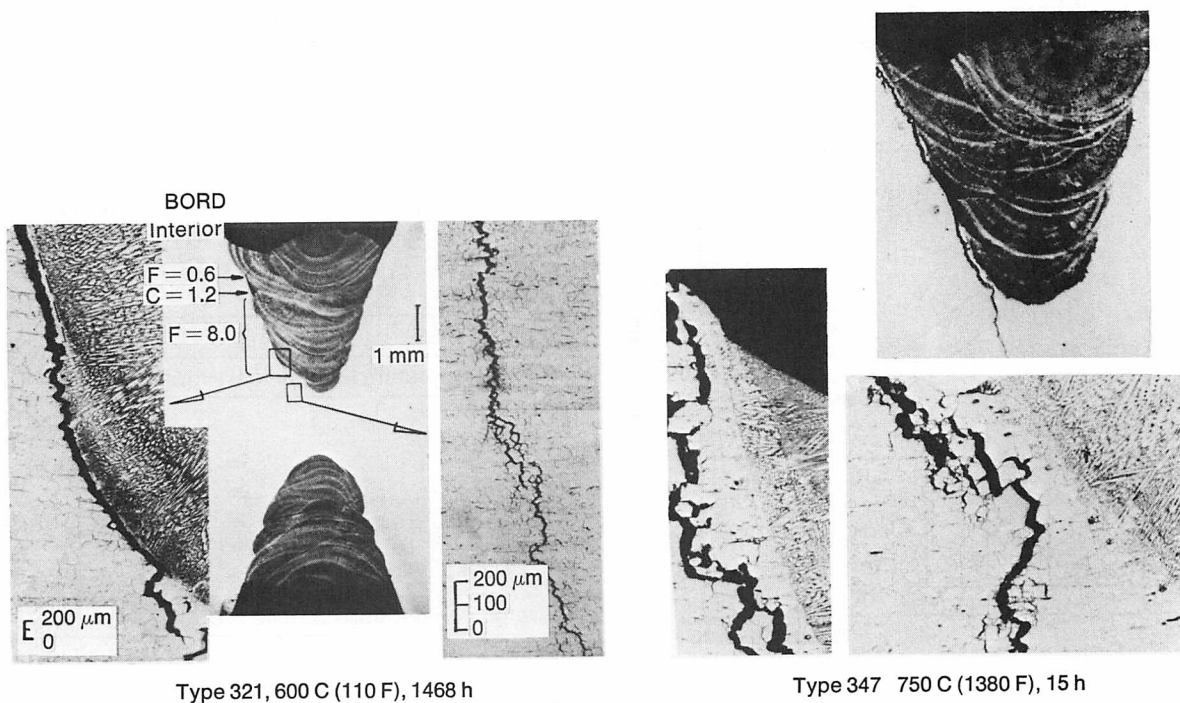


Type 321, 600 C (110 F), 1468 h

Type 347   750 C (1380 F), 15 h

FIGURE 6—*Stress reheat cracking of austenitic stainless steels.*
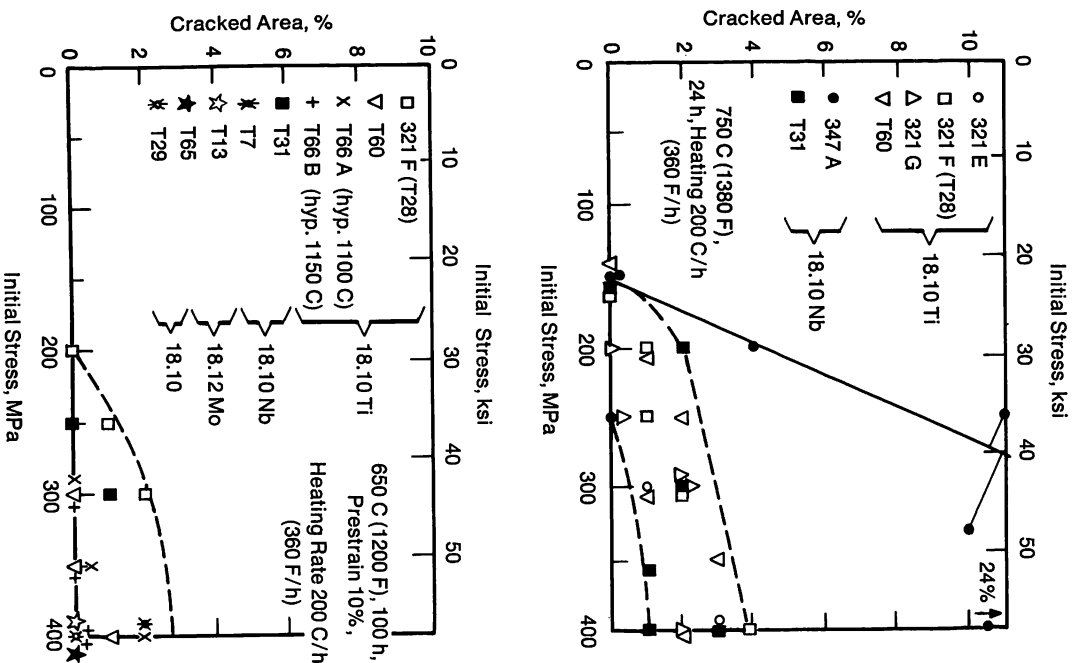
*FIGURE 7—Reheat cracking of austenitic steels; results of implants tests.*

welding and precipitation on stacking fault plates during stress relief treatment or in service. The latter causes considerable hardening of the matrix and localization of deformation at the grain boundaries giving intergranular rupture.

To meet the toughness and sensitization criteria, it was tempting to use a titanium stabilized steel, but there was a possible risk of cracking on reheating. The tendency toward this type of cracking was therefore studied by comparison with the SPH steel. Two methods were used. The first is based on a technique used by the BWRA.[2] An incompletely filled circular joint is made on a piece of metal to be tested. The filler metal is as refractory as possible (16-13 cobalt steel) so that the HAZ is under maximum stress. After a holding period between 600 and 800 C (1110 and 1470 F), the specimen is examined for crack formation under the bead. Figure 6 gives typical examples of results on Types 347 and 321.

With the second technique, based on the implant method developed by Granjon of the French Welding

**Table II**—Comparison of Some Characteristics of Sodium-Cooled Fast Breeder Reactors

| Reactor | | BN 350 USSR 1973 (350 MW) | Phenix France 1973 (250 MW) | PFR GB 1974 (250 MW) | SNR RFA (282 MW) | BN 600 USSR (600 MW) | Super Phenix France (1200 MW) | Clinch River USA (350 MW) |
|---|---|---|---|---|---|---|---|---|
| Tube Material | Evaporator | 2¼ Cr-1 Mo | 2¼ Cr-1 Mo 2¼ Cr-1 Mo-1 Nb | 2¼ Cr-1 Mo-1 Nb | 2¼ Cr-1 Mo-1 Nb | 2¼ Cr-1 Mo | Alloy 800 | 2¼ Cr-1 Mo |
| | Superheater | 2¼ Cr-1 Mo | 18-10 Ti (321) | 18-10 Mo (316) | 2¼ Cr-1 Mo-1 Nb | 18-10 (304) | Alloy 800 | 2¼ Cr-1 Mo |
| Sodium Temperature, C (F) | Enter | 455 (850) | 550 (1020) | 530 (990) | 520 (970) | 515 (960) | 525 (980) | 500 (940) |
| | Exit | 275 (520) | 350 (660) | 370 (700) | 375 (710) | 320 (610) | 345 (650) | 345 (650) |
| Water Temperature, C (F) | Enter | 160 (315) | 245 (475) | 290 (550) | 255 (490) | 240 (465) | 235 (455) | 230 (450) |
| Steam | Exit Temperature, C (F) | 380 (715) | 510 (955) | 515 (960) | 500 (930) | 505 (940) | 490 (915) | 480 (900) |
| | Pressure, KPa (psi) | 4000 (580) | 16,800 (2440) | 16,600 (2400) | 16,650 (2410) | 16,000 (2320) | 18,400 (2670) | 10,200 (1480) |

**Table III**—Steels Considered for Tubes for Fast Breeder Reactors

| Grade | Treatment | C | Si | Mn | P | S | Cr | Ni | Mo | Ti | Al | V | Nb | B | Cu |
|---|---|---|---|---|---|---|---|---|---|---|---|---|---|---|---|
| 10 CD 9.10 | 925/975 C (1695/1785 F) AC | ≤ | 0.10 | 0.30 | ≤ | ≤ | 2.0 | — | 0.9 | — | — | — | — | — | — |
| 2¼ Cr-1 Mo | plus 650-775 C (1200-1425 F) | 0.15 | 0.50 | 0.60 | 0.03 | 0.03 | 2.5 | — | 1.1 | — | — | — | — | — | — |
| 10 CD Nb 9.10 | 970/1030 C (1780/1885 F) AC | ≤ | 0.15 | 0.40 | ≤ | ≤ | 2.0 | 0.3 | 0.9 | — | — | — | ≧ | — | — |
| 2¼ Cr-1 Mo-1 Nb | plus 680-750 C (1255-1380 F) | 0.10 | 0.50 | 0.80 | 0.02 | 0.02 | 2.5 | 0.8 | 1.1 | — | — | — | 10xC | — | — |
| Z 10 CD 9 | 900/1000 C (1650/1830 F) AC | ≤ | 0.25 | 0.30 | ≤ | ≤ | 8.0 | — | 0.9 | — | ≤ | — | — | — | — |
| 9 Cr-1 Mo | plus 700-800 C (1290-1470 F) | 0.15 | 1.00 | 0.60 | 0.03 | 0.03 | 10.0 | — | 1.1 | — | 0.02 | — | — | — | — |
| Z 10 CD Nb-V 9.2 | 1050/1125 C (1920/2055 F) AC | ≤ | 0.20 | 0.80 | ≤ | ≤ | 8.5 | — | 1.7 | — | — | 0.2 | 0.30 | — | — |
| 9 Cr-2 Mo-Nb-V | plus ~775 C (~1425 F) | 0.15 | 0.65 | 1.30 | 0.03 | 0.03 | 10.5 | — | 2.3 | — | — | 0.4 | 0.55 | — | — |
| Z5 NC 35-20 | 980 ± 20 C (1795 ± 35 F) | 0.03 | ≤ | ≤ | — | ≤ | 19 | 30 | — | 0.15 | 0.15 | — | — | — | ≤ |
| Alloy 800 | Rapid Cooling | 0.06 | 1.0 | 1.5 | — | 0.015 | 23 | 35 | — | 0.60 | 0.60 | — | — | — | 0.75 |
| Z6 CNT 18-12 B | 1075-1125 C (1965-2055 F) | 0.04 | ≤ | ≤ | ≤ | ≤ | 17 | 10 | — | 4xC | — | — | — | 0.001 | — |
| 18-10 Ti (321) | Rapid Cooling | 0.08 | 1.0 | 2.0 | 0.04 | 0.03 | 19 | 13 | — | 0.60 | — | — | — | 0.006 | — |

Insitute,[3] steels are compared on a more quantitative basis on graphs of the kind shown in Figure 7, where cracking is plotted against initial applied stress after reheating the implant.

From this investigation, it emerged that Type 321 steels behave better on reheating than Type 347 steels but tend to crack nevertheless. No such phenomenon was ever observed for 316 and 316L. The use of 321 for this kind of application has therefore been delayed.

## Steam Generator Exchange Tube

Owing to the risk of reaction between sodium and water, the steam generators of sodium-cooled fast neutron reactors are generally considered to be one of the most critical parts of the installation. To the general selection criteria already mentioned must be added specific criteria connected with problems of corrosion in water and sodium should a sodium reaction occur.

Taking these various criteria together, it appears that no material meets the standards required to make it the obvious choice. This is shown by the wide variety of materials chosen for steam generators of working or planned fast reactors throughout the world (Table II).[4] Those used or contemplated are mainly ferritic steels (2¼ Cr-1 Mo, niobium stabilized or not, 9 Cr-1 Mo and 9 Cr-2 Mo-Nb-V, austenitic steels of the 18-10 family, or 35 Ni-20 Cr alloy, Alloy 800). Table III lists the compositions of these various alloys.

With respect to the above criteria, each of these materials possesses different properties which must be known exactly when the choice is made for a given project, a choice liable to restrictions on the specified composition range and subject to extra requirements where the thermomechanical treatment of the tubes is concerned. Such an evaluation requires numerous studies and close collaboration among the laboratories of the organizations concerned. For this purpose, a Working Group on fast reactor plant materials was founded in 1969 by Electricité de France and the Commissiariat à l'Energie Atomique. Steel plants, builders and more recently tube manufacturers have been closely associated with this enterprise and have taken part in the joint development studies. The ideas summed up here on materials for steam generator tubes, deduced from the many results of French and foreign laboratories, are the fruits of this collaboration.

**Availability and experience.** Some of these steels are widely used in similar applications such as steam generators and superheaters in conventional power stations and in various heat exchangers. This industrial background is a guarantee against difficulties that cannot always be anticipated from laboratory work which is restricted to a limited number of casting grades tested under conditions that cannot always be made representative. For example, test times are shorter than those planned for the plants themselves.

This is the case for 2¼ Cr-1 Mo steels which are extensively used in many countries. The niobium stabilized grade is more recent and not as fully developed as the previous grade. It has only been used in a small number of applications such as the evaporator tubes in the Phenix and PFR reactors. It also may not be readily available.

Alloys 9 Cr-1 Mo and 9 Cr-2 Mo-Nb-V have been widely used for superheaters in conventional power stations. The latter steel was chosen for superheaters operating at temperatures of about 600 C (1110 F) in some twenty French power stations. It is worth noting that the only incidents experienced with these tubes have been attributed to excessive local temperatures resulting from improper adjustment of the burners or to the steam cycle.

Austenitic steels, 18-10, 18-10 Ti, 18-10 Mo, are extensively used as materials for superheaters, and they are readily available when their specifications comply with the various standards. Alloy 800 in its present form is a more recent development. Because of its mechanical properties and corrosion resistance in a variety of media, it has been adopted or considered for a number of applications, in particular for steam generator tubes in pressurized water of high temperature nuclear reactors. However, each type of application has its own requirements. Although operating experience with sodium/water exchangers at 550 C (1020 F) is negligible, a considerable amount of development work has been carried out with this alloy in recent years, and there are abundant laboratory data on many casting compositions. There is no particular difficulty with respect to supply.

**Mechanical properties of tubes at high temperature.** This is an essential criterion because of high primary stresses. The allowable stresses of candidate alloys, established on the same basis, are plotted against temperature in Figure 8. These curves show that at elevated temperatures, for instance 550 C (1020 F), allowable stresses for 2¼ Cr-1 Mo and 9 Cr-1 Mo steels are very low compared with those for 9 Cr-2 Mo-Nb-V and the austenitic steels. These stresses are considered too low for steam generators designed for use with sodium at elevated temperatures (in the vicinity of 540 C, 1005 F). These materials could only be used for the exchanger unit, superheater included, if the highest temperature did not exceed some 500 C (930 F). For elevated temperatures, the superheater must be either in an austenitic alloy (Alloy 800, which could also be used for the economizer-evaporator, or 18-10 which would only be used for the superheater because of corrosion in the evaporator) or in steel 9 Cr-2 Mo-Nb-V with a ferritic-martensitic structure.

As for the vessel, the stainless steels selected will be preferably grades 18-10 stabilized with titanium or low carbon Type 316 to ensure good creep resistance
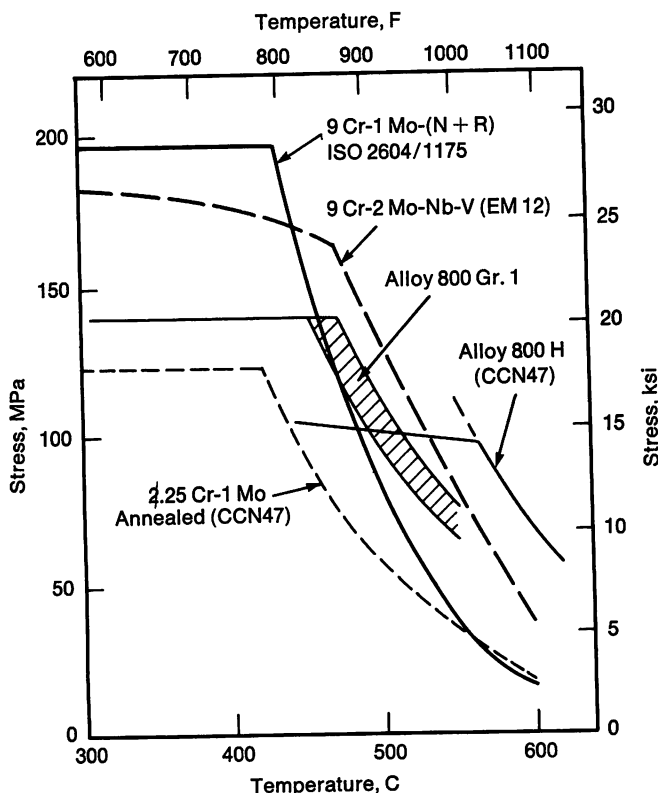


FIGURE 8—Allowable stresses for candidate steam generator tube materials.
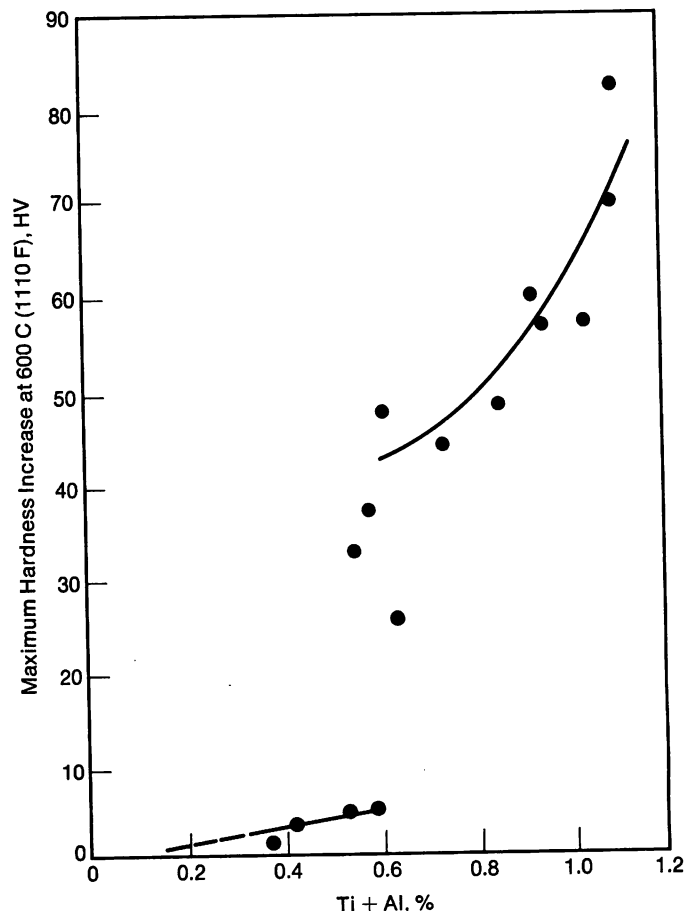


FIGURE 9—Hardening of Alloy 800 with γ′ precipitation.
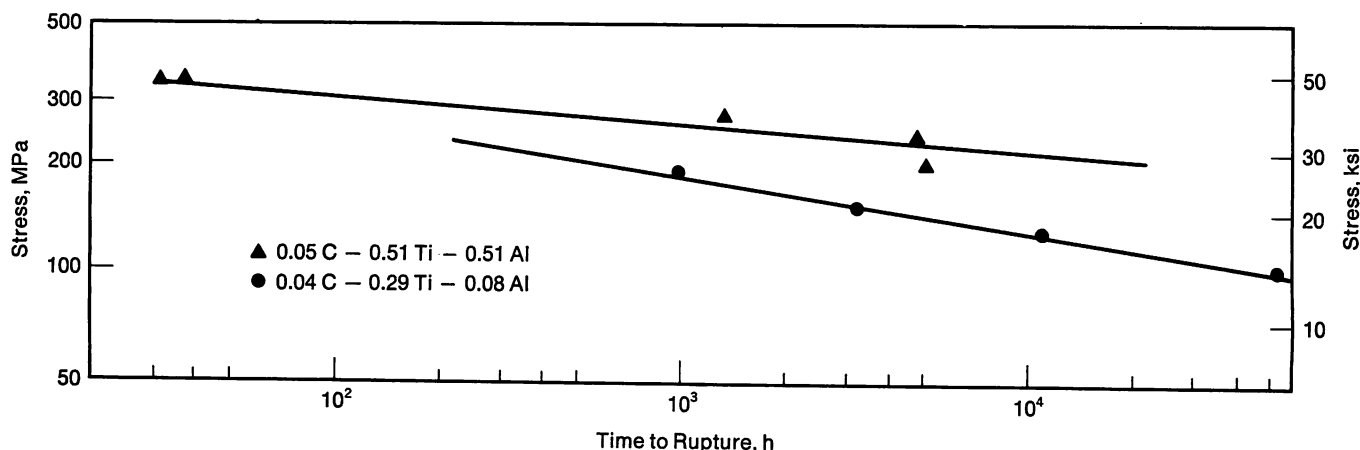
FIGURE 10—Effect of Ti + Al on creep strength of Alloy 800 Grade 1.
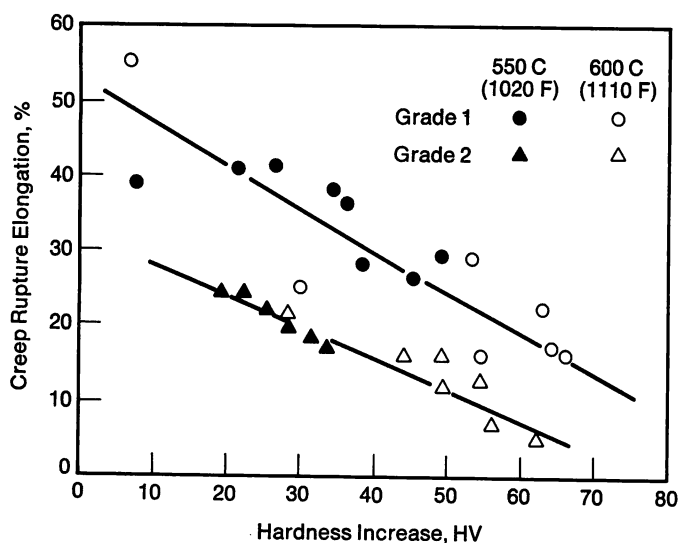


FIGURE 11—Effect of hardening by $\gamma'$ precipitation on creep ductility of Alloy 800 and 800 H.

and prevent or reduce chromium depletion at the grain boundaries (sensitization to intergranular corrosion) which may occur during welding or in service.

The optimum chemical composition of steel 316L SPH (Table I) chosen for the vessel and the structures operating at elevated temperatures in Super Phenix appears to satisfy this dual requirement, and at the same time does not result in embrittlement in service.

Alloy 800 has variable mechanical properties depending on chemical composition and final heat treatment. Because of these variations, ASTM has defined two grades, 1 and 2, differing essentially in the temperature of the final heat treatment.

Grade 1, which is annealed at a lower temperature (980 C, 1795 F), has better mechanical properties below 550 C (1020 F) than Grade 2 which is solution annealed at (1150 C, 2100 F) and intended for applications above 550 C (1020 F). Recent terminology now distinguishes between Alloy 800, the former Grade 1, and Alloy 800 H intended for applications where creep occurs which must satisfy additional requirements (C > 0.05% and grain

size < 5 ASTM). This paper deals only with Grade 1 but draws attention to the fact that the more complete resolutioning of the carbides in the weld affected zones modifies the properties considerably to approximately those of Grade 2.

Note that the ASME Code, in Code Case N 47, only considers Alloy 800 H and not Alloy 800, Grade 1.

It is now well established that the good high temperature properties of Alloy 800 in the temperature range under consideration is the result of precipitation of the $\gamma'$ phase, $Ni_3$ (Ti, Al).[5] Figure 9, taken from the works of Persson and Egnell,[6] confirms that the alloy undergoes a hardening that is directly related to its titanium and aluminium contents. Counteracting its beneficial effect on creep resistance (Figure 10), this hardening considerably lowers creep ductility, whereas instantaneous ductility is practically unmodified by the presence of the $\gamma'$ phase. Figure 11 shows that fracture elongations may be less than 5%, especially in the case of Grade 2 (similar values seem to be obtainable with Grade 1, and even lower values may be achieved with products that have been previously cold worked). Attempts were then made with a view to limiting the Ti and Al contents to improve ductility without excessively diminishing creep resistance. The starting point of these investigations was the curves of the type shown in Figure 9. The best policy would seem to be to use Alloy 800, where the precipitation of the $\gamma'$ phase can be put to advantage, while ensuring against the risk of low ductility by a detailed calculation of the deformation of the most highly stressed zones (thermal sleeves, for instance) and by meticulous fabricating processes (quality of the welds in particular).

This led to more restrictive composition ranges for titanium and aluminium in the Alloy 800 considered for Super Phenix (Ti = 0.30-0.50%, Al = 0.10-0.25%) while Ti + Al had to be higher than 0.55% to ensure the beneficial effect of the $\gamma'$ phase on creep resistance.

Many tests have been carried out in the approval procedure for the 9 Cr-2 Mo-Nb-V steel for superheater tubes in French Electricity Board Thermal Power Sta-

tions. As a result, its creep properties at 550 and 600 C (1020 and 1110 F) are now well known.

A knowledge of the low cycle fatigue resistance at high temperature of the steels used in steam generators is essential considering the conditions under which they must operate. Operating temperatures are high, heat fluxes considerable and several transient operating states occur. In addition, sodium, which has an excellent heat exchange coefficient, transmits any of its temperature fluctuations to the tube wall. In the presence of a combination of sodium flows at different temperatures under unfavorable hydraulic conditions, the metal may be subjected to a much greater number of fatigue cycles than those due simply to the closing down and starting up of the plant, which can generally be forecast quite accurately. It is consequently advisable to take creep into account when analyzing fatigue in steam generators. Apart from computation difficulties, one of the main difficulties here is the lack of fatigue data for temperatures above 400 C (750 F). For instance, Code Case N 47 of the ASME Code Section III provides no information on most of the materials under consideration here, and the only available curves refer to 18-10 steels, with and without molybdenum, and to Incoloy 800 H.

As a result, the EDF/CEA Work Group undertook an extremely well-implemented research program which first provided results on 18-10 molybdenum steel with low carbon and the corresponding weld filler metal.[7] For steam generator materials and the associated weld filler metals, the test program in progress on Alloy 800 and planned on ferritic steels should provide results to enable the determination of curves of low cycle fatigue resistance and cyclic consolidation and an influence of the frequency or the duration of the cycles with respect to stresses. From the results of all these tests, it should be possible to reasonably extrapolate the actual operating conditions in service.

In calculating the stresses on the tubes, it is generally considered that the effect of sodium on mechanical properties of the materials should be taken into account, for instance embrittlement by the liquid metal. However, results obtained to date by different laboratories are not in accord. They do show, however, that there is no risk of embrittlement by liquid metals, the effect noted on certain mechanical properties being the result of carburization or decarburization. The purity of the sodium is in fact one of the primary factors in these tests, and this does not facilitate the experimental work.

In creep tests on Alloy 800, the life of the material appears to be decreased in a sodium environment and the fracture ductility lowered, but only at temperatures above 650 C (1200 F) according to some authors.[8, 9] Sodium would also appear to have an unfavorable effect on the occurrence of tertiary creep at 550 C (1020 F) with stainless steels,[10] but other authors claim that sodium has a favorable effect on the life of these steels at 700 C

(1290 F).

For the fatigue resistance of austenitic steels, sodium appears to increase the number of fracture cycles at 500 C (930 F) for steels 18-10 and 18-10 Mo, but to have apparently the opposite effect for 18-10 steel in the case of considerable plastic deformations if the sodium is very pure.[7]

Further tests in large test loops are under way in several laboratories to clarify these points.

**Sensitization.** In the same way as the steels used for the vessel, the stainless steels for the Super Phenix tubing should stand up well to the standardized tests used to detect chromium depletion at the grain boundaries (sensitization to intercrystalline corrosion). Any stainless steel considered for the superheater would need to comply with the same requirement.

An identical phenomenon is likely to occur with Alloy 800 by precipitation of $Cr_{23}C_6$ at the grain boundaries. However, with this alloy, the quantity of free carbon that can precipitate in service is generally much lower than the carbon content of the alloy, since the final heat treatment at 980 C (1795 F) cannot dissolve the intergranular carbides precipitated during earlier heat treatments. The sensitivity region of the time/temperature diagram is therefore very limited and is more dependent on the temperature of the final heat treatment than the total carbon content. Chromium depletion can be detected by a test in boiling copper sulfate solution identical to that used for 18-10 stainless steels.[11]

A traditional heat treatment of 30 minutes at 700 C (1290 F) followed by cooling at a rate of 60 C/hour (110 F/hour) can also be used with Alloy 800 to detect any large amount of carbon in solution. As for 18-10 steels, this test should not be considered as an accelerated test on susceptibility in service but as a test to guarantee the good homogeneity of the chromium content, the lack of anomalies in the heat treatment of the tubes or of accidental contamination by carbon. However, during welding, solution of carbon and the grain growth which will occur in the heat affected zone will greatly increase tendency toward sensitization. This sensitization of zones affected by welding can be limited by a relatively low total carbon content (0.03 to 0.06%), an appropriate titanium content, a good welding technique ensuring very narrow heat affected zones and, if necessary, heat treatment of the welds to precipitate the titanium carbides.

**Weldability and properties of welded joints.** Austenitic steels such as 18-10 stainless steels and Alloy 800 for steam generator tubes are generally considered to have good welding properties provided certain precautions are taken.

The weldability of ferritic steels is generally considered to present more problems than austenitic steels since more precautions must be taken, and heat treatments are often necessary to prevent hydrogen cracking.

Slow cooling (preheating) and stress relieving treatments are often required to normalize the structure of the heat affected zones or restore toughness.

Nevertheless the welding of 2¼ Cr-1 Mo steel can be carried out under good conditions, and the behavior of the welds in service is satisfactory as extensive experience proves. The niobium stabilized grade also has good weldability, but the welds and heat affected zones show some niobium carbide eutectic films[12] which have often been accused of affecting the risk of fracture in service (due to fatigue in particular). No proof of their possible harmful influence has ever been put forward.[13] With respect to the metal flux weld, these eutectics have a beneficial "self-healing" effect on high temperature cracking,[14] but the range of C and Nb contents for which this effect can occur is as yet unknown. Finally, it must be noted that the weld affected zones of 2¼ Cr-1 Mo-Nb steel have a relatively high transition temperature (about 150 C, 300 F) with no possibility of normalizing by stress relieving treatment.

Some additional welding problems arise with the 9 Cr-2 Mo-Nb-V steel because of its extreme hardenability which requires preheating and stress relieving. However this last operation is facilitated by the good behavior of the material with respect to cracking on reheating. There may nevertheless be a risk of cracking at high temperatures when welding without filler metal or with a filler metal having the same composition as the base metal. This effect is also visible for 2¼ Cr-1 Mo-Nb-V steel. The fact that the 9 Cr-2 Mo-Nb-V steel is used successfully in a large number of superheaters in traditional power plants shows that these problems can be mastered.

**Decarburization of ferritic steels.** The decarburization of certain ferritic steels in sodium was considered a major obstacle to their use at elevated temperatures. Steels such as 2¼ Cr-1 Mo in particular are subject to decarburization with subsequent deterioration of mechanical properties. Again, the carbon may be transferred by the sodium to the parts in austenitic stainless steels such as the intermediate exchanger and modify their ductility appreciably. Many investigations have dealt with the kinetics and mechanism of this carbon transfer.

By grouping the data obtained over periods of some thousand of hours, Krankota and Armijo[15] were able to

plot the decarburization constants for 2¼ Cr-1 Mo versus temperature (Figure 12).

Assuming that decarburization obeys simple diffusion laws, the use of this curve shows that, up to 500 C (930 F), decarburization should remain low. In fact, experiments in test loops[16] have shown that carbon transfer between the economizer-evaporator part of Phenix (475 C, 885 F maximum) and the austenitic steel tubes of the intermediate exchanger and the superheater was extremely limited and presented no risk.

For long periods at higher temperatures, the simple diffusion hypothesis is not sufficient to define the behavior of 2¼ Cr-1 Mo steel. As shown in Table IV, the decarburization constants may be very different for steels
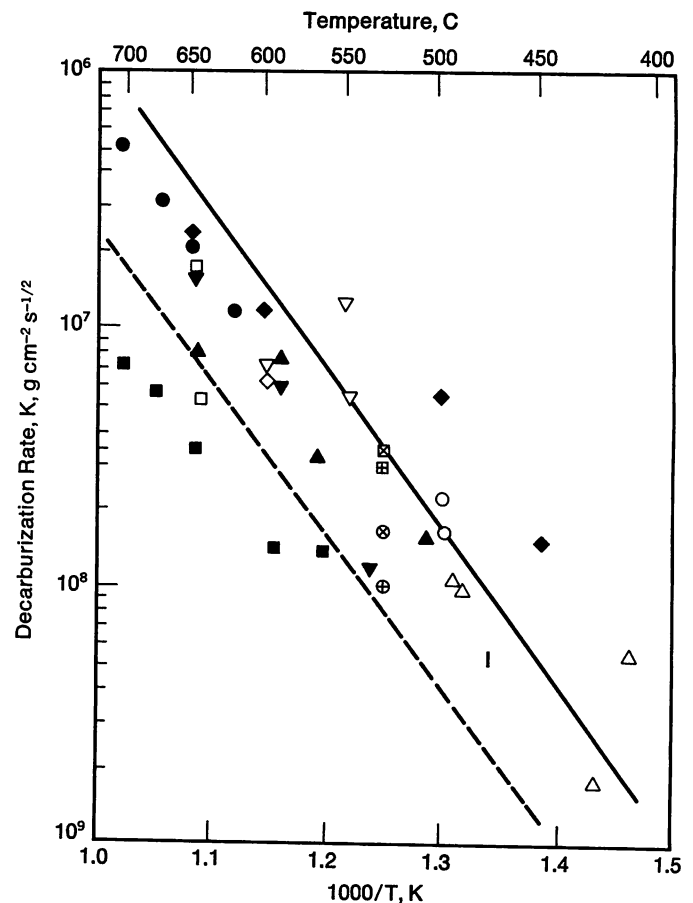


*FIGURE 12—Decarburization constants for 2¼ Cr-1 Mo steel as a function of temperature.*

**Table IV**—Decarburization Constants (g cm$^{-2}$ s$^{-½}$) for 2¼ Cr-1 Mo Steel at 530 C (985 F)

|  | 3300 h | 6000 h | 9300 h |
|---|---|---|---|
| Tube 1, 925 C (1695 F) plus 675 C (1245 F) Principal carbide: $Fe_3C$ | $3.77 \times 10^{-8}$ | $3.32 \times 10^{-8}$ | $3.11 \times 10^{-8}$ |
| Tube 2, 980 C (1795 F) plus 700 C (1290 F) Principal carbides: $M_{23}C_6$-$Mo_2C$ | $1.66 \times 10^{-8}$ | $1.14 \times 10^{-8}$ | $1.11 \times 10^{-8}$ |
| Plate, 925 C (1695 F) plus 710 C (1310 F) Principal carbides: $M_{23}C_6$-$Mo_2C$ | $1.07 \times 10^{-8}$ | $1.01 \times 10^{-8}$ | $0.94 \times 10^{-8}$ |

tempered at different temperatures, and they also decrease with time. This may be explained by the fact that the carbon loss kinetics are governed by the decomposition of carbides present in more or less stable forms.[17-19] Different tempering temperatures may produce different carbides, as shown on Figure 13, thereby modifying decarburization kinetics. On the other hand, the transformation of unstable carbides at operating temperatures into more stable carbides may explain the decreasing rate of carbon loss.[18]

Therefore, it seems that, subject to a suitably selected heat treatment and a rather low initial carbon content (C = 0.07%), these steels could be used at a temperature close to that at which their use is precluded due to their low creep resistance. If such is the case, the interest in 2¼ Cr-1 Mo-Nb steel, which does not decarburize in sodium at these temperatures, would be slight, considering the apparently lower strength of this steel at elevated temperatures compared with the nonstabilized steel and the doubts remaining with respect to the properties of the welds and the problems of its supply.

**Corrosion.** In the water/steam circuit under normal operating conditions, the first preventive action against the risk of corrosion consists of following general rules on the operation of steam generators. In the first place, it is essential to control the purity of the process water. 18-10 stainless steels cannot be used for the evaporators of single throughput systems because of their susceptibility to stress corrosion when chlorides are concentrated in the evaporation zones. On the other hand, Alloy 800, because of its higher nickel content, reacts well to stress corrosion in a chloride-containing medium. In superheated steam, Alloy 800 could be affected by intergranular corrosion in the case of extreme chromium depletion at the grain boundaries.[20]

The kinetics of generalized corrosion must be known
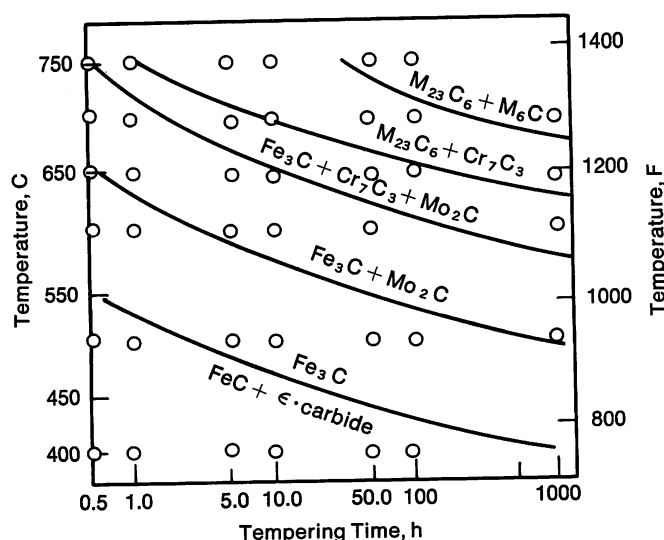
to calculate the extra thickness needed for the tubes. Generally corrosion rates have been determined under isothermal conditions. While they are very low in water for austenitic stainless steels, they increase at a rapid linear rate for low alloy ferritic steels. The slope of the line is highly dependent on the circulating velocity of the water and the temperature.[21] In superheated steam, oxidation kinetics are parabolic under isothermal conditions. For tubes subjected to a thermal flux and therefore temperature fluctuations, a greatly increased corrosion rate is possible for low alloy ferritic steels. [22]

General corrosion of low alloy steels, even if it presents no risk for the material, is a serious handicap in operating the reactor. The hydrogen formed by oxidation of the steel by water diffuses either totally or partially toward the sodium. This hydrogen accumulates in the form of sodium hydrides in the cold traps which must therefore be large or easily regenerated. Moreover the leak detectors which measure the hydrogen that is released in the case of a sodium/water reaction have a high background noise, which may diminish their sensitivity.[23]

The curves of Figure 14 show the reduction in the quantities of hydrogen diffusing toward the sodium in the three loops of Phenix.[24] These quantities stabilize, after 400 to 800 equivalent days at full power, at a value corresponding to a corrosion rate of 0.2 mg $dm^{-2}h^{-1}$. The corrosion rate of the superheater in stainless steel is taken to correspond to a law of the type $M^2 = 22\ t$ at 500 C (930 F) (in mg $dm^{-2}$, t in hours),[25] which corresponds to a negligible corrosion rate after 300 days compared with the corrosion of the economizer-evaporator parts in ferritic steel. These values are in good agreement with the anticipated mean values.

In the event of leakage, the formation of sodium hydroxide in the circuits produces a much more corrosive media, which means that the behavior of the materials must be studied over the whole concentration range from pure sodium to water (pure steam).



FIGURE 13—Successive carbides through the tempering of quenched 2¼ Cr-1 Mo steel.
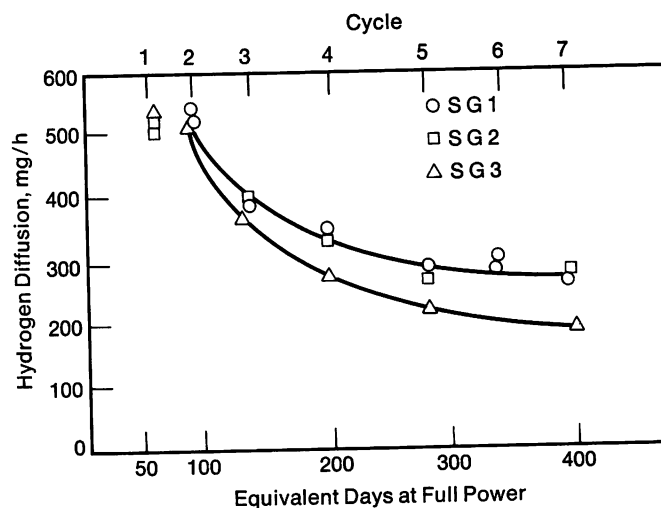


FIGURE 14—Hydrogen diffusion through steam generator tubing of Phenix Plant.

It is, in fact, possible that a relatively violent sodium/ water reaction will enable a certain quantity of sodium to penetrate the water/steam circuit. The concentration of sodium hydroxide in this circuit may be very high during a short time corresponding to the draining and cleaning of the loop after the incident.

In sodium hydroxide solutions, ferritic steels such as 2¼ Cr-1 Mo only experience cracking corrosion under very high stresses and generally at low temperatures.[26] These conditions seem very improbable in practice, and any general corrosion that may occur appears less dangerous during short contamination periods, in particular since it should be attenuated if hydrogen formed by the oxidation reaction diffuses toward the sodium, which is the case here.[27]

On the contrary, austenitic steels are sensitive to stress corrosion in a caustic environment. This sensitivity depends for each alloy on the concentration of sodium hydroxide in the solution and on the applied stresses.[28]

The curves in Figure 15 define the cracking corrosion region for 500 hours at 350 C (660 F) for Alloy 800 and 18-10 Mo steel. Stresses greater than 120 MPa (17.4 ksi) are necessary to crack Alloy 800 in 500 hours in a 50% concentration medium which is considered the most corrosive for this alloy. On the other hand, 18-10 steels crack rapidly at low stresses in a much wider concentration range.

When water or steam penetrates the sodium, the sodium/sodium hydroxide medium may also give rise to intergranular stress corrosion of austenitic steels and Alloy 800.[29]

The curve in Figure 16 shows the corrosion region for Alloy 800 at 500 C (930 F) at 500 hours. The associated risk depends on the possibility of maintaining locally high NaOH concentrations in Na for a long period, which is doubtful. At 350 C (660 F), no cracking occurs, even at

high stresses and prolonged periods.

Steel 2¼ Cr-1 Mo in sodium plus 10% sodium hydroxide suffers a very low loss in weight at 350 C (660 F) and a loss of approximately 60 mg cm$^{-2}$ in 500 hours at 550 C (1020 F). Steel 9 Cr-2 Mo-Nb-V suffers a loss in weight some 3 or 4 times greater under the same conditions, which is explained by the harmful influence of the chromium in this environment. However, the decrease in thickness is not a problem for contaminations of short duration. A rapid and complete purification of the sodium after a sodium/water reaction is essential to prevent considerable corrosion of all the materials, and above all, stress corrosion of austenitic steels if the stresses exceed thresholds of the order of those indicated in Figures 15 and 16. Pressure stresses are generally higher than this threshold for 18-10 Ti steel, but less for Alloy 800. However, to evaluate the stress level of the external and internal skin of the tube, both residual stresses and thermal stresses and their stress relief in service must be analyzed. Total and partial stress relieving of residual stresses in austenitic alloy bundles may be considered advisable.

The different behaviors of ferritic and austenitic steels in these media also give rise to different development processes of small leaks in exchanger tubes.[30] A small crack creating a contact between the sodium and the water or steam will widen under the effect of general corrosion of the metal in the crack for a ferritic steel. The edges of the crack on the water side have a tendency to be clogged by magnetite, then to be unclogged by reaction with the sodium when it is purified by diffusion of the sodium hydroxide (Figure 17a).

With 18-10 austenitic steels and Alloy 800, intergranular corrosion of the metal in the crack occurs which can lead to rapid unclogging of the embrittled part without any detection of the sodium reaction (Figure 17b). However, although the development processes are different for the two types of material, the important factor is the knowledge of the kinetics to detect any small leaks
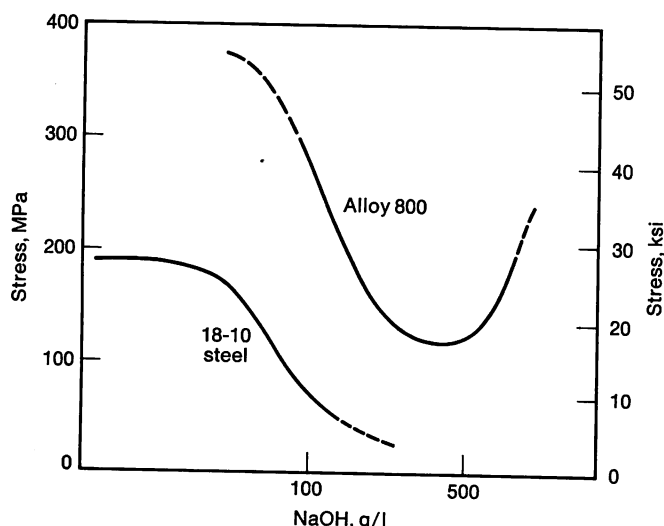


FIGURE 15—Stress corrosion cracking in caustic solutions at 350 C (660 F).
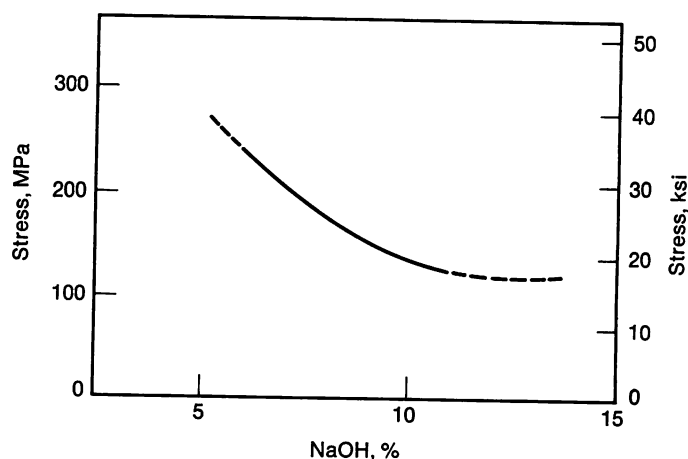


FIGURE 16—Stress corrosion cracking of Alloy 800 in Na-NaOH solution (500 h at 550 C, 1020 F).

(75 X)                    (50 X)                    (200 X)

a                        b                         c
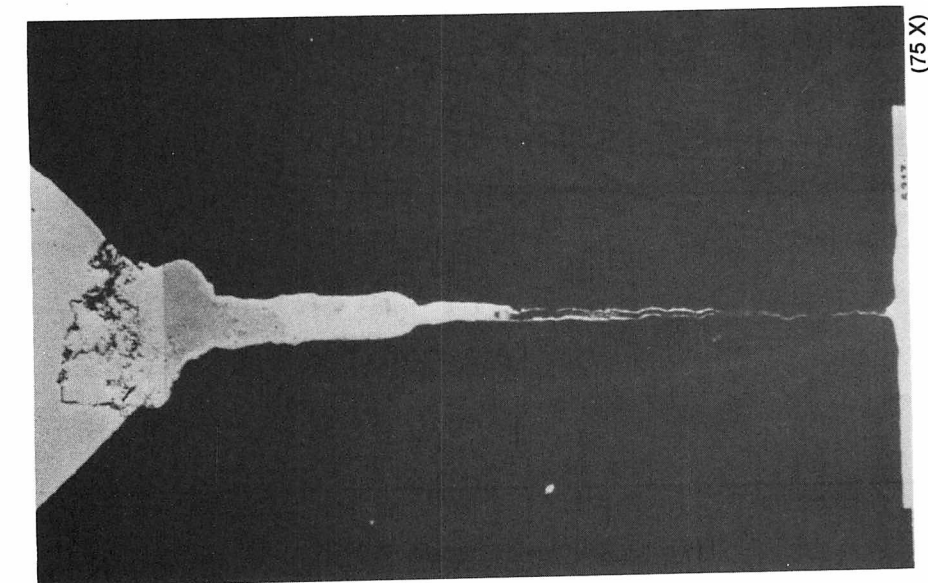
Microwastage test with a through-thickness fatigue     Same for 316 tube.     Stress corrosion on Alloy 800 in Na + 10% NaOH.
crack on 2¼ Cr-1 Mo steel tube.
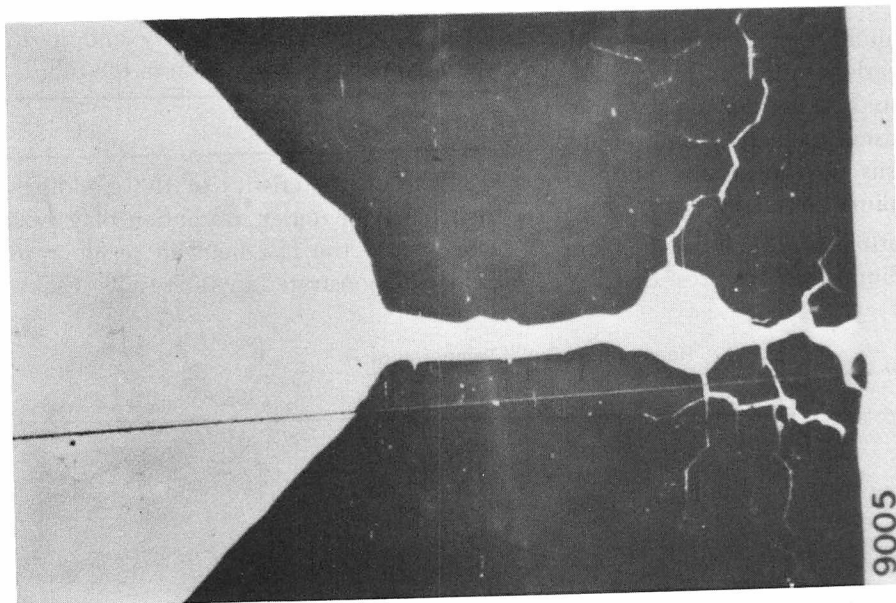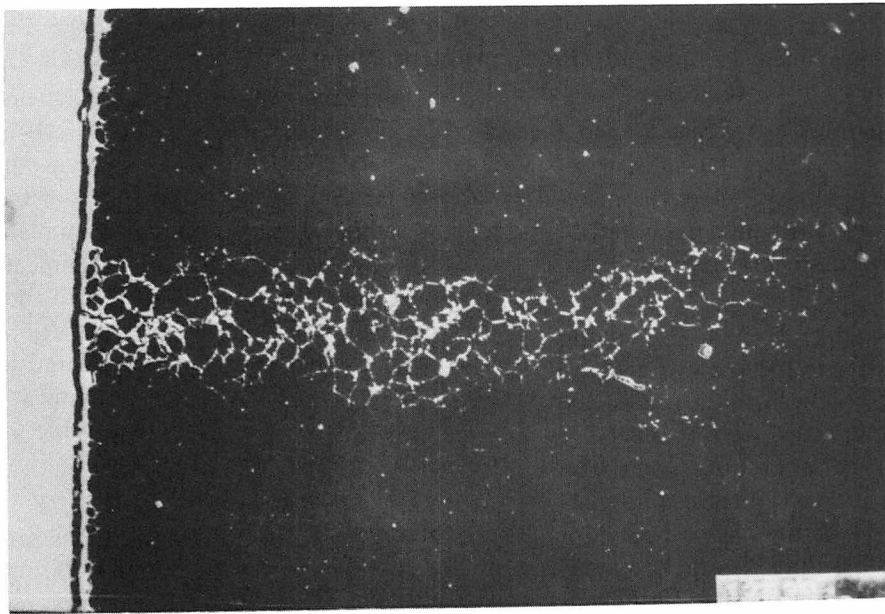
*FIGURE 17—Corrosion of different materials in Na + H₂O or Na + NaOH media.*

very rapidly. Comparison of these kinetics requires a great number of investigations which are currently in progress.

To reduce the risks of sodium/water reactions to a minimum and avoid the consequences on subsequent operation of the plant, it is essential to select the materials for the tube bundles with particular care, and to design and construct the entire steam generator plant with the same attention.

The choice of materials depends on the operating conditions, principally the temperature of the sodium. If this temperature is not very high, in the region of 500 to 520 C (930 to 970 F) for instance, ferritic steel 2¼ Cr-1 Mo will easily satisfy mechanical requirements. The industrial background of this product, its price and market availability are all in favor of the choice of such a steel. The loss of carbon in sodium can be kept to a minimum, in particular by a suitable adjustment of the chemical composition and heat treatment of the tubes.

Steel 9 Cr-1 Mo offers an additional guarantee with respect to the risks of decarburization and especially corrosion in water which could be high in the evaporating zones in the case of thermal oscillation, and, in any case, could hinder operations by the accumulation of diffused hydrogen in the sodium circuit.

Should optimized operating conditions for the plant lead to secondary hot sodium temperatures that are higher than 540 to 550 C (1005 to 1020 F), the choice of materials is limited to Alloy 800 and 9 Cr-2 Mo-Nb-V.

A great many laboratory tests have been carried out on Alloy 800, and it has been used in the mock-up. It is a satisfactory solution. However, its use implies certain requirements on the reproductibility of the product, i.e. narrow composition ranges for certain elements and precise conditions for the thermomechanical treatment of the tubes. These precautions guarantee good creep resistance while ensuring that ductility does not fall below the value that has been carefully calculated for the type of plant under consideration. In the same way, the design of the plant will have to eliminate the known risks of stress corrosion of this material in the media resulting from a sodium/water reaction.

Steel 9 Cr-2 Mo-Nb-V, which has proved its worth in the superheaters of traditional EDF power plants, seems able to satisfy the various requirements for use in sodium/water exchangers. Particular care is needed to obtain a reproducible quality and in the subsequent welding and weld inspection of the tubes.

## Core Materials

The characteristics of the cladding materials and their behavior under irradiation play a vital part in the economy of the fast neutron reactor program. This is clearly demonstrated by the results (Figure 18) of a com-
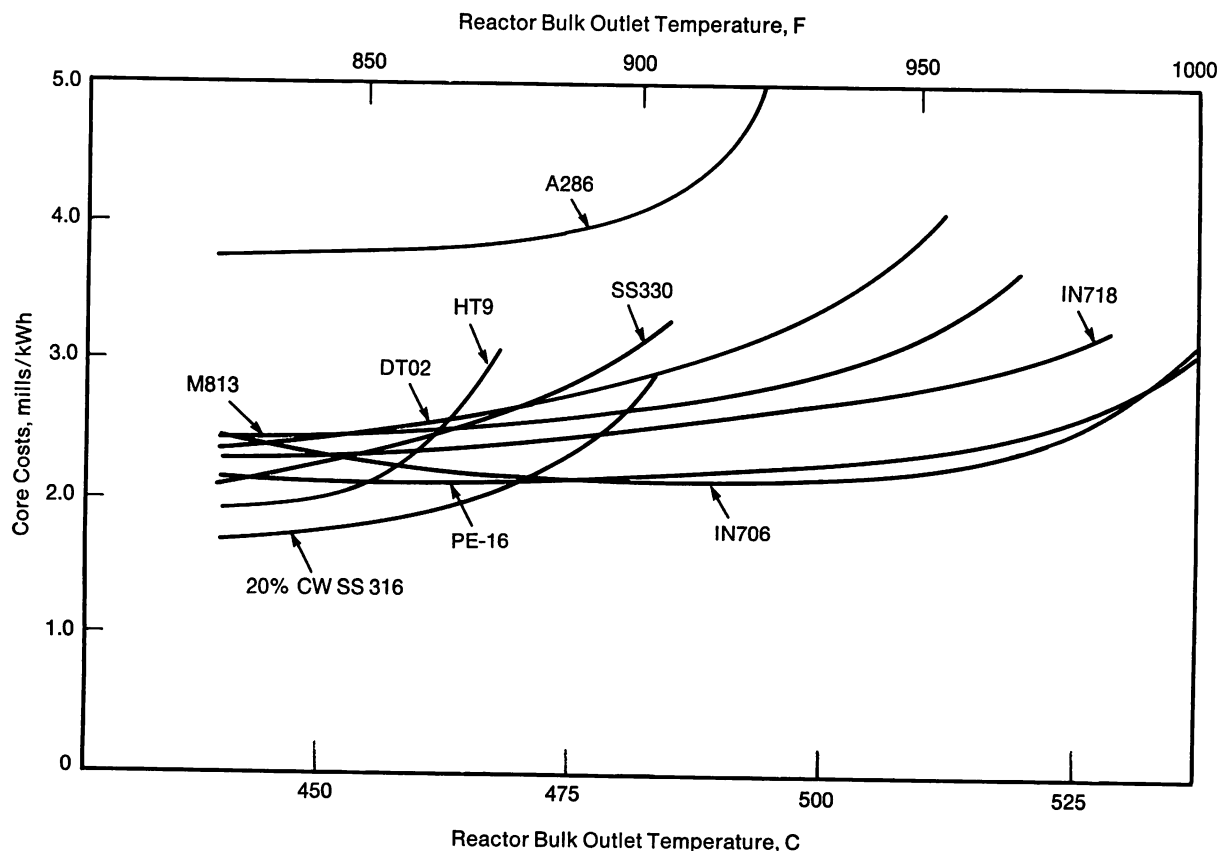


FIGURE 18—Optimum core cost vs. bulk outlet temperature.

plicated optimization calculation[31] where the performances of different cladding materials are compared on the basis of influence on cost per kWh, which can vary by a factor 2 according to the nature of these materials. The results of such an operation should not be taken too literally since they depend on the characteristics of the materials used. They merely show that the unit cost depends primarily on two factors, maximum acceptable cladding temperature and burn-up.

## Maximum Cladding Temperature

To have a reasonable steam cycle, close to that of a conventional thermal station given all the exchange coefficients, the existence of a double sodium circuit, the temperature distribution in the core, etc., the maximum cladding temperature should be around 650 C (1200 F). In view of such inevitable constraints as the presence

of primary stresses from the internal pressure of gaseous fission products and the compatibility with sodium, the outcome has been an almost universal choice of austenitic steels, and, among these, of Type 316 because of good creep resistance.

## Burn-up

In a fast neutron reactor, the burn-up values necessary to the good economy of the system are very high, above 100,000 MWd/t. Given the high neutron fluxes and long in-pile periods necessary, this corresponds to a very large damage factor (expressed in number of times each atom is displaced, the dpa) of about 200. Such changes in the periodic arrangement of atoms lead to macroscopic alterations which can drastically limit in-pile life.

Two kinds of interdependent phenomenon are:
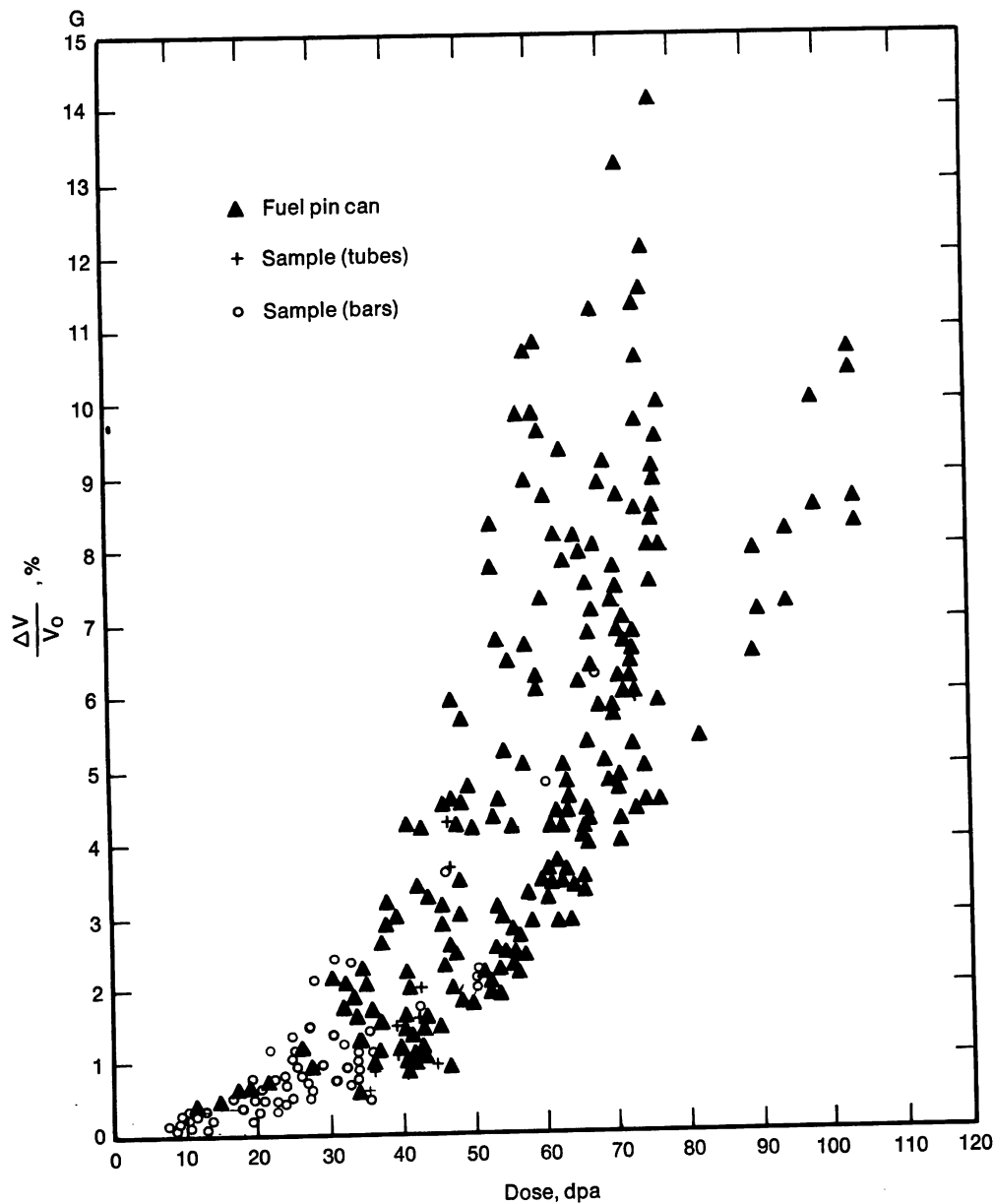


FIGURE 19—Swelling at SA 316 ($\theta \sim 500\,C$, 930 F).

1. Those leading to size changes involving irradia-
tion creep swelling, and

2. Those causing changes in the alloy structure.

## Swelling

This is one of the typical effects associated with high
fast neutron fluxes which produce a large number of
Frenkel pairs, i.e. vacancies and interstitials of which
most recombine immediately, so that almost nothing is
left of the initial population. This *je ne sais quoi et ce
presque rien* is responsible for the swelling problem.
Since interstitials are much more easily attracted by dis-
locations than a small excess of vacancies (which are
therefore left behind and tend to precipitate as small
cavities or holes), these can then grow by absorption of
vacancies increasing the volume and reducing the
density.

The swelling, G, is equal to the number of cavities,
Nc, multiplied by their mean volume, $\overline{V}$. As in any
growth/germination process, G obeys a rate law with a
maximum [between 300 and 700 C (570 and 1290 F) for
steels].

A fast neutron reactor fuel element is a very compact
set of fuel pins of 5 to 8 mm (0.20 to 0.31 in.) diameter.
Swelling can give rise to diameter changes which, even
when limited to a few percent of the original value, can
disturb the thermohydraulics of the cluster and lead to
unacceptable overheating. Moreover, the sodium flow in
an assembly is channelled by a wrapper tube, usually

hexagonal, which; if deformed by swelling, can involve
handling problems.

Swelling of the austenitic steels used for these ap-
plications depends on the temperature and neutron flux.
This means that a structural part subjected to a strong
thermal gradient will experience a swelling gradient that
could lead to considerable plastic deformation and frac-
ture in irradiation embrittled materials.

The control of swelling will be examined essentially
in reference to the behavior of series 300 austenitic steels
and more especially Type 316, the basic composition
used almost unanimously as a reference material for fast
neutron reactor fuel element cladding.

A word is necessary first on the scatter of results ob-
tained on a batch of cladding tubes from an industrial
manufacture. Figure 19 gives an idea of the dimension
of this phenomenon on a solution annealed 316 steel. It
shows the order of magnitude of the swelling produced
in these steels even under moderate doses. The practical
impact of such scatter is considerable, and, if perform-
ances are not to be limited to the worst case, it is abso-
lutely essential to analyze the reasons for its occurrence.
Another obvious result of this scattering effect, not often
mentioned in the technical literature, is that research
based on the comparative behavior of isolated samples
is meaningless. One reason for scatter may be found in
the irradiation conditions, but the influence of this factor,
though not to be neglected, should not be exaggerated.
Figure 20 shows a set of diametric profile measurements
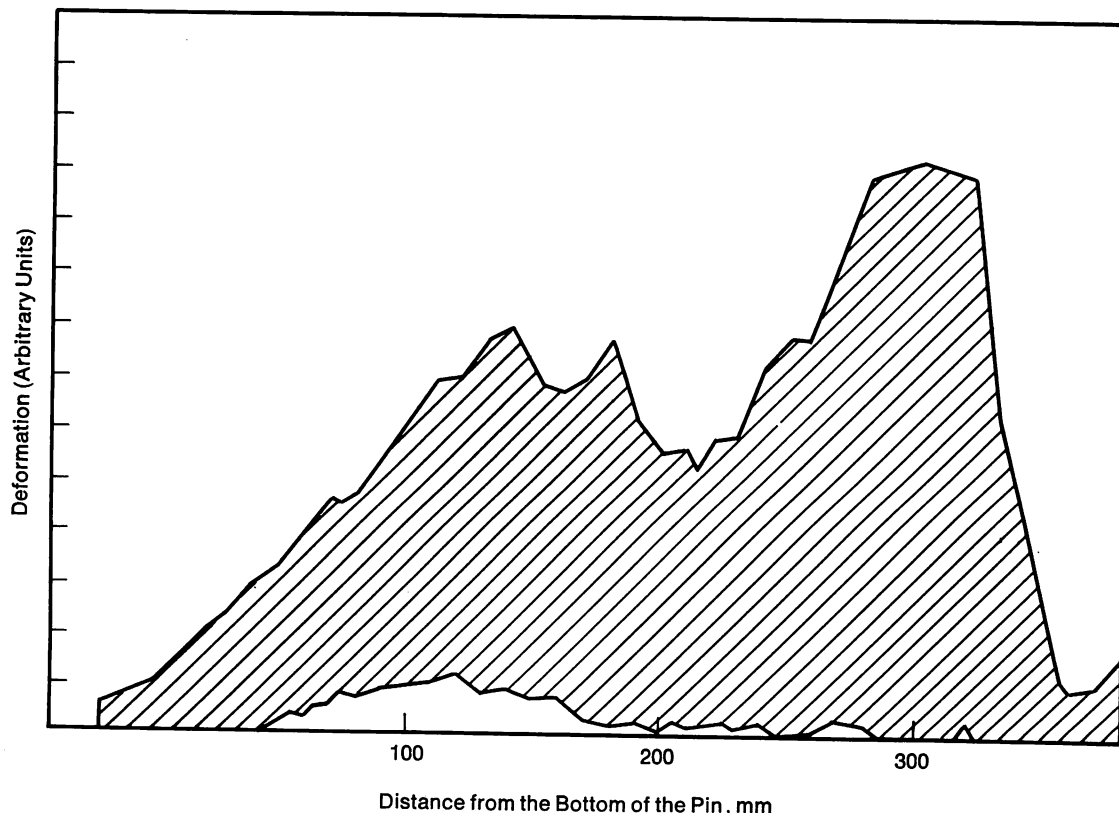


FIGURE 20—Diameter deformation range of pins of a complete Rapsodie bundle.

obtained on solution annealed Type 316 cladding *of the same fuel assembly* irradiated in Rapsodie, and the scatter is still considerable even excluding the colder peripheral pins.

Another tendency is toward a two-peak swelling. It is interesting to enquire into the metallurgical origins of such variability by analyzing the factors likely to govern swelling.

The effect of cold work was recognized very early and used in practice. Nearly all the teams concerned recommend the use of limited cold work (about 20%) for cladding tubes. Figure 21 gives examples of the benefits expected, mainly owing to reduction of the mean cavity volume, $\bar{V}$.

The effect of cold work was foreseen by simple swelling theories and was associated chiefly with the high initial density of dislocations resulting from plastic deformation. However, the disturbing fact, mentioned by Delaplace[32] among others and, in our opinion, still unexplained, is that the original dislocations quickly disappear at the start of irradiation although their effect appears to last a very long time, at least in irradiation with ions.

A systematic comparison of swelling versus degree

of cold work is difficult. Busboom[33] gives a particularly clear example of 304 steel (Figure 22) where the main effect of cold work is to shift the incubation dose.

The effect of carbon content in the matrix of a 316 steel is considerable, especially at low temperatures (Figure 23). Swelling was shown to depend not on the total carbon content but on the quantity in metastable solution in the matrix. It is now known that previous carbide precipitation treatments have a catastrophic effect on swelling (Figures 24 and 25).
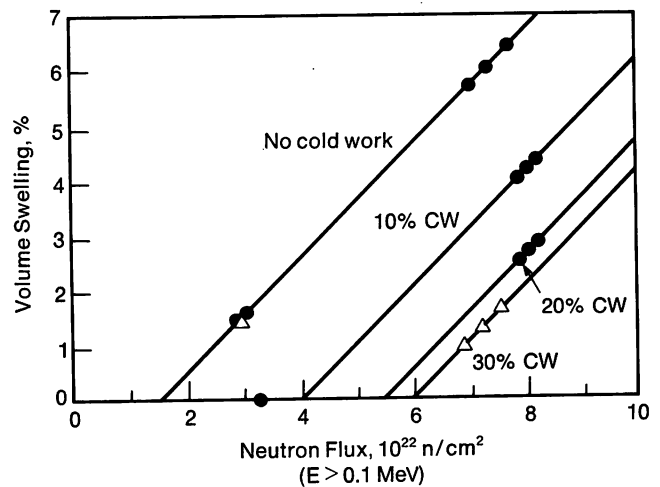


FIGURE 22—*Dependence of swelling in Type 304 stainless steel at 450 C (840 F) on cold work.*



FIGURE 21—*Swelling vs. temperature for 0.021% C Type 316 grades.*
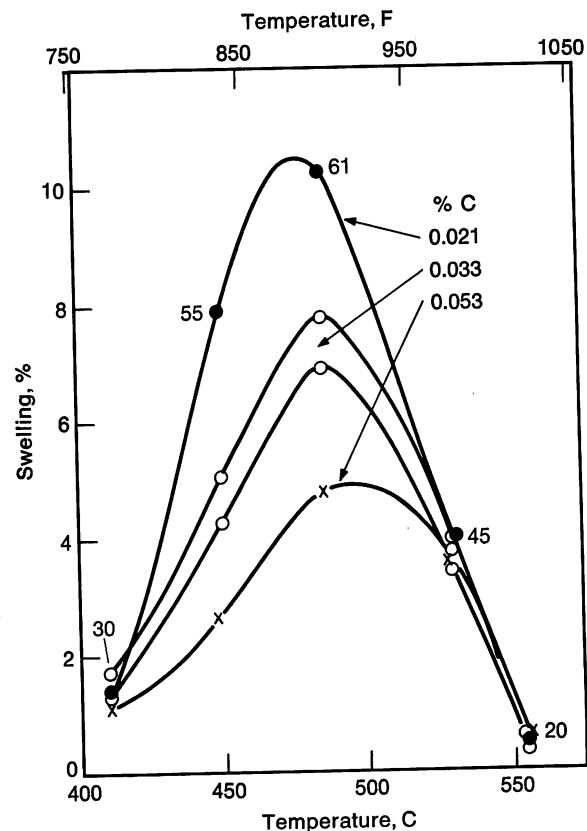


FIGURE 23—*Swelling of steels of three different carbon contents (solution annealed).*

Early test results seemed to indicate a highly beneficial influence of molybdenum. Appleby et al.[34] showed that molybdenum tends to shift the swelling peak of austenitic steels toward high temperatures without affecting the maximum swelling. No really convincing explanation has been advanced to account for this phenomenon. It could be advocated that molybdenum in solid solution reduces swelling at 450 C (840 F). At higher temperatures, the heavy precipitation of carbides and Laves phase lowers the molybdenum content in the matrix and with it the swelling resistance.

Phenomena of this type have been held responsible for the so-called second swelling peak observed in solution annealed (SA) 316 steel, where the carbon content reduction in the matrix by carbide precipitation is blamed for swelling above 500 C (930 F). This approach has been treated mathematically by Dupouy et al.[35] who introduced the carbide precipitation kinetics through a
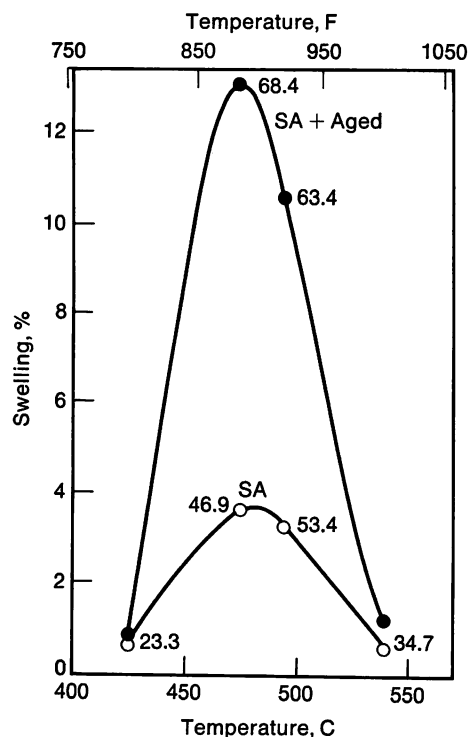


FIGURE 24—Swelling of a low carbon Type 316. The aging treatment was 100h at 750 C (1380 F).
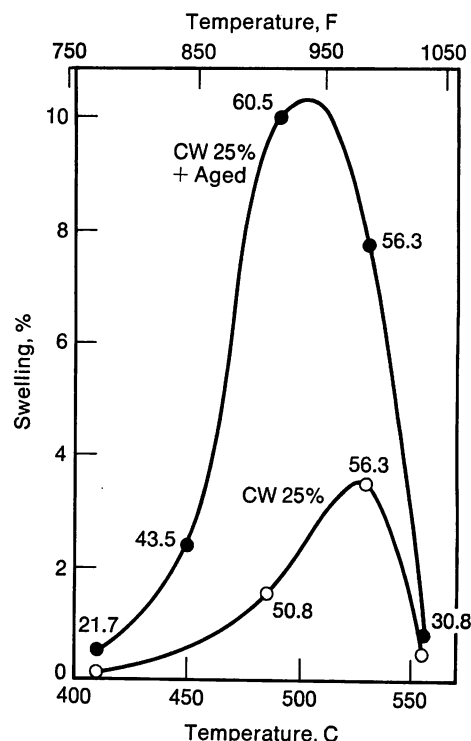


FIGURE 25—Swelling of a 0.05% carbon Type 316. Aging treatment was 100h at 750 C (1380 F).
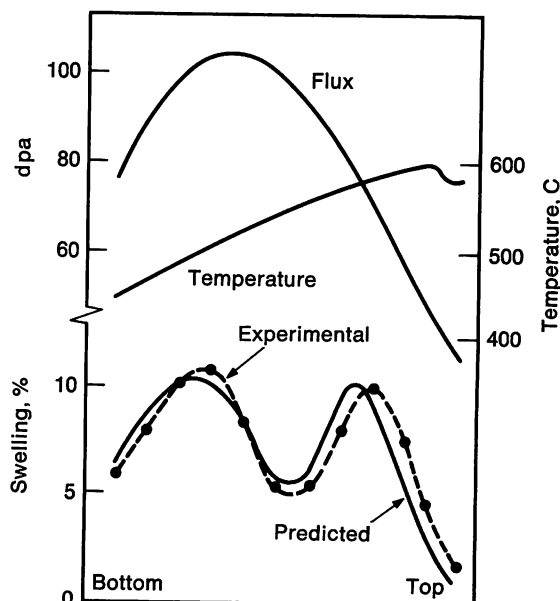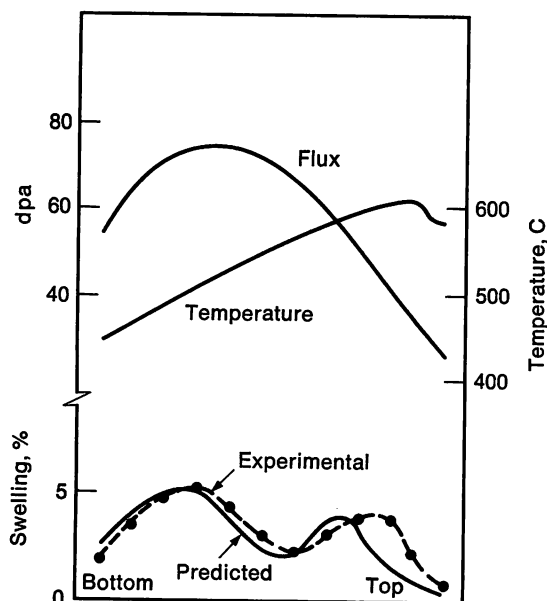


FIGURE 26—Comparison between measured and predicted swelling of SA 316 based on Johnson-Mehl equation for carbon precipitation.

Johnson-Mehl type equation into their swelling equation with some success, as shown in Figure 26 for SA 316.

Bates and Johnson,[36] using a simulation technique
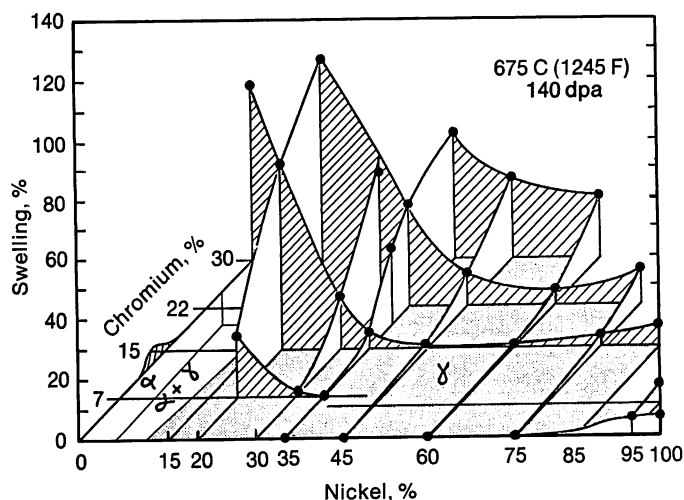


FIGURE 27—*Swelling in the Fe-Cr-Ni system.*
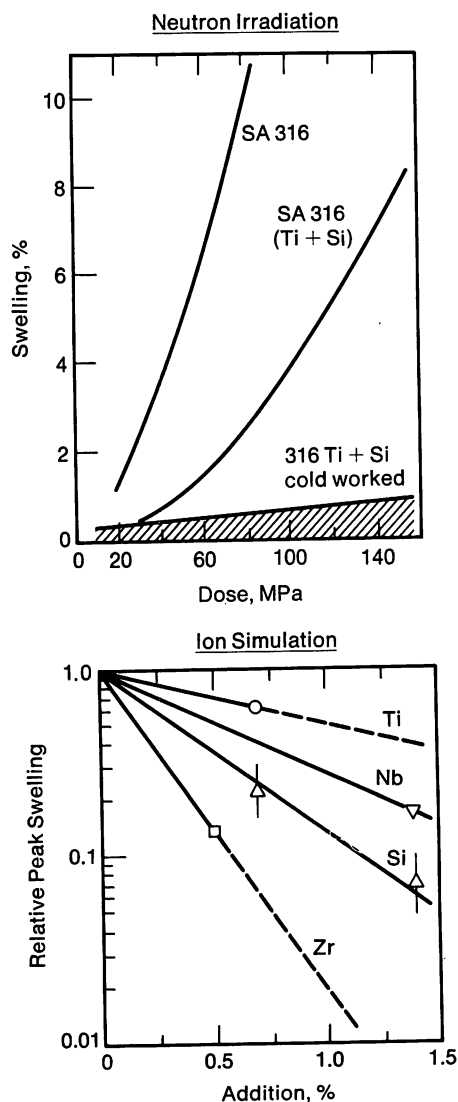


FIGURE 28—*Synthetic representation of the effects of addition elements on swelling of Type 316 steel.*

(5 MeV Ni ion bombardment), systematically studied a wide composition range in the Fe-Cr-Ni ternary region and established the diagram reproduced as Figure 27. Raising the Ni content above 30% appears extremely promising, but it seems more difficult to limit the chromium content to the values suggested by this diagram. These general tendencies are confirmed by studies on industrial nickel alloys such as PE 16 in Great Britain and IN 706 in the U.S. and France.

A certain number of elements which, in low concentrations, seem to have a strong influence on the swelling of austenitic steels have been identified. Carbon has already been mentioned. Boron and niobium[37] are apparently beneficial at high concentrations (a few hundred ppm), probably too high for good weldability. At higher concentrations, Ti, Si and Zr would also seem to be beneficial (Figure 28).

Harries[38] observed that all alloys subject to much swelling lie within the $\gamma + \sigma$ region and blames this behavior on $\sigma$ formation and depletion of the matrix in favorable elements. Watkin[39] defends the same hypothesis but shows that the best correlation is obtained with $N_v$, the number of electron vacancies per atom, which is known to have been a parameter often used to define superalloys free of sigma phase.

It seems that most beneficial elements are $\gamma$ forming with the particular exception of Cr. Favorable gamma forming elements are carbon and nickel. Here we are concerned with observations rather than explanations. The way in which swelling can be influenced by the metastability of the alloy and in particular by changes in the matrix composition during periods at high temperature has already been shown. Fundamental and applied studies have recently been devoted to the metallurgical stability of alloys under irradiation and will probably yield a clue to the chemical composition effects on the swelling phenomenon. A brief outline of this work follows.

It was long assumed that phase transformations under irradiation were connected with local disorder (cascades) or with accelerated diffusion related to the point defect density which would enable a system to reach equilibrium more quickly. Recent work has clearly shown that these are only two extreme cases of possible irradiation effects and that experimental observations can be represented, as suggested by Adda,[40] on a particle flux/temperature diagram. In the intermediate range, where supersaturation is high and point defects mobile, alloys can display structures quite different from those corresponding to out-flux thermodynamic stability. The result is a variety of precipitates unknown by orientation, morphology, nature and composition.

Many theoretical models have been developed, one of the most popular being the kinetic approach to influx stability. This irradiation-induced precipitation of subsaturated solution has been observed and related to

solute flows toward point defect sinks or saturable traps.[40-42] Many examples of such induced precipitations now exist both in simple subsaturated systems, Ni-Si, Ni-Ge, Ni-Be, Al-Zn, W,[43-51] and in complex alloys such as 316 steels[52-57] or nickel-base alloys.[58]

The flux/temperature diagram region in which each phase lies depends not only on the composition of the alloy but also on the initial microstructure.

As mentioned above, the swelling of alloys at high temperatures is interpreted in terms of changes in the matrix composition. Thus, the swelling of 316 steels has recently been related to elimination of the Ni-Si matrix associated with precipitation of $\gamma'Ni_3Si$.[56]

## References

1. L. Vaïbus, Specialist Meeting, P.A.E., IWGFR/22, Bergisch Gladbach, 1977.

2. Métaux Corrosion Industrie, October 1974, 590, January 1977, 617.

3. H. Granjon and S. Debiez, Revue de Métallurgie, 12 December 1973, 1033.

4. R. A. Müller and H. Schauder, Atomic Energy Review, 13, 1975, 215.

5. A status review of Alloy 800, Conference de la BNES, Reading, 25-26 September 1974.

6. N. G. Persson and L. Egnell, "Creep rupture characteristics of Alloy 800 around 600 C," Communication au Colloque des Communautés Européennes sur l'Alliage 800, Brussels, September 1976.

7. P. Petrequin, et al., "Prise en compte de la fatigue oligocyclique dans les constructions des réacteurs rapides refroidis au sodium," Journées d'étude sur la fatigue oligocyclique, ENSTA, Paris, 1976.

8. J. E. Cordwell and R. D. Nicholson, CEGB Report RD/B/N 3195, 1975.

9. M. J. Collins, CEGB Report RE/L/N 25/74, 1974.

10. E. te Heesen and E. D. Grosser, Conference Materials for Nuclear Steam Generators, Gatlinburg, Tennessee, September 1975.

11. Ph. Berge, J. R. Donati, D. Guttmann, P. Spiteri and L. Vaïbus, Mém Scient, Rev. Métallurg, 72 (11), 1975, 837.

12. J. R. Donati, L. Vaïbus and C. Zacharie, Mém. Scient., Rev. Métallurg, 71 (3), 1974, 187.

13. E. D. Grosser and H. Lorentz, Communication F 3.2, Conference Materials for Nuclear Steam Generators, Gatlinburg, Tennessee, September 1975.

14. C. Colombe, S. Debiez, J. R. Donati, P. Petrequin and C. Zacharie, Communication au Congrès sur les aciers ferritiques pour générateurs de vapeurs de réacteurs rapides, London, June 1977.

15. J. L. Krankota and J. S. Armijo, Nuclear Technology, 24, 1974, 225.

16. L. Champeix, et al., "Carbon transfer between 2¼ Cr-1 Mo alloy and austenitic steels," International Conference, Liquid Metal Technology in Energy Production, Champion, Pennsylvania, May 1976.

17. R. L. Klueh and J. M. Leitnaker, Met. Trans, A, 6 A, 1975, 2089.

18. R. G. Baker and J. Nutting, J. Iron and Steel Inst, 192, 1959, 257.

19. K. O. Natesan, O. K. Chopra and T. F. Kassner, Conference, Materials for Nuclear Steam Generators, Gatlinburg, Tennessee, September 1975.

20. J. Blanchet et al., Com. Nuclex, Colloque A, series 1, Bâle, 1976.

21. Ph. Berge, Colloque EDF-ADERP Chimie de l'eau et corrosion aqueuse dans le générateur de vapeur, Ermenonville, 13-17 March 1972.

22. H. E. Homig, Combustion, 40, 1968, 4.

23. E. Benoist, M. Campillard and J. L. Quinet, International Conference, Liquid Metal Technology in Energy Production, Champion, Pennsylvania, May 1976.

24. A. Lacroix, ibid.

25. M. Warzee and Ph. Berge, "Corrosion des aciers inoxydables et des alliages riches en nickel dans la vapeur surchauffée à haute température," Rapport des Communautés européennes de l'Energie atomique, EUR 3387.

26. J. J. Cantens, F. Dabosi and Ph. Berge, Comm. présentée aux Journées d'Automne de la Société Française de Métallurgie, Paris, October 1976.

27. Ph. Berge, C. Ribon and P. Saint-Paul, Corrosion, 32, 1976, 61.

28. Ph. Berge, J. R. Donati, B. Prieux and D. Villard, 66ème congrès international sur la corrosion métallique, Sydney, December 1975.

29. Ph. Berge, C. Oberlin and P. Saint-Paul, Journal of Nucl. Mat., 57, 1975, 283.

30. J. R. Donati, M. Grand and P. Spiteri, Journal of Nucl. Mat., 54, 1974, 217.

31. D. P. Johnson et al., Trans. ANS, November 1976, 145.

32. J. Delaplace and N. Azam, Apport de techniques de simulation à l'étude du gonflement des aciers austénitiques, Conference Internationale, Ajaccio, June 4-8, 1979.

33. H. J. Busboom, Headline 75, 1975, 32.

34. W. K. Appleby, E. E. Bloom, J. E. Flinn and F. A. Garner, Swelling in Neutron-Irradiated 300-Series, International Conference, Radiation Effects in Breeder Reactor Structural Materials, Scottsdale, Arizona, June 1977, 524.

35. J. M. Dupouy, L. Lehmann and J. L. Boutard, Swelling and Irradiation Creep of 316 Stainless Steel, Conference, Alushta, 1978, Vol. 5, 280.

36. J. F. Bates and W. G. Johnson, Effects of Alloy Composition on Void Swelling, International Conference, Radiation Effects in Breeder Reactor Structural Materials, Scottsdale, Arizona, June 1977, 630.

37. ibid., 637.

38. D. R. Harries, Void Swelling in Austenitic Steels and Nickel Base Alloys: Effects of Alloy Constitution and Structure, Proc. Harwell Conf. on the Physics of Irradiation Produced Voids, AERE-R-7934, 1975, 287.

39. J. S. Watkin, Dependence of Void Swelling on the Electron Vacancy Concentration, Irradiation Effects on the Microstructure and Properties of Metals ASTM STP 611, 1976, 271.

40. Y. Adda, M. Beyeler and G. Brebec, Thin Solid Films, 25, 1975, 107.

41. R. A. Johnston and N. Q. Lam, Phys. Rev., B 13/B 15, 1976/1979, 4364/1794.

42. L. E. Rehn, P. R. Okamoto, B. I. Potter and H. Wiederich, J. Nucl. Mat., 74, 1978, 242.

43. H. Wiederich, P. R. Okamoto and N. Q. Lam, Radiation Effects in Breeder Reactor Structural Materials, Scottsdale, Arizona, June 1977, 801.

44. R. Cauvin and G. Martin, J. Nucl. Mat., 83, 1979, 67; and Phil. Mag, to be published.

45. A. Barbu and A. J. Ardell, Scripta Met, 9, 1975, 1233.

46. A. Barbu and G. Martin, Scripta Met., 11, 1977, 771.

47. C. Silvestre, A. Silvent, C. Regnard and G. Sanfort, J. Nucl. Mat., 57, 1975, 125.

48. A. Barbu, Proceeding of Conference, *Irradiation Behavior of Metallic Materials for Fast Reactor Core Components*, Ajaccio, June 4-8, 1979, 69.

49. P. R. Okamoto, A. Taylor and H. Widersich, "Fundamental Aspects of Radiation Damage in Metals," U. S. ERDA Report, Conf. 75.1006, 1975, 1188.

50. K. Farrell, Unpublished results.

51. R. K. Williams, J. O. Stiegler and F. W. Wiffen, ORNL Report J.M. 450052, 1974.

52. H. R. Brager and F. A. Garner, *Trans. ANS, 28,* 1978, 151.

53. H. R. Brager and J. L. Stralsund, *J. Nucl. Mat., 73,* 1973, 46.

54. E. E. Bloom and J. O. Stiegler, "Effects of Radiation on Substructure and Mechanical Properties of Metals and Alloys," ASTM STP 529, 1973, 360.

55. H. R. Brager and F. A. Garner, *J. Nucl. Mat., 73,* 1978, 9.

56. H. R. Brager and F. A. Garner, HEDL SA 1412, 1978.

57. E. H. Lee, A. F. Rowcliffe and E. A. Keink, *J. Nucl. Mat., 83,* 1979, 79.

58. M. L. Bleiberg, R. Bajaj, W. L. Bell and L. E. Thomas, WARD AD 3045-4, 1977.

## Discussion

C. T. SIMS, *General Electric Company.* An earlier paper described a device for producing rapidly solidified powder characterized by very fine grains and unusual properties. There must be more disorder and more disclocations in these materials than could be produced by simple cold working. Would not these materials be of interest for a reduction in the swelling problem?

M.WEISZ.I think this has been tried at Oak Ridge. The problem is that if there is too much energy in the material, recrystallization can result during service. Amorphous materials have been tried, but they can become crystalline in service. The materials need to be stable in the 450 to 650 C (840 to 1200 F) range.

# Materials Selection for Gas Cooled and Fusion Reactor Applications

by D. I. Roberts, S. N. Rosenwasser and J. F. Watson
General Atomic Company

Among the many advanced energy systems under development in the United States and world-wide, gas cooled reactors and magnetic confinement fusion reactors offer the potential to make significant contributions to the world's intermediate and long-term energy needs. However, these advanced systems pose a number of interesting materials challenges, and the purpose of this paper is to highlight some of these issues.

Since numerous papers have been published describing the features and advantages of both gas cooled reactor and fusion reactor systems,[1-5] this information will not be reviewed in detail here. However, the principal features of the systems will be briefly described.

The versions of the gas cooled reactor which are currently under development in the United States, the Federal Republic of Germany and Japan are listed in Table I. The common feature of all these systems is that they utilize high pressure helium coolant to transfer heat from the reactor core to the heat exchangers. The thermal gas cooled reactor systems (referred to hereafter as TGRs) all utilize a graphite-moderated core fueled with uranium and thorium oxide or carbide. The gas cooled fast breeder reactor (GCFR), on the other hand, utilizes a metal clad Pu/U oxide fuel similar to the fuel being developed for the liquid metal fast breeder reactor (LMFBR) program. The maximum temperatures to which structural (non-core) materials are exposed within these systems are shown in Table II. A schematic presentation of a typical process heat TGR of the type that might be used for SynFuels applications is shown in Figure 1.

Materials of construction in these systems are exposed to relatively high temperatures. Thus, where metallic materials are employed, design is strongly influenced by effects such as creep, high temperature corrosion, fatigue, etc., and assessment of these properties is a key development task.

The family of magnetic confinement fusion reactors also contains a wide variety of different designs. A typical Tokamak design[5] is shown in Figure 2. One of the principal features of a fusion reactor is that a very high flux of very high energy neutrons is emitted from the plasma. These neutrons bombard the structures immediately surrounding the plasma, where they give up their energy to generate heat. The components subject to this intense irradiation are known as the first wall and blanket structures. Irradiation damage resistance is a major consideration in material selection for these components in fusion reactors. In pulsed Tokamaks, resistance to fatigue

**Table I**—Helium Gas Cooled Reactor Programs

| Thermal Reactors | Fast Reactor |
|---|---|
| HTGR—Steam Cycle (HTGR-SC) HTGR—Process Heat (HTGR-PH) HTGR—Gas Turbine (HTGR-GT) HTGR—Steamer | Gas Cooled Fast Breeder Reactor (GCFR) |

**Table II**—Highest Nominal Temperatures to Which Noncore Components Are Exposed in Helium Gas Cooled Reactors

| Reactor Type | Temperature, C (F) | Temperature of Hottest Thermal Barrier, C (F) | Temperature of Hottest Regions of Heat Exchangers, C (F) |
|---|---|---|---|
| HTGR—Steam Cycle | 750 (1380) | 750 (1380) | 700 (1290) |
| HTGR—Process Heat | 850-1000 (1560-1830) | 850-1000 (1560-1830) | 800-950 (1470-1740) |
| HTGR—Gas Turbine | 850 (1560) | 850 (1560) | 600 (1110) |
| HTGR—Steamer | 600 (1110) | 600 (1110) | 520 (970) |
| GCFR | 650 (1200) | 650 (1200) | 550 (1020) |
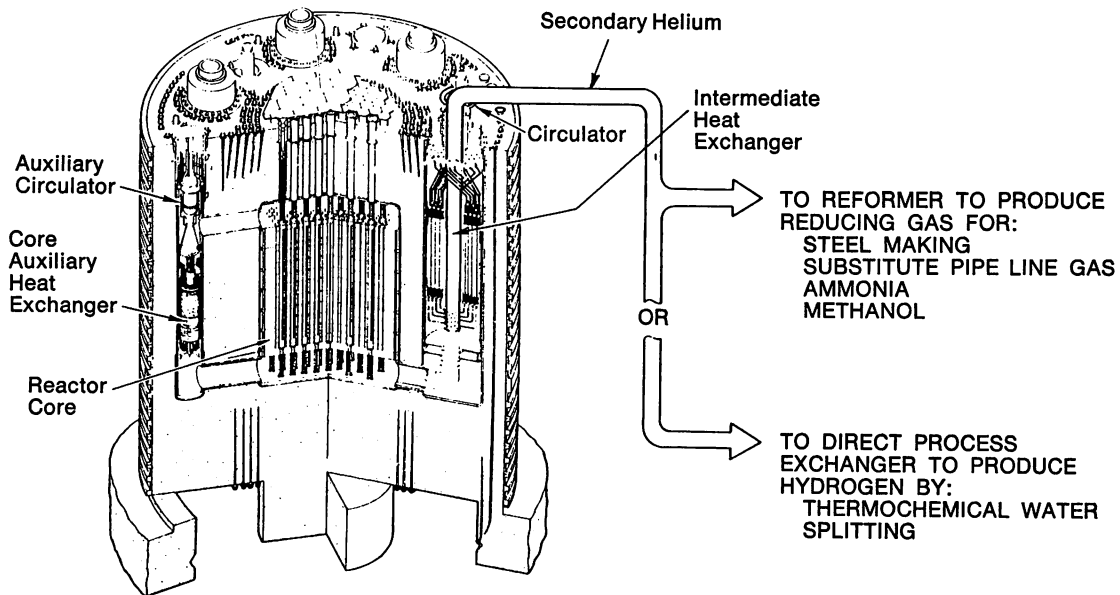
FIGURE 1—Nuclear heart of a process heat TGR.
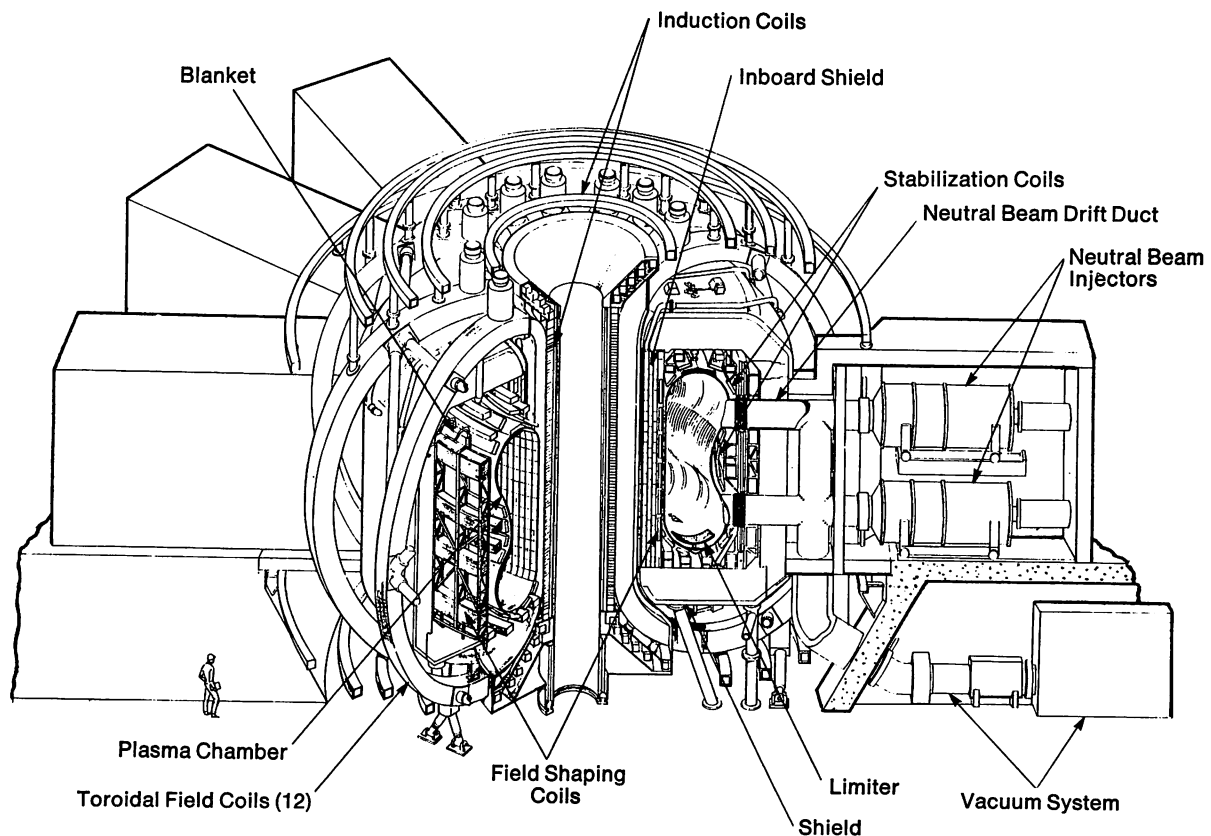


FIGURE 2—Schematic of power generating fusion reactor assembly.

stresses from thermal cycling is another important material requirement.

Some variations of the fusion reactor feature structures that operate at significantly elevated temperatures. For these structures, high temperature effects, such as creep and corrosion, are important in addition to irradiation considerations. Magnetic confinement fusion reactors also frequently contain superconducting magnet systems where materials are exposed to cryogenic temperatures.

To meet the design needs of the various components of fusion and gas cooled reactor systems, a very wide variety of materials is employed. These include structural ceramics (such as alumina, silicon nitride, silicon carbide and graphite), fibrous insulation materials, and a wide variety of metallic alloys ranging from carbon

steels to the nickel-base superalloys. In keeping with the context of this conference, this paper will be confined to the steels and high temperature alloys used in these systems and, where appropriate, to how the use of molybdenum enhances the properties of these materials that are of engineering interest.

## Materials for Gas Cooled Reactor Applications

### Important Properties

The principal considerations that influence the selection of materials for gas cooled reactor applications are indicated in Table III. Clearly, the importance of each of these aspects varies from reactor to reactor. In the reactor systems that feature the highest temperatures, elevated temperature strength (resistance to creep, creep-fatigue, etc.) and reaction between materials and coolant impurities are vitally important considerations. On the other hand, irradiation effects are more significant in fast reactor systems. Fabricability and cost are significant considerations for all reactor systems since economics are of major importance.

**Table III**—Behavior Considerations Important in Selection of Materials for Use in High Temperature Components of Gas Cooled Reactors

1. Tensile, Creep, Low Cycle Fatigue and Creep-Fatigue Interaction Behavior.
2. Interaction of Materials with Environments (Impure Helium, Steam/Water, Irradiation, Temperature) and Effects on Mechanical Properties.
3. Thermal Aging and Embrittlement.
4. Fabricability (Weldability, Bendability, Availability in Required Product Forms, etc.); Matching or Appropriate Properties in Welds; Cost.
5. ASME Code Qualification (where applicable).

**Table IV**—Major High Temperature Alloys of Interest for Gas Cooled Reactors

| | |
|---|---|
| 2¼ Cr-1 Mo | IN  100 |
| 9-12Cr/Mo Steels | IN  713LC |
| Type 304 SS | IN  738 |
| Type 316 SS | MA 754 |
| Alloy 800H | MA 956E |
| Hastelloy X | |
| Inconel 617 | |

The design and construction of many reactor components must comply with the rules of the ASME Code. When these components operate at elevated temperature, the rules of Section III, Class 1, Code Case N-47 may apply. These rules require that very sophisticated analyses of designs be performed with particular attention to time-dependent failure modes such as creep, creep-fatigue, ratchetting, etc. Thus, for materials used in these components, it is necessary to generate large

amounts of detailed property information to qualify materials to these Code rules and permit the required design analyses to be performed.

The major alloys of interest for gas cooled reactor applications are shown in Table IV. An inspection of the list reveals that molybdenum will play an important alloying role in the applications of these materials. In the following sections, some of the activities under way in each of the areas noted in Table III will be highlighted.

### Elevated Temperature Strength

As indicated above, when component design is governed by ASME Code rules such as those contained in Code Case N-47, a very high degree of analysis is required, which in turn necessitates the existence of a very large and complete data base for both time-independent and time-dependent phenomena. One of the difficulties encountered in designing to these rules is that it is necessary to extrapolate behavior because components typically have a design life of 20 to 40 years, whereas the data that exist rarely exceed 3 to 6 years in duration. Moreover, it is necessary not only to extrapolate in time but, in many cases, to extrapolate backward in temperature. That is, it is necessary to provide a basis for assessing how materials will behave between the temperature at which creep is nonexistent and the temperature at which creep is very significant. For example, Alloy 800H exhibits essentially no creep (from an engineering standpoint) at temperatures below 425 C (800 F). On the other hand, it is clear that creep is occurring at a significant rate at 595 C (1100 F). For designing to Code Case N-47, it is necessary to provide a basis for assessing how the material will behave at temperatures of, for example, 480 or 510 C (900 or 950 F). Thus, the need for "backward extrapolation."

It is also necessary for elevated temperature design purposes to make some assessment of "minimum strength properties." To do this, it is necessary to perform statistical analyses in which the behavior of a large number of heats of material is represented. By this method, it is possible to obtain some estimate of the probable minimum strength material likely to be obtained.

Over the years, numerous methods have been utilized for the extrapolation of, for example, creep and rupture properties. An example of a Larson-Miller type analysis performed on one set of Hastelloy X data is shown in Figure 3. Such analyses can be used to estimate long time or lower temperature behavior for design purposes (although great care must be exercised where it is necessary to extend the master curve beyond the realm of the data).

The majority of existing elevated temperature creep and rupture data have been generated in an air environment. In a gas cooled reactor, however, components are operating in a helium environment containing low levels of impurities. Since it is known that creep and rupture

properties are environmentally sensitive, it is necessary to assess the effect this environment may have on elevated temperature strength. Figure 4 compares the stress rupture data for annealed 2¼Cr-1Mo that were obtained
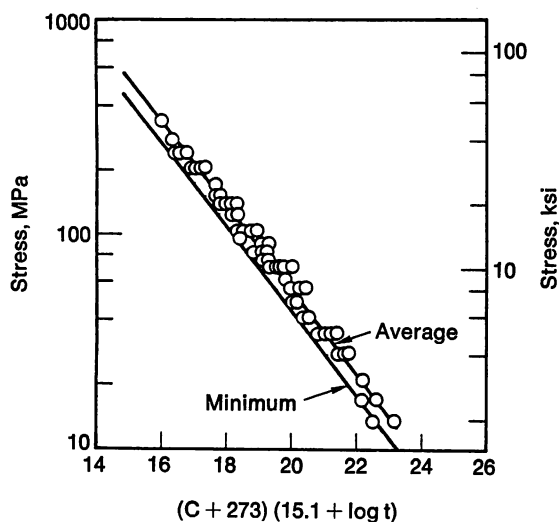


FIGURE 3—Typical Larson-Miller master curve for Hastelloy X stress rupture in air.

$(C + 273)(15.1 + \log t) = 5.6344 - 1.9486 \times 10^{-4} \log \sigma$
t = time, h
$\sigma$ = stress, MPa

in TGR helium and the scatter band of air data for this alloy. As indicated, the effects of the environment are not large enough to cause gross disagreement between the helium and the air data. However, when specific comparisons are made between the creep-rupture behavior of one heat of material in air and in helium, some differences are apparent, as shown in Figure 5.[6] Typically, the effect of the helium environment is to shorten the tertiary creep period, to reduce the rupture strain and to shorten the rupture life.

Design of elevated temperature structures requires the performance of creep-fatigue analyses, and recommendations regarding the analytical approach to use are contained in a nonmandatory appendix to Code Case N-47. Since fatigue and creep-fatigue are also environmentally sensitive phenomena, it is necessary to assess the effects of TGR helium on these properties. Data available thus far indicate that there is an environmental effect as illustrated in Figure 6.

## Compatibility with Coolants

The effects of environment on both creep and fatigue strength are, in part, related to the chemical interactions that occur between the low levels of impurities in the helium environment and the materials being tested. For the last 15 to 20 years, there has been extensive study of these interaction mechanisms as they relate to TGR
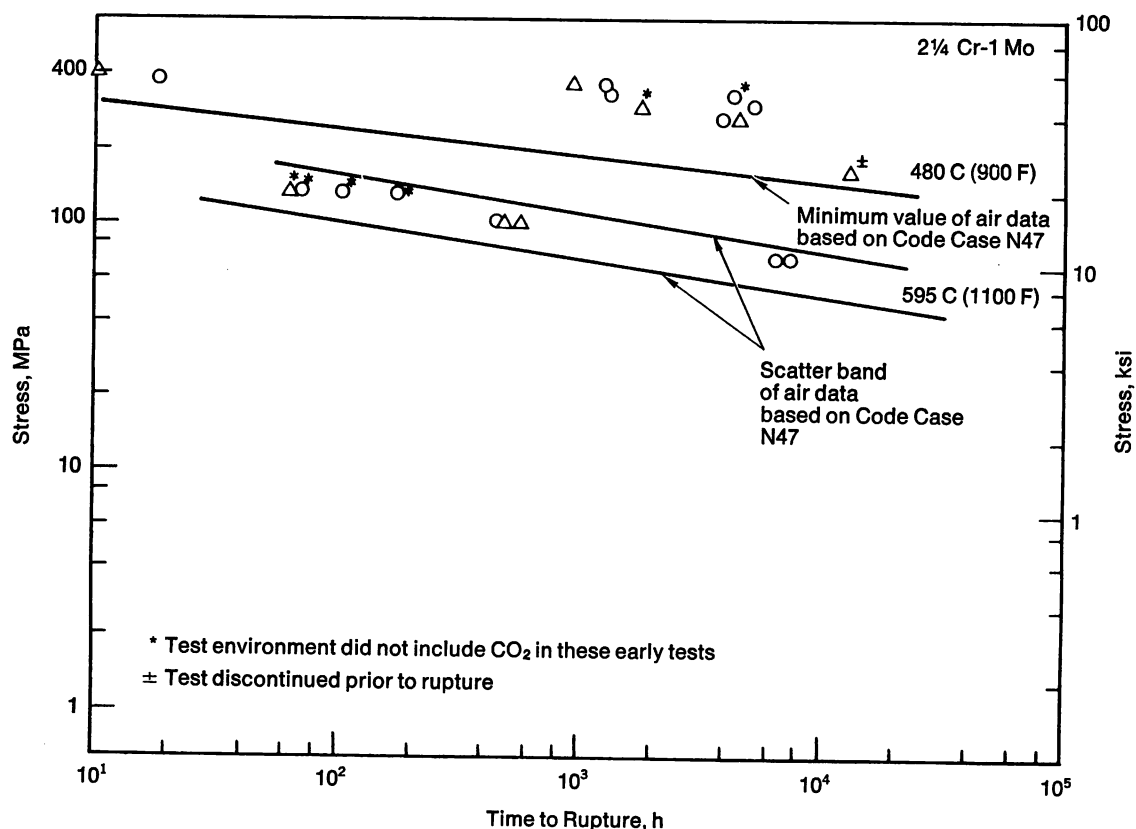


FIGURE 4—Comparison of stress rupture behavior of several heats of annealed 2¼Cr-1Mo steel in TGR helium and the scatter band of air data for the alloy.

helium. Impurities that may be expected in gas cooled reactor systems are shown in Table V. Review of these environments indicates that they can be oxidizing or reducing and carburizing or decarburizing with respect to the major alloying elements in iron- and nickel-base high temperature alloys.[7] In GCFRs, decarburization is



FIGURE 5—*Comparison of creep rupture behavior of specimens from a single heat of annealed 2¼Cr-1Mo in air and TGR helium.*
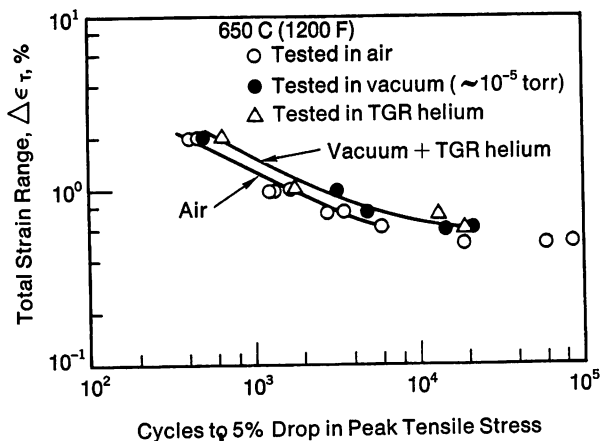


FIGURE 6—*Number of cycles to a 5% decrease from the maximum value of the peak tensile stress as a function of the total axial strain range for Alloy 800H specimens tested in air, vacuum and TGR helium.*

**Table V**—Impurity Levels Expected in Primary Coolant of Gas Cooled Reactors

| Impurity | HTGR-SC | HTGR-GT and HTGR-PH | GCFR |
|---|---|---|---|
| $H_2O$ | 10 ppm | 0.5 ppm | 4000 ppm |
| $H_2$ | 200 | 500 | 1000 |
| CO | 10 | 50 | <1 |
| $CH_4$ | 20 | 50 | <1 |
| $CO_2$ | <1 | <1 | <1 |
| $N_2$ | 15 | 15 | |
| $O_2$ | <<<1 | <<<1 | |

potentially a more significant concern in view of the relatively high moisture level that can occur in this essentially graphite-free system. On the other hand, in TGRs featuring a large, hot graphite core, carburization is of greater potential significance.

Both carburization and decarburization rates are very sensitive to temperature. Rates of carburization, for example, increase significantly as temperature rises, as shown in Figure 7. The wrought alloys clearly can carburize relatively rapidly in TGR helium at temperatures above about 700 to 800 C (1290 to 1470 F). The cast nickel-base superalloys, on the other hand, exhibit much greater resistance to carbon uptake under these conditions.



FIGURE 7—*Comparative carburization behavior of metals in TGR helium.*

The exact mechanisms of carburization under TGR conditions are not yet fully understood. However, it is known that important factors include the catalytic and transport characteristics of oxides formed on the surface, the carbon potential of the gas relative to the carbon activity in the metal under test, and the diffusion of carbon in the metal.

The observation of significant carburization rates at temperatures pertinent to the higher temperature gas cooled reactor systems has led to increased efforts to develop carburization resistant coatings and alloys for the high temperature applications. Some of the major coating systems currently under study are shown in Table VI.

Some of the heat exchangers in gas cooled reactor systems contain water/steam as a secondary coolant fluid. Thus, it is also necessary, for design purposes, to know the oxidation rates of materials in high pressure steam. Substantial work in this direction has been under way for many years at Oak Ridge National Laboratory,[8] and Figure 8 illustrates these results on several alloys of interest.

**Table VI**—Carburization Resistant Coatings Under Study

| Aluminized Coatings | Preformed Oxide Coatings |
|---|---|
| Al | In air |
| Al + Cr | In controlled environments |
| Al + Pt | |
| Al + Rh | |
| | |
| M-Cr-Al-Y Coatings | Claddings |
| M = Fe or Ni | Fe-Cr-Al-Mo-Hf |
| | Fe-Cr-Al-Y |
| Silicide Coatings | Udimet 720 |
| Cr-Si | Inco Clad 671/800H |
| Cr-Si-Ni | |



FIGURE 9—Effects of thermal aging at 650 C (1200 F) on the Charpy impact toughness of several high temperature alloys.



FIGURE 8—Corrosion rates of candidate TGR heat exchanger materials in superheated steam.[8]
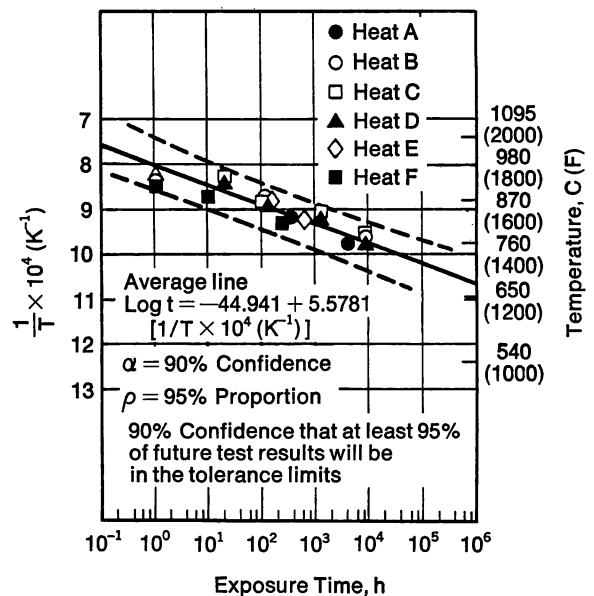


FIGURE 10—Temperature-time envelope for the onset of recrystallization in 20% prestrained alloy 800H.

## Thermal Aging and Embrittlement

At the temperatures that prevail in gas cooled reactors, many of the high temperature alloys of interest undergo microstructural changes that may cause embrittlement, which occasionally can be serious.[9] Because it is necessary to show that reactor structures can absorb high strain rate events (such as seismic loads) after extended high temperature operation, it is important to understand the extent to which aging causes changes in properties. Figure 9 illustrates the results obtained from long time aging of a number of alloys of interest for gas cooled reactor applications. The Charpy V-notch data shown in Figure 9 conveniently illustrate changes that occur. However, for design purposes, more quantifiable fracture toughness information (such as that generated by compact tension testing) is required, and such data are currently being generated.

## Fabricability/Costs

As indicated previously, many of the components of high temperature gas cooled reactors are large and complex in configuration. To be fabricated, materials must be capable of being formed into the required shapes. Material costs are also important. Thus, it is essential to understand the overall cost and fabricability of candidate materials. The effects of fabrication factors on expected service behavior may also be important. For example, the effects of fabrication-induced cold work on the properties of materials can be significant, and it is essential, among other things, to avoid onset of recrystallization in service (Figure 10).[10] Similarly, it is important to know the elevated temperature strength of the weld metals used to join materials for elevated temperature nuclear service. It is becoming clear that weld metal strengths may not always live up to those of the base metal, and special precautionary methods may be required if satisfactory long time service is to be assured.

## Materials for Fusion Reactor First Wall/Blankets

### Introduction

First wall/blanket lifetime has been identified as a

key issue in the ultimate commercialization of fusion power. Because of the considerable cost and time involved in first wall/blanket changeouts, the structural materials employed must exhibit a long life under severe operating conditions, and low activation materials should be employed wherever possible. The current U.S. program to develop materials for commercial reactors is focused on several classes of metallic materials, including austenitic stainless steels, precipitation hardened Fe-Ni-Cr alloys, reactive metal alloys (titanium) and refractory alloys (vanadium with niobium). Recent results from fission reactor irradiation experiments in the United States and Europe suggest that another group of alloys, the Fe-Cr martensitic stainless steels, might offer the potential of significantly greater first wall/blanket lifetimes and therefore should be given serious consideration. The following sections of this paper report the results of preliminary experiments and analyses to assess the feasibility of incorporating ferromagnetic martensitic steels in fusion reactor designs and an evaluation of the possible advantages of this class of material with respect to first wall/blanket lifetime. Again, it is noted that molybdenum will play a significant alloying role in this application.

The general class of alloys under consideration is ferritic steels containing about 9 to 13% chromium with small but important additions of carbide stabilizing and/or strengthening elements such as molybdenum and vanadium. These steels are conventionally used in the normalized-and-tempered condition for high temperature applications.[11] As discussed below, they can compete favorably with austenitic alloys up to about 600 C (1110 F). Although the heat treatment can result in either a tempered martensite or bainite structure, depending on the alloy and thermal treatment parameters, this general class of materals will be referred to as "martensitic" stainless steels for simplicity. These steels have been employed successfully in such high temperature applications as steam turbines, jet engines and gas turbines. The 12Cr-1Mo-0.3V alloy has been used commercially for high temperature applications in Europe for over 10 years. The tungsten-containing alloy specified in the Federal Republic of Germany as DIN X 20 CrMoWV 12 - Material No. 1.4935 (marketed by Sandvik in the United States as alloy HT-9), is currently being considered for a number of thermal and fast reactor components, including steam generators, recuperators, auxiliary heat exchangers and steam piping.

On the basis of irradiation test results, HT-9 was among a group of six prime advanced candidate materials identified by the United States National FBR Cladding/Duct Materials Development Program and is in fact the only commercial candidate alloy. Because of the encouraging and rapidly expanding data base from the FBR Program, the significant application history, and the current interest in the alloy, HT-9 was selected as a representative martensitic alloy for evaluation for fusion applications.

The nominal composition of alloy HT-9 is given in Table VII. For high temperature, extended time service, the alloy is usually heat treated at 1050 C (1920 F) for one-half hour, air cooled, and then tempered at 780 C (1435 F). Although higher strengths are obtainable in 12Cr steels with lower tempering temperatures, the 780 C (1435 F) treatment ensures long time stability of the tempered martensite and strengthening carbide precipitates to about 600 C (1110 F) service.

## Mechanical Behavior

The strength of HT-9 is compared with that of several other candidate first wall/blanket alloys in Figure 11. The variations of minimum ultimate tensile strength with temperature is plotted for HT-9, 20% cold worked and annealed Type 316 stainless steel, Inconel 718, titanium alloys Ti-6Al-4V and Ti-6Al-2Sn-4Zr-2Mo, vanadium
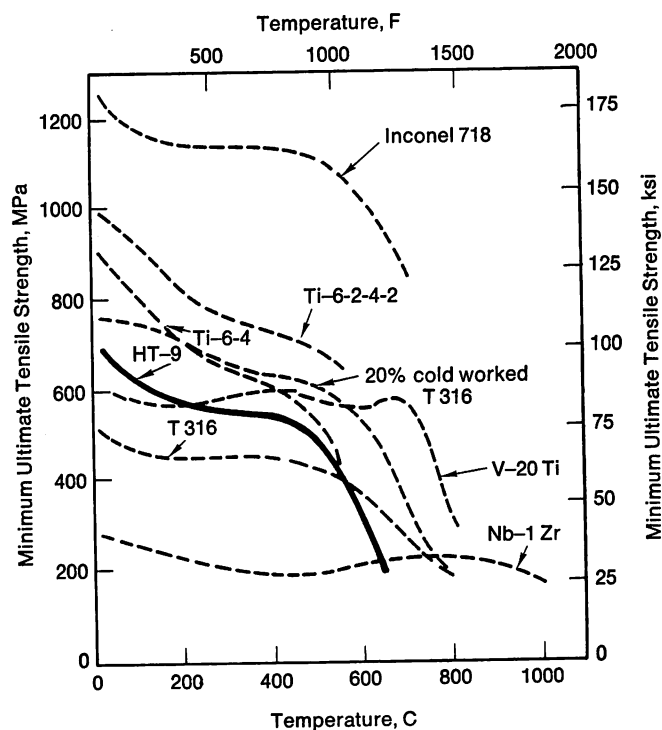


FIGURE 11—*Minimum ultimate tensile strength of HT-9 and other candidate first wall/blanket materials.*

**Table VII**—Nominal Composition of Alloy HT-9

| Element, % | | | | | | | | |
|---|---|---|---|---|---|---|---|---|
| Cr | Ni | Mo | W | V | Si | Mn | C | Fe |
| 11.5 | 0.5 | 1.0 | 0.5 | 0.3 | 0.25 | 0.5 | 0.20 | Bal |

**Table VIII**—Estimated Allowable 300,000-Hour Design Stresses ($S_{mt}$) for HT-9 and Type 316 Based on the Criteria of ASME Code Case N-47 (Elevated Temperature Service)

| Material | $S_{mt}$, MPa (ksi) | | | | | |
|---|---|---|---|---|---|---|
| | R.T. | 400 C  (750 F) | 500 C  (930 F) | 550 C  (1020 F) | 600 C  (1110 F) | 650 C  (1200 F) |
| HT-9 | 227  (32.9) | 196  (28.4) | 110  (16.0) | 62  (9.0) | 32  (4.6) | 14  (2.0) |
| Type 316 | 138  (20.0) | 110  (16.0) | 108  (15.7) | 87  (12.6) | 50  (7.3) | 31  (4.5) |

alloy V-20Ti, and niobium alloy Nb-1Zr.[12-16] It is evident that the short term strength of HT-9 is between that of Type 316 and cold worked Type 316 to about 500 C (930 F) and is equivalent to that of Type 316 and Ti-6Al-4V at about 550 C (1020 F). Above 500 C (930 F), the short term strength of HT-9 decreases rapidly.

Estimated allowable stress intensities, $S_{mt}$, for HT-9 and Type 316, defined using the criteria employed by ASME Boiler and Pressure Vessel Code Case N-47, are shown for a 300,000-hour lifetime as a function of temperature in Table VIII. The allowable design stress intensities take into account both time-independent and time-dependent creep strength behavior and indicate that for lifetimes on the order of 40 years, which are desirable for commercial power plants, the maximum nominal design temperature for HT-9 components is about 600 C (1110 F).

In fusion reactors, as in gas cooled reactors, thermal stresses are an important source of cyclic fatigue and creep-fatigue damage, particularly in pulsed fusion systems. The comparative resistance to thermal stress can be estimated by a parameter, M, which is a function of thermal conductivity, thermal expansion coefficient, Poisson's ratio, Young's modulus and yield strength. Thermal stress resistance increases with increasing M. The thermal stress resistance of HT-9 at 500 C (930 F) is

**Table IX**—Thermal Stress Resistance of Candidate Fusion Alloys at 500 C (930 F)

| Alloy | Thermal Stress Resistance, M, (W/m) x 10$^{-3}$ |
|---|---|
| Annealed Type 316 | 1.3 |
| Type 316 Cold Worked 20% | 4.9 |
| HT-9 | 8.5 |
| Ti-6Al-4V | 10.2 |
| Ti-6Al-2Sn-4Zr-2Mo | 10.4 |
| Inconel 718 | 10.7 |
| V-20Ti | 12.3 |
| Nb-1Zr | 19.8 |

Note: $M = \dfrac{2\sigma_y K(1-\nu)}{\alpha E}$,

where $\sigma_y$ = yield strength,
  K = thermal conductivity,
  $\nu$ = Poisson's ratio,
  $\alpha$ = thermal expansion coefficient,
  E = Young's modulus.

compared with that of other candidate materials in Table IX. The significantly higher thermal conductivity and lower thermal expansion coefficient of ferritic HT-9 relative to austenitic Type 316 provides the former with a significantly greater resistance to thermal stress effects. The thermal stress resistance of HT-9 is slightly lower than that of the titanium alloys and the precipitation-strengthened nickel alloy Inconel 718.

**Radiation Damage**

The primary reason for investigating the application of HT-9 is its apparent resistance to neutron radiation damage. Most of the pertinent information with respect to void swelling, in-reactor creep, and embrittlement has been developed in the U.S. FBR program and has not yet been generally released. Although discussion of the radiation damage resistance of HT-9 must therefore be qualitative, a number of relevant observations can be made on the basis of EBR II data to greater than $1 \times 10^{23}$ n/cm² (E > 0.1 MeV).

Void swelling in HT-9 is at least an order of magnitude less than in cold worked Type 316. Current results indicate that swelling is even lower than the 3.7%, 500 C (930 F) peak swelling at 150 dpa previously reported for HT-9 under heavy ion bombardment.[17] The currently published equation for cold worked Type 316[18] predicts peak swelling of about 35% at 580 C (1075 F) and 150 dpa. In addition, the in-reactor creep resistance of HT-9 appears better than that of cold worked Type 316 to temperatures in excess of 600 C (1110 F).[19]

Although only low helium levels and low helium/dpa ratios relative to fusion neutron conditions have been evaluated, the tensile ductility retention of HT-9 appears superior to that of cold worked Type 316 (particularly when tested above the irradiation temperature) and vastly superior to that of the precipitation-strengthened nickel alloys up to 600 C (1110 F). Furthermore, the microstructure of HT-9 appears stable under irradiation in the temperature range of interest, but the shift in ductile/brittle transition temperature (DBTT) after irradiation must be determined.

**Application Experience**

The class of 9Cr-12Cr steels has been used extensively in power generation applications throughout Europe for over 25 years.[20] While most of these applications have been directed toward superheaters, reheaters and evaporators for oil and coal fired power plants,

much experience and performance history information pertinent to fusion applications has been generated. In addition to fossil power plant applications, this class of steel has been employed in nuclear power plants. In the Hinkley Point "B" AGR in the United Kingdom, super-heaters and reheaters are 9Cr and 12Cr steels.[21] The Fort St. Vrain HTGR employs standard 410 and 422 (12Cr) stainless steel grades in the helium circulators and com-pressors.[22] Other applications have included gas and steam turbine components, aircraft and missile thin wall pressure vessels, and petroleum industry pressure vessel linings.[23]

Proposed nuclear applications for 9Cr-12Cr steels presently under consideration include ducts, cladding and steam generators for the U.S. LMFBR and GCFR; steam generators for the Japanese FBR; ducts and steam generators for the French Super Phenix; steam genera-tors, helium/helium heat exchangers, helium circulators and steam piping for the U.S. HTGR; and steam genera-tors for the U.S. LWR.

Two of the largest users for fossil plants in Europe have been Sulzer Brothers (Switzerland) and the United Kingdom Central Electricity Generating Board (CEGB). Table X indicates the performance and failure histories for these two organizations. In the United Kingdom, CEGB has 25 operating fossil power plants which use 9Cr and 12Cr steels. Application temperatures were as high as 850 C (1560 F), but successful long term operation temperatures were limited to the range from 600 to 650 C (1110 to 1200 F) maximum. At the higher temperatures, overheating contributed to a significant amount of creep damage with correspondingly shorter rupture lives. Of particular interest are the relatively few weld failures. Welding must be performed following a careful proce-dure involving pre- and post-weld heat treatments. Only two failures have been reported which related directly to welding.

The lower part of Table X shows the countries and

total tonnages reported for Sulzer Brothers fossil power plants.[24] Again, excellent operating performance with only limited failures has been observed.

### Metallurgical Performance Evaluation of HT-9

To qualify the long term high temperature service performance of candidate martensitic stainless steel for fusion application, General Atomic, in conjunction with Sulzer Brothers, evaluated the behavior of HT-9 super-heater tubing from a welded boiler in the Reutlingen, FRG, coal fired power plant.[25] Tubes were removed from service after 80,000 hours at temperatures near 600 C (1110 F). In addition to 720 normal operating starts/shut-downs (50 from room temperature), the tube had also experienced six off-normal thermal shocks related to power failures at the plant. The tubes were subjected to relatively low stresses of approximately 20 to 50 MPa (2.9 to 7.3 ksi).
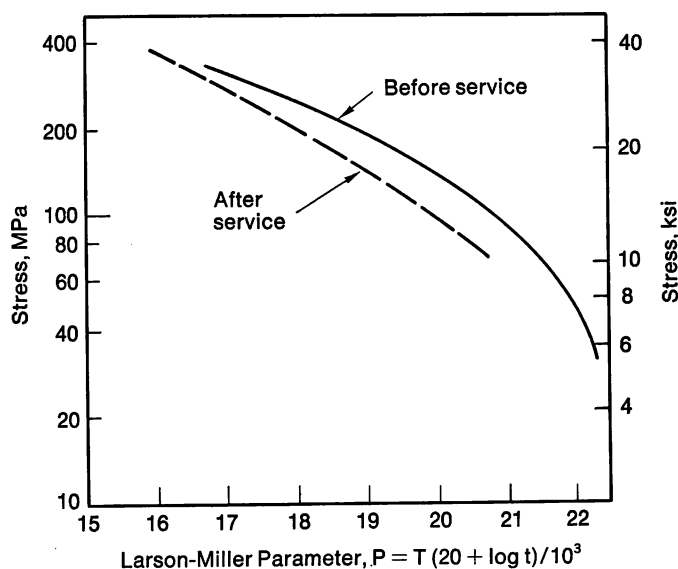


FIGURE 12—Effect of 80,000-hour, 600 C (1110 F) service exposure on the stress rupture properties of HT-9.

**Table X**—Foreign Usage and Performance of 9Cr-12Cr Steels in Fossil Power Plants

| Location | Usage | Alloy | Temperature, C (F) | Service Status, $10^3$ h | Failure History |
|---|---|---|---|---|---|
| United Kingdom | 13 plants | 9CrMo (V) | 450-660 (840-1220) | ≤110 | 1 faulty weld 1 faulty weld repair Fireside corrosion |
| | 12 plants | 12CrMo | 430-850 (805-1560) | ≤45 | Overheating > 650 C (1200 F) |
| Austria Belgium Czechoslovakia Germany Switzerland Turkey Yugoslavia | 96 tons | 9CrMo | ≤610 (≤1130) | ≤110 | 1 faulty weld repair |
| | >250 tons | 12CrMo (V, W) | ≤610 (≤1130) | ≤130 | Fireside corrosion |
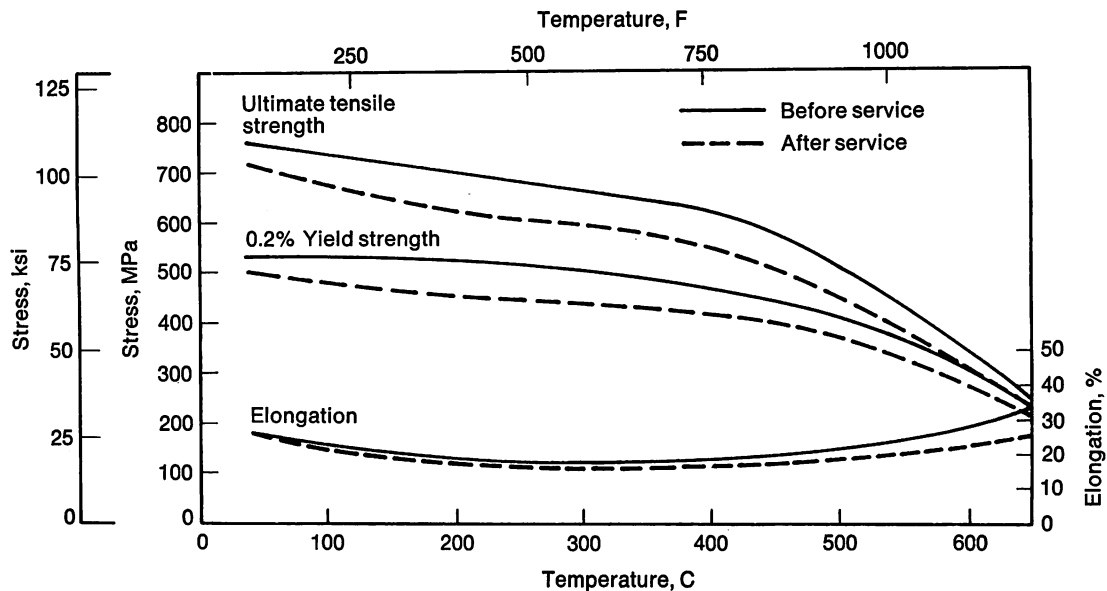
FIGURE 13—Effect of 80,000-hour, 600 C (1110 F) service exposure on the tensile properties of HT-9.

The interrupted-service evaluation included stress rupture, tensile strength from room temperature to 600 C (1110 F), Charpy V-notch impact toughness and microstructural examination. The properties of unexposed tubing were determined simultaneously for comparison.

Figure 12 shows the curves obtained in the stress rupture tests with stress plotted as a function of the Larson-Miller parameter.[26] Overaging of carbides after 80,000 hours of in-service exposure decreased stress rupture lifetimes, particularly at the higher stress levels. As indicated by Figure 12, the residual creep properties remained quite good. It should also be mentioned that total creep strains did not change significantly. Figure 13 shows the room and elevated temperature tensile properties determined. Again, strength properties were only slightly reduced after long term service, and the tensile ductilities remained quite close to values before service over the entire test temperature range. Figure 14 shows the impact toughness values obtained at room temperature and −45 C (−50 F) for half-width specimens. Impact toughness decreased; however, substantial toughness remained even at −45 C (−50 F). Alloy HT-9 undergoes a transition in impact fracture behavior from ductile to brittle with decreasing temperature, and, following the service exposure, the DBTT shifted to a somewhat higher temperature, although the precise DBTT was not determined in these tests.

Transmission electron microscopy was employed to study the microstructural changes occurring with service exposure. Overall structural stability appeared to be excellent, the most prominent feature noted being the enhanced precipitation of $M_{23}C_6$ carbides at martensite inter-lath boundaries. Some precipitation of an $Fe_2Mo$ Laves phase was also noted but was not found to be morphologically detrimental to the mechanical properties. The decrease in impact toughness properties was
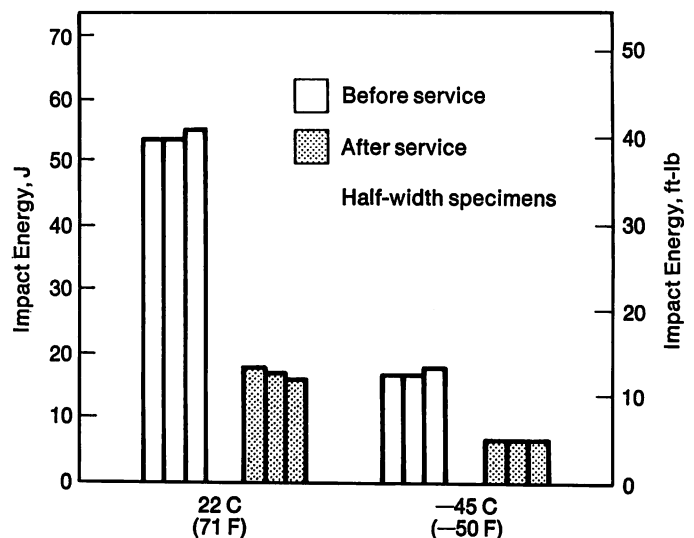


FIGURE 14—Effect of 80,000-hour, 600 C (1110 F) service exposure on the impact properties of HT-9.

most likely associated with the carbide precipitation. Thus, the effects of a long term service exposure did not lead to dramatic reductions in mechanical properties which is consistent with the overall good thermal stability of HT-9.

## Identification of Key Issues and Major Requirements

Based on a detailed evaluation of the known data bases for martensitic steels and fusion design requirements, the key issues which must be resolved have been identified as follows:

1. Fracture resistance, particularly the change of fracture toughness at lower temperature as a result of the ductile-to-brittle transition behavior characteristics of these steels.

2. The effect of the fusion reactor environment on structural properties, including the effects of displacement damage and transmutation products from interaction with fusion 14-MeV neutrons and the compatibility with candidate coolants.

3. Weldability/fabricability, specifically pre- and post-weld heat treatment requirements, cracking susceptibility, and repair procedures in configurations pertinent to fusion applications and the sensitivity of weld procedures to microstructure and properties.

A comprehensive testing program to address these issues is currently in progress.

## Concluding Comments

The preceding discussion has illustrated some of the materials challenges that lie before us in our quest for the energy benefits that will result from the development of gas cooled and fusion reactors. Resolution of these issues will undoubtedly challenge our technical and innovative abilities. Nevertheless, it seems highly probable that the work currently under way and that which will be performed in the next several years will provide the required materials engineering solutions, and we will be able to bring these much-needed advanced systems to the market place.

In closing, it seems appropriate to note the past, present and future contributions that the use of molybdenum makes to the engineering application of a wide variety of alloys that will play a key role in "Alloys for the 80s."

## References

1. J. W. Landis and J. F. Watson, "Materials and Design Concepts of Gas Cooled Reactor Systems," *Gulf-GA-A12248*, General Atomic Co., 1972.

2. P. R. Kasten, "Gas Cooled Reactors—The Importance of Their Development," *ORNL-5515*, Oak Ridge National Laboratory, 1979.

3. T. Moffette, et al., "GCFR Commercial Plant Parameter Interim Selection," *GA-A15397*, General Atomic Co., 1979.

4. C. F. McDonald, "The Nuclear Closed Cycle Gas Turbine—A Utility Power Plant of the Future," *GA-A15082*, General Atomic Co., 1978.

5. "GA TNS Project—Status Report for FY78 (Vol. I-VIII)," *GA-A15100*, General Atomic Co., 1978.

6. G. Y. Lai, and R. J. Wolwowicz, "Creep-Rupture Behavior of 2¼Cr-1Mo Steel, Alloy 800H and Hastelloy X in a Simulated HTGR Helium Environment," *GA-A15572*, General Atomic Co., 1979.

7. F. N. Mazandarany and G. Y. Lai, "Corrosion Behavior of Selected Structural Materials in a Simulated Steam-Cycle HTGR Helium Environment," *GA-A14446*, General Atomic Co., 1977.

8. J. R. D. Stefano, Oak Ridge National Laboratory, private communication, 1978.

9. O. F. Kimball, W. R. Pieren and D. I. Roberts, "Effects of Elevated Temperature Aging on the Mechanical Properties and Ductility of Ni-Cr-Mo-Cb Alloy 625," *GA-A12683*, General Atomic Co., 1973.

10. G. Y. Lai and A. B. Smith, "Recrystallization Behavior of Alloy 800H," *Characterization of Materials for Service at Elevated Temperatures, MPC-7*, ASME, New York, 1978, 225.

11. R. T. King, et al., "Alternate Structural Materials for Liquid Metal Fast Breeder Reactors," Symposium, *Structural Material for Service at Elevated Temperatures in Nuclear Power Generation*, Houston, Texas, November 1975, ASME, New York, 375.

12. J. E. Chafey and J. B. Wattier, "Estimation of Allowable Design Stress Values for 12Cr-1Mo-0.3V Steel," *GA-A14610*, General Atomic Co., 1978.

13. J. C. Spanner (Ed.), "Nuclear Systems Materials Handbook, Volume 1, Design Data," *TID 26666*, Handford Engineering Development Laboratory, 1976.

14. "Metallic Materials and Elements for Aerospace Vehicle Structure," *HIL-HBKC-5B*, Sections 5.3.3 and 5.4.3, USAF, 1975.

15. R. E. Gold, et al., "Technical Assessment of Vanadium Base Alloys for Fusion Reactor Applications," *COO-4540-1*, Westinghouse Electric Corp., 1978, 112.

16. J. W. Davis and G. L. Kulcinski, "Assessment of Titanium for Use in the 1st Wall/Blanket Structure of Fusion Power Reactors," *EPRI ER 386*, McDonnell Douglas Astronautics Co., 1977, 10.

17. F. A. Smidt, et al., "Swelling Behavior of Commercial Ferritic Alloys, EM-12 and HT-9, as Assessed by Heavy Ion Bombardment," *Irradiation Effects on the Microstructure and Properties of Metals*, ASTM STP #611, American Society for Testing and Materials, 1976, 227.

18. J. C. Spanner (Ed.), *op. cit.*, Section 5.

19. B. A. Chin, et al., "A Comparison of the In-Reactor Creep Behavior of Selected Commercial Alloys at a Temperature of 593°C," *9th ASTM International Symposium on Effects of Radiation on Structural Materials*, Richland, Washington, 1978.

20. L. D. Thompson and S. N. Rosenwasser, "Ferritic Stainless Steels for Fusion Applications," to be published in the Sixth Alloy Development for Irradiation Performance Task Group Quarterly Progress Report for the Period Ending June 30, 1979.

21. L. M. Wyatt, "The Performance of Cr-Mo Steels in the Boilers of CEGB Power Stations, in Ferritic Steels for Fast Reactor Steam Generators," Proceedings of an International Conference held by the British Nuclear Energy Society at the Institution of Civil Engineers, London, May 30 through June 2, 1977.

22. A. Smith, General Atomic Co., private communication.

23. J. Z. Briggs and T. D. Parker, "The Super 12% Cr Steels," Climax Molybdenum Co., 1965.

24. H. Fricker, "Sulzer Experience with High Chromium Ferritic Steels," *TA 2730*, Sulzer Brothers, 1977.

25. J. E. Chafey and L. D. Thompson, "Post-Service Evaluation of the Properties of a 12 Cr-1 Mo Steel Superheater Tube," to be presented at the 1980 ASME Winter Annual Meeting, Chicago, Illinois, November 16-21, 1980.

26. B. Walser, "The Metallurgical and Mechanical Properties of X 20 CrMoWV 12 1 After Service Exposure in a Fossil Fired Boiler," 222/1511, Sulzer Brothers, 1977.

## Discussion

**V. K. SIKKA, *Oak Ridge National Laboratory*.** In Figure 14, you showed that an 80,000-hour exposure in air or in steam degraded the impact strength of HT-9. Would not superimposed irradiation further degrade impact properties?

Regarding your comment that you see this problem being addressed in the 80s, are you referring to chemistry modifications or changes in temperature?

J. F. WATSON. To take the second question first, it is minor changes in chemistry. On the first question, there will be an additive effect, and this may be the problem that puts a limit on the extent that these alloys can be used. At the moment we do not have the test data because these intensely energetic neutrons will cause 150 displacements per atom, let's say, and I don't think we have any results (maybe a few cyclatron tests using helium ion injection) to go by. So we will be standing here perhaps ten years from today to assess the data that have been gathered.

V. K. SIKKA. Is much known about the fabrication of this material?

J. F. WATSON. Yes, that was the point of Table X that showed the experience throughout 25 CEGB plants, steam piping mostly, and the Sulzer experience in 5 or 6 foreign countries. The experience had all been very good of course with careful attention to welding.

G. H. WALTER, *International Harvester Company*. Speakers have given data for Charpy U tests and Charpy V-notch tests. Are these used to rank materials or are they design criteria?

J. F. WATSON. Charpy tests are strictly qualitative. Design criteria are based on J-interval and similar tests. The question you raise is, by the way, not just applicable to the nuclear industry.

V. K. SIKKA. Charpy U-notch tests are being used for stainless steel, and there is some correlation with J-interval measurements so it can be used to evaluate long term aging effects.

D. A. CANONICO, *Oak Ridge National Laboratory*. As far as radiation damage goes, we have designed based on appendix G, which requires a minimum 67 J (50 ft-lb) at 33 C (60 F) above the nil ductility temperature. So those low values would not be allowed today in or near any of those types of reactors. We are doing quite a bit of work on the gas crude program looking at materials in relation to appendix G. This kind of information is good, but the areas of concern are those involving parts under stress where the code would be concerned with allowable stresses.

# Heavy-Wall Pressure Vessels for Energy Systems

by D. A. Canonico
Oak Ridge National Laboratory

The 1980s must be dedicated to the development of the technology required to assure an adequate supply of economically acceptable energy. Of particular concern is the availability of petroleum during the next decade. It may be in short supply because (1) reserves are depleted or (2) there is an oil embargo. Regardless of the cause, a shortage of petroleum will result in a crisis of major proportions.

In 1978, 78.0 quads of energy were consumed in the United States.[1] The energy usage was in three categories: residential-commercial, industrial and transportation. The portion of total energy consumed by each of these categories was 36.5, 37.1 and 26.4%, respectively. The sources of the energy in 1978, as well as for the prior five years, are given in Table I. It is important to note that oil was the source of nearly 50% of the energy consumed over the six years covered in Table I, and its usage increased (by nearly 4%) from 1973 through 1978. In 1978, oil supplied 37.8 quads of energy. Transportation accounted for nearly 53% (20 quads) of the petroleum consumed in the U.S. Only 3.9 quads (10.3%) of the oil was consumed by the electric utilities, and it was the energy source for 16.6% of the electricity produced. Much of this 16.6% can be supplied by nuclear and/or coal. Such is not the case for transportation. This category is nearly totally dependent upon petroleum products.

During the next decade, we must assure the transportation industry the energy that it requires. This may necessitate the increased use of electric vehicles at the present state of technology of storage batteries. If such a means of transportation is promoted, the electric energy can be supplied by nuclear or coal facilities. Even with an increase in the use of electric vehicles, the demand for petroleum for transportation will continue.

The availability of crude oil in the next decade depends on (1) recoverable resources and (2) the world political climate. In 1973, it was reported[2] that the U.S. had 8 and 11 years of proven crude oil and natural gas reserves. In 1978, demonstrated recoverable crude oil reserves were reported[3] to be 4.3 years. (Dry natural gas reserves were reported[4] to be 10.7 years.) These figures may be extremely conservative. Proven reserves are economically controlled, and higher priced crude oil will no doubt extend the "years of demonstrated reserves." Such a conclusion is based on past experience; fear of "running out of oil," was expressed[5] as early as the 1920s. Although the time period may not be precisely predicted, it is a fact that the U.S. oil and gas reserves are finite. Perhaps of more concern is the fact that most western nations are importers of crude oil. (In 1978 43.7% of the petroleum products consumed[1] in the U.S. was imported!) If this imported oil should become unavailable for any reason, the impact would be serious.

For the above reasons, it is necessary that the development of alternate sources of petroleum products be the primary goal of the 1980s. Advanced energy sources such as solar and fusion are technologically challenging, but their commercialization is considerably beyond the next decade. It is mandatory that proven energy sources be promoted, and, where necessary, the technology to fully commercialize a system be developed. (Primarily this is the area of coal conversion. Liquefaction and gasification of coal have been proven to be feasible. During the next decade, we must emphasize their commercialization.) Commercialization of coal conversion requires large reaction and gasifier pressure vessels. This is an area where engineering skills must be focused to assure that these vessels operate safely and reliably for their design lives. Concurrent with the commercialization of the coal conversion processes, we

**Table I**—Major Sources of the Energy Consumed in the United States for the Years 1973-1978[a]

| Year | Total Consumption, quads[b] | Percent of Total | | | | |
|------|------|------|------|------|------|------|
| | | Coal | Gas | Oil | Hydro | Nuclear |
| 1973 | 74.61 | 17.8 | 30.2 | 46.7 | 4.0 | 1.2 |
| 1974 | 72.35 | 17.8 | 30.0 | 45.7 | 4.6 | 1.8 |
| 1975 | 70.71 | 18.1 | 28.2 | 46.3 | 4.6 | 2.7 |
| 1976 | 74.16 | 18.5 | 27.4 | 47.0 | 4.1 | 2.9 |
| 1977 | 76.66 | 18.4 | 26.0 | 48.5 | 3.4 | 3.5 |
| 1978 | 78.01 | 18.1 | 25.4 | 48.4 | 4.1 | 3.8 |

[a] U.S. Department of Energy, Information Administration, Annual Report to Congress, 1978, DOE/EIA-0173/2 (April 1979).
[b] 1 quad = $1.055 \times 10^{18}$ J = $10^{15}$ Btu.

**Table II**—Comparison of Sizes of Pressure Vessels for Comparable Plants

| Reactor Type | BWR | PWR |
|---|---|---|
| Identification | Hartsville–1 | Palo Verde–1 |
| Net Electrical Output, MW | 1205 | 1235 |
| Coolant Pressure, MPa (psi) | 7.2 (1040) | 15.3 (2250) |
| Cylinder Wall Thickness, mm (in.) | 145 (5.7) | 231 (9.1) |
| Inside Diameter, m (in.) | 6.045 (238) | 4.623 (182) |
| Height, m (ft) | ~22 (~73) | ~15 (~48) |

have the opportunity of advancing the concepts of vessel design, developing improved materials and improving fabrication procedures. This is a rare opportunity afforded to the metallurgical community, and it is a challenge that must be met. This is an opportunity to conduct premortem studies, an approach to safety that, to the best of my knowledge, was first achieved in the Heavy-Section Steel Technology (HSST) Program,[6] a program that is sponsored by the U.S. Nuclear Regulatory Commission and administered by the Oak Ridge National Laboratory.

The HSST Program is an integral part of a comprehensive effort under way in the U.S. to assure the integrity of light-water nuclear reactor pressure vessels throughout their useful lives. Nuclear pressure vessels weigh about 450 metric tons (500 tons), approach 6.1 m (20 ft) in diameter, and are over 21 m (70 ft) in height. Vessel sizes in recent years have increased to the point where a vessel weighing about 910 metric tons (1000 tons) is not uncommon. Table II compares typical vessel sizes for boiling and pressurized water reactors. The dimensions of nuclear pressure vessels pale, however, when compared with those proposed for commercial coal gasification processes. A gasifier vessel for a conceptual two-train, 6.1 MW (500 × $10^9$ Btu/day) HYGAS commercial coal conversion plant[7] is nearly 76 m (250 ft) tall, varies in inside diameter from 7.6 to 9.4 m (25 to 31 ft), and weighs nearly three times as much as a boiling water reactor (BWR) or a pressurized water reactor (PWR). The nominal operating pressures in the HYGAS process are similar to those for a BWR, but the process temperature is considerably higher, 930 vs 290 C (1700 vs 550 F). A great deal of energy will be contained in an operating pressure vessel the size of that shown in Figure 1. A cursory calculation based on a nominal design pressure of 9.0 MPa (1300 psi), a temperature of 930 C (1700 F), and a gas composition of 25% $H_2$, 25% $CH_4$, 30% $H_2O$, 10% CO and 10% $CO_2$, showed that the energy stored in the conceptual HYGAS gasifier is about 5.9 × $10^{10}$ J (4.4 × $10^{10}$ ft-lb), which is equivalent to nearly 13,200 kg (29,000 lb) of TNT. The potential destruction if the vessel were to rupture instantaneously is comparable to 58 conventional 455 kg (1000 lb) bombs. The instantaneous release of this much energy would literally destroy the entire coal conversion facility in
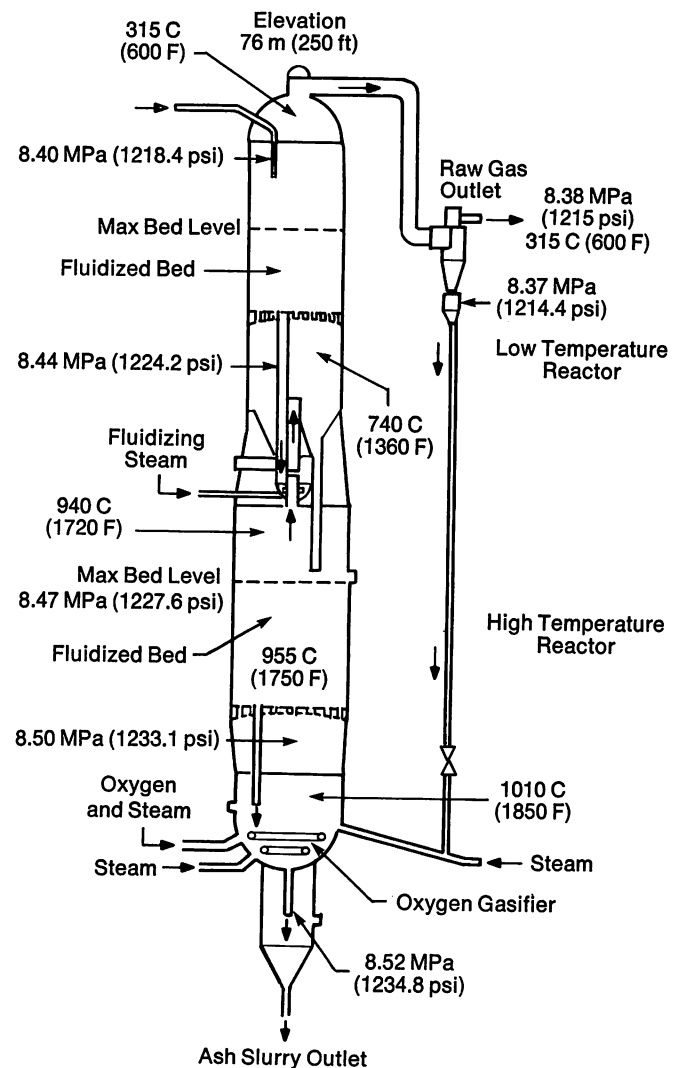


*FIGURE 1—Conceptual design for a pressure vessel for a two-train 6.1 MW (500 x $10^9$ Btu/day) commercial gasifier for the HYGAS process. Pressures are absolute.*

which it operated and could hurl fragments of steel hundreds of feet. Needless to say, such an incident is intolerable, and owners and manufacturers alike will strive to prevent such an occurrence.

The challenge of the 80s is to assure that we can build pressure vessels of the sizes that are required for commercialization of coal conversion processes. Perhaps the biggest challenge is to achieve this goal within the limits of current technology.

Working within the confines of current metallurgical technology permits us to:

1. review present rules whereby pressure vessels are designed,

2. utilize melting practices that provide improved ingot quality while increasing ingot yield,

3. develop improved alloys based on current pressure vessel steels, and

4. improve current welding procedures to provide higher deposition rates with improved weld

**Table III**—U.S. and Canadian Jurisdictions Requiring the Application of at Least One Section of the ASME Boiler and Pressure Vessel Code

| U.S. States and Territories | | |
|---|---|---|
| Alabama | Kentucky | Oklahoma |
| Alaska | Louisiana | Oregon |
| Arizona | Maine | Panama Canal Zone |
| Arkansas | Maryland | Pennsylvania |
| California | Massachusetts | Puerto Rico |
| Colorado | Michigan | Rhode Island |
| Connecticut | Minnesota | South Dakota |
| Delaware | Mississippi | Tennessee |
| Dist. of Columbia | Montana | Texas |
| Georgia | Nebraska | Utah |
| Guam | Nevada | Vermont |
| Hawaii | New Hampshire | Virginia |
| Idaho | New Jersey | Washington |
| Illinois | New York | West Virginia |
| Indiana | North Carolina | Wisconsin |
| Iowa | North Dakota | Wyoming |
| Kansas | Ohio | |

| U.S. Cities and Counties | | |
|---|---|---|
| Albuquerque, NM | Miami, FL | Spokane, WA |
| Buffalo, NY | Milwaukee, WI | Tacoma, WA |
| Chicago, IL | New Orleans, LA | Tampa, FL |
| Dearborn, MI | New York, NY | Tucson, AZ |
| Denver, CO | Oklahoma City, OK | Tulsa, OK |
| Des Moines, IA | Omaha, NB | University City, MO |
| Detroit, MI | Phoenix, AZ | White Plains, NY |
| E. St. Louis, IL | St. Joseph, MO | Arlington Co., VA |
| Greensboro, NC | St. Louis, MO | Dade Co., FL |
| Kansas City, MO | San Francisco, CA | Fairfax Co., VA |
| Los Angeles, CA | San Jose, CA | Jefferson Parish, LA |
| Memphis, TN | Seattle, WA | St. Louis, Co., MO |

| Provinces in Canada | | |
|---|---|---|
| Alberta | Newfoundland and | Prince Edward Island |
| British Columbia | Labrador | Quebec |
| Manitoba | Northwest Territory | Saskatchewan |
| New Brunswick | Nova Scotia | Yukon Territory |
| | Ontario | |

Information extracted from: *Tabulation of the Boiler and Pressure Vessel Laws of the United States and Canada,* Data Sheet, Uniform Boiler and Pressure Vessel Laws Society, Inc., Hartford, Connecticut, June 1979.

metal and heat affected zone quality.

Each of these four areas will be discussed in the following sections.

## Vessel Design

Currently large pressure vessels are designed in accordance with the rules of the *ASME Boiler and Pressure Vessel Code* (Code). (The United States and Canadian jurisdictions that require, by law, the application of at least one section of the Code are listed in Table III.) The basis for establishing maximum allowable stress values or design stress intensity values is related to a number of factors, the most important of which are:

1. design philosophy and criteria,

2. the type of construction permitted,

3. the degree of analysis required, and

4. the amount of nondestructive examination required.

Nuclear pressure vessels are designed and built in accordance with Section III of the Code. Because of the serious nature of a breach of the primary containment, the philosophy of design for Class 1 (Subsection NB) nuclear pressure vessels requires a greater degree of design analysis for all construction details. Procedures are given for classifying stresses and evaluating cyclic loading. A factor of 3 is used on tensile strength when establishing the design stress intensity values.

Currently it appears that pressure vessels for coal conversion processes will be designed in accordance with the rules of Section VIII of the Code. There are two Divisions in Section VIII. The allowable stresses in Division 1 are lower than those in Division 2. The design philosophy in Section VIII, Division 1 is based on the following:

**Table IV**—Criteria for Calculation of Allowable Stresses (Nonbolting Conditions)

| Standard | Fraction of Minimum | | | | |
|---|---|---|---|---|---|
| | Ultimate Tensile | Yield Stress | Creep Stress[a] | Rupture Stress[b] | Uniaxial Strain Cycling Fatigue |
| ASME Section VIII Division 1 | 1/4 | 2/3[c] | 100% ave | 67% ave 80% min | — |
| ASME Section VIII Division 2 | 1/3 | 2/3[d] | [e] | [e] | [f] |

[a] To give 0.01% strain per 1000 h.

[b] To give rupture in 100,000 h.

[c] Above room temperature, these values can be exceeded for some materials when the application involves components where greater deformation is not objectionable, but they cannot exceed 90% of minimum yield stress at temperature.

[d] Above room temperature, this value could be 90% of yield stress at temperature for materials (i.e., austenitic stainless steels and certain nickel-base alloys), but it cannot exceed 2/3 of specified minimum yield stress at room temperature.

[e] Criteria not established.

[f] Fatigue properties are not always required. Need for fatigue analysis is determined by designer in accordance with para. AD-160 of ASME Section VIII Division 2 rules.
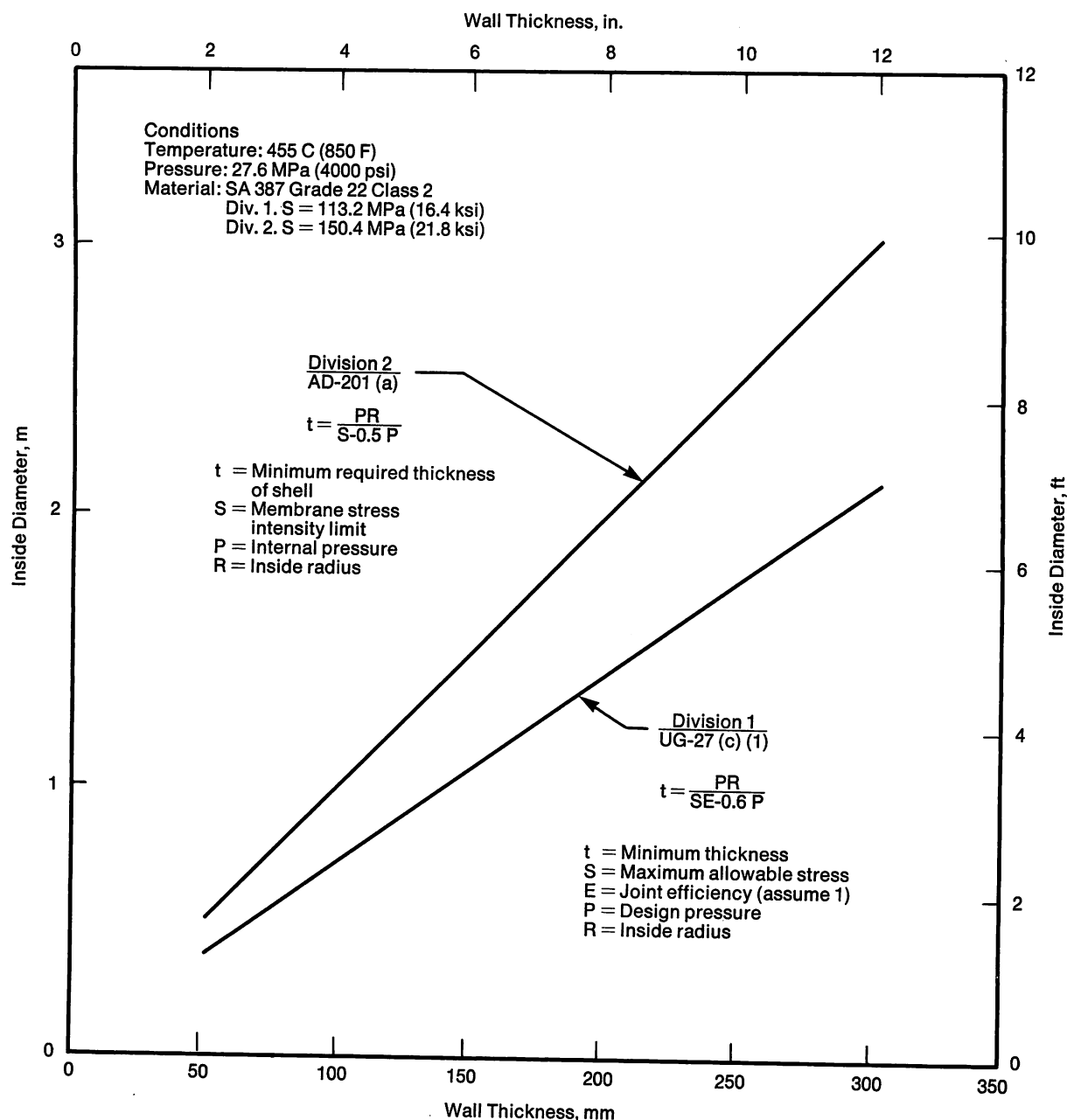
FIGURE 2—Comparison of the effect of the allowable stresses in Section VIII, Divisions 1 and 2 on the diameter of vessel that can be fabricated from a given thickness of SA-387 Grade 22 Class 2. The design conditions are identical for both vessels.

1. The basis for calculating wall thicknesses and allowable pressures is membrane stress. Secondary bending and stress concentrations are not considered.

2. The formulae used in the design calculations and the allowable stresses include sufficient margins of conservatism to limit bending or peak stresses to safe levels.

3. A factor of 4 on tensile strength is used for establishing allowable stresses.

The design philosophy in Section VIII, Division 2 is identical to that in Section III, Subsection NB. Table IV compares the bases for determining allowable stresses. The differences in the stresses are reflected in the size of the pressure vessel that can be designed and built. Figure 2 allows a comparison between a Division 1 and

Division 2 vessel designed to identical pressure and temperature conditions. There is a decided size advantage to a Division 2 design; based on a 305 mm (12 in.) wall thickness, the vessel inside diameters are approximately 2 and 3 m (7 and 10 ft) for Divisions 1 and 2, respectively. The increase in diameter permitted in Division 2 doubles internal volume. This volume increase may result in a cost advantage; however, this advantage may be offset by the increased cost of the more rigorous rules of analysis and inspection required in Division 2. Indeed the analysis and inspection in Section VIII, Division 2 are essentially identical to those in Section III, Subsection NB. Personnel safety and vessel integrity are of foremost concern; however, a breach of a coal conversion pressure vessel is not as serious an event as that of a

nuclear vessel. Therefore, requiring identical analysis and inspection, both extremely costly activities, does not seem warranted. Two areas in Section VIII require further attention. One area in which the rules of Section VIII are inadequate is toughness. This concern is recognized by reputable fabricators and/or owners and is discussed in the literature.[8,9] A new section of the Code could be developed to recognize that the stringent requirements mandated by nuclear applications may not be necessary for coal conversion vessels. The development of such a section of the Code will require data that support allowable stresses that are higher than those in Division 1 without the more demanding requirements of Division 2. Liquefied coal will be acceptable only if it can be competitive, and any effort to reduce cost will improve its economic position in the world market.

The second area where Section VIII is inadequate is the absence in Division 2 of design stress intensity values for temperatures in the creep range. This void is evident in Table IV. Effort must be put forth to develop a basis for establishing design stress intensity values at temperatures where time-dependent properties become controlling. Currently some coal liquefaction processes that require that the reaction vessels be designed for temperatures near 480 C (900 F) are being based on the design stress intensity values in Code Case N-47. This Code Case[10] was developed for breeder reactor design and contains only five alloys, one of which (2¼ Cr-1 Mo) is a candidate for coal conversion reaction and gasifier vessels. Further, only the 205-415 MPa (30-60 ksi) strength class is permitted for 2¼ Cr-1 Mo in Code Case N-47. Section VIII of the Code should be encouraged to develop criteria for assigning design stress intensity values in the creep range. Further, one should be cognizant that the materials will be used to fabricate coal

conversion pressure vessels, the breach of which does not have the same consequences as a breach of a nuclear pressure vessel.

Finally, improved materials that will be discussed later must be Code-approved if they are to be used for Code construction. Usually, mechanical property data from three to five commercial heats are desired for setting allowable stresses. This imposes no particular hardship when the alloy has been correctly developed, and the required allowable stress values are in the temperature range where tensile properties control. It is considerably more difficult and time consuming to obtain the desired data for setting stresses in the creep range. The latter requires data for time periods up to $10^4$ hours for three to five heats. Further, at least one heat should be tested to $3 \times 10^4$ hours, a period of about 3.5 years. If a promising alloy is currently under development, Code approval will not be forthcoming before the middle of this decade. New material requires 4 to 6 years for Code approval, and that assumes that the data are sufficient to satisfy the Code requirements for establishing allowable stresses.

## Melting Practice

Recent advancements in melting practices should be employed in the preparation of materials for pressure vessels. The processes of interest are electroslag remelting (ESR), low sulfur conventional processing (LSC), low sulfur vacuum carbon deoxidized processing (LSVCD) and central zone remelting (CZR).

The CZR process[11,12] is unique in that it employs the ESR process to improve the quality of the central region of a conventional ingot. Figure 3 describes how the process operates. Briefly the center region (which contains

**Table V**—Compositional Ranges for Nuclear Pressure Vessel Steels

| Specification | Element, % [a,b] | | | | | | | | | |
| | C | Mn | P | S | Si | Mo | Ni | Cu | Cr | V |
|---|---|---|---|---|---|---|---|---|---|---|
| *Plate* | | | | | | | | | | |
| SA 533 Grade B Class 1 | 0.25 | 1.15-1.50 | 0.035 (0.012)[c] | 0.040 (0.015)[c] | 0.15-0.30 | 0.45-0.60 | 0.40-0.70 | (0.010)[c] | — | (0.05)[c] |
| 20 Mn-Mo-Ni 55 | 0.25 | 1.15-1.50 | 0.035 | 0.040 | 0.15-0.30 | 0.45-0.60 | 0.40-0.70 | — | — | — |
| *Forging* | | | | | | | | | | |
| SA 508 Class 3 | 0.15-0.25 | 1.20-1.50 | 0.025 (0.012)[c] | 0.025 (0.015)[c] | 0.15-0.40 | 0.45-0.60 | 0.40-1.00 | (0.10)[c] | 0.25 | 0.50 |
| SA 508 Class 2 | 0.27 | 0.5-1.00 | 0.025 (0.012)[c] | 0.025 (0.015)[c] | 0.15-0.40 | 0.55-0.70 | 0.50-1.00 | (0.10)[c] | 0.25-0.45 | 0.050 |
| 22 Ni-Cr-Mo 37 | 0.17-0.23 | 0.50-1.00 | 0.02 | 0.02 | 0.35- | 0.50-0.80 | 0.60-1.20 | — | 0.30-0.50 | 0.05 |

a Single values are maximum limits.
b Compositional limits are for heat analysis; the limits for product analysis are more broad.
c Restricted values for heat used at the beltline.
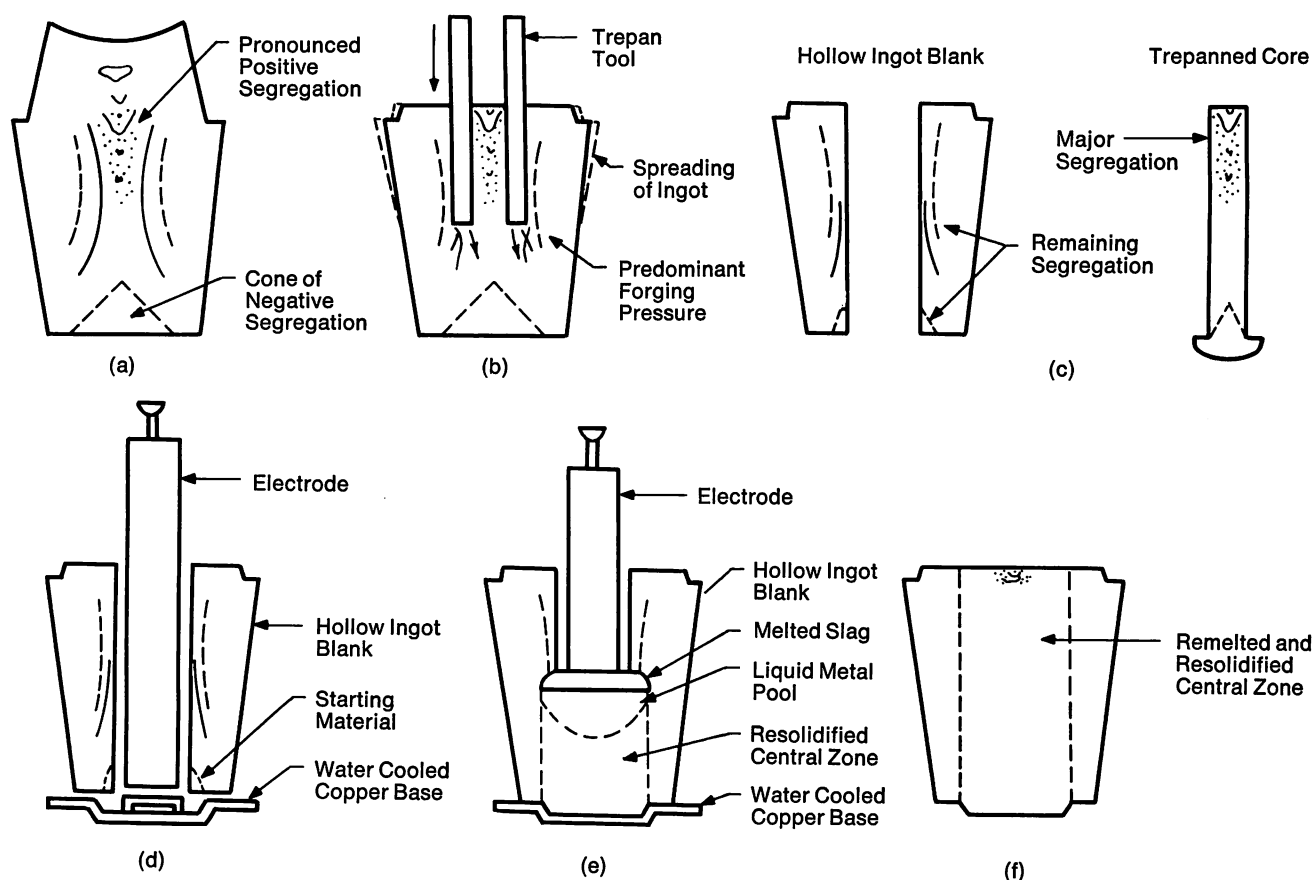
*FIGURE 3—Central zone remelting process. (a) An as-cast air melted ingot. (b) Center core region is removed. (c) Cross section of ingot after removal of the core. (d) and (e) Refilling of the central region by electroslag remelting. (f) Final ingot.*

the segregates) of a conventional ingot is trepanned. The central region is then refilled by using an electroslag remelting casting procedure. This procedure results in a more uniform, higher quality final product. The process lends itself to providing cylindrical forged courses for pressure vessels whose inner walls can be of a chemical composition that will resist the environments in which the vessels must operate. In the case of a coal conversion pressure vessel, this region can be enriched with those elements (chromium and molybdenum) that provide resistance to hydrogen attack. For nuclear applications, the inner core can be of an analysis that is resistant to irradiation embrittlement. For example, the air melted ingot body can be somewhat higher in Cu, P and V. The inner core can be cast from an electrode low in those elements thereby providing excellent toughness even at the end of its useful life (the time of operation that is used for determining the probability of a nuclear pressure vessel failure from thermal shock in the event of a loss-of-coolant accident). The CZR process is also attractive for large tubesheets because of the high quality of the central portion of the ingot.

The other three processes (ESR, LSC and LSVCD) all provide ingots that have extremely low sulfur contents. All three are capable of providing sulfur levels of less than 30 ppm, and LSC reportedly provides levels as low as 7 ppm. The largest ESR ingots are currently

available from Röchling-Burbach in the Federal Republic of Germany. They reportedly have cast ESR ingots of greater than 100 metric tons (110 tons). Such facilities are now being developed in the U.S. Bethlehem Steel has a facility capable of producing ingots 1525 mm (60 in.) in diameter. National Forge is installing one of similar size.

The LSC method of casting ingots was developed by Japan Casting and Forging Corporation. The LSCVD process is a development of Japan Steel Works (JSW). The LSCVD process also provides an ingot with extremely low phosphorus ($<0.003\%$) and low silicon (about $0.05\%$). The low silicon content was selected by JSW along with low phosphorus to minimize segregation streaks.

All four of these melting processes provide steels that should exhibit superior toughness. Sulfur has a deleterious effect on Charpy V-notch upper shelf impact energy.[13] Obtaining an upper shelf energy of 68 J (50 ft-lb) or greater is required[14] to establish the $RT_{NDT}$. Phosphorus was shown by Rineholt[15] to drastically increase the 20 J (15 ft-lb) Charpy V-notch temperature. Decreasing these two elements does not sacrifice a steel's hardenability. Reducing them will improve resistance to hot cracking and embrittlement during service.

Moreover, the utilization of these advanced melting processes and their higher yields from a given ingot are in
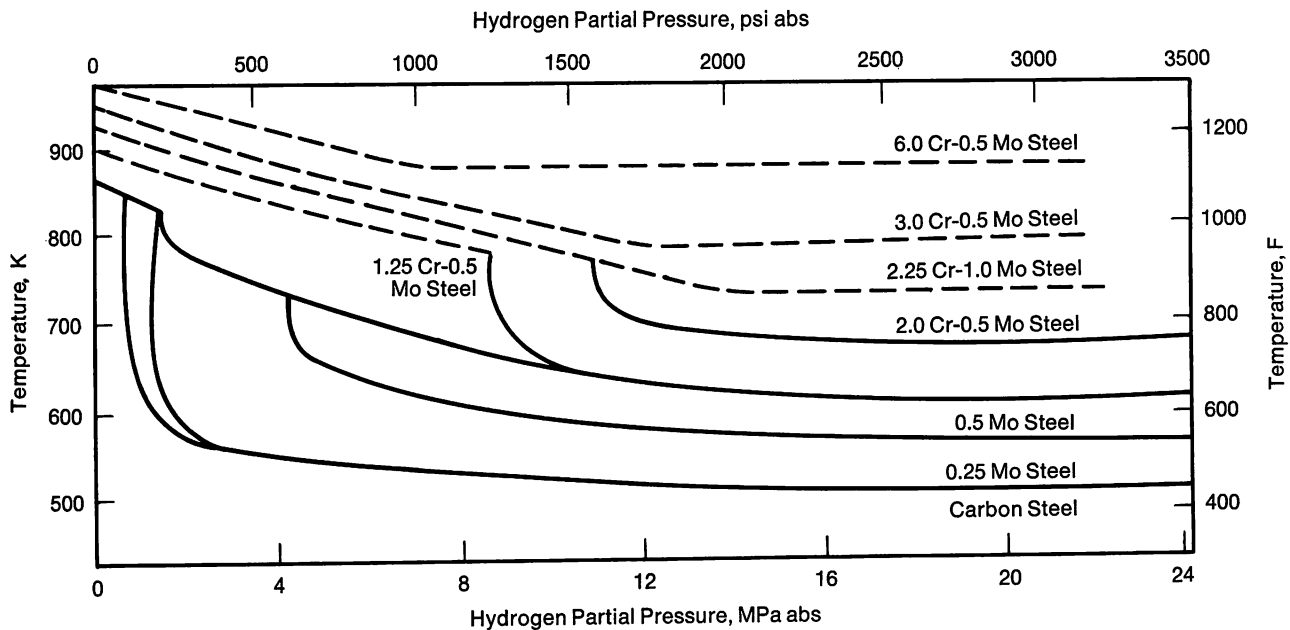
FIGURE 4—The Nelson Diagram that provides the recommended operating limits to avoid methanation and decarburization for high temperature high pressure service in hydrogen-rich environments.

themselves creditable from an energy conservation viewpoint. Currently the yield from a large conventional air melted ingot can be as low as 50%. The ESR process and the CZR process yields are reportedly 85 to 95%.

## New Materials

New materials may be a misnomer. Probably improvements (hopefully) of current materials may be more descriptive. At the present time, there are essentially only two alloys used in the manufacture of the primary containment for nuclear reactors. These are the SA-533 Grade B Class 1 plate and its forging counterpart SA-508 Class 3 and SA-508 Class 2. Table V contains the composition ranges permitted in the SA specifications and their counterpart Federal Republic of Germany specifications. These steels satisfy the LWR pressure vessel needs. Unless there is a resurgence of interest in larger LWR facilities, such as there was in the late 1960s and early 1970s,[16] it is doubtful that these steels will be replaced with stronger and/or tougher steels. It is likely, however, that advantage will be taken of the improved melting practices discussed previously, and the quality of the steel from which the LWR vessels are fabricated will be improved. This improvement in quality will be reflected in a lower sensitivity to irradiation. Stabilizing mechanical properties, in particular fracture toughness, will end the concern that a loss-of-coolant accident accompanied by a thermal shock from activating the emergency core cooling system may result in a breach of the primary containment.

Such is not the case for steels for coal conversion systems. Currently the top candidate for the fabrication of large gasifiers and reaction vessels is 2¼ Cr-1 Mo steel.

This steel is of interest because of its resistance to hydrogen attack as predicted from Nelson curves (Figure 4). The range for chromium and molybdenum in most specifications that cover 2¼ Cr-1 Mo steel is from 2.0 to 2.5% and 0.90 to 1.10%, respectively. A lean heat, one containing near 2.0% Cr and 0.90% Mo, may not have the desired resistance to hydrogen attack if used in a high pressure liquefaction process operating above 425 C (800 F). Further, the hardenability of 2¼ Cr-1 Mo steel appears to be too low to provide tensile properties much in excess of 575 MPa (75 ksi) after a nominal postweld heat treatment (PWHT). Figure 5 illustrates this point. The DATA TRAK, a method for duplicating the cooling rate after austenitizing obtained in thick sections in 12 mm (½ in.) square bars, was used to obtain the results shown in Figure 5. This procedure is permitted in Paragraph NB 2212 of Section III and Paragraph AM 202 of Section VIII, Division 2. The tensile data in Figure 5 for 2¼ Cr-1 Mo steel cooled from either 925 or 1040 C (1700 or 1900 F) at a rate representing that of the quarter-thickness depth location in water quenched 305 mm (12 in.) plate indicate that, after a 40 hour PWHT, the steel will barely satisfy the Class 2 strength requirement for the SA-387 Grade 22 specification. These results suggest that the use of the higher strength classes of 2¼ Cr-1 Mo steel (such as SA-542 Classes 1 through 4) is not likely.

Considerable work is being done to develop steels that exhibit improved mechanical properties. Most of this work is based on adaptations of current Code-approved specifications, and this should aid in acceptance of the steels by the Code if they should prove worthy of being used for the fabrication of large pressure vessels.

Japan Steel Works[17] is modifying 2¼ Cr-1 Mo steel

**Heat Treatment**

Austenitized 925 C (1700 F) for 1 h
Q — Quench — "Data Trak" simulated cooling rate
T — Temper — 705 C (1300 F) for 1 h, air cool
S — Stress relief — 675 C (1250 F) for 40 or 120 h



(a)
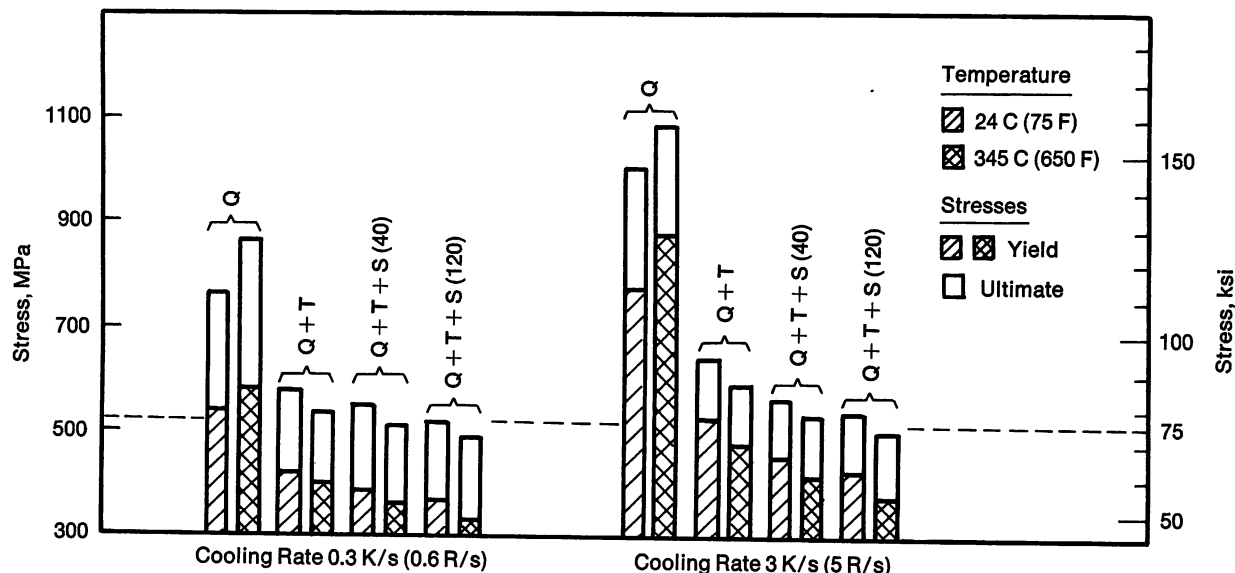
**Heat Treatment**

Austenitized 1040 C (1900 F) for 1 h
Q — Quench — "Data Trak" simulated cooling rate
T — Temper — 705 C (1300 F) for 1 h, air cool
S — Stress relief — 675 C (1250 F) for 40 or 120 h
A — Aged — 345 C (650 F) for 1000 h



(b)
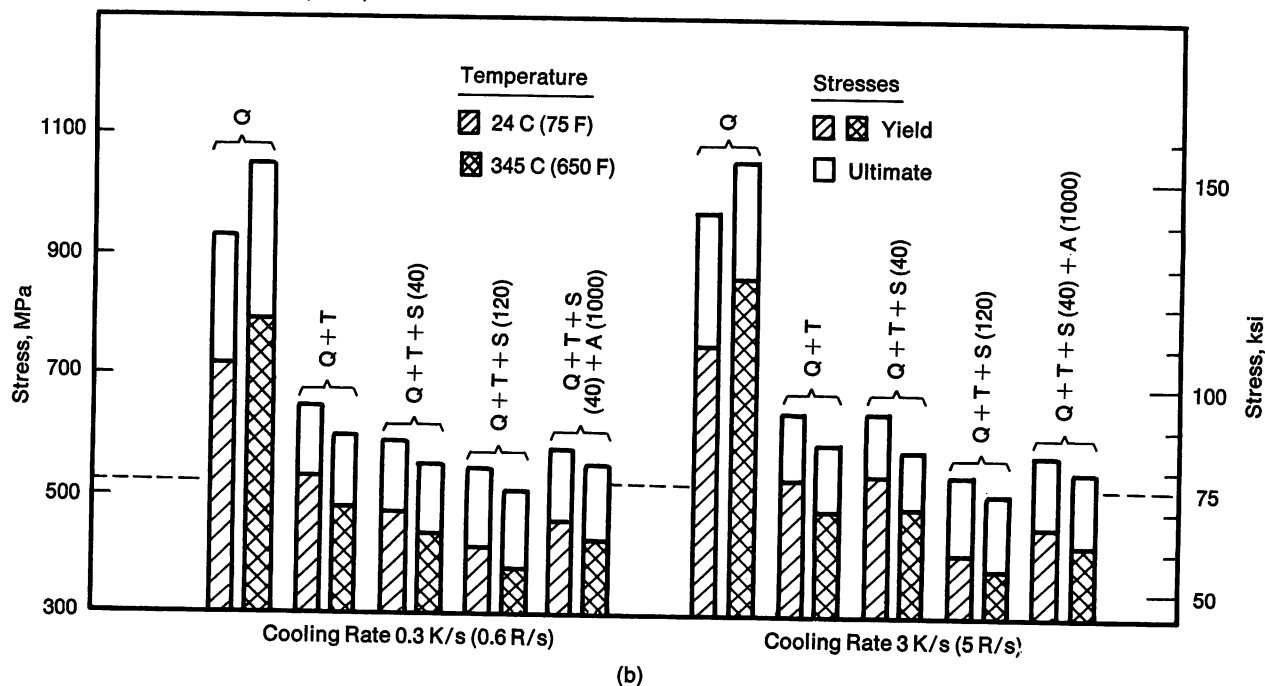
*FIGURE 5—Effect of heat treatment on the 24 and 345 C
(75 and 650 F) tensile properties of 2¼ Cr-1 Mo steel. (a)
925 C (1700 F) austenitizing temperature. (b) 1040 C (1900 F)
austenitizing temperature. The 0.3 and 3 K/s (0.6 and 5 R/s)
cooling rates represent the quarter-thickness and surface loca-
tions, respectively, in 305 mm (12 in.) plate.*

by decreasing the Si and adding V, Ti and B. Deliberate additions of these elements at nominal amounts of 0.30, 0.022 and 0.0023% considerably increased the hardenability of conventional 2¼ Cr-1 Mo steel. This modification resulted in increased strength in the creep range; at 480 C (900 F) there was approximately a 50% increase in creep rupture strength for failure in $10^5$ hours. This improvement was achieved with no apparent loss of fracture toughness. Japan Steel Works has simulated weld heat cycles on the modified base metal, and the results indicate that the heat affected zone properties should be equal or superior to those of conventional 2¼ Cr-1 Mo steel. This work is in its early stages, and the results appear promising.

The U.S. Department of Energy is sponsoring the development of improved alloys for coal conversion pressure vessels. Work is under way at the University of California and at Oak Ridge National Laboratory (ORNL). The UC studies[18,19] have been directed toward the modification of Mn-Mo-Ni steel (SA-533 Grade B) and Cr-Mo steel (SA-542). The modification of the Mn-Mo-Ni steels involved additions of 1% Cr and 0.7% Mn. (The Mn-Mo-Ni specification, SA-533 Grade B, currently permits up to 1.5% Mn. This Mn addition is aimed at increasing its level to nearer 2%.) The addition of the

Cr and Mn have increased the hardenability of the SA-533 Grade B steel. The researchers report that the increased hardenability has resulted in improved strength and toughness for specimens heat treated to represent the quarter-thickness depth location in both 200 and 305 mm (8 and 12 in.) thick plate.

Zackay and Parker[18,19] are also studying modifications of 2¼ Cr-1 Mo steel with 0.5% Mn and 0.5% Ni. They report that these additions retard the transformation of austenite to proeutectoid ferrite. This results in a more uniform microstructure for thicker sections. This more uniform microstructure is reflected in improved Charpy V-notch toughness. Both transition temperature and upper shelf energy were improved.

The work at the University of California, although in its early stages, does show considerable promise. The modifications to the SA-533 Grade B analysis should improve that steel's resistance to hydrogen attack, but whether it is improved sufficiently to permit use at typical liquefaction temperatures must be established. The reported results[18,19] for the modifications of the two steels are based on tempering times of 4 hours. This time period is too short when considering the extended PWHT times that are encountered during the fabrication of large pressure vessels. These time periods often exceed
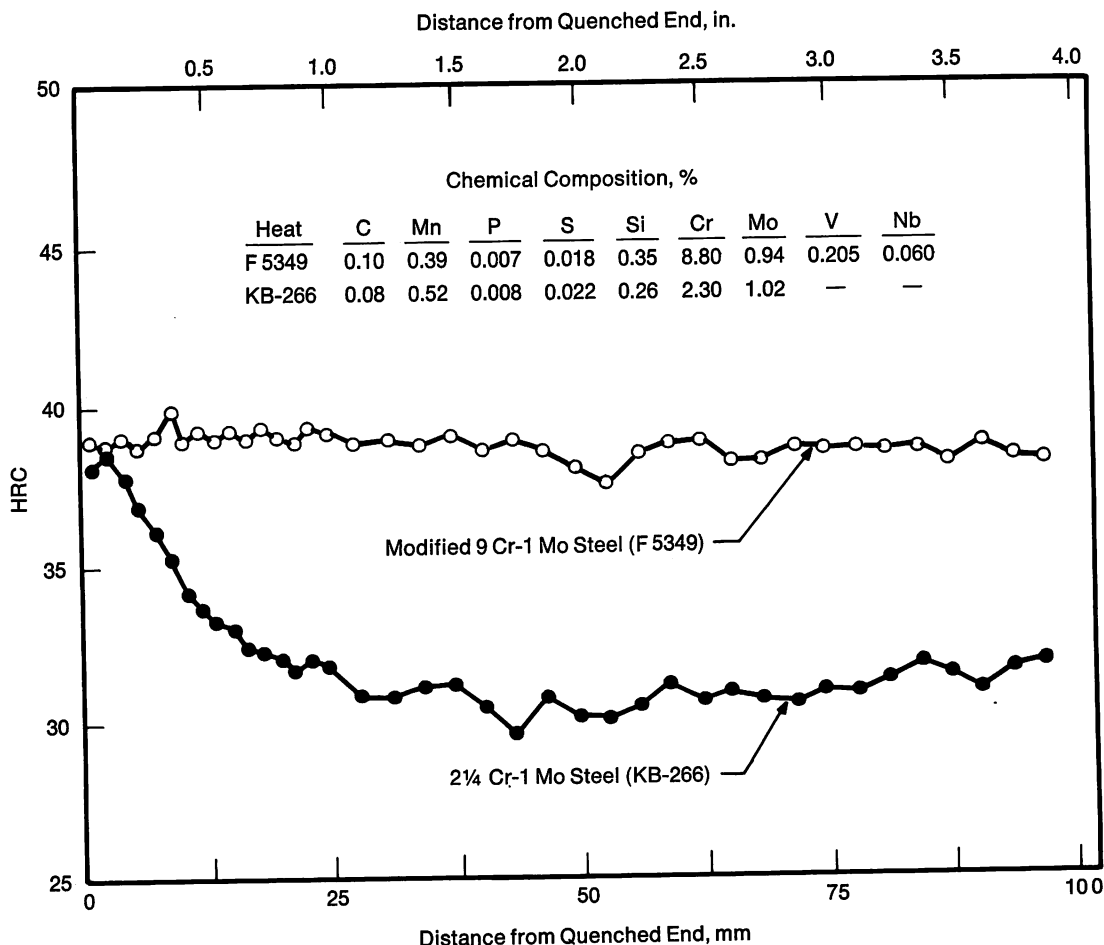


FIGURE 6—Comparison of the hardenability of conventional 2¼ Cr-1Mo steel and modified 9 Cr-1 Mo steel.

40 hours and can be as long as 100 hours.

In cooperation with Combustion Engineering Inc., ORNL is involved in the development of an improved high temperature alloy based on the 9 Cr-1 Mo analysis.[12] The modification in this case consists of the addition of Nb and V at levels of near 0.1 and 0.2%, respectively. The conventional 9 Cr-1 Mo steel has considerably greater hardenability than 2¼ Cr-1 Mo.[20] This hardenability is not affected by the Nb and V modifications. This is evident in the Jominy end-quench results obtained by Climax Molybdenum for modified 9 Cr-1 Mo and conventional 2¼ Cr-1 Mo steels.[21] These results are shown in Figure 6. The 9 Cr-1 Mo steel is air hardenable and will transform to martensite even at section sizes greater than 200 mm (8 in.). Further, there is no evidence that proeutectoid ferrite will be present in thick sections, and, therefore, the microstructure should be uniform even in section sizes greater than 200 mm (8 in.). This conclusion is based on studies conducted at Lehigh University that correlated the cooling rates at various Jominy end quench distances with those obtained experimentally in thick water quenched plate.[22] The ORNL researchers report that the creep strength of the modified 9 Cr-1 Mo alloy is similar to that of type 304 stainless steel up to about 625 C (1150 F).

Weldability studies are being conducted on the modified 9 Cr-1 Mo alloy.[23] Early results indicate that hot cracking will not be a problem. Also, Gleeble studies involving simulated weld thermal cycles show that the heat affected zone toughness is independent of cooling rate over the range from 14 to 55 C/s (25 to 100 F/s).

The alloys discussed above are all modifications of existing specifications already approved for Code construction. This fact will expedite their acceptance into the Code. Of course, this assumes that all the development data are substantiated through testing programs that provide the needed confirmatory results required for the commercialization of these alloys.

The development of improved alloys should be commended. Also, much can be achieved with current alloys. The ability of modern melting methods to decrease sulfur and phosphorus to near 30 ppm in large commercial heats is noteworthy. Even in ingots poured from air melted heats, the S and P levels can be limited to 0.01% and lower. In view of this capability, it is ludicrous to tolerate ASTM and ASME pressure vessel steel specifications that permit S and P levels of 0.035 to 0.045%. A review and update of these specifications should be undertaken.

## Fabrication

All large pressure vessels are fabricated by welding. Economics dictate this method of fabrication. The entire chemical, petroleum and energy-producing industries

depend on high quality weldments. A large pressure vessel of the size suggested in Figure 1 will contain over 305 m (1000 ft) of weld. Welding and its related activities (joint preparation, inspection and examination, postweld heat treating, etc.), are responsible for over 50% of the fabrication cost of a large pressure vessel. Currently, a 910 metric ton (1000 ton) vessel is the largest that can be shop fabricated. The size is attainable in only three or four shops in the U.S., and this limit is set by crane capacities. Vessels heavier than 910 metric tons (1000 tons) must be field fabricated. The size of shop-fabricated vessels is further restrained by the ability to deliver them. The dimensions of pressure vessels that can be transported on land are limited to about 4.3 m (14 ft) in diameter and 725 metric tons (800 tons) in weight. Lengths up to 30 m (100 ft) have been transported. Large shop-fabricated vessels such as those listed in Table 2 are shipped by barge; however, this requires navigable waterways. This mode of transportation is generally limited to the eastern half of the U.S.

All joining is done by fusion welding processes. Currently two welding processes are employed for most vessel fabrication; these are the submerged arc (SA) and shielded metal arc (SMA) processes. The SA process employs a granular flux covering the weld arc and until recently has had this limitation. The SA process has been primarily used for shop fabrication. Field fabrication, because of the need for welding in all positions [flat (1G), horizontal (2G), vertical (3G), and overhead (4G)], is accomplished primarily with the SMA process.

These generalizations are being challenged by recent improvements and advancements in joining procedures. Submerged arc welding procedures that permit the use of this process in positions other than 1G are being developed by Chicago Bridge and Iron Company.[24] The company has procedures that permit the containment of the flux even in the overhead (4G) position. This development will greatly increase the field fabrication deposition rate, thereby decreasing costs.

A considerable effort is being directed to adapting the electron beam (EB) process for joining thick sections. This process is normally confined to use in vacuum chambers and is considerd an "exotic" joining procedure more commonly encountered in applications for the aerospace and electronic industries. It is being developed for out-of-chamber welding of thick sections and has shown promise. The goal is to produce a high quality joint typical of an EB weld without the need for a full heat treatment such as is necessary for electroslag welds. This development work is being done independently by Babcock and Wilcox Company[25] and Sciaky Brothers, Inc.[26] The B&W program is sponsored by the Department of Energy. It has achieved sound welds in 200 mm (8 in.) thick plate of 2¼ Cr-1 Mo steel using simulated field fabrication procedures. The procedure requires welding from both sides. Sciaky Brothers has successfully welded
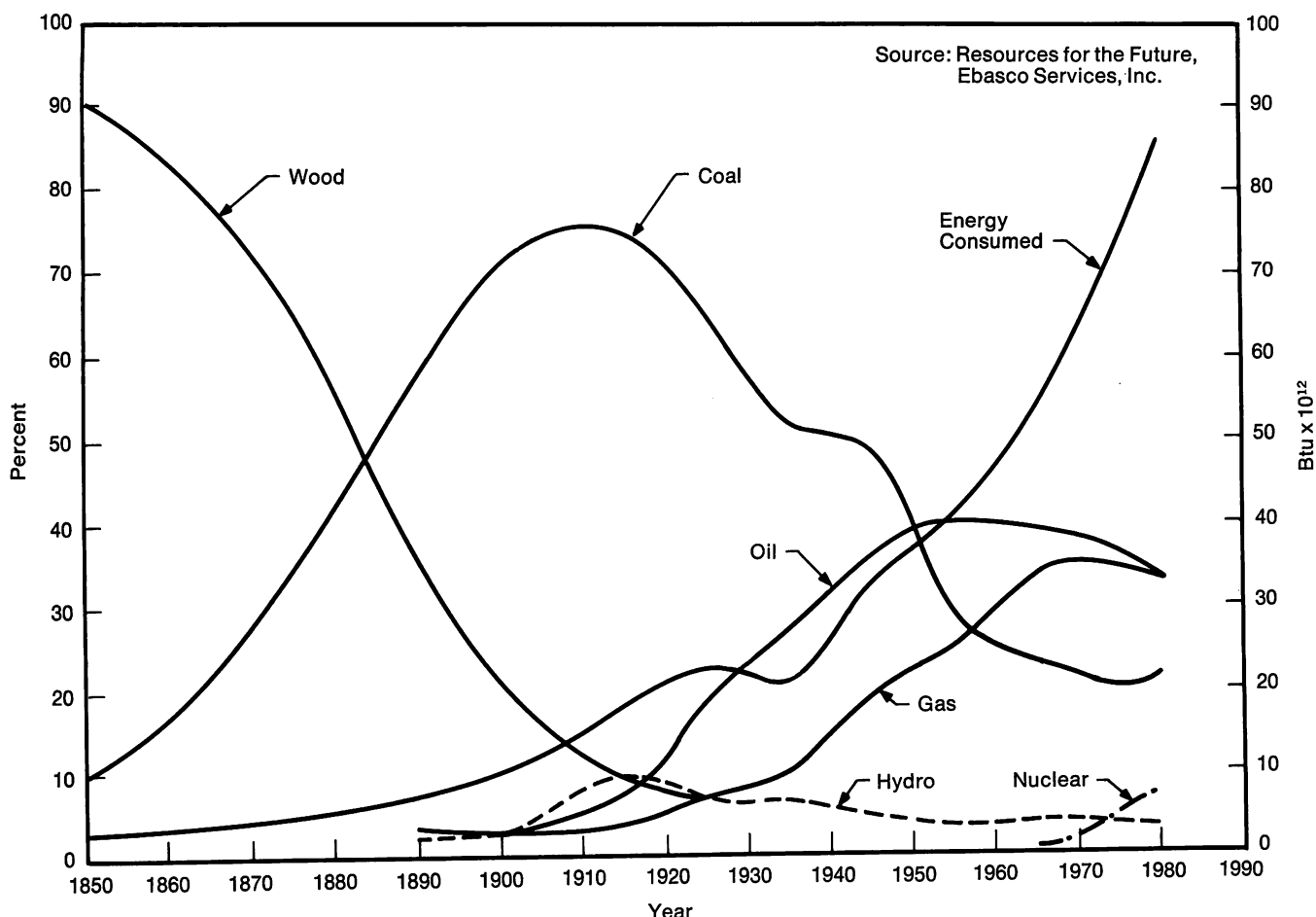
FIGURE 7—*Energy sources and consumption in the United States since 1850.*

135 mm (5 3/16 in.) thick A-533 Grade B steel rings.

The adaptation of the EB welding procedure for thick-walled pressure vessel steels appears promising. Additional metallurgical studies must be conducted to assure that the properties, in particular toughness, are adequate for the vessel's intended use after PWHT.

## Conclusions

The challenge of the 1980s will be to assure that the western world has an adequate supply of energy. Conservation is commendable and perhaps can be made to work, but, in recent years, the only time that the U.S. underwent a sustained reduction in energy growth was during the 1930s, a period of a severe depression not only in the U.S. but in the entire world. This is clearly seen in Figure 7. More recently, the U.S. decreased its energy growth, and that was, as can be seen in Table I, during 1974 and 1975, two years in which the U.S. had a somewhat severe recession. Further, even if the western world can curtail energy consumption, the world needs will grow. The standard of living in most third world countries will increase in the years ahead, and this growth will require energy.

In the U.S., transportation places the greatest demand on petroleum products. These demands can be met through the liquefaction of coal. Commercializing the coal conversion processes will impose an unprecedented demand for large pressure vessels. This demand can be met through modernization of the Code to meet the needs of an evolving industry. This was accomplished for nuclear pressure vessels; it can be done for coal conversion vessels. Advantage should be taken of modern melting practices. The steels produced by these processes should be of higher quality, exhibit improved fracture toughness, and be less susceptible to in-service degradation. Modifications of steels currently accepted in the Code appear to provide improved mechanical properties. These steels may permit the fabrication of larger diameter vessels with thinner section sizes and improved reliability and integrity. Adapting current specifications should expedite Code approval. Finally, the challenge of improving welding procedures and adapting processes for field applications will result in higher quality weldments.

The challenge of the 1980s lies in assuring that the world has adequate energy. This can only be achieved through the assurance that, when the industry requires large pressure containment systems, the technology exists to satisfy that need—immediately.

## Discussion

J. F. WATSON, General Atomic, Inc. Is there a role for the prestressed concrete pressure vessel? What factors are important when considering the prestressed concrete pressure vessel?

D. A. CANONICO. Oak Ridge National Laboratory has looked at prestressed concrete pressure vessels for gasification and liquefaction applications and found that they do have much to offer. One advantage is the potential for easier field fabrication. The economics are more attractive the larger the plant.

J. LESSELLS, British Steel Corporation. In the 2¼ chrome-1 moly steel and the Japanese derivative of it, it is difficult to obtain an increase in strength without a sacrifice in toughness. We have had trouble both with toughness and welding. Do you have any information on these aspects of the Japanese steel?

D. A. CANONICO. No, but their work looks attractive and we are planning a cooperative program. Our results with the modified 9 chrome-1 moly steel looked good from the toughness standpoint. Most people want to design for operation at 480 C (900 F), and they would like to go to 495 C (925 F) with a higher working pressure. Under these conditions, the regular 2¼ chrome-1 moly steel is borderline. With just a little more hardenability, assuming the Nelson diagram can be satisfied, the code requirements at 480 C (900 F) could be very easily satisfied. The Japanese steel and the 9 chrome-1 moly steel appear to do this.

R. STEVENSON, General Motors Corporation. What sulfur content would you like to see in the steels for pressure vessels in light of current melting practices?

D. A. CANONICO. I believe nuclear requirements are currently 0.015% sulfur and 0.012% phosphorus. I certainly think that 0.01% sulfur could readily be achieved. It is ludicrous to have 0.035% sulfur as the permissable level in A533, Grade B and A 387, Grade 22 for pressure vessel applications.

## References

1. J. Blue and J. Arehart, A Pocket Reference of Energy Facts and Figures, Oak Ridge National Laboratory, October 1979.
2. Federal Energy Administration, Project Independence Report, November 1974, 66.
3. American Petroleum Institute, Basic Petroleum Data Book, April 1978.
4. American Gas Association, Gas Facts, 1977, 1978.
5. Federal Energy Administration, Project Independence Report, November 1974, 25.
6. D. A. Canonico, Met. Prog., 116(2), July 1976, 32.
7. W. L. Greenstreet, C. B. Oland, J. P. Callahan and D. A. Canonico, Feasibility Study of Prestressed Concrete Pressure Vessels for Coal Gasifiers, ORNL-5312, August 1977.
8. D. A. Canonico et al., Assessment of Materials Technology for Gasifier and Reaction Pressure Vessels and Piping for Second Generation Commercial Coal Conversion Systems, ORNL-5238, August 1978, 87.
9. D. A. Canonico, Structural Integrity of Vessels for Coal Conversion Systems, ORNL/TM-6969, September 1979.
10. ASME Boiler and Pressure Vessel Code Cases, Nuclear Components, Case N-47-16, American Society of Mechanical Engineers, New York, 1977, 105.
11. L. R. Cooper, U.S. Patent 3,603,374, September 7, 1971.
12. P. Patriarca et al., Nucl. Technol., 28, March 1976, 516.
13. Metals Handbook, Ninth Edition, Volume 1, Properties and Selection: Iron and Steels, American Society for Metals Park, Ohio, 1978, 694.
14. ASME Boiler and Pressure Vessel Code, Sect. III, Nuclear Power Plant Components, Div. 1, Subsection NB, Para. NB 2330, American Society of Mechanical Engineers, New York, 1977.
15. J. R. Rinebolt, "Effect of Metallurgical Structures on the Impact Properties of Steels," Symposium on Effect of Temperature on the Brittle Behavior of Metals with Particular Reference to Low Temperatures, ASTM Spec. Tech. Publ. 158, American Society for Testing and Materials, Philadelphia, 1953.
16. R. H. Sterne, Jr. and L. E. Steele, Nucl. Eng. Des., 10, 1969, 259.
17. D. A. Canonico, private communication from J. Watanabe, Japan Steel Works, October 1, 1979.
18. V. F. Zackay et al., "Alloy Design for Several Critical Components in Fossil Fuel Energy Conversion Systems," Third Annu. Conf. Materials for Coal Conversion and Utilization, Gaithersburg, Maryland, October 10-19, 1978, CONF-781018, U.S. Department of Energy.
19. V. F. Zackay and E. R. Parker, "Low Alloy Steels for Thick-Walled Pressure Vessels," Fourth Annu. Conf. Materials for Coal Conversion and Utilization, Gaithersburg, Maryland, October 9-11, 1979, CONF-791014, U.S. Department of Energy.
20. J. Orr, F. R. Beckitt, and G. D. Fawkes, "The Physical Metallurgy of Chromium-Molybdenum Steels for Fast Reactor Boilers," Proc. Int. Conf. Ferritic Steels for Fast Reactor Steam Generators, May 30-June 2, 1977, Vol. 1, pe. 4, by S. F. Pugh and E. A. Little, British Nuclear Energy Society, 1978.
21. V. K. Sikka, ORNL, private communication from P. J. Grobner, Climax Molybdenum Company, April 30, 1980.
22. E. H. Kottcamp, D. A. Canonico and R. D. Stout, Weld. J. 41 (8), August 1962, 350S.
23. D. P. Edmonds and P. L. Sturgill, Weldability of Modified 9 Cr-1 Mo Steels, ORNL/TM-6890, August 1979.
24. D. P. Edmonds, ORNL, Private Communication from J. E. Sims, Chicago Bridge and Iron Company, March 11, 1980.
25. C. M. Weber, "Development of Automated Welding Processes for Field Fabrication of Thick-Walled Pressure Vessels — Electron Beam Method," Third Annu. Conf. Materials for Coal Conversion and Utilization, Gaithersburg, Maryland, October 10-19, 1978, CONF-781018, U.S. Department of Energy.
26. D. A. Canonico, ORNL, Private Communication, W. J. Farrell, Sciaky Brothers Inc., April 16, 1980.

# Characteristics of Hardenable 12% Cr Steels for Energy Conversion Systems

by N. G. Persson
Sandvik AB

Hardenable steels with 9 to 12% chromium and additions of other alloying elements, mainly molybdenum and vanadium, are widely used in plants for electric power generation. In conventional fossil fueled units, such steels are used for a variety of components including superheater and reheater tubing in boilers, main steam pipes, shells, bolting and turbine blades and rotors. The 9Cr-1Mo steel is found world-wide as boiler tubing because of its superior oxidation resistance compared with lower chromium steels such as 2¼Cr-1Mo. However, the increase in chromium up to about 9% does not confer any appreciable improvement in elevated temperature strength. In fact, the standard 9Cr-1Mo steel has similar long-term creep properties to 2¼Cr-1Mo.[1] To arrive at a significantly higher rupture strength, 9Cr-1Mo must be modified by increasing molybdenum up to 3%,[2-4] employing other alloying additions,[5,6] or the chromium level has to be raised to about 12%.

The 12Cr-1Mo steel and variants thereof have been used since the 1960s, primarily in Europe, and long-term ($\sim$ 100,000 hours) operating experience has now been achieved. Depending upon alloy additions other than chromium and molybdenum and the heat treatment, the mechanical properties of these steels can be varied within wide limits. The high hardenability provides through hardening in large section sizes even when air cooling is employed. The high tempering resistance lends good structural stability at temperatures typical of steam plants, an essential for installations designed to operate for 10, 20 or even 30 years.

Recently, the 9-12Cr-Mo grades have received growing attention for possible future use in nuclear reactor systems such as the fast breeders and fusion reactors. The 9Cr-1Mo steel has already been selected for steam generator tubing in the British prototype fast reactor, and variants of the 12Cr-1Mo steel are being studied for the next generation of fast reactors.

There are several reasons why the transformable 9-12Cr-Mo steels with additions of V, W and Nb attract growing attention. They fill a gap in long-term strength at intermediate temperatures between ferritic steels of lower chromium content and the austenitic chromium-nickel steels. Because of higher creep strength, section sizes can be reduced, hence the thermal gradients and corresponding stresses in components subject to high heat fluxes such as steam generator and superheater tubes can also be reduced. The high thermal conductivity and low thermal expansion coefficient of ferritic steels compared with the austenitics contribute to the same effect and also minimize stresses created during plant start-up and shutdown.

General corrosion resistance in steam is enhanced compared with grades of lower chromium content, and the ferritic steels are much less prone to stress corrosion cracking in halide environments than the austenitic steels. Chromium also confers improved corrosion resistance on the flue gas side with the exception that there is little advantage of 12% over 2¼% chromium in oil fired units.

A sound knowledge of transformation characteristics is a prerequisite to the successful use of the chromium-molybdenum steels. This is necessary to obtain the desired long-term properties as well as avoiding difficulties during fabrication and welding. This paper presents some aspects of the physical metallurgy and structure/property relationships in steels with about 12% chromium. The procedures used in steel manufacture and fabrication, particularly welding, of components are touched upon. Most comments are related to tube and pipe components in steam plants. Experience regarding long-term service and the changes in structure and properties during such exposure concludes the paper.

## Physical Metallurgy of 12% Chromium Steels

### Transformation Characteristics

The plain chromium steels with about 12% Cr and 0.1 to 0.2% C are characterized by being fully transformable, and air hardening takes place even in large section sizes. The tempering resistance of this steel is rather low, however, and the long-term structural stability at ele-

vated temperatures consequently rather poor. Despite high oxidation resistance, its usefulness is limited because of poor creep strength. The thermodynamic stability can be greatly improved by additions of alloying elements, notably carbide formers such as molybdenum, vanadium, tungsten and niobium. This can be done without violating the basic transformation characteristics, i.e. without introducing large amounts of delta ferrite which would reduce the hardenability.

The physical metallurgy of this class of steels, often referred to as the super 12% chromium steels, is now well understood and has been described in numerous publications.[7-10] The transformation upon cooling from the austenitising temperature, typically 1000 to 1070 C (1830 to 1960 F), invariably leads to a martensitic structure which may contain some delta ferrite. The reason is that the pearlitic reaction preceded by carbide precipitation is extremely slow, and the bainitic reaction is completely suppressed (Figure 1). Some undissolved carbides are likely to be found in the lath martensite, particularly if strong carbide forming elements such as titanium and niobium are present. Martensite formation starts at or below about 300 C (570 F) and is completed within a temperature interval of about 150 C (300 F). Tempering resistance is usually high enough to prevent any auto-tempering during cooling, i.e. no carbide precipitation occurs within the martensite on cooling. The result is a hard and brittle product which must be softened. From what has been said, it is evident that isothermal transformation is not a practical means of softening these steels. The best route to achieve full control of properties involves normalizing with cooling in air or oil followed by tempering. In selecting suitable temperatures for these treatments, their influence on the mechanical properties must be considered.

The solution treating temperature determines the prior austenite grain size and the dissolution of carbides. A coarse austenite grain size is undesirable as it confers low impact properties.[11] To restrict grain growth, steels not containing titanium or niobium are austenitized at about 1050 C (1920 F) maximum, while those alloyed with titanium or niobium can be treated at higher temperatures because of the pinning of grain boundaries by carbides. Grain refinement is also achieved once an appreciable amount of delta ferrite is present in the structure. This is utilized in some duplex structure variants.[12,13]

With increasing tempering parameters (temperature and time), martensite decomposes and forms a succession of carbide types starting with the least stable $M_3C$ and ending with $M_{23}C_6$, $M_6C$, $M_2N$ and MX phases close to the $Ac_1$ temperature (Figure 2). These precipitation reactions are complex and involve in-situ transformations from one type to another as well as dissolution/reprecipitation processes. Except for the plain 12% Cr steel, all variants exhibit a secondary hardening which has its peak at 450 to 500 C (840 to 930 F). Tempering in this range should be avoided since it confers poor mechanical properties (low yield to tensile ratio and low impact strength). To achieve a thermodynamically stable structure suitable for high temperature components, it is customary to temper at above 650 C (1200 F) and often close to the maximum allowable temperature without risking reformation of austenite. As will be shown later, it is possible to obtain an attractive combination of mechanical properties at high and low temperatures.

The microstructure that results from tempering of 12Cr-Mo-V steels at approximately 750 C (1380 F) is tempered martensite with a dispersion of carbides, predominantly type $M_{23}C_6$, located at prior austenite grain boundaries and martensite lath boundaries. Steels containing titanium or niobium[8] or an increased vanadium content[14] exhibit a fine intragranular dispersion of MX
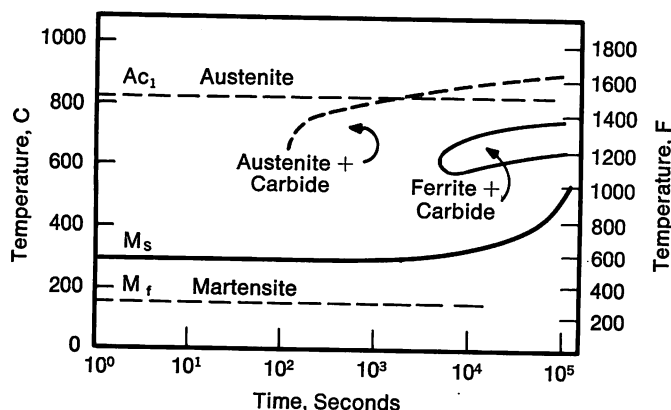


FIGURE 1—Continuous cooling diagram for a steel with composition 0.2% C, 12% Cr, 1% Mo and 0.3% V, austenitized at 1050 C (1920 F) to yield an austenite grain size of ASTM 4 to 5.
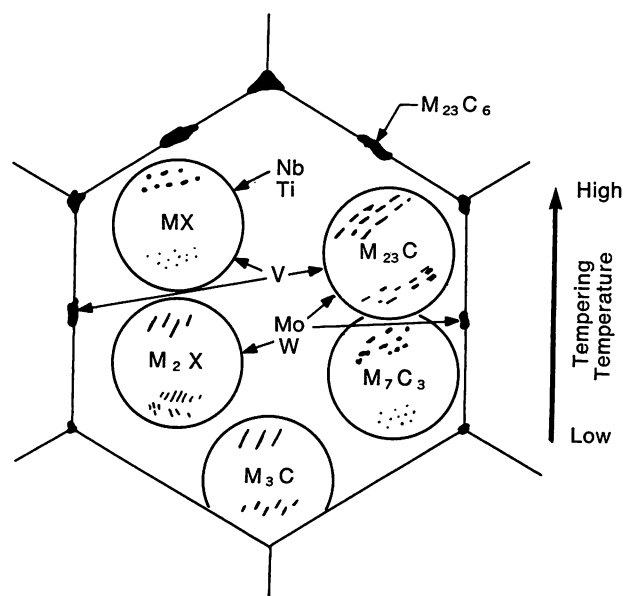


FIGURE 2—Types of carbides formed during tempering steel containing 12% Cr and additions of strong carbide formers.

particles. During service at above 500 C (930 F), further precipitation of metastable compounds may occur if the tempering treatment is not carried out to yield close to equilibrium precipitation. Some experimental steels containing high amounts of molybdenum and tungsten produce intermetallic compounds such as Laves phase in addition to the carbides.[15]

### Influence of Alloying Elements

The influence of all major alloying elements on transformation characteristics and the resulting properties has been extensively studied and is well understood. Only a few important aspects will be mentioned here.

To retain a fully transformable steel on the basis of 12% Cr when increasing the content of alloying elements, it is essential to control the propensity for delta ferrite formation. The following elements, in order of increasing influence, expand the delta ferrite domain:[7] Si, W, Mo, V and Al. The opposite effect is exerted by the austenite forming elements Mn, Cu, Co, Ni, C and N, Mn having the weakest and N the strongest influence.

Elements like Ti and Nb, which have a very high carbon and nitrogen affinity, affect the austenite/ferrite equilibrium by two mechanisms. They increase the delta ferrite content by shifting the phase boundary while removing carbon and nitrogen from solution, which increases the ferrite content still further. In most commercial steels like 12Cr-Mo-V-(W), the alloy additions are balanced in such a way that these steels are fully transformable although traces of delta ferrite may be present as a result of segregations. However, there are some commercial and developmental steels with carbon on the low side, typically 0.10%, such as 9Cr-2Mo, 9Cr-2Mo-V-Nb, and 12Cr-2Mo, which contain up to about 40% delta ferrite.

Another important aspect which has to be considered is the shift in $Ac_1$ and $M_S$ temperatures imposed by alloy additions. The $Ac_1$ temperature, which for the plain 12% Cr steel is about 740 C (1360 F), is depressed by additions of Mn and particularly Ni, while V, Mo, Si and Al have the opposite effect. Since reformation of austenite must be avoided during tempering and since the best combination of mechanical properties is obtained at a high tempering temperature, the $Ac_1$ should not be allowed to drop below 700 C (1290 F) but rather should be of the order of 800 C (1470 F). For commercial steels like 12Cr-Mo-V-(W), $Ac_1$ is about 820 C (1510 F). The $M_S$ and $M_f$ temperatures are important because they govern the final structure. The combined effect of all

alloying elements in depressing the $M_S$ temperature should be controlled such that $M_S$ does not drop below about 200 C (390 F). With a temperature interval of about 150 C (270 F) for completion of the martensite transformation, $M_f$ will be sufficiently high to ensure that the steel becomes fully transformed when cooled to ambient temperature. A steel with a lower $M_S$ would require refrigeration which would be very impractical from a manufacturing point of view.

The addition of several carbide forming elements to the base composition is essential in view of the desired long-term stability of the carbide dispersion. Although elements like V, Mo and W enter the chromium carbides existing in the normalized and tempered condition rather than introducing new carbide types, they effectively retard the coalescence and growth of these carbides and prolong the serviceable life of the component.

## Mechanical Properties

The design of high temperature components such as pressure vessels is generally based either on the minimum proof stress, the tensile strength or the mean creep rupture strength, each being reduced by a factor of safety. Other properties of importance, although not directly utilized in design, are good short- and long-term ductility and adequate toughness, the latter essential for ease of fabrication and servicing as well as safety of operation during the start-up and closedown of a plant. These properties will be discussed with reference to the internationally standardized 12Cr-Mo-V-(W) pressure vessel steel with the composition shown in Table I.

### Tensile Properties

The tensile properties of a standardized steel like 12Cr-Mo-V-(W) largely depend on the choice of tempering parameters. This is examplified in Table II where the minimum properties for two delivery conditions of tubes are given.[16] A statistical evaluation of a large number of tests conducted on tubes in superheater sizes in the delivery condition (1050 C, 1920 F, 30 min, A.C. + 780 C, 1436 F, 120 min, A.C.) shows the following variation of tensile properties measured at room temperature:

| | | |
|---|---|---|
| 0.2% Yield Strength | 577 MPa | ( 83.7 ksi) |
| Standard Deviation | 25 MPa | ( 3.6 ksi) |
| Tensile Strength | 809 MPa | (117.0 ksi) |
| Standard Deviation | 26 MPa | ( 3.8 ksi) |
| Elongation (5d) | 21% | |
| Standard Deviation | 1.4% | |

**Table I**—Chemical Composition for Steel 12Cr-Mo-V-(W)

| | Element, % | | | | | | | | |
|---|---|---|---|---|---|---|---|---|---|
| | C | Si | Mn | P | S | Cr | Mo | V | W |
| Minimum | 0.17 | — | — | — | — | 10.00 | 0.80 | 0.25 | 0.40 |
| Maximum | 0.23 | 0.50 | 1.0 | 0.030 | 0.030 | 12.50 | 1.20 | 0.35 | 0.60 |

**Table II**—Mechanical Properties at Room Temperature for Boiler Tube of Steel 12Cr-Mo-V-(W)

| Condition | Yield Strength, MPa | Yield Strength, (ksi) | Tensile Strength, MPa | Tensile Strength, (ksi) | Elongation, % | Impact Strength (ISO, V-notch), J/cm² | Impact Strength (ISO, V-notch), (ft-lb/cm²) |
|---|---|---|---|---|---|---|---|
| As Delivered | 564 | (81.8) | 750 | (109) | 24 | 75 | (55) |
| After 80,000 h | 509 | (73.8) | 736 | (107) | 24.5 | 40 | (29) |
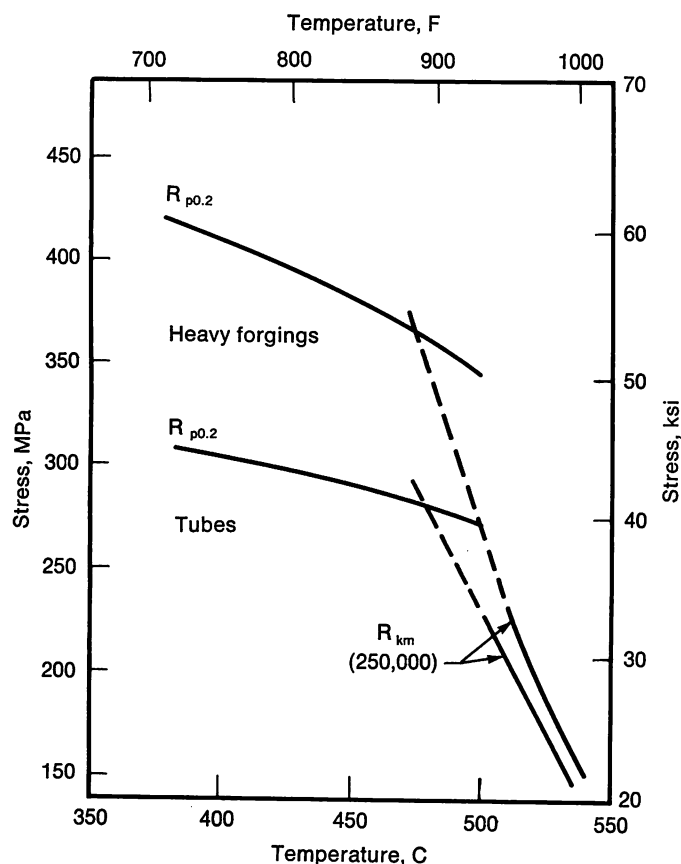
FIGURE 3—Proof and rupture stress according to ISO for two product forms of a steel with 0.2% C, 12% Cr, 1% Mo and 0.3% V.

Yield and tensile strengths at elevated temperature for the same type of product are given in Figure 3 together with the minimum values according to ISO.[1] The influence of heat treatment is reflected in the internationally agreed assessments of ambient and elevated temperature proof stress values published by ISO. Here two sets of data were established based on the two levels of minimum tensile strength of 690 MPa (100 ksi) for tubes and 780 MPa (113 ksi) for heavy forgings.

So far only the standardized 12Cr-Mo-V steel and the modified tungsten-alloyed variant have been considered. The addition of 0.5% tungsten to 12Cr-Mo-V confers a marginal 3% increase in tensile strength from

ambient temperature to at least about 400 C (750 F).[17] More substantial differences in tensile properties are observed when delta ferrite appears in the structure due to a reduction of carbon or a further addition of molybdenum, vanadium or niobium. The presence of delta ferrite *per se* reduces the tensile strength, but this reduction can, in many cases, be offset by a modification of the normalizing and tempering procedure to take advantage of the dispersion strengthening produced by strong carbide formers such as niobium.[11,13] Nitrogen may be utilized to replace carbon up to at least 0.10%. It confers the same tensile strength but at a slightly improved ductility.

**Impact Strength**

Toughness depends largely on the strength level as governed by the heat treatment. It is also influenced by alloying additions and the presence of delta ferrite. The upper shelf energy as measured by half-sized Charpy
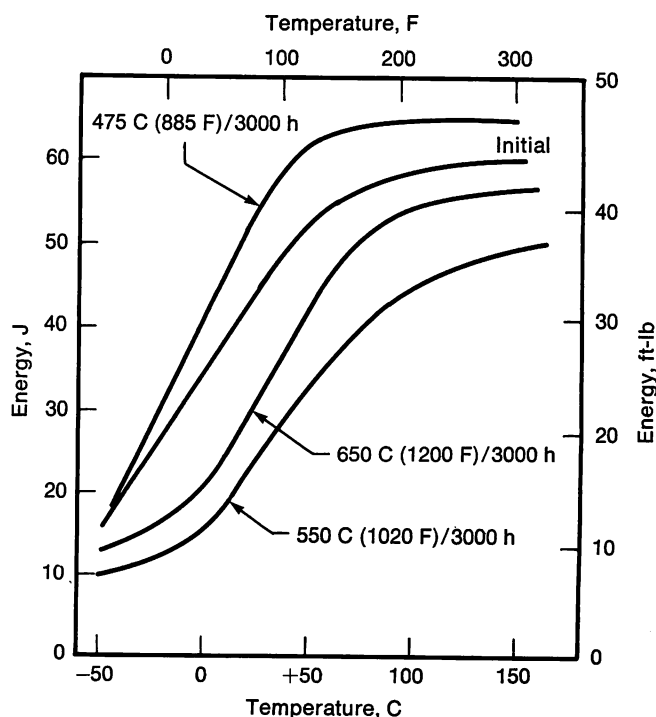
FIGURE 4—Impact strength (measured with half-sized Charpy V-notch specimens) of a steel with 0.2% C, 12% Cr, 1% Mo, 0.3% V and 0.5% W. The influence of aging at 475 to 650 C (885 to 1200 F) is demonstrated.

V-notch specimens is approximately 60 J (44 ft-lb) (Figure 4), and there is no dramatic change after aging the material for up to 3000 hours at 475 to 600 C (885 to 1110 F). The impact transition temperature falls in the range from −20 to +20 C (−4 to 68 F) for these conditions. Both the upper shelf energy and the ITT can be shifted by varying microstructural parameters and tempered strength. A refinement of prior austenite grain size reduces the ITT but has no obvious effect on the upper shelf energy.[11] The introduction of a certain amount of delta ferrite by reducing carbon and increasing molybdenum does not seem to change impact properties compared at a given strength. A certain directional anisotropy is often observed which is related to the presence of non-metallic inclusions, primarily MnS, elongated in the rolling direction. This anisotropy can be reduced by inclusion shape control, e.g. addition of rare earth metals which brings about an increase in the upper shelf energy.

Above all, the tempered strength governs the impact properties. Reducing the strength by altering the tempering parameters produces a decrease in ITT, typically 2 to 5 C per 10 MPa (4 to 9 F per 1 ksi), and an increase in the upper shelf energy values.[11]

## Creep Properties

The short-term yield strength and the long-term, 250,000-hour rupture strength coincide at about 480 C (900 F) for the standardized 12Cr-1Mo-V-(W) steel. The creep data on which ISO Commitee TC 17, Subcommittee SC 18 made this evaluation covered the range from 500 to 650 C (930 to 1200 F), and the number of data points beyond 30,000 hours was limited. More data have now become available covering both the limited section sizes typical of superheater tubes and larger components.

Creep strength is governed by elements in solid solution retarding dislocation movements and by carbide particles, the principal role of which is to maintain the high dislocation density created by the martensite reaction. The pinning action of the particles gradually decreases as particles coarsen during high temperature service and dislocations become mobile and interact to form subboundaries. This process is associated with a drop in creep resistance, and alloy additions are, therefore, aimed at stabilizing the carbide dispersion. The effects of individual elements have been studied by many authors.[8,11,14,15,17,18] Elements such as V, Mo and W do not introduce new carbide types but mainly become incorporated in the chromium carbides and reduce their rate of growth. The addition of a small amount of W confers a marginal 5 to 10% increase in rupture strength.[17,19] Larger amounts of these elements may result in the formation of intermetallic compounds such as Laves phase and introduce delta ferrite. Steels with up to 3% molybdenum and less carbon than the standard steel contain 20 to 40% delta ferrite.[12] The rupture strength on the basis of a few thousand hours is higher than the standard steel and comparable to that of AISI Type 304 at around 600 C (1110 F). The long-term properties remain to be confirmed.

The effect of a strong carbide former like niobium is to refine the particle dispersion and to retain the dislocation density at a very high level. As a result, niobium-alloyed variants exhibit a high rupture strength in short-term testing and a pronounced drop in strength when exposed at lower stresses for longer times. This drop is caused by the coalescence of niobium carbides and occurs within about 10,000 hours at 600 C (1110 F), after which the rupture strength falls close to that of the niobium-free steel.[8]

Rupture ductility is generally high and is maximized if the steel is tempered to a low tensile strength. The ductility is often observed to decrease with decreasing stress, and some variants such as the niobium-alloyed grades display a ductility trough. Pressure tests on notched superheater tubes made from 12Cr-Mo-V steel have demonstrated that this material is highly tolerant to stress concentrations under creep conditions.[20] Ductility was also found to be adequate under the conditions of multiaxial stresses.

## Corrosion Properties

The oxidation kinetics of ferritic steels with an alloy content up to 9Cr-1Mo do not vary much, and it is only when the chromium content is increased to 12% that some improvement is observed. Results from both plant and laboratory trials show that these steels oxidize in dry steam in accordance with the parabolic rate law forming a duplex scale containing $Fe_3O_4$ and $Fe_2O_3$.[21] Oxide spalling is less frequently observed in the 12Cr steels but may occur at the layer interfaces as a result of cooling and system strains. The adherence of the oxide scale can be improved by surface cold work which promotes the formation of a thin chromium-rich protective layer.[21] This is in contrast to the poor results obtained on ferritic steels of lower chromium content and is more in line with the effect observed on austenitic steels.

The resistance of the 12Cr steels to fire-side corrosion depends on the type of fuel. In oil fired units, all ferritic steels with more than about 2% chromium exhibit approximately the same weight loss. When coal is fired, the corrosion rate decreases with increasing chromium content. Under conditions of low oxygen activity often prevailing in such units, carburization may occur in all steels, but the depth decreases as chromium increases.

## Steel and Component Manufacture

### Melting

Melting the 12% Cr steels normally follows standard

practice and typically involves melting in electric arc furnaces and refining in an AOD converter followed by continuous casting of slabs or casting into ingots. The gas content and the amount of nonmetallic inclusions is often reduced by vacuum degassing which also improves the homogeneity of the steel. For demanding applications, an additional improvement in cleanliness can be imparted by high vacuum remelting or electroslag refining.

As was pointed out earlier, the anisotropy of impact strength is directly related to the presence of elongated sulfides, and additions of rare earths, magnesium or zirconium redistribute and alter the shape of such harmful inclusions. Deoxidation practices should also be selected in such a way that the excess amount of deoxidants such as aluminum dissolved in the matrix is low otherwise the toughness and high temperature ductility may be impaired.

### Hot and Cold Working

Breakdown of billets, hot forging and rolling of bar and hot extrusion of tube is normally carried out at 1000 to 1300 C (1830 to 2370 F). These steels are sensitive to cracking when cooled from hot working temperatures unless cooling is slow and is followed by a process anneal at 700 to 800 C (1290 to 1470 F). It is also customary to transport the material hot between certain production steps.

Hot reducing and forging of components is carried out in the lower half of the above temperature range, but the temperature should not be allowed to drop below approximately 950 C (1740 F) because of the increased risk of cracking at the lower temperatures. Components manufactured by hot processes should be given a complete normalizing and tempering treatment to fully control the properties.

Cold forming operations like tube bending do not present problems as long as the local deformation does not exceed the fracture strain. Suitable choice of tooling makes it possible to fabricate tube bends with radii of 2d. Cold-bent superheater tubes were formerly stress relieved at about 740 C (1360 F), but this is no longer generally done.[22] Creep tests conducted on cold worked (stretched and compressed) material demonstrated that cold work caused a marginal reduction of rupture strength which was recovered after a stress relief treatment.

### Welding

Welding is considered the most complicated fabrication process for the 12% Cr steels because of the high hardenability of these steels. The martensite formed in the weld metal and heat affected zone (HAZ) is hard and brittle and must be tempered. The usual way of avoiding these brittle structures is to use a high preheat temperature of at least 430 C (805 F) and an interpass temperature in the range 430 to 500 C (805 to 930 F). After welding, the component should be cooled below the $M_f$ temperature of approximately 150 C (300 F) and subsequently tempered at 700 to 800 C (1290 to 1470 F). Cooling to room temperature should only be allowed when the section size is of the order of 10 mm (0.4 in.) or less and in the absence of stress raisers. When welding large sections, lower preheat and interpass temperatures are sometimes prescribed which allow each individual layer to transform into martensite which then becomes tempered during the application of subsequent layers. With this technique, sections up to 270 mm (10.6 in.) have been successfully welded.

Except for strict temperature control, welding does not pose any special problems. It is common practice to use filler metals with the same composition as the steel to be welded. The root pass is normally made using the TIG process with filler metal added. Because of the high hardness during some stages of operation, there exists a risk for hydrogen cracking if the welding consumables are not properly dried and the welded component is not immediately tempered.

The welding metallurgy of the 12Cr-Mo-V steels is well known. When considering the toughness of welded structures, it is important to observe that the most sensitive area is located in the HAZ at a certain distance from the fusion line. The reason is that grain coarsening of the austenite is most pronounced at an intermediate temperature whereas, at the higher temperatures occurring in the weld metal and close to the fusion line, delta ferrite restricts grain growth.[23]

As the main concern regarding weldability of the 12Cr-Mo-V-(W) steel is the high martensite hardness, less crack sensitivity can be expected at a lower carbon content. Variants with 0.05 to 0.10% C and 2% Mo seem to offer a good combination of weldability and high temperature strength. These steels can probably be welded without preheating, and the hardness of the as-welded structure equals that of the welded and tempered 12Cr-Mo-V steel with 0.2% C. The duplex structure is also advantageous in restricting grain growth in the HAZ.

### Practical Experience in Power Plants

The 12Cr-Mo-V-(W) steel has been used in fossil fueled boilers for at least 20 years. The longest experience exist with superheater tubes which were installed as early as in 1957.[16] Later this steel was also employed in reheater and evaporator tubes in coal fired boilers[24] and in larger components such as steam pipes and headers. A niobium-alloyed variant is commonly used in gas turbines.

Operating experience with boiler tubes is excellent, and operating times of up to 92,000 hours have been re-

ported with no signs of specific material failures. A detailed investigation of a boiler tube after 80,000 hours of service at 610 C (1130 F) showed that the mechanical properties measured at room temperature were very little affected (Table II).[16] The impact strength was reduced, but the material still had adequate toughness. Creep tests demonstrated a drop in strength at high stresses at 600 C (1112 F) as a result of the exposure, an effect attributed to the coarsening of carbides during service. These observations underline the excellent thermal stability of the 12Cr-Mo-V-W steel which is further corroborated by experiments in which the influence of temperature excursions up to 750 C (1382 F) on the microstructure and creep properties was elucidated.[25]

Superheater and reheater tubes of type 12Cr-Mo-V installed in British coal fired boilers have shown improved performance over 9Cr-Mo steel and lower alloy grades which they have replaced.[24] Failures during service have generally been attributed to severe over heating up to 850 C (1562 F). Service times up to 35,000 hours are reported.

# Conclusions

A wealth of experience exists for 12Cr-Mo-V-(W) steel in various product forms in power plants, particularly in Europe. The fabrication problems have been solved, and the general experience from in-plant service is favorable. This class of steel, whether according to its original composition or modified by reducing carbon, increasing molybdenum or making other additions, presents an attractive combination of properties. These steels should be an interesting alternative to both lower alloyed hardenable steels and higher alloyed austenitic steels in the construction of conventional power plants as well as advanced nuclear power systems. An extended use can be expected provided that complementary information regarding properties is created when called for and appropriate code approvals are obtained.

# References

1. D. O. Burton, J. Orr and J. B. Marriott, "Elevated Temperature Properties of 2¼Cr-1Mo, 9Cr-1Mo and 12Cr-1Mo-V Steels for International and National Standards," International Conference, *Ferritic Steels for Fast Reactor Steam Generators,* British Nuclear Energy Society, London, May 30-June 2, 1977.

2. T. Yukitoshi, K. Nishida, T. Oda and T. Daikoku, ASME Winter Annual Meeting, Nov. 1975, Paper 75—WA/PVP-2.

3. T. Yukitoshi, K. Yoshikawa, K. Tokimasa, T. Kudo, Y. Shida and Y. Inaba, "Behavior of Low Alloy Steel in Sodium Environment," International Conference, *Ferritic Steels for Fast Reactor Steam Generators,* British Nuclear Energy Society, London, May 30-June 2, 1977.

4. P. J. Grobner and T. Wada, Climax Molybdenum Co., Unpublished data, 1977.

5. M. Caubo and J. Mathonet, *Rév. de Métallurgie, 66* (5), 1969, 345.

6. S. D. Harkness, et al., "Development of a 9Cr Steel with Improved Strength and Toughness," International Conference, *Ferritic Steels for Fast Reactor Steam Generators,* British Nuclear Energy Society, London, May 30-June 2, 1977.

7. K. J. Irvine, D. J. Crowe and F. B. Pickering, *J. Iron and Steel Institute, 195,* 1960, 386.

8. A. Hede and B. Aronsson, *Ibid., 207,* 1969, 1241.

9. J. Orr, F. R. Beckitt and G. D. Fawkes, "Physical Metallurgy of Steels for Fast Reactor Boiler Circuits," International Conference, *Ferritic Steels for Fast Reactor Steam Generators,* British Nuclear Energy Society, London, May 30-June 2, 1977.

10. J. Z. Briggs and T. D. Parker, The Super 12% Cr Steels, Climax Molybdenum Co., 1965.

11. E. A. Little, D. R. Harries and F. B. Pickering, "Some Effects of Heat Treatment on Structure and Properties of 12Cr Steels," International Conference, *Ferritic Steels for Fast Reactor Steam Generators,* British Nuclear Energy Society, London, May 30-June 2, 1977.

12. T. Wada, Climax Molybdenum Co., Unpublished data, 1978.

13. P. J. Grobner and T. Wada, Climax Molybdenum Co., Unpublished data, 1979.

14. J. Koutsky, J. Bacharova and J. Jezek, *Archiv Eisenhüttenwesen, 45* (3), 1974, 155.

15. J. Koutsky and J. Jezek, *J. Iron and Steel Institute, 203,* 1965, 707.

16. H. W. Fricker and B. Walser, "Experience with 12Cr Steels," International Conference, *Ferritic Steels for Fast Reactor Steam Generators,* British Nuclear Energy Society, London, May 30-June 2, 1977.

17. G. Oakes, J. Orr and P. W. Taylor, "Effect of Tungsten on Tensile and Rupture Strength of 12Cr Steel," International Conference, *Ferritic Steels for Fast Reactor Steam Generators,* British Nuclear Energy Society, London, May 30-June 2, 1977.

18. T. Fujita and N. Takahashi, *Trans. Iron and Steel Institute of Japan, 18,* 1978, 702.

19. L. O. Egnell and N. G. Persson, "On Creep Properties of Sandvik HT7 and HT9," International Conference, *Ferritic Steels for Fast Reactor Steam Generators,* British Nuclear Energy Society, London, May 30-June 2, 1977.

20. J. A. G. Hutchings and J. C. Guest, "Observations on Bursting Behavior of Boiler Tubes Made from Three Chromium-Molybdenum Steels," International Conference, *Ferritic Steels for Fast Reactor Steam Generators,* British Nuclear Energy Society, London, May 30-June 2, 1977.

21. M. I. Manning and E. Metcalfe, "Oxidation of Ferritic Steels in Steam," International Conference, *Ferritic Steels for Fast Reactor Steam Generators,* British Nuclear Energy Society, London, May 30-June 2, 1977.

22. J. A. Board, *British Nuclear Energy Society Journal, 13,* 1974, 211.

23. R. S. Fidler and D. J. Gooch, "Hot Tensile Properties of Simulated Heat Affected Zone Structures in 9Cr-Mo and 12Cr-Mo-V Steels," International Conference, *Ferritic Steels for Fast Reactor Steam Generators,* British Nuclear Energy Society, London, May 30-June 2, 1977.

24. L. M. Wyatt, "Performance of Chrome-Molybdenum Steels in Boilers of CEGB Power Stations," International Conference, *Ferritic Steels for Fast Reactor Steam Generators,* British Nuclear Energy Society, London, May 30-June 2, 1977.

25. B. Walser, P. Brezina and T. Geiger, *Arch. Eisenhüttenwesen, 50* (6), 1979, 249.

## Discussion

Y. E. SMITH, *Climax Molybdenum Company.* Do you see the better weldability of the lower carbon 12 chrome steel as being effective in bringing it to practical application, or is there some other limitation that is going to prevent this steel from being in common usage.

N. G. PERSSON. I believe that that kind of material might well become a very interesting engineering material, but I think there is still a lack of long-term data which should really be the basis for judgment. Certainly the welding characteristics are much better than for the high carbon grade.

# Stainless Steels for Solar Energy Conversion

by J. D. Redmond and R. M. Davison
Climax Molybdenum Company

Low temperature solar energy conversion provides space heating, domestic water heating and swimming pool heating. Without the need of concentration of solar radiation to produce high temperatures, the system required to convert solar energy to usable heating forms can be quite simple. The problem is then to design a unit and select materials that will provide performance and durability within the economic constraints imposed by alternative energy sources.

The critical component of the solar heating system is the absorber panel within the collector. Over the full lifetime of the system, on the order of 10 to 20 years, the absorber panel must be resistant to internal corrosion, and its selective surface must be stable and undisturbed by substrate corrosion. Although plastics, steel, copper and aluminum have been considered for absorber panels, experience is rapidly accumulating in support of the conclusion that type 444 (18Cr-2Mo) ferritic stainless steel is the optimal absorber material in terms of performance, safety, reliability, durability and cost.

Stainless steel absorber panels are manufactured very inexpensively. Two sheets of light gauge type 444 stainless steel, as thin as 0.38 mm (0.015 in.), are embossed with the flow pattern, faced together, and welded by electrical resistance spot and seam welding. As shown in Figure 1, this design is the limiting case for closely spaced collecting tubes. It is highly efficient because the transfer fluid is in contact with over 90% of the collecting surface. The short thermal path eliminates the importance of the difference of thermal conductivities among



a) Fin-Tube Construction

b) Sheet Construction
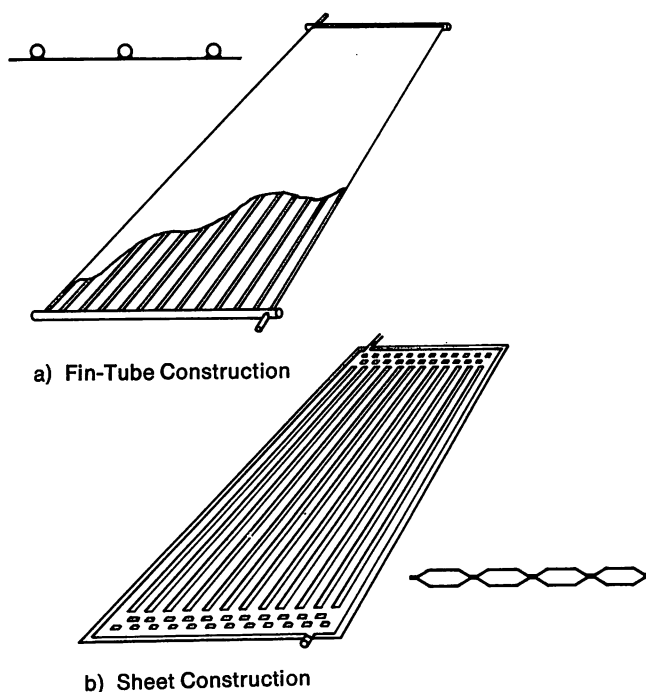
FIGURE 1—Alternative absorber panel designs for low temperature thermal conversion of solar energy.

**Table I—Stainless Steels Evaluated for Application in Solar Collectors**

| Grade* | Element, % | | | | | |
|--------|------------|-----|-----|-----|-----|-------|
| | Cr | Mo | Ni | C | N | Other |
| 304 | 18.00-20.00 | — | 8.00-10.50 | 0.08 max | 0.10 max | — |
| 316 | 16.00-18.00 | 2.00-3.00 | 10.00-14.00 | 0.08 max | 0.10 max | — |
| 409 | 10.5 -11.75 | — | — | 0.08 max | — | Ti = 6 x C min = 0.75 max |
| 439 | 17.00-19.00 | — | 0.50 max | 0.07 max | — | Ti = 12 x C min = 1.10 max |
| 444 | 17.50-19.50 | 1.75-2.50 | 1.00 max | 0.025 max | 0.035 max | (Nb + Ti) = 0.2 + 4 (C + N) min = 0.8 max |

* Types 304, 316 and 409 are recognized and designated in the AISI numbering system. Types 439 and 444 are commercially available grades more recently introduced that do not have AISI recognition at this time. The naming, type 439 and type 444, used in the text represents common usage and not AISI designation.

the various materials. This method of construction produces a tight metal-to-metal crevice in the panel. The grade of stainless steel selected must be able to resist crevice corrosion.

Stainless steel solar heating systems can use untreated tap water or swimming pool water as the heat transfer medium. Use of water (1) avoids toxic chemicals and the expense of "double-wall" heat exchangers designed to prevent leakage to the user circuit, (2) avoids the expense of monitoring and maintaining a chemical system, (3) makes optimal use of the high thermal conductivity and low viscosity of water, and (4) shortens the response time of a panel because draindown reduces the thermal mass of a nonoperating panel. For space heating and domestic water heating, the transfer fluid reaches 80 to 90 C (175 to 195 F). The panel can easily exceed 150 C (300 F) if drained during full sunlight, a condition which can lead to corrosion problems through concentration of the transfer fluid. Pool water is more corrosive than tap water, but a pool heating system is typically limited to 30 to 40 C (85 to 105 F) by system design.

If a glycol solution is used, type 444 stainless steel is still appropriate. Recent corrosion studies[1] concluded that type 444 was unaffected by glycol or its degradation products, as might be typical of severe operating conditions or poor system maintenance, but copper, aluminum and steel were attacked.

The forms of corrosion that must be avoided by stainless steels are (1) pitting and crevice corrosion, (2) intergranular attack, (3) stress corrosion cracking, (4) galvanic corrosion, and (5) atmospheric corrosion. The grades of stainless steel that have been considered for solar heating service are shown in Table I.[2]

As shown in Table II, type 444 has excellent resistance to crevice corrosion even at very high chloride levels as might be encountered during a dryout condition. It is observed that the distilled water solutions used in laboratory testing are more aggressive than natural waters because of their mineral content, as is consistent with long-term field experience.

Intergranular attack is very unlikely because the high temperature exposure in resistance welding is extremely brief, and because the ferritic stainless steels considered are required to be stabilized with titanium or niobium, or both.

Because all environmental conditions leading to stress corrosion cracking are present in the solar panel, a material not susceptible to SCC must be selected. As shown in Table III, type 444 shows practical immunity to SCC even in boiling 42% $MgCl_2$. These observations have been confirmed in field tests where austenitic stainless steels have failed by stress corrosion cracking but not the ferritic steels.

**Table II**—Crevice Corrosion Resistance of Stainless Steels for Solar Energy Conversion[a]

| Solution | Type 304 | Type 439 | Type 444 |
|---|---|---|---|
| 200 ppm $Cl^-$ deionized water[b] | P (0.020)[e] | P (0.100) | NP[f], NP, NP, P (0.040) |
| 500 ppm $Cl^-$ deionized water[b] | P (0.250) | P (0.100) | NP, NP, NP, P (0.030) |
| 1000 ppm $Cl^-$ Ann Arbor tap water[c] | P (0.090), NP | — | NP, NP, NP |
| 2000 ppm $Cl^-$ Ann Arbor tap water[c] | — | — | NP |
| 1000 ppm $Cl^-$ Simulated well water[d] | P (0.100) | — | NP, NP |
| 2000 ppm $Cl^-$ Simulated well water[d] | — | — | NP, NP |

[a] Metal-to-metal crevice, 90 C (195 F), $O_2$-saturated solutions, 45 days.
[b] pH 5-6.
[c] pH 9-10.
[d] 24 ppm $NO_3^-$, 14 ppm $SO_4^=$, 180 ppm $HC_3^-$, pH 8.3.
[e] P = pitting observed; ( ) = penetration in mm.
[f] NP = no penetration.

**Table III**—Stress Corrosion Cracking Resistance of Stainless Steels

| Test | Time to Failure for Indicated Stainless Steels, h | | | |
|---|---|---|---|---|
| | Type 304 | Type 316 | Type 439 | Type 444 |
| Boiling 42% $MgCl_2$ | <8 | <24 | >1700* | >1700* |
| Boiling 25% NaCl (pH 1.5) | <16 | <144 | >2000* | >2000* |
| NaCl Wick Test | <120 | <360 | >1440* | >1440* |

* No failure observed.

It may be necessary to insulate the stainless steel absorber panel from the copper plumbing because type 444 has been shown to be more noble.[1] On the other hand, connections of type 444 and copper in field installations have not revealed interactions of practical consequence.

For best performance, the absorber needs a black coating that absorbs radiation of visible wavelengths and does not reemit the energy as infrared wavelengths. Black chromium oxide is generally recognized as the industry standard for effectiveness and stability. It is necessary that the metal substrate show no atmospheric corrosion that would disrupt the absorptive coating. For metals other than stainless steel, a thin layer of nickel is plated on the substrate to provide corrosion resistance, and then chrome oxide is electrolytically deposited. This system is cheaper with stainless steel because the nickel flash is not required.

Chromium oxide can be produced on stainless steel by controlled oxidation using a system developed at Climax,[3] based on a process originally developed by Armco.[4] This surface, produced by dipping the panel for five minutes in molten sodium dichromate, shows excellent selectivity undiminished by temperature, humidity and ultraviolet radiation exposure. Samples placed in test by Armco when the coating system was originally developed for architectural decoration show no degradation after thirty-years exposure in a severe industrial atmos-

phere. The chemical black chrome system is now in use by several manufacturers.

A review of laboratory corrosion test results indicates that type 444 ferritic stainless steel is the cost effective material for low temperature solar collectors. This conclusion has been confirmed in commercial experience in Japan, the United States, South Africa, Australia and Europe. Type 444, in conjunction with the chemical black chrome coating method, provides a solar collector of outstanding performance and extraordinary durability. Stainless steel solar collectors provide an economical and practical method of using a renewable energy source to reduce dependence on scarce and costly fossil fuels.

## References

1. R. B. Diegle, "Corrosion Studies of Aluminum, Copper, and Steel Under Simulated Solar Collector Conditions," NACE Symposium Corrosion/80, Chicago, March 3-7, 1980.

2. J. D. Redmond, E. A. Lizlovs and R. M. Davison, "The Application of Stainless Steel to Solar Collectors," American Section Meeting of the International Solar Energy Society, Orlando, Florida, June 1977.

3. J. D. Redmond, J. D. Baker and R. M. Davison, "A New Selective Black Coating for Solar Collectors," American Section Meeting of the International Solar Energy Society, Denver, Colorado, August 1978.

4. Armco Fabricating Data Bulletin, "The Armco Stainless Steel Ebonizing Process," Armco, Inc., Middleton, Ohio, August 31, 1959.

# Heavy-Duty Gas Turbines; Challenge and Response for the Next Decade

by C. T. Sims
General Electric Co.

The first record and illustration of the concept to utilize combustion gas to spin a shaft and thereby derive power from the shaft appears to have occurred in the 17th Century in Europe[1] (Figure 1). Centuries later, World War II provided the impetus to apply this principle of generation to gaseous thrust, and thus was born the aircraft jet engine. However, the original use to spin a shaft and derive useful energy through operation of equipment to move gas or liquids, to move vehicles, or to make electricity has continued as a significant parallel development in man's technology. Gas turbines for industrial power generation were becoming known in the first half of the 20th Century, and during the second half of the Century have grown to become a major contributor to world power needs.

Presently, such heavy-duty gas turbines (often also called "industrial" gas turbines, and at one time "land" gas turbines) fall into two major categories, those for direct electric power generation and those for a variety of other energy uses, often also now called "industrial" applications.

For instance, heavy-duty gas turbines driving electric generators now account for a 9% share of electrical power capacity in the United States. Much of this is directed toward "peaking" use, where the rapid start capability of gas turbines is an essential ingredient. In large industrial gas turbines, horsepower from the shaft drives the pumps for a host of world pipe lines, provides propulsion for ships, drives locomotives, and provides similar energy where the mechanical output is desired.

For all these applications, the principal features brought to the job by gas turbines are high efficiency of energy conversion, rapid start capability, short cycle time between order and delivery and high mobility to site location resulting from their relatively light weight compared to diesels and steam power plants. Heavy-duty gas turbines are an integral and increasing factor in plans for advanced power plants, such as those burning coal gas, oil from coal or coal directly. Examples of some present-day cycles[2,3] are shown in Figure 2, together with a cutaway view of a contemporary gas turbine.

It is the objective of this paper to attempt to identify the major challenges facing the continuing advance of the materials technology for these turbines and to generate some observations on how these challenges will be met.



FIGURE 1—Early illustration of gas turbine principle applied to industrial energy needs. From Bishop Williams, Mathematical Magick, England, 1648, Courtesy W. B. Wilson, GE Co.

## Metallurgy of Heavy-Duty Gas Turbines

The metallurgical construction[4] and the operating conditions of a typical gas turbine are described below to clarify the requirements their materials must meet.
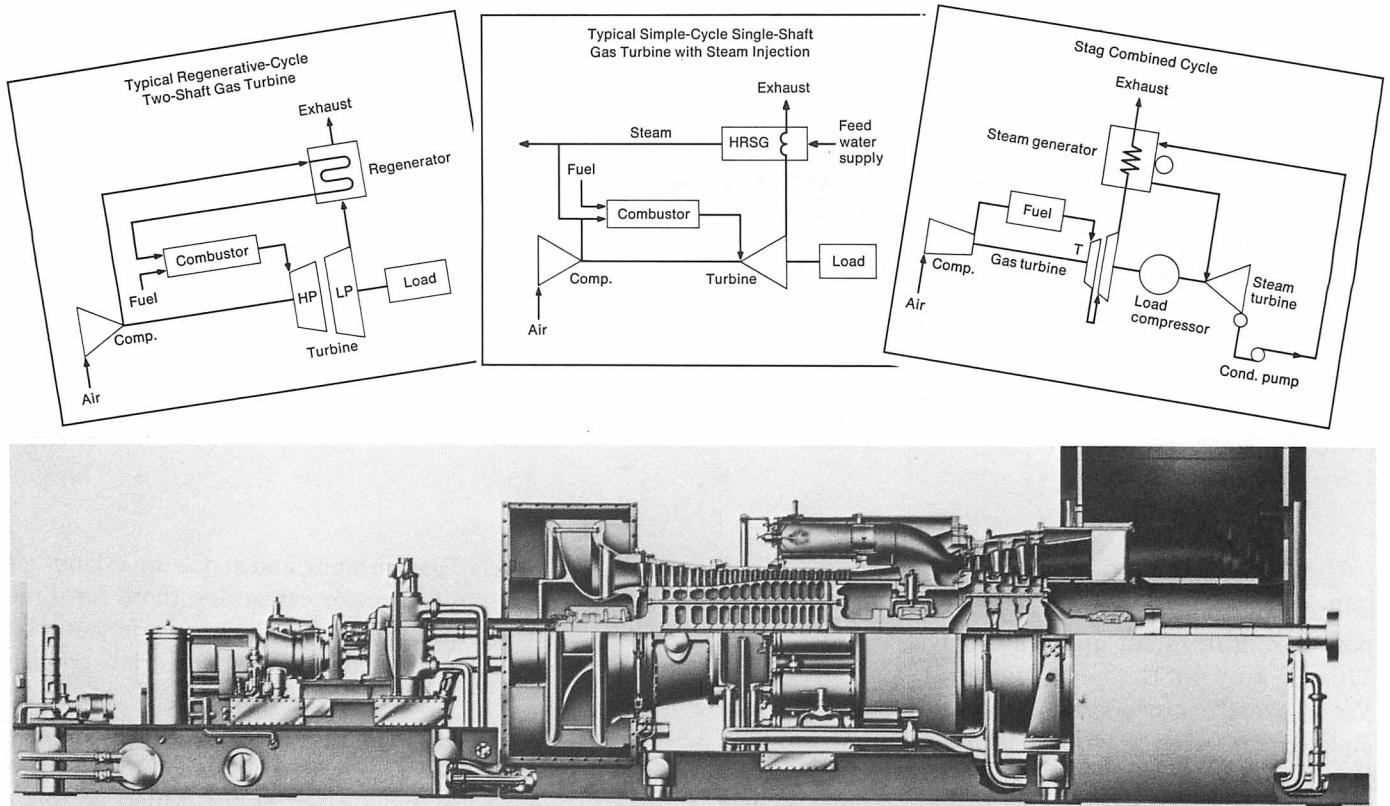
FIGURE 2—70 MW heavy-duty single-shaft gas turbine with examples of some gas turbine cycles.
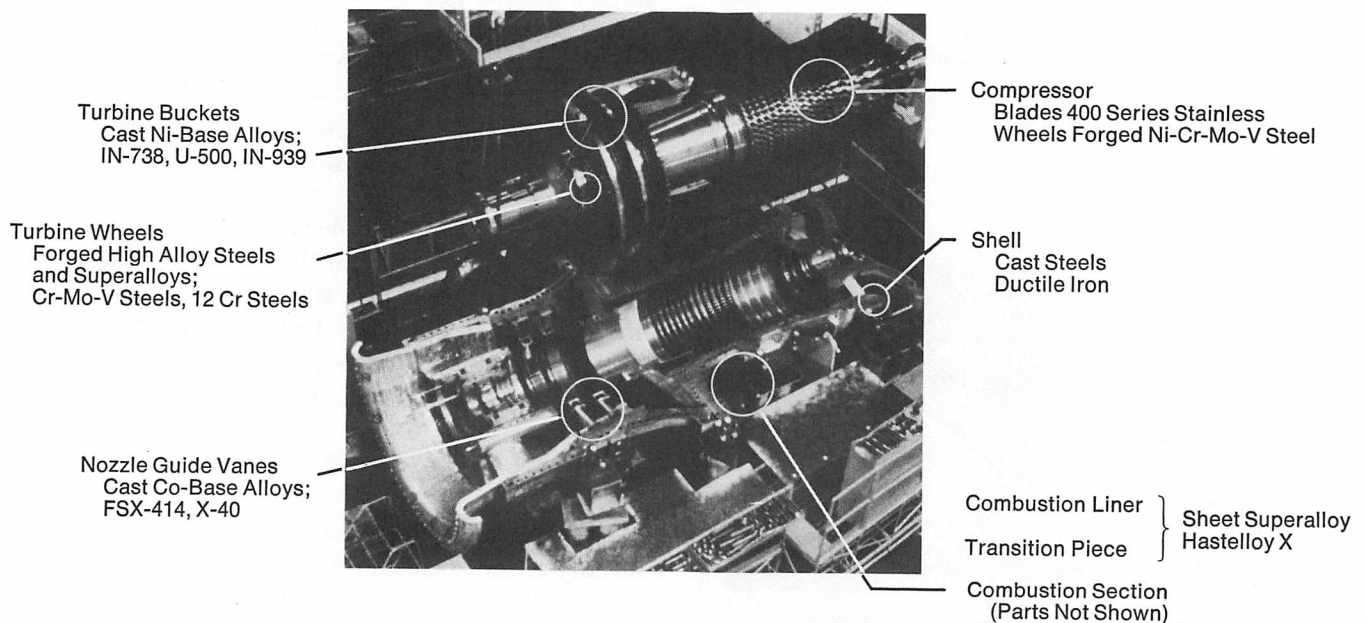


FIGURE 3—A heavy-duty gas turbine in assembly; typical materials for major components identified for class and examples.

## Alloys Utilized

Figure 3 broadly identifies the leading alloy types typically used in major gas turbine components. While other heavy-duty gas turbine designs may vary somewhat from the turbine shown here, it can be considered broadly typical. The picture also illustrates the relatively massive construction and large size of heavy-duty gas turbines, an important feature related to economy and durability.

**Turbine Shell.** These components, somewhat similar to shells for steam turbines, but lower in pressure containment, are usually cast iron or low alloy steel. Ductile cast iron currently serves well. Service temperature rarely exceeds about 315 C (600 F).

**Compressor.** The compressor wheels are usually a forged low alloy steel of high integrity and toughness. Ni-Cr-Mo-V steels are typical, although Ni-Cr-Mo also has been used. Compressor blading is often a 400-series martensitic stainless steel to optimize strength and corrosion at moderate temperatures. Compressor discharge for heavy duty turbines is about 250 to 350 C (480 to 660 F) at present.

**Combustor and Transition Sections.** The combustion chamber, of course, must contain the fuel, highly compressed air and their combustion products during the critical combustion phase; the transition ducting carries the resultant high temperature flame directly into the first stage of static airfoils. Typically, combustion system components are made of sheet metal products from very high temperature corrosion resistant wrought alloys, such as Hastelloy X. Oxidation resistance, corrosion resistance, strength and fatigue resistance all are critical to performance. Combustion section alloys, depending on cooling design, operate up to about 870 C (1600 F).

**Turbine Wheels.** Turbine wheel materials technology, as in all high temperature rotating equipment, is critical. Heavy-duty gas turbines have used a variety of forged wheel materials, with some reaching toward diameters of 2.1 m (7 ft). Depending on design and location, wheels range from Cr-Mo-V alloy steels through 12 chrome steels such as M-152; superalloy wheels such as IN-706 have been considered. It is almost classic that the critical properties are high tensile strength and ductility, giving high fracture toughness. Wheel rim temperatures are usually kept low (compared to aircraft

turbines) to maintain creep resistant dovetail sections and to allow the most economic choice of materials possible.

**Nozzle Guide Vanes.** The gas stream, currently in the order of 1100 C (2000 F) in peaking heavy-duty gas turbines, sees its first aerodynamic interaction with the nozzle guide vanes, airfoils which turn the gas stream to drive the buckets and wheels. In most large heavy-duty gas turbines, nozzle guide vanes are investment castings (Figure 4) constructed so that several vanes are in a group for sealing and for economy.[5] They are cobalt- or iron-base alloys, with the first stages usually a cobalt alloy such as FSX-414. These alloys are characterized by good castability, high corrosion resistance, good metallurgical stability and long time creep strength, and (very importantly) manufacturing and field repair weldability.

**Turbine Buckets.** Turbine buckets are the focus of metallurgical accomplishment in gas turbines (Figure 5).[6] The materials capability of the buckets usually limits the capability of the turbines. Buckets require an unusual combination of high tensile strength and toughness in their dovetail connection with the wheels, high creep and rupture strength in the airfoil portion and the greatest possible resistance to oxidation and corrosion. They also must be easily cast and readily coated. Usually buckets are vacuum cast from nickel-base alloys such as IN-738, IN-939 or Udimet-500. Most turbine manufacturers now coat early stage bucketing to obtain maximum oxidation and corrosion protection.

**Exhaust Section.** The gas stream, cooled, losing pressure ("exhausted!"), leaves the turbine through fabricated steel passages. Considerable condensate type corrosion can occur here, so the trend is toward a protected steel or perhaps a 12% chromium steel.

### Operating Conditions

Heavy-duty gas turbines for industrial service are designed and built to insure maximum performance at minimum cost. However, the cost includes not only machinery but fuel, and obviously now, the latter is more significant than ever. The state-of-the-art at present is that peaking heavy-duty gas turbines are beginning to be fired to gas stream temperatures (in Stage I nozzles) of about 1100-1200 C (2000-2200 F). The hot metal parts are cooled to a maximum of 870-1040 C (1600-1900 F), and pressures in the range of 1.0 to 1.4 MPa (10-14 atm) are common. It should be borne in mind that long life, low cost and parts durability are prime needs in a heavy-duty gas turbine design. Peak load turbines are designed for about 5000 to 10,000-hour service, while turbines for continuous or base load service are designed for 100,000-hour life.

Of special significance is that heavy-duty gas turbines must be prepared to burn a wide variety of fuels. Some of the combustion products are highly corrosive in nature, and can create fouling in the turbine or even
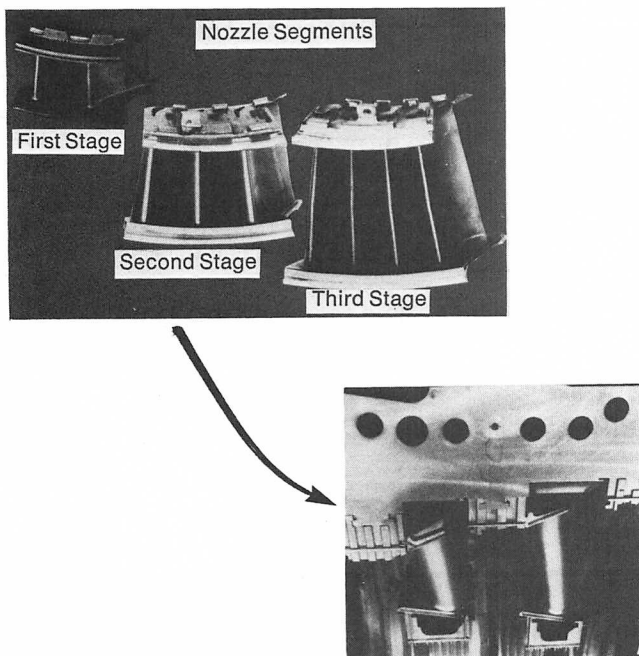


*FIGURE 4—Investment cast nozzle guide vane segments for 35 MW heavy-duty gas turbine. As castings and with second and third stages mounted. Third stage nozzle about 280 mm (11 in).*

First, Second, Third Stage Buckets

Construction Features Second & Third Stage

Integral Shroud

Gas Path

Bucket Vane

167 C (300F) 3rd Stage Temperature Drop

Extended Shank

Dovetail

First-Stage Turbine Buckets Radial View

Cross Section of a Cooling Hole in Bucket

Cooling Air Inlet Holes

First Stage Bucket
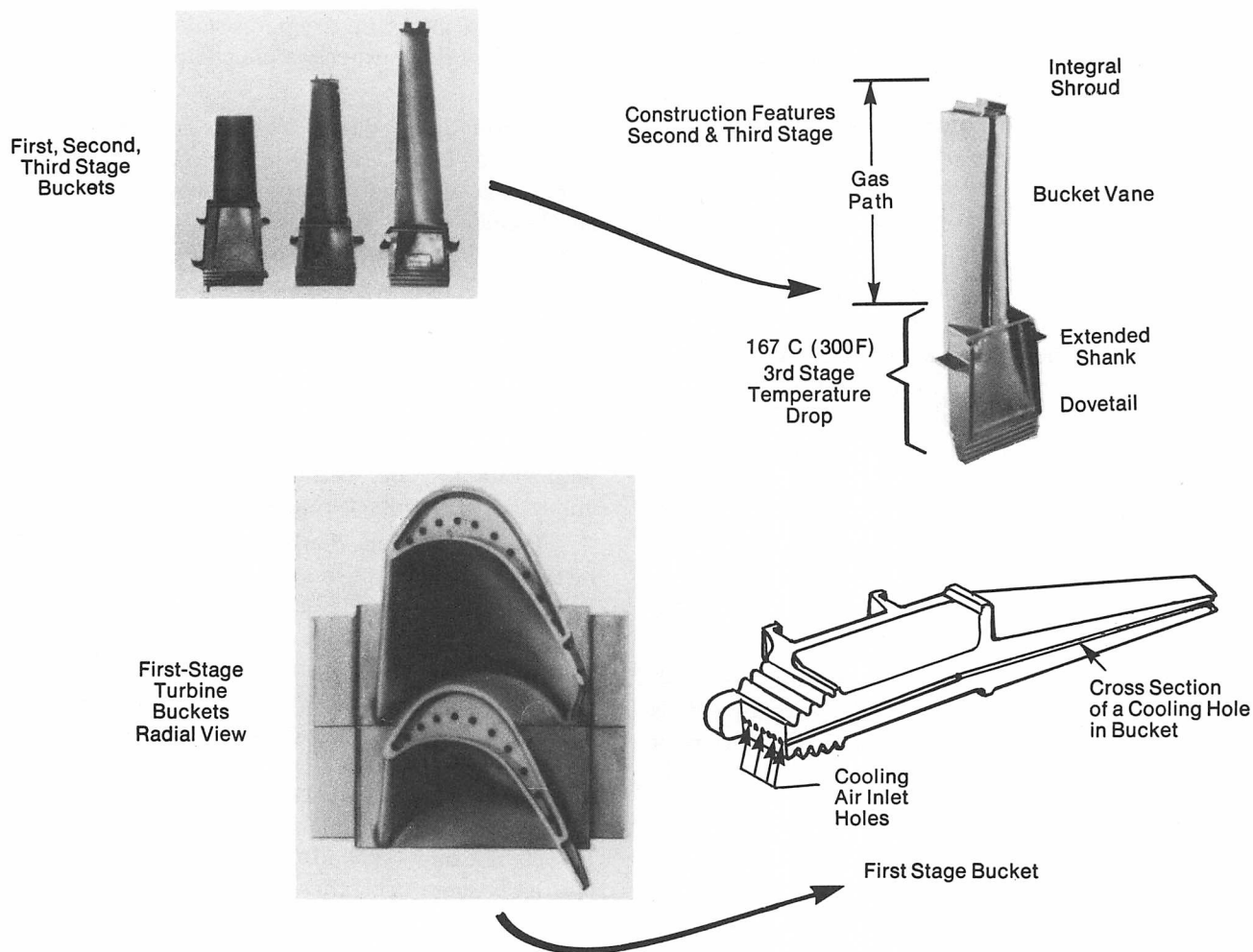
FIGURE 5—Bucket features for 75 MW single-shaft gas turbine.

**Table I**—Some Properties of Gaseous and Liquid Turbine Fuels

| | | | | | Liquid Fuels | | |
| | | Gaseous Fuels | | | True Distillates | Ash-Bearing | |
| | | Natural Gas | Low Btu Coal Gas | Coke Oven Gas | Kerosene | No. 2 Distillate | Blended Residuals and Crudes | Heavy Residuals |
|---|---|---|---|---|---|---|---|---|
| Heat Values $TJ/m^3$ / $Btu/ft^3$ | | 2.14-2.62 / 950-1150 | 0.18-0.37 / 50-200 | 1.22-1.46 / 500-900 | 10,150 to 10,900 kcal/kg / 18,300 to 19,700 Btu/lb | | | |
| Specific Gravity (vs. Air or Water) | | 0.58-0.72 | 0.80-0.92 | 0.40-0.45 | 0.78-0.83 | 0.82-0.88 | 0.80-0.92 | 0.92-1.05 |
| Ash, ppm | | — | — | — | 1-5 | 2-50 | 25-200 | 100-1000 |
| Major Components | $CH_4$ | 75-100% | 0.5-4.5% | 28-32% | Na | | | |
| | $H_2$ | — | 12-16 | 50-55 | + 0.0-0.5 ppm | 0-1 ppm | 1-100 ppm | 1-350 ppm |
| | CO | — | 2-30 | 5-7 | K | | | |
| | $N_2$ | 1-16 | 30-55 | 1-6 | V 0-0.1 | 0-0.1 | 0.1-80 | 5-400 |
| | $CO_2$ | ~0.1 | 5-10 | 2-3 | Pb 0-0.5 | 0-1 | 0-1 | 0-25 |
| | | | | | Ca 0-1 | 0-2 | 0-10 | 0-50 |

erosion. Thus, fuels become a key factor in gas turbine technology.

**Fuels.** Heavy-duty gas turbines utilize two basic types of fuels at present, gaseous fuels and liquid fuels. Table I summarizes briefly the most obvious character-istic properties of some of these fuels.[7]

Probably over one-third of the world's gas turbines have been operated on natural gas. With few exceptions, the gas stream from this clean fuel requires only oxida-tion resistance in hot stage parts, unless unusual or

*FIGURE 6—Example of fouling in heavy-duty gas turbines.*

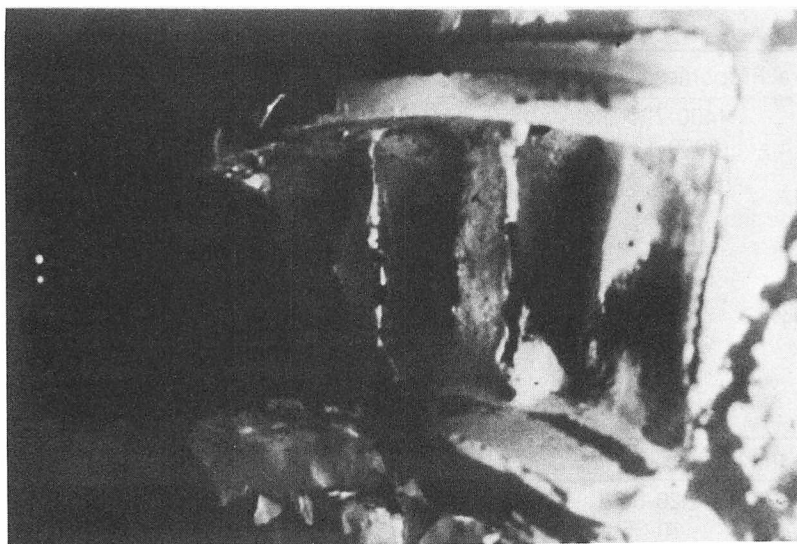stray contaminants (such as salt dust or spray ingested with compressor air) enter the gas stream. However, our future supplies of natural gas are now in question. While future turbines will operate on gas made from coal (or other sources), additional challenges are bound to arise, as described in the next section.

A large number of turbines in the world operate on liquid fuels of kerosene or distillate nature. Many of these fuels generate essentially noncorrosive gas streams, although general opportunity for corrodents to be present in liquid fuels is somewhat higher than for gaseous fuels. Still, for these types of fuels, major concern in turbine hot stages is maintaining resistance to oxidation attack. Thus, in recent years, it has become common for industrial gas turbine manufacturers to utilize coatings to assist oxidation resistance. However, a significant number of gas turbines also are operated on the more highly corrosive and ash-bearing crude and residual fuels. These fuels contain sulfur, sodium, potassium, vanadium and lead at levels which cause attack of the hot stage superalloys. Alkaline metal (Na & K) attack is the most common problem. To protect against alkaline metal attack, the fuel can be water-washed to reduce the alkaline metal to below about 1 ppm, a critical level. If vanadium is present, the fuel must be treated with magnesium compounds to render the vanadium contaminant harmless. While reducing the corrosion attack, a certain amount of solid matter is created by this treatment which, together with any natural inorganic ash which occurs following combustion of a heavy liquid fuel, can tend to collect on the turbine hot stage parts. This fouling eventually can clog gas and cooling channels (Figure 6).[8, 9]

To combat this problem, it is industrial practice to inject the turbine with ground nutshells which abrade off the ash, or to water-wash the turbine. Water hydrates and loosens the ash so that subsequent turbine startup will clean much of it from the hot stage parts.

The experience achieved by industrial gas turbine manufacturers in handling such problem-causing fuels is excellent background for the possible troubles which could be generated by the onset of future coal-derived fuels, as discussed below.

## The 80s Challenge

It is the intent of this section to identify the materials challenges expected to face heavy-duty gas turbines in the decade of the 1980s. We will attempt first to identify the turbine applications expected and the demands on performance that will occur, then review the challenges to industrial turbine materials in an orderly fashion.

### Application Expected

Heavy-duty gas turbines will, of course, continue to be utilized in electric power and industrial service, where the primary fuels are fossil fluids (gas and oil). However, it is commonly accepted that the solid fossil fuel (coal) will soon assume a much larger role in energy generation. Heavy-duty gas turbines will be a vital, critical part of this technology. Following, we will attempt to focus on the action involving heavy-duty gas turbines and on the use of coal. Table II[10] shows some properties of coal. The potential problems from its composition should be obvious.

**Combined Cycles.** It is basic that (whatever the fuel source) by combining gas turbines with steam turbines to form a "combined cycle," greater fuel-to-output efficiencies can be obtained. The concept of combined cycles has already been applied to simple, contemporary steam boiler plants for some time and will be an integral part of the more advanced processes discussed below. The gas turbine acts as a "topping cycle" to the steam turbine system, raising the critical upper combined-cycle temperature and increasing efficiency significantly.

**Table II**—Properties of Solid Coal Fuel

| General Properties | |
|---|---|
| Higher Heating Value | 4400-7200 kcal/kg (8000-13,000 Btu/lb) |
| Chemical Species | Complex hydrocarbon, plus Shales Clays Sulfides, Sulfates Carbonates Silicates Oxides, others |
| Ash | 10-25% |

| Typical Ash Analyses, % | |
|---|---|
| $SiO_2$ | 20-60 |
| $Al_2O_3$ | 10-35 |
| $Fe_2O_3$ | 5-35 |
| CaO | 1-20 |
| $TiO_2$ | 0.5-2.5 |
| MgO | 0.3-4.0 |
| $K_2O$ | 0.2-3.0 |
| $Na_2O$ | 0.2-0.9 |
| $SO_3$ | 0.1-12 |
| —plus Cl, P, others | |

Steam/gas turbines operating in combined cycles will be the major rotating electrical generating equipment integrated into both moderately advanced and more time-distant energy generating systems such as coal gasification, fluid bed combustion, certain types of reactors and conventional boilers. Thus, while discussed separately here, combined ST/GT cycles not only exist as unique plants, but will be found married with many other rather complex systems eventually. By combining a steam plant with an efficiency of perhaps 36% and a gas turbine plant with simple-cycle efficiency of 32%, the combined-cycle plant will yield efficiencies of the order of 41%.

**Goal Gasification Power Plants.** The major thrust in the United States to generate electric power from coal is now called the "IGCC—Integrated Gasification Combined Cycle." This means a combined-cycle plant integrated with a coal gasification process. Coal gasification is not new; the Lurgi process of Germany has been in use for years. Now, modern, more efficient gasification systems are under development by Texaco, Allis-Chalmers, and others.

The idea is to produce large quantities of low or medium Btu gas, and utilize it directly to drive gas
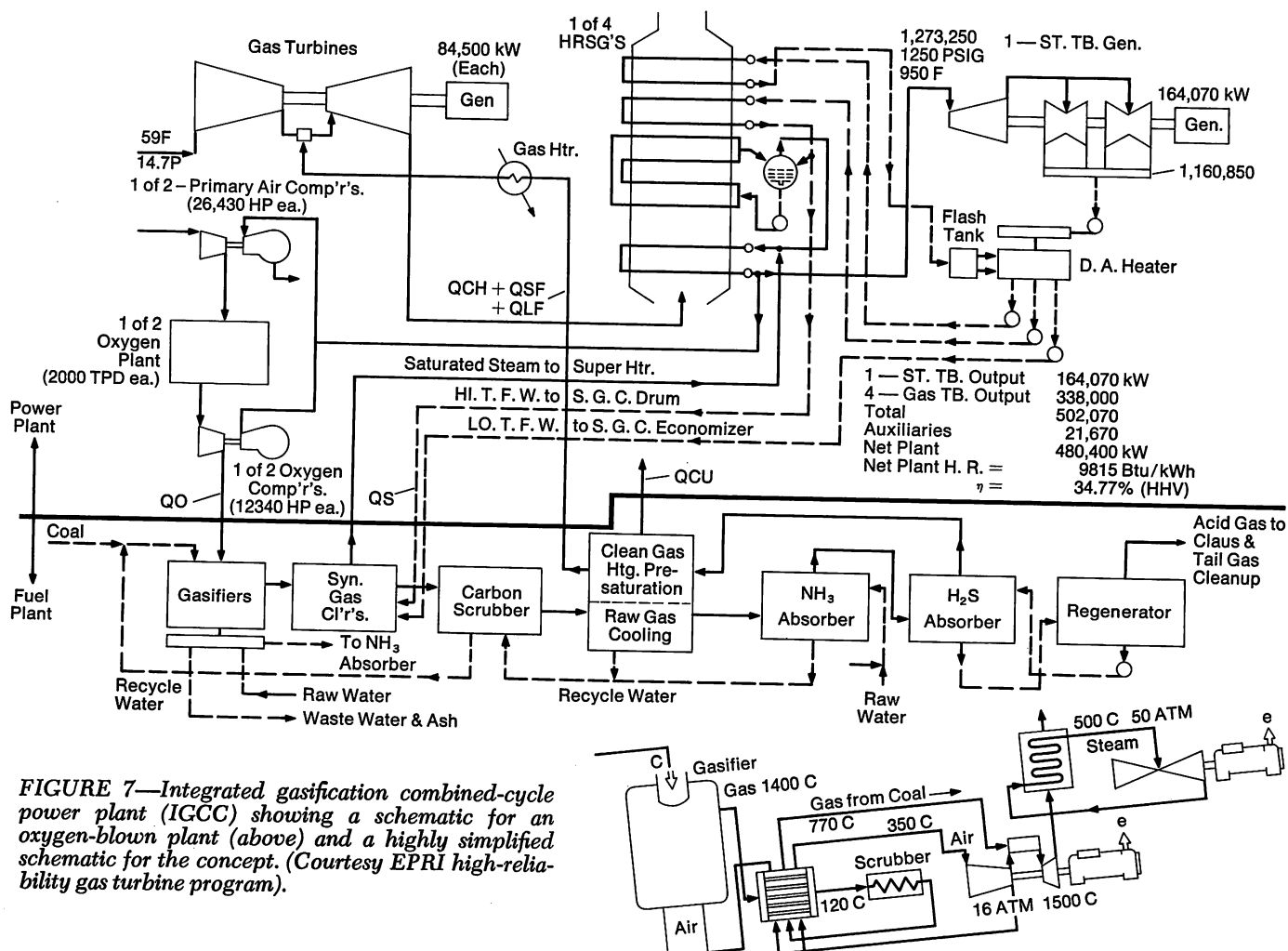


*FIGURE 7—Integrated gasification combined-cycle power plant (IGCC) showing a schematic for an oxygen-blown plant (above) and a highly simplified schematic for the concept. (Courtesy EPRI high-reliability gas turbine program).*
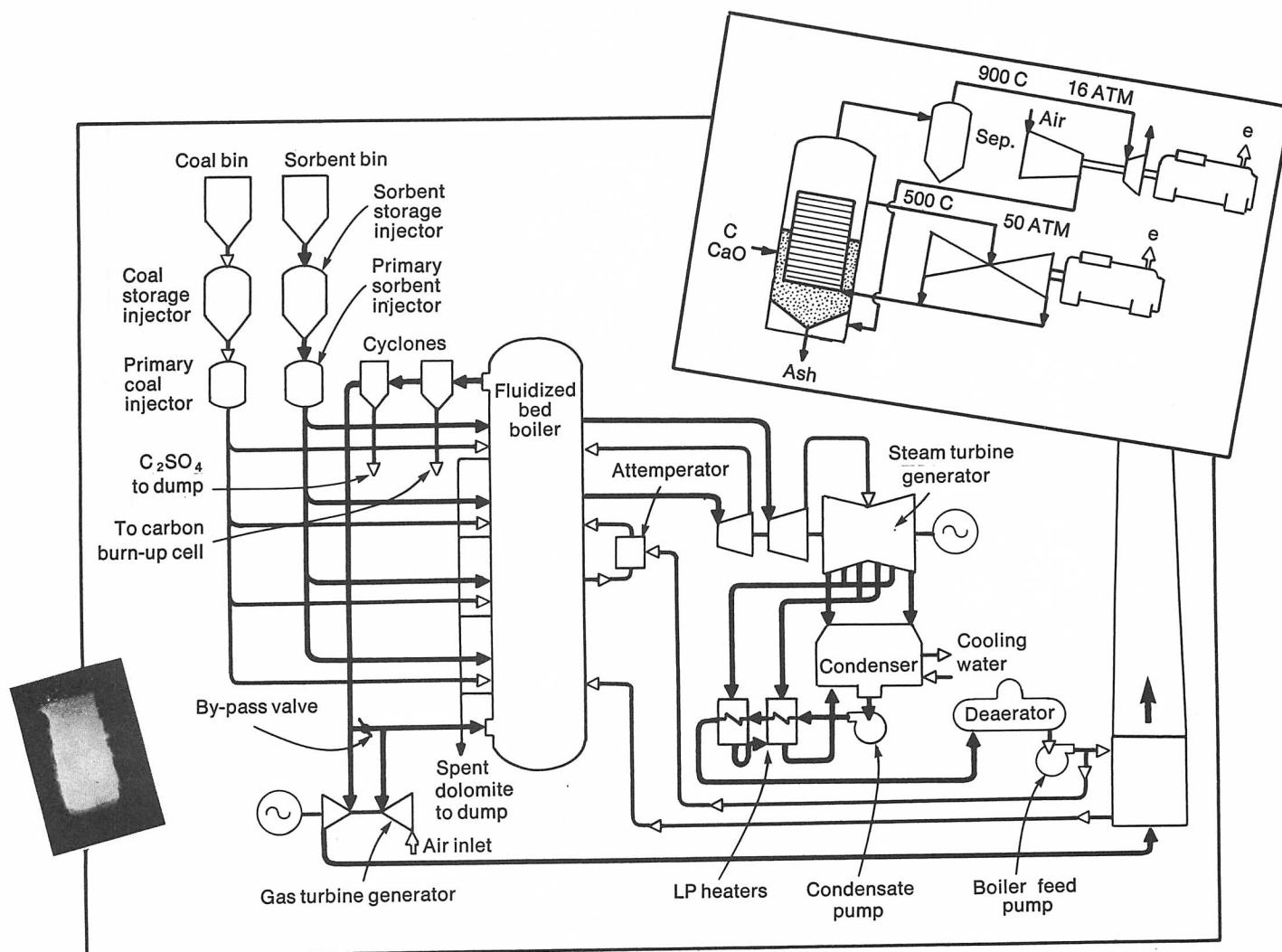
FIGURE 8—*Pressurized fluid bed combustion power plant with gas and steam turbine combined cycle.*

turbines in the combined cycle. By way of example, Figure 7 shows a low Btu IGCC power plant in simplified fashion complimented with a diagram of the whole system. Gasifier exhaust temperatures can run up to 1540 C (2800 F). The gas turbine may well face gas turbine inlet temperatures of 1430 C (2600 F).

These conditions, complexed by corrosive, erosive and fouling fuel conditions as described below give some idea of the challenge. Importantly also, a glance at Figure 7 should give a feeling for the difficulty of controlling such a system.

**Pressurized Fluid Bed Power Plants.** An alternate method of generating energy also under widespread investigation in the United States and elsewhere is that of direct-cycle fluid bed combustion (FBC). In the major thrust of this process, coal is burned under pressure (PFBC) in a fluidized bed column to produce a hot gas stream which can drive gas turbines. Boiler tubes crisscross within and immediately above the fluid bed for steam generation. The hot high pressure gases are never cooled and drive the gas turbine directly, so no loss of sensible heat occurs. However, this also means the gas is not easily cleaned before use. Complete and simplified flow diagrams for a PFBC system are given in Figure 8.

PFBCs will operate with bed temperatures up to about 950 C (1700 F) and will be fed by coal mixed with dolomite for desulfurization. Combustion will take place at about 1.0-1.5 MPa (10-15 atm). Systems will be designed for about a 200,000-hour life. However, to avoid use of intermediate heat exchangers, the hot gases pass directly from the combustion zone through several stages of filtration before entering the gas turbine.

Thus, the gas turbines will be required to accept gases only at temperatures of about 870 C (1600 F). However, the concern is with corrosion, erosion and fouling (Figure 9).[10] If the filtration systems do not do a virtually perfect job of removing the copius ash carried over from the bed and gaseous species containing S, Na, K and Pb, hot gas path part life could be extremely short indeed.

**Industrial Applications.** In the 80s, gas turbines will continue to find and expand applications in industrial
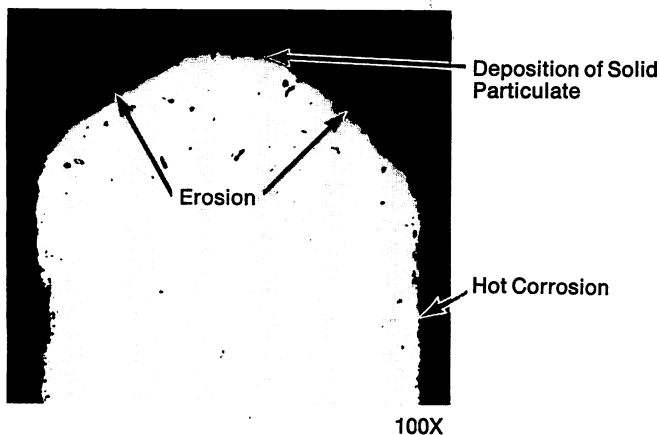
FIGURE 9—Simultaneous corrosion, deposition and fouling on IN-738 following 565-hour exposure in Exxon PFBC test rig. (Courtesy Grey/GE-ESPD.)

power service. However, the changes in the gas turbines probably will be not so marked as those expected for electric power generation, although there will be a continuation of demand for increased performance-to-cost ratios. This means that heavy-duty gas turbines, principally of the two-shaft variety, will continue to be utilized for pumping gas, operating chemical plants and providing mechanical power in a variety of applications.

Importantly, combined-cycle arrangements will increase, such as in pumping gas through pipe lines. The unprecedented cost increases for fuel are putting more emphasis on thermal efficiency of the systems, and the combined cycles, of course, signficantly improve utilization of the energy available. However, this alone will have little effect on materials problems.

## Performance Demands

The heavy-duty gas turbine business is a competitive one. Large, technically competent companies are designing and building turbines of increasingly improved performance-to-cost factors. Depending upon specific applications, costs of fuel and other market factors (such as monetary considerations and political needs), the triple factors of efficiency, output and reliability all will be expected to improve in the next decade. While many external forces affect the specifics of these factors, it is difficult and frustrating to attempt predictions. We might expect something like the following.

**Gas Turbine Output.** Heavy-duty gas turbines currently range in output up to about 100 MW, or that equivalent in mechanical power. While increased size/output usually also connotes increases in improvement and performance, it also dictates less flexibility. Accordingly, it is probable that gas turbine size will not increase very rapidly for the next decade. Combining and multiplying unit arrangements will be used to provide large amounts of power from a given plant or utility site.

**Efficiency Increase.** Fuel costs continue to increase. A major offsetting factor to that increased cost is increased efficiency. One measure of efficiency improvement is increased temperature of operation. Figure 10 shows that the average turbine inlet temperature of gas turbines has grown historically at a rate of about 15 C (27 F) per year.[4] For air cooled designs, the growth potential remaining is not great. However, further advances in cooling technology do appear possible, and the advent of water cooling will create a step-function increase in operating temperatures to about 1450 C (2000 F).
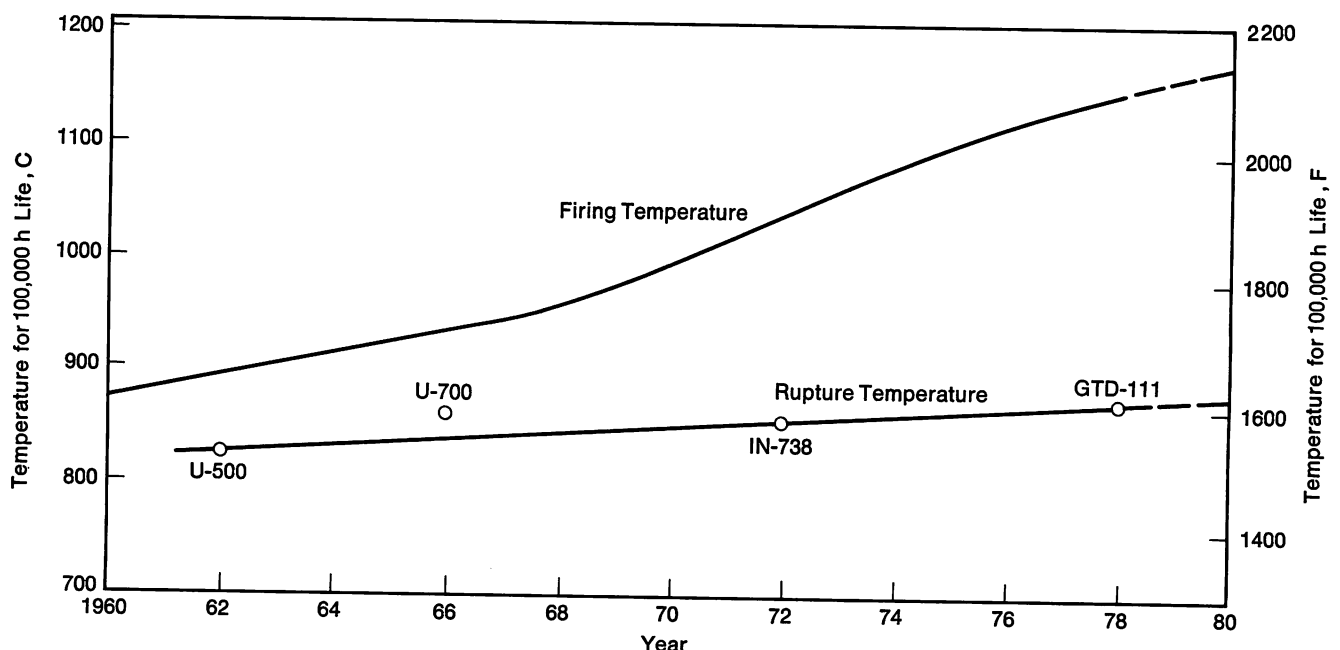


FIGURE 10—Firing temperature and bucket material improvement for heavy-duty gas turbine.

## Materials Challenges

Following, an attempt is made to identify a series of "challenges" to be faced by industrial gas turbine materials engineers in the 80s. Some grow from the continuum of challenges and needs of heavy-duty turbines, and some are new.

**Challenge I—Increased Physical Conditions.** Unlike steam turbines, industrial gas turbines have not reached a plateau in operating temperature and pressure. There will be a continued, constant effort to increase temperature and pressure of the operating gas stream. Emphasis on these factors may vary as market demands change, but, in the total sense, the move will continue to be upward. Ultimately, upper goals in temperatures can be considered to be, at a minimum, the stoichiometric combustion temperature for low Btu gas, which is about 1650 C (3000 F).

Aircraft engines, with their more complex design and cooling configurations, are operating at pressures about 30% over industrial turbines, and (in military engines) short time temperatures are around 1650 C (3000 F). In limited respects, as time goes on, more of this aircraft engine technology will be introduced into heavy-duty gas turbine design. Pressure ratios up to 1.6-1.8 MPa (16-18 atm) may come into place by about 1990.

In making these observations, however, some pertinent facts should be identified. For instance, the *incremental* efficiency changes with temperature increase less and less rapidly, and, while power increases above 1370-1430 C (2500-2600 F), absolute efficiency starts to drop off. Thus, the need now is for significant advances in air cooling, or step-type cooling improvements, such as by water. The challenge to materials, then, is obvious. The materials will need to face these gas stream temperatures and to handle the increased mechanical burden.

**Challenge II—Facing New Fuels.** While the fuels utilized for high temperature fossil fired energy generating systems until now have been natural fluids, the major efforts in place to increase sharply the use of coal can create significant problems.

First, coal is more versatile than gas or oil since it can be used as a solid fuel (coal itself) or converted to liquid fuels (coal-derived liquids, CDL) and gaseous fuels (high, medium or low BTU gas). When the solid fuels is directly combusted in fluid bed combustion systems, the impurities which compose the ash (Table II) obviously contain elements of highly corrosive nature to gas turbines; in fact, the ash level alone is of high concern because of its potential for fouling and eroding, although it appears not to be as erosive as ash from coal combusted in conventional fashion.

Table III compares coal-derived liquids to their petroleum-derived equivalents.[10] It can be seen that there is indeed a rough equivalency, and CDLs are ex-

**Table III**—Selected Properties of Liquid Fuels

|  | Petroleum Fuels | Coal-Derived Fuels |
|---|---|---|
|  | Petroleum No. 2 | Medium Distillates |
| Viscosity at 38C (100F) | 1.4-2.2 | 2-6 |
| HHV, Btu/lb | 19,300 | 18,500 |
| Sulfur, % | 0.2 | 0.1 |
| Sodium, ppm | 1.0 max. | 1.0 max.* |
| Ash, ppm | 2-50 | 100 |
|  | Heavy Distillates | Heavy Distillates |
| Viscosity at 38C (100F) | 6-60 | 10-100 |
| HHV, Btu/lb | 19,200 | 17,500 |
| Sulfur, % | 0.2-1.0 | 0.2-0.5 |
| Sodium, ppm | 1.0 max. | 5.0 max.* |
| Ash, ppm | 2-50 | 300 max. |

* Na + K.

pected to be available with a range of physical and chemical properties in the approximate range of petroleum fuels. This is certainly not surprising since prior technology—like that in Germany during World War II—generated such fuels. Low Btu gas tends (Table I) to generate new technology, since its heating value is so much below natural gas. In fact, variations of this fuel have also been known and used for years in some areas.

However, chemical compositions of the fuels have significant dissimilarities, and it is certain that this will create some materials challenges. For instance, unlike petroleum fuels, coal contains high quantities of potassium, and studies to date, such as those on the DOE Fireside I program,[9] have amply demonstrated that potassium (with sodium) appears to be a more aggressive corrodent for high temperature alloys than fuels containing sodium alone. Additionally, solid and liquid fuels contain large amounts of inorganic matter which converts to ash upon combustion. The ash itself can significantly reduce turbine performance by fouling.

**Challenge III—Hot Component Size.** To achieve logical economy and efficiency of size, industrial gas turbines have grown to about 100 MW. One can expect there will be some continued emphasis on increasing size. Critical components such as combustors, wheels, nozzle guide vanes and buckets may grow somewhat larger. Examples of such components were shown in Figures 4 and 5; the size of latter stage buckets is extremely large. As turbines grow, the size will increase still further. Achieving an acceptable level of properties in the increasing cross sections of superalloy hot stage parts requires constant attention.

Buckets and nozzle guide vanes, made of superalloy investment castings, are the most critical components in the turbine. With time, they are becoming more complex

consistent with air cooled design requirements. In recent years, constant technical interaction has been required between casting houses and the turbine manufacturers to assure delivery of reliable cast products. The large sizes create slow cooling rates, large grains, heavy segregation, and they encourage metal/mold reactions. Porosity can become a plague. If uncontrolled, these effects can lead to reduced mechanical properties and to poor surface stability resulting from poor grain boundary corrosion resistance. Clearly, metallurgists and designers must continue to surmount this increasing challenge in the 80s.

**Challenge IV—Critical Element Supply.** Unfortunately, we are now solidly submerged in a new era—that of rampant scarcity for many of the critical elements in high temperature alloys. Elements can be considered "critical" for geopolitical reasons, cost reasons, or both. This problem will only get worse as some true natural thinning-out of resources occurs, and as the increasing geographic concentration of resources allows generation of increased cartel action among producers. In the United States, new defense requirements further exacerbate the problem. Critical elements for gas turbines that can expect to be foci of difficulty will be chromium, molybdenum, tungsten, tantalum, nickel and, of course, cobalt.

Figure 11 shows the incredible price performance of cobalt metal between early and late 1978. The price rise was caused by several factors including (1) social turmoil and engineering neglect of the mining operation in Zaire (The Congo), (2) a gradual worldwide demand increase for cobalt, (3) a decrease of world demand for copper (Co is a byproduct of Cu mining), and (4) a sudden cessation of sales from the U.S. stockpile, which probably triggered the action. This cobalt price increase may have cost U.S. business a total approaching $0.5 bil-
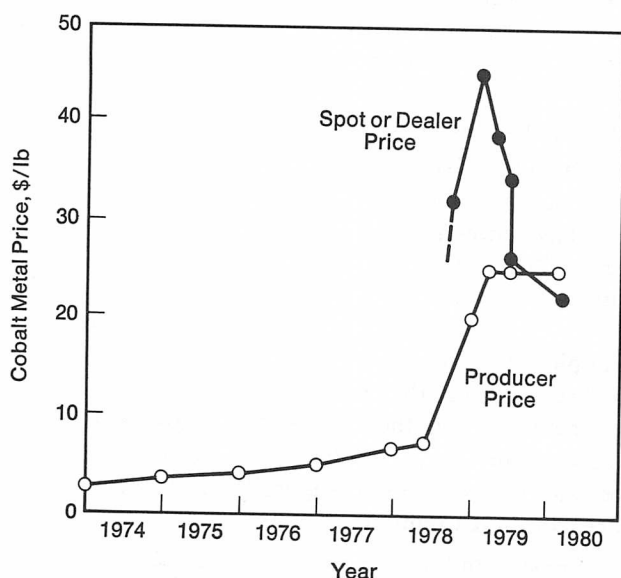
lion compared to original levels in 1978 alone; the extraordinary prices are continuing.

The price of molybdenum and tantalum have also more than doubled recently, but in the long run, the most critical element of all is chromium, absolutely essential in high temperature alloys. The only significant sources are Rhodesia and South Africa. The generation of effective oxidation and corrosion resistance for superalloys in gas turbines by use of chromium as an alloying element is a crucial matter.

Clearly, metallurgical developments and changes to ameliorate the problems of critical elements will be a vital, continuing chord through the next decade.

## Facing the Challenges

To meet and surmount these challenges, materials effort and development will be significant. Specific approaches and developments, of course, can be difficult to detail without involving proprietary problems. However, for the benefit of the alloy and process suppliers for heavy-duty gas turbines, it is important to outline the possible avenues of attack. Views from both design and materials direction will be covered, since they are interchangeable.

### Advances in Air Cooling

Prior to a discussion of hot stage material requirements, it is appropriate to summarize the design trend, since this functions to define material requirements. In this respect, significant advances will be made in air cooling for heavy-duty gas turbines.

From the standpoint of hot part air cooling design, heavy-duty gas turbines have aircraft engines forging ahead of them as a major guide to solutions of their cooling needs. As an example, an advanced air cooled part from an aircraft engine is shown in Figure 12. Currently, industrial turbines use direct convection cooling (Fig-

FIGURE 11—Price behavior of cobalt metal melting stock in recent years.
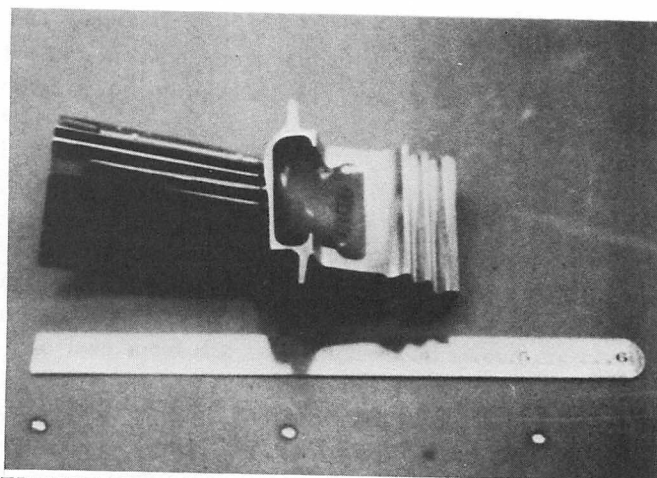
FIGURE 12—Advanced air cooled bucket.

ure 5) and a certain degree of trailing edge cooling, a somewhat simpler approach.

Service considerations, particularly the corrosion and fouling resistant requirements caused by heavy fuel usage, cause heavy-duty gas turbines to move more slowly. However, the 80s will see significant steps forward toward turbines where more extensive air cooling is utilized to maintain metal temperatures at low levels.

## Advent of Water Cooling

Water cooled heavy-duty gas turbines are a new major technology rushing into the 1980s. Following early development on a small 1 MW water cooled turbine, utility-sized nozzle vanes, combustors and buckets are being demonstrated in rig tests. Figure 13 shows the relative performance characteristics of air cooled versus water cooled electric power plants for a fixed bed gasification system utilized in integrated combined cycles fired at 1100, 1320 and 1650 C (2000, 2400 and 3000 F). Water cooled gas turbine technology is shown here at 1650 C (3000 F). For each 55 C (100 F) increase in firing temperature over the range described, a cost improvement of about 1.1 mils per kWh (2-3%) is achieved.
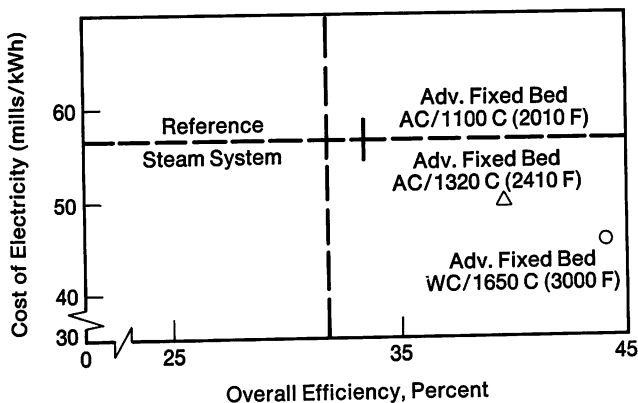


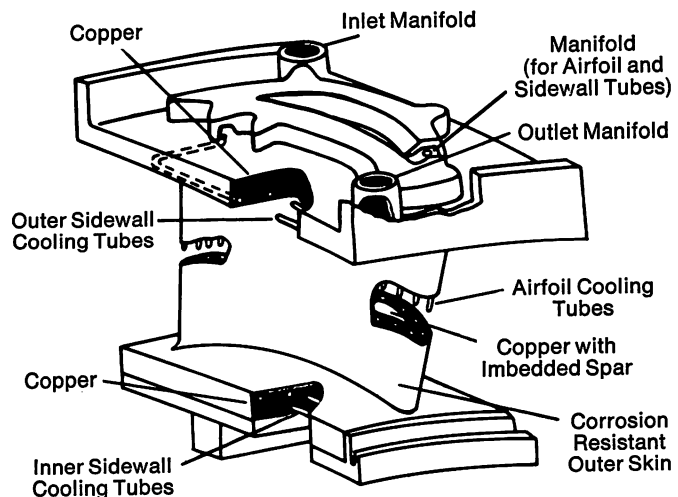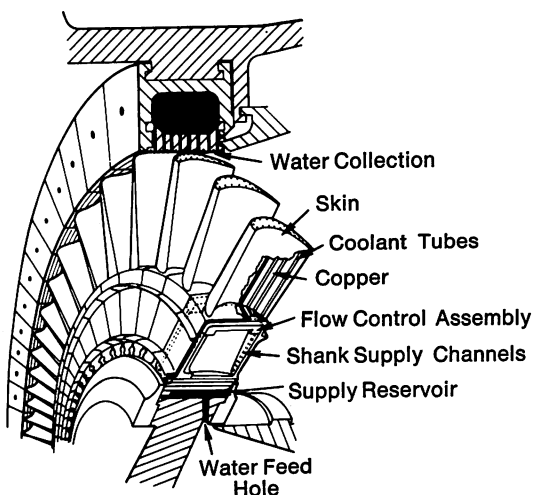*FIGURE 13—Performance of water cooling. (Courtesy R. Sheldon, GE-GTD.)*

Thus, the advantages of such a very high temperature system are obvious. The water cooled gas turbine offers the opportunity to burn contaminated petroleum and coal-derived fuels at high thermal efficiency and specific output. The low metal surface temperatures made possible by the desirable coolant properties of water are expected to be significantly more tolerant to contaminants (corrosion and deposition) than is the case with air cooling.

The first application of water cooling is expected to occur in water cooled turbine nozzle designs, as shown in Figure 14. The nozzle is shown with a high conductivity copper sublayer for application at turbine firing temperatures in the range of 1260-1650 C (2300-3000 F). For lower firing temperatures, a similar concept is employed in a monolithic structure. A pressurized closed-circuit water system is used at subcritical conditions, and with no boiling present. Recently, a water cooled nozzle operated at a gas stream temperature of 1430 C (2600 F) for about 60 hours.

The second step in the application of water cooling is the incorporation of an unpressurized, open-circuit water cooled bucket (Figure 14). The configuration shown is for 1260-1650 C (2300-3000 F) firing temperature applications. As for nozzles, a monolithic structure would be utilized for lower firing temperatures. Full-sized water cooled buckets are expected to go on test in the mid 1980s.

Water cooled turbine materials requirements re-emphasize some old needs and identify some new. For instance, the need for oxidation/corrosion resistant coatings or claddings of very high capability to face aggressive gas streams continues. On the other hand, thermal conductivity has become a dominating physical factor in such composites, and the need for high strength, high conductivity copper alloys has been identified and is under development.



*FIGURE 14—Water cooled components for the 1430 C (2600 F) gas turbine.*

Certainly for latter stages and "lower" temperatures in such turbines, advanced superalloys like those now used in air cooled parts represent the type of metallurgical technology that will be required.

## Alloy Development for Hot Stages

Obviously, major demand is for castable superalloys with high structural stability, creep, rupture and tensile strength, fatigue strength, and corrosion and oxidation resistance. All these properties are needed for operation in air cooled heavy-duty gas turbines and latter stages of water cooled turbines under the stringent mechanical and chemical conditions expected. One can expect that emphasis will occur in the following areas.

**Minor Elements.** The broad work to optimize generally familiar nickel and cobalt superalloy compositions through control of minor elements such as carbon, boron, hafnium, manganese, yttrium and the like will continue and probably increase. Current alloys will be modified and some new alloys probably issued based on minor element additions. This will include the effect of these minor elements on the mechanical and fatigue properties, such as low cycle and thermal fatigue. Recent examples are the interest in boron and hafnium additions.

However, increased attention will also be given the effect of minor elements on oxidation and corrosion resistance. Efforts will be extended to identify more precisely those compositions which generate the most stable environmentally resistant oxide films to protect the alloys for use in coatings and claddings.

**Critical Elements.** Changes in alloy design to conserve critical elements are occurring now. By the middle of the 80s, changes from new alloy design should be felt as critical element supply becomes even more of a problem. First, emphasis will be on creep and fatigue resistant alloy bases, using, if possible, the elements plentiful in the North American continent such as iron, molybdenum, aluminum and titanium. Coatings, claddings and other protective means will become more commonplace to reduce the use of chromium required for environmental resistance.

## Alloy Process Development for Hot Stages

Property advances for superalloys possible through chemistry changes are becoming very limited, and, during the 70s, processing for alloying improvement moved to the center of the stage with the advent of DS, single crystals, powder metallurgy and HIP. Also, new alloys and tailored alloys to fit these new processes are becoming evident, such as PWA-1452 for DS and monocrystal processing. Tailoring alloy compositions to optimize effects of processing will become a strong factor in heavy-duty turbine metallurgy by the end of the 1980s.

**Composite Components.** To circumvent restrictions caused by large part size and the expense and availability of critical elements, significant steps will be made in the 80s to generate hot stage parts composed of several alloys bonded together. For instance, over 21,000 hours of commercial service have been achieved with clad buckets in medium-sized gas turbines. Now, a program sponsored by EPRI at GE will develop claddings for large power generation size turbines. These will be placed in field test by 1983. The principle of the concept is shown in Figure 15a, which also illustrates how different alloys can be utilized for airfoil vanes and for dovetails in buckets for air cooled service.

The concept, of course, is aimed at optimized properties where needed at the various locations in large gas turbine buckets. For instance, a bucket dovetail segment could be composed of a fine grained powder metallurgy forging or fine grained casting to give high tensile and high cycle fatigue properties. An airfoil vane core section (or spar section) might be directionally solidified to produce optimized creep rupture and low cycle fatigue

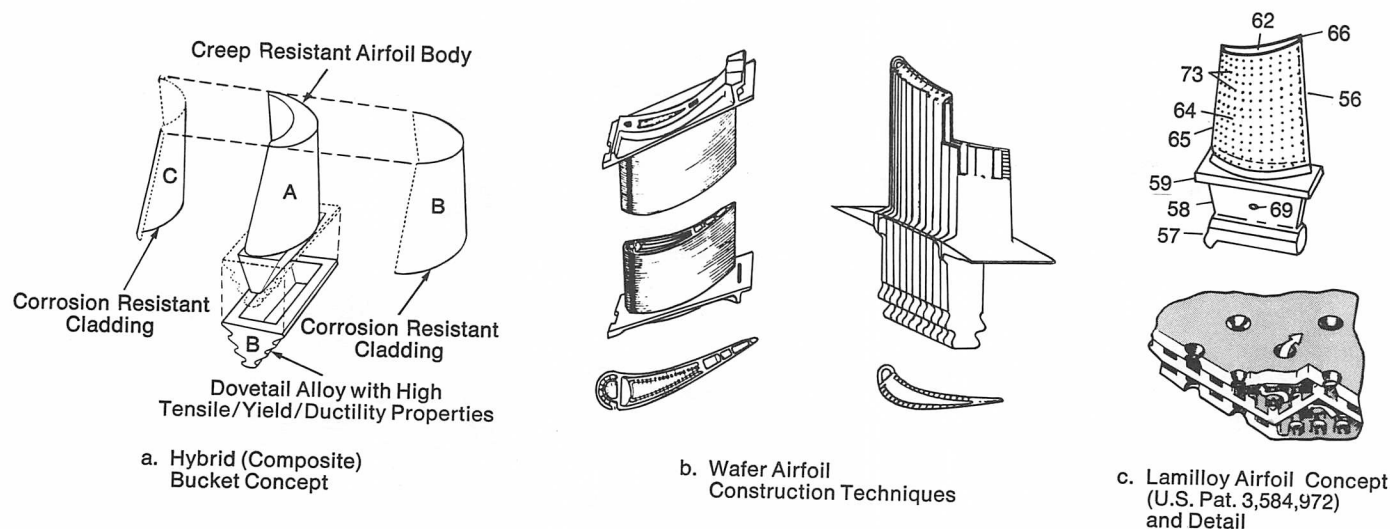

a. Hybrid (Composite) Bucket Concept

b. Wafer Airfoil Construction Techniques

c. Lamilloy Airfoil Concept (U.S. Pat. 3,584,972) and Detail

FIGURE 15—*Three approaches to improve performance of airfoil structure in heavy-duty turbine service.*

properties. Of course, the entire surface of the part exposed to the gas stream will be protected with an oxidation/corrosion resistant cladding. Thick coatings also are a potential.

Striking examples of composite components are the turbine hot stage parts now being developed for operation from 1100-1650 C (2000-3000 F) for the DOE HTTT water cooled turbine program discussed above. In these composites, structures composed of sharply different base metals, such as copper alloys, stainless steels and superalloy materials bonded into unified structures, are being brought to full-size test status.

**Wafer Process.** DOE is also sponsoring a program at a major manufacturer for construction of hot stage parts for aircraft type units applied to industrial/utility service.[12] The wafer method of construction consists of fabricating turbine airfoils from thin plates, or wafers, which can be aligned in either the radial or chordwise direction (Figure 15b). Cooling passages are photoetched into the individual wafer surfaces prior to bonding the wafers together. Surface airfoil contours and attachment areas are then machined. Thus, the wafer approach achieves high cooling efficiencies through the use of intricate cooling schemes not possible to produce by normal investment casting techniques. Applications of wafered components to heavy-duty gas turbines relates to their potential ability to improve air cooling capability without use of surface holes which could plug from heavy fuel fouling.

**Lamilloy Process.** Another concept to improve air cooling effectiveness, yet still permit hot stage part operation in combustion products from heavy fuels is "Lamilloy," developed by Detroit Diesel Allison[13] and supported by EPRI (Figure 15c). Lamilloy consists of a laminated or ply-type approach to create a controlled flow of coolant from a cast load-carrying spar to the airfoil surface. Bonded layers of thin sheet materials, separated by studs, with photoetched or chemical-milled cooling holes are attached to the spar to form the cooling arrangement. The labyrinth path taken through the laminations by the cooling air combines the effects of transpiration cooling and more conventional convection/impingement cooling techniques. It will be important to establish whether the transpiration cooling holes resist plugging from ash in ash-bearing fuels.

**Alloy Protection**

Superalloys for buckets in industrial gas turbines have outrun their innate oxidation resistance and have fallen prey to the insidious attack of hot corrosion; almost universally, early hot stages now are coated to improve this factor. Nozzle guide vanes may not be far behind. Ensuing problems with coal-derived fuels will further emphasize the necessity for protection of hot stage parts in this fashion. One example of the improvements ob-
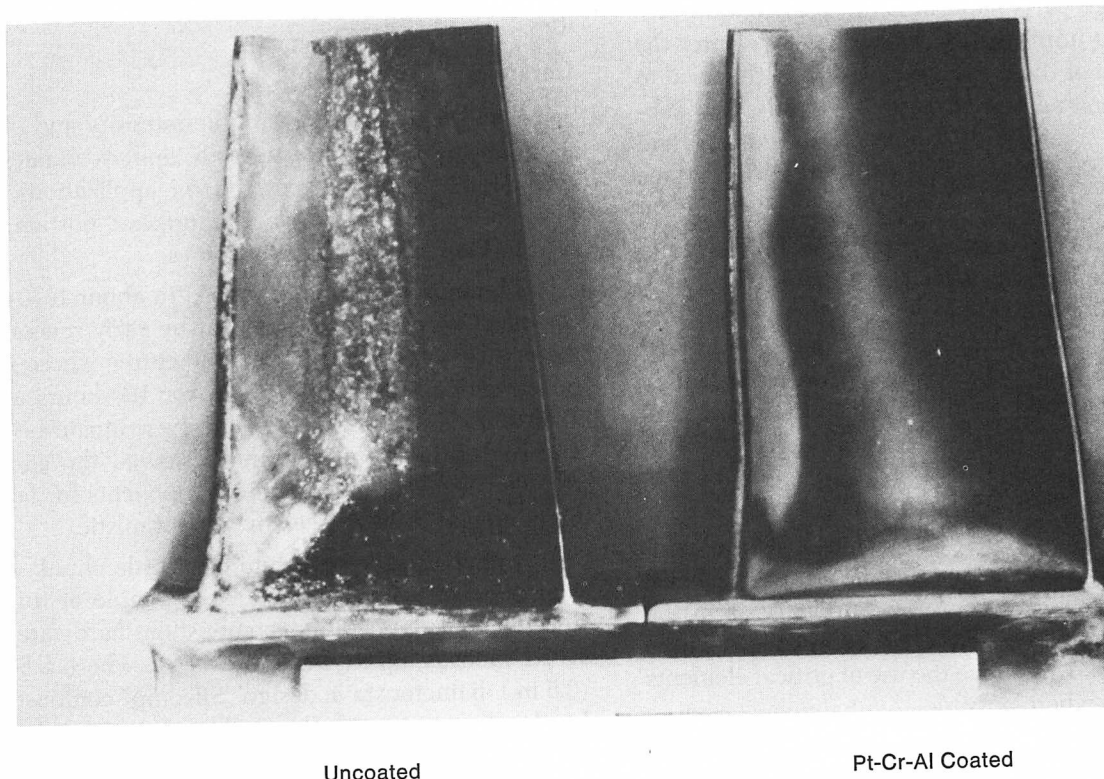


Uncoated                    Pt-Cr-Al Coated

*FIGURE 16—Improvement in protection from coating of typical Stage-I gas turbine bucket (IN 738) after 25,000 hours in corrosion-prone service.*
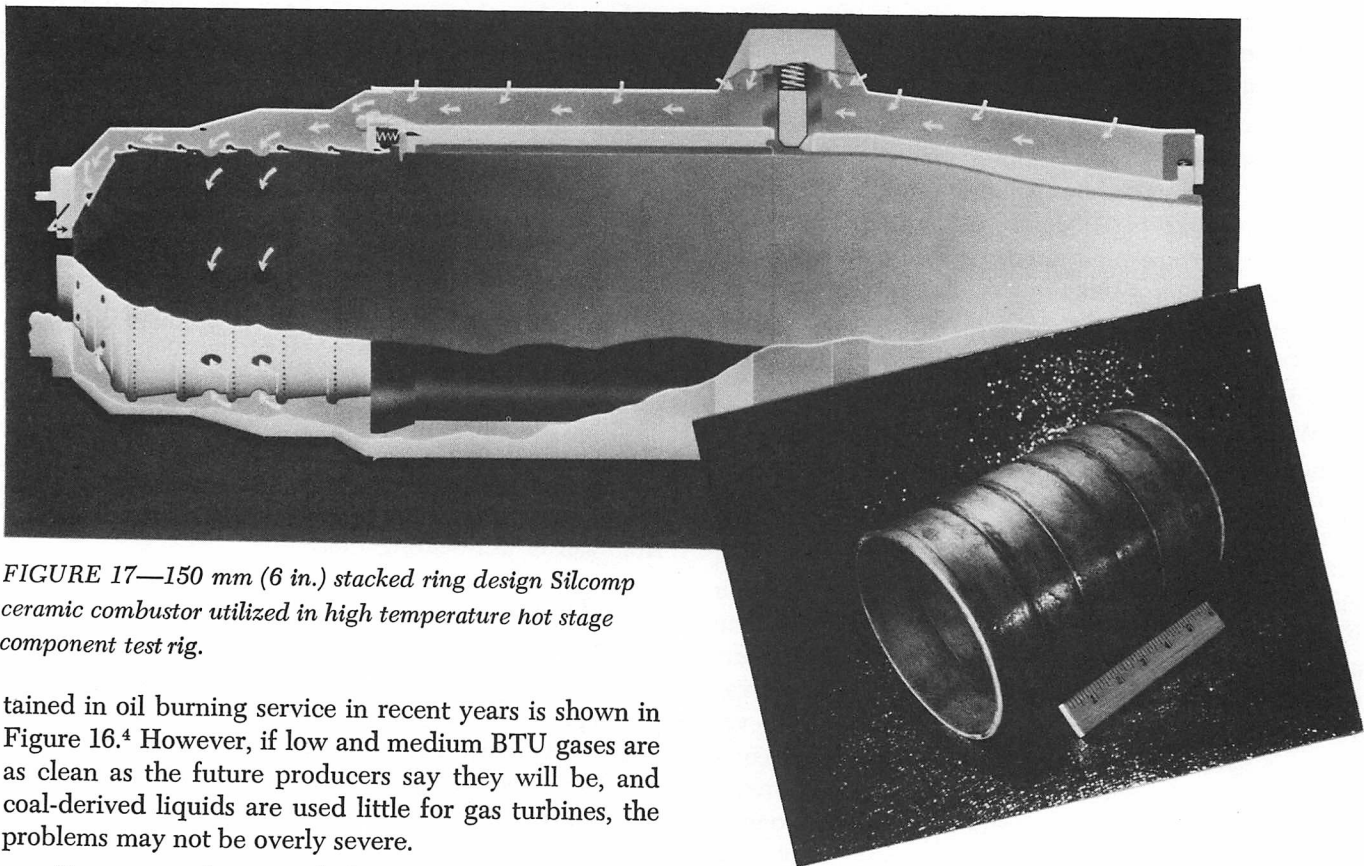
FIGURE 17—150 mm (6 in.) stacked ring design Silcomp ceramic combustor utilized in high temperature hot stage component test rig.

tained in oil burning service in recent years is shown in Figure 16.[4] However, if low and medium BTU gases are as clean as the future producers say they will be, and coal-derived liquids are used little for gas turbines, the problems may not be overly severe.

To repeat, the critical element problem raises its head here. Until recently, at least, the general approach has been to utilize the most corrosion resistant alloys possible for hot stage parts hand-in-hand with coating protection to further improve performance. As we enter the 80s, conservation of the critical elements and the need to meet further demands on strength will cause the substrate to become significantly less corrosion resistant, and much more of the protection load will shift to the surface coating.

Also, this will be consistant with a general shift from "diffusion type" to "overlay type" coatings. Overlay types, applied by electron beam, plasma or other techniques, represent a significant advance, since almost unlimited thickness can be applied providing for considerably longer lives. Claddings, a development toward still greater protection, have been discussed above.

### Alloys for Turbine Structure

The alloying approaches for turbine structural components, wheels, compressor, turbine frame, exhaust components, etc., will be gently evolutionary as in the past. Emphasis will be toward larger components. There will be tendencies to minimize the use of critical elements such as chromium where possible.

An example of alloy change may be in compressor, exhaust components or other accessory components where 12 Cr steels might replace stainless steels with higher chromium content. Selected savings in chromium level creating reduced criticality of components can

occur from careful considerations of corrosion resistance needs. Cr-rich protective coatings are further possibilities.

### Ceramics

The broad effort of variable intensity and objective today in the U.S. and overseas to apply ceramics to gas turbines is presently centered on applications toward automotive use, although a significant portion also is devoted to heavy-duty gas turbines.

These programs were started in about 1970-72, and the effort was spurred somewhat by early successes at a major heavy-duty turbine manufacturer where ceramic nozzle guide vanes were tested for 100 hours at about 1260-1320 C (2300-2400 F). However, innate brittleness and high fabrication costs have slowed the effort, and steps toward rotating ceramic components for large turbines appear to have been overly optimistic.

A new attitude is to bite off a little chunk, chew it well, then take another step. An example of this is the development in ceramic combustion hardware under EPRI sponsorship at General Electric where a 88.9 mm (3.5 in.) diameter stave design "Silcomp" combustor liner has been operating as the "bill of materials" combustor for a small very high temperature test rig for about three years. This combustor runs at gas stream temperatures up to 1650 C (3000 F). Subsequently, several successful runs up to 30 hours have been made on a 153 mm (6 in.) stacked ring design Silcomp combustor. Here, also, the

combustion liner is ceramic because of necessity. A picture of this combustor is shown in Figure 17.

Accordingly, for the 80s, it is felt that a more conservative approach to ceramics will be seen than for the 70s. There will be continued study of the basic properties of ceramics, development of compositions and processing (in ceramics "composition" and "processing" are essentially synonymous) and a gradual movement toward test equipment evaluation of static parts. In heavy-duty gas turbines, replacement of superalloys by ceramics in hot stage parts will not occur in the 1980s, but some significant testing may start near the end of the decade.

## Summary

Heavy-duty gas turbine materials engineers must face and must solve significant challenges during the decade between 1980 and 1990. These challenges will arise principally from the increased demands on the turbines in their roles as topping machinery in large power plants fired with oil, coal and coal-derived fuels, as well as in continued industrial applications.

The challenges are:

1. *Increased Physical Conditions.* To increase power and efficiency, turbines must operate at higher temperatures and pressures.

2. *New Fuels.* Coal-derived fuels can bring additional corrosion, erosion and fouling problems to turbine hot stages.

3. *Hot Component Size.* Gas turbine hot stage parts will continue to grow in size, moderately.

4. *Critical Element Supply.* Restrictions in availability and price increases for economically and strategically available elements will effect alloy choice and design significantly.

To meet these challenges, we can expect activity in most or all of the following materials and design technical areas:

- *Air Cooling.* Alloys and processing will be fitted and tailored to take advantage of increased air cooling.

- *Water Cooling.* Advances will be rapid in water cooling, and some turbines will be operating on at least one water cooled stage by 1990.

- *Alloy Development.* Effects of minor elements will be optimized and alloy changes made to meet critical element cost and supply problems.

- *Process Development.* New processes will develop to combine alloys to optimize performance in previously monolithic components and to accommodate water cooling and increased air cooling.

- *Ceramics.* A new, more realistic conservative approach may lead to demonstration of static combustion components by 1990.

- *Alloy Protection.* Coatings will increase in thickness, claddings will come into use, and compositions improved by minor element changes.

- *Structural Alloys.* Changes will be slow, responsive to critical element demands.

## Acknowledgments

## References

1. B. Wilkins, *Mathematical Magick,* 1648.
2. R. Gessner and W. Gibbons, General Electric Gas Turbine Publication GER-2509A, 1979.
3. R. Lang, General Electric Gas Turbine Publication GER-3098, 1978.
4. F. Lordi and A. Foster, General Electric Gas Turbine Publication GER-2182M, 1979.
5. A. Ludwig and J. Jermanok, ASME Paper 79-GT-14, 1979.
6. R. Junge, General Electric Gas Turbine Publication GER-3116, 1979.
7. A. D. Foster, H. vonE. Doering and J. W. Hickey, General Electric Gas Turbine Publication GER-222L, 1977.
8. "Fireside I," High-Temperature Gas Turbine Engine Components Materials Testing Program, Task I, DOE Contract No. EX-76-C-01-1765, Final Report, 1978.
9. C. T. Sims, H. vonE. Doering and D. P. Smith, ASME Paper 79-GT-160, 1979.
10. C. T. Sims, Proceedings, *4th Annual Conference on Materials for Coal Conversion and Utilization,* Gaithersburg, Maryland, 1979.
11. A. Caruvana, et al, ASME Paper 79-GT-39, 1979.
12. R. Sellers, D. Dohlberg and G. Calvert, Proceedings, *AIAA/ SAE 13th Propulsion Conference,* Orlando, Florida, 1977.
13. R. E. Strong, ASME Paper 77-WA/ENER-14, 1977.

# Linepipe Requirements in the Eighties

by A. B. Rothwell and R. J. Cooke
Foothills Pipe Lines (Yukon) Ltd.

Experience has shown that technological forecasting is generally as prone to error as that in the economic or, for that matter, meteorological fields. Nevertheless, each new decade precipitates its epidemic of prognostications, and the eighties are clearly no exception. In the context of the pipe line industry, the forecaster is perhaps at some considerable advantage since the lead times associated with major capital projects are now such that much of what will happen in the next decade is already well on the way to being determined. Drawing courage from this, and from the fact that we believe it is the major user companies that will ultimately decide future technological directions (albeit under constraints from many different sources), the authors hope to indicate the principal alternatives for the next few years of development in large diameter linepipe.

Any attempt to project into the future must rely heavily on an understanding of the past; the expression of this understanding can vary in sophistication from the simplistic exponential growth laws which have been used quite widely (and often misleadingly) in predicting supply and demand to quite complex models involving all the diverse economic, technical and, increasingly, social factors that condition a particular area of development. In the context of the pipe line industry, past, present and future are intimately linked, since many major projects which were conceived, and began to influence material development, in the early seventies will not come to fruition until the mid-eighties. For this reason, we shall devote some considerable space in this paper to an examination of the historical trends in the metallurgy of pipeline steels.

This paper will deal essentially with gas transmission pipe lines since, with a few qualifications, this represents the most demanding form of pipe line service from a materials point of view.

In keeping with our background, we shall concern ourselves primarily with the technological issues. In general, however, choices between different avenues of development must be based on the economics of the overall system, and it will thus be impossible totally to ignore these aspects. Similarly, it would be naive in this day and age to ignore the social and political forces that impact upon the selection and growth of the technology.

With this background, and on the premise that the aim of all material and process development is to provide the most economic realization of the system design, we shall first consider the design requirements for pipe line systems and attempt to relate these to specific material properties.

## Design Requirements and Material Properties

The primary design requirements for a pipe line system may be summarized under the general headings of throughput, safety and reliability, and feasibility of installation.

### Throughput

The long distances typical of many of the current frontier and offshore projects have led to a need for massive reserves and correspondingly high throughputs to achieve economic viability. While the overall economics of a system designed for a given throughput are a complex function of pipe dimensions, strength level, compression capacity, availability of existing facilities, energy market prices and associated fuel costs, developments to date have generally followed a consistent trend toward higher pressures and larger diameters.

Typical of the present state of the art is the design of the Alaska Highway project, which envisages 1422 mm (56 in.) O.D. pipe operating at 7450 kPA (1080 psi) and 1219 mm (48 in.) O.D. pipe operating at 8690 kPa (1260 psi).

This trend toward higher operating pressures and larger diameters can be met only by using higher strength steels or by increasing wall thickness. As Figure 1 shows in a qualitative fashion, the yield strength level most commonly used has increased steadily over the last twenty-five years,[1] suggesting that the former rather than the latter option has been traditionally favored. It is legitimate to ask, at this stage, whether this trend will continue, or whether we stand at some kind of watershed in linepipe technology. In any event, the effect of inflation on the economics of capital investment, the likelihood of

continuing higher fuel costs and, in some cases, the desirability of transporting associated liquids make it unlikely that the trend toward higher operating pressure will be reversed. Unless there are very significant changes in the technology and economics of linepipe production and installation, it is improbable that the most prevalently used yield stress will fall below the current level of 483 MPa (70 ksi). Some factors affecting the potential for even higher strength materials will be discussed in a later section, both in terms of the materials technology available and the rate factors, technical and external, that may influence developments.

## Safety and Reliability

The concerns for safety and reliability in any pipeline system are obvious; the balance between these concerns may, however, change somewhat for the long distance, largely remote pipe lines which will condition the material developments of the near future. Clearly, for such lines, the dangers of third party damage and the potential hazards to persons and property are reduced. This is reflected, and should continue to be addressed, by code design requirements based on decreasing stress levels (increasing wall thicknesses) with increasing population density or risk. On the other hand, the logistic aspects of restoring a failed line to service in remote areas may be considerably more demanding, although the long

distances between the more remote parts of such a pipe line and the markets which it supplies reduce the impact in terms of continuity of supply. The fracture control design of the various segments of the Alaska Highway project in Canada, for example, has involved detailed consideration of these issues.[2] In this case, the primary fracture design is aimed at minimizing the probability of failure during the intended service life, with additional consideration of the consequences of failure in the event of its accidental occurrence. In terms of materials specifications, this implies a consideration of fracture initiation control and fracture propagation control, each of which may impose distinct notch toughness requirements.

In the design of gas pipe lines today, a prerequisite for both fracture initiation and fracture propagation control is the specification of pipe materials whose dynamic, full scale ductile-to-brittle transition temperature is below the minimum design temperature.* On the basis of extensive work at Battelle[3] and, later, in the UK,[4] this requirement is adequately addressed by the specification of 85% minimum shear area at the design temperature in the drop-weight tear test, a level which is easily

---

* It is worth noting that, even for the so-called "Arctic" projects, the minimum design temperature is rarely below −10 C (14 F) for buried pipe lines; this is not the case for station piping and other above ground facilities, which may experience much lower temperatures.
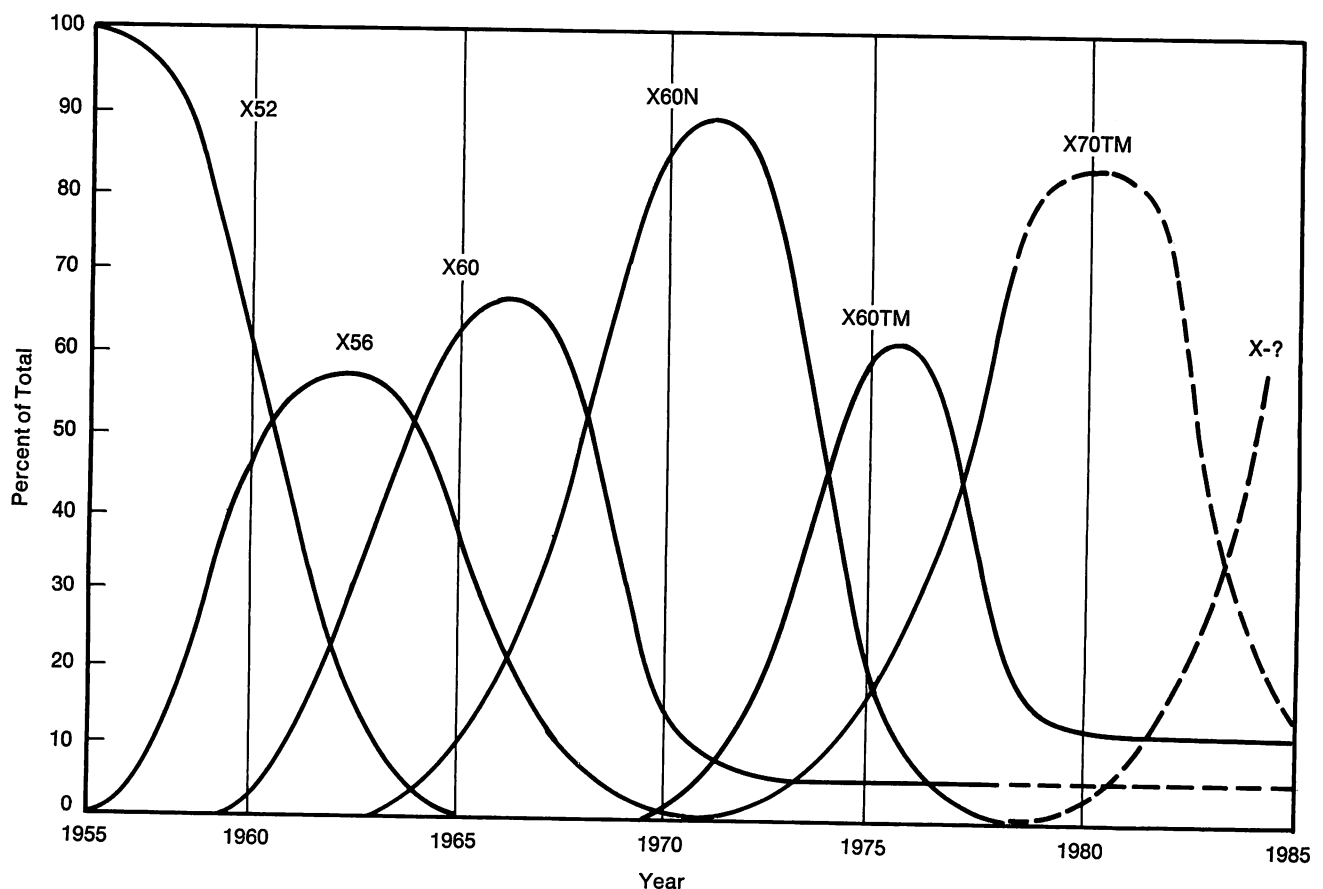


FIGURE 1—Increase in Linepipe yield strength over the past 25 years.

achieved and generally exceeded by a wide margin in presently available HSLA linepipe steels.

Having ensured that the materials are only subject to ductile fracture, the next step is to determine the necessary toughness for fracture initiation control. The approach in general use by the gas pipe line industry is based on the analysis developed by Battelle for the American Gas Association.[5,6] Figure 2 illustrates schematically the predicted relationship between critical defect size and Charpy impact energy which arises from this analysis; at infinite toughness, failure is flow stress controlled and a maximum attainable critical defect size is thus reached. Toughness is then specified to give a minimum critical defect size which is some fraction of the flow stress dependent defect size, typically 80-90%. As an example, these principles applied to the mainline sections of the Alaska Highway pipe line yield minimum toughness levels of 68 J (50 ft-lb), with associated critical, through-wall defect sizes of over 150 mm (6 in.). It is perhaps of interest to note that, in the late sixties, when guarantees of impact energy first began to be required for pipe line steels, the values specified were in the order of 30 J (22 ft-lb). In the smaller, lower pressure lines then being built, even this energy level would have assured a critical defect size of over 100 mm (4 in.). This is a graphic illustration of the way in which the advances in service conditions, coupled with a more rigorous defect tolerance analysis, have led to significantly higher demands on material quality which have, in turn, dictated fundamental changes in production technology.

The topic of fracture propagation control is considerably more complicated; Battelle,[5] the British Gas Corporation[7] and others have developed methods for predicting the level of 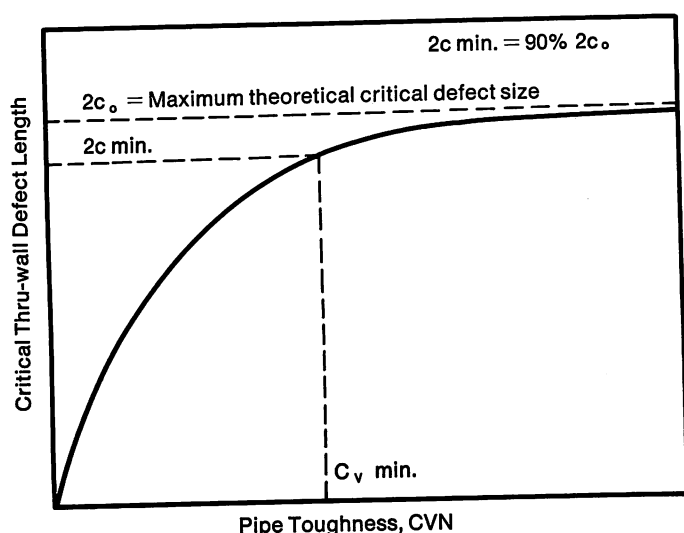Charpy toughness necessary to arrest a running ductile fracture. All of these analyses proved adequate for conventional pipe line design (say, up to 1067 mm, 42 in. diameter, Grade 414, 6900 kPa, 1000 psi, single phase decompression). However, with the simultaneous advent of larger sizes, higher operating pressures, richer gases giving two phase decompression, and heavily controlled rolled steels showing marked fracture surface separations and strongly sloping shelf behavior in impact tests, predictions based on these models became unreliable.[8] It is outside the scope of this paper to discuss the various attempts currently being made to solve this problem; these were dealt with in full in a recent publication.[9] The resulting perplexity has led to a variety of approaches to fracture propagation control. It is possible, for instance, to adopt the most conservative measure of arrest toughness as the minimum specification value (or minimum all-heat average), but for current major projects, this leads to levels which are beyond that which can be economically supplied, even with the most recent steelmaking developments. One reaction to this dilemma is to adopt a design based on the use of independent crack arresters, generally in the form of loose-fitting sleeves. Aside from the questions of installation costs and long-term integrity, it is debatable whether crack arresters spaced at, say, 300 m (1000 ft) intervals will have a significant effect on expected maximum fracture lengths. As an alternative, a more integrated approach to fracture length control may be adopted, as has been the case for the Canadian section of the Alaska Highway pipeline. In practice, fracture arrest occurs as a result of a number of naturally-occurring features, including field girth welds, valve assemblies, heavy wall pipe and bends, as well as high toughness pipe. A probabilistic analysis, using all or some of these arrest mechanisms with the distribution of toughness levels determined by the specified minimum (and, where appropriate, an all-heat average), can be used to predict anticipated fracture lengths. The acceptability of these lengths can be assessed on a facility-specific basis, giving consideration to the reliability specifically required by a given facility. The fact that outage time appears to be independent of fracture length up to at least 75 m (250 ft), and relatively insensitive to fracture length below 300 m (1000 ft) indicates that the issue is somewhat academic in many instances. These concepts have been discussed in detail in a recent paper[2] and have received regulatory approval for the southern sections of the Alaska Highway pipe line in Canada.

Clearly, fracture control (and its relationship to system safety and reliability) is a complex topic that could well form the basis of a separate paper. However, we shall restrict ourselves at this point to emphasizing that the increasing demands for notch toughness have led, over the past fifteen years, to some quite revolutionary changes in steelmaking technology. We shall examine these, together with some probable directions for the future, in a later section.
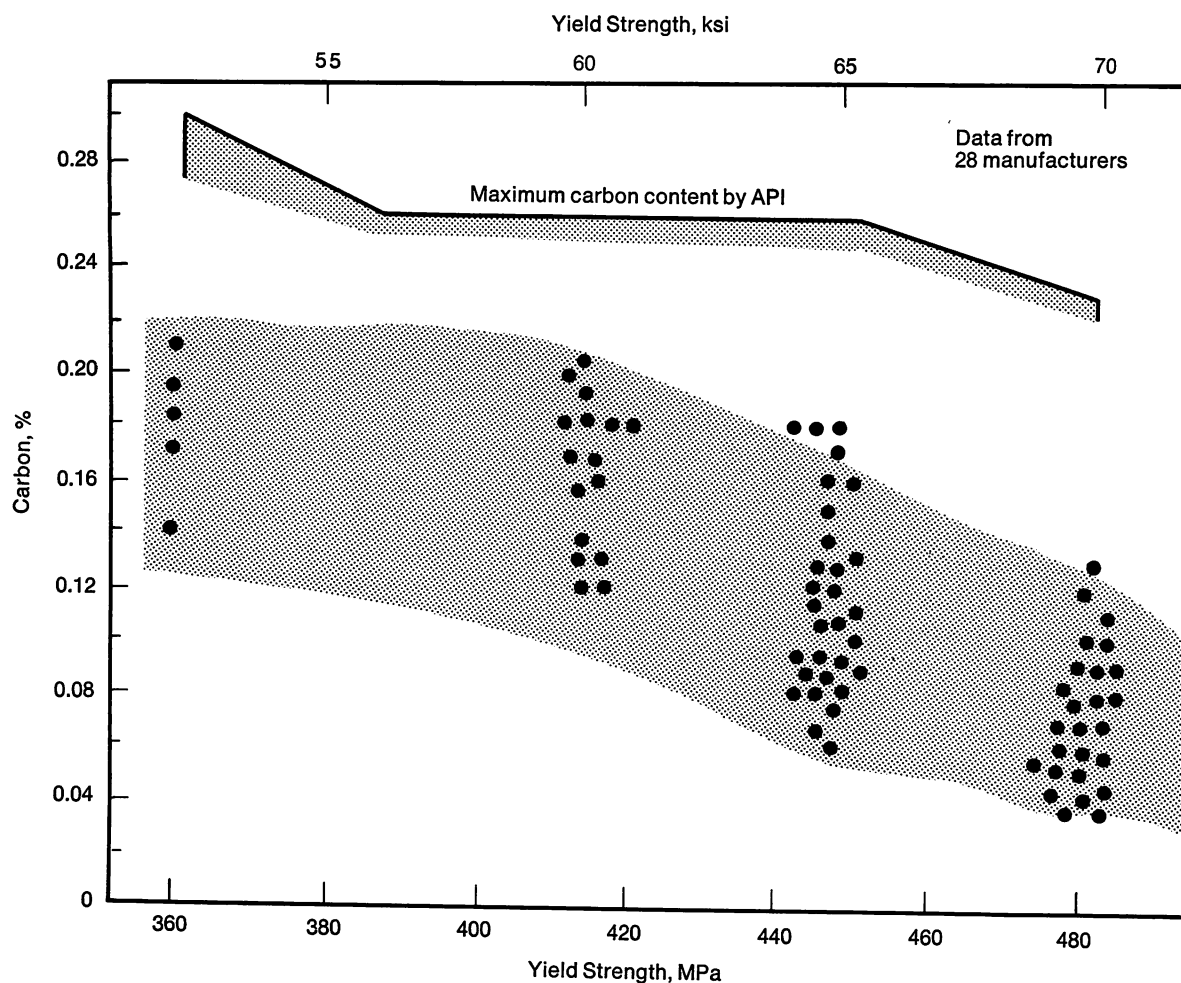


*FIGURE 2—Schematic illustration of the relationship between Charpy V-notch properties and through-wall defect length.*

FIGURE 3—*Trend of declining carbon content with increasing strength grade over the last fifteen years.*

## Installation

A number of closely interrelated factors influence the ease with which a pipe line can be installed in the field. Among these are the size (weight and wall thickness of the individual joint), ease of cold bending and other field manipulation and, above all, weldability. In keeping with its paramount economic importance, we shall concentrate here on the latter.

Field weldability involves so many different factors that the most appropriate test still appears to be a full-scale simulation.[10] However, certain clear relationships with chemical composition do exist, and it is no exaggeration to state that the major changes in pipe line steel formulation over the last ten to fifteen years have been largely conditioned by the prevalent technique of field welding using cellulosic electrodes.[11] We shall speculate in a later section as to whether these trends are likely to continue or whether developments in welding technology which are, in themselves, economically attractive will arrest or even reverse the recent directions. Whatever the future may hold, some current specifications, such as those developed by Foothills, acknowledge the dominant role of low carbon contents in assuring freedom from cold cracking problems through the allowance of pro-

gressively higher carbon equivalents as the carbon content is reduced below the maximum permitted in the applicable standard or specification.

## Current Trends in Pipe Line Steels

As a direct result of the evolution of system requirements summarized in the preceding section, the technology of pipe line steels has been in a state of constant development through the last fifteen years.

As has already been pointed out, the prevalent strength level has increased from 360 to 483 MPa (52 to 70 ksi) over this period. At the same time, contrary to the tendency of earlier years to equate strength with carbon content, and in response to the requirements for improved field weldability, carbon contents have steadily declined. These interrelated trends are graphically illustrated in Figure 3, while Figure 4 is indicative of the influence which some major project specifications have had in bringing about these changes.[11]

This steady reduction in carbon content and simultaneous increase in strength and toughness were made possible by some quite fundamental changes in production technology. The conviction that high levels of tough-
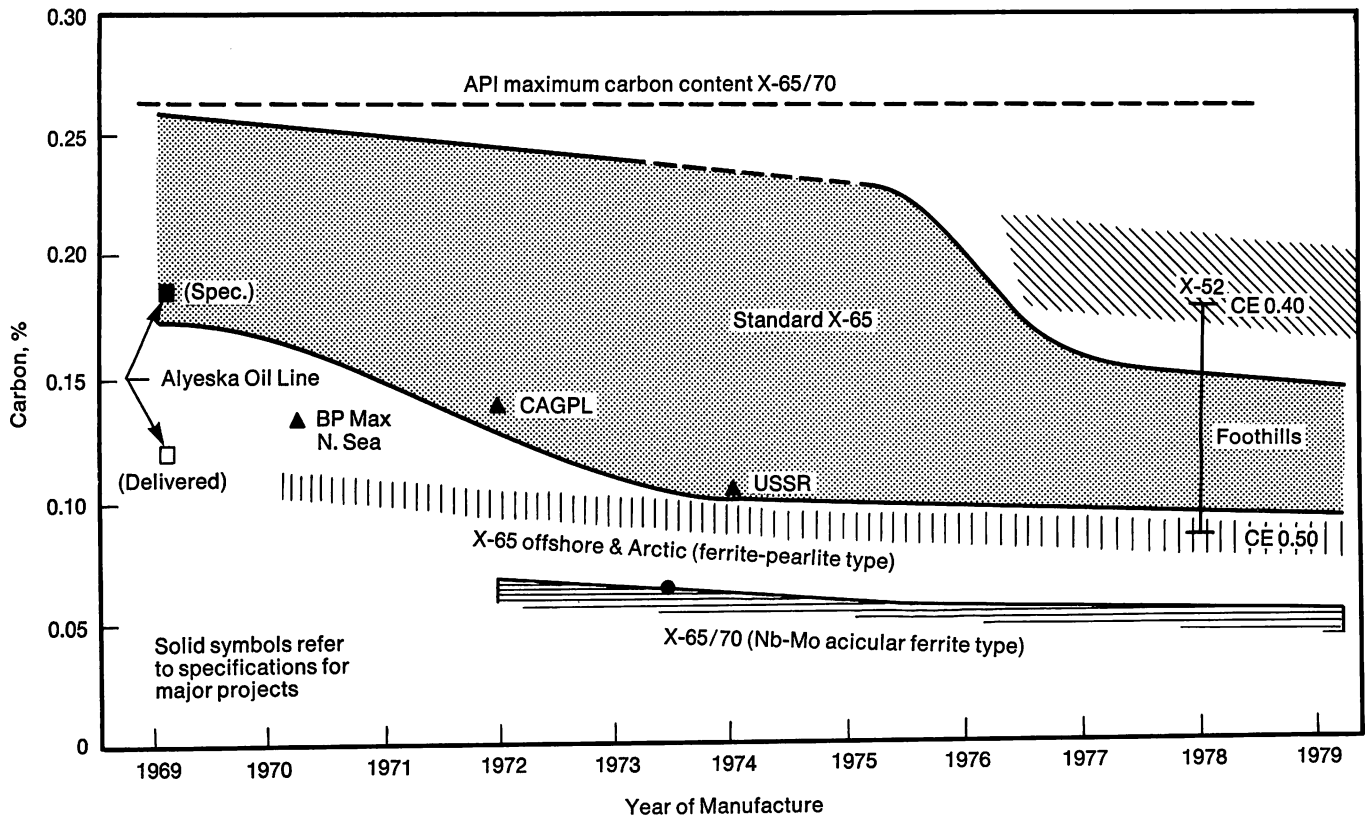
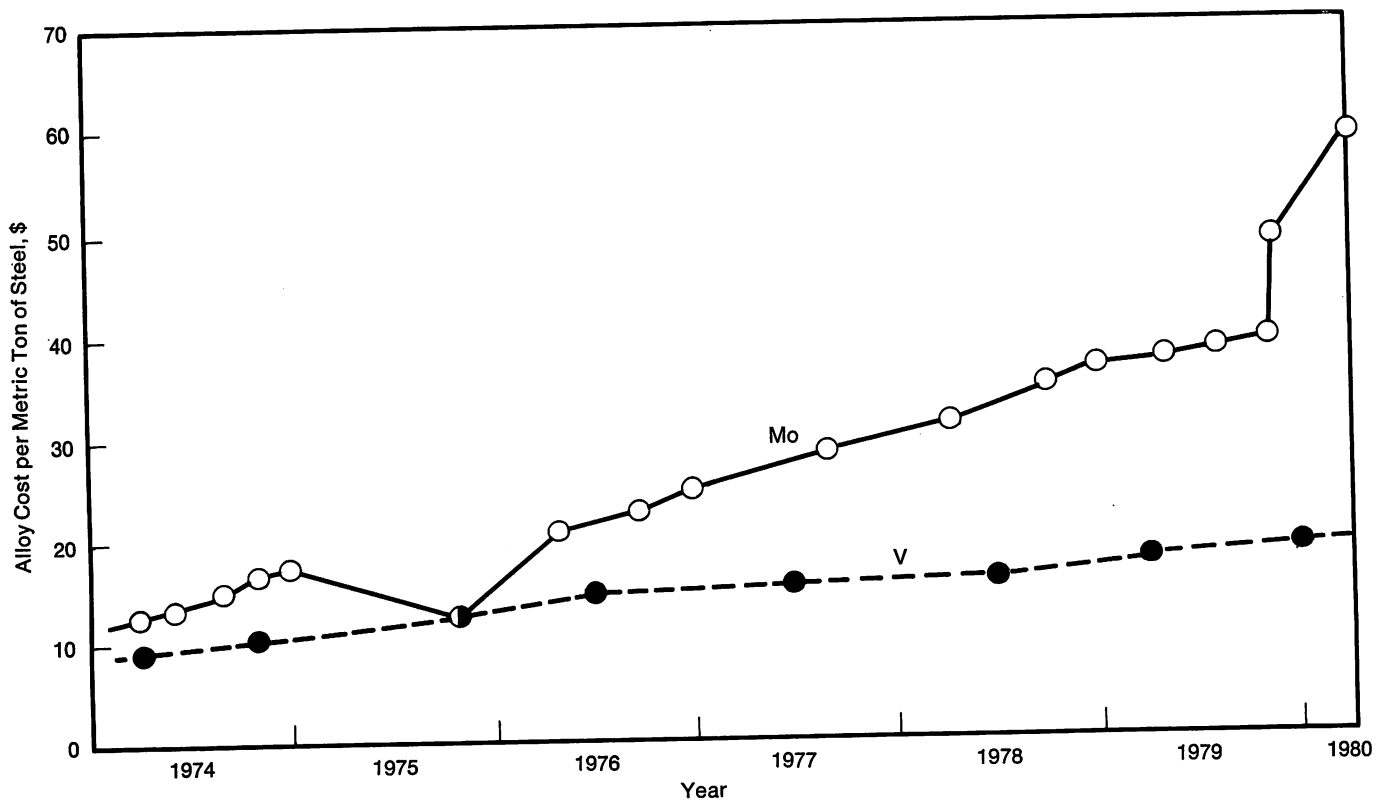FIGURE 4—*Trend of decreasing carbon content with year of manufacture.*



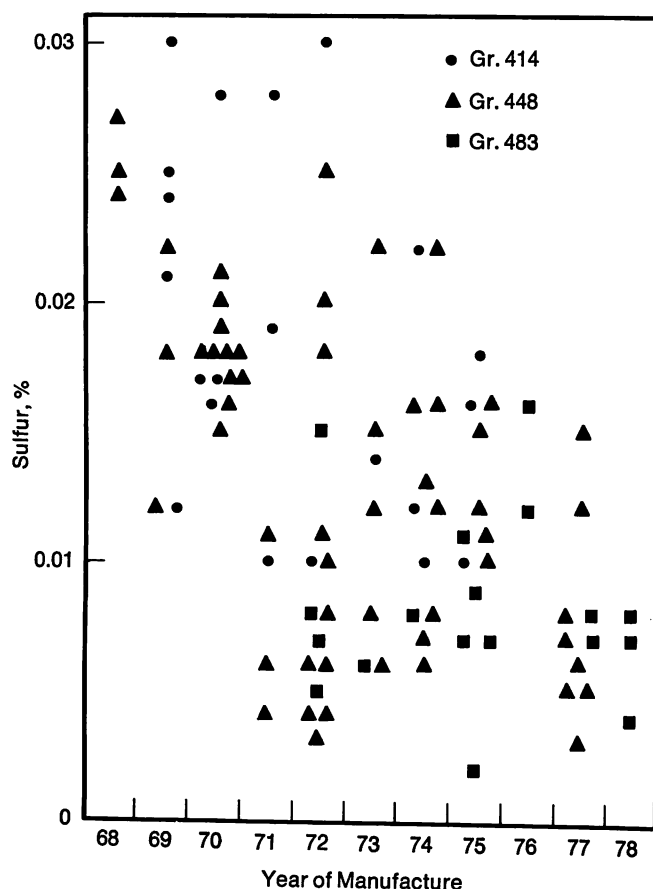FIGURE 5—*Alloy costs for typical Gr. 483 chemistries.*

*FIGURE 6—Variation of sulfur content with pipe grade and year of manufacture.*

ness could only be achieved by the use of a normalizing treatment was overturned by the development of controlled rolling in the sixties, allowing leaner chemistries to be used for equivalent and higher strength levels.[12,13] A further step was taken with the introduction in the early seventies of the low carbon, molybdenum niobium steels, initially championed by Climax researchers.[14] For some years, these steels, either of the extremely low carbon, acicular ferrite type, or the 0.08-0.12% C, pearlite reduced type, were the predominant class of high strength, high toughness steels being produced worldwide. Since 1978, as a result of increasing molybdenum prices, there has been a significant shift toward niobium-vanadium steels. Figure 5 illustrates the recent growth of the cost per metric ton of molybdenum and vanadium in typical Grade 483 pipe line steels. The differential is even greater if "trader" prices for molybdenum are considered.[2] Clearly, the economics of molybdenum-bearing pipe line steels have become less attractive.

It is worth pointing out that the ability to produce Grade 483 niobium-vanadium steel suitable for current major projects is the result of a considerable investment in time and expertise, as well as in hardware,[1] and it may prove difficult to reverse this recent trend when the molybdenum market situation returns to normal.

Molybdenum suppliers may draw comfort from the fact that major users of linepipe still have some preference for the readily weldable, lower carbon molybdenum steels and that the limited capacity for controlled rolling of some of the most efficient North American linepipe suppliers virtually precludes the alternative solutions in the heavier wall thicknesses required by major project specifications.

The second consistent trend which has characterized the past decade, apart from that toward lower carbon contents and higher levels of alloying and microalloying, has been toward lower sulfur levels. In high quality steels deoxidized with aluminum, it is primarily elongated sulfide inclusions that account for the anisotropy of ductility. In the late sixties, the realization that long, ductile fracture was possible and could in principle be controlled by specification of an adequate level of transverse impact energy,[5] initiated a sequence of changes in steelmaking aimed at reducing this anisotropy and, ultimately, at raising the overall toughness level. Figure 6 illustrates the range of sulfur contents in longitudinally welded pipe supplied against a large number of orders, worldwide, over a ten-year period.[15] A number of observations can be made concerning this diagram. First, there is a steady trend toward lower sulfur contents; the current API 5LX limit of 0.05% was already irrelevant by the early seventies. Second, the use of external desulfurization techniques to produce very low sulfur levels (<0.01%) dates from the early seventies[16] and was more or less coincident with the widespread introduction of Gr. 483 steels. A further factor, which is not apparent in this figure, is the rise and fall of sulfide shape control, typically using rare earth metals. This technique gave the possibility of achieving high transverse toughness without the need for extreme desulfurization[17] (the rare earth treatment itself generally leads to some reduction in sulfur content). However, the increasing demand for steels having high levels of toughness has made it economically feasible for many steelmakers to install desulfurization equipment. In addition, laboratory and field experience indicating that rare earth levels over approximately 0.02% could have a detrimental effect on GMA welding[18] (tack welding in the pipe mill or semiautomatic or automatic field welding) has also contributed to a general technological preference for desulfurized steels.

In spiral welded pipe, largely because the critical transverse-to-pipe-axis orientation no longer coincides with the minimum toughness direction in the skelp, the trend toward inclusion shape control and/or lower sulfur contents has been slower. However, the general demand for higher quality levels, and a perceived concern regarding the possibility of alternative fracture propagation modes which exploit the low toughness orientation, have led the major suppliers of spiral welded linepipe to incorporate desulfurization into their repertoire of produc-

tion technology.

The topic of advanced controlled rolling methods has been briefly alluded to above. Most wide plate mills installed in the last ten to fifteen years were designed for extremely high separating forces and torques and incorporate a substantial degree of computer control capability.[19] All of these factors can combine to assure the reproducible application of very severe controlled rolling schedules with finishing temperatures in the inter- or subcritical range. While these techniques certainly allow leaner chemistries for a given thickness and strength level,[1,20] there are clear indications that the fracture propagation resistance of such materials, as assessed by conventional quality control tests, may be illusory. A fuller understanding of the way in which this aspect of toughness must be approached may well dictate a retreat from the more extreme controlled rolling procedures, with finishing temperatures being limited to levels at or about the start of transformation. Such a step should not be considered retrograde, but simply a recognition of the possibility that we have not always, in the past, had the knowledge to incorporate the most appropriate test techniques into our specifications.

# Future Developments

It has already been suggested that we may well stand at some kind of a threshold in linepipe technology in terms of strength/toughness/chemistry trade-offs which can be achieved with the existing, conventional technology of controlled rolled HSLA steels. We should also point out, however, that what is now considered conventional would have been outrageously uneconomical, in the context of tonnage steels, a mere decade ago. The changing economics of the energy industry have irreversibly altered the concept of linepipe steels as relatively unsophisticated materials, which make few additional demands on good run-of-mill practice. It is thus legitimate to speculate on what the next decade may bring, and whether, to break through the apparent barrier posed by current production technology, further fundamental changes will be made. In this section, a number of developments which are already well researched on a laboratory or pilot production scale will be considered in relation to their potential for future development.

## Low Carbon Bainitic Steels

It has long been understood that bainitic microstructures offer the prospect of attaining higher levels of strength in the air cooled state than were possible in ferrite-pearlite or acicular ferrite steels. However, the toughness of bainite is extremely sensitive to carbon content;[22] in addition, the higher levels of alloying necessary to achieve a bainitic microstructure militate against weldability. McEvily and coworkers suggested the possibility of extra low carbon bainitic steels in the sixties,[23] and

further work in Europe[24-26] and Japan[27] confirmed that good toughness and weldability could be achieved even at strength levels close to 700 MPa (100 ksi). However, the necessary carbon contents ($\sim$0.02%) could not be consistently achieved without vacuum degassing, facilities for which were not available in tonnage steelworks at that time. Recently, the more widespread introduction of degassing has opened up the possibility of producing these grades commercially; it also allows the use of very small, closely-controlled amounts of boron to promote the bainitic structure rather than much larger amounts of elements such as chromium, nickel or molybdenum. This precise control (normally to within 0.0005%), necessitated by the extremely detrimental effect of free boron on notch toughness,[28] was not generally possible in the absence of vacuum degassing. It thus appears that a new family of pipe line steels may be ready to be launched; the outstanding question is the economic viability of the product, which, in turn, depends on production costs and the capacity of the industry effectively to utilize the increased strength levels. In this regard, limitations may arise, in the short term, from the unavailability of matching components in equivalent strength levels[2] and, in the longer term, from the inability of the pipe line designer to cope with and justify either higher operating pressures or higher diameter/wall thickness ratios.

## Quenched and Tempered Steels

On the assumption that greater strength/thickness capabilities would ultimately be required than could be achieved in controlled rolled HSLA steels, the possibility of a quench-and-temper (QT) heat treatment has been studied by a number of producers. Two distinct lines of development have been followed. The first of these is the more conventional, being derived from the technology of high strength seamless pipe for oil country applications involving the heat treatment of formed and welded pipe using prevalent induction heating and spray quenching.[29] Welding consumables must be selected with this heat treatment in mind, but, given this proviso, few problems with weld zone strength and toughness need be anticipated. Special heat treatments involving two quenching operations have also been proposed by some Japanese producers for applications requiring extreme toughness at low temperature.[29] Because of the problems of productivity and the obvious application of this type of product to heavy wall, high toughness requirements rather than higher strength *per se*, it is likely to be restricted to station piping and other specialty items rather than to linepipe.

The second approach, the metallurgical background to which has been widely studied in the UK[30] and Canada,[31,32] is the quenching of conventional low carbon HSLA steels in the plate mill directly after rolling, followed by an appropriate tempering treatment. Produc-
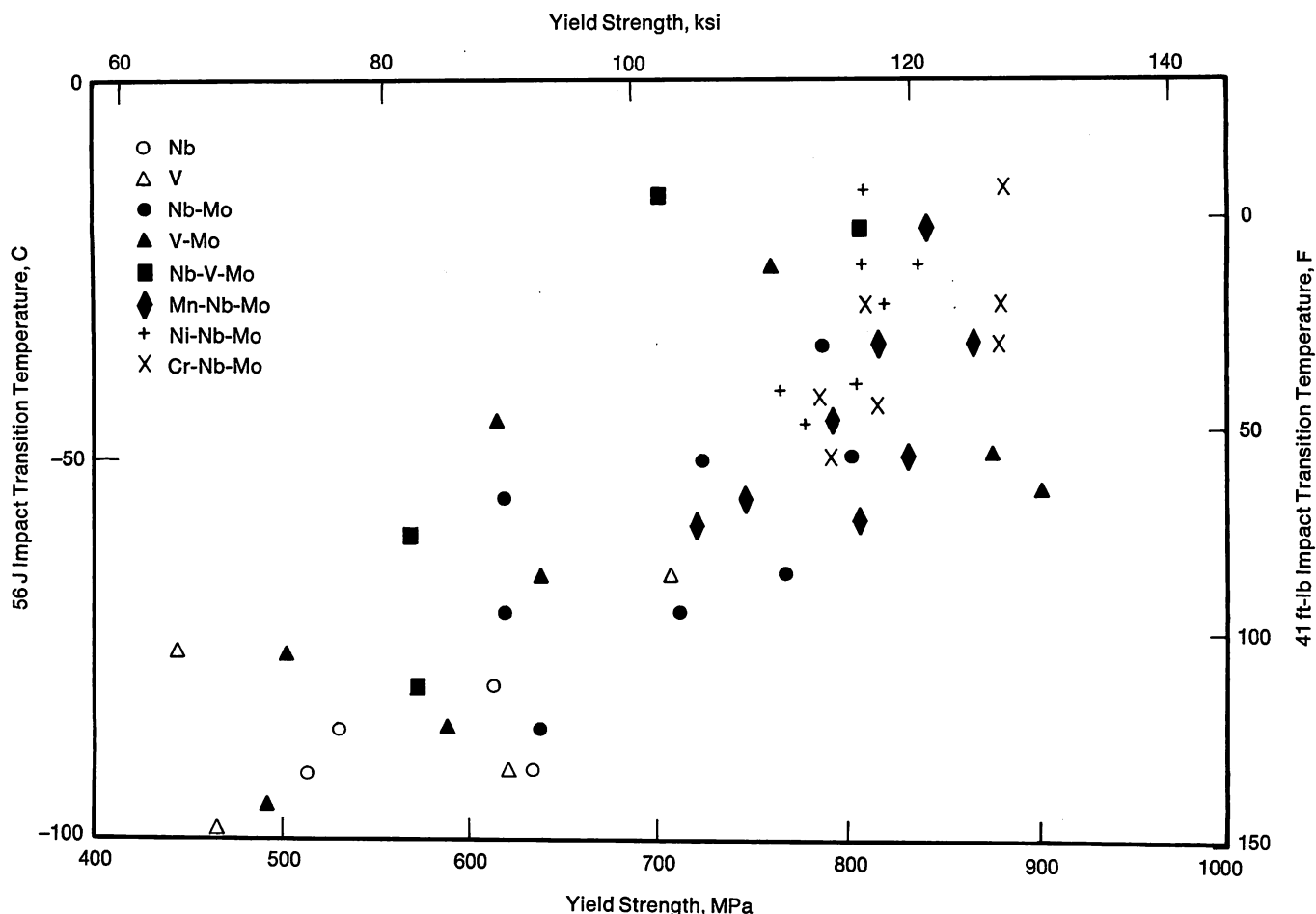
FIGURE 7—Range of yield strength and toughness attainable in direct-quenched-and-tempered HSLA steels.

tivity can be made to match that of the plate mill, and some very attractive combinations of strength and toughness can be achieved (Figure 7).[32] The options exist of attaining currently-used strength levels at very low alloy contents, or, where higher yield strengths can be utilized, of reaching these at alloy contents similar to those of existing Gr. 483 steels. Weld zone properties remain a potential problem with these materials, but it is unlikely that any insurmountable technical problems exist. Because of the paucity of experience, little is known as yet of the economic trade-offs of this technology, but such a product has been supplied commercially,[33] and more information should soon be available. Again, the alloy supply industry should be acutely aware of the economics of this type of production. Since considerable capital investment is involved, the activation energy for such a change in fundamental technology is extremely high; however, once the "hump" has been passed, the need to amortize the investment dictates that any return to previous technology would be extremely difficult to promote.

## Seam Weld HAZ Toughness

The development of welding techniques and consumables which will produce acceptable properties for

today's high strength, high toughness linepipe has been the subject of a large volume of research during the last decade.[34] We feel that it is worthwhile to discuss briefly the toughness of the seam weld heat affected zone, since this can have an effect on the choice of technology for skelp production.

First, it is necessary to consider what level of toughness is appropriate to the seam weld HAZ. It has recently been shown that fracture propagation can take place along the HAZ in both spiral and longitudinal seam pipe.[35] However, in practice, such an event would only increase the fracture length in the event of rupture by one joint since the position of seam welds is always staggered. It is implicit in the requirements of specifications such as Foothills' P100, however, that the fracture initiation resistance of the weld should be equivalent to that of the pipe body, due account being taken of orientation. While these requirements are quite readily met in the fusion zone, and in tests which sample a wide range of microstructures[36] (Figure 8a), there is little doubt that regions of low toughness exist in any conventional linepipe HAZ whenever the heat input exceeds about 2.5 kJ/mm (64 kJ/in.),[37] (corresponding to a wall thickness of something over 13 mm, 0.5 in., with conventional tandem, two-pass submerged arc welding). Even at lower
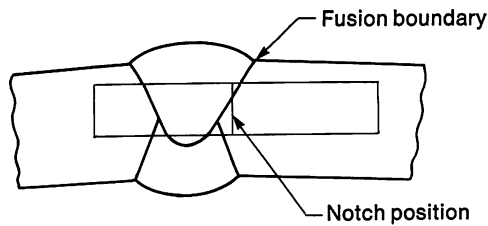
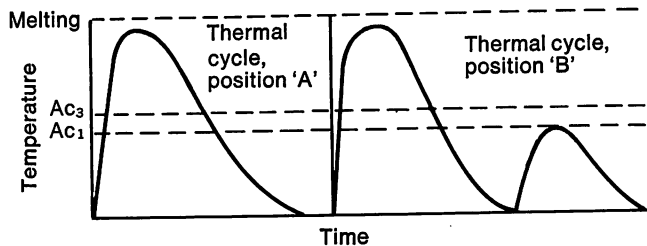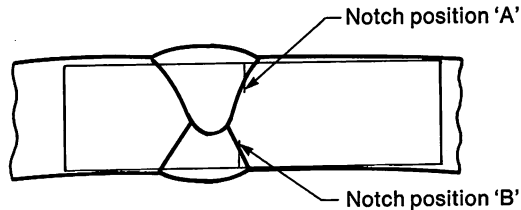FIGURE 8a—Typical configuration for seam weld HAZ Charpy test.





FIGURE 8b—Configuration of COD Testpiece sampling and low toughness regions of seam weld HAZ and associated thermal cycles.

heat inputs, there may be a region near the inside of the pipe wall showing a low toughness level as a result of the double thermal cycle experienced in this area. Figure 8b and Table I illustrate some of these points.[38,39] It can be seen that extremely poor local toughness may be expected in conventional, pearlite reduced Gr. 483 steels. These results refer to test pieces in which thermal cycles typical of particular regions of the HAZ were simulated, in blanks from which crack opening displacement (COD) test pieces were subsequently machined. Similar data can be obtained in COD test pieces from real welds if the crack tip is appropriately located (Figure 8b).

The significance of these highly localized zones of low toughness is not entirely clear, but they have caused a certain amount of concern and brought about a number of developments in linepipe technology. Some proposed changes in welding technology, by reducing the heat input or effectively converting the process to a multipass operation[29,40] could conceivably eliminate the problem. In light of the results shown in Table I, trends toward lower carbon contents are certainly beneficial. One of the most effective techniques for improving HAZ toughness, however, appears to be the incorporation of very small quantities of titanium into the steel. Work in the UK in the sixties established the effectiveness of fine dispersions of titanium nitride in controlling austenite grain size and established the ground rules for its use.[41,42] It was found that very small volume fractions ($\sim$10$^{-4}$) of TiN particles, typically of $\sim$20 nm dimensions, were capable of

**Table I**—COD Transition Temperatures in Simulated Seam Weld Heat Affected Zones

| Steel | Element, % * | | | | Carbon Equiva- lent, % | Position (Fig. 8b) | 0.2 mm (0.008 in.) Transition Temperature, | |
| | C | Mn | Mo | Ni | | | C | (F) |
|---|---|---|---|---|---|---|---|---|
| A | 0.09 | 1.38 | 0.015 | — | 0.323 | A | −30 | (−20) |
|  |  |  |  |  |  | B | +25 | (+75) |
| B | 0.09 | 1.37 | 0.305 | — | 0.379 | A | +25 | (+75) |
|  |  |  |  |  |  | B | +125 | (+255) |
| C | 0.085 | 1.62 | 0.40 | — | 0.435 | A | +35 | (+95) |
|  |  |  |  |  |  | B | +110 | (+230) |
| D | 0.09 | 1.56 | 0.34 | 0.45 | 0.448 | A | +35 | (+95) |
|  |  |  |  |  |  | B | +125 | (+255) |
| E | 0.04 | 1.29 | 0.345 | — | 0.324 | A | −10 | (+15) |
|  |  |  |  |  |  | B | +30 | (+85) |
| F | 0.05 | 1.48 | 0.455 | — | 0.388 | A | +5 | (+40) |
|  |  |  |  |  |  | B | +85 | (+185) |
| G | 0.04 | 1.60 | 0.355 | 0.47 | 0.409 | A | +5 | (+40) |
|  |  |  |  |  |  | B | +55 | (+130) |
| H | 0.04 | 2.10 | 0.38 | 0.47 | 0.497 | A | −5 | (+25) |
|  |  |  |  |  |  | B | +70 | (+160) |

* All steels contain 0.12-0.33% Si, 0.02-0.03% Al, ≦0.005% S, 0.007-0.019% P and 0.055-0.07% Nb.

**Table II**—Effect of Titanium on COD Transition Temperatures in Simulated Seam Weld Heat Affected Zones

| Steel | Element, % | | | | | | Carbon Equivalent, % | Position (Fig. 8b) | 0.2 mm (0.008 in.) Transition Temperature, C | (F) |
|---|---|---|---|---|---|---|---|---|---|---|
| | C | Mn | Mo | Ni | Ti | N | | | | |
| I | 0.080 | 1.34 | 0.35 | — | 0.033 | 0.015 | 0.373 | A | 0 | (+30) |
| | | | | | | | | B | +100 | (+210) |
| B | 0.090 | 1.37 | 0.305 | — | — | — | 0.379 | A | +25 | (+75) |
| | | | | | | | | B | +125 | (+255) |
| J | 0.075 | 1.52 | 0.49 | — | 0.027 | 0.015 | 0.426 | A | −5 | (+25) |
| | | | | | | | | B | +85 | (+185) |
| C | 0.085 | 1.62 | 0.40 | — | — | — | 0.435 | A | +35 | (+95) |
| | | | | | | | | B | +110 | (+230) |
| K | 0.045 | 1.49 | 0.31 | 0.485 | 0.020 | 0.014 | 0.387 | A | −25 | (−15) |
| | | | | | | | | B | +55 | (+130) |
| G | 0.040 | 1.60 | 0.355 | 0.47 | — | — | 0.409 | A | +5 | (+40) |
| | | | | | | | | B | +55 | (+130) |

restraining grain growth for periods of some hours, at temperatures up to 1300 C (2370 F); prolonged or repeated high temperature treatment did reduce their effectiveness, however, as did nitrogen contents below stoichiometry.

Further work in Japan[43] and elsewhere[44-46] demonstrated the possibility of utilizing this technique to restrain HAZ grain growth. Since austenite grain size or, more properly speaking, the resultant bainite colony size, is one of the most potent factors in determining HAZ toughness,[47] the presence of titanium nitride should bring about significant improvements. Table II shows that these are indeed observed.[39,46] The current trend toward the increasing use of continuous casting is highly beneficial, since it eliminates the slow solidification and high temperature soaking typical of large slabbing ingots. It thus seems quite likely that, wherever seam weld HAZ toughness is perceived to be problematic, titanium additions can be quite conveniently used to give worthwhile improvements.

**Advances in Field Welding Technology**

A final topic which should be considered is the expectation of considerable advances in field welding technology over the next decade. While these do not, of themselves, represent changes in linepipe production practice, they may have an influence on future developments in some unexpected directions.

While the traditional "stovepipe" technique, using cellulosic electrodes, is still the predominant field welding method, increasing use has been made of GMA welding over the last decade. Initial applications involved semiautomatic welding. The fully automatic equipment which has been developed over this period is beginning to look attractive from an economic and technical point of view.[48] Experience in the practical application of automatic GMA welding is growing, and there is little doubt that an increasing proportion of field welding will be

carried out in this way over the next few years. The Foothills project, for example, will attempt to maximize its usage.

The significance of this change from the point of view of materials technology may be considerable; it has already been pointed out that much of the thrust toward lower carbon contents has resulted from concerns over field weldability (specifically, hydrogen-assisted cold cracking) particularly as strength levels and the dimensions of pipe joints have increased. Current low carbon Gr. 483 steels are extremely resistant to HAZ cold cracking, and welding procedures (in particular, preheat and inter-pass times) are probably dictated more by a need to control weld metal cold cracking and microfissuring than by the traditional limitations imposed by the parent metal.[11] Reduction of the hydrogen content of the deposited metal from the >40 ppm typical of Exx10 stick electrodes to 5-10 ppm which is achieved in GMA welding greatly reduces the danger of cold cracking, as does the reduction or elimination of delay between root and hot pass. The overall result is that there will be much less of a premium on very low carbon contents in materials to be used for projects in which automatic GMA welding is extensively used. This, in turn, may influence the choice of alloy or microalloy systems preferred since, as has been pointed out before, it is normally possible to produce Gr. 483 steel (at a given thickness) with lower carbon contents in niobium-molybdenum steels than in niobium-vanadium steels. This is particularly true if the use of severe controlled rolling is precluded by considerations of fracture propagation resistance.

A final topic which may be worth mentioning is the on-going development, in different parts of the world, of a number of field joining techniques which do not involve arc welding. These include flash-butt, laser, electron beam and friction welding. One of the most interesting, both because of its implications and because it is at an advanced phase of development, is the explosive sys-

tem being developed by CIL in conjunction with Trans-Canada Pipelines and Stelco. It appears that this technique is reaching a point at which a package of equipment for field preparation (forming of bell end and surface cleaning), welding, heat treatment and inspection can be assembled, and a full-scale field trial may be anticipated in the near future. The metallurgical implications of this rather revolutionary approach to field welding are considerable. Clearly, weldability as traditionally understood will no longer be at issue; furthermore, since it is anticipated that the bell-and-spigot configuration will have a high probability of arresting any service fracture, it may well be that fracture propagation considerations become irrelevant. On the other hand, it will be necessary to establish that the pipe line steel used is compatible with the specified post-weld heat treatment. These changes in perspective could have a profound effect on the metallurgy of linepipe steels and could ultimately lead to a reversal of many of the trends toward higher technology materials which have been discussed in the preceding sections.

## Nontechnical Factors Influencing Linepipe Development

To this point, we have assumed that the development of linepipe technology will be predominantly influenced by the requirements of major or so-called "mega" projects, and that trends toward higher system efficiency, as reflected in increasing diameter, wall thickness and operating pressure, will dictate such project requirements. Therefore, it follows that nontechnical factors affecting these projects may influence the direction and rate of linepipe development.

Based on the experience of the Foothills Group of Companies in developing one such project during the last decade, the authors feel it is appropriate to note two such factors that will likely influence the nature of linepipe development in the eighties. These are the influence of the regulatory processes and the influence of national objectives on procurement practice and industrial benefit.

With respect to the regulatory process, the job of determining and protecting the "public interest" has assumed unprecedented proportions, and no indication presently exists that it will moderate in the eighties. Given that this involvement does represent the will of the democracies in which we live, the authors suggest that the development of technology will have to understand and accommodate such involvement, hopefully in a more effective manner than in the past.

Turning to the specific influences that the regulatory processes may have on linepipe development, the simple existence of well funded and technically staffed agencies will increase their depth of interest and may result in the application of requirements, perhaps belatedly, over and above those established by the user. Traditionally, this type of input has been biased toward the use of "proven" technology and away from the innovations we may seek to apply. Furthermore, this may be coupled with a desire to finalize and settle on the technology as early in the project development process as possible, rather than make provision for advances which can be reasonably anticipated in the time frames available. This technical conservatism, coupled with the long regulatory gestation periods required by major projects, can serve to delay technical progress and, perhaps of more concern, diminish the user's motivation to encourage such progress. He may simply take the path of least resistance and propose only what has been accepted in the past which will ultimately result in higher transportation costs to the consumer.

So that these influences do not seriously impede technological development, it is important that those involved rigorously research and document the technology so that it can be supported with a minimum of debate and challenge. A particularly effective method of doing this is for users and suppliers, preferably jointly, to conduct full-scale trial demonstration or test programs. Our experience suggests that the time and additional expense of this approach is worthwhile and can produce more timely, informed and relevant regulatory decisions.

The second external factor that may have an effect on linepipe development is the adoption, by major projects, of social objectives and, more specifically, objectives related to domestic procurement and industrial benefit. For example, the Foothills Group of Companies has, from the outset, endeavored to maximize domestic content and to use our requirements as a stimulus for lasting industrial development in Canada. Similar objectives have been applied to the American sections of the project, and a reciprocity of procurement practice has been established by international agreement between the two countries.

The effect of this trend on linepipe development, while not necessarily being a dominant factor, may influence what specific paths are followed and where changes take place. It is important for those interested in the advancement of the technology to understand this and to direct their efforts toward ensuring that the optimum technology becomes available within the political boundaries where it may most advantageously be applied. In effect, we should look to increased technological transfer among users and suppliers perhaps through mechanisms such as licensing of technology and cooperative research and development programs.

## Conclusions

We have discussed the rationale behind recent developments in linepipe steels and emphasized that the driving force behind all such developments must be over-

all system economics. It has been suggested that, after more than a decade of progress, we now stand at a threshold in the metallurgy of linepipe steels; it seems likely that we have reached a limit in terms of what can be achieved with conventional HSLA technology. We have examined some avenues for future advances which are currently well researched on a laboratory or pilot scale; understandably, we have tended to concentrate on those with which we have had some direct involvement, and, in the hallowed tradition of technological forecasting, we have probably missed the one major potential breakthrough which will revolutionize the industry. Finally, we have discussed some current and prospective developments in field welding methods which could conceivably have far reaching effects on future material technology.

As a general assessment of the present situation, it seems clear that the range of conventional HSLA linepipe steels having yield strength levels up to 483 MPa (70 ksi) in wall thicknesses up to 20 mm (0.79 in.) will continue to meet the vast majority of needs through the next decade; no doubt the advances in quality which have been made to satisfy the stringent requirements of frontier and offshore projects will be incorporated into the general production technology with resulting benefits in efficiency of installation and reliability in service. Major changes will only come about under the pressure of new, high technology projects whose demands cannot be economically met in any other way. The prospects for such projects in the coming decade, in the present regulatory, social, political and economic climate, constitute a topic more adapted to crystal gazers (or, perhaps more appropriately for this conference, molybdomancers) than to metallurgists.

## Acknowledgments

## References

1. W. W. Wiedenhoff, P. A. Peters, W. B. Kretzschmann and W. M. Hof, "Vanadium in High-Strength Steels", Paper D; Chicago, November 1979.

2. R. J. Cooke and T. C. Slimmon, "Materials Selection for the Alaska Highway Pipeline Project". Proceedings of the Canadian Council of ASM Conference on Materials to Satisfy the Energy Demand, Harrison Hot Springs, B. C., May 1980.

3. R. J. Eiber, Fourth Symposium on Linepipe Research, AGA, New York, 1966, 83.

4. G. D. Fearnehough, D. W. Jude and R. T. Weiner, "Practical Applications of Fracture Mechanics to Pressure Vessel Technology", Institution of Mechanical Engineers, London, 1971, 156.

5. W. A. Maxey, Fifth Symposium on Linepipe Research, AGA, Arlington, 1974, J-1.

6. W. A. Maxey, J. F. Kiefner, R. J. Eiber and A. R. Duffy, ASTM STP 514, 1972, 70.

7. W. A. Poynton, Proceedings of I.G.E. Symposium on Crack Propagation in Pipelines, Paper 14, Newcastle-upon-Tyne, 1974.

8. R. J. Eiber and W. A. Maxey, "Materials Engineering in the Arctic," ed. M. B. Ives, ASM, Metals Park, 1977, 306.

9. A. B. Rothwell, M. Urednicek and A. Gilroy-Scott, "Requirements for Control of Ductile Fracture Propagation in Large-Diameter Gas Transmission Pipelines". Proceedings of the Canadian Council of ASM Conference on Materials to Satisfy the Energy Demand, Harrison Hot Springs, B. C., May 1980.

10. B. Phelps, Microalloying 75, Union Carbide Corp., New York, 1977, 570.

11. J. M. Gray and A. B. Rothwell, "How Welding Affects Pipeline Steels", Proceedings AWS Conference, Pipeline Welding and Inspection, Houston, February 1980.

12. J. J. Irani, D. Burton, J. D. Jones and A. B. Rothwell, ISI Publication 104, The Institute, London, 1967, 110.

13. K. J. Irvine, T. Gladman, J. Orr and F. B. Pickering, JISI, 208, 1970, 717.

14. A. P. Coldren, Y. E. Smith and R. L. Cryderman, "Processing and Properties of Low-Carbon Steel," TMS-AIME, New York, 1973, 163.

15. J. M. Gray, Personal communication.

16. H. Pircher and W. Klapdar, Microalloying 75, Union Carbide Corp., New York, 1977, 232.

17. L. Luyckx, J. R. Bell, A. McLean and M. Korchnisky, Met, Trans., 1, 1970, 3341.

18. H. Gondoh, S. Yamamoto, M. Nakayama, H. Nakasugi and H. Matsuda, Microalloying 75, Union Carbide, New York, 1977, 453.

19. T. Suzuki, K. Nishizawa and Y. Asai, ibid., 442.

20. P. E. Repas, ibid., 387.

21. K. J. Irvine and F. B. Pickering, JISI, 201, 1963, 518.

22. K. J. Irvine and F. B. Pickering, ISI Special Report 93, The Institute, London, 1965, 110.

23. A. J. McEvily, R. G. Davies, C. L. Magee and T. L. Johnston, Transformation and Hardenability in Steels, Climax Molybdenum Company, Ann Arbor, 1967, 179.

24. A. Massip and L. Meyer; Stahl und Eisen, 98 (19), 1978, 989.

25. B. Serin, Y. Desalos, Ph. Maitrepierre and J. Rofes-Vernis, Mém. Sci. Rev. Mét., LXXV, 1978, 355.

26. A. B. Rothwell, Centro Sperimentale Metallurgico, Rome. Unpublished reports 1705R, 1973 and 1932R, 1974.

27. H. Nakasugi, H. Matsuda and H. Tamehiro, this conference.

28. A. P. Coldren, R. L. Cryderman and M. Semchyshen, Die Verfestigung von Stahl, Climax Molybdenum Company, Zurich, 1969, 17.

29. H. Matsubara, B. Sakai and T. Itaoka, "Materials Engineering in the Arctic," ed. M. B. Ives, ASM, Metals Park, 1977, 190.

30. J. J. Irani and G. Tither, ISI Publication 104, The Institute, London, 1967, 135.

31. J. D. Boyd, "Materials Engineering in the Arctic," ed. M. B. Ives, ASM, Metals Park, 1977, 200.

32. A. B. Rothwell, Can. Met. Quarterly, 16, 1977, 195.

33. M. LaFrance, Private communication.

34. J. M. Gray, "Development of Superior Notch Toughness in High-Dilution Weldments of Microalloyed Steel." CBMM International, Pittsburgh, 1980.

35. Foothills Pipe Lines (Yukon) Ltd., Unpublished work.

36. G. Bernard, Microalloying 75, Union Carbide Corp., New York, 1977, 552.

37. A. B. Rothwell, J. T. McGrath, A. G. Glover, B. A. Graville and G. C. Weatherley, IIW Report IX, 1147, 80.

38. A. B. Rothwell, A. G. Glover, J. T. McGrath and G. C. Weatherley, Proc. 5th Bolton Landing Conference, General Electric Co., Schenectady, 1978, 257.

39. A. B. Rothwell, Noranda Research Centre, Unpublished work.

40. E. Miyoshi, Y. Ito, H. Iwanaga and T. Yamura, "New Development in Weldability and Welding Technique for Arctic-Grade Linepipe." AWS Conference, Houston, May 1974.

41. T. George and J. J. Irani, *J. Aus. I.M.*, *13*, 1968, 94.

42. H. Stuart, D. Burton and A. B. Rothwell, BISRA Open Reports MG/C/54/69 and MG/C/55/69.

43. T. Ikeno, S. Kanazawa, A. Nakashima, K. Okamoto and K. Kanaya, *Tetsu-to-Hagane*, *59*, 1973, 146.

44. J. M. Sawhill, T. Wada and D. E. Diesburg, WRC Monograph "Welding of Linepipe Steels," New York, 1977, 86.

45. N. E. Hannerz, "Welding of HSLA (Microalloyed) Steels," ed. A. B. Rothwell and J. M. Gray, ASM, Metals Park, 1978, 365.

46. A. B. Rothwell, A. G. Glover, J. T. McGrath and G. C. Weatherley, "The Potential of Titanium for Improving the HAZ Toughness of High-Strength Linepipe Steel," presented at TMS-AIME Fall Meeting, Milwaukee, September 1979.

47. R. E. Dolby and J. F. Knott, *JISI*, *210*, 1972, 857.

48. G. L. Archer, P. H. M. Hart and A. Q. Stalker, WRC Monograph "Welding of Linepipe Steels," New York, 1977, 147.

# Discussion

J. L. MIHELICH, *Climax Molybdenum Company*. X-70 production is presumably going to continue at some high level, but how high a strength level can we expect? When are we going to see higher strength steels?

A. B. ROTHWELL. This is a very difficult question to answer because the design of a pipeline system is quite a complicated balancing act between a lot of different requirements, only one of which is the strength/thickness equation. If you have to choose between greater wall thickness and higher strength, there are some sound reasons from the point of view of installability why you'd go to the higher strength. There are some limitations in terms of maximum diameter-to-thickness ratios, and these are very complex equations that the pipeline system designer has to keep in mind. I would be surprised to see wide usage within the next decade or so of anything beyond X-80.

R. T. HILL, *Metallurgical Consultants, Inc.* I think that you will probably see up to X-100 for the deep water applications. In fact, a paper presented recently at the Offshore Technology Conference mentioned that X-100 was being considered.

J. P. TRALMER, *Shell Development Company*. With respect to your illustration that showed the quenched-and-tempered grades of pipe, you said that there was no concern over welding. Does this refer to field welding or seam welding only?

A. B. ROTHWELL. I was strictly referring to the seam weld. The point that I was trying to make was that if you quench and temper the whole pipe as opposed to making the pipe out of quenched-and-tempered plate (provided you tailor the consumables for the seam weld in such a way that they respond in the right way to the heat treatment process), you have nothing to worry about with the seam weld.

J. LESSELLS, *British Steel Corporation*. Could you comment on the toughness of weld heat affected zones?

A. B. ROTHWELL. Basically, it may be a concern. It is implicit in our specifications and I think probably most others that the seam weld should be as tough with respect to crack initiation as the pipe body. If you run Charpy tests, which sample a wide range of different structures across the heat affected zone, there is no problem in getting this level of toughness. But if you look with a fine fatigue crack in a COD test for regions of low toughness, you'll find them. One of the techniques which looks very promising in dealing with this is the use of very small amounts of titanium. An Australian/British development from the sixties of using titanium nitride for grain control at very high temperatures can be used very effectively in weld heat affected zones.

P. BOUSSEL, *Climax Molybdenum Company*. What do you think about the effect of transmitting sour gas in pipelines on the specification requirements? This is particularly important for offshore applications.

R. J. COOKE, *Foothills Pipe Lines (Yukon) Ltd.* There is an area of technological development in sour gas applications considering the amount that is being found and the locations. I think for the first time we are going to see a lot of effort to have high strength sour gas pipe in large diameters. Today, at least in Canada, sour gas systems are rarely above X-52 or X-60, so the sour gas development in terms of strength is trailing behind the high tonnage applications.

# The Metallurgy of Steels for Large Diameter Linepipe

by H. W. Paxton
U.S. Steel Corporation

A little more than 10 years ago, the mechanical property and metallurgical requirements for large diameter UOE linepipe were rather rudimentary, consisting essentially of minimum tensile properties and maxima on the chemical composition—the latter primarily to assure acceptable weldability. At that time, API Grade X-60, with a small tonnage of API Grade X-65, represented the maximum strength being offered commercially. Pipe was made from hot-rolled semikilled plate steels having base compositions in the range of about 0.20 to 0.25% carbon and 1.25% manganese with additions of niobium (up to about 0.05%) and/or vanadium (up to about 0.08%) depending on the combination of strength and gauge.

Over the last decade, the specification requirements for linepipe have become more stringent. These include (1) a greater demand for higher strength pipe—up to API Grade X-70—to increase product throughput and thus improve the operating economy of pipe lines, (2) the inclusion of notch toughness requirements in specifications to assure that if an operating failure occurs, the fracture would behave in a ductile manner, and the pipe steel would have sufficient fracture energy to preclude a long running fracture and thus improve the safety of the pipe line, and (3) the demand for better weldability to reduce the construction costs of pipe lines and also to improve their integrity and thus their safety. Typical requirements for large diameter pipe to be used in a severe environment such as the Arctic include 480 MPa (70 ksi) minimum yield strength, a ductile-to-brittle transition temperature below −18 C (0 F), a Charpy V-notch (CVN) upper shelf energy of 95 J (70 ft-lb) or more at −18 C (0 F) and a carbon equivalent of 0.43% maximum.

The desire for improved weldability and fracture energy dictated a shift to lower carbon steels, such that today linepipe for the more critical applications is generally produced from steels containing 0.10% carbon or less. Although these lower carbon steels inherently have higher fracture energies than the earlier classes of linepipe steels, the increase in energy was not sufficient to attain the desired higher levels. Therefore, it became necessary to resort to the use of very low sulfur steels coupled with inclusion shape control and an overall high degree of cleanliness to raise the CVN shelf energy to the levels being required in the most stringent specifications. The demand for ductile-to-brittle transition temperatures substantially lower than those achieved by normal plate-mill hot-rolling practices could not be met by the usual approaches of normalizing or quenching and tempering. The reasons for not considering heat treatment include the relatively high cost, the lack of sufficient heat treating facilities for the large tonnages generally required for a pipe line, and the reluctance of customers to use a heat treated product for which little or no operating experience exists. This problem was overcome by a change in deoxidation practice (semikilled to silicon-aluminum killed) coupled with the development of controlled rolling practices. The changes resulted in a refined grain size such that fully ductile fracture behavior well below −18 C (0 F) is now routinely obtained. Even though there is a contribution to yield strength from the grain refinement resulting from controlled rolling, the increase in strength from this source for these low carbon steels is partially offset by the reduction in carbon content from the 0.20 to 0.25% level of the previously used linepipe compositions. To make up this difference, strengthening additions of copper, nickel, chromium and/or molybdenum are used, which, in conjunction with the precipitation strengthening from microalloying additions of niobium and/or vanadium, enable API Grade X-70 strengths to be attained.

Thus, these weldable high strength high toughness linepipe steels are the result of the development of a new class of low carbon low sulfur HSLA steels and the associated controlled rolling practices. The highlights of the studies at U.S. Steel Research leading to these developments are outlined in this paper. The transfer of this technology to other steel products as well as studies to develop the next generation of linepipe are also outlined.

## Metallurgical Developments and Their Influence on Properties and Behavior

### Alloy Development

The class of low carbon, low alloy steels used for current large diameter linepipe is generally restricted to

those steels containing 0.05 to 0.10% C, 1 to 2% Mn, 0.02 to 0.10% Nb, 0.05 to 0.15% V, and Mo, Ni, Cu and Cr in amounts of 0.10 to 0.30%. These steels generally also have low sulfur contents in the range of 0.002 to 0.010%. The steels may also contain 0.20 to 0.30% Si and 0.012% N, but these elements are the result of steelmaking practice and are not deliberate additions.

In the present section, the general contributions of the major alloying elements will be described based on our own experience and also that of other laboratories. This information, along with the effects of rolling practice discussed subsequently, has served as a basis for the alloy design of the Mn-Mo-Nb Arctic grade linepipe steel.

**Carbon.** Restriction of the carbon content to the range of 0.05 to 0.15% is dictated by the need for good weldability and high shelf energies. The effect of higher carbon contents on increasing the amount of weld under-bead cracking is well documented[1-3] and will be discussed later in some detail. The effect of higher carbon contents in lowering the shelf energy is also well documented.[4-6]

Because of the above considerations, the carbon in linepipe steels was further lowered to the 0.05 to 0.10% range.[7] The small decrease in yield strength caused by this lowering of the carbon content can easily be compensated for by the use of other strengthening mechanisms.

**Manganese.** Addition of manganese to linepipe steels has a number of important effects. First, addition of 1 to 1.5% Mn lowers the temperature at which austenite transforms to polygonal ferrite by 50 C (90 F).[8] This results in a significant ferrite grain size refinement, and a consequent increase in strength and a lowering of the transition temperature. Increasing the manganese content to 1.5 to 2.0% lowers the transformation still further, but this causes the austenite to transform to acicular rather than polygonal ferrite.[9]

It was decided early in the alloy development studies that the manganese content of the steels would be restricted to 1 to 1.5% to maintain a polygonal ferrite matrix. This lower manganese content also has some advantages from a steelmaking viewpoint.

Manganese strengthens steel both by grain refinement and solid solution hardening. The dual strengthening effects of manganese can most easily be seen by comparing the strength of steels with and without manganese for different grain sizes. Such data from an early study[10] are shown in Figure 1. The different grain sizes were established by controlled rolling and finishing at different temperatures. The marked increase in strength at low finishing temperatures is a separate effect caused by warm working of the ferrite and will be discussed later. The data for the C-Mn steel (0.06% C, 1.2% Mn) are displaced to finer grain sizes compared to the C steel
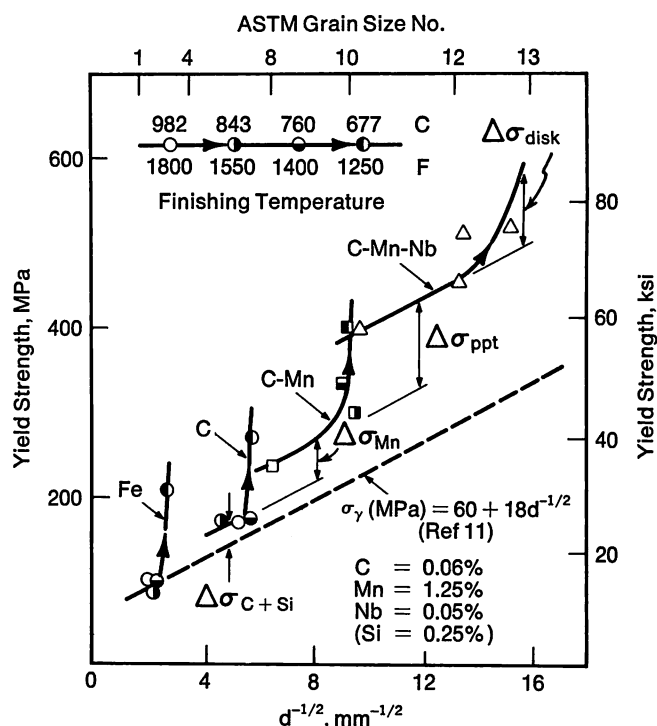
FIGURE 1—Alloying element effects on strength in controlled rolled linepipe steels.

(0.06% C) because of the effect of manganese on the transformation temperature, but extrapolation of the data for the C steel on a $d^{-1/2}$ basis[11] shows that a substantial solid solution hardening effect, $\Delta\sigma_{Mn}$, is required to account for the increased strength of this steel. The value of $\Delta\sigma_{Mn}$ is 34 MPa (5 ksi) per 1% Mn, in agreement with other investigations.[12]

The marked refinement of grain size by manganese additions lowers the transition temperature because of the (normal) well established dependence on $d^{-1/2}$. However, another beneficial effect of manganese on transition temperature results from the reduction in the amount and thickness of grain boundary carbides.[5,10,13-15] These carbides can be particularly harmful because they can and do crack at low temperatures during plastic straining. These microcracks can then propagate into the ferrite matrix and cause a marked increase in transition temperature.

The improvement in transition temperature with manganese additions of about 1% is illustrated in Figure 2. These data are taken from the same series of steels described previously.[10] The decrease in transition temperature of the C steel (0.06% C), $\Delta T_{Mn}$, by addition of 1.2% Mn, is quite marked and results primarily from the reduction in the amount and thickness of the grain boundry carbide film. When compared at the same finishing temperature of 875 C (1550 F) (same austenite grain size), it can be seen that manganese still further reduces the transition temperature by grain size refinement according to the usual $d^{-1/2}$ dependence.[16] (The increase in transition temperature at low finishing temperatures

**Figure 1 data:**

ASTM Grain Size No.: 1  4  8  10  12  13

| 982 | 843 | 760 | 677 | C |
|-----|-----|-----|-----|---|
| 1800 | 1550 | 1400 | 1250 | F |

Finishing Temperature

$\Delta\sigma_{disk}$
C-Mn-Nb
$\Delta\sigma_{ppt}$
C-Mn
$\Delta\sigma_{Mn}$
C
Fe
$\Delta\sigma_{C+Si}$

$\sigma_y$ (MPa) = 60 + 18$d^{-1/2}$ (Ref 11)

C = 0.06%
Mn = 1.25%
Nb = 0.05%
(Si = 0.25%)

Yield Strength, MPa (axis: 200, 400, 600)
Yield Strength, ksi (axis: 20, 40, 60, 80)
$d^{-1/2}$, mm$^{-1/2}$ (axis: 0, 4, 8, 12, 16)

is caused by warm working of the ferrite and is subsequently discussed.)

The effect of manganese on both strength and transition temperature can be illustrated by replotting the data of Figures 1 and 2 in the manner shown in Figure 3. From Figure 3, it can be seen that though the general strength level is increased, the overall effect of manganese is to drastically lower the transition temperature.

**Niobium and Vanadium.** Niobium combines with carbon or nitrogen to form a fine dispersion of Nb(C, N) in the austenite, thereby retarding grain growth and recrystallization during controlled rolling.[5,17,18] As a result, a considerably finer austenite grain size and a subsequent finer ferrite grain size are achieved in controlled rolled steels containing niobium. The fine dispersion of Nb(C, N) that has formed in the austenite, or in the ferrite during or after transformation, also results in a significant increase in strength.

Vanadium also interacts strongly with carbon and nitrogen to form V(C, N), but this interaction is weaker than in the case of niobium. As a result, precipitation of V(C, N) occurs at lower temperatures in the austenite region than in the case of niobium. As for niobium, vanadium has a beneficial effect in controlling the recrystallization behavior of the austenite and in providing a strengthening increment from precipitation hardening, especially in steels with higher nitrogen contents.[19] Although much of our alloy development work was concerned with additions of both niobium and vanadium,[20] the present discussion is focused on niobium. However, many of the effects of this element are similiar to those obtained with vanadium additions.

The level of niobium in the alloy studies was such that Nb(C, N) would dissolve upon reheating prior to rolling but would subsequently precipitate during controlled rolling at lower temperatures. From the solubility products for NbC[21] and NbN,[22] it can be shown that for a 0.06% C steel with 0.01% N, all the Nb(C, N) will be dissolved at 1195 C (2180 F) if the niobium content of the steel was 0.03%. Further additions of niobium were not beneficial.[23]

The strengthening effects of niobium arise from both grain size refinement and precipitation hardening. As shown in Figure 1, the grain size range for a C-Mn-Nb steel (0.06% C, 1.2% Mn, 0.05% Nb) is significantly lower than for a C-Mn steel (0.06% C, 1.2% Mn), and the strengthening increment for this decrease in grain size follows the standard $d^{-1/2}$ relationship. However, over and above this strengthening effect, there still remains a strengthening effect, $\Delta\sigma_{ppt}$, which arises from the precipitation of Nb(C, N) in the ferrite. The value of $\Delta\sigma_{ppt}$ of 103 MPa (15 ksi) is an appreciable fraction of the total strength of the steel. The other strengthening increments are 252 MPa (37 ksi) from grain size refinement, 34 MPa (5 ksi) from manganese solid solution
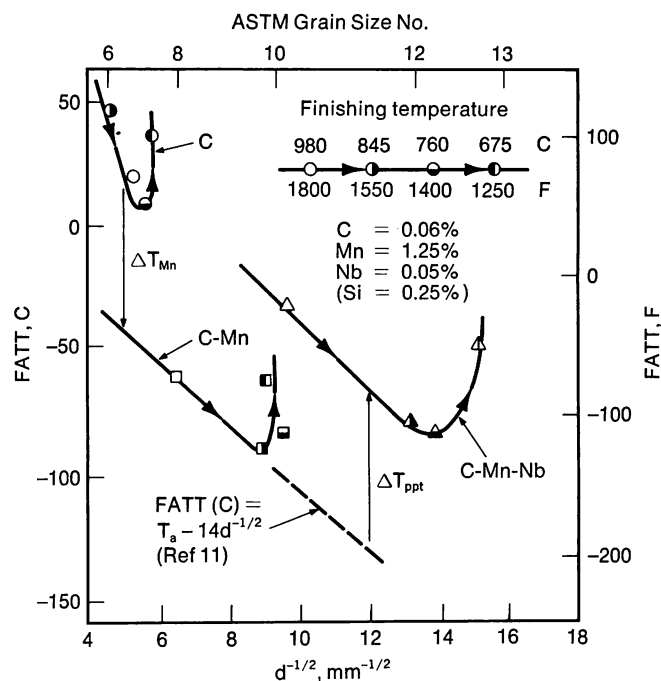


FIGURE 2—Alloying element effects on transition temperature in controlled rolled linepipe steels.
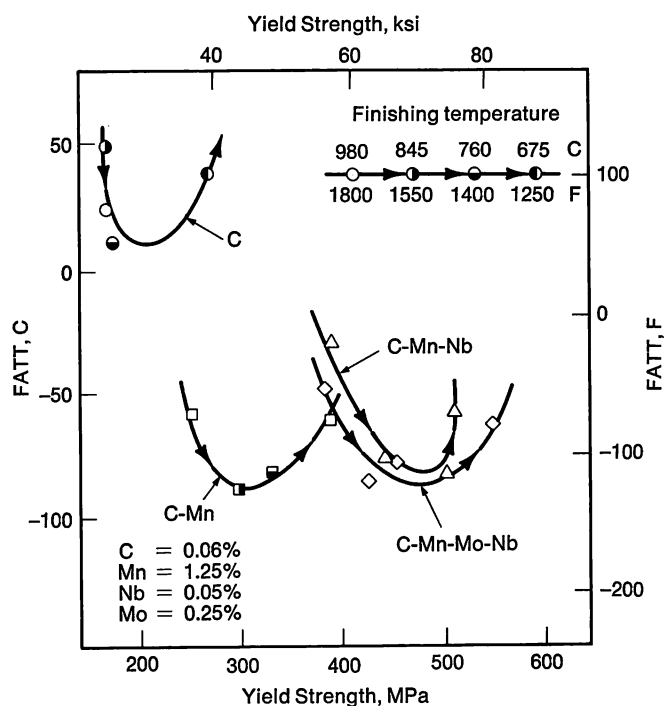


FIGURE 3—Alloying element effects on yield strength and transition temperature in controlled rolled linepipe steels.

hardening, 28 MPa (4 ksi) from pearlite and silicon solid solution hardening combined, and 60 MPa (9 ksi) from the frictional stress of pure iron. The total of these strengthening increments is 477 MPa (69 ksi) which is the yield strength of the steel when finished near 760 C (1400 F).

At finishing temperatures below 760 C (1400 F), ferrite may form during the rolling operation, and the
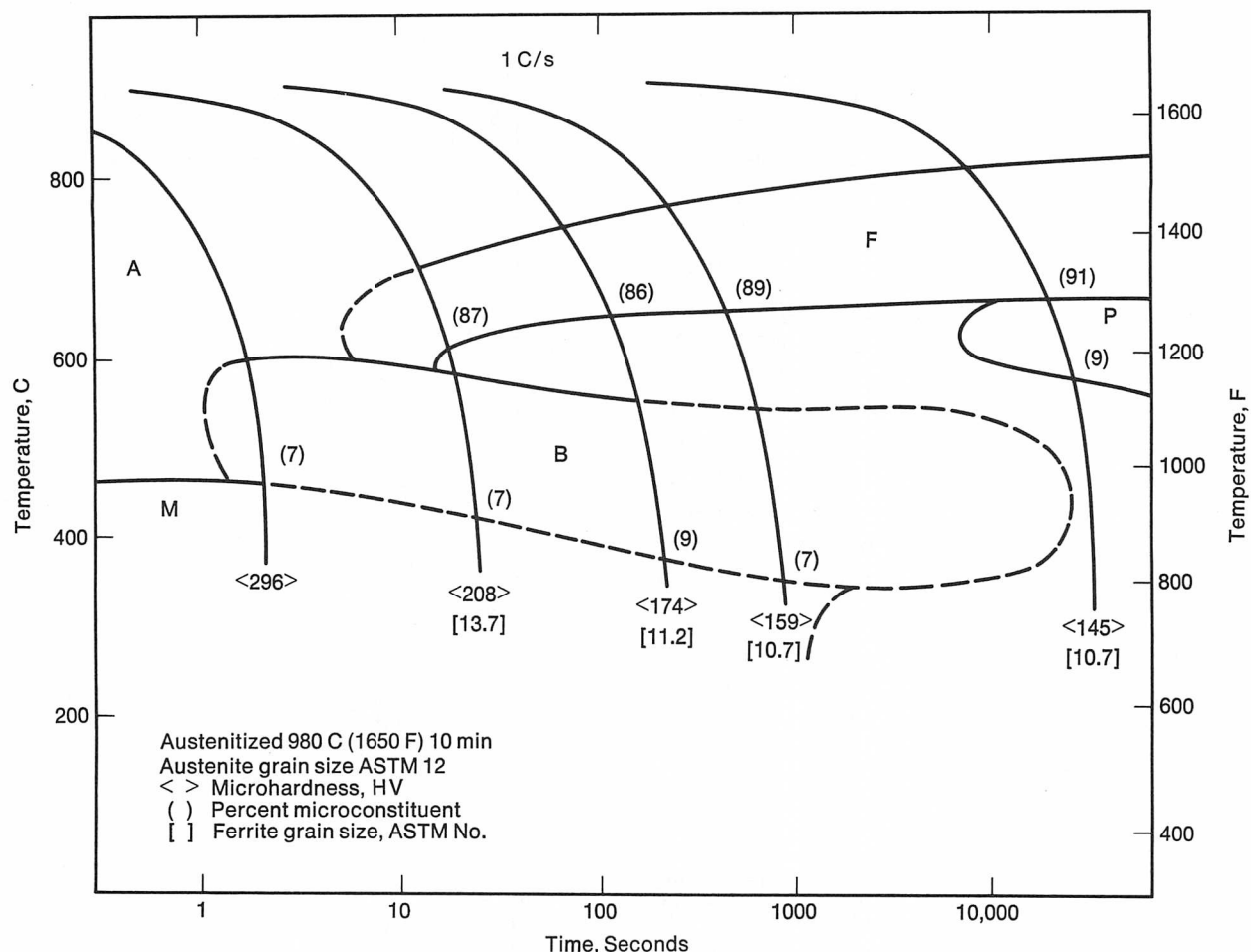
a. Continuous cooling diagram
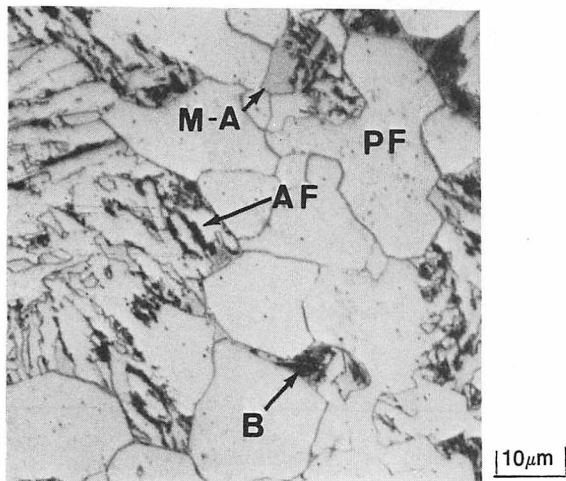


b. Microstructure of specimen cooled at 1 C/S (1.8 F/S)

FIGURE 4—Continuous cooling diagram and microstructure of 0.10C-Mn-Mo-Nb steel.

strength of the steel is further increased because of the warm working and resultant higher dislocation density of the ferrite. The strength increase, $\Delta\sigma_{disl}$, can amount to about 70 MPa (10 ksi) but is obviously dependent on the amount of work introduced into the steel at this low temperature.

The effect of niobium on the transition temperature also arises from two separate causes. As shown in Figure 2, although the grain refining action of niobium tends to lower the transition temperature, the effect of precipitation of NbC is to increase the transition temperature. The value of the relative effects can be estimated from Figure 2. The refinement of the grain size from ASTM No. 9.5 to 12.5 lowers the transition temperature by 70 C (125 F). The value of $\Delta T_{ppt}$ is +80 C (145 F). As a result, these effects tend to counterbalance each other, and there is a slight increase in transition temperature. However, as shown in Figure 3, this means that a large strength increase can be obtained with only a small increase in transition temperature. As a result, linepipe steels with a yield strength of 480 MPa (70 ksi) and with a transition temperature of −75 C (−105 F) can be obtained by controlled rolling of C-Mn-Nb steels if the finishing temperature is near 760 C (1400 F).

The effect on the transition temperature of finishing at temperatures below 760 C (1400 F) is complex because of the development of splitting fracture and deformation of the ferrite. Discussion of this topic is deferred to the section on rolling practice.

**Molybdenum.** Molybdenum kinetically suppresses ferrite formation and therefore slightly lowers the trans-

formation temperature. This can cause a slight reduction in grain size and less precipitation of Nb(C, N) during or subsequent to transformation. These two effects offset each other so that there is little change in strength or transition temperature with molybdenum additions. As a result, the strength and transition temperature of a C-Mn-Mo-Nb steel (0.06% C, 1.2% Mn, 0.5% Nb and 0.25% Mo) is similar to that of the C-Mn-Nb steel previously described, as shown in Figure 3.

More significantly, molybdenum suppresses the formation of pearlite. As a result, in steels that contain 0.25% Mo, the austenite remaining after polygonal ferrite formation will transform to lower temperature products such as acicular ferrite, bainite and a martensite-austenite constituent.[8, 24-26] As shown in Figure 4a, air cooling 13 mm (½ inch) plates, giving typically a rate of about 1 C/s (1.8 F/s), results in transformation of austenite to about 80% polygonal ferrite (PF), followed by transformation of the remaining austenite to acicular ferrite (AF), bainite (B) and a martensite-austenite constituent (M-A). A typical microstructure is shown in Figure 4b.

Although controlled rolling and the presence of different amounts of residual elements can alter the relative fractions of acicular ferrite, bainite and M-A constituent, the basic microstructure of these steels is not changed by controlled rolling (compare Figure 4b with Figure 5).

The formation of these lower transformation products has an important effect on the stress/strain behavior of these steels. When the amount of the M-A constituent exceeds 5%, the yield point is eliminated and a continuous stress/strain curve is obtained, as shown in Figure 6.[25] Steels with this type of stress/strain curve exhibit rapid work hardening when strained only a few percent. This behavior is desirable in plate product used to make UOE pipe because the pipe-forming strains can be utilized to increase the strength of the pipe over that of the plate. This increased strength can more than compensate for the Bauschinger effect which arises when tension test specimens cut from the pipe are flattened and tested.[27-29]

The term M-A constituent arises from the presence of appreciable amounts of retained austenite contained within the small martensite particles.[25] The change in the nature of the stress/strain curve with small amounts of the M-A constituent is very similar to that observed with dual phase steels. The elimination of the yield point is related to the presence of residual stresses about the small martensite particles.[29] The rapid work hardening of these steels can be attributed to either the gradual lowering of the peaks in these residual stresses as plastic straining progresses or to the normal work hardening of two-phase composites which contain hard particles in a soft matrix.[30]

**Copper, Nickel and Chromium.** Copper and nickel are expected to have effects on the transformation behavior similar to that of manganese, in that they lower the transformation temperature. These two elements may thus refine the grain size slightly and lead to less precipitation of Nb(C, N), in the ferrite phase. They may also contribute to a small solid solution hardening effect.[5] The effect of copper and nickel on transition temperature in these steels is not well documented, although nickel



(750 X)

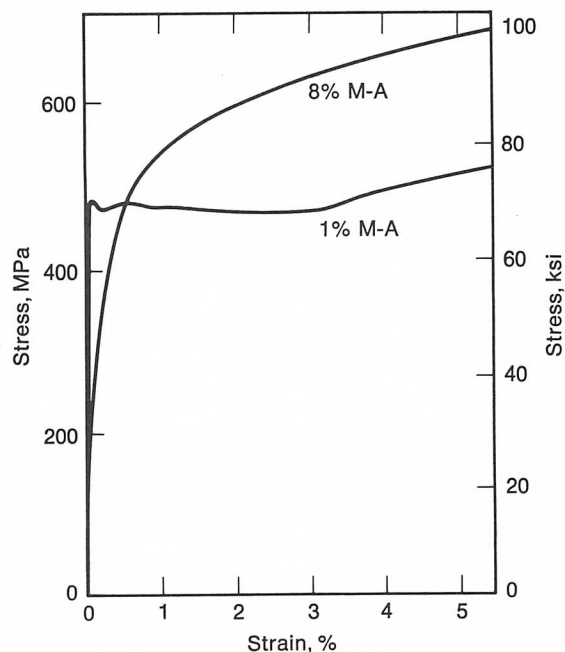FIGURE 5—Microstructure of control rolled Mn-Mo-Nb steel. 2% Nital etch.



FIGURE 6—Change in stress/strain behavior with increasing amount of M-A constituent.

FIGURE 7—*Schematic representation of controlled rolling process in Mn-Mo-Nb steel.*
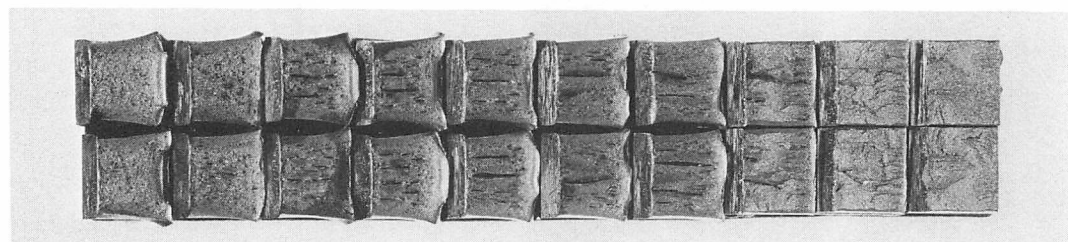
## Rolling Practice

In general, the deformation sequence in the controlled rolling process for plate designed for use in large diameter linepipe consists of (1) an initial high temperature rolling, (2) a delay to allow the plate to cool to lower temperatures, and (3) a final low temperature rolling. To achieve the very fine grain sizes that are required for low transition temperatures, deformation is generally extended to temperatures below Ar$_3$. As a result, ferrite may form during the later stages of the rolling process.

The metallurgical changes that occur in the austenite during controlled rolling are schematically shown in Figure 7. These changes can be classified into several regimes.[5, 32] At high temperatures, rapid recrystallization of the austenite occurs with some grain refinement. At intermediate temperatures, only partial recrystallization of the austenite occurs, and the unrecrystallized austenite grains become flattened in the rolling plane. At low temperatures, no recrystallization occurs, and the grains are flattened still further. Upon cooling after rolling, ferrite nucleates at the boundaries of the flattened austenite grains and grows inward, and, as a result, the ferrite grain size is essentially determined by the thickness of the austenite grains.[33] Niobium of course, plays a central role in the controlled rolling operation, because the precipitation of NbC retards recrystallization and grain growth of the austenite.

The strength and transition temperature of this class of steels varies with the final finishing temperature in a manner previously described (see Figures 1 to 3). The present discussion is restricted to the change in properties at the lowest finishing temperatures.

Although ferrite formed from the deformed austenite is relatively dislocation free, ferrite that forms during the rolling process at low temperatures is warm worked and may have a relatively high dislocation density. Because of the high temperature, some of these dislocations may be recovered to form a subboundary network.[32]

in larger amounts has a beneficial effect in lowering the transition temperature because of its effect on cross slip.[31] It has been reported that copper reduces the corrosion rate of the steel and that this decreases the tendency for the generation of hydrogen that might form voids at inclusion sites. As a result, some investigators suggest that copper should be added to linepipe steels. This subject is discussed later.

Chromium has been studied the least of all the alloying additions, but it is expected that its major effect, in conjunction with molybdenum, is to alter the transformation characteristics of the steel and promote the formation of the M-A constituent.



| Test Temp., C | | 93 | 65 | 27 | 4 | −18 | −40 | −62 | −84 | −95 | −106 |
|---|---|---|---|---|---|---|---|---|---|---|---|
| | F | 199 | 149 | 81 | 39 | 0 | −40 | −80 | −119 | −139 | −159 |
| Energy, | J | 108 | 97 | 94 | 106 | 95 | 72 | 69 | 20 | 15 | 5 |
| | ft-lb | 80 | 72 | 69 | 78 | 70 | 53 | 51 | 15 | 11 | 3.7 |
| Shear, % | | 100 | 100 | 100 | 100 | 100 | 100 | 99 | 60 | 5 | 0 |

FIGURE 8—*Effect of test temperature on the Charpy V-notch properties of a Mn-Mo-Nb steel plate after low temperature controlled rolling.*

A more important result of the low temperature rolling is the development of splits (or separations) on the fracture surface of CVN impact specimens as shown in Figure 8. The splits run parallel to the rolling plane and separate the impact specimens into a number of smaller specimens. The effect of these splits on the impact energy at different test temperatures is shown in Figure 9. At high test temperatures in the shelf region, no splits are observed. As the test temperature is lowered, splits appear in the specimen even though the rest of the specimen is still fracturing in a 100% shear mode. As the test temperature is lowered below the ductile-to-brittle transition, the splits disappear.

Because splits form prior to the passage of the crack front,[35] splitting has the effect of dividing the specimens into several thinner specimens. As the plastic volume associated with ductile fracture is proportional to specimen thickness,[36] the Charpy impact energy is decreased. This results in a decreasing shelf energy as shown in Figure 9. It is not yet clear whether the shelf energy or the lower impact energy corresponding to 100% shear is the correct criterion for resistance to ductile crack propagation.[37]

Although splitting may lower the shelf energy, it may be beneficial in that it also lowers the ductile-to-brittle transition temperature.[37] This is a result again of the separation of the specimen into a number of thinner specimens which relaxes the hydrostatic tension component at the root of the notch, and causes a decrease in the transition temperature.

The metallurgical reasons for splitting that have been suggested are numerous. Because splitting develops only when the finishing temperature is below Ar3, a number of authors have proposed that the deformation of the

ferrite results in development of an unfavorable (001) [011] crystallographic texture that promotes cleavage on planes parallel to the rolling plane.[38-40] Others have proposed that the mixture of fine and coarse grains associated with controlled rolled steels that are finished at low temperatures contributes to splitting fractures.[41] Other studies indicate that splitting fractures are caused by fracture along the flattened ferrite grain boundaries that are associated with low temperature controlled rolling.[34, 42] Our own studies suggest that all of these factors enter into splitting and that it is not possible to separate the individual contribution of these various effects.[10, 35] In general, however, most investigators agree that splitting fractures result from low finishing temperatures and can be eliminated by normalizing, quenching and tempering, or recrystallization anneals.[10, 41]

It is not surprising that agreement has not been reached on the effect of finishing at temperatures below Ar3 on the transition temperature. Different investigators have found a decrease,[32, 34] no change,[17] and an increase[10] in the transition temperature. In general, the increased strength level caused by the higher dislocation density in ferrite would be expected to increase the transition temperature.[5, 10] However, if the higher dislocation density is recovered into a subgrain network, some lowering of the transition temperature might be expected.[27] Splitting associated with the low temperature rolling might be expected to lower the transition temperature. The combined effect of these three different contributions on the transition temperature is probably sensitive to the amount of deformation, the temperature and the strain rate in the last part of the controlled rolling schedule.

Rolling practices generally adopted for Mn-Mo-Nb steels have been designed so that the finishing temperature is slightly below Ar3 to achieve the maximum grain size refinement but not so far below Ar3 that the propensity for splitting is very great.

## Microcleanliness Studies

Studies by Battelle Memorial Institute,[43-45] and the American Iron and Steel Institute[46] have established the need for high toughness in linepipe steels for gas transmission lines. Not only must the pipe steel have a low ductile-to-brittle transition temperature so that during all conditions of use the pipe temperature is above the transition temperature of the steel, but also the energy absorbing capability of the steel above the transition temperature (shelf energy) must be high to avoid long running fractures in lines operating at high gas pressures. This had led to specifications[47] for Arctic linepipe requiring minimum Charpy V-notch energy absorption at −18 C (0 F) of as high as 143 J (105 ft-lb).

The ductile fracture process occurs by the nucleation of cavities at inclusions, second phase particles or grain intersections, the growth of the cavities, and eventual coalescence and fracture.[48] The metallurgical factors
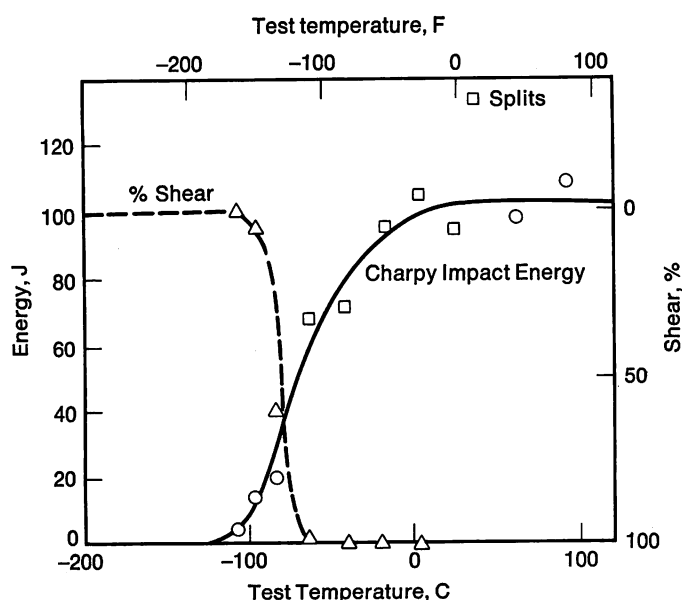


FIGURE 9—*Charpy V-notch impact properties of Mn-Mo-Nb steel after low temperature controlled rolling.*

affecting ductile fracture and thus shelf energy may be divided into two categories, those associated with the steel matrix, i.e., the strength of the steel and the manner in which the strengthening is achieved, and those associated with steel cleanliness, i.e., the number, size, shape and distribution of sulfides, oxides and carbonitrides. The alloy development and rolling studies described earlier have shown the importance of optimizing the strengthening of the steel to provide the best possible combination of high strength and low ductile-to-brittle transition temperature. This was accomplished by obtaining the desired strength at the lowest practical level of carbon in the steel and by developing the finest possible ferrite grain size. Fortunately this optimization also optimizes the toughness of the steel matrix at temperatures above the transition temperature.*

**Influence of Nonmetallic Inclusions on Notch Toughness.** The category still to be addressed is that of microcleanliness. Steelmakers recognized very early that steels with high volume fractions of nonmetallic inclusions exhibit low ductility, and that, as the strength of the steel increased, the importance of improving microcleanliness increased. However, quantitative results were scarce prior to 1960. One of the early papers providing quantitative information which arrived at some important generalizations regarding the influence of inclusions (second phase particles) on the ductility of metals was by Edelson and Baldwin in 1962.[49] They found that, for a number of dispersion alloys of copper, ductility depended upon the volume fraction of the second phase particles and was independent of particle size, shape or composition. As shown in Figure 10, the ductility appears to be a hyperbolic function so that major improvements in ductility occur when the volume of second phase is reduced to a very low value. The relative insensitivity of the results to the nature of the second phase is noteworthy. Holes lead to the same relation as hard, strong particles such as alumina.

In the study by Edelson and Baldwin, the range of particle sizes was 127 to over 20,000 $\mu$m. Inclusions in steels cover a wide range of sizes, but they are mostly in the size range of 1 to 10 $\mu$m, inclusions in this size range behave according to the predictions of Edelson and Baldwin. Kiessling has classified inclusions in steel based on their chemistry[50] and, in working with inclusions, has made some generalizations regarding the effect of inclusions on the properties of steels well worth noting. He concludes that it is technically impossible to make steel free of inclusions so we must learn to optimize the properties of the composite matrix.[51] He also concludes that, for each steel type, there exists a critical inclusion size. Oxide and sulfide inclusions larger than the critical
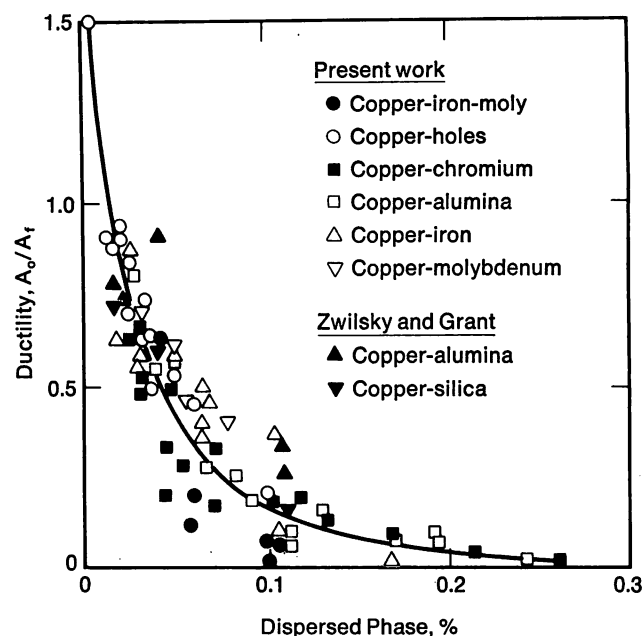


FIGURE 10—Tensile ductility of several copper dispersion alloys versus volume fraction of the dispersed phase.

size reduce steel ductility and toughness independent of inclusion size, composition or properties. Inclusions smaller than this critical size do not reduce ductility and toughness and may even result in strengthening, grain refinement, creep resistance, etc.

Experimental studies on steels confirm the hyperbolic dependence of ductility and toughness on volume fraction of inclusions over 1 $\mu$m in size. Results also show that both inclusions and carbides of about 5 nm or smaller do not participate in initial nucleation of ductile fracture although they may aid in extending ductile fracture by acting as secondary void nucleating sites.[52] In addition, experiments show that inclusion shape is an important variable. When inclusions become flattened and elongated in the longitudinal direction during the rolling process, the ductility and toughness of specimens oriented in the transverse and through-thickness direction is low compared to that of longitudinally oriented specimens.

Studies of the influence of microcleanliness on toughness in steel intensified at U.S. Steel during the development of high strength quenched-and-tempered plate steels for submarine hulls (HY130 and 10Ni-Cr-Mo-Co steel). These high strength steels required resistance to fracture under explosive shock loading and, as a result, required a level of toughness higher than that achievable with then conventional levels of nonmetallic inclusions. As seen in Figure 11, studies of the influence of sulfur content and oxygen content showed that the toughness followed the exponential form observed by Edelson and Baldwin. At levels over 0.015%, sulfur was found to control the notch toughness, and variations in oxygen content had little effect. At sulfur levels below 0.015%, variations

---

* Hereafter in this section, the term toughness or notch toughness will refer to the Charpy V-notch energy absorption in the region of ductile fracture, i.e., on the upper shelf of the Charpy V-notch energy versus testing temperature curve.
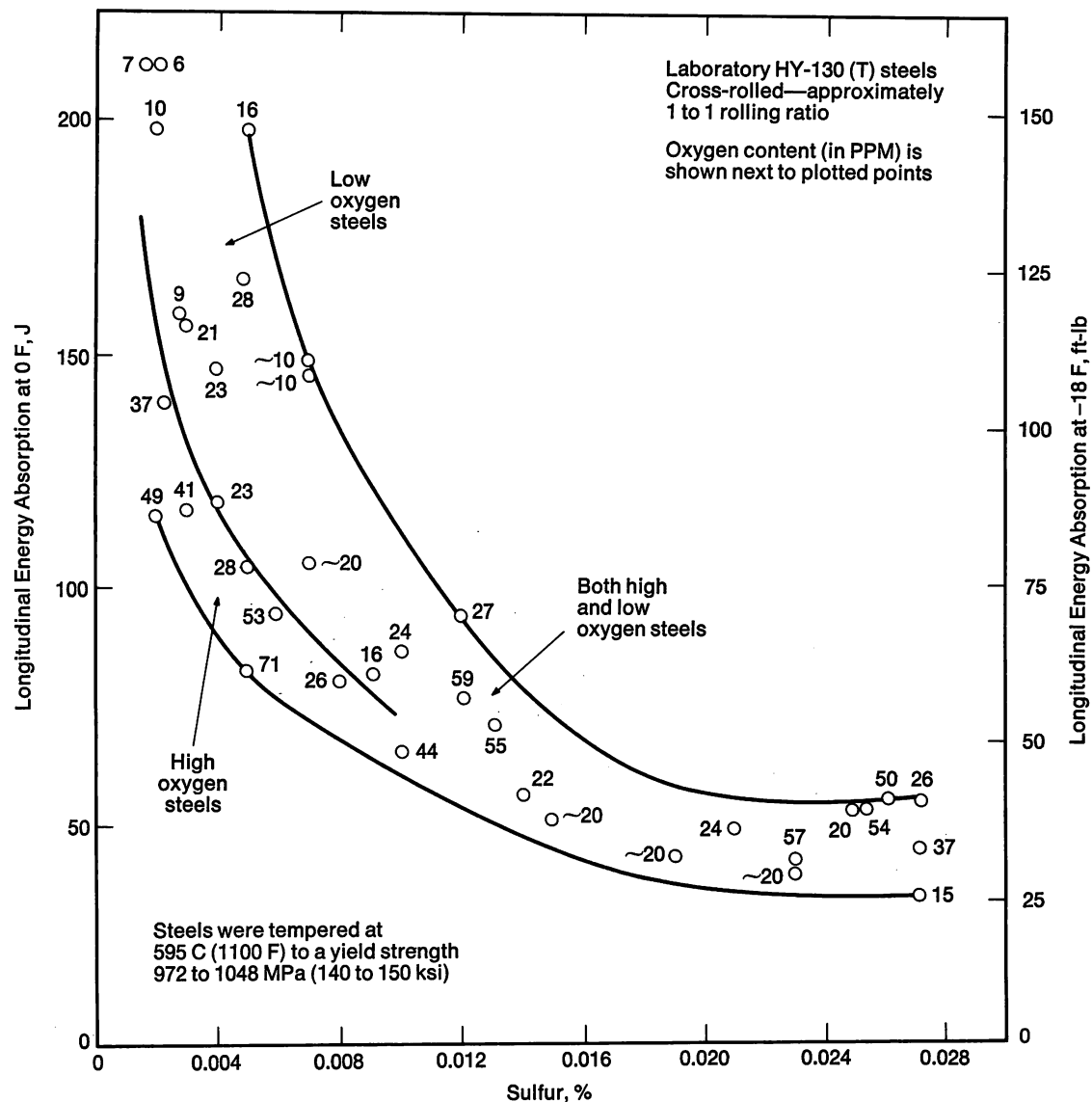
*FIGURE 11—Effect of sulfur and oxygen content on the shear energy absorption of 12.7 mm (0.5 in.) thick water-quenched-and-tempered plates.*

in oxygen content had a marked effect on toughness. For example at 0.002% sulfur, notch toughness can vary from 241 J (178 ft-lb) when oxygen content is 7 ppm to 116 J (85 ft-lb) when oxygen content increases to 49 ppm. These effects of sulfur and oxygen arise from void nucleation by manganese sulfides and alumina inclusions. Using these data, Gray & Wilson[53] showed (Figure 12) that, when sulfur and oxygen content is converted to the calculated volume fraction of sulfide and oxide inclusions, $CVN = 9.84\,V^{-0.75}$.

When interest in the development of Arctic grade linepipe intensified in the early 1970s, there was a need to know to what extent information on the effect of inclusion content on the notch toughness of high yield strength quenched-and-tempered steels could be applied to hot-rolled ferrite-pearlite steels of much lower strength. The effect of sulfur content on the notch toughness of several lower strength (241 to 483 MPa or 35 to 70 ksi yield

strength) carbon steels with and without niobium was determined. As indicated by the results in Figure 13, these lower strength hot-rolled steels exhibited the same general behavior as the high strength quenched-and-tempered steels, i.e., marked increase in notch toughness as sulfur level was reduced below about 0.015%. These steels also exhibited a smooth reduction in notch toughness as the strength of the steel increased (Figure 14). The increased strength was achieved either by increasing carbon content or increasing cooling rate after hot rolling. However, the strength/toughness relationship of these steels is not necessarily typical of production steels nor is it optimum. The 15 to 25 ppm oxygen achieved by laboratory vacuum-induction melting is lower than the oxygen contents of 30 to 70 ppm typical of production heats. The inclusions formed in 135 and 225 kg (300 and 500 lb) rapidly solidified laboratory ingots are small, and, because of the low reduction ratio in hot rolling the
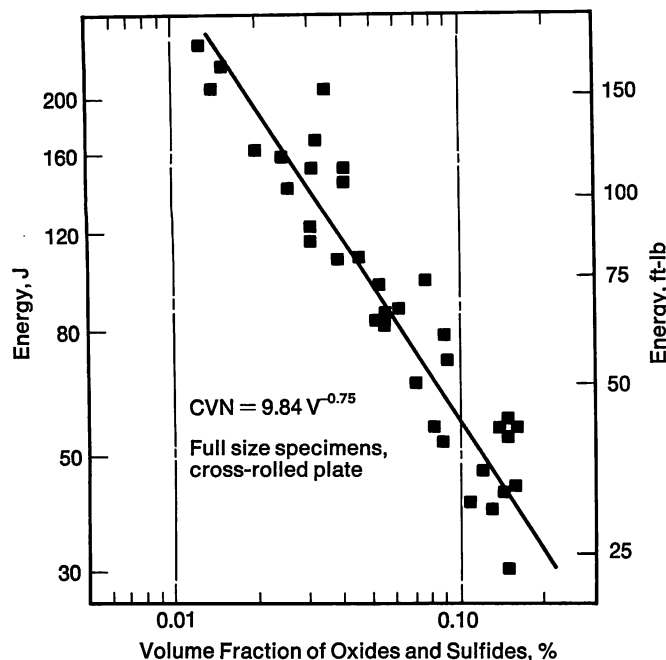
FIGURE 12—Relation between Charpy V-notch shelf energy and volume fraction of oxides and sulfides in 5Ni-Cr-Mo-V 896 MPa (130 ksi) quenched-and-tempered steel.

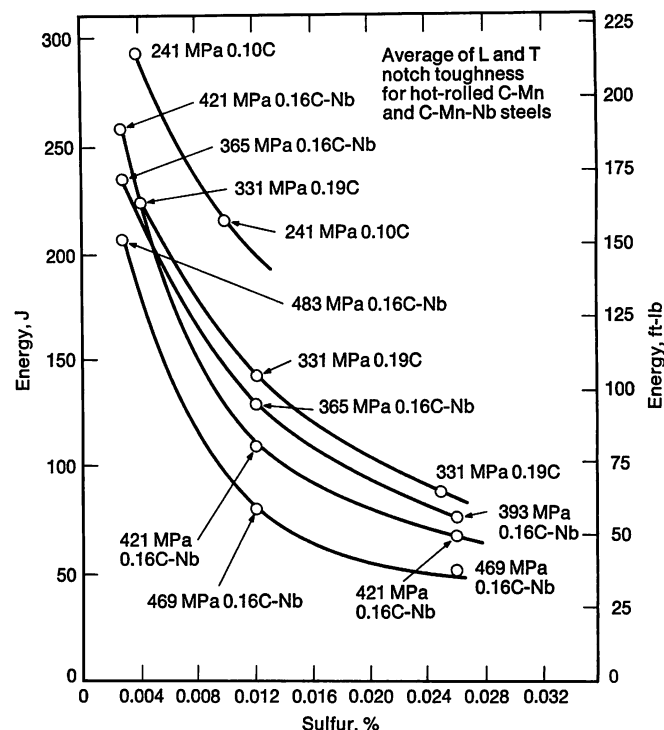CVN = 9.84 V^{-0.75}

Full size specimens, cross-rolled plate



FIGURE 13—Relation between Charpy V-notch shelf energy and sulfur content for 241 to 483 MPa (35 to 70 ksi) C-Mn-Nb hot-rolled steels.
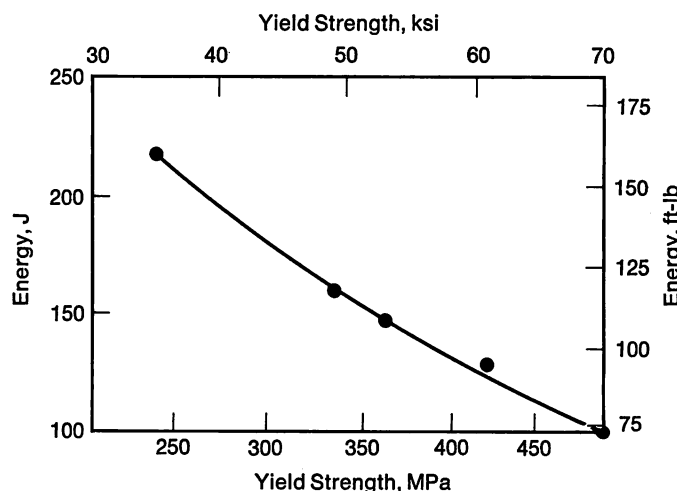


FIGURE 14—Relation between Charpy V-notch shelf energy at 0.010% sulfur and yield strength for C-Mn and C-Mn-Nb hot-rolled steels.

ingot to plate, the extent to which inclusions are elongated or stringered is low compared to production plates. These factors increase the toughness of laboratory steels over that obtained in production steels. The development of optimum linepipe compositions and controlled rolling schedules results in steels with low carbon contents (typically 0.08%) and very fine grain sizes as described earlier. Steels with this optimized structure have higher toughness at a given level of sulfur and oxygen than the higher carbon hot-rolled steels. The net effect is that improvements in microstructure are counterbalanced by reductions in microcleanliness so that the results shown in Figures 13 and 14 are quite typical of what might be expected in production steels for Arctic linepipe.

**Inclusion Stringering and the Influence of Cross Rolling.** The information presented above establishes the need to reduce the volume fraction of nonmetallic inclusions to a minimum in Arctic grade linepipe steels. However, this is not the only consideration. The tendency for inclusions to form in clusters and to elongate as stringers, as mentioned earlier, is also an important consideration. High strength linepipe steels are aluminum killed to minimize oxide formation. As a result, the manganese sulfide inclusions formed in the ingot are the Type II inclusions described by Sims.[54] Type II sulfides precipitate as a eutectic at the end of the solidification process and thus form as clusters at austenite grain intersections and along austenite grain boundaries in the cast structure. Moreover, Type II inclusions are readily deformable at hot-rolling temperatures. As a result, clusters of highly elongated and flattened inclusions are formed in the plate.[55] Likewise, alumina inclusions precipitate from

liquid steel in the form of dendritic clusters, and, although the individual inclusions do not deform at hot-rolling-temperatures, the clusters form stringers in the plate.

Clustering and elongation or stringering of nonmetallic inclusions markedly influence the anisotropy of ductility and notch toughness in plate steels. Accordingly, generalizations which suggest that the volume fraction of the larger nonmetallic inclusions is the only inclusion variable influencing ductility and notch toughness require modification. Baker and Charles[56] show that the

effect of inclusion shape can be rationalized by using the projected length of inclusions per unit area to comprehend the effect of both volume fraction and inclusion shape on fracture toughness as measured by crack opening displacement. A similar parameter is the area fraction of inclusions parallel to the direction in which the crack is running. Clustering of inclusions also affects ductility and notch toughness. However, the influence of clustering, which has been shown to be particularly detrimental to through-thickness ductility, is only now beginning to be quantitatively studied in any detail.

At U.S. Steel, the effect of longitudinal-to-transverse rolling ratio on the notch toughness of silicon-aluminum killed C-Mn plate steels has been studied. The results show that, by cross rolling plates so that the longitudinal-to-transverse rolling ratio is 1 to 0.75 (depending on sulfur content), anisotropy in notch toughness can be eliminated. Cross rolling lowers the longitudinal toughness to the same extent that it raises the transverse toughness so that the resulting CVN shelf energy of the cross-rolled plate is the average of longitudinal and transverse toughness in the straightaway rolled plate.

The influence of sulfur content on the shelf energy of cross-rolled (L/T = 1) and straightaway rolled 13 mm (½ in.) thick plates is shown in Figure 15, and the influence of both sulfur content and rolling ratio on anisotropy in notch toughness is shown in Figure 16. At sulfur levels of 0.004%, anisotropy is reduced from that observed for 0.012 and 0.025% S but is still present to some extent. The study also showed that elimination of pearlite banding by a short time debanding heat treatment at 1330 C (2425 F) improved the level of notch toughness but did

not change the degree of anisotropy.

In another laboratory study, the effect of sulfur content and cross rolling (L/T = 1 versus straightaway rolling) on reduction of area in longitudinal, transverse and through thickness specimens was determined. As shown in Figure 17, the results were similar to those for notch toughness. The most significant result was the very marked reduction in through-thickness ductility with increasing sulfur content and the not unexpected insensitivity of through-thickness ductility to cross-rolling ratio.

**Inclusion Shape Control.** Cross-rolling studies show that rolling ratios of from 0.75 to 1.0 are required to optimize transverse notch toughness. Because of length and width requirements for plates to be used in forming linepipe, cross-rolling ratios in the range of 0.75 to 1.0 are not practical (cross-rolling ratios for production plates rolled from continuously-cast slabs are generally in the range of 2.0 to 3.0 for plates spread to width and then rolled straightaway and 4.0 to 7.0 for plate rolled to width and then turned and cross-rolled to length). Moreover, if flattened and elongated nonmetallic inclusions could be avoided and clustering of sulfides and oxides reduced, the through thickness ductility and notch toughness could be increased and, as a result, the resistance of linepipe plates to hydrogen sulfide cracking increased. The above considerations dictate the need for additional research and development to optimize transverse notch toughness, i.e., the development of effective methods of sulfide shape control. Several elements are capable of converting the Type II manganese sulfides to alloy sulfides which are compact and do not deform readily during hot rolling. Additions such as zirconium, rare earths and calcium have been used to control sulfide shape in steel. Zirconium is effective when its use is properly controlled, but this element has the disadvantage that it also has a strong affinity for carbon, nitrogen and oxygen, forming carbides, nitrides and oxides detrimental to toughness. These detrimental inclusions (particularly carbonitrides in steels of high nitrogen content) partially offset the benefits of forming hard sulfides which can improve transverse notch toughness. Moreover, zirconium is not effective in reducing the sulfur content of the steel. In contrast, rare earths and calcium are effective not only in controlling the sulfide shape but also in reducing sulfur content.

Rare earths have the potential of markedly improving transverse and through-thickness ductility and notch toughness, but, like zirconium, their use also requires careful control. Steelmaking practices are complicated by the very strong affinity of rare earths for oxygen, by the low difference in density between rare earth sulfides and molten steel, which hampers desulfurization resulting from separation of the sulfides formed at steelmaking temperatures from the molten steel, and by the need to provide stirring or agitation to the steel when rare earths are added to assure thorough mixing. The use of rare
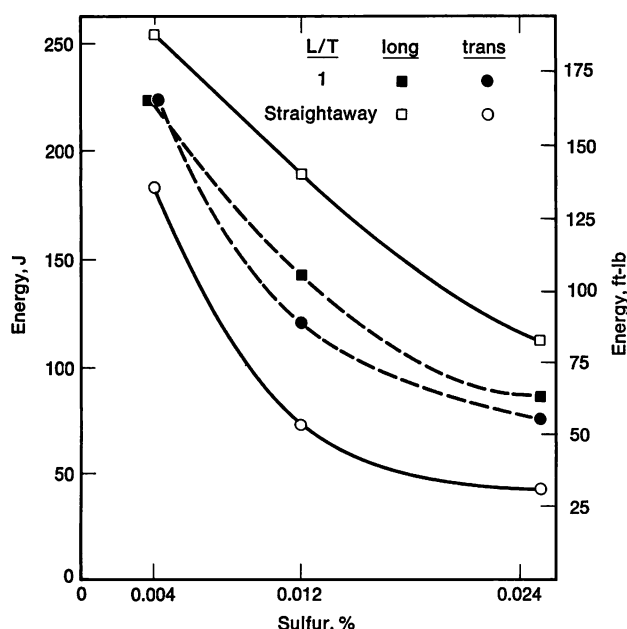


FIGURE 15—Effect of sulfur content on Charpy V-notch shelf energy absorption in silicon-aluminum killed 0.19C-1.2Mn hot-rolled steel.
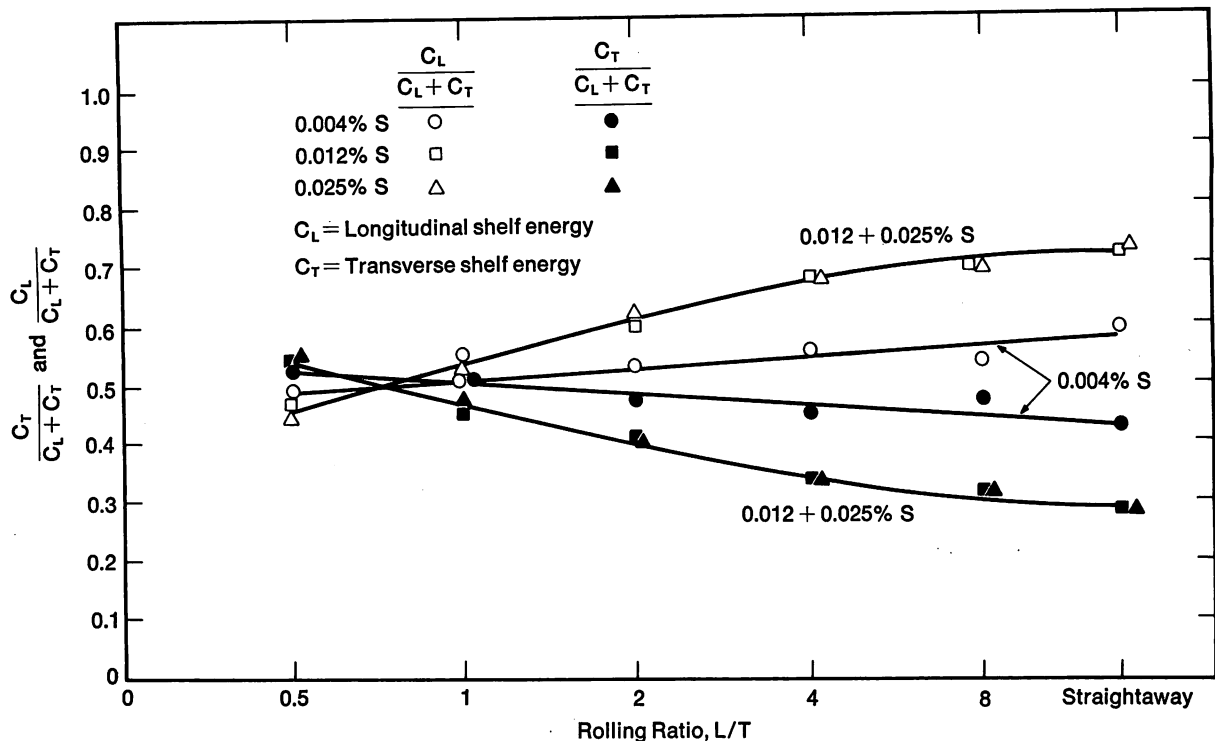
FIGURE 16—Effect of longitudinal-to-transverse rolling ratio on toughness anisotropy of silicon-aluminum killed 0.19C-1.2Mn hot-rolled steels.

earths for desulfurization and sulfide shape control has been extensively studied in recent years; these studies are summarized in a recent review by Waudby.[57] The problem of substantial segregation of rare earth sulfides and oxysulfides to the bottom of the ingot and the resulting occurrence of low toughness in plates from bottom cuts has been studied by Sanbongi.[58] Independent studies at U.S. Steel on the development of rare earth addition practices for sulfide shape control generally substantiate results summarized by Waudby and Sanbongi. For compact rare earth oxysulfide inclusions that are uniformly distributed in the ingot and do not form stringers during hot rolling of the plate, the sulfur content of the steel at the time of addition should not be in excess of 0.012%, and the rare earth/sulfur ratio should be 3/1. In addition, the steel must be thoroughly deoxidized with aluminum before the rare earth addition, reoxidation of the rare earth treated steel from refractories or air must be minimized, and the rare earth must be well mixed with the steel at the time of addition. When the addition is properly made, the sulfur content of the steel will be reduced (the sulfur content of the rare earth treated steel will be 0.003 to 0.005% lower than that of the steel before treatment), and rare earth sulfides or oxysulfides that do not deform on hot rolling will be formed.

The rare earth treatment of a straightaway-rolled 0.1 C-Mn steel with a yield strength of 235 MPa (34 ksi) raised the through-thickness notch toughness from 43 to 170 J (36 to 125 ft-lb) and the transverse notch toughness from 133 to 243 J (102 to 183 ft-lb) but had little or no
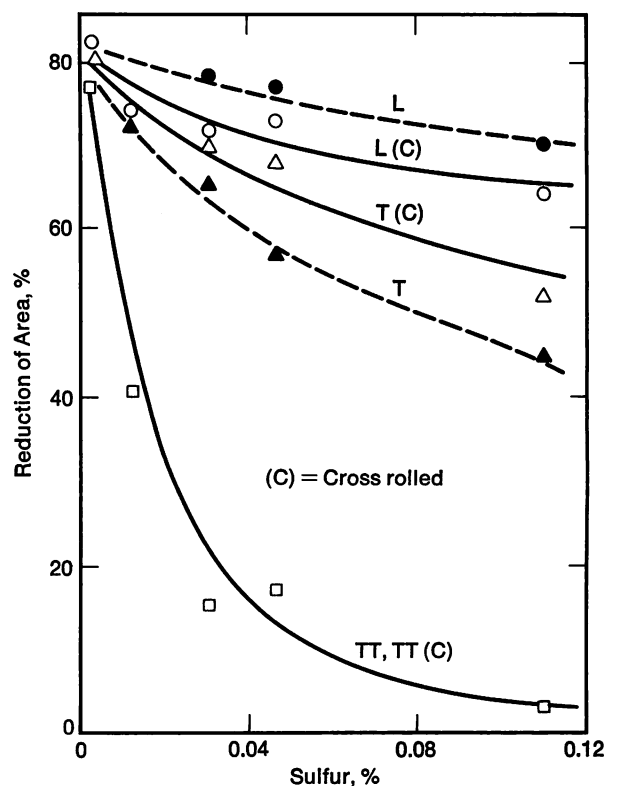


FIGURE 17—Effect of sulfur content on reduction of area in straightaway and cross-rolled (rolling ratio = 1) Mn-Nb steels.
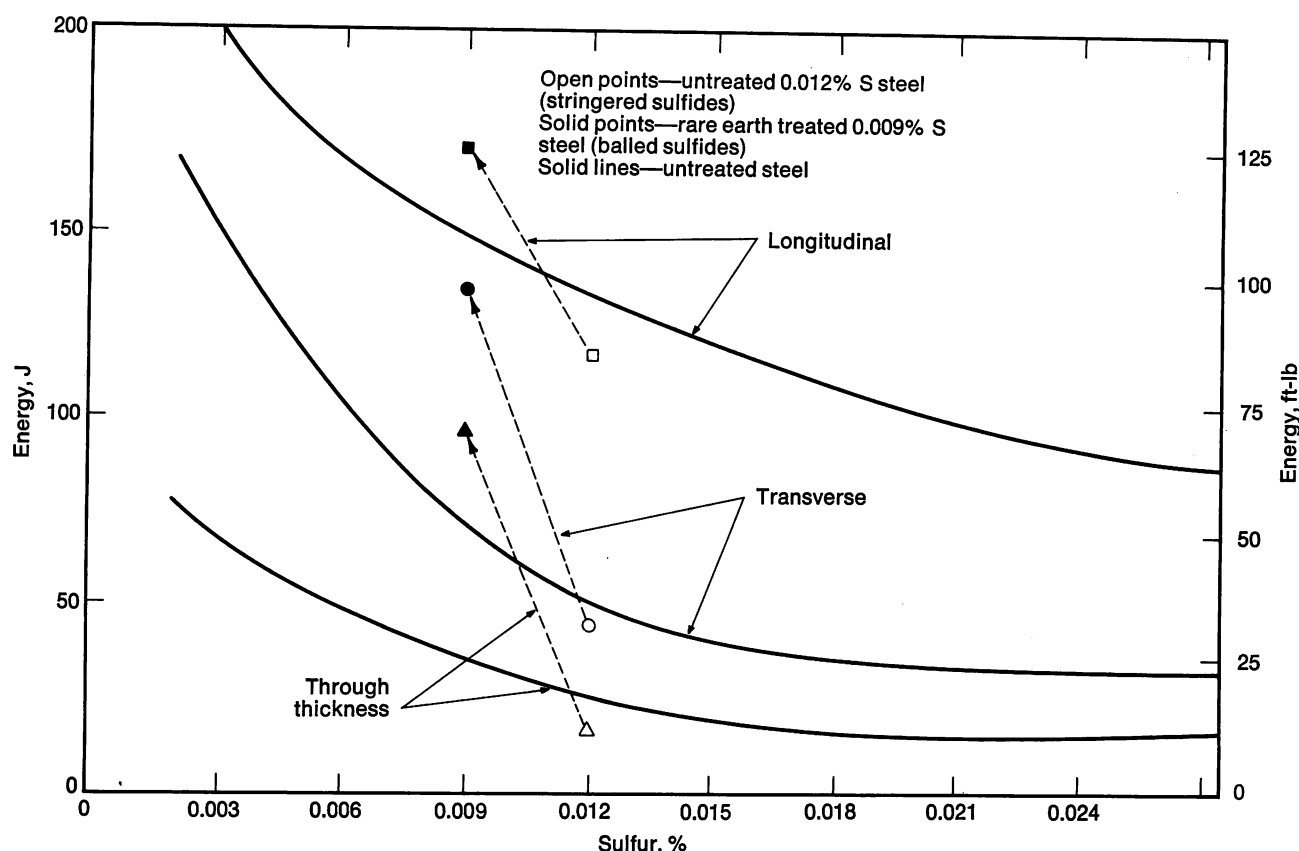
FIGURE 18—*Effect of sulfur content and rare earth treatment on the shelf energy of straightaway-rolled carbon steel plate.*

effect on longitudinal notch toughness or ductile-to-brittle transition temperature. Similar effects are shown for high strength low alloy 0.19 C-Mn line pipe steel in Figure 18. Note that the rare earth treatment reduced the sulfur from 0.012 to 0.009%, and the resulting steel had notch toughness similar to that achieved at sulfur contents of 0.004% without rare earth treatment. Figure 19 shows the appearance of sulfides present in longitudinal views (500 X) in the above mentioned steel without rare earth treatment and with rare earth treatment.

The use of calcium for desulfurization and sulfide shape control has several advantages over zirconium or rare earths. A major advantage is that calcium treatments can readily reduce sulfur contents from levels of 0.020% to below 0.003%. Moreover, the remaining sulfides, which consist of calcium aluminate particles surrounded by a layer of calcium sulfide, are not elongated on subsequent hot rolling. The formation of calcium aluminate is also an advantage because this eliminates the dendritic alumina $(Al_2O_3)$ inclusions that are responsible for clusters and stringers of angular inclusions in plate steels. Such clusters and stringers contribute to low transverse and through-thickness ductility and toughness.[59] Finally, because calcium sulfide and calcium aluminate are of much lower density than rare earth sulfides, they separate more readily from the steel, and the problem of bottom segregation of sulfides and oxides in ingots is much

reduced.

The major disadvantage of calcium is its very low solubility in molten steel and its high vapor pressure at steelmaking temperatures (162 kPa, 23 psi). When calcium is plunged into steel, the reaction is violent. It quickly vaporizes, leaves the melt and burns in air. The short contact time between calcium and molten steel wastes calcium and does not allow chemical reactions to go to completion. To slow down the reaction and improve the efficiency of calcium as a desulfurizer, calcium is usually added as CaSi or more complex ferroalloys such as CaBaSiAl to lower the fugacity. Saxena and Engh[60] claim that these complex ferroalloys are inefficient because of vaporization and escape of calcium from the bath. They suggest that injection of powdered $CaO\text{-}CaF_2$ provides the desired desulfurization, results in the formation of calcium aluminate and produces sufficient calcium dissolved in the steel to provide for the formation of CaS on cooling of the molten steel during solidification.

The advantages of calcium as a desulfurizer and sulfide shape control agent would appear to outweigh its disadvantages and, where injection equipment is available, make it a preferred addition over rare earths. At U.S. Steel, calcium injection using the Thyssen Niederrhein (TN) process[61] is preferred and has been adopted

a. Base composition, 0.013% sulfur.    (500 X)
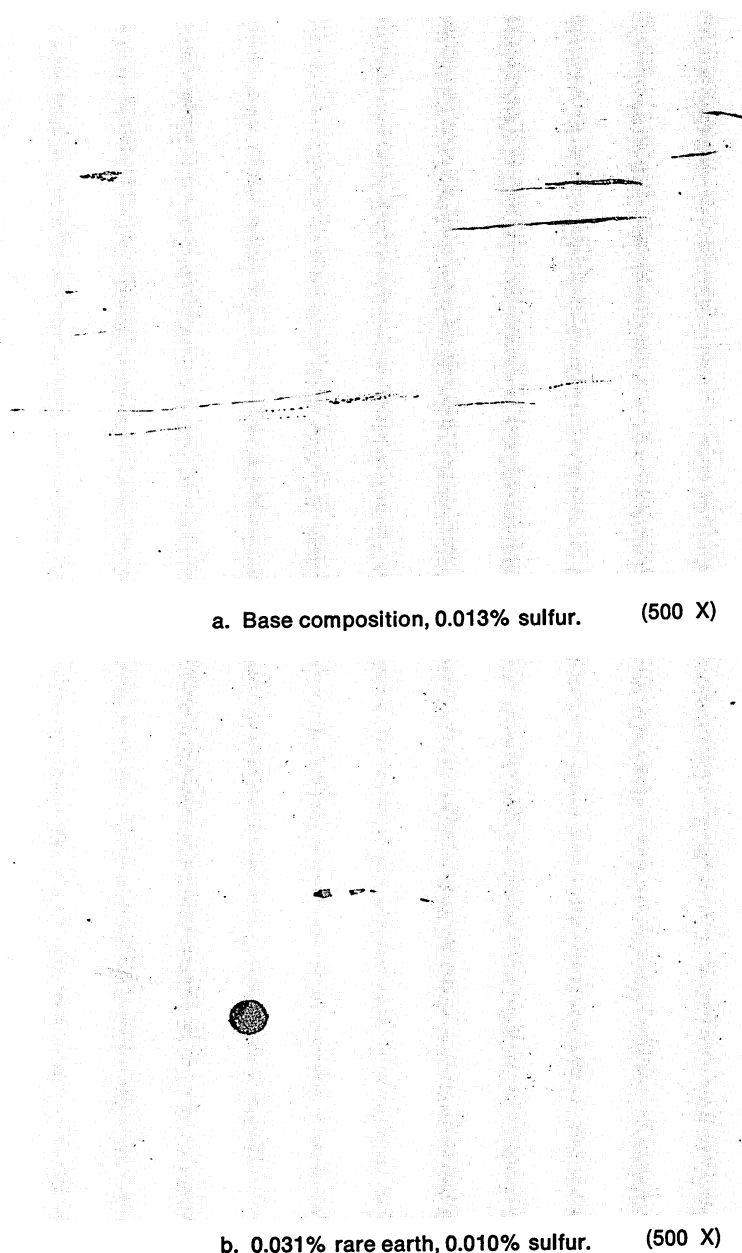
b. 0.031% rare earth, 0.010% sulfur.    (500 X)

*FIGURE 19—Typical inclusion morphologies in straight-away-rolled C-Mn-Cb steels. Longitudinal view. Unetched. (500 X)*

for linepipe steels at the Texas Works. When properly controlled, this process is capable of producing plate steels with sulfur levels below 0.004%. These steels have the added advantages that the few inclusions observed are globular and that the steel is free of clustered alumina particles. This provides high and uniform levels of notch toughness in plate with very little anisotropy even when they are controlled rolled with rolling ratios as high as 7.0.

## Welding Studies

In the welding of linepipe, two areas that must be considered are (1) the longitudinal seam weld that is used to join the long edges of the formed plate into a cylinder,

which is commonly done by multiwire submerged arc welding (SAW) with a single pass from each side, and (2) circumferential or girth welding to join the pipes together in the field, which is commonly done by multipass shielded metal arc welding (SMAW) although gas metal arc welding (GMAW) is also being used.

**Seam Welding.** Because the longitudinal seam weld in linepipe is usually made by two-pass SAW, a high energy input process, this weld cooling rate is lower than that of the girth weld; thus high heat affected zone (HAZ) hardness or hydrogen-induced cold cracking are seldom a problem. The SAW process is considered a low hydrogen welding process, and hydrogen is introduced only if the consumables or plate edges become contaminated with moisture or foreign material.

Most specifications for Arctic grade linepipe state that the pipe shall meet the requirements of API 5LX[62] plus additional requirements. 5LX specifies such factors as dimensional tolerances, weld shape, weld soundness and tensile and bend properties. The additional requirements usually restrict the 5LX requirements with respect to weld soundness and impose additional mechanical property requirements, particularly minimum notch toughness and maximum hardness of the weld metal and HAZ. Most specifications impose a maximum hardness of HV 260 in the weld metal and HAZ. Specified minimum average CVN energy absorption values for the weld metal and HAZ have varied from 54 J at −25 C (40 ft-lb at −13 F) in an early specification[63] to 95 J at −18 C (70 ft-lb at 0 F) in a more recent specification.[47] Because of the low carbon content of the plate, the hardness and toughness requirements of the HAZ have not been difficult to meet. However, the electrodes and fluxes traditionally used for the seam welding of linepipe were not suitable for obtaining the higher notch toughness required in the weld metal.

In a typical linepipe seam weld, the weld bead is comprised of about ⅔ fused base metal and about ⅓ fused electrode. Thus, the concentration of the less reactive elements in the weld bead can be expressed by the relation:

$$M_w = \frac{1}{3} M_e + \frac{2}{3} M_p$$

where $M_w$, $M_e$ and $M_p$ are the concentrations of the element in the weld, the electrode and the plate, respectively. The results of laboratory investigations indicate that this relationship is reasonably valid for such elements as Cu, Ni, Cr, Mo and Nb. However, the concentrations of the more reactive elements, such as C, Mn, P, S, Si, Al, N and O, are dependent on both their initial concentrations and the chemical reactions that occur during welding.

The microstructure of the weld metal, and thus its notch toughness, is determined by the cooling rate after welding and by the chemical composition, which affects both the microstructure and the amount of nonmetallic
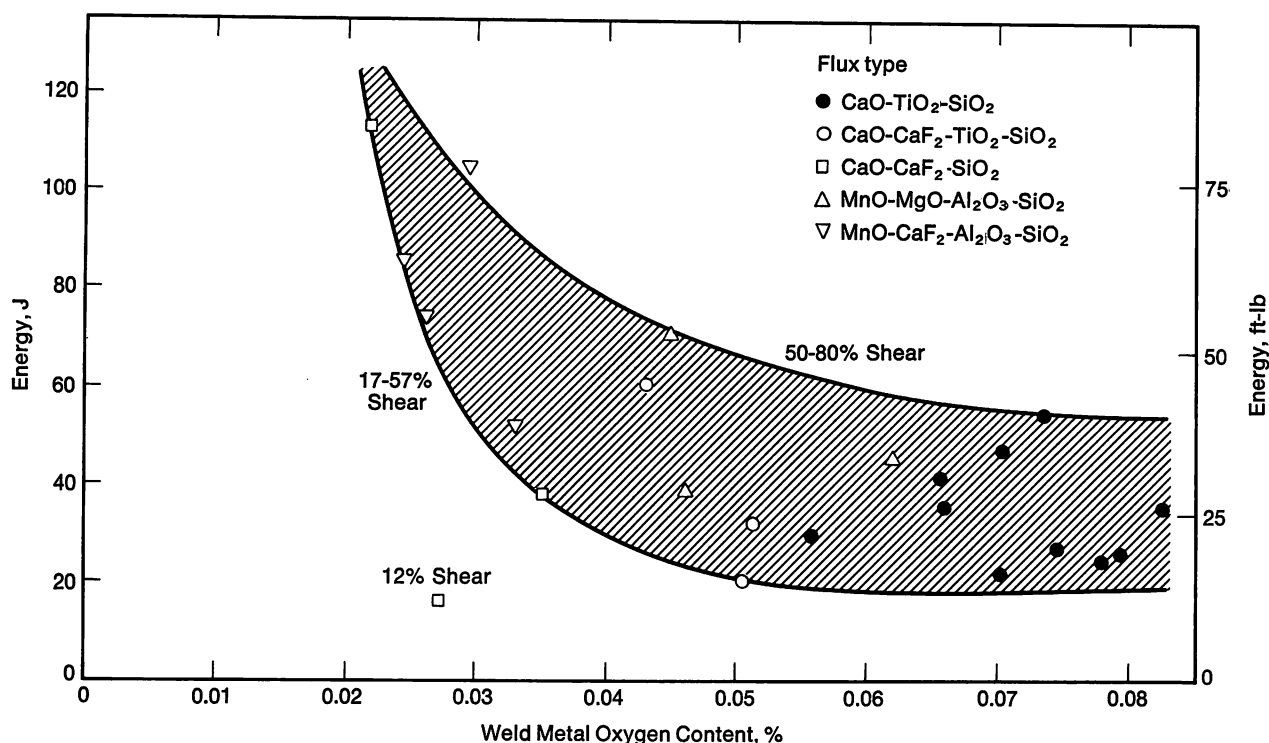
*FIGURE 20—Effect of oxygen content on notch toughness of submerged arc weld metals at −25 C (−13 F).*

inclusions. It is desirable to have a weld metal with a low volume fraction of inclusions to maximize the shelf energy absorption, and with a matrix of fine, interlocking acicular ferrite to improve the cleavage resistance and thus lower the transition temperature.[64] The presence of proeutectoid ferrite segregated on prior austenite grain boundaries should be avoided, as well as pearlite, upper bainite and clusters of coarse, blocky lath martensite because they provide paths of easy crack propagation. Excessive hardness due to solid solution strengthening or precipitation hardening should also be avoided because of the tradeoff of toughness for strength.[64]

The inclusion content of weld metal, which is related to the oxygen content, affects the shelf energy. This effect is apparent in Figure 20, in which the energy absorption of several submerged arc weld metals is plotted as a function of oxygen content. Although the weld metals were not on the upper shelf, the effect of lower oxygen content in improving notch toughness is apparent.

In general, the oxygen content of the weld metal is lowered by increasing flux basicity as defined by the formula:

$$B = \frac{CaO + MgO + CaF_2 + \frac{1}{2}(MnO + FeO)}{SiO_2 + \frac{1}{2}(Al_2O_3 + TiO_2 + ZrO_2)}$$

Fluxes in which B is less than 1 are considered acidic, fluxes with B between 1 and 1.5 are considered neutral, and fluxes with B greater than 1.5 are considered basic.

The most commonly used flux for SAW linepipe in the U.S. is a fused, acid calcium-titanium silicate flux

because of its good operating characteristics, good resulting weld bead appearance and soundness, and good recycling ability. (It can be reused repeatedly without flux particle breakdown or moisture pickup.) Because of the acidic nature of this flux, it results in a weld metal oxygen content of about 600 to 800 ppm. The oxygen is present primarily in the form of manganese silicate inclusions which lower the shelf energy absorption.

The most commonly used electrodes for seam welding are AWS EM-12K (1% Mn, 0.2% Si) or EH-14 (2% Mn). These electrodes result in weld metal relatively lean in alloy content and thus of low hardenability. The microstructures show significant amounts of proeutectoid ferrite on the prior austenite grain boundaries and coarse ferrite platelets resembling upper bainite. A typical microstructure of weld metal in a low C, Mn-Mo-Nb linepipe steel made with an acidic calcium-titanium silicate flux and EM-12K electrode is shown in Figure 21a. This weld metal exhibited only 24 J CVN energy absorption at −25 C (18 ft-lb at −13 F).

The cleavage resistance of weld metal can be improved by additions of manganese, nickel and molybdenum which act to increase the proportion of fine, interlocking acicular ferrite.[64] Such a microstructure is shown in Figure 21b, in which an electrode containing 2.3% manganese, 0.9% nickel and 0.5% molybdenum (AWS EF 3) was used with the same steel and flux. The energy absorption of this weld metal was 54 J at −25 C (40 ft-lb at −13 F), which was a modest improvement as compared to the EM-12K electrode, but still not sufficient to
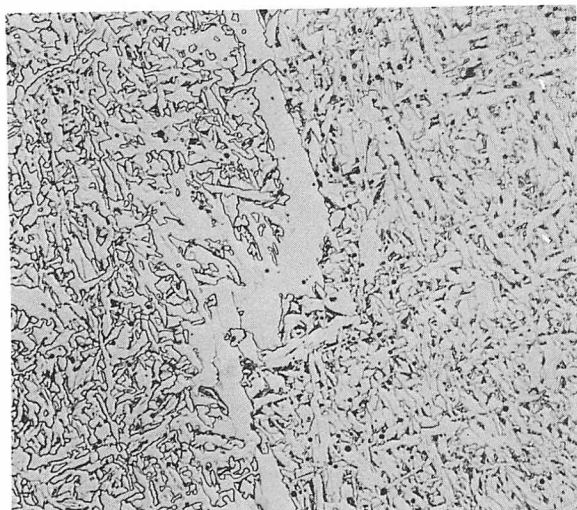
a. C-Mn electrode with acidic flux. 24 J (18 ft-lb) CVN energy at –25 C (–13 F).
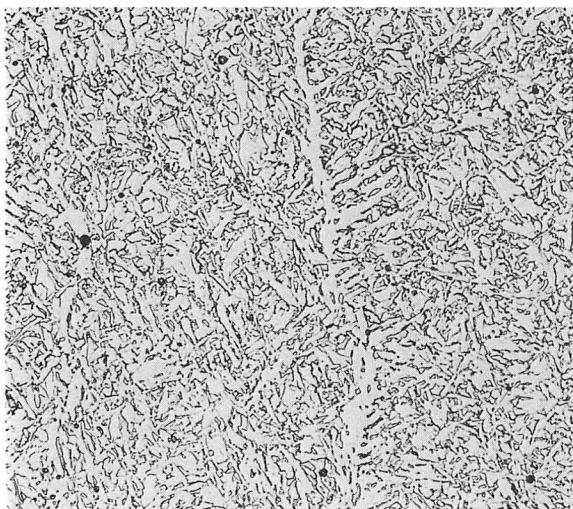


b. Mn-Ni-Mo electrode with acidic flux. 54 J (40 ft-lb) CVN energy at –25 C (–13 F).
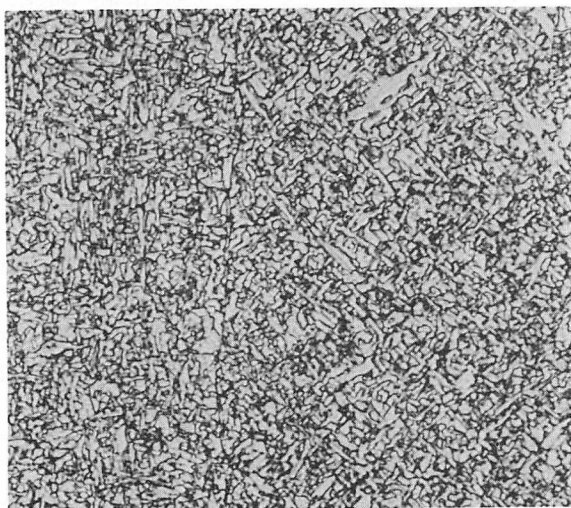


c. Mn-Mo-Ti-B electrode with basic flux. 217 J (160 ft-lb) CVN energy at –18 C (0 F).

FIGURE 21—Typical microstructures in SAW metal in low C, Mn-Mo-Nb linepipe steel. Nital etchant.

meet the 95 J at –18 C (70 ft-lb at 0 F) required in the most recent specification. The improvement in notch toughness given by this microstructure is partially offset by the high inclusion content of the weld metal from the acidic flux and solid solution strengthening from the relatively high alloy content.

The failure to attain sufficiently high toughness levels with conventional alloy electrodes and fluxes spurred several new developments in welding consumables for linepipe. One manufacturer developed an agglomerated $MnO-SiO_2-Al_2O_3$ flux, also known as an alumina-basic flux, resulting in lower levels of oxygen in the weld metal (about 300 ppm) and also in added manganese to the deposit. The amount of acicular ferrite was increased, which improved cleavage resistance. When used with an AWS EM-12K electrode on low C, Mn-Mo-Nb steel, this flux resulted in about 81 J CVN at –18 C (60 ft-lb at 0 F). However, because of the high weld metal manganese content and admixture of other alloys from the plate, the hardness of the weld metal often approached or exceeded the specified HV 260 maximum, depending on the amount of alloy in the plate.

Another manufacturer modified fused acidic flux to produce a weld metal with a lower oxygen content (300 to 500 ppm) and recommended the use of either of two high silicon electrodes, depending on plate alloy content: 1.8% Mn—0.65% Si—0.5% Mo and 1.6% Mn—1.0% Si, which are classified as AWS E708-G and E708-6, respectively. According to their theory, silicon promotes a thin vein of proeutectoid ferrite on the prior austenite grain boundaries which prevents nucleation of brittle lath type constituents, and, as a result, the remaining matrix transforms to acicular ferrite. CVN values of about 54 to 108 J at –18 F (40 to 80 ft-lb at 0 F) have been attained with these electrode/flux combinations. Because the flux is fused acidic, it performs well in production, and this electrode/flux combination has been used extensively for commercial linepipe production orders having moderate CVN requirements, e.g., 47 J at 0 C (35 ft-lb at 32 F). However, the HV 260 maximum can be approached or exceeded when these electrodes are used on plates with high alloy content.

To obtain the optimum weld metal microstructure (acicular ferrite with little or no proeutectoid ferrite) at low hardness, a new electrode has been developed.[64] This electrode contains nominally 1.3% Mn, 0.3% Mo, 0.02% Al, 0.03% Ti and 0.004% B. The electrode contains aluminum and titanium to minimize the loss of boron by formation of oxides or nitrides during welding, thereby inhibiting its effectiveness in retarding formation of proeutectoid ferrite. In addition, the electrode should be used with a basic flux to maintain a low oxygen potential in the weld pool. This electrode was designed to provide a weld metal with hardenability sufficient to produce the desired acicular ferrite microstructure at a low alloy content with a correspondingly low weld metal hardness.

Such a microstructure is shown in Figure 21c. When used with a fully basic flux and low C, Mn-Mo-Nb plate, CVN values of 217 J at −18 C (160 ft-lb at 0 F) were attained. However, the basic flux is agglomerated, which could result in potential problems with moisture absorption or flux particle breakdown during recycling. In addition, the weld bead appearance was not as good as that obtainable with fused acidic fluxes.

Limited studies have shown that the Mn-Mo-Ti-B electrode could be used with other fluxes that may be more suitable for use under pipe mill operating conditions. When used with an agglomerated alumina basic flux, a fused neutral flux and a fused basic flux, CVN values of 127, 122 and 161 J at −18 C (94, 90 and 119 ft-lb at 0 F), respectively, were obtained. Although these values are lower than attainable with the agglomerated fully basic flux, they readily meet the 95 J (70 ft-lb) minimum specified for Arctic grade linepipe.

**Girth Welding.** Because girth welding is usually a multipass process, the chemical composition and thus mechanical properties of the deposited weld metal are determined essentially by the electrode composition and welding technique. Electrode manufacturers have been developing new or improved electrodes to meet the mechanical property requirements of girth welds in pipe lines for Arctic service.

The mechanical properties of the HAZ are determined by the plate composition and the cooling rate after welding. Because field girth welding is a relatively low energy input process, the HAZ cooling rate in heavy wall pipe can be quite high. This can result in low temperature transformation products (martensite and bainite) with high hardness, low toughness and increased susceptibility to hydrogen-induced cracking. The most common method of field girth welding of linepipe is SMAW with cellulose-covered electrodes, which introduce a substantial amount of hydrogen into the weld region thus increasing the danger of hydrogen-induced cold cracking. However, the steels being developed for Arctic or other high toughness applications are very low in carbon content which is beneficial in terms of HAZ hardness, toughness and cracking susceptibility. In addition, preheating of the pipes during girth welding, which lowers

the weld cooling rate, is often used in critical applications. Thus, in practice few problems have been encountered in girth welding of Arctic grade pipe lines.

However, pipe line designers are attempting to ensure good field weldability of the steel by specifying a maximum carbon equivalent (C.E.).[47,63,65] For example, two recent specifications[63,65] for Arctic grade linepipe proposed a maximum C.E. value of 0.40 based on the formula:

$$C.E. = C + \frac{Mn}{6} + \frac{Cr + Mo + V}{5} + \frac{Ni + Cu}{15}$$

U.S. Steel's low C, Mn-Mo-Nb steel compositions with typical electric furnace levels of residual elements may have C.E. values that exceed 0.40, depending on the specified strength and pipe wall thickness. However, such specifications generally indicate that linepipe with C.E. values somewhat higher than 0.40 would be acceptable if satisfactory field weldability can be demonstrated.

Another method of evaluating weld cracking susceptibility is the cracking parameter, $P_{cm}$,[66] which is based on the formula:

$$P_{cm} = C + \frac{Si}{30} + \frac{Mn + Cu + Cr}{20} + \frac{Ni}{60} + \frac{Mo}{15} + \frac{V}{10} + 5B$$

A program was conducted to evaluate the weldability of six Arctic grade linepipe steels from recent heats produced at the Texas Works. The conventional underbead cracking test[67] was performed, which is a measure of the relative susceptibility of the steel to weld HAZ cracking. In addition, simulated girth welds were made in plate samples, and mechanical properties were obtained.

The chemical compositions of the six steels investigated are shown in Table I. All were low carbon Mn-Mo-Nb steels, with the heaviest plate thicknesses, 20 mm (0.79 in.), containing purposeful additions of chromium. Two indices of weld cracking susceptibility, the carbon equivalent (C.E.) and the cracking parameter ($P_{cm}$), were calculated from the chemical composition and are shown in Table II.

**Underbead Cracking Tests.** The variations in maximum underbead cracking with carbon content, C.E. and

**Table I**—Chemical Composition of Linepipe Steels Investigated

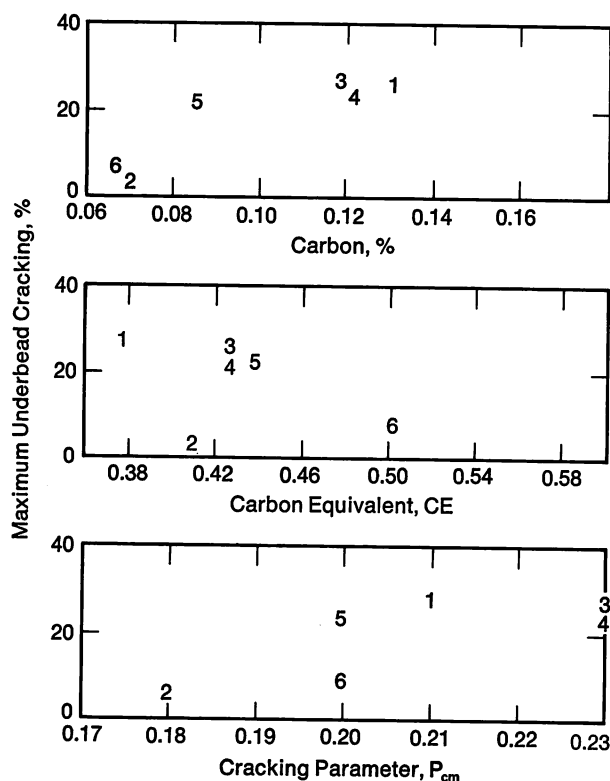| Steel No. | Plate Thickness, mm (in.) | Element, % | | | | | | | | | | |
|-----------|---------------------------|------|------|-------|-------|------|------|------|------|------|-------|-------|
| | | C | Mn | P | S | Si | Cu | Ni | Cr | Mo | Nb | Al* |
| 1 | 16 (0.63) | 0.13 | 1.24 | 0.002 | 0.012 | 0.22 | 0.08 | 0.03 | 0.06 | 0.05 | 0.035 | 0.023 |
| 2 | 19 (0.75) | 0.07 | 1.52 | 0.007 | 0.003 | 0.24 | 0.08 | 0.03 | 0.08 | 0.31 | 0.046 | 0.024 |
| 3 | 19 (0.75) | 0.12 | 1.35 | 0.009 | 0.004 | 0.22 | 0.10 | 0.04 | 0.08 | 0.32 | 0.049 | 0.021 |
| 4 | 19 (0.75) | 0.12 | 1.32 | 0.005 | 0.005 | 0.24 | 0.12 | 0.07 | 0.11 | 0.30 | 0.047 | 0.023 |
| 5 | 20 (0.79) | 0.09 | 1.42 | 0.011 | 0.006 | 0.24 | 0.10 | 0.04 | 0.26 | 0.27 | 0.057 | 0.020 |
| 6 | 20 (0.79) | 0.07 | 1.46 | 0.008 | 0.005 | 0.22 | 0.11 | 0.05 | 0.53 | 0.36 | 0.052 | 0.021 |

* Total aluminum.

**Table II**—Carbon Equivalents and Cracking Parameters of Steels Investigated

| Steel No. | Carbon Content, % | Carbon Equivalent, C.E.[a] | Cracking Parameter, $P_{cm}$[b] |
|---|---|---|---|
| 1 | 0.13 | 0.37 | 0.21 |
| 2 | 0.07 | 0.41 | 0.18 |
| 3 | 0.12 | 0.43 | 0.23 |
| 4 | 0.12 | 0.43 | 0.23 |
| 5 | 0.09 | 0.44 | 0.20 |
| 6 | 0.07 | 0.50 | 0.20 |

$$^a \text{C.E.} = C + \frac{Mn}{6} + \frac{Cr + Mo + V}{5} + \frac{Ni + Cu}{15}$$

$$^b P_{cm} = C + \frac{Si}{30} + \frac{Mn + Cu + Cr}{20} + \frac{Ni}{60} + \frac{Mo}{15} + \frac{V}{10} + 5B$$

**Table III**—Results of Transverse Weld Tension Tests on Simulated Field Girth Welds

| Steel No. | Tensile Strength, MPa (ksi) | Fracture Location |
|---|---|---|
| 2 | 566 (82.2) | Base metal |
|   | 557 (80.9) | Base metal |
|   | 565 (82.0) | Base metal |
|   | 566 (82.1) | Base metal |
| 3 | 605 (87.8) | Base metal |
|   | 597 (86.6) | Base metal |
|   | 601 (87.2) | Base metal |
|   | 601 (87.3) | Base metal |
| 5 | 550 (79.8) | Weld metal[a] |
|   | 586 (85.1) | Base metal |
| 6 | 591 (85.8) | Weld metal[b] |
|   | 602 (87.4) | Base metal |

[a] The fracture initiated at a fusion imperfection at the weld toe.

[b] This specimen exhibited very little weld reinforcement.



FIGURE 22—Effects of carbon content, carbon equivalent, and cracking parameter on underbead cracking in Arctic grade linepipe steels.

$P_{cm}$ are shown graphically in Figure 22. Although only six steels were studied, some general trends were observed: (1) Underbead cracking increased with increased carbon content. The two steels with the lowest carbon content (0.07%) had the least amount of cracking. (2) There was no correlation between underbead cracking and C.E. This is in agreement with other studies[68] with steels having carbon contents less than about 0.10%. (3) There appeared to be a critical value of $P_{cm}$ necessary to minimize underbead cracking.

The degree of cracking that occurred during this study will undoubtedly differ from that which will occur in an actual production weld because of differences in the location and design of the joint, the welding process and welding procedure. For satisfactory field girth welding of the linepipe, a maximum cracking level of 50% in the underbead cracking test has been proposed; this is based on demonstrated satisfactory performance of linepipe with 54% underbead cracking.[69] It should be noted that at least one potential pipe line fabricator had designated a 50% maximum underbead cracking level as acceptable weldability in their specification for linepipe fittings.[70] On the basis of this criterion, all six steels investigated, with carbon equivalents ranging from 0.37 to 0.50, would be satisfactorily weldable by field girth welding procedures using cellulose-covered electrodes.

**Transverse Weld Tension Tests.** The results of transverse weld tension tests made in accordance with API Standard 1104[71] on simulated field girth welds in plates from Steels 2, 3, 5 and 6 are shown in Table III. All but two of the fractures occurred in the base metal. The two weld metal fractures were associated with a fusion imperfection and with an insufficient weld reinforcement respectively, and are thus related to weldment soundness and geometry rather than to material properties. API Standard 1104 requires that the tensile strength of each specimen be equal to or greater than the specified minimum tensile strength for the grade, which is typically 531 and 565 MPa (77 and 82 ksi) for grades X-65 and X-70, respectively.[63, 65] Thus, Steel No. 2 would meet the weld tensile requirements for grade X-65, and Steels 3, 5 and 6 would meet the weld tensile requirements for grade X-70 (assuming a successful retesting of another tension specimen from Steel No. 5).

**Side Bend Tests.** The side bend test is used to determine both soundness and ductility in the weld region. The results of the side bend tests on the simulated girth welds are shown in Table IV. Two of the specimens failed because of imperfections in the weld metal, most likely associated with the weld soundness and not a material deficiency. Although the 98 mm (3⅞ inch diameter) mandrel was slightly larger than the specified 89 mm (3½ inch) diameter, the significant ductility exhibited

**Table IV—Results of Side Bend Tests on Simulated Field Girth Welds**

| Steel No. | Individual Test Results* |
|---|---|
| 2 | 8 passed |
| 3 | 7 passed, 1 failed (5 mm long tear in weld metal) |
| 5 | 4 passed |
| 6 | 3 passed, 1 failed (6 mm long root tear) |

The specimens were bent 180 degrees around a 98 mm (3⅞ in.) diameter mandrel.

* To pass the test, the specimens shall exhibit no cracks or other defects in the weld metal exceeding 3.175 mm (⅛ in.) in length. Edge cracks shall not exceed 6.35 mm (¼ in.) in length unless obvious defects are observed (API Standard 1104).

**Table V—Results of Nick Break Tests on Simulated Field Girth Welds**

| Steel No. | Individual Test Results |
|---|---|
| 2 | Pass |
| | Pass |
| | Pass |
| | Pass |
| 3 | Pass |
| | Pass |
| | Pass |
| | Fail: lack of fusion |
| 5 | Pass |
| | Fail: slag inclusions* |
| 6 | Fail: slag inclusions* |
| | Fail: slag inclusions* |

* Slag inclusions in excess of that permitted in API Standard 1104.

in the weld region for the four steels should be sufficient to pass the side bend test in API Standard 1104.

**Nick Break Tests.** The nick break test is used only to determine weld soundness. The results of the API Standard 1104 nick break tests are shown in Table V. All failures were associated with weld soundness and not material properties.

**Charpy V-Notch Tests.** The CVN energy absorption of the weld metal (made with AWS E8018-G electrodes) in each of the four steels joined is shown in Table VI. Although API Standard 1104 does not require notch toughness testing, notch toughness data were obtained. Notch toughness values of 34 and 31 J (25 and 23 ft-lb) were attained at temperatures as low as –40 C (–40 F) in the weld metal for joints in Steels 2 and 3, respectively. In the weld metal for joints in Steels 5 and 6, notch toughness values of 32 and 42 J (24 and 31 ft-lb) were attained at –25 C (–13 F).

Because the SMAW girth welds are deposited by multipass welding, the admixture from the base metal is relatively low. Thus, the mechanical properties of the weld metal would be determined primarily by the electrode type and welding parameters and, to a lesser extent, by the base metal composition. Electrode manufacturers are continuing development of improved SMAW electrodes for Arctic applications; thus, the properties obtained with the AWS E8018-G electrodes used in this study may not represent the optimum attainable.

**Hardness Traverses.** The diamond pyramid hardness of the weld region in the four simulated girth welds is plotted in Figures 23 and 24. There was little difference in average hardness of the base metals, with individual values ranging from HV10 177 to 216. The HAZ's were generally slightly harder than the corresponding base metals, with the highest individual reading of HV10 238 located adjacent to the root pass in Steel No. 3. There was considerable variation in hardness throughout the weld metals—HV10 169 to 242. The softest region was always located in the traverses at the midthickness; this was probably the result of the tempering effect of several weld passes during the multipass welding. The hardest regions were in the root pass and the capping passes, which received little or no tempering. However, the hardness in any part of the weld region was well below

**Table VI—Results of Charpy V-Notch Impact Tests of Simulated Field Girth Welds Joined with E8018-G Electrodes**

| Steel No. | Test Temperature, C (F) | | | | | | | | | | | |
|---|---|---|---|---|---|---|---|---|---|---|---|---|
| | –62 | (–80) | –40 | (–40) | –25 | (–13) | –18 | (0) | –5 | (23) | 26 | (78) |
| | Energy Absorption, J (ft-lb)* | | | | | | | | | | | |
| 2 | 14 | (10) | 34 | (25) | 39 | (29) | 46 | (34) | 52 | (38) | 94 | (69) |
| 3 | 19 | (14) | 31 | (23) | 34 | (25) | 38 | (28) | 56 | (41) | 81 | (60) |
| 5 | 8 | (6) | 23 | (17) | 33 | (24) | — | | 43 | (32) | 85 | (63) |
| 6 | 9 | (7) | 14 | (10) | 42 | (31) | — | | 35 | (26) | 84 | (62) |

* Average of duplicate specimens.

the HV 260 maximum imposed for the longitudinal seam weld in some proposed specifications.[63, 65]

General Discussion. The results of the laboratory tests herein described—underbead cracking, tension, side bend, nick break, Charpy V-notch and hardness— demonstrate, within the limits of laboratory tests, the satisfactory weldability of the steels investigated. Confirmation by actual field girth welding of full size pipe sections was beyond the scope of this investigation. However, the tests conducted as part of this investigation did not reveal any significant potential problems with any of the various types of steels investigated.

### Hydrogen-Induced Blister Cracking

Since the service failure of an ARAMCO sour gas transmission pipe line,[72] hydrogen-induced blister cracking (HIBC) has been recognized as an important potential mechanism for initiating failures in linepipe, and HIBC resistance has become a new requirement for linepipe steels for sour gas transmission. It is generally agreed

that HIBC is the result of nascent hydrogen (generated by corrosion) being absorbed into the steel and precipitating at certain sites as gaseous hydrogen.[73, 74] Since the fugacity of hydrogen generated during corrosion in a sour environment is extremely high ($10^6$ to $10^7$ kPa, 150 to 1500 ksi), molecular hydrogen precipitated in the steel readily causes internal cracks.

To determine the factors controlling the propensity to HIBC, a scanning electron fractographic investigation[74] was conducted on the internal surface of hydrogen-induced cracks formed during the British Petroleum (BP) test.[72] In addition, some samples immune to HIBC in the BP test were examined metallographically. The fractographic examinations revealed that the surface of cracks formed in the BP test always contained a significant amount of certain types of inclusions, indicating that HIBC was caused by the precipitation of hydrogen at these detrimental inclusions. In this investigation, three types of detrimental inclusions were identified as (1) elongated glassy silicates, (2) elongated manganese sulfides,
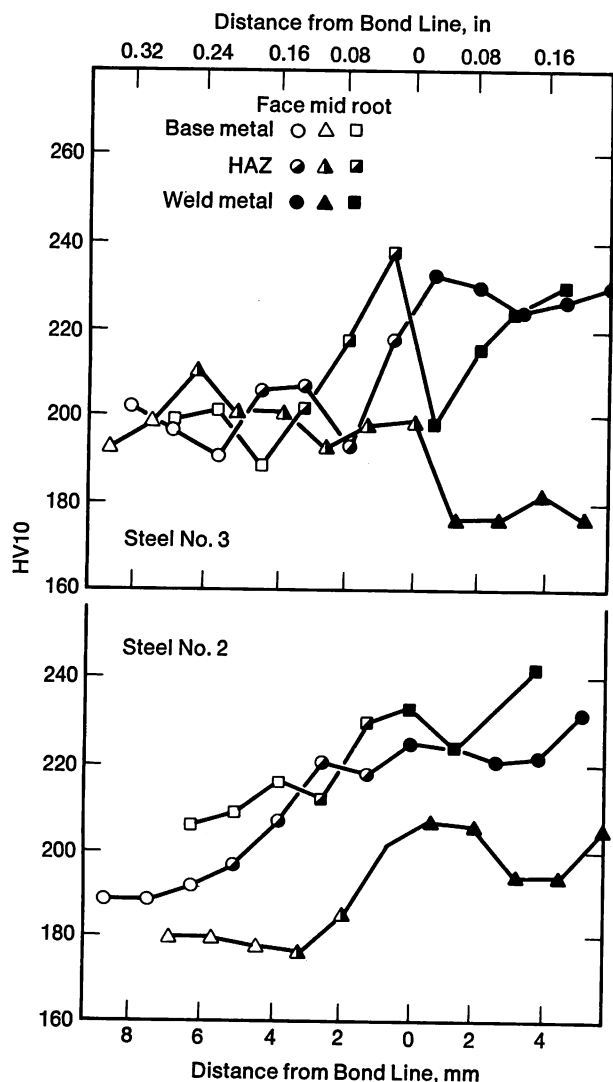


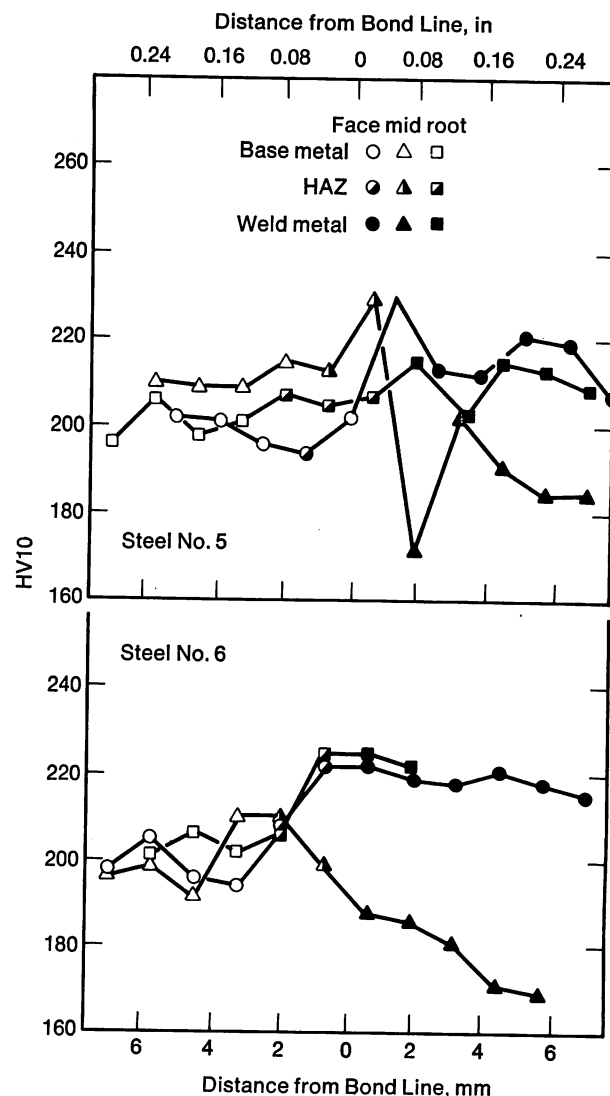FIGURE 23—Hardness traverses on simulated field girth welds in Arctic grade linepipe steels.

FIGURE 24—Hardness traverses on simulated field girth welds in Arctic grade linepipe steels.

and (3) massive niobium carbonitrides. It has been found that decreasing the sulfur content to below 0.006% did not always provide immunity to HIBC in the BP test, especially when elongated sulfides were localized in a small region. Alumina type inclusions and globular inclusions appeared to be much less harmful to HIBC performance.

Although Japanese investigators[75-79] reported that additions of copper greater than 0.20% completely suppressed HIBC by reducing the corrosion rate and thus the amount of hydrogen absorbed, our test results showed no beneficial effect of copper on HIBC performance and also that copper additions (up to 0.5%) did not affect either the corrosion rate or the amount of hydrogen absorbed. Italian investigators[80] also reported no beneficial effect of copper but claimed a beneficial effect from the addition of chromium. Our experience shows, however, that chromium additions (up to 0.5%) have no effect on HIBC performance. Therefore, we believe the HIBC resistance can be improved primarily by improving the cleanliness of the steel and by eliminating the detrimental inclusions mentioned above such as elongated glassy silicates, elongated manganese sulfides and massive niobium carbonitrides. Alloying elements have very little effect, if any, on HIBC performance.

Environmental factors also have important influences on the HIBC performance. For example, decreased $H_2S$ content in the environment decreases the HIBC susceptibility of a given material. Table VII shows the effect of $H_2S$ content in the exposure solution on HIBC performance.[74] When using the standard 100% $H_2S$ environment for the BP test, all the specimens exhibited cracking (cracking sensitivity ratio [CSR] ranging from 0.1 to 4), whereas in the 5% $H_2S$ environment, none of the companion specimens showed any cracking.

**Table VII**—Effect of $H_2S$ Content in Exposure Solution on the HIBC Performance

| Sample Number | Cracking Sensitivity Ratio, | |
|---|---|---|
| | BP Test[a] | Low $H_2S$ Test[b] |
| A | 4 | 0 |
| B | 3 | 0 |
| C | 2 | 0 |
| D | 2 | 0 |
| E | 1 | 0 |
| F | 0.7 | 0 |
| G | 0.2 | 0 |
| H | 0.1 | 0 |

a 100% $H_2S$ gas bubbled.
b 5% $H_2S$ + 95 $N_2$ gas bubbled.

The exposed area of the test specimen is another variable influencing the susceptibility to HIBC as indicated by recent work evaluating variables in BP testing procedures. Although the entire surface area of a speci-

men is usually exposed to the sulfide solution in the BP tests conducted at our laboratory, some investigators[75,76] expose only the top and bottom faces of specimen (that are parallel to the pipe wall) by coating the sides. The effect of side coating on the HIBC performance is shown in Table VIII. In this study, when the specimen was side coated, the measured CSR value was reduced by factors of 2 to 5. Thus, side coating of the specimen obviously reduces the amount of hydrogen absorbed during exposure and thereby lowers the cracking tendency.

**Table VIII**—Effect of Side Coating in BP Test

| Sample Number | Cracking Sensitivity Ratio | |
|---|---|---|
| | No Side Coating | With Side Coating |
| 105 | 11 | 4 |
| 626 | 5 | 1 |
| 651 | 3 | <0.1 |
| 656 | 1 | 0.8 |
| 943 | 0 | 0 |

## The Next Decade for Linepipe Steels

Linepipe with minimum yield strengths up to 483 MPa (70 ksi) having excellent notch toughness and weldability is now readily available. UOE pipe in diameters up to about 1625 mm (64 inches) is also available. Although it is not expected that there will be any need for pipe with diameters beyond those presently available, the economics and history of pipe lines point toward higher strengths and toughnesses than presently produced. Because of metallurgical restraints and facility limitations, controlled rolling cannot be expected to provide strength/toughness combinations much beyond the present maximum levels. Therefore, it is expected that any substantial increase will have to be achieved by quenching and tempering.

There are two approaches to the production of quenched-and-tempered ultrahigh strength large diameter linepipe. These are to fabricate pipe from heat treated plate, or to heat treat pipe fabricated from as-rolled plate. Consideration of these approaches indicates that the latter is preferred because (1) as-rolled plate would be much easier to form into pipe than high strength quenched-and-tempered plate, and (2) the embrittled zone of the longitudinal high heat input submerged-arc seam weld would be eliminated by the final heat treatment. High volume production of quenched-and-tempered tubular products is generally accomplished by furnace austenitizing, progressively quenching and then tempering with the pipe in the horizontal position through these operations. However, studies have shown for pipe with large diameter-to-wall thickness

ratios, austenitizing in the conventional manner (horizontally) cannot be successfully accomplished because the pipe will sag (lose roundness) excessively.[81] One alternative is to autenitize and quench the pipe vertically. Limited trials have shown that although this approach eliminates the sagging problem, it is not suited to the processing of large tonnages. One approach that appeared to offer the advantages of treating the pipe horizontally and yet avoid the sagging problem was to progressively austenitize using induction heating and then progressively quench. With this approach, only a short length of the pipe would be at the austenitizing temperature at any time, and also the time at temperature would be minimized.

A number of laboratory studies were conducted to evaluate the metallurgical response and resulting mechanical properties of linepipe steels when quenched and tempered using induction heating. One of these[82] involved a series of five steels with a base composition of 0.18% C, 1.40% Mn and 0.06% V. To increase harden-

ability, small additions (see Table IX) of one or more of the following elements were added: copper (up to 0.45%), nickel (up to 0.24%), chromium (up to 0.25%), molybdenum (up to 0.17%) and boron (up to 0.002%). Straightaway-rolled 13 mm (0.5 inch) plates of each steel were induction heated to 885 C (1625 F), progressively spray quenched and furnace tempered at 565, 620, or 675 C (1050, 1150 or 1250 F). Furnace tempering was used as previous studies indicated sagging of the pipe was not a problem at these lower temperatures.[81] The results of this study, Table X, indicated that excellent combinations of strength and toughness were generally obtained by this approach.

Subsequently, it was decided to determine the engineering feasibility of induction heat treating 1220 mm (48 in.) OD linepipe.[83] Therefore, 6 m (20 ft) lengths of 1220 mm (48 in.) OD by 12 mm and 16 mm (0.468 and 0.625 in.) wall submerged arc welded pipe were fabricated for heat treating. These pipes were made from a BOP heat of C-Mn-V steel containing additions of copper,

**Table IX**—Chemical Composition of Steels Investigated

| Steel | Element, % | | | | | | | | | | | | | |
| | C | Mn | P | S | Si | Cu | Ni | Cr | Mo | V | B | Al* | Ti | N |
|---|---|---|---|---|---|---|---|---|---|---|---|---|---|---|
| A | 0.18 | 1.38 | 0.007 | 0.011 | 0.39 | — | — | — | — | 0.058 | 0.0018 | 0.042 | 0.015 | 0.007 |
| B | 0.17 | 1.36 | 0.009 | 0.010 | 0.39 | 0.32 | 0.24 | 0.25 | 0.06 | 0.056 | — | 0.046 | — | 0.007 |
| C | 0.17 | 1.35 | 0.012 | 0.010 | 0.38 | 0.31 | 0.23 | 0.24 | — | 0.058 | 0.0022 | 0.042 | 0.017 | 0.006 |
| D | 0.19 | 1.36 | 0.009 | 0.010 | 0.39 | 0.31 | — | 0.24 | — | 0.059 | 0.0022 | 0.038 | 0.016 | 0.006 |
| E | 0.19 | 1.38 | 0.009 | 0.010 | 0.39 | 0.45 | 0.24 | — | 0.17 | 0.059 | — | 0.042 | — | 0.006 |

* Total aluminum.

**Table X**—Effect of Tempering Temperature on the Transverse Mechanical Properties of 13 mm (0.5 in.) Plates of 0.18C-1.4Mn-0.06V Base Steel Induction Austenitized Spray Quenched and Furnace Tempered

| Steel | Alloying Addition | Tempering Temperature, C (F) | | Yield Strength, MPa (ksi) | | Tensile Strength, MPa (ksi) | | Charpy V-Notch Properties | | | |
| | | | | | | | | Shelf Energy Absorption, J (ft-lb) | | 50% Shear Temperature, C (F) | |
|---|---|---|---|---|---|---|---|---|---|---|---|
| A | B | 565 | (1050) | 814 | (118) | 848 | (123) | 54 | (40) | −48 | (−55) |
| | | 620 | (1150) | 718 | (104) | 786 | (114) | 72 | (53) | −51 | (−60) |
| | | 675 | (1250) | 594 | (86) | 676 | (98) | 88 | (65) | −60 | (−75) |
| B | Cu, Ni, Cr, Mo | 565 | (1050) | 820 | (119) | 890 | (129) | 62 | (46) | −37 | (−35) |
| | | 620 | (1150) | 738 | (107) | 820 | (119) | 68 | (50) | −43 | (−45) |
| | | 675 | (1250) | 642 | (93) | 731 | (106) | 90 | (66) | −62 | (−80) |
| C | Cu, Ni, Cr, B | 565 | (1050) | 882 | (128) | 917 | (133) | 38 | (28) | −4 | (+25) |
| | | 620 | (1150) | 786 | (114) | 835 | (121) | 43 | (32) | −32 | (−25) |
| | | 675 | (1250) | 696 | (101) | 759 | (110) | 62 | (46) | −60 | (−75) |
| D | Cu, Cr, B | 565 | (1050) | 910 | (132) | 958 | (139) | 42 | (31) | −23 | (−10) |
| | | 620 | (1150) | 842 | (122) | 876 | (127) | 50 | (37) | −12 | (+10) |
| | | 675 | (1250) | 683 | (99) | 752 | (109) | 73 | (54) | −73 | (−100) |
| E | Cu, Ni, Mo | 565 | (1050) | 924 | (134) | 972 | (141) | 54 | (40) | −62 | (−80) |
| | | 620 | (1150) | 848 | (123) | 897 | (130) | 68 | (50) | −73 | (−100) |
| | | 675 | (1250) | 649 | (94) | 724 | (105) | 84 | (62) | −93 | (−135) |

**Table XI**—Chemical Composition and Transverse Mechanical Properties of Induction Austenitized, Quenched-and-Tempered 1220 mm (48 in.) OD Linepipe

| Element, % | | | | | | | | | | |
|---|---|---|---|---|---|---|---|---|---|---|
| C | Mn | P | S | Si | Cu | Cr | Mo | V | Al* | N |
| 0.14 | 1.42 | 0.014 | 0.006 | 0.24 | 0.26 | 0.19 | 0.07 | 0.046 | 0.033 | 0.004 |

* Total aluminum.

### Mechanical Properties

| Wall Thickness, mm (in.) | | Yield Strength, MPa (ksi) | | Tensile Strength, MPa (ksi) | | Charpy V-Notch Properties | | | |
|---|---|---|---|---|---|---|---|---|---|
| | | | | | | Shelf Energy Absorption, J (ft-lb) | | 50% Shear Temperature, C (F) | |
| 12 | (0.468) | 627 | (91) | 724 | (105) | 121 | (89) | −57 | (−70) |
| 16 | (0.625) | 593 | (86) | 689 | (100) | 123 | (91) | −46 | (−50) |

chromium and molybdenum (Table XI). These pipes were heat treated on a pilot induction heat treating facility, Figure 25, constructed and operated by the Westinghouse Electric Corporation. Sections of pipe were progressively heated by axially conveying them through a 0.76 m (2½ ft) long 60-hertz induction coil and subsequently quenched by a water spray ring located at the exit end of the induction coil. These pipes were heated at an average rate of 9.5 C (17 F) per second to an austenitizing temperature of 925 C (1700 F), and the spray quench had a severity of quench (Grossman) value of about 50 mm$^{-1}$ (2 in.$^{-1}$). Because there was no furnace of sufficient size readily available to temper the pipes, they were also induction tempered by heating at 9.5 C (17 F) per second to 675 C (1250 F) and then air cooled. No major problems were encountered during the operation, and the pipe did not sag indicating that it is feasible to heat treat large diameter thin wall pipe using induction heating. The mechanical properties obtained on these pipes are shown in Table XI. Although the properties

were fairly impressive, they were not as good as those obtained in the earlier laboratory studies. The results were not unexpected, however, as a previous laboratory study[84] showed that for as-quenched samples of this steel (1) the mechanical properties of furnace tempered plates were consistently superior to those of induction tempered plates, and (2) the mechanical properties of induction tempered plates were essentially independent of tempering temperature in the range evaluated (565 to 675 C, 1050 to 1250 F). Therefore, it was concluded that furnace tempering would be preferable to induction tempering of induction-austenitized-and-quenched material.

Seamless linepipe is usually furnished in the hot-rolled condition, and therefore, generally has a relatively high ductile-to-brittle transition temperature. The service performance of seamless linepipe, however, has been excellent. In spite of this, the notch toughness properties currently being required for UOE linepipe are beginning to be specified for seamless linepipe. Because ultrahigh
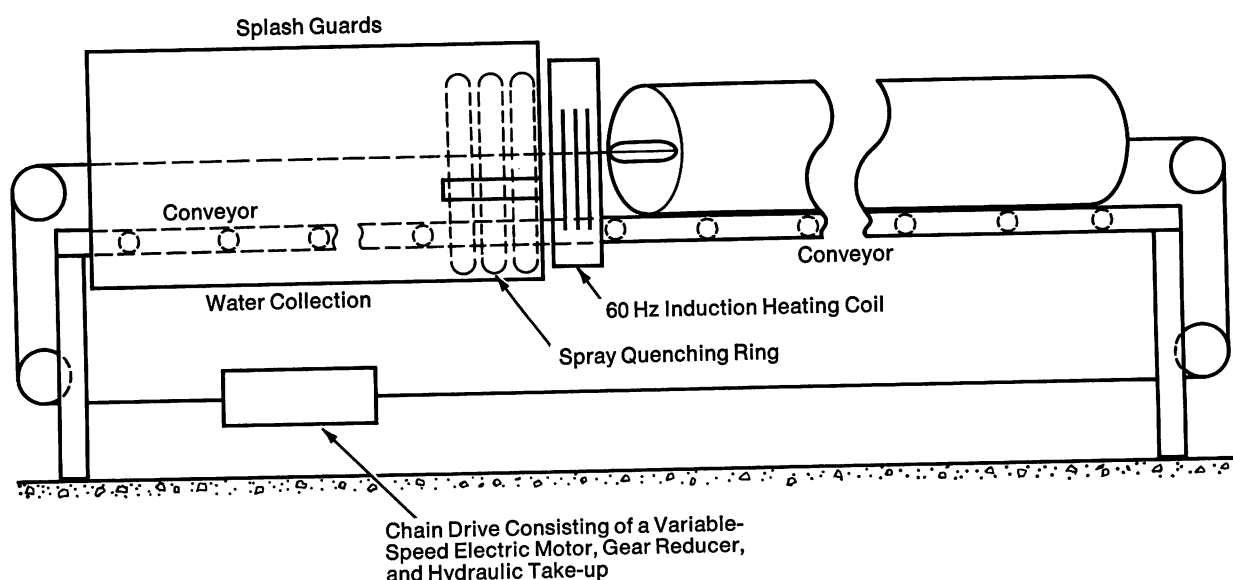


*FIGURE 25—Schematic of pilot induction heat treating facility.*

**Table XII**—Chemical Composition and Transverse Mechanical Properties of Hot-Rolled and Normalized Vanadium-Nitrogen Steel Plates

| | | | | | Element, % | | | | | | | |
|---|---|---|---|---|---|---|---|---|---|---|---|---|
| C | Mn | P | S | Si | Cu | Ni | Cr | Mo | V | Nb | Al[a] | N |
| 0.19 | 1.28 | 0.011 | 0.024 | 0.21 | 0.05 | 0.02 | 0.07 | 0.01 | 0.09 | 0.03 | 0.018 | 0.019 |

a Total aluminum.

### Mechanical Properties

| Plate Thickness, mm (in.) | Yield Strength, MPa (ksi) | | | Tensile Strength, MPa (ksi) | | | Charpy V-Notch Properties | | | | | |
|---|---|---|---|---|---|---|---|---|---|---|---|---|
| | | | | | | | Shelf Energy Absorption, J (ft-lb) | | | 50% Shear Temperature, C (F) | | |
| | HR[b] | FN[c] | IN[d] | HR | FN | IN | HR | FN | IN | HR | FN | IN |
| 13 (0.5) | 524 (76) | 421 (61) | 552 (80) | 710 (103) | 565 (80) | 662 (96) | 24 (18) | 38 (28) | 34 (25) | 38 (100) | -48 (-55) | -37 (-35) |
| 25 (1.0) | 538 (78) | 379 (55) | 510 (74) | 745 (108) | 559 (81) | 621 (90) | 33 (24) | 46 (34) | 35 (26) | 99 (210) | -21 (-5) | -32 (-25) |

b Hot-rolled.
c Furnace normalized.
d Induction normalized.

strength was not a consideration, induction normalizing rather than quenching and tempering was chosen as the method to improve toughness. A laboratory study[85] was conducted to determine the extent of any improvement in mechanical properties from induction normalizing. Plates of a vanadium-nitrogen steel, Table XII, commonly used for high strength linepipe fittings were evaluated in two thicknesses, 13 and 25 mm (½ and 1 in.). The plates were evaluated in the hot-rolled condition after furnace normalizing at 905 C (1660 F) and after induction normalizing at the same temperature. In the latter case, the plate samples were heated at 11 C (20 F) per second and then air cooled. The mechanical properties of these plates, Table XII, show that whereas furnace normalizing reduces the yield strength and improves the transition temperature of the hot-rolled material, induction normalizing also improves transition temperature

but retains the high as-rolled yield strength.

These results indicated that induction normalized vanadium-nitrogen steels can be used to produce high strength seamless pipe with good notch toughness. Because of these promising results, 6 m (20 ft) long sections of 610 mm (24 in.) OD by 12.7 mm (0.500 in.) and 22.2 mm (0.875 in.) wall thickness pipe of vanadium-nitrogen steel (see Table XIII for composition) were induction normalized on the Westinghouse pilot heat treating facility for evaluation.[86] The pipe was progressively treated by axially conveying through a 760 mm (30 in.) long 60-hertz induction coil and then air cooling. The pipe was heated to 900 C (1650 F) and the heating rate varied from 7 to 11 C (13 to 20 F) per second depending on wall thickness. No major problems were encountered during heating, and the pipe did not sag.

As summarized in Table XIII, the average yield

**Table XIII**—Chemical Composition and Transverse Mechanical Properties of Hot-Rolled and Induction Normalized 610 mm (24 in.) OD Seamless Linepipe

| | | | | | Element, % | | | | | | | |
|---|---|---|---|---|---|---|---|---|---|---|---|---|
| C | Mn | P | S | Si | Cu | Ni | Cr | Mo | V | Nb | Al[a] | N |
| 0.20 | 1.29 | 0.009 | 0.012 | 0.24 | 0.018 | 0.016 | 0.025 | 0.018 | 0.079 | 0.012 | 0.036 | 0.026 |

a Total aluminum.

### Mechanical Properties

| Wall Thickness, mm (in.) | Yield Strength, MPa (ksi) | | Tensile Strength, MPa (ksi) | | Charpy V-Notch Properties | | | |
|---|---|---|---|---|---|---|---|---|
| | | | | | Shelf Energy Absorption, J (ft-lb) | | 50% Shear Temperature, C (F) | |
| | HR[b] | IN[c] | HR | IN | HR | IN | HR | IN |
| 12.7 (0.500) | 503 (73) | 482 (70) | 717 (104) | 607 (88) | 34 (24) | 46 (34) | 104 (220) | -21 (-5) |
| 22.2 (0.875) | 531 (77) | 448 (65) | 710 (103) | 565 (82) | 46 (34) | 54 (40) | 107 (225) | -26 (-15) |

b Hot-rolled.
c Induction normalized.

strength (469 MPa or 68 ksi versus 517 MPa or 75 ksi) of the induction normalized pipe was lower than that noted for the hot-rolled pipe. However, the 50% shear transition temperatures were significantly improved (average −23 C or −10 F versus 105 C or 222 F) by heat treating. Thus, induction normalizing appears to be a viable method of producing high strength high toughness seamless linepipe.

## Other Applications of Linepipe Steel Technology

### Plate

There has been a modest transfer of linepipe steel technology to other applications involving plate products. The transfer has been largely in the controlled rolling processing methods developed for linepipe to obtain improved ductile-to-brittle transition temperatures. For example, some mills now make use of controlled rolling to help meet the AASHTO notch toughness requirements for steel for bridges.

Classically, improved transition temperature behavior in plate product has been achieved by heat treatment. With the development of linepipe controlled rolling procedures, however, some mills have been able to take advantage of such practices for improving notch toughness whereas others have not. Controlled rolling slows production to various degrees depending upon the local conditions. Also, it is more difficult to implement for items where sizes change continually than for repetitive sizes typical of linepipe orders. The cost of decreased production must, therefore, be weighed against the cost of heat treatment. Controlled rolling is generally economically feasible on new mills designed for the purpose and interestingly, on very old mills, whose production rate is sufficiently slow that controlled rolling restrictions do not seriously hamper production. Also, controlled rolling becomes less economical or practical as plate thickness increases because of the increased mill delay times involved plus the increased loads on the mill.

In the future, as the cost of energy continues to climb, it is expected that controlled rolling will be used to an even greater extent as a replacement for heat treatment. Mills will be designed for controlled rolling to achieve certain notch toughness properties instead of requiring heat treatment to achieve such properties (as is frequently the case at present).

With regard to compositions, the Mn-Mo-Nb Arctic grade linepipe analysis has not been used as plate in other applications because more economical compositions are available providing the necessary combinations of strength and toughness. Niobium and vanadium treated grades of plate steel (ASTM A572) are used extensively, but it should be noted that these grades were developed concurrently with the pipe grades of similar composition, rather than being derived from them.

### Sheet

As discussed earlier, the presence of martensite-austenite constituents in Mo-Nb steels accounts for a continuous yielding behavior in linepipe plate. In turn, the continuous yielding characteristics give rise to high work hardening of the steel during pipemaking operations such that reliable increases in strength can be obtained for known levels of forming strain. The high work hardening rate of martensite-containing steels has already been exploited in developing the new class of formable high strength steel sheets called dual phase steels. By careful control of composition and processing, steel sheets containing soft, ductile ferrite and 5 to 20% martensite are produced which work harden to specific strength levels after relatively light deformations in customer forming operations. Because of the excellent combination of good formability and high strength obtained after part forming, dual phase steels are attracting much attention from steel producers and from automakers where a large potential application for lighter weight components such as wheels, bumpers, frame members and pillars is forecast. As a result, substantial considerable further developments in ferrite-martensite (dual phase) steels are foreseen. Further research on the nature of the ferrite-martensite interface and on methods of controlling the dispersion of martensite is likely to result in steels having higher formability and higher strength.

Although we have come a long way in optimizing composition and processing to produce fine grained hot-rolled steels for Arctic grade linepipe, many of the studies have been empirical in nature, and further development will depend on improving our understanding of the basic principles governing the strength and toughness of these steels. Already we see extensive basic research in progress to understand how temperature, composition, strain and strain rate act to influence the deformation, recovery and recrystallization of austenite during hot rolling. Such studies should further optimize controlled rolling schedules and will hopefully lead to more latitude in such schedules.

A factor tending to counteract the improvements in ductile-to-brittle transition temperature resulting from grain refinement is the formation of iron carbide at ferrite grain boundaries. Additional basic research is needed to understand the influences of steel composition, grain orientation and the kinetics of carbide precipitation on the formation of such carbides.

Finally, in anticipation of the need for economical linepipe steels with strengths above 552 MPa (80 ksi), additional basic research on transformation characteristics of low carbon low alloy steels is needed so that new and innovative thermomechanical treatments, such as accelerated cooling on the rolling mill, can be reduced to practice.

Developments to date have resulted in hot-rolled steels with superior strength and toughness, but these may be only the first steps in a long series of truly remarkable developments that will stem from the basic research suggested by the present Arctic linepipe steel.

## References

1. C. B. Valdrich, Welding Journal, Research Supplement, 26 (3), 1947, 153.
2. J. Dearden and H. O'Neill, Trans. Inst. Welding (U.K.), 3, 1940, 203.
3. K. Winterton, Welding Journal, 40 (6), 1961, 253.
4. K. W. Burns and F. B. Pickering, J. Iron and Steel Inst., 202, 1964, 899.
5. J. D. Baird and R. W. Preston, Processing and Properties of Low-Carbon Steel, Met. Soc. AIME, New York, 1972, 1.
6. A. R. Rosenfield, G. T. Hahn and J. D. Embury, Met. Trans., 3, 1972, 2797.
7. M. F. Baldy, Offshore Technology Conference, Dallas, 1976, OTC 2667.
8. C. R. Speich and A. J. Schwoeble, U. S. Steel Corp., Monroeville, Pa., unpublished research, 1977.
9. M. A. Cevallero, C. Parini and N. Pizzimento, Microalloying 75, Session 2B, Vanitech, London, 1975, 81.
10. C. R. Speich and D. S. Dabkowski, The Hot Deformation of Austenite, Met. Soc. of AIME, New York, 1977, 557.
11. W. B. Morrison, ASM Transactions Quarterly, 59, 1966, 824.
12. J. H. Bucher, J. D. Grozier and J. F. Enrietto, "Fracture, an Advanced Treatise," Vol. VI, Fracture of Metals, Academic Press, New York, 1967, 248.
13. B. Mintz, W. B. Morrison and A. Jones, Metals Technology, 6, 1979, 252.
14. W. Jolley, J. Iron and Steel Inst., 206, 1968, 107.
15. T. C. Lindley, G. Oates and C. E. Richards, "Effect of Second Phase Particles on the Mechanical Properties of Steel," Iron and Steel Inst., London, 1971, 54.
16. J. Heslop and N. J. Petch, Phil Mag., 2, 1957, 649.
17. R. B. C. Yeo, A. G. Melville, P. E. Repas and J. M. Gray, Journal of Metals, 20 (9), 1968, 33.
18. J. M. Gray, Met. Trans., 3, 1972, 1495.
19. A. M. Sage and D. S. Dabkowski, Vanitech, London and U. S. Steel Corp., Monroeville, Pa., Unpublished research, 1979.
20. P. E. Repas, Microalloying 75, Session 2B, Vanitech, London, 1975, 38.
21. R. P. Smith, Trans. AIME, 236, 1966, 221.
22. R. P. Smith, Trans. AIME, 224, 1962, 190.
23. D. S. Dabkowski, U. S. Steel Corp., Monroeville, Pa., Unpublished research, 1979.
24. L. Habraken and M. Economopolus, Transformation and the Hardenability of Steels, Climax Molybdenum Company, 1967, 69.
25. V. Biss and R. L. Cryderman, Met. Trans., 2, 1971, 2267.
26. D. S. Dabkowski and C. R. Speich, Proceedings of the 19th Mechanical Working and Steel Processing Conference, AIME, New York, 1977, 557.
27. T. Taira, T. Osuka and Y. Ishida, Proceedings of the 15th Mechanical Working and Steel Processing Conference, AIME, New York, 1973, 3.
28. A. K. Shoemaker and K. D. Ives, ibid, 51.
29. G. Tither and M. Lavite, J. Metals, 27 (9), 1975, 15.
30. C. R. Speich and R. L. Miller, Structure and Properties of Highly Formable Dual-Phase Steels, AIME, New Orleans, 1979.
31. W. C. Leslie, R. J. Sober, S. G. Babcock and S. J. Green, Trans. ASM, 62, 1969, 690.
32. T. Tanaka, N. Tabata, T. Hatomura and C. Shiza, Microalloying 75, Session 1, Vanitech, London, 1975, 88.
33. L. J. Cuddy, U. S. Steel Corp., Monroeville, Pa., Unpublished research, 1979.
34. B. L. Bramfitt and A. R. Marder, "Processing and the Properties of Low-Carbon Steel," TMS, AIME, New York, 1973, 191.
35. D. S. Dabkowski, P. J. Konkol and M. F. Baldy, Met. Eng. Quarterly, 16, 1976, 22.
36. W. A. Backofen, Deformation Processing, Addison-Wesley, Reading, Mass., 1972, 308.
37. R. J. Eiber, W. A. Maxey and A. R. Duffy, Proceedings of the 16th Mechanical Working and Processing Conference, AIME, New York, 1974, 353.
38. E. Miyoshi, M. Fukuda, H. Iwanaga and T. Okazawa, Proceedings of the Conference on Crack Propagation in Pipelines, British Gas Corporation, England, 1974.
39. J. H. Little, J. A. Chapman, W. E. Morrison, and B. Mintz, Proceedings of the Third Int. Conf. on Strength of Metals and Alloys, Institute of Metals and the Iron and Steel Inst., London, 1973, 80.
40. T. Coleman, D. Dulieu and A. Couch, ibid, 70.
41. R. Schofield, G. Rowntree, N. V. Sarma, and R. T. Werner, Metals Technology, 1, 1974, 325.
42. B. L. Bramfitt and A. R. Marder, Met. Trans. A, 8A, 1977, 1263.
43. G. M. McClure, R. J. Eiber, F. T. Hahn, F. W. Boulger and K. M. Masubuchi, Research on the Properties of Linepipe, American Gas Association, New York, 1962, 1.
44. G. M. McClure, C. T. Hahn, A. R. Duffy, R. J. Eiber and L. L. Elder, Symposium on Linepipe Research, American Gas Association, New York, 1966, 17.
45. W. A. Maxey, 5th Symposium on Linepipe Research, American Gas Association, Arlington, Virginia, 1974, 110.
46. Anon., Running Shear Fractures in Linepipe Subcommittee Summary Report—AISI Committee of Large-Diameter Line-pipe Producers, American Iron and Steel Institute, New York, 1974, 5.
47. Anon., Specification SP-4680-50-26, Northwest Alaskan Pipeline Company, 1979.
48. J. Gurland and J. Plateau, Trans. ASM, 56, 1963, 442.
49. B. I. Edelson and W. M. Baldwin, Jr., ASM Trans. Quarterly, 55, 1962, 230.
50. R. Kiessling and N. Lange, Non-metallic Inclusions in Steel, Parts I-IV, The Metals Society, London, 1978.
51. R. Kiessling, J. of Metals, October 1969, 48.
52. T. B. Cox and J. R. Low, Jr., Ph.D. Thesis, Carnegie-Mellon University, NASA Grant 33-087-003, Tech. Report No. 5, May 1973.
53. J. M. Gray and G. M. Wilson, Pipeline and Gas Journal, December 1972, 50.
54. C. E. Sims, Trans. AIME, 215, 1959, 367.
55. T. J. Baker and J. A. Charles, J. Iron & Steel Institute, 210, 1972, 680.
56. T. J. Baker and J. A. Charles, Effect of Second Phase Particles on the Mechanical Properties of Steel, The Iron and Steel Inst., London, 1971, 74.
57. P. E. Waudby, International Metals Review (2), 1978, 229, 74.
58. K. Sanbongi, Trans. ISIJ, 19, 1979, 1.
59. M. Fukuda, T. Hashimoto and Y. Kitagawa, Sumitomo Search No. 14, November 1975.
60. S. K. Saxena and T. A. Engh, Scandinavian J. of Metallurgy, 5, 1976, 105.
61. H. Pircher and W. Klapdar, Microalloying '75, Union Carbide Corporation, 1977, 232.
62. Anon., Specification for High-Test Linepipe, API Spec. 5LX, American Petroleum Institute, 22nd Edition, March 1978.
63. Anon., Specification for Main Linepipe, Canadian Arctic Gas Study, Ltd., Specification No. 2950-6-6, August 1973.

64. J. G. Garland and P. R. Kirkwood, *Metal Construction, 1* (5), 1975, 320.

65. Anon., Proposed Specification for Linepipe, El Paso Natural Gas Co., Alaskan LNG Project, Revised June 1973.

66. Y. Ito and K. Bessyo, International Institute of Welding Document No.1X-576-68.

67. R. D. Stout and W. D. Doty, *Weldability of Steels,* 2nd Edition, Mack Printing Co., Easton, Pa., 1971, 252-254.

68. J. Gordine, *Welding Journal, Research Supplement, 56,* 1977, (7), 201-s.

69. A. G. Barkow, Natural Gas Pipeline Company of American Engineering Division, Report No. NG-70-3, January 1971.

70. Anon., Specification for Butt-Welded Fittings 12 Inches or Larger for Use with High Yield Pipe, Canadian Arctic Gas Study, Ltd., Specification No. 2950-6-11, Rev. 5, January 1973.

71. Anon., Standard for Welding Pipelines and Related Facilities, API Standard 1104, American Petroleum Institute, 14th Edition, 1977.

72. E. M. Moore and J. J. Warga, *Materials Performance, 15* (5), 1976, 18.

73. J. L. Robinson, *Welding Research Institute, Research Bulletin, 18* (5), 1977, 121.

74. B. E. Wilde, C. D. Kim and E. H. Phelps, "Some Observations on the Role of Inclusions in the Hydrogen-Induced Blister Cracking of Linepipe Steels in Sulfide Environments," to be published in *Corrosion.*

75. M. Kowaka, F. Terasaki, S. Nagata and A. Ikeda, *The Sumitomo Search, 14* (v), 1975, 36.

76. E. Miyoshi, T. Tanaka, F. Terasaki and A. Ikeda, *Trans. ASME, 98,* Sr. B, (4), 1976, 1221.

77. T. Taira, Y. Kobayashi, M. Inagaki and T. Watanabe, "Sulfide Corrosion Cracking of Linepipe for Sour Gas Service," Paper No. 171, presented at Corrosion/79, Atlanta, Georgia, March 1979.

78. M. Itohk, M. Inagaki and T. Taira, "Hydrogen Sulfide Corrosion Cracking of Large Diameter Linepipe," Paper presented NACE/Middle East, Bahrain, April 1979.

79. Y. Nakai, M. Kurahashi, T. Emi and O. Maida, *Trans. Iron and Steel Inst. of Japan, 18,* (3), 1979, 149.

80. A. DeVita and C. Parrini, "Experience in the Development of Steels Resistant to Stress Corrosion and Hydrogen-Induced Cracking," Paper presented at the International Conference <<HSLA Steels>> — <<Experiences in Applications>>. Joint AIME-SFM Meeting, Versailles, France, January 1979.

81. J. A. Scott, U.S. Steel Corp., Monroeville, Pa., Unpublished research, 1965.

82. D. S. Dabkowski and M. F. Baldv, U.S. Steel Corp., Monroeville, Pa., Unpublished research, 1973.

83. D. S. Dabkowski, M. F. Baldv and L. F. Porter, U.S. Steel Corp., Monroeville, Pa., Unpublished research, 1973.

84. D. S. Dabkowski and M. F. Baldv, U.S. Steel Corp., Monroeville, Pa., Unpublished research, 1972.

85. D. S. Dabkowski and M. F. Baldv, U.S. Steel Corp., Monroeville, Pa., Unpublished research, 1973.

86. D. S. Dabkowski, U.S. Steel Corp., Monroeville, Pa., Unpublished research, 1974.

# Discussion

G. R. PRESCOTT, *C. F. Braun & Company.* Would the author comment on the thicknesses of plate that can be handled in the controlled rolling process.

H. W. PAXTON. That depends very much on the type of plate mill that you have. Some of the more modern ones perhaps can handle 35 or 40 mm (1.4 or 1.6 in.). I think 25 mm (1 in.) would be a reasonable number. When you get above that then it depends on the mill.

F. BORIK, *Climax Molybdenum Company.* You showed two types of stress/strain curves, the rounded one reflecting the MA constituent and the one with a square shape. Do you have information on the stress corrosion resistance of these two types of materials?

J. D. DEFILIPPI, *U. S. Steel Corporation.* We have looked at the effects of adding copper or chromium on the stress corrosion resistance of this class of steel and did not find any significant effects.

J. L. MIHELICH, *Climax Molybdenum Company.* Several authors have mentioned (or will mention) steelmaking techniques resulting in consistently low carbon contents in the order of 0.01 to 0.02%. Do these techniques have a place in the manufacture of linepipe steels?

H. W. PAXTON. We have not pushed these methods in the linepipe area up to now. The principle application that we have seen for very low carbon contents is in magnetic alloys rather than in steels where combinations of strength and toughness were important.

# Development of Controlled Rolled Ultra Low Carbon Bainitic Steel for Large Diameter Linepipe

by H. Nakasugi, H. Matsuda and H. Tamehiro
Nippon Steel Corporation

With the discovery of huge oil and gas reserves in the coastal areas of the Arctic Ocean and West Siberia, the demand for large diameter linepipe to transport oil and gas over long distances is increasing as an economic mass transportation method.

High strength linepipe used in a cold climate requires not only good low temperature toughness but also excellent weldability because field welds must be made under severe environmental conditions. Recent increasing demand for higher strength, heavier wall thickness and superior weldability beyond the current level, however, makes it difficult to satisfy the required properties of linepipe with traditional ferrite-pearlite or even with acicular ferrite steels. For this purpose, bainitic steel can offer the possibility of producing such high strength linepipe from the point of view of both metallurgy and economy.

Nippon Steel Corporation (NSC) undertook fundamental research on as-rolled bainitic steel in the late 1960s[1] and has now successfully developed controlled rolled ultra low carbon bainitic steel (ULCB steel) suitable for Arctic service by means of complete control of processing parameters from steelmaking to plate rolling. This ULCB steel can be characterized by a newly-developed composition and plate rolling method.

In this paper, the effects of various alloying elements such as C, Mn, Nb, N, etc. and processing parameters on the mechanical properties of ULCB steel are discussed with regard to their microstructures. The results of actual production tests and various availability tests for Arctic grade linepipe are also presented.

## Summary

Table I shows the comparison between newly-developed and conventional bainitic steels.

In general, conventional bainitic steel is expensive, and the weldability and toughness are not sufficiently good for Arctic grade linepipe owing to the large amount of alloying additions required to achieve a bainitic micro-

structure in the air cooled condition and to insufficient grain refinement.

Extremely low carbon content and a low carbon equivalent conspicuously improve the weldability of ULCB steel (Figure 1). $P_{cm}$ is the most reliable carbon equivalent formula at present for low carbon HSLA steels.[2,3]

For improving the toughness of bainitic steel, it is necessary to minimize the austenite grain size prior to the bainitic transformation, since the effective grain size for cleavage fracture of bainitic steel has a strong dependence on the austenite grain size compared with ferrite-pearlite steel.[4]

The newly-developed plate rolling method effectively refines the austenite grain size and markedly improves low temperature toughness.

Fine titanium nitride (TiN) particles dispersed in the steel slab also improve the toughness in both the base metal and the heat affected zone (HAZ) in welds.[5]

## Fundamental Experiments on ULCB Steel

### Effects of Alloying Elements

A number of laboratory tests were performed to examine the effect of alloying elements on the mechani-



$$P_{cm} = C + \frac{Mn+Cu+Cr}{20} + \frac{Si}{30} + \frac{V}{10} + \frac{Mo}{15} + \frac{Ni}{60} + 5B \ (\%)$$
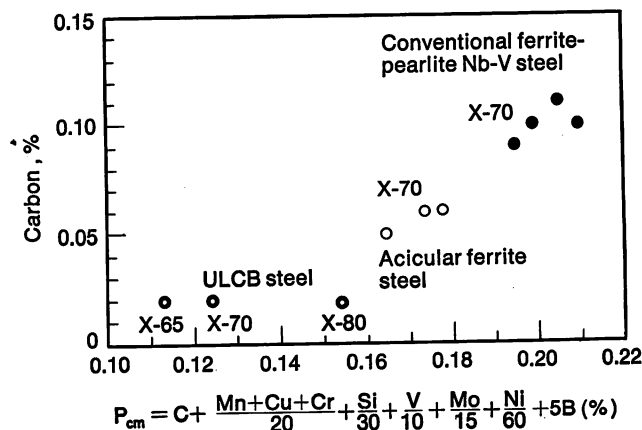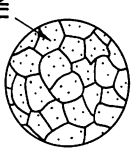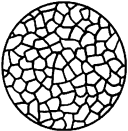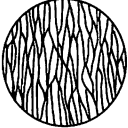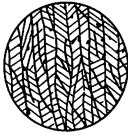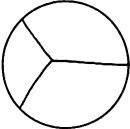
FIGURE 1—Indication of weldability of ULCB steel.

**Table I**—Comparison Between Newly-Developed and Conventional Bainitic Steels

| Steel | Chemical composition | Plate rolling | | | Microstructure | Properties |
|---|---|---|---|---|---|---|
| | | Slab heating | Rough rolling | Finish rolling | | |
| Newly-developed ULCB steel | 1. Extremely low carbon content, approximately <0.03%. <br> 2. Utilization of maximum benefit of grain refinement with fine dispersed TiN particles. <br> 3. Optimal combinations of alloying elements, such as Mn, Nb, B, etc. <br> 4. Low carbon equivalent. | Inhibition of austenite grain growth with application of fine dispersed TiN particles and low temperature heating. <br><br> Fine and homogeneous austenite grain. <br><br> TiN <br><br> ASTM No. 5 to 6 | Refinement of austenite grain through repeating recrystallization. <br><br> Fine and homogeneous recrystallized austenite grain. | Elongation of austenite grain and formation of deformation bands with large amounts of reduction in non-recrystallization region of austenite. | Highly substructured, fine and homogeneous structure. | Good toughness in both base metal and HAZ. <br><br> As a result, excellent combination of strength, toughness and weldability. |
| Conventional bainitic steel | 1. High carbon content, approximately 0.10%. <br> 2. Large amounts of alloying elements, such as Mn, Cr, Mo, etc. <br> 3. High carbon equivalent, more than 0.55%. | Coarse and heterogeneous recrystallized austenite grain. <br><br> ASTM No. —3 to 0 | Coarse and heterogeneous austenite grain. | Insufficient reduction in non-recrystallization region of austenite. | Coarse bainite. | Poor toughness in both base metal and HAZ. <br><br> Poor weldability. |

cal properties of ULCB steel. Some of them are described here.

The steel was melted in a 50 kg (110 lb) electric furnace, and the ingots were rolled to 20 mm (0.8 in.) thick plate. Mechanical tests were carried out in the transverse direction.

Figure 2 shows the effect of carbon content on the strength and Charpy V-notch properties. Increasing carbon content elevates tensile strength but decreases low temperature toughness because of the increasing high carbon martensite islands in the microstructure. Since excessively low carbon contents seem to degrade toughness, carbon contents ranging from 0.01 to 0.03% are most desirable for toughness. Recent progress in steelmaking enables us to produce ultra low carbon steel commercially.

A low carbon content is also desirable from the standpoint of weldability as shown in Figure 3. Although boron additions increase the hardness in the HAZ, it is possible to eliminate this detriment by restricting the

carbon content to extremely low levels.

Figure 4 shows the effect of manganese on strength and Charpy V-notch transition temperature. Manganese is the major alloying element in this steel and is added in the range from 1.5 to 2.0% depending on plate thickness and required strength level. Increasing manganese content elevates strength through the depression of the ferrite-pearlite transformation without a large loss in toughness.

Figure 5 shows the effect of niobium on the strength and Charpy V-notch transition temperature. Niobium improves both strength and toughness through grain refinement, as shown in Figure 6. In the case of ultra low carbon steel, a small amount of niobium is in solid solution in the slabs heated at low temperature such as 1000 C
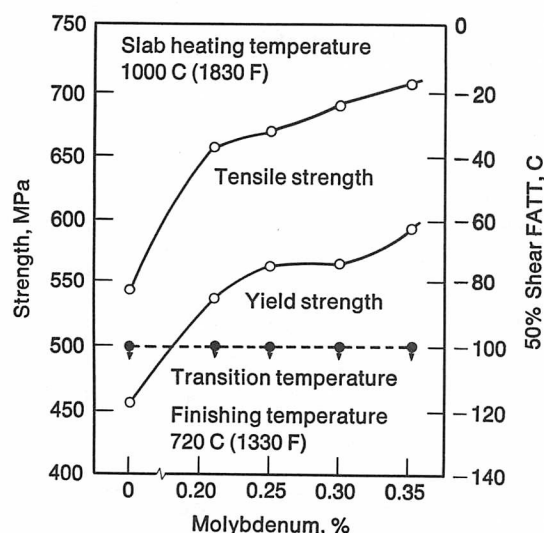


FIGURE 4—Effect of manganese content on the strength and Charpy V-notch transition temperature. The base composition is 0.02% C, 0.04% Nb, 0.01% Ti and 0.001% B.



FIGURE 2—Effect of carbon content on the strength and Charpy V-notch properties. The base composition is 1.75% Mn, 0.04% Nb, 0.18% Mo, 0.01% Ti and 0.001% B.
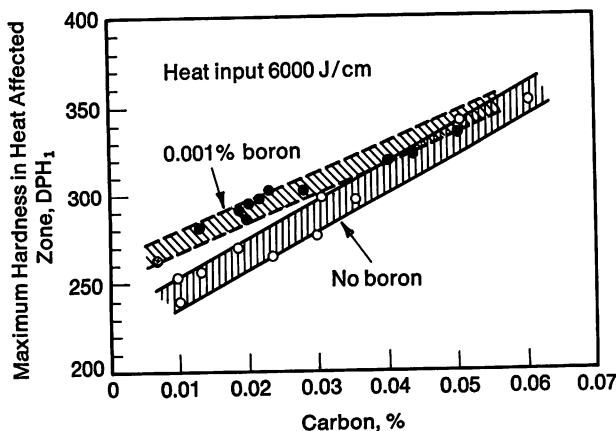


FIGURE 3—Effect of carbon content on the hardness of heat affected zone.
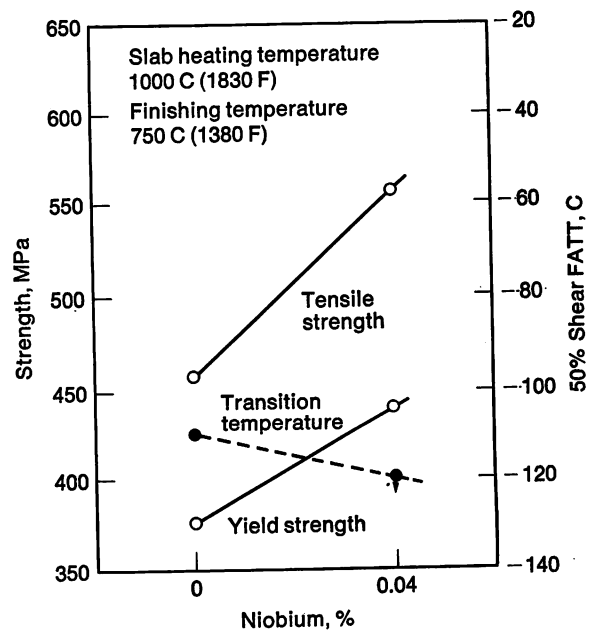


FIGURE 5—Effect of niobium on the strength and Charpy V-notch transition temperature. The base composition is 0.02% C, 1.70% Mn, 0.01% Ti and 0.001% B.

(1830 F), and it seems to contribute to the development of a bainitic microstructure as well as to precipitation hardening.

Figure 7 shows the effect of molybdenum on the strength and Charpy V-notch transition temperature. Molybdenum also increases strength without a loss in toughness. This element is important for producing a fine grained bainitic microstructure in conjunction with manganese and other elements. The amount of molybdenum required also depends on the strength and plate thickness. Although molybdenum can be replaced by other elements such as manganese, nickel and copper, some molybdenum is required for producing a higher strength steel beyond API grade X-70.

Figure 8 shows the effect of nitrogen on strength and Charpy V-notch transition temperature. The behavior of mechanical properties in Figure 8 can be explained with regard to the hardenability effect of boron. Boron is an indispensable element for this kind of bainitic steel. To assure the hardenability effect of boron, it is necessary to fix nitrogen with other elements which have stronger affinity for nitrogen than boron. When titanium is used for this purpose, it must be added to satisfy the relationship: Ti—3.4 N $\geqq$ O.

Excessive titanium forms titanium carbide which is detrimental to toughness. Under optimum conditions, titanium combined with nitrogen improves toughness in both the base metal and HAZ to prevent austenite grain growth during slab heating, hot rolling and welding.

Although boron also combines with nitrogen, the resulting boron nitride (or boron constituent) degrades toughness. It is therefore desirable to restrict boron and nitrogen contents to as low a level as possible.

The effects of individual elements in ULCB steel on the mechanical properties were examined separately thus far. As shown in Figure 9, the tensile strength of ULCB steel can be correlated with the calculated $D_I$ value which is defined as follows:

$$D_I \text{ (inches)} = \sqrt{C/10}\, [5.1\,(\text{Mn-1.2}) + 5]\, (1 + 0.7\,\text{Si})$$
$$(1 + 3\,\text{Mo})\,(1 + 0.36\,\text{Ni})$$

within a limited range of chemical compositions



0% niobium                    0.04% niobium    50μm
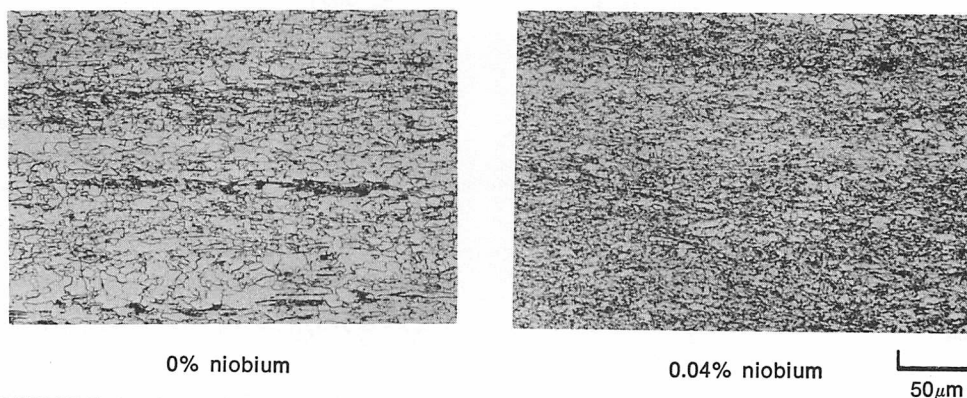
FIGURE 6—Optical micrographs showing the effect of niobium on the microstructure.



FIGURE 7—Effect of molybdenum content on the strength and Charpy V-notch transition temperature. The base composition is 0.02% C, 2.0% Mn, 0.05% Nb, 0.01% Ti and 0.001% B.
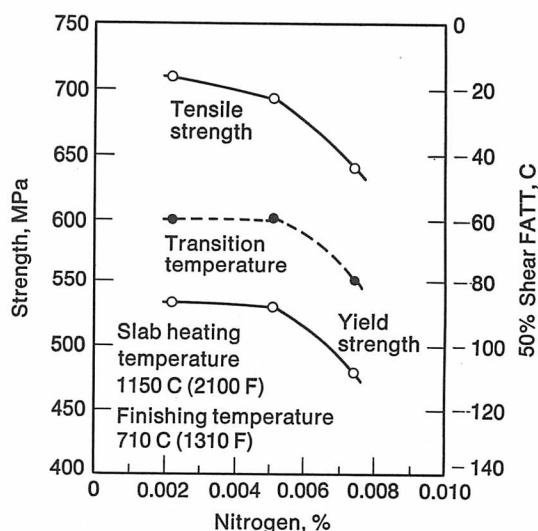


FIGURE 8—Effect of nitrogen content on the strength and Charpy V-notch transition temperature. The base composition is 0.03% C, 1.75% Mn, 0.04% Nb, 0.18% Mo, 0.01% Ti, and 0.001% B.

(Mn > 1.2%) and processing parameters. This relation is based on the premise that boron contributes significantly to the development of the bainitic microstructure.

However, it is very difficult to obtain the relationship between toughness and chemical composition because of the complicated and important effects of processing parameters.

## Effects of Heating and Rolling Conditions

The effect of heating temperature on mechanical properties was examined with a 22 mm (0.87 in.) plate rolled from a 210 mm (8.3 in.) slab. The chemical com-



FIGURE 9—Relationship between calculated $D_I$ and tensile strength for ULCB steel.



FIGURE 10—Effect of slab heating temperature on the strength, BDWTT transition temperature and Charpy V-notch energy of ULCB steel.

position was 0.02% carbon, 1.72% manganese, 0.04% niobium, 0.18% molybdenum, 0.01% titanium and 0.001% boron.

Figure 10 shows the effect of slab heating temperature on the strength and Charpy V-notch properties. Figures 11 and 12 show the changes in austenite grain size and acid-soluble niobium in the slab during heating. Figure 13 shows the change in microstructure and cleavage fracture appearance with slab heating temperature.

Decreasing the heating temperature from 1150 to 950 C (2100 to 1740 F) lowers the strength but increases toughness. This decrease in strength can be explained by the decreasing amount of niobium in solid solution during heating and by the austenite grain size prior to transformation.

The microstructure of plate rolled at a low heating temperature of 950 C (1740 F) comprises a mixture of fine grained ferrite and elongated island martensite, but that of plates rolled at heating temperatures of 1050 and 1150 C (1920 and 2100 F) mainly comprises bainite (Fig-



FIGURE 11—Effect of slab heating temperature on the austenite grain size for ULCB steel.



FIGURE 12—Effect of slab heating temperature on acid-soluble niobium.

Slab heating temperature 950 C (1740 F)

20 μm

10 μm
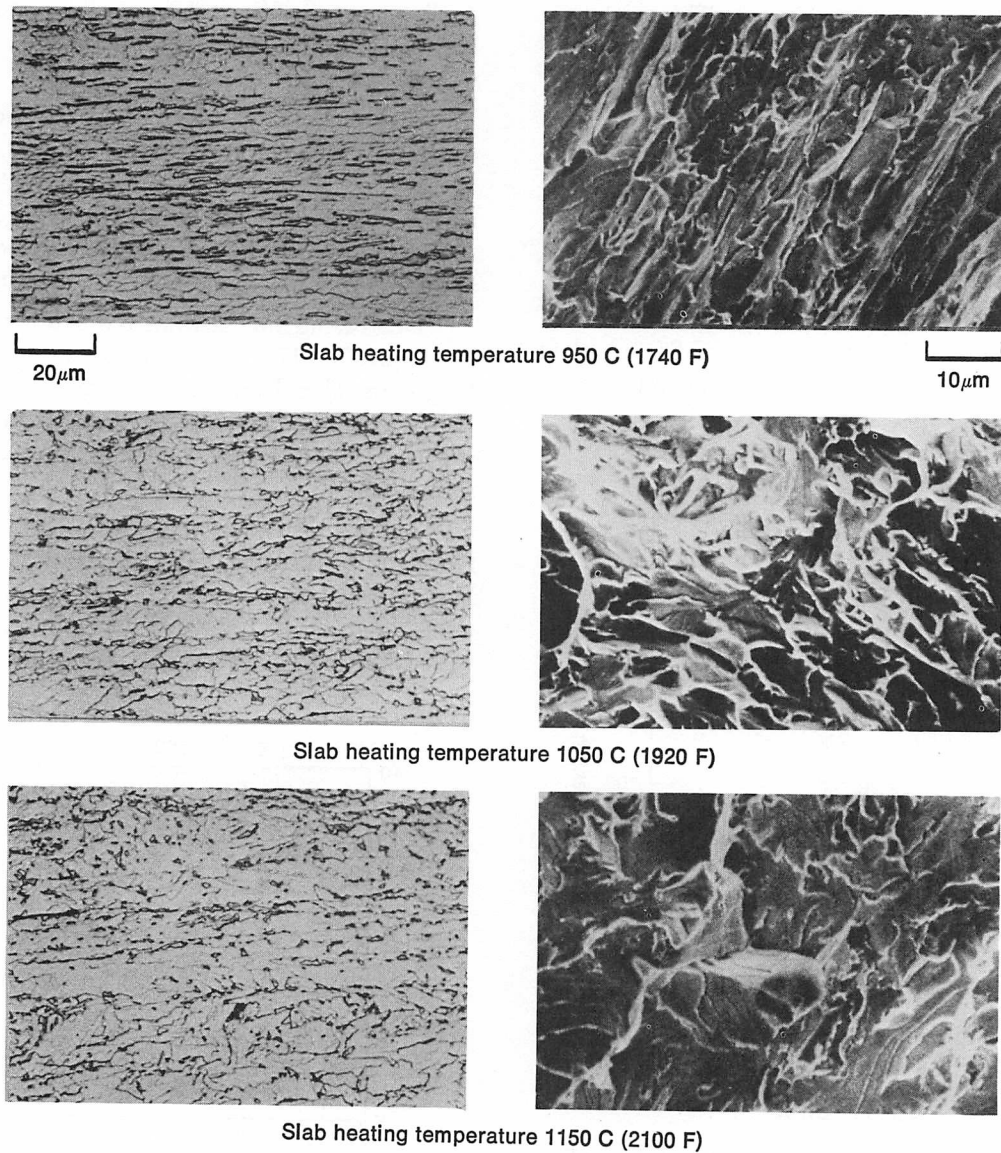
Slab heating temperature 1050 C (1920 F)

Slab heating temperature 1150 C (2100 F)

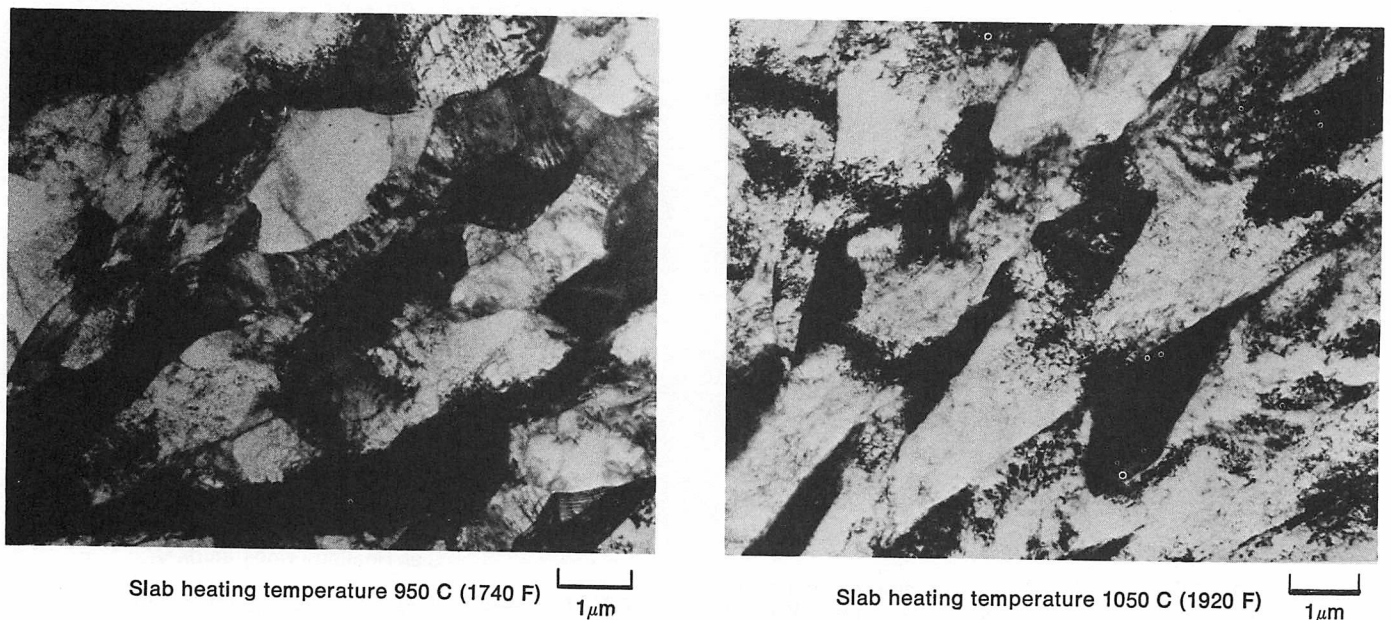FIGURE 13—*Change of microstructure and cleavage fracture appearance with slab heating temperature for ULCB steel.*



Slab heating temperature 950 C (1740 F)    1 μm

Slab heating temperature 1050 C (1920 F)    1 μm

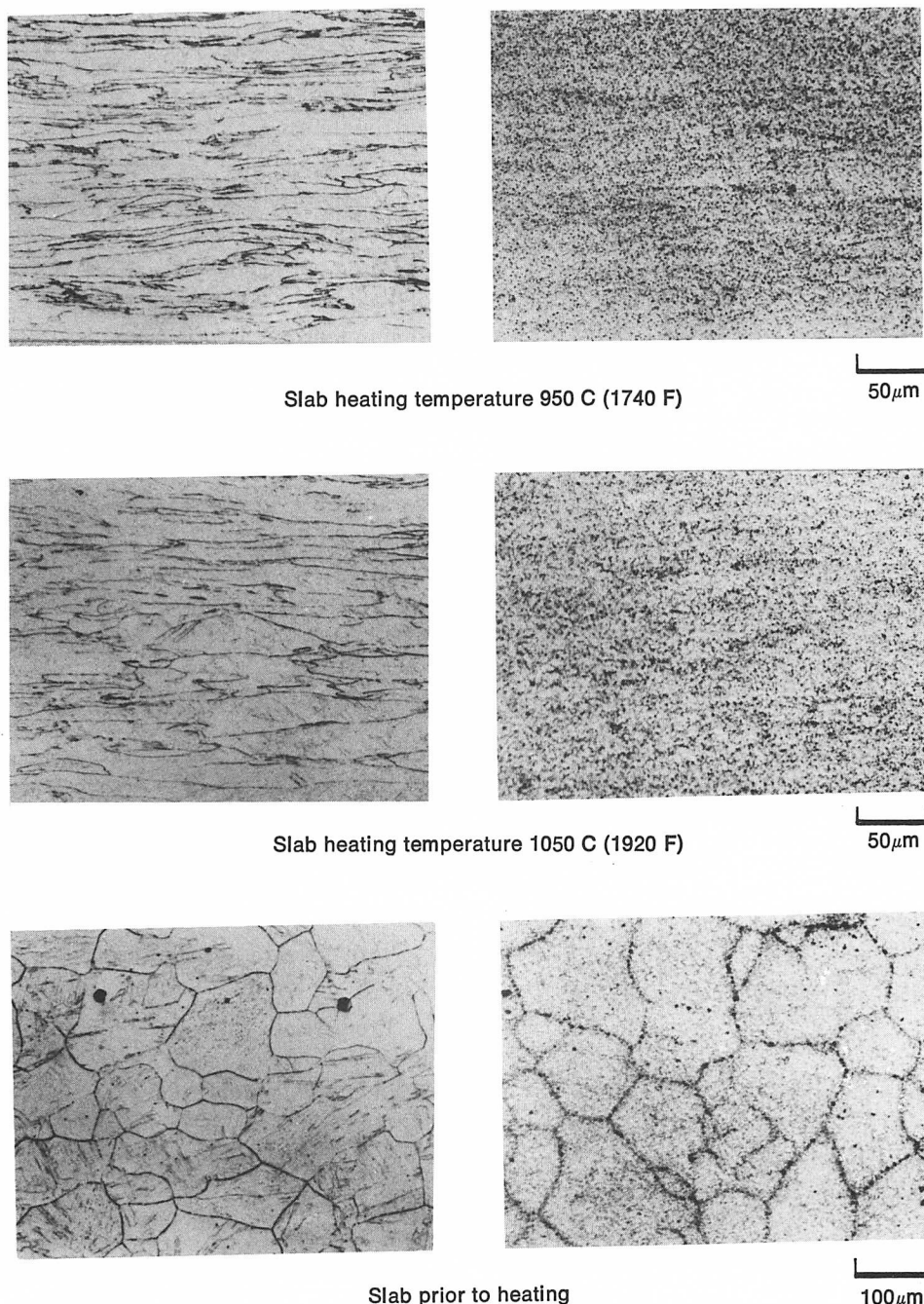FIGURE 14—*Transmission electron micrographs showing the effect of slab heating temperature on microstructure.*

Slab heating temperature 950 C (1740 F)                      50μm

Slab heating temperature 1050 C (1920 F)                     50μm

Slab prior to heating                                        100μm

FIGURE 15—*Optical micrographs and images of boron by fission track etching method in ULCB steel.*

ure 13). Figure 14 clarifies this feature in the microstructure. Ferrite grains of plate rolled from extremely low temperature heating at 950 C (1740 F) are strongly deformed and have cell structures.

Figure 15 shows the distribution of boron atoms in plate determined by a fission track etching method and the corresponding austenite grain at an intermediate thickness of 35 mm (1.4 in.) during rolling, as compared with a slab prior to heating.

Although it is thought that boron segregates not only at nonrecrystallized austenite grain boundaries but also at deformation bands formed by low temperature rolling, the distribution of boron in plates rolled from heating

temperatures of 950 and 1050 C (1740 and 1920 F) is similar.

It can be concluded that the differences in austenite grain size prior to transformation and amounts of niobium in solid solution during heating cause the differences in microstructure.

On the other hand, the change of toughness with slab heating temperature can be explained by the difference of effective grain size for cleavage fracture, as found in Figure 13. It is a well-known fact that the transition of microstructure from ferrite-pearlite to bainite increases effective grain size.
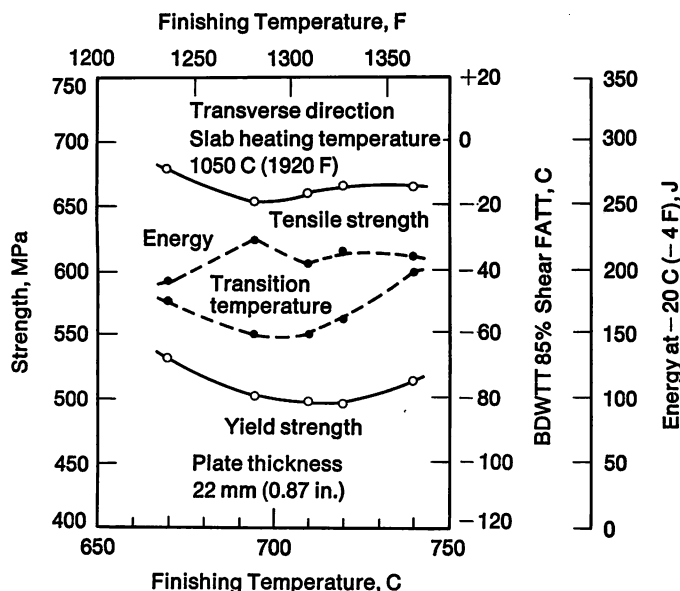
FIGURE 16—Effect of finishing temperature on the strength, BDWTT transition temperature and Charpy V-notch energy of ULCB steel.
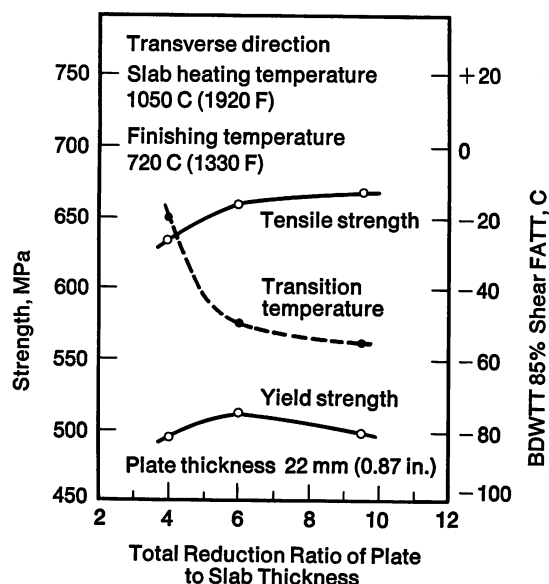


FIGURE 17—Effect of total reduction ratio of plate to slab thickness on the strength and BDWTT transition temperature under the condition that reduction below 900 C (1650 F) is kept constant.

Low temperature heating ranging from 1000 to 1050 C (1830 to 1920 F) is most desirable for toughness in this steel to achieve the good combination of strength and toughness.

Excessive low temperature heating decreases the impact energy because of the high separation density on fracture surfaces.

Figure 16 shows the effect of finishing temperature on the strength and impact properties. Although the variation in finishing temperature has little effect on strength, a preferable temperature range exists for toughness. This temperature is approximately 700 C (1290 F) which is slightly above the bainitic transformation temperature.

Even if low temperature heating is employed and the austenite grain size during heating is kept small, good toughness cannot be obtained unless sufficient total reduction is employed (Figure 17). This fact indicates that deformation in the austenite recrystallization region plays an important roll in grain refinement.

## Properties of ULCB Steel Pipe for Arctic Service

NSC has successfully developed ULCB steel through a number of fundamental experiments and actual production tests. This steel makes it possible to produce high strength linepipe from API X-60 to X-80 grades for Arctic service.

Properties of this steel as a 20 mm (0.79 in.) wall pipe of 1420 mm (56 in.) diameter will be detailed hereunder.

**Production Process and Chemical Compositions.** Figure 18 schematically shows the production process for linepipe. Table II shows typical chemical compositions of X-70 and X-80 ULCB steels. The steels were
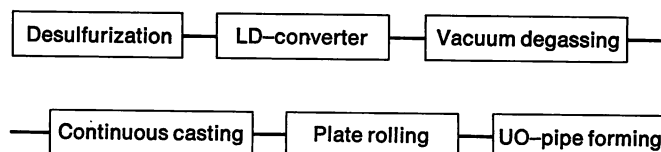


FIGURE 18—Production process for ULCB steel for Arctic service.

**Table II**—Chemical Compositions

| Grade | Element, % | | | | | | | | | | | | | |
| | C | Si | Mn | P | S | Ni | Mo | Nb | Ti | B | Al | N | $C_{eq.}$ [1] | $P_{cm}$ [2] |
|---|---|---|---|---|---|---|---|---|---|---|---|---|---|---|
| X-70 | 0.020 | 0.13 | 1.89 | 0.020 | 0.002 | — | — | 0.048 | 0.016 | 0.001 | 0.044 | 0.0025 | 0.335 | 0.124 |
| X-80 | 0.018 | 0.16 | 2.01 | 0.019 | 0.003 | 0.32 | 0.30 | 0.052 | 0.018 | 0.001 | 0.041 | 0.0024 | 0.434 | 0.154 |

[1] $C_{eq.} = C + \dfrac{Mn}{6} + \dfrac{Cr+Mo+V}{5} + \dfrac{Ni+Cu}{15}$

[2] $P_{cm} = C + \dfrac{Mn+Cu+Cr}{20} + \dfrac{Si}{30} + \dfrac{V}{10} + \dfrac{Mo}{15} + \dfrac{Ni}{60} + 5B$

**Table III**—Mechanical Properties of 1420 mm (56 in.) Diameter Pipes

| Grade | Direction of Test | Yield Strength, MPa (ksi) | | Tensile Strength, MPa (ksi) | | Elongation in 50.8 mm (2 in.), % | Yield Ratio, % | Energy at −20 C (−4 F) J (ft-lb) | | 50% Shear FATT, C (F) | | BDWTT Shear Fracture Area at −20 C (−4 F), % |
|---|---|---|---|---|---|---|---|---|---|---|---|---|
| X-70 | Longitudinal | 520 | (75.4) | 630 | (91.4) | 38 | 83 | 202 | (149) | <−80 | (<−110) | — |
| | Transverse | 542 | (78.6) | 653 | (94.7) | 38 | 83 | 141 | (104) | <−80 | (<−110) | 100 |
| X-80 | Longitudinal | 591 | (85.7) | 716 | (103.8) | 35 | 83 | 176 | (130) | <−80 | (<−110) | — |
| | Transverse | 633 | (91.8) | 746 | (108.2) | 33 | 85 | 131 | (97) | <−80 | (<−110) | 100 |
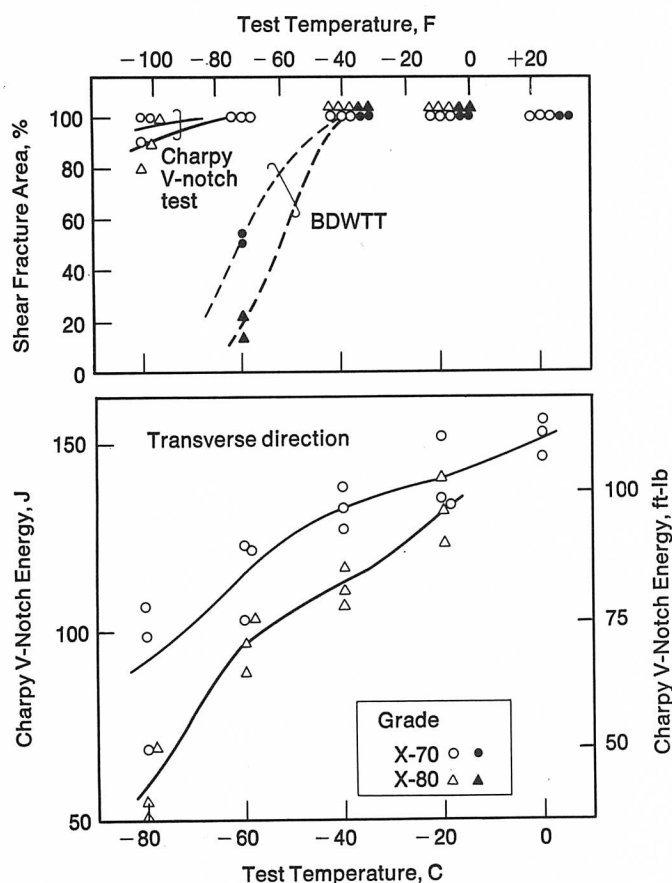


FIGURE 19—*Typical energy and fracture appearance transition curves for pipes.*



FIGURE 20—*Optical micrographs of ULCB steels.*

melted in a 250-ton LD converter and cast continuously into a 210 mm (8.3 in.) slab. The slabs were rolled to 20 mm (0.79 in.) plate by a newly-developed controlled rolling method.

Because the chemical composition and controlled rolling in the plate mill are very important factors, the ranges of alloying elements and heating and rolling conditions are strictly controlled.

**Base Metal Properties of Pipe.** Table III shows the mechanical properties of ULCB steel pipes. Figure 19 shows typical energy and fracture appearance transition

temperature curves. Figure 20 shows optical micrographs.

In spite of ultra low carbon content, the effective use of boron results in high strengths as in API X-70 and X-80 requirements. High impact energy and low transition temperature can be attributed to ultra low carbon contents and fine grained bainite as shown in Figure 20.

Stress/strain curves for ULCB steel exhibit a continuous yielding behavior, and therefore yield strength increases by UO pipe forming as shown in Figure 21.
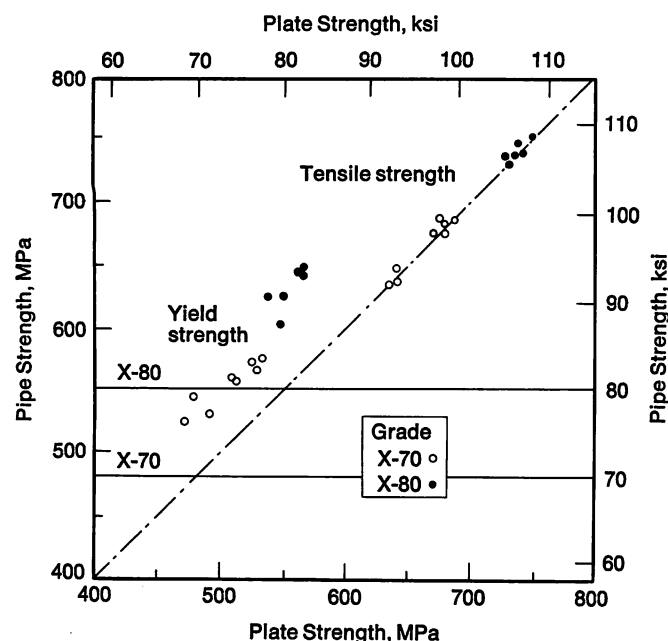
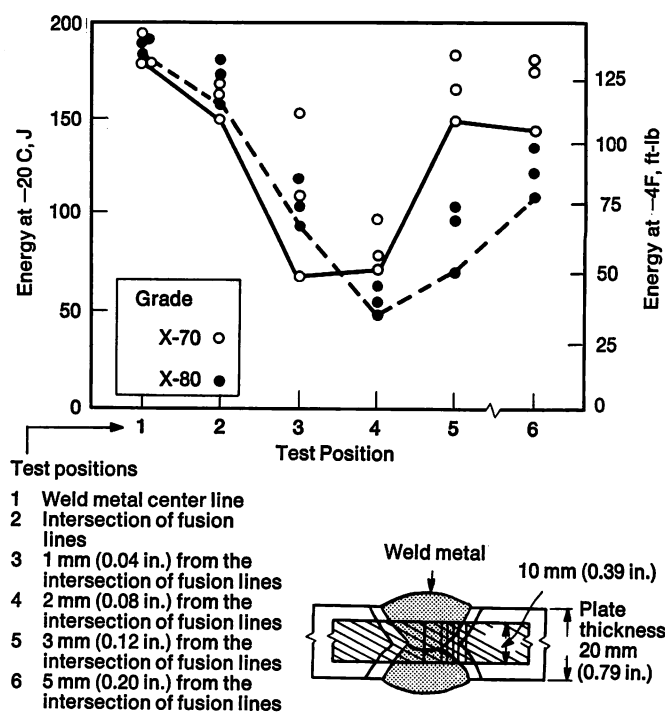FIGURE 21—*Change of strength resulting from pipe forming.*



**Test positions**

1  Weld metal center line
2  Intersection of fusion lines
3  1 mm (0.04 in.) from the intersection of fusion lines
4  2 mm (0.08 in.) from the intersection of fusion lines
5  3 mm (0.12 in.) from the intersection of fusion lines
6  5 mm (0.20 in.) from the intersection of fusion lines

FIGURE 22—*Charpy V-notch energy of submerged arc weld joint at different test positions.*

**Table IV**—Mechanical Properties of Submerged Arc Weld Joint

| Grade | Tensile Properties (Transverse Weld) | | | Charpy V-Notch Impact Properties | | |
|---|---|---|---|---|---|---|
| | Tensile Strength, MPa (ksi) | Elongation in 50.8 mm, % | Location of Fracture | Test Position[1] | Energy at −20 C (−4 F), J (ft-lb) | 50% Shear FATT, C (F) |
| X-70 | 681 (99.0) | 36 | Base metal | Weld metal center line | 184 (136) | −60 (−75) |
| | | | | 2 mm from the intersection of fusion line | 83 (61) | −35 (−30) |
| X-80 | 758 (110.2) | 30 | Base metal | Weld metal center line | 187 (138) | −60 (−75) |
| | | | | 2 mm from the intersection of fusion line | 57 (42) | −30 (−20) |

[1] Reference to Figure 22.

**Properties of Seam Welds.** Longitudinal seam welds were made with a single pass on each side, employing a submerged arc welding procedure. Heat input was approximately 39 kJ/cm (99 kJ/in.) for inside and 49 kJ/cm (124 kJ/in.) for outside passes.

Table IV gives the mechanical properties of submerged arc welded joints. Figures 22 and 23 show the change in Charpy V-notch energy of submerged arc welded joints with test position and the distribution of hardness across the joints.

Good toughness in the HAZ can be achieved with grain refinement from fine, dispersed TiN particles and from the decrease in high carbon martensite islands resulting from the lowered carbon content.

These results confirm that ULCB steel has good weld metal toughness and is suited for Arctic grade linepipe.

**Field Weldability.** Table V shows Battelle underbead cracking test results. No cracking occurs in this test because of the ultra low carbon content and the low carbon equivalent.

To ascertain the properties of actual pipe joints, Y-butt welding of short pipes was performed. Welding was made with six passes, with heat input ranges from 25 to 34 kJ/cm (64 to 86 kJ/in.).

Table VI and Figure 24 show the properties of girth weld joints. The hardness in the HAZ can be kept very low.
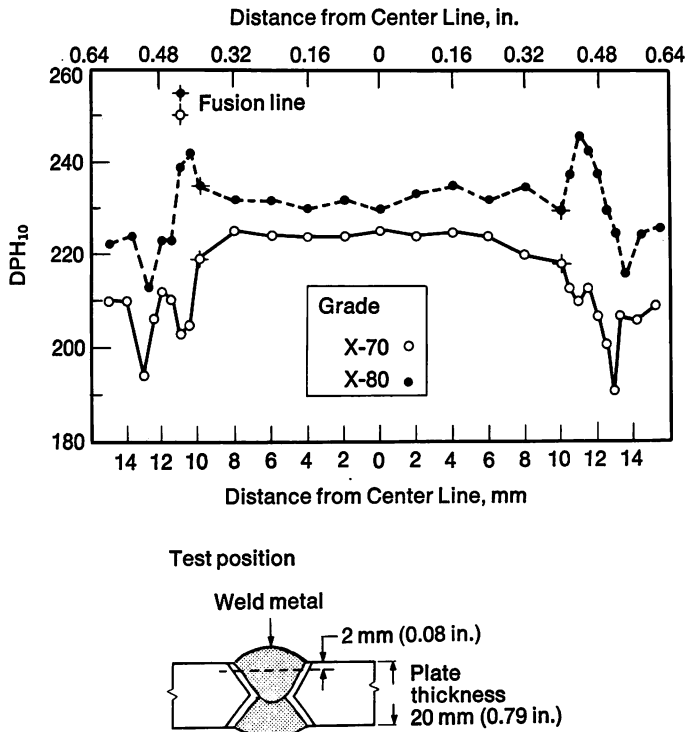
Distance from Center Line, in.



FIGURE 23—Distribution of hardness across submerged arc weld joint.

**Table V**—Battelle Under-Bead Cracking Test Results

| | Preheat Temperature, C (F) | | | | |
|---|---|---|---|---|---|
| Grade | 5 (40) | 25 (75) | 50 (120) | 75 (165) | 100 (210) |
| X-70 | O | O | O | O | O |
| X-80 | O | O | O | O | O |

O No cracking.

Welding conditions
Current: 100 amps.
Voltage: 25 volts.
Travel speed: 24 cm/min (9.4 in./min).
Heat input: 6.0 kJ/cm (15 kJ/in.).
Filler metal: 3.2 mm (0.13 in.) dia.
Phoenix Cel-80.
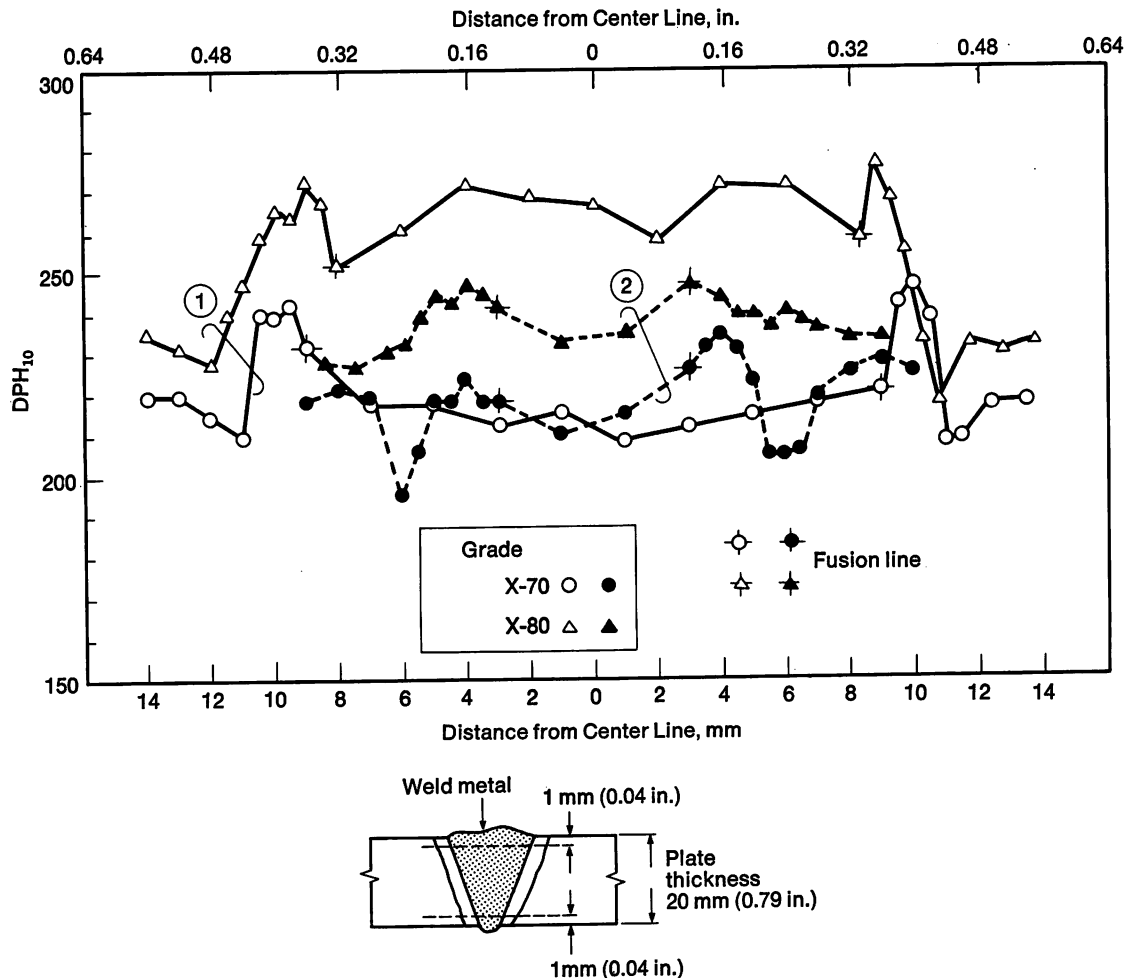


FIGURE 24—Distribution of hardness across simulated girth weld joint.

**Table VI**—Mechanical Properties of Simulated Girth Weld Joint

| Grade | Tensile Properties (Transverse Weld) | | | | Side-Bend Test | Charpy V-Notch Impact Properties | | |
|-------|------|------|------|------|------|------|------|------|
| | Tensile Strength, MPa (ksi) | | Elongation in 50.8 mm (2 in.), % | Location of Fracture | 50.8 mm (2 in.) Dia. Pin | Test Position | Energy at −20 C (−4 F), J (ft-lb) | 50% Shear FATT, C (F) |
| X-70 | 657 | (95.3) | 36 | Base metal | Good | Weld metal center line | 98 (72) | −20 (−4) |
| | | | | | | Heat affected zone | 122 (90) | −30 (−20) |
| X-80 | 732 | (106.2) | 28 | Base metal | Good | Weld metal center line | 88 (65) | −45 (−50) |
| | | | | | | Heat affected zone | 107 (79) | −25 (−15) |

Welding conditions
  Welding rod type: Low hydrogen (4 mm, 0.16 in. diameter).
  Heat input: 25 to 34 kJ/cm (64 to 86 kJ/in.).

## Conclusions

To improve the low temperature toughness and weldability of bainitic steel for linepipe, NSC has developed ULCB steel which has a new chemical composition. NSC's ULCB steel, produced by a newly-developed controlled rolling method, is well suited for API X-60 to X-80 grade linepipe for Arctic service. This steel exhibits an excellent combination of strength, toughness and weldability.

## References

1. T. Terazawa, et al., *Toward Improved Ductility and Toughness,* Climax Molybdenum Company, Kyoto, 1971, 101.

2. Y. Ito and K. Bessyo, IIW Document IX-576-68, 1968.

3. R. E. Dolby, *Low Carbon Structural Steels for the Eighties,* May 1979, IIIB-1.

4. F. B. Pickering, *Microalloying 75,* Session 1, Vanitech, London, 1975, 3.

5. H. Gondon, et al., Nippon Steel Technical Report No. 14, 1979, 55.

## Discussion

R. STEVENSON, *General Motors Corporation.* Why is there anisotropy in the properties of plate produced from vacuum degassed stock of low sulfur content?

H. TAMEHIRO. Sulfur does contribute to directionality even at a content as low as 0.003%. When sulfur is extremely low, about 0.001%, there is very little directionality.

# Materials Technology for Oil and Gas Production

by R. D. Kane and W. K. Boyd
Battelle-Houston Operations

To fulfill the energy demands of our modern industrial society, it is necessary to maintain ample supplies of hydrocarbon fuels. Through several decades of gas and oil production, however, many of the existing large domestic reservoirs have reached maturity and are either in or approaching periods of declining production. Consequently, it is necessary to

1. develop methods to extract gas and oil more efficiently and completely from these existing reservoirs, and

2. develop the technology involved in producing gas and oil from greater depths and in increasingly more hostile environments.

In addition, methods of producing hydrocarbons from unconventional sources (tar sands, oil shales, coal deposits, etc.) must also be explored.

The development of these sources of hydrocarbons involves new materials frontiers. It requires the identification of areas where economic or engineering benefit will be gained through application of materials technology. In the production of oil and gas, the paramount materials needs are centered around the necessity for higher strength and/or corrosion resisting materials. These downhole environments can have pressures exceeding 138 MPa (20 ksi) and temperatures exceeding 205 C (400 F) and can contain hydrogen sulfide and/or carbon dioxide gas, sulfur compounds, organic acids and concentrated brine solutions.

This paper discusses several areas of gas and oil production where application of new materials technology has been considered and applied. These areas are

1. deep well production,

2. sour (H$_2$S) gas production, and

3. enhanced recovery methods such as CO$_2$ injection, steam injection and *in situ* combustion.

## Deep Well Production

It is increasingly necessary to produce deep hydrocarbon-containing formations. In the past, many of these deep reservoirs were overlooked because there was an abundance of shallower deposits available that could be produced inexpensively. For example, as shown in Figure 1, the number of wells drilled and completed to depths in excess of 4570 m (15,000 ft) has increased dramatically since 1950.[1] This increase is primarily the result of the need to obtain greater amounts of hydrocarbons to fulfill energy requirements. However, it also reflects the development of engineering capabilities which allow wells to be routinely drilled and completed to depths exceeding 6,060 m (20,000 ft) as indicated in Figure 2.[1]

Tubulars developed for today's deep wells must be designed to have high strength to insure resistance to tensile failure under high axial load as well as resistance to collapse and burst.[2] A list of the observed casing grade
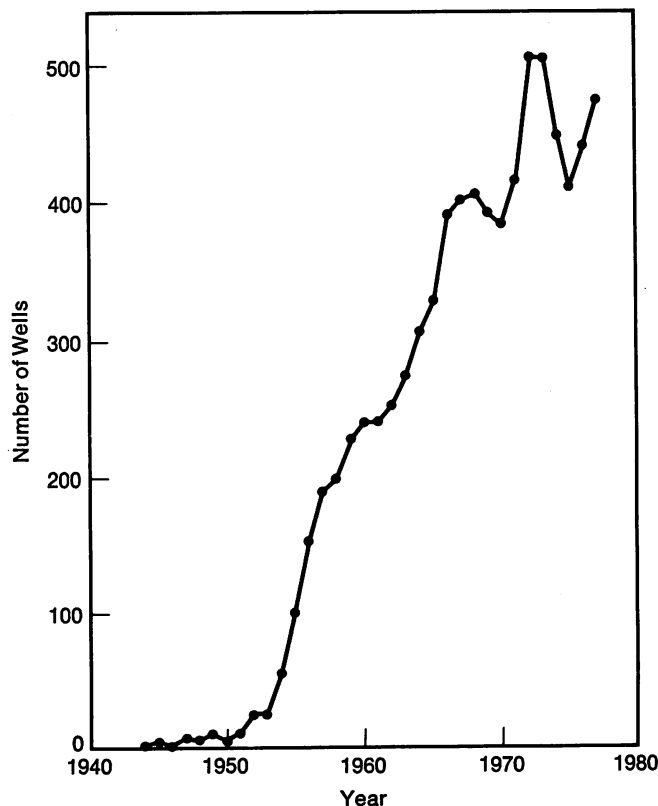


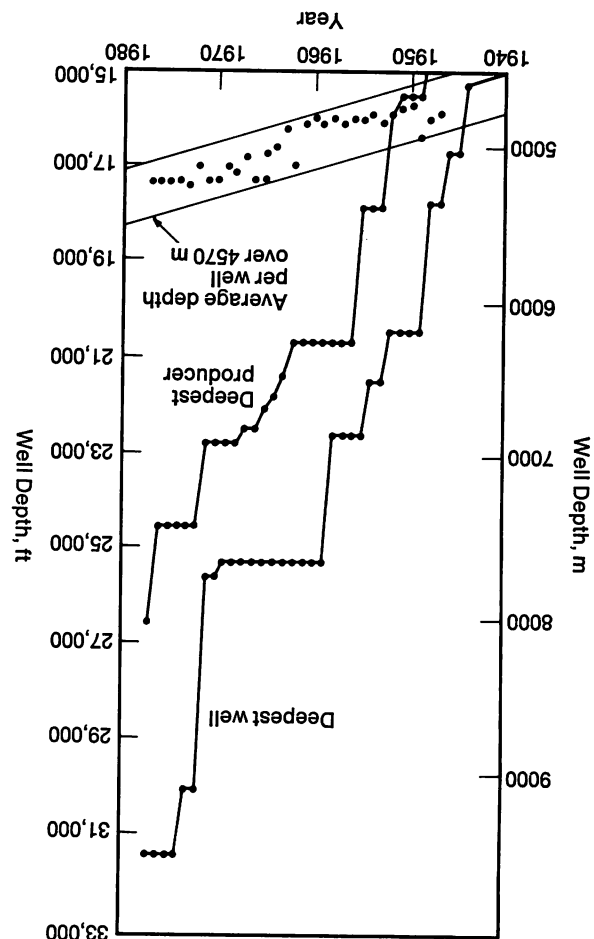FIGURE 1—Wells completed per year to 4570 m (15,000 ft) and deeper.

steels is shown in Table I. The higher strength tubular grades (L-80 through V-150) are typically based on Mn-Cr-Mo-C alloying technology and are processed in the quenched and tempered condition. These materials have yield strengths in the range 550 to 1240 MPa (80 to 180 ksi). As will be discussed later, the most significant factor which can limit the use of the high strength steels is the presence of $H_2S$. Deep wells have been completed to formations con-

**Table I—Standard API and Non-API High Strength Steel Casing and Tubing Grades**

| Grade | Minimum Yield Strength, MPa (ksi) | Maximum Yield Strength, MPa (ksi) |
| --- | --- | --- |
| C-75* | 520 (75) | 655 (95) |
| L-80* | 550 (80) | 655 (95) |
| N-80 | 550 (80) | 760 (110) |
| C-90* | 620 (90) | 725 (105) |
| S-95 | 655 (95) | 760 (110) |
| P-110 | 760 (110) | 965 (140) |
| S-125 | 860 (125) | 1035 (150) |
| S-140 | 965 (140) | 1140 (165) |
| V-150 | 1035 (150) | 1240 (180) |

* Specified for use in sour environments.



FIGURE 2—Wells drilled, completed and produced at depths of 4570 m (15,000 ft) and deeper.

taining pressures in excess of 138 MPa (20 ksi) with temperatures greater than 205 C (400 F). Current trends indicate that well depths will continue to increase and will eventually result in wells with bottomhole temperatures in excess of 260 C (500 F). As these temperatures increase, they approach a range where strength properties of steel and other materials of construction become affected. Similar effects have already been observed in geothermal wells. Elevated temperature tensile data on high strength casing grade steels at 370 C (700 F) indicate that over 20% strength loss occurs from room temperature values.[3]

## Sour Gas Production

In oil field operations, it is often necessary to produce hydrocarbon reservoirs that contain significant amounts of $H_2S$ and $CO_2$ in addition to brine solutions. When these species are present in the environment, corrosive degradation of the exposed materials can occur. This degradation can take many forms; e.g., weight loss corrosion, (pitting, crevice and general corrosion), and environmentally induced embrittlement (sulfide stress cracking, hydrogen induced cracking, hydrogen embrittlement and stress corrosion cracking).

### Weight Loss Corrosion

Weight loss corrosion often limits the potential usefulness of commonly used oilfield materials by removing metal and thereby reducing load and pressure-sustaining capabilities of equipment. This is particularly critical in downhole applications because components must typically be designed with minimum wall thicknesses for clearance considerations which maximizes axial and burst loading.

Formations containing 28 to 46% $H_2S$, 3 to 8% $CO_2$ and 51 to 69% methane at 205 C (400 F) and 138 MPa (20 ksi) have been encountered. These levels of $CO_2$ and $H_2S$ coupled with high pressures and temperatures constitute a very aggressive corrosive environment that few materials can withstand. In many instances, these downhole corrosion problems can be handled with chemical inhibition in periodic batch treatments. Under severe conditions, however, the successful inhibition of corrosion has to be based on circulation of inhibitor and a carrier oil to saturate the sour gas with oil. This provides a continuously inhibited liquid hydrocarbon phase on the metal surface. The main drawback for such a system is the large expense associated with injection and reclamation of the carrier oil and inhibitor. In addition, as temperatures and pressures increase, it becomes increasingly difficult to saturate the gas with the carrier oil and inhibitor to establish the protective inhibited oil layer on the metal surface.[4,5]

Alternate means of providing a protective inhibited layer on the metal surfaces are being examined. One method which incorporates the use of water soluble
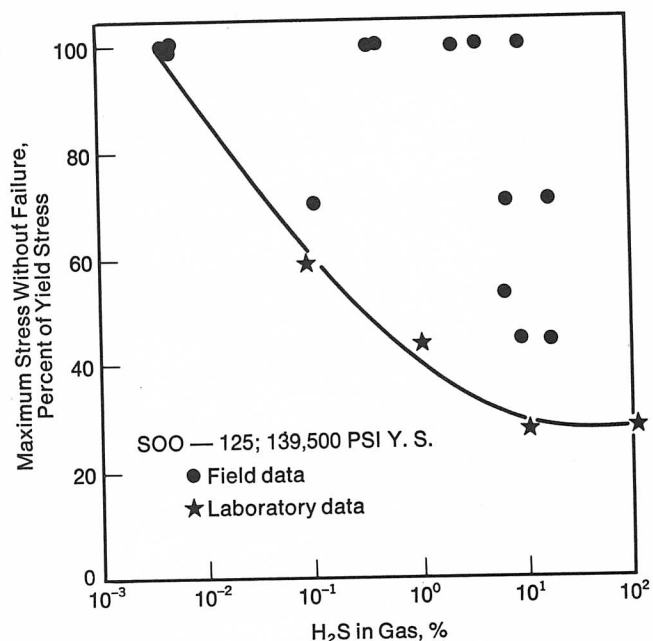
FIGURE 3—Corrosion of steel in sour field environment.



FIGURE 4—Typical sulfide stress cracking data for low alloy casing grade steels in aqueous laboratory and field environments containing $H_2S$.

inhibitors appears attractive. During production, some of the water contained in the produced gas condenses. Therefore, very little inhibitor and carrier solution is needed to provide a continuous protective inhibitor/water layer on the metal surface.

In some cases, however, as shown in Figure 3, chemical inhibition is not effective because of either environmental or engineering limitations. This has recently brought about the use of corrosion resisting alloys in a number of applications from downhole tubulars to valve and specialty components. Some of the materials being considered for these applications are shown in Table II. As indicated in this table, they typically contain significant amounts of chromium, nickel and molybdenum which enhance their corrosion resistance. In some cases, titanium alloys are also being considered.

### Environmental Embrittlement

**Sulfide stress cracking of steels.** When $H_2S$ is present, embrittlement can occur in high strength steels (greater than or equal to 550 MPa, 80 ksi minimum yield strength) commonly used in completing and producing gas and oil wells. This phenomenon, called sulfide stress cracking (SSC), constitutes the principal problem associated with the production of sour hydrocarbons. SSC results in failures at stresses less than the material yield strength (Figure 4). It is a hydrogen embrittlement phenomenon resulting from the simultaneous action of tensile stress and hydrogen produced on the metal surface by the iron/$H_2S$ corrosion reaction. SSC is the single most important limitation in the use of high strength steels in some oil field environments.

High strength tubular steel grades designed for use in $H_2S$ service include C-75, L-80 and C-90. These grades have been shown to exhibit the necessary resistance to SSC for use in sour field operations. The highest strength grade of those indicated, C-90, is the result of extensive development work conducted by both steel manufacturers and oil companies. It is a Cr-Mo-C alloy (similar to AISI 4130) processed by sophisticated quenching and tempering facilities to produce a uniform, nearly completely martensitic structure capable of being tempered at relatively high temperatures and retaining yield strength levels of 620 to 725 MPa (90 to 105 ksi).

The use of higher strength steels in $H_2S$ environments is governed by (1) environment temperatures, (2) $H_2S$ concentration, and (3) material yield strength.[6] As shown in Figures 5 and 6, regions of performance have been identified where SSC is and is not anticipated. Typically, the higher strength steels (yield strength greater than or equal to 758 MPa, 110 ksi) have been used effectively at temperatures above 80 C (175 F) because of the beneficial effect of elevated temperature on promoting resistance to SSC. Currently, research is being conducted to develop higher strength steels with greater resistance to SSC. Materials with specified composition (control of elements such as Mn, Cr, Mo, S and P) and/or reduction in the levels of heat treatment are being examined.[7] However, much work needs to be done to

**Table II**—Typical High Alloy Materials Being Considered for Corrosive Oilfield Service

| Type | Materials | Element, % | | | | | | | | |
|---|---|---|---|---|---|---|---|---|---|---|
| | | Fe | Ni | Cr | Mo | Cb + Ta | Ti | Al | Cu | Other |
| **Stainless Steels** | | | | | | | | | | |
| Martensitic | 12 to 13 Cr | Bal | — | 12 | — | — | — | — | — | — |
| | CA6NM | Bal | 4 | 12 | 0.70 | — | — | — | — | — |
| Precipitation Hardened | 17 – 4 PH[a] (martensitic) | Bal | 4 | 17 | — | — | — | — | 4 | — |
| | Custom 450[b] (martensitic) | Bal | 6 | 15 | 0.75 | — | — | — | 1.5 | — |
| | A-286 (austenitic) | Bal | 26 | 15 | 1.3 | — | 2.0 | 0.2 | — | B – 0.015 |
| Austenitic | 20 Cb – 3[b] | Bal | 33 | 20 | 2.5 | 1.0 max. | — | — | — | — |
| | 2 RK 65[c] | Bal | 25 | 19 | 4.5 | — | — | — | 1.5 | — |
| | Sanicro 28[c] | Bal | 31 | 27 | 3.5 | — | — | — | 1.0 | — |
| Duplex (Austenitic/ Ferritic) | AF – 22[d]/SAF – 2205[c] | Bal | 5.5 | 22 | 3 | — | — | — | — | N – 0.14 |
| | Uranus 50 | Bal | 7 | 21 | 2.5 | — | — | — | 1.5 | — |
| | Ferralium[e] | Bal | 5.5 | 26 | 3 | — | — | — | 3 | N – 0.1 min. |
| **Nickel Alloys** | | | | | | | | | | |
| Cold Reduced | Hastelloy Alloy C-276[e] | 6 | Bal | 15 | 16 | — | — | — | — | Co – 2.5 max. W – 4.0 |
| | Hastelloy Alloy G[e] | 20 | Bal | 22 | 6 | 2 | — | — | 2.0 | Co – 2.5 max. W – 1.0 max. |
| | Inconel Alloy 625[f] | 25 | Bal | 21 | 9 | 3.5 | 0.2 | 0.2 | — | — |
| | Incoloy Alloy 825[f] | 30 | 42 | 22 | 3 | — | 0.9 | 0.1 | 2.25 | — |
| | Incoloy Alloy 800[f] | 45 | 32 | 21 | — | — | 0.4 | 0.4 | 0.38 | — |
| Precipitation | Inconel Alloy 718[f] | 19 | Bal | 19 | 3 | 5.0 | 0.9 | 0.5 | 0.15 | — |
| | Pyromet 31[b] | 15 | Bal | 23 | 2 | 0.85 | 2.3 | — | 1.3 | B – 0.005 |

[a] ARMCO Steel Corporation.
[b] Carpenter Technology Corporation.
[c] Sandvik, Inc.
[d] Mannesmann Steel.
[e] Cabot Corporation, Stellite Division.
[f] Huntington Alloys.
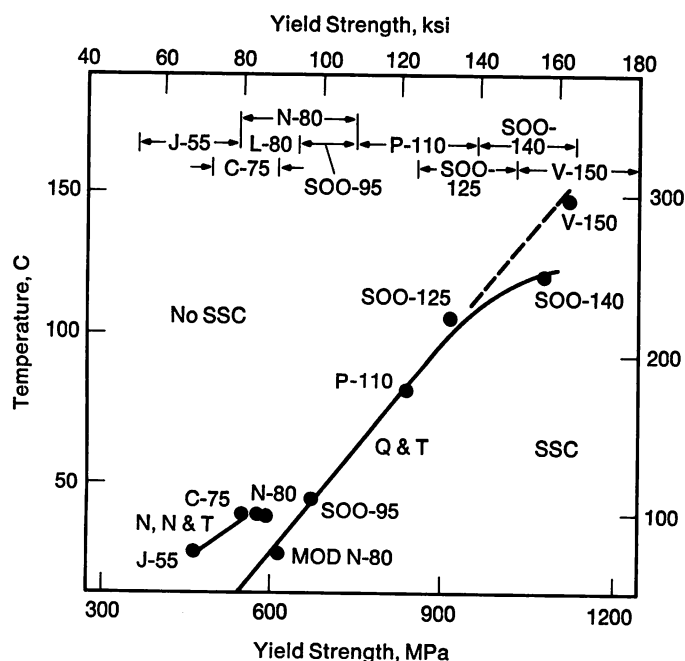


FIGURE 5—Effect of temperature on sulfide stress cracking of high strength steels.
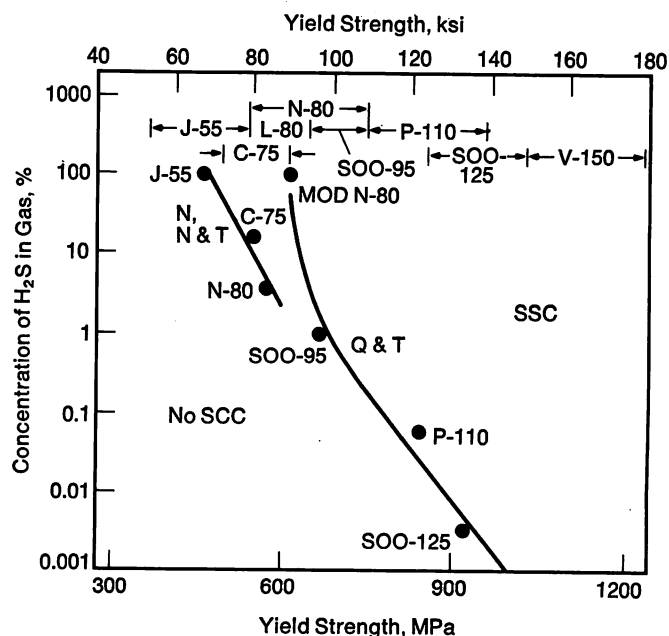


FIGURE 6—Effect of $H_2S$ concentration on sulfide stress cracking of high strength steels.
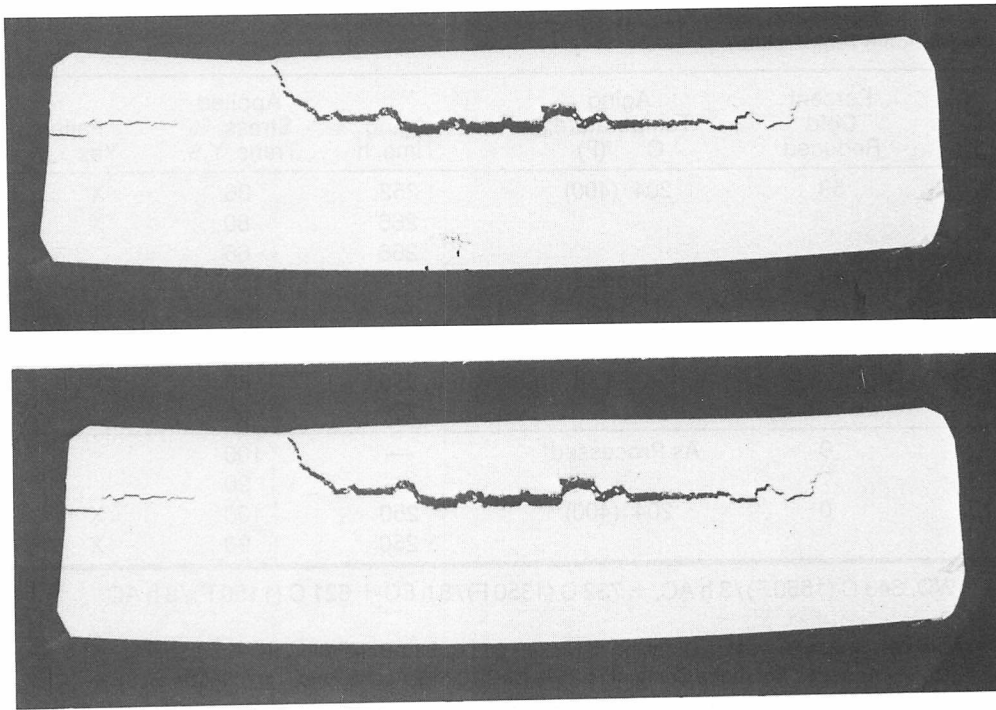
FIGURE 7—Hydrogen-induced cracking of linepipe steel in laboratory seawater solution saturated with $H_2S$.

extend the useful yield strength range of steels in sour gas applications.

**Hydrogen-induced cracking of steels.** Linepipe steels (less than or equal to 550 MPa, 80 ksi yield strength) commonly used in oilfield service can be susceptible to embrittlement in $H_2S$ by a phenomenon called hydrogen-induced cracking (HIC) or blister (stepwise) cracking. It differs from SSC in that it occurs by the accumulation of hydrogen, which is produced by sulfide corrosion, along internal interfaces such as manganese sulfide inclusions or low temperature transformation structures (see Figure 7).[8]

HIC has produced surprisingly few failures in sour gas pipe line. However, the currently unpredictable and catastrophic nature of the failures presents a significant problem to pipe lining sour environments. Typically, the problem is mitigated by control of the environment to minimize corrosion and uptake of hydrogen into the steel (i.e., dehydration to remove water and chemical inhibition). In some cases, susceptibility to HIC has been reported to be reduced by controlling the shape and distribution of nonmetallic inclusions in the steel through special metal practice (low S steel) and deoxidation practice. Also, additions of Cu may have a beneficial effect on reducing susceptibility to HIC. Controversy currently exists, however, regarding the factors which control the behavior of pipe line materials in the sour service environments.

**The embrittlement of high alloy materials.** With the increasing trend toward mitigating corrosion and obtaining high strength with stainless steels and nickel alloys, there has been much interest recently in the corrosion



FIGURE 8—Hydrogen embrittlement of Hastelloy Alloy C-276 in 5% NaCl, 0.5% acetic acid saturated with $H_2S$. C-ring specimen galvanically coupled to steel.

and embrittlement behavior of these alloys in environments containing $H_2S$, $CO_2$ and chlorides. As shown in Table III, high strength nickel alloys can exhibit hydrogen embrittlement (HE) in these environments.[9] Figure 8 reveals a typical fracture appearance of a cold-worked nickel alloy resulting from HE. Such failures are the result of cathodic (hydrogen) charging of the nickel-base alloy in the aqueous $H_2S$ environment. This phenomena is accelerated greatly by galvanic coupling of these materials to steel. The amount of hydrogen charg-

**Table III**—Hydrogen Embrittlement of Nickel Base Alloys (C-Ring Specimens Coupled to Steel, Tested in NACE Solution at Room Temperature)

| Material | Percent Cold Reduced | Aging Temperature, C    (F) | Aging Time, h | Applied Stress, % Trans. Y.S. | Failure Yes | No | Exposure, Days |
|---|---|---|---|---|---|---|---|
| Hastelloy Alloy C-276 | 59 | 204  (400) | 252 | 96 | X | | 4 |
| | | | 266 | 80 | X | | 29 |
| | | | 266 | 66 | | X | 97 |
| | 59 | Unaged | — | 100 | | X | >100 |
| | 37 | Unaged | — | 100 | | X | >100 |
| Inconel Alloy 625 | 59 | 204  (400) | 250 | 96 | X | | <3 |
| | | | 250 | 80 | X | | <3 |
| | | | 250 | 66 | | X | >100 |
| Inconel Alloy 718 | 0 | As Processed* | — | 100 | | X | >100 |
| | | | — | 90 | | X | >100 |
| | 0 | 204  (400) | 250 | 100 | X | | 42 |
| | | | 250 | 90 | X | | 82 |

* 1052 C (1925 F)/1 h WQ, 843 C (1550 F)/3 h AC, + 732 C (1350 F)/8 h FC + 621 C (1150 F)/8 h AC.

**Table IV**—Stress Corrosion Cracking of Nickel- and Cobalt-Base Alloys (C-Ring Specimens Tested in Aqueous Solutions Containing 25% NaCl, 0.5% Acetic Acid, 1 g/l Sulfur, $H_2S$)

| Material | % Trans. Y.S. | 175 (350) 70% | 90% | 205 (400) 70% | 90% | 290 (550) 70% | 90% |
|---|---|---|---|---|---|---|---|
| Hastelloy Alloy C-276 (37% CR) | | O | X | X | X | X | X |
| MP35N (59% CR) | | X | X | X | X | X | X |
| Hastelloy Alloy G (59% CR) | | — | — | X | X | — | — |

O — Passed.

X — Failed.

Time-to-failure by SCC of 100 days in some cases. Test duration needed to obtain data shown in this table was 150 days.
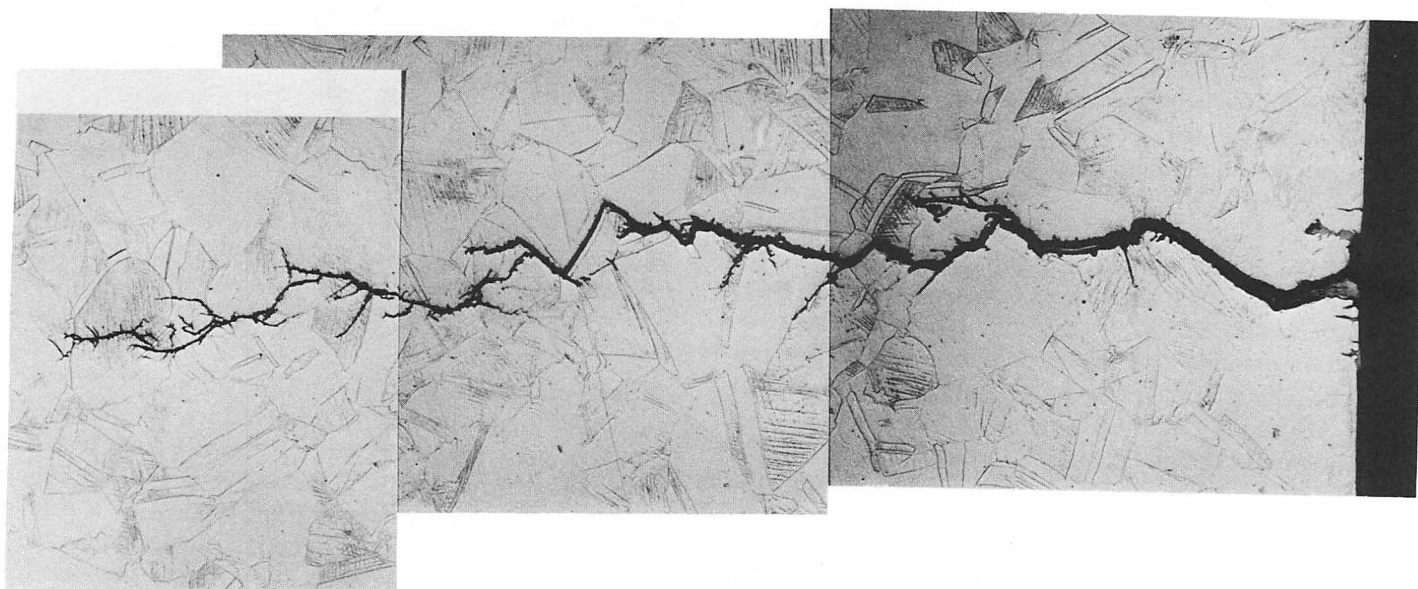


FIGURE 9—*Stress corrosion cracking of Hastelloy Alloy C-276 in aqueous solution of 25% NaCl, 0.5% acetic acid, 1 g/l sulfur, saturated with $H_2S$ at 205 C (400 F).*

ing produced by the nickel alloy/steel galvanic couple in an aqueous H₂S environment is sufficient in many cases to produce HE in a susceptible material. Increased susceptibility to HE in nickel alloys has been found to be associated with elevated temperature heat treatments (260 to 595 C, 500 to 1100 F), higher material strength and stress levels, and transverse stresses (relative to the cold-working direction). Similar to SSC in steels, HE of the nickel alloys is less severe at elevated temperatures.[9] Consequently, the current use of these materials is based on the control of strength levels, eliminating high temperature heat treatments, and control of the environment by minimizing galvanic interactions.

In addition, the susceptibility of stainless steels and nickel alloys to SCC in elevated temperature H₂S/sulfur-containing brines is greater than once realized.[10] As shown in Table IV, nickel alloys can exhibit SCC at temperatures greater than 175 C (350 F). The susceptibility to SCC appears related to alloy content; the materials containing higher Cr and Mo levels exhibiting better performance. The nature of the SCC found in these alloy systems is shown in Figure 9. Similar behavior for the lower alloy stainless materials to that shown here for the nickel alloys has been reported. Unfortunately, there are currently no comprehensive guidelines available for the use of these materials over a range of downhole environments. The use of these materials is currently limited and is typically based on the results of laboratory autoclave tests.

## Enhanced Recovery Methods

The petroleum industry has conducted extensive research on the development of methods for enhanced recovery since the 1930s. From this research, several processes, referred to as tertiary recovery methods, have been developed and field tested. The processes that show significant promise beyond conventional secondary waterfloods are (1) chemical flooding, (2) CO₂ injection, and (3) thermal methods. Currently, the thermal methods in use are steam injection and *in situ* combustion (fire flooding). The two processes which involve application of new oilfield materials technology are CO₂ injection and the thermal recovery methods.[11]

### CO₂ Injection

This recovery technique involves the injection of CO₂ gas to miscibly displace crude oil, thus permitting recovery of more of the oil from the reservoir rock than is presently possible with conventional techniques. Successful CO₂-enhanced recovery requires a supply of large quantities of CO₂. Therefore, CO₂ source wells (those capable of producing large quantities of high percentage CO₂ gas) must be drilled, completed and produced. This gas must then be processed, transported and injected into the production reservoir. The primary factor limiting the

performance of engineering materials is the corrosion of components exposed to aqueous environments containing CO₂.

The material requirements for CO₂ recovery varies considerably, however, depending on the location in the CO₂ recovery system. For example, in the CO₂ source well, very high concentrations of CO₂ gas are present at high pressures. This leads to a highly acidic downhole environment by the formation of carbonic acid when CO₂ and liquid water combine. To eliminate corrosion problems in CO₂ source wells, the application of high alloy materials has taken place. Materials such as Incoloy 825, containing nickel, chromium, iron and molybdenum, are being considered for such service. Other materials being considered include 12-13% chromium stainless steels and duplex stainless steels. The basis for the use of materials containing high levels of nickel and chromium in aqueous CO₂ environments can be seen in Figures 10 and 11. These figures indicate the beneficial effects of both chromium and nickel on corrosion resistance in CO₂ condensate well service.[12]
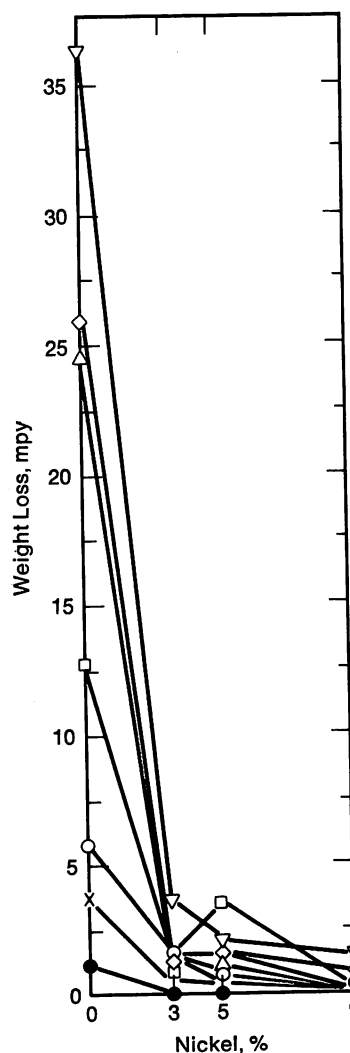


FIGURE 10—*Effect of nickel content on the CO₂ corrosion of steels in gas condensate well service.*

Following production, the $CO_2$-rich gas is processed and dehydrated. Dehydration is a necessary step since this allows the use of conventional steel pipeline materials in the transportation and injection of the $CO_2$ without excessive corrosion occurring.[14] Corrosion problems can arise, however, in the injection system particularly if a water alternate $CO_2$ gas (WAG) recovery method is used. Plastic coated and/or nickel plated steel or AISI 410 stainless steel construction is often used. Severe corrosion of carbon steel, however, has been reported at locations of coating damage.[13] Pitting corrosion of AISI 410 stainless steel wellhead components has also been observed.

In the production system associated with a $CO_2$ recovery, the extent of corrosion is generally related to the degree of water production. As water production increases, the severity of corrosion also increases. Production well corrosion is further complicated by the presence of other aggressive species such as $H_2S$ and chlorides in

the produced hydrocarbons. In most production well applications, corrosion can be mitigated satisfactorily with corrosion inhibitors or plastic coated tubing. However, for some production well applications where high temperatures are encountered, high alloy materials such as the duplex stainless steels, 12-13% chromium stainless steels and nickel alloys appear as attractive alternatives to conventional low alloy steels.

There is a recovery process similar to $CO_2$ injection, whereby combusted boiler (inert) gas is injected into the hydrocarbon reservoir to enhance recovery. This gas contains high concentrations of nitrogen along with $CO_2$, CO and $NO_x$. Problems associated with this process include corrosion of steel components from the $CO_2$ gas and a form of stress corrosion cracking in steel caused by the presence of CO and $CO_2$ in the aqueous environment.

### Thermal Recovery Methods

Thermal recovery constitutes one of the most highly developed of the enhanced recovery techniques in terms of field experience. Basically, thermal processes add heat to the hydrocarbon reservoir (by either steam or in situ combustion) which reduces oil viscosity or in some cases vaporizes the oil. These techniques increase the mobility of viscous crude oils or tars so they can be more effectively produced. [11]

**Steam injection.** Steam injection has been used effectively to enhance viscous oil deposits in a number of locations in the United States West Coast since the early 1960s. This technique has also been used effectively in Venezuela. Standard carbon steel casing and tubing have been used successfully in these projects. The temperatures encountered during production from wells in these steam injection projects generally were limited to approximately 205 C (400 F). The lack of major corrosion problems in these projects appears related to the relatively low temperatures and natural inhibition by the heavier hydrocarbon constituents.

Steam injection projects conducted at temperatures in excess of 250 C (480 F) have encountered some problems with acid gas ($H_2S$ and $CO_2$) production. After production for one year, levels of $H_2S$ and $CO_2$ in the produced gases in one of these projects reached 31% and 78%, respectively. The $H_2S$ is produced by reactions with sulfur in the hydrocarbons or breakdown of pyrites. The presence of these acid gases in conjunction with high downhole temperatures can lead to severe corrosion problems with steel components. In addition, during periods when temperatures return to near ambient, production of $H_2S$ can cause SSC of high strength steels. Consequently, the use of SSC resisting materials must be considered in these cases. Similar experiences have been encountered during steam injection conducted for the purpose of producing hydrocarbons from tar sands in Canada. In these projects, highly alloyed material such
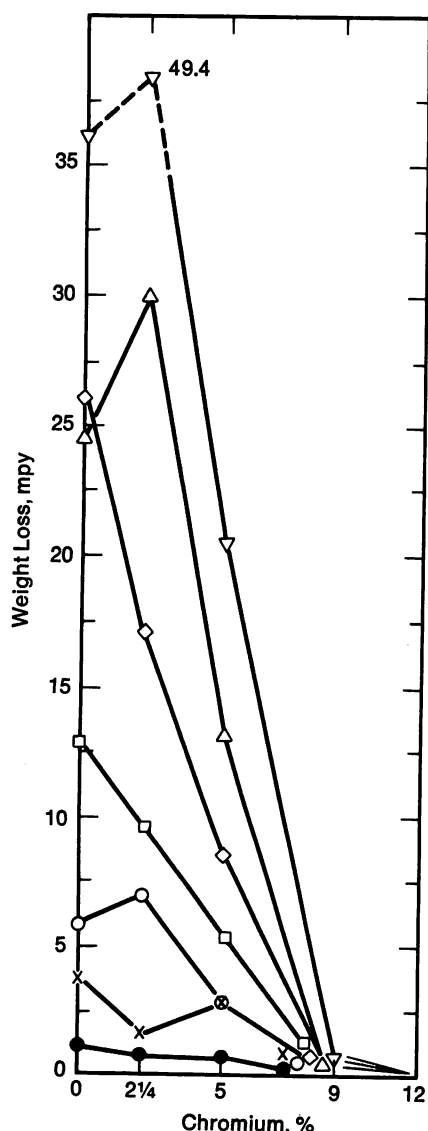


FIGURE 11—Effect of chromium content on the $CO_2$ corrosion of steels in gas condensate well service.

as Hastelloy Alloy C-276 have been used for downhole liners in the high temperature production zones to significantly reduce corrosion.

### In Situ Combustion

In situ combustion (also referred to as fireflooding) consists of injecting air into the formation to maintain a controlled burning of a portion of the hydrocarbon deposit. The heat generated by this burning along with steam, hot water and gas drive the hydrocarbons to production wells. These techniques have been extensively used in the production of high viscosity oil. However, it is currently being used in tar sand production and in situ coal gasification.

As the burning formation zone approaches a production well, temperatures increase dramatically. Temperatures between 205 C and 425 C (400 F and 800 F) can be encountered. Production rates also increase significantly as the burn zone approaches the production well. Therefore, it appears advantageous to maintain production as long as possible from a particular well to maximize production efficiency. However, a major limiting factor in production is corrosion of steel tubulars in this high temperature environment which may contain $H_2S$, $CO_2$ and various organic and inorganic acid constituents. At these very high temperatures, organic inhibitors are ineffective in mitigating corrosion resulting in frequent equipment changes being necessary to prevent failures. Oxidation and sulfidation of the materials of construction can occur. In addition, the production often contains solid particles such as sand, coke and iron sulfide corrosion products which combine errosion with corrosion.

There has been some limited use of high alloy liners for combustion projects in hopes of extending the life of production wells. Materials such as stainless steels, Incoloy 800, Incoloy 825 and Hastelloy Alloy C-276 have been employed in this service.

### Conclusions

In coming years, gas and oil production will depend more heavily on new sources of hydrocarbons and enhanced recovery of hydrocarbons from existing formations. As indicated in this review, special materials technology often necessary to exploit these sources of gas and oil can result in considerable benefit.

The use of higher strength and more corrosion resistant materials is taking place. Consequently, there is considerable need for additional design data to better define the limits of acceptable performance for high strength steels, stainless steels and nickel alloys in environments which may contain corrosive species and may involve high pressures and temperatures. New inhibitor systems must be developed which can extend the use of steel components into increasingly more hostile environments.

### References

1. R. McNally, Petroleum Engineer International, March 1978, 19.
2. J. A. Straatmann, Petroleum Engineer International, March 1978, 35.
3. R. E. Snyder, "Geothermal Well Caping Design: A Study of Failure Modes and Cementing Limitations," Prepared under Contract 13-2297, Sandia Laboratories, Albuquerque, New Mexico, May 1979, 90.
4. T. W. Hanby, Jr., "Development of High Pressure Sour Gas Technology," Preprint 8309, SPE Fall Meeting, September 1979.
5. M. C. Place, Jr., "Corrosion Control—Deep Sour Gas Production," Preprint 8310, SPE Fall Meeting, September 1979.
6. R. D. Kane and J. B. Greer, Journal of Petroleum Technology, 29, November 1977, 1483.
7. G. M. Waid and R. T. Ault, "The Development of a New High Strength Casing Steel with Improved Hydrogen Sulfide Cracking Resistance of Sour Oil and Gas Well Applications," Preprint 180, NACE Corrosion/79, March 1979.
8. A. Ikeda and M. Kowaka, Chemical Economy and Engineering Review, 10 (5-9), May/June 1978, 117.
9. R. D. Kane, M. Watking, D. F. Jacobs and G. L. Hancock, Corrosion, 33 (9), September 1977, 309.
10. R. D. Kane, J. B. Greer, D. F. Jacobs, H. R. Hanson, B. J. Berkowitz and G. A. Vaughn, "Stress Corrosion Cracking of Nickel and Cobalt-Base Alloys in Chloride Containing Environments," Preprint 174, NACE Corrosion/79, March 1979.
11. J. T. Miskell, Energy, Spring 1977, 21.
12. National Associaiton of Corrosion Engineers, "The Field Testing of 32 Alloys in The Flow Stream of Seven Condensate Wells," Publication No. 50-3, July 1950, 103.
13. L. E. Newton, Jr. and R. A. McClay, "Corrosion and Operational Problems, $CO_2$ Project," SACROC Unit, Preprint 6391, Permian Basin Oil and Gas Recovery Conference, Society of Petroleum Engineers, March 1977.

# Fireflooding — A Materials Challenge for the Eighties

by G. B. Kohut, J. R. Caldwell and R. A. Morris
Gulf Science and Technology Company

In recent years, there has been much discussion con-
cerning future crude oil availability in the United States.
Decreasing levels of crude oil production have stimulated
the search for alternate sources of energy as well as tech-
nologies to improve oil recovery from known reserves.
Figure 1 shows the expected distribution of U.S. produc-
tion of crude reserves, both past and present.[1] About
24% has already been produced; 9% is considered read-
ily producible by conventional techniques; 13% is tagged
as EOR (enhanced oil recovery) potential; 14% is con-
sidered producible in the future by presently developing
technology; while 40% will be left in the ground unless
a major breakthrough in technology occurs. This paper
deals with the barrel fraction tagged EOR potential.

## What Is Enhanced Oil Recovery?

Crude oil lies beneath the earth's surface in rock or
sand formations and not in large lakes or pools as artists
sometimes conceptualize. An analogy to the existence of
crude oil can be made with a tray of ordinary sand into
which a beaker of oil is poured. The oil saturates the sand
and occupies the space between the sand grains. Simi-
larly in oil reservoirs, oil is contained in the voids or
spaces between the actual sand or rock particles.

Normally formation oil is displaced from the reser-
voir by a water and/or gas drive mechanism into a pro-
duction well. Enhanced Oil Recovery techniques refer
to processes that aid or enhance the normal formation
recovery mechanisms. Fireflooding is one such EOR
process that shows considerable potential for improving
oil production in the 1980s and beyond.

## What Is a Fireflood?

Oil recovery is a displacement process. Water or gas
sweeps the oil from the rock or sand toward producing
wells. After the natural drive mechanism decreases, fire-
flooding is sometimes used to recover additional oil.

Figure 2 schematically shows a typical fireflood
operation. One well in a pattern of wells is designated
as an injection well. Others in the field are designated as
producers. After completing the wells with proper ma-
terials, the crude oil at the injection well is ignited with
a downhole heating device. Air is continuously injected
to maintain combustion. The formation oil is caused to
burn in a radial pattern toward the production wells.
During the burning process, steam and other gaseous
materials of combustion move radially outward from the
injection well toward the producing wells, displacing oil



% Original Oil-in-Place

| | |
|---|---|
| Produced | 24 |
| Reserves* | 9 |
| EOR Potential | 13 |
| Future Technical Developments | 14 |
| Considered Finally Unrecoverable | 40 |

*Conventional Recovery
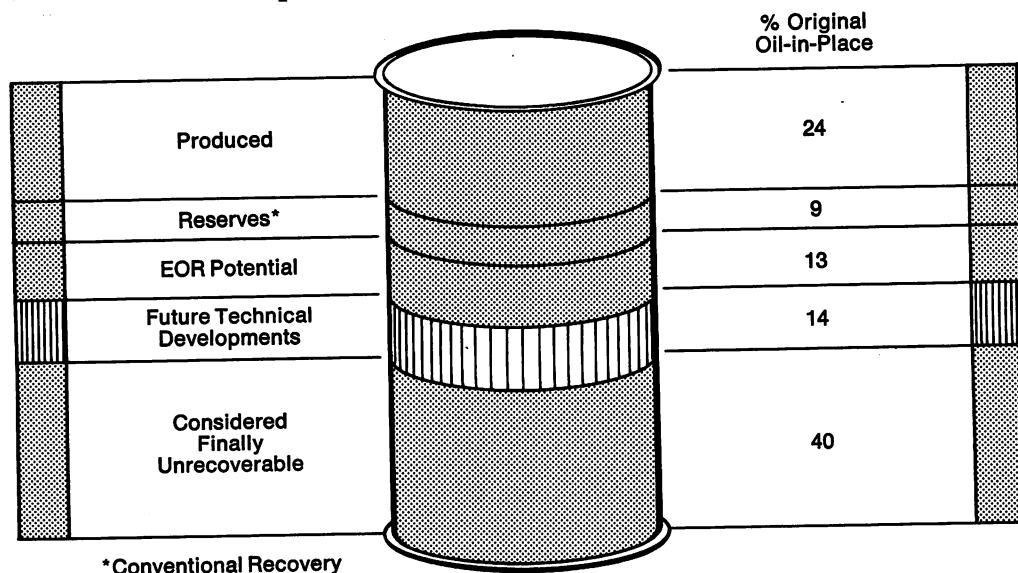
FIGURE 1—Representation of U.S. crude oil barrel.

and connate water ahead of the firefront. Heat from the combustion zone also reduces the oil viscosity and its resistance to flow. Water and oil are vaporized near the combustion zone and transported to cooler regions in the formation ahead of the combustion front where they condense. The temperature decreases ahead of the combustion front and levels out at between 95-315 C (200-600 F) at the steam plateau, ahead of which is located still another zone of warm fluids. The combustion zone moves through the reservoir at a speed which is a function of both air rate and the amount of oil burned; it travels at a speed less than the advance of the steam plateau.

Relatively high temperatures after steam breakthrough can accelerate corrosion and/or failure of downhole equipment and cause premature shutdown or loss of production wells. Selection of materials to withstand the temperature rise and corrosive conditions in the well vicinity is critical to maximize production.

## Corrosivity of Firefloods

A cursory look by the corrosion engineer at the fireflood process will alert him to the corrosion potential in a fireflood operation. Potential corrosives in producing wells are:

Oxygen

Organic acids

Carbonic acid

Chlorides

Sulfides

Oxygen is not normally present in conventional oil-producing formations. It is, however, a potential problem in firefloods since air is injected to support the combustion.

Organic acids are formed as a product of crude oil combustion. Formic and acetic acid would be the most probable constituents.

Carbonic acid ($CO_2$ dissolved in water) is present in many oil reservoirs or is formed in a fireflood as a combustion product of hydrocarbons. Carbonic acid is corrosive to conventional oilfield materials.

Chlorides are present in brines or saltwater naturally occurring in many formations and wells. At elevated temperatures, brine solutions become very corrosive to conventional materials. In fact, austenitic stainless steels can experience stress corrosion cracking in chlorides as shown in Figure 3.

Sulfides and sulfur compounds in fireflooding result from naturally occurring $H_2S$ in the gas, sulfur compounds released during combustion or from naturally occurring pyrites in the rock formation.

### Fireflood Production Well Environments

As stated above, corrosive gases and fluids are predicted for fireflood production wells. To identify qualitatively the types of constituents or corrosives in a fireflood environment, laboratory tests are sometimes performed
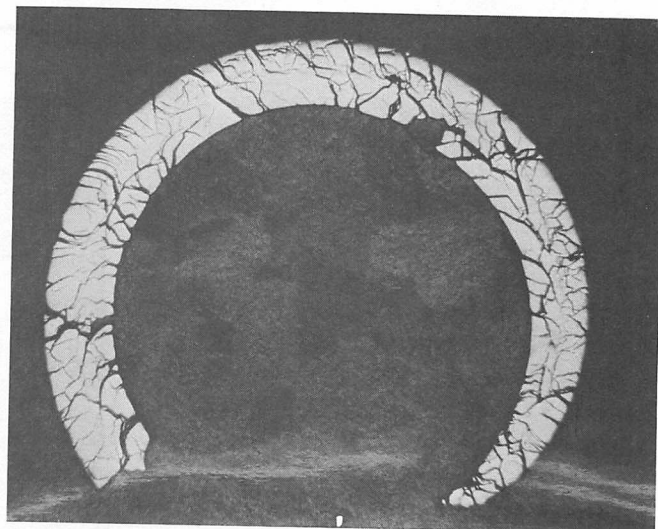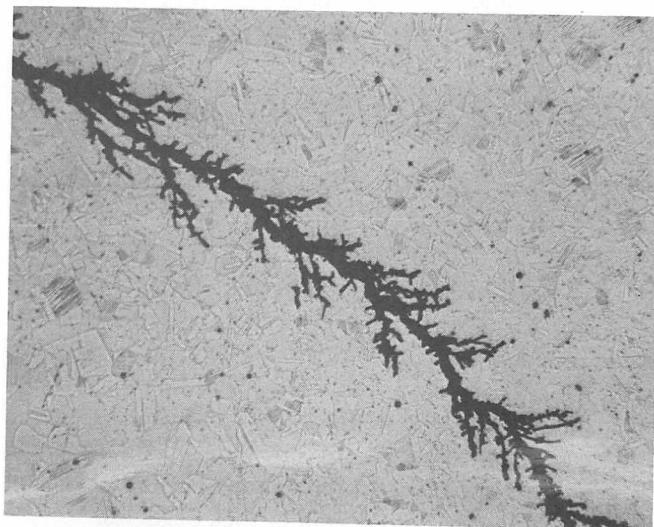




FIGURE 3—Chloride stress corrosion cracking in Type 316 stainless steel—spring (upper); production tubing packer component (lower).



FIGURE 2—Schematic diagram of a fireflood operation showing the various thermal zones in the reservoir during combustion.
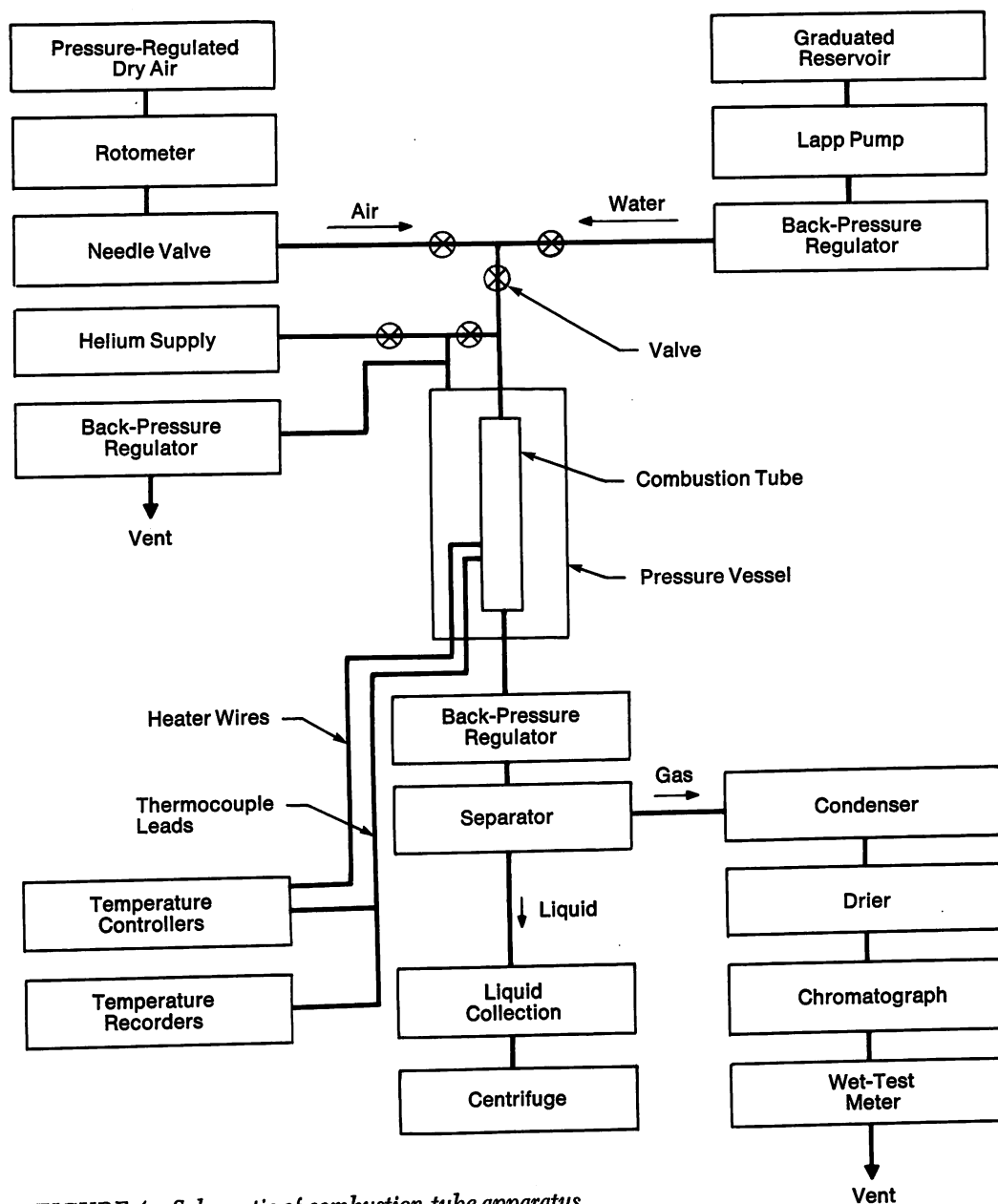
*FIGURE 4—Schematic of combustion tube apparatus.*

in an apparatus known as the combustion tube. This apparatus is schematically shown in Figure 4. The combustion tube consists of an inner chamber where sand, crude oil and water from a particular reservoir are packed. This tube is contained in a heated medium. Air is injected into the combustion tube, the oil-bearing sand is ignited and a burn is maintained by throttling the air. The effluent gases from the tube run through a condenser, and the liquid phase is centrifuged so that the oil and water fractions can be collected and analyzed. The gas fraction is passed through a chromatograph to identify various compounds and constituents.

Table I lists the results of several analyses of effluents from various combustion tube runs. Several points are noteworthy: (1) pH ranges are on the acid side primarily because of the presence of formic and acetic acids, (2) chloride concentrations are variable and de-

pendent upon saltwater or brine composition in the formation water, (3) sulfates are detectable in the water phase, and (4) $H_2S$ and other sulfide materials are present in the effluents.

## Materials for Firefloods

A screening program was conducted, to develop a data base for selecting materials for corrosive fireflood conditions. This program was designed to screen materials in three different manners with an attempt to develop correlations between field and laboratory tests. Tests were performed in combustion tubes, autoclaves and downhole.

Table II lists alloys that were screened for corrosion performance. Carbon steel (C-steel) represents the con-

**Table I**—Analysis of Combustion Tube Effluents from Various Reservoir Fluids

|  |  | Reservoir | | | |
|---|---|---|---|---|---|
|  |  | AA | BB | CC | DD |
| Water | pH | 4.0-7.0 | 3.8-7.2 | 3.7-7.4 | 4.5-7.3 |
|  | CL$^-$ | 65% | 11% | 7.2% | 6.3% |
|  | SO$_4$= | 0.22 | 0.16 | 0.44 | 0.3 |
|  | Acetic | <0.03 | 0.03-0.32 | 0.01-0.08 | ND |
|  | Formic | <0.03 | ND | ND | <0.03 |
| Oil | Acetic | <0.03 | ND | <0.03 | Tr |
|  | Formic | <0.03 | ND | <0.03 | ND |
| Gas | H$_2$S | Tr | ND | ND | ND |
|  | S= | 1.5 | 1.1 | 7 | 3.7 |
|  | Corrosion Rates at 90 C (195 F), mpy | | | | |
|  | Carbon Steel | 34.7 | — | 57.6 | 87 |
|  | Incoloy 825 | <0.1 | — | 1.6 | — |
|  | Inconel 625 | <0.1 | — | 1.1 | — |

ND = Not determined.
Tr = Trace.

**Table II**—Chemical Composition of Alloys Screened for Fireflood Service

| Alloy | Element, % | | | | |
|---|---|---|---|---|---|
|  | Cr | Ni | Mo | Fe | Other |
| Carbon Steel | — | — | — | Bal | — |
| T 410 | 13 | — | — | Bal | — |
| T 316 | 18 | 8 | 2.5 | Bal | — |
| Incoloy 800 | 20 | 32 | — | Bal | — |
| Incoloy 825 | 20 | 45 | 3 | Bal | 2.3 Cu |
| 20 Cb 3 | 20 | 32 | 2.5 | Bal | 3.5 Cu |
| 2 RK 65 | 20 | 25 | 4.5 | Bal | 1.5 Cu |
| Inconel 600 | 15 | Bal | — | 8 | — |
| Inconel 625 | 20 | Bal | 9 | 5 | — |
| Inconel 617 | 22 | Bal | 9 | — | 12.5 Co |
| Hastelloy C-276 | 15 | Bal | 16 | 6 | 4 W-2.5 Co |
| Hastelloy G | 22 | Bal | 6 | 20 | 2 Co |
| MP 35 N | 20 | 30 | 9.5 | — | 34 Co |
| MP 159 | 20 | 25 | 7 | 9 | 3 Ti-34 Co |
| Ti | — | — | — | low | — |
| Ti-Pd | — | — | — | — | 1.5 Pd |
| Ti-Mo-Ni | — | 0.8 | 0.3 | — | — |
| Ti-Al-V | — | — | — | — | 6 Al-4 V |

ventional ferritic steel materials used in oil production; 12 Cr (410 stainless) is conventionally the first alloy level above the carbon or low alloy steels; Type 316 is representative of the austenitic stainless steels. Iron base nickel-chromium alloys are represented by Incoloy 800; Inconel 625 and the Hastelloys represent nickel-base alloys containing chromium and molybdenum. Several titanium alloys were also tested.

**Combustion Tube Results**

To demonstrate that firefloods can be extremely corrosive, initial tests using corrosion coupons were carried out in the effluent from the combustion tube apparatus.

Table III lists the data obtained in two different test runs with coupons inserted in several zones of the effluent stream condenser at various temperature levels. Significant corrosion rates are obtained on various alloys in a simulated fireflood test-tube burn. Higher temperatures generally promote higher corrosion rates.

**Autoclave Test Results**

Since combusion tube tests are rather expensive to perform, and the amount of corrosive effluent is relatively small, autoclaves tests were conducted to obtain corrosion rates at various temperature levels. The first step in such testing involved standardizing a typical fireflood pro-

**Table III**—Corrosion Rates in Combustion Tube Effluent Stream

| Zone Tempera-ture, C (F) | Reservoir | | | | | |
|---|---|---|---|---|---|---|
| | AA | | | EE | | |
| | 150 (300) | 205 (400) | 150 (300) | 95 (200) | 150 (300) | 95 (200) |
| Incoloy 825 | 1.0 mpy | 16.0 mpy | 3.3 mpy | <0.1 mpy | 0.4 mpy | <0.1 mpy |
| Inconel 625 | 0.2 | 7.7 | 0.2 | <0.1 | <0.1 | <0.1 |
| Hastelloy C-276 | <0.1 | 0.5 | 1.9 | <0.1 | 0.3 | 0.1 |
| MP 35 N | <0.1 | 11.6 | 11.6 | — | — | — |
| Ti 50 A | 1.1 | 0.6 | 0.4 | — | — | — |
| Inconel 600 | — | — | — | 4.4 | 22.2 | 7.6 |
| Carbon Steel | — | — | — | 80.9 | 73.7 | 82.4 |

**Table IV**—Corrosion Rates in Various Laboratory Environments at 175 C (350 F)

| | Environment | | | |
|---|---|---|---|---|
| | A | B | C | D |
| Incoloy 825 | 21 mpy | 2.1 mpy | 11.8 mpy | 22.4 mpy |
| Inconel 625 | <0.1 | 2.3 | 1.0 | 0.1 |
| Hastelloy C-276 | 0.3 | 1.9 | 1.4 | 2.6 |
| MP 35 N | 4.2 | 2.4 | 1.2 | 4.8 |
| Sandvik 2 RK 65 | 26 | 2.7 | 12.0 | — |

A = 100 psi $CO_2$, produced brine, 60 ppm $H_2S$, 0.5% formic acid.
B = As A except 0.1% formic acid.
C = As A except synthetic brine.
D = 100 psi $CO_2$, produced brine, 0.1% acetic, 0.1% formic, 0.1% $SO_2$, 0.2% organic compounds.

ducing well environment. Table IV lists four test runs in four simulated environments. Note that significant corrosion rates are achieved on various materials in these tests. Analysis of the data and past experience indicate that environment D is a typical case for a severe, aggressive fireflood environment. The corrosivity of this environment results from salts and acids.

Table V summarizes data on selected alloys. Note that the conventional steel material had an extremely high corrosion rate of about 100 mm (4 in.) per year and that the chromium and austenitic stainless steels are not suitable in this aggressive environment. Above 140 C

(280 F), corrosion performance is improved with nickel and moly alloy materials. At 175 C (350 F), a significant corrosion rate for Incoloy 825 shows the effect of increasing temperature. Comparison of the data at 175 C (350 F) and 205 C (400 F) also shows the substantial temperature effect. In general, alloys containing nickel, chromium and molybdenum have the lowest corrosion rates in simulated fireflood environments over a wide temperature range.

**Field Tests**

Tables VI and VII show comparative results between laboratory autoclave tests and field performance. Temperatures listed here are the average temperatures during exposure of the test coupons in the field compared with static temperatures in the autoclaves. Note the good correlation between the autoclave tests and field performance.

**Conclusions**

The laboratory and field corrosion rate screening program on various materials confirmed that fireflood producing well environments can be extremely corrosive to conventional oil field materials such as carbon and low alloy steels. Downhole environments vary in corrosivity depending upon several factors including the

**Table V**—Autoclave Corrosion Test Results in Simulated Fireflood Environment "D"

| Test Tempera-ture, C (F) | 140 (280) | 175 (350) | 205 (400) |
|---|---|---|---|
| Carbon Steel | 2900-4000 mpy | — | — |
| T 410 | 120-400 | — | — |
| Inconel 600 | 140-300 | — | — |
| Incoloy 800 | 28 | — | — |
| Incoloy 825 | 0.4-1.1 | 22-46 mpy | — |
| Inconel 625 | — | <0.1 | 0.9-6.4 mpy |
| Hastelloy C-276 | — | 2.6 | 0.8-1.4 |
| MP 35 N | — | 3.6-4.8 | 14.1 |
| Hastelloy G | — | 5.5 | 27.4 |
| Ti 50 A | — | — | 0.7-66.1 |

**Table VI**—Comparison of Corrosion Rates in Field and Laboratory Environments (Reservoir "AA" at 60 C, 140 F)

|  | Field | Laboratory |
|---|---|---|
| Carbon Steel | Corroded Away | 2640 mpy |
| 12 Cr Stainless | 824 mpy | 960 |
| Incoloy 800 | 0.6 | 1.2 |
| Incoloy 825 | 0.2 | 0.1 |
| Inconel 600 | 477 | 334 |

**Table VII**—Comparison of Corrosion Rates in Field and Laboratory Environments (Reservoir "DD")

| Test Temperature, C (F) | Field | | Laboratory |
|---|---|---|---|
|  | 30 (90) | 90 (195) | 90 (195) |
| Carbon Steel | 47-59 mpy | 114 mpy | 87 mpy |
| 12 Cr Stainless | 5.6 | 14.9 | — |
| Incoloy 800 | <0.1 | 0.7 | — |
| Inconel 625 | <0.1 | <0.1 | <0.1 |

composition of the crude oil and the sand. Because of this relationship, it is difficult to generalize on the corrosivity of a specific downhole fireflood environment unless field experience or data, such as that from the combustion tube, is available. Laboratory tests have confirmed field test results and show that Incoloy 825 or nickel-base molybdenum-containing alloys such as Inconel 625 and Hastelloy C-276 are the most corrosion resistant under the conditions studied. Many other proprietary alloys of these general compositions would probably perform satisfactorily if chemical composition is matched to the tested grades and microstructural features are similar. Use of Incoloy 825 has been satisfactory in many fireflood applications at temperatures less than 150 C (300 F). Relatively high nickel alloys, such as the Inconel 625 and Hastelloy C-276, would likely outperform the Incoloy 825 at higher temperatures.

In selecting materials for fireflood producing wells, the corrosion engineer must consider sand, water, crude oil compositions and the maximum probable operating temperature. Further testing is required to investigate propensity to chloride-induced stress corrosion cracking in fireflood environments. Other means of mitigating corrosion, such as nonmetallic and metallic coatings and chemical corrosion inhibitors, may be alternatives to alloys. These techniques must be proven by laboratory and field tests.

# Reference

1. T. M. Geffen, *World Oil*, *180* (4), 1975, 53.

# A New Rock Bit Steel

by S. R. Scales, Hughes Tool Company and
D. E. Diesburg, Climax Molybdenum Company

Rotary drilling currently is the standard process for making holes in the earth's crust. Rotary drilling is used for oil, gas and water wells, for blast holes in the mining industry and for holes required for other purposes. Prior to the invention of the rolling conical cutter rock bit in 1909, the use of the rotary method of drilling was greatly restricted because hard rock was difficult to drill with a drag bit's scraping action.

A two-cone bit introduced in 1909, shown in Figure 1, was the first successful oilfield bit to use cutters that rolled on the bottom of the hole. With the introduction of self-cleaning cones in 1925, shown in Figure 2, two-cone bits were able to effectively drill a greater range of formations.
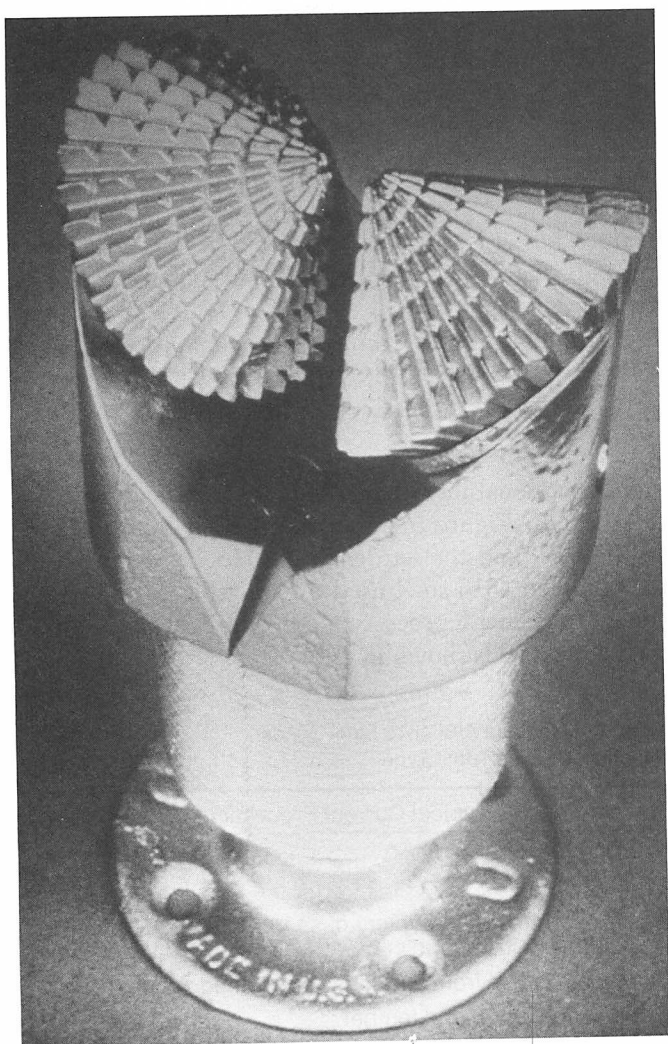


FIGURE 1—First successful oilfield bit to use cutters that roll on the bottom of the hole. [Gauge diameter 149 mm (5⅞ in.)]
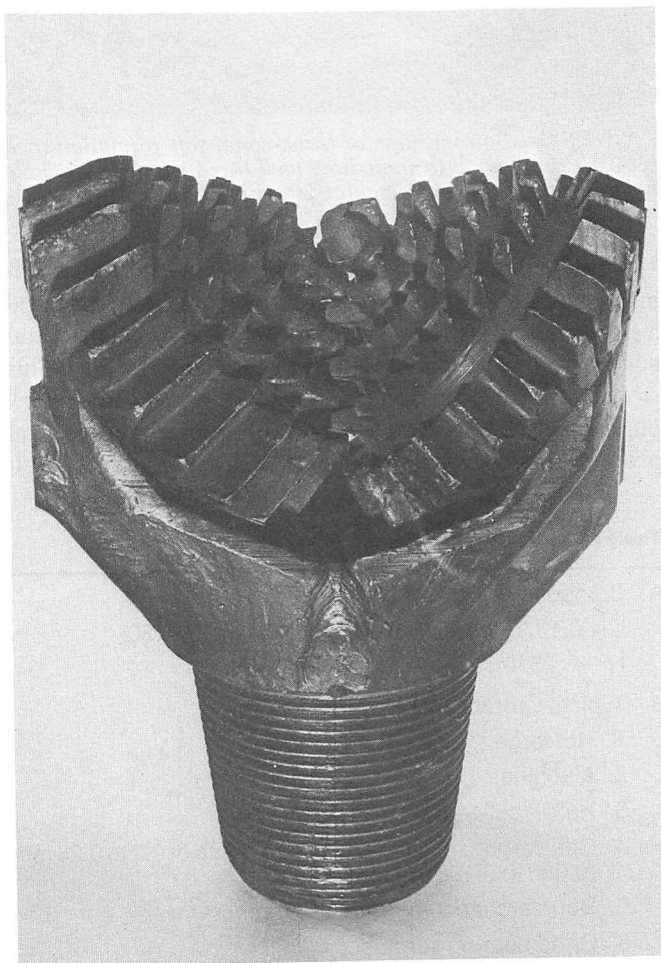


FIGURE 2—Self-cleaning two-cone rock bit. [Gauge diameter 229 mm (9 in.)]

Three-cone bits were introduced from 1931 through 1933. The basic design of a three-cone bit still used today provides the maximum number of relatively large cutting teeth and bearing capacity for a specified diameter of hole to be drilled. Figure 3 is a bottom view of a soft formation rock bit with a ring gauge to indicate how well three cones fill the hole being drilled.
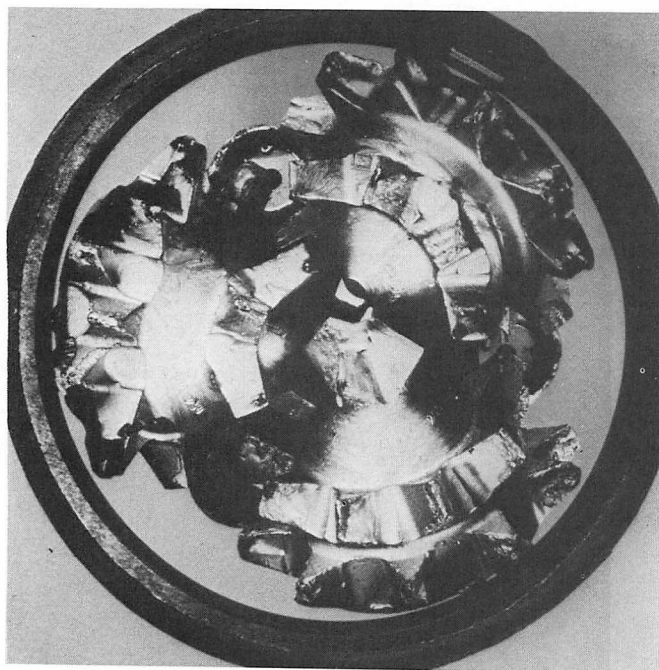
FIGURE 3—Bottom view of three-cone, soft formation rock bit with ring gauge to show how well three cones fill the hole being drilled. [Gauge diameter 200 mm (7⅞ in.)]

In the late 1930s, as a result of a joint effort by a primary rock bit manufacturer (Hughes Tool Company) and a steel producer, SAE-AISI 4815 steel was developed and adopted for rock bit cones (all were steel tooth type). This steel is still the standard composition for steel tooth rock bit cones. The typical composition range and general processing procedures for AISI 4815 are given in Table I.

**Table I**—AISI 4815 Steel Cones, Steel Tooth Type

A. Composition, %:
   C—0.13/0.18, Mn—0.40/0.60, Si—0.15/0.30, Ni—3.25/3.75, Mo—0.20/0.30.

B. Typical Current Processing:
   1. Hot forge.
   2. Machine.
   3. Hardface teeth.
   4. Gas carburize to a typical case depth of 0.2 to 0.25 mm (0.080 to 0.100 in.) and cool.
   5. Double quench harden and temper.
   6. Grind bearing surfaces.

In 1951, the first rolling cone rock bits with cemented tungsten carbide teeth were marketed. The first tungsten carbide teeth were cylinders with a hemispherical cutting end. A typical rock bit with such teeth is shown in Figure 4. The cylindrical portion of each tungsten carbide tooth was pressed into a drilled and reamed hole with an uncarburized surface. An interference fit was maintained between the tungsten carbide tooth and the reamed hole. A modified AISI 4815 steel with slightly



FIGURE 4—Tungsten carbide tooth, hard formation bit manufactured about 1960. Note the cemented carbide jet nozzles introduced in 1953. [Gauge diameter 220 mm (8¾ in.)]

higher hardenability than AISI 4815 was adopted for these cones. Figure 5 shows the hardenability of AISI 4815H steel and the hardenability Hughes required for the modified 4815 steel used for tungsten carbide tooth cones. The general processing procedure for the modified SAE 4815 steel is shown in Table II.

**Table II**—Modified AISI 4815 Steel Cones, Tungsten Carbide Tooth Type

| Typical Current Processing |
| --- |

1. Hot forge.
2. Machine.
3. Gas carburize to a typical case depth of 0.20 to 0.25 mm (0.080-0.100 in.) and cool.
4. Machine case from surfaces to be drilled and reamed.
5. Quench harden and temper.
6. Drill and ream holes and press tungsten carbide teeth into holes.
7. Grind bearing surfaces.
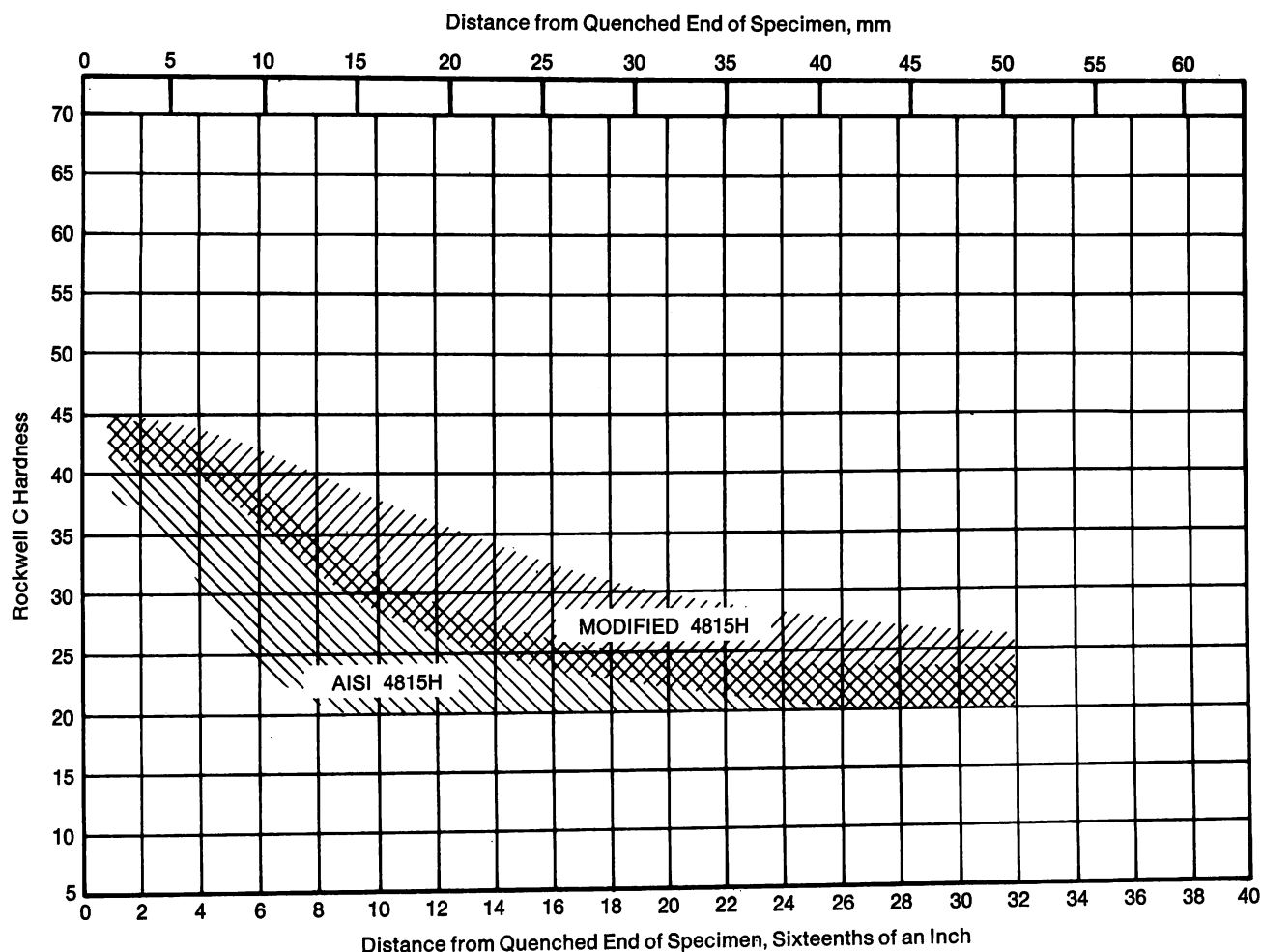
FIGURE 5—*Hardenability ranges for AISI 4815H and modified 4815H.*

In 1972, a need was recognized for a new, higher hardenability carburizing grade of steel for tungsten carbide tooth cones because:

1. Tungsten carbide teeth with greater projection and a variety of shapes for the cutting ends were being used. See Figure 6 for variations currently used. High yield strength steel is required for good tungsten carbide tooth retention in interference press fits.

2. Large sizes of tungsten carbide tooth bits and large tungsten carbide tooth cutters were becoming more popular, respectively, for blast holes in open pit mining and for shaft drilling of underground mines. Higher core yield strength for good tungsten carbide tooth retention was desired.

3. The journal bearing tungsten carbide tooth bit had been introduced in 1970 for the first time giving the oilfields a bearing that lasted as long as the carbide teeth. Journal bearing cones have thicker sections than roller bearing cones, and, therefore, a higher hardenability steel was needed to provide the yield strength necessary for good carbide tooth retention. Figure 7 shows a sealed

journal bearing rock bit with chisel-shaped tungsten carbide teeth.

Starting in 1970, Hughes Tool personnel had worked with Climax Molybdenum personnel in the adoption of SAE EX30 steel as a head-section steel. (Each body and inner bearing part of a rock bit is called a head-section.) Climax personnel had developed EX30 as a reduced nickel replacement for 4815 steel, and it did prove to be slightly superior to AISI 4815 and much superior to AISI 8720 steel as a head-section steel. Both AISI 4815 and 8720 had been used as standard steels for head-sections. As a head-section steel, EX30 replaced two steels, reducing inventory cost while improving performance.

Hughes personnel again worked with Climax personnel, starting in 1972, to develop a new high hardenability carburizing grade of steel for tungsten carbide tooth rock bit cones and shaft cutters. Climax personnel furnished Hughes with sample bars (64 and 83 mm, 2½ and 3¼ in. diameter) that they melted, cast and forged in their laboratory in Ann Arbor, Michigan. There were some minor composition variations in the samples. Included in the Hughes program were end quench hardenability tests to determine both hardenability and aus-

INNER                    HEEL

(a) Soft rock formation

INNER                    HEEL

(b) Medium rock formation

INNER            HEEL            INNER            HEEL

(c) Hard rock formation
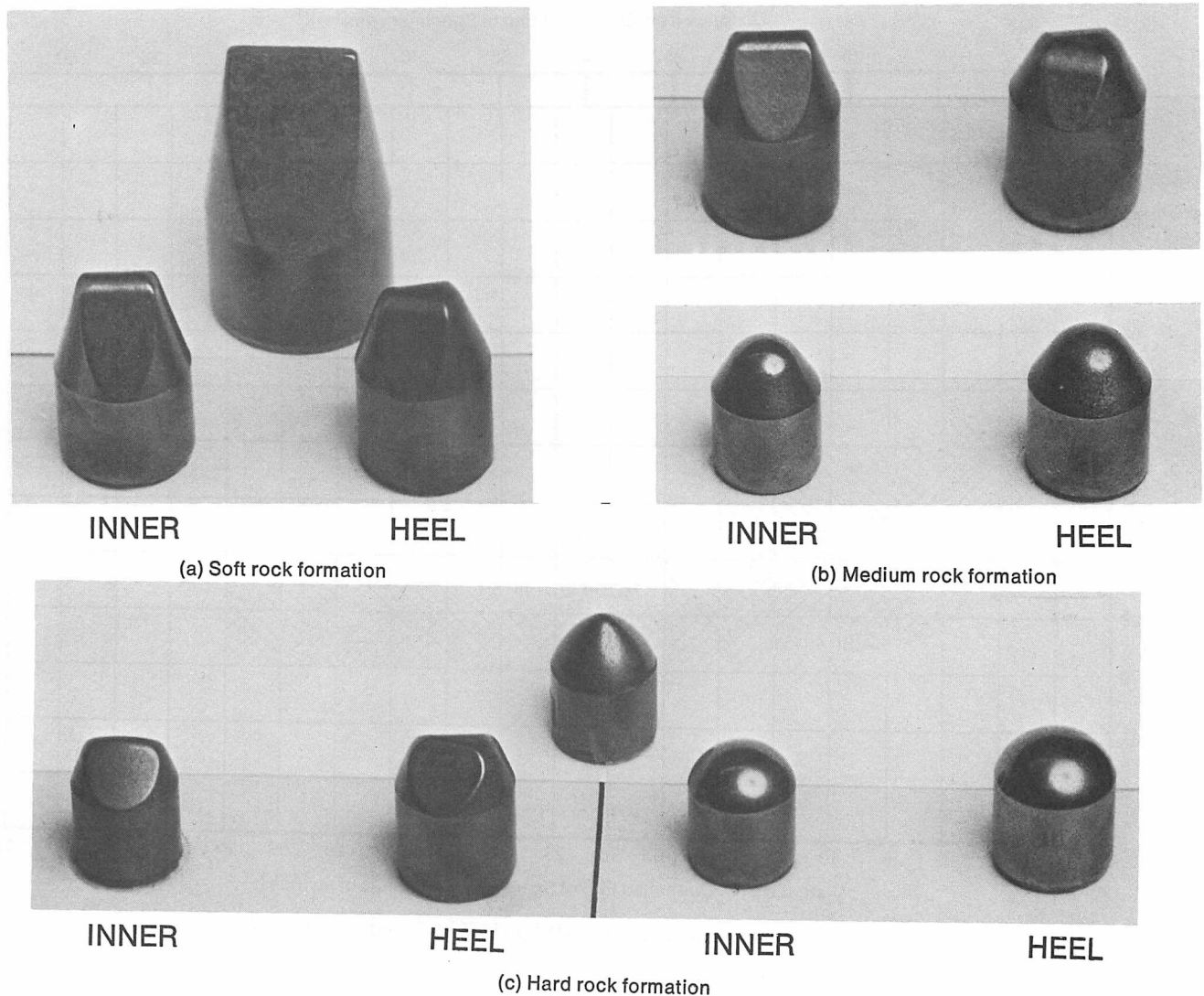
FIGURE 6—*Tungsten carbide teeth for various indicated rock formations.*

tenitizing temperature, tests for mechanical properties and field testing of two cones. The steel is now known as SAE EX55.

All of the test results were encouraging and resulted in the purchase of an experimental heat (about twelve tons) of EX55 steel for the manufacture and field testing of tungsten carbide tooth cones and tungsten carbide tooth cutters. These tests were successful, and today EX55 steel is a Hughes standard material for large tungsten carbide tooth cones and cutters. Tungsten carbide tooth cones of EX55 steel are processed the same as shown in Table II. The composition of EX55 steel in weight percent is as follows:

C—0.15/0.20, Mn—0.70/1.00, Ni—1.65/2.00, Cr—0.45/0.65, Mo—0.65/0.80.

Figure 8 shows a hardenability band for EX55 which includes fifty consecutive heats (approximately 4000 tons) of steel purchased by Hughes.

Figures 9 and 10 show the case and core microstructures of a carburized, hardened and tempered EX55 steel cone.

## Laboratory Evaluation of Carburized Steels for Rock Bits

As can be seen in Figure 11, EX55 exhibits extra high hardenability compared to AISI 4815H and AISI 9310H. The alloy content was chosen to take advantage of a known synergistic effect on hardenability by combining nickel and molybdenum,[1] while at the same time maximizing the manganese and chromium contents to reduce the alloy cost. Subsequent evaluation of the fracture resistance of carburized steels using laboratory tests showed that EX55 exhibits excellent fracture properties in the carburized condition, similar to the properties of AISI 4817 and AISI 9310.
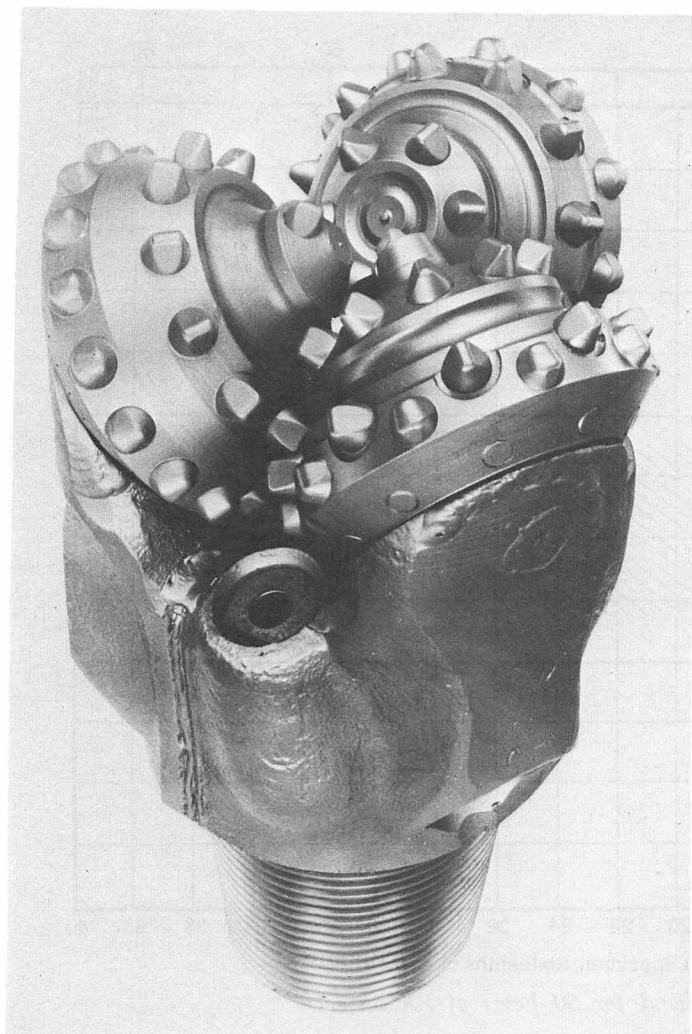
FIGURE 7—*Modern sealed journal bearing rock bit with chisel-shaped tungsten carbide teeth. [Gauge diameter 200 mm (7⅞ in.)]*

Alloy content can influence the fracture toughness of carburized cases as illustrated in Figure 12. Shown in Figure 12 is the fracture toughness in the carburized cases of EX55 and AISI 4817 compared to that of low alloy steels including AISI 8620. Differences in residual stress that may have existed in the carburized cases of these steels were eliminated by measuring the residual stress with x-ray diffraction and subtracting its contribution. Having accounted for the residual stress contribution, the fracture toughness values shown in Figure 12 represent only differences in microstructural fracture toughness.

Knowing that alloy content can influence the fracture resistance of carburized cases from Figure 12, an extensive program was initiated at Climax to evaluate the fracture properties of carburizing steels. A test specimen having a simplified geometry of a gear tooth was designed. The dimensions of the specimen are given in Figure 13. A "tooth" at each end permits two tests to be performed with the same specimen. The specimen is held upright in a Charpy impact machine similar to the testing of Izod specimens (ASTM Testing Procedure E23). Instead of measuring the total energy required to completely break each tooth, the maximum load is measured and used to calculate the stress required for fracture. Total energy absorbed during fracture evaluates both the properties of the case and the core, and the results can be completely dominated by a soft tough core and, in effect, can mask important differences in the fracture resistance of carburized cases. Testing the "tooth" specimen in bending and measuring the load to cause fracture allows the calculation of an outer fiber stress at the fracture location. Such a measurement is interpreted as the stress required to crack the carburized case and is, therefore, a measure of the case fracture properties, essentially independent of core properties. With adequate case depths, the core behaves elastically at the bending loads needed to crack the case. (Inadequate case depths can permit yielding in the core before the fracture stress of the case is exceeded.) Although the core behaves elastically and does not contribute directly to the fracture stress, the core can indirectly influence the fracture properties of the case by influencing the buildup of compressive residual stresses in the case. Residual stresses are known to be important to fracture resistance. Figure 14 shows that residual stresses contribute directly to the fracture stress values.[2] The combined effect of microstructural fracture toughness and residual stress on fracture behavior is indeed the very property of interest, and no adjustment to account for residual stresses is required when measuring impact fracture stress values of carburized cases.

Figure 15 shows the effect of various alloy combinations on the impact fracture stresses of carburized cases.[3] Figure 15a shows how the combination of molybdenum and nickel leads to improved impact fracture stress. Increasing the nickel content in a low molybdenum steel did not improve the fracture stress (Figure 15b), just as adding molybdenum to a low nickel, low manganese steel did not improve the fracture stress (Figure 15a). In general, manganese did not improve the fracture stress in molybdenum-free steels as shown in Figure 15c. Combining 0.25% Mo with 1.12% Mn resulted in a 25% increase in the impact fracture stress. With 0.8% Mn, the best fracture stress was obtained with low chromium contents (~ 0.5% Cr). Chromium additions generally decreased the impact fracture stress except when added to high nickel (> 3.0% Ni) steels where its presence was neutral, as illustrated in Figure 15d for AISI 9310 containing 1.2% Cr. High nickel content can offset any detrimental effect that chromium may have.

The combination of alloys in EX55 not only gives extra high hardenability but also results in excellent fracture resistance (Figure 15a). To further demonstrate the excellent fracture resistance of EX55, carburized "tooth" specimens were repeatedly impact loaded using a constant energy impact of 4 J (35 in.-lb). EX55 withstood
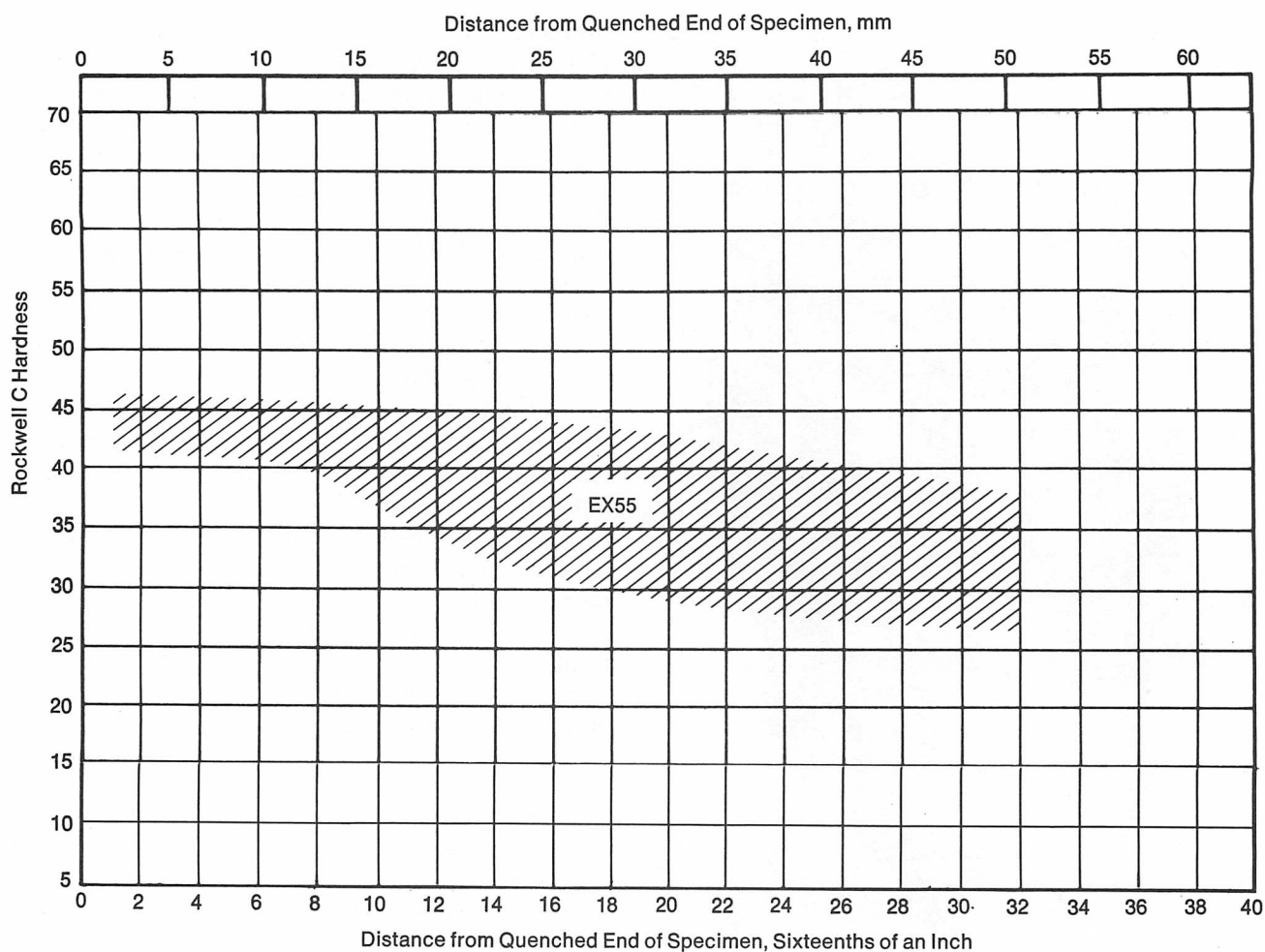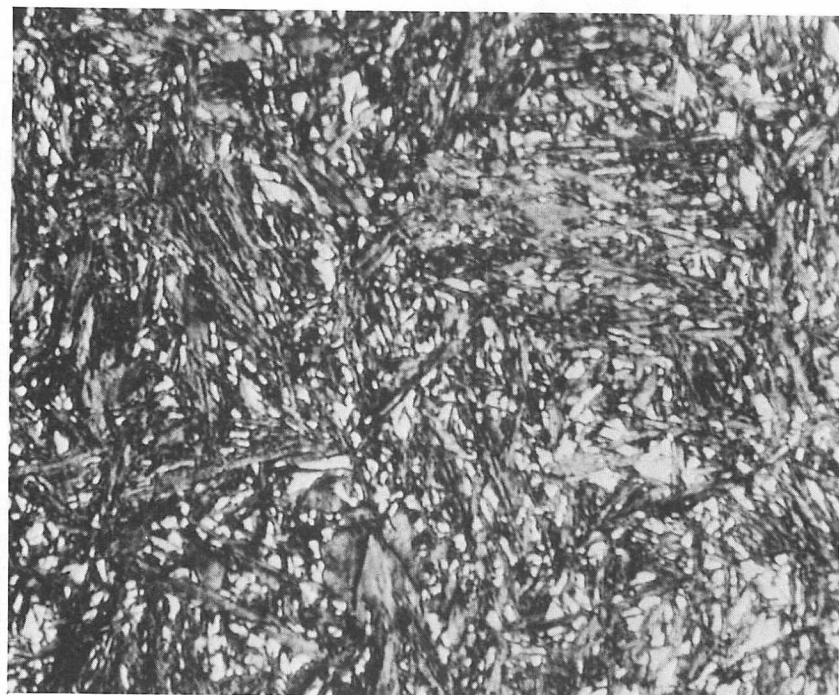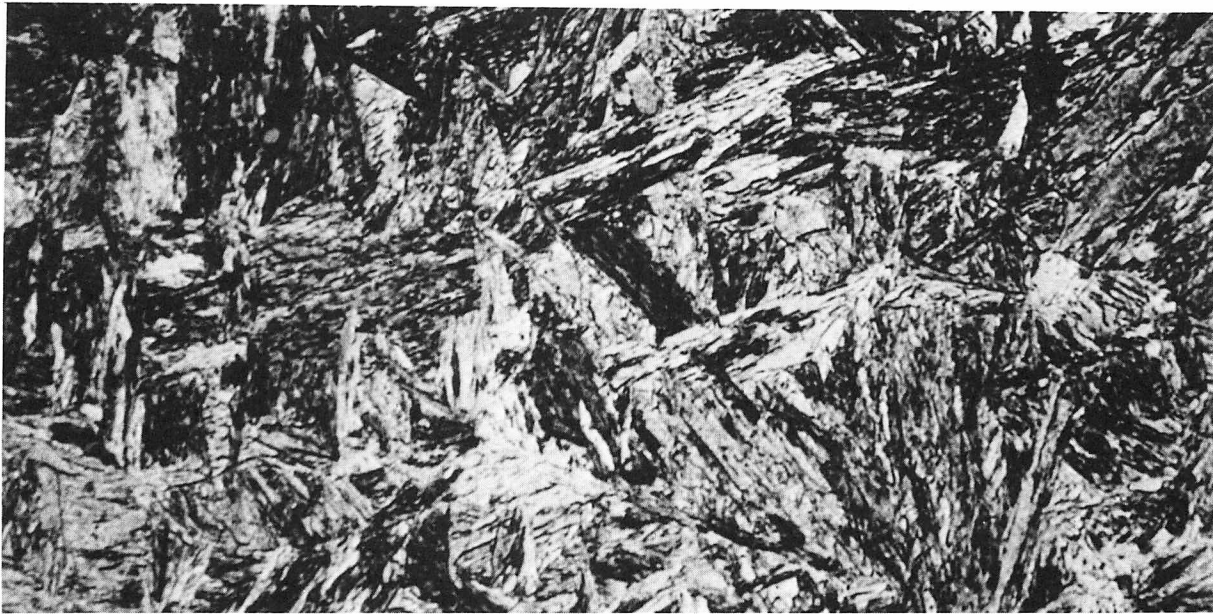
FIGURE 8—Hughes hardenability band for 50 heats of EX55 steel.



2% Nital                               (1000 X)

FIGURE 9—Quenched-and-tempered carburized case of EX55 steel cone. Properties: File hard (56 HRC min.)

2% Nital                                                    (1000 X)

FIGURE 10—Quenched-and-tempered core of EX55 steel cone.

Typical properties:  Hardness        —41 HRC
                     Tensile strength —1303 MPa (189 ksi)
                     Yield strength   —1103 MPa (160 ksi)
                     Impact strength  —71 J (53 ft-lb)
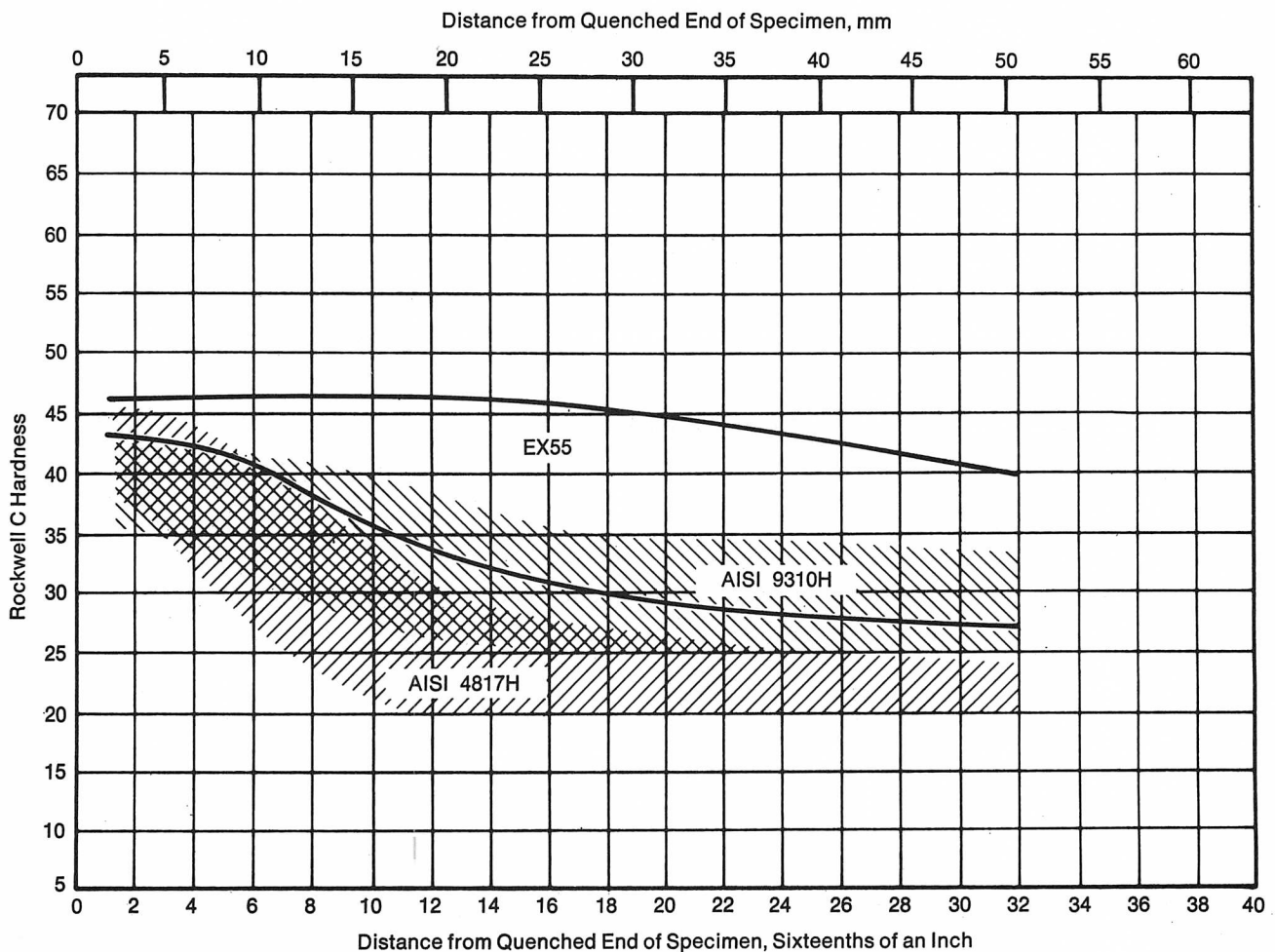


FIGURE 11—Core hardenability of laboratory heats (high and low side chemistries)
of EX55 compared with the hardenability bands for
commercial AISI 4817 and AISI 9310 steels.
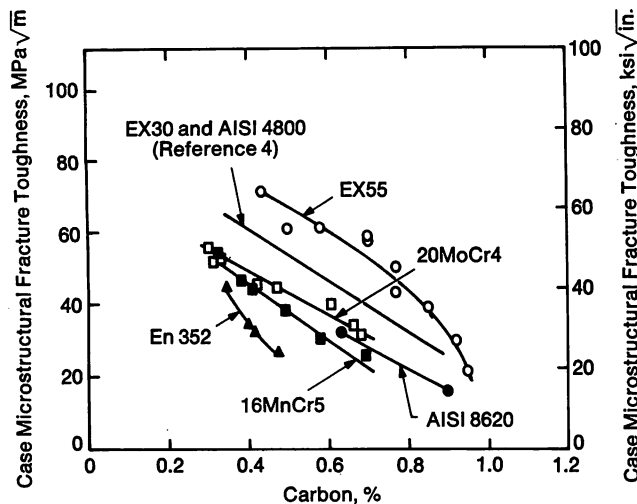
FIGURE 12—Fracture toughness at various carbon contents within carburized cases (corrected for presence of residual stress).
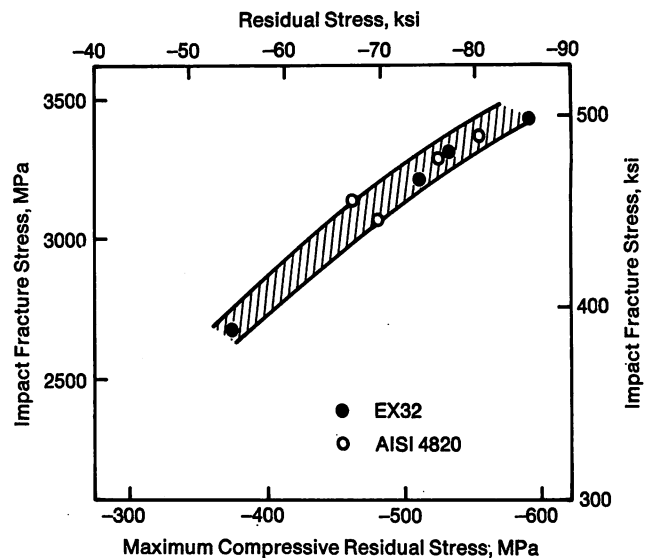


FIGURE 14—Relationship between impact fracture stress and compressive residual stress in the outer 0.76 mm (0.030 in.) of the carburized case.[2] (All cases contained <50% retained austenite.)
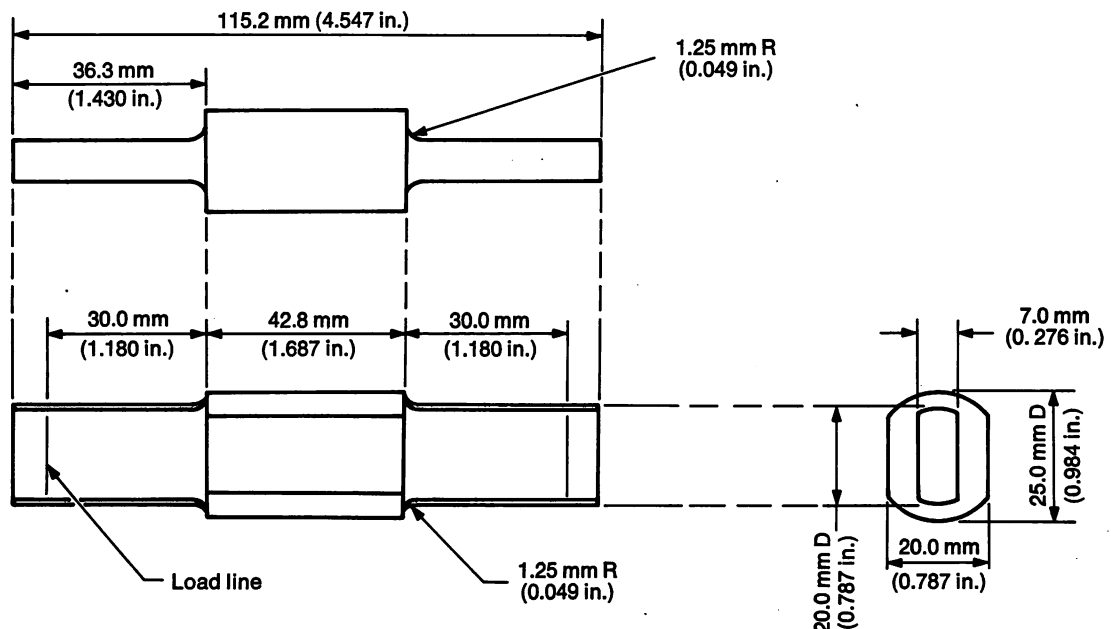


FIGURE 13—Specimen geometry used for determining the impact fracture stress of carburized steels.

1000 impacts before fracture. AISI 4817 withstood 550 impacts while steels such as AISI 8620 broke with 8 impacts.

## Summary

The brief history of the development of three-cone rock bits with tungsten carbide teeth has been pre-sented. A high hardenability EX55 steel was developed to meet the requirements of the carburized cones for these rock bits. The performance of EX55 as a cone steel for tungsten carbide tooth bits has been excellent. Laboratory evaluations of the relative fracture resistance of carburized cases has verified the high impact fracture resistance of carburized EX55. The alloy combination responsible for the excellent fracture resistance was concluded to be 1.8% Ni and 0.75% Mo.
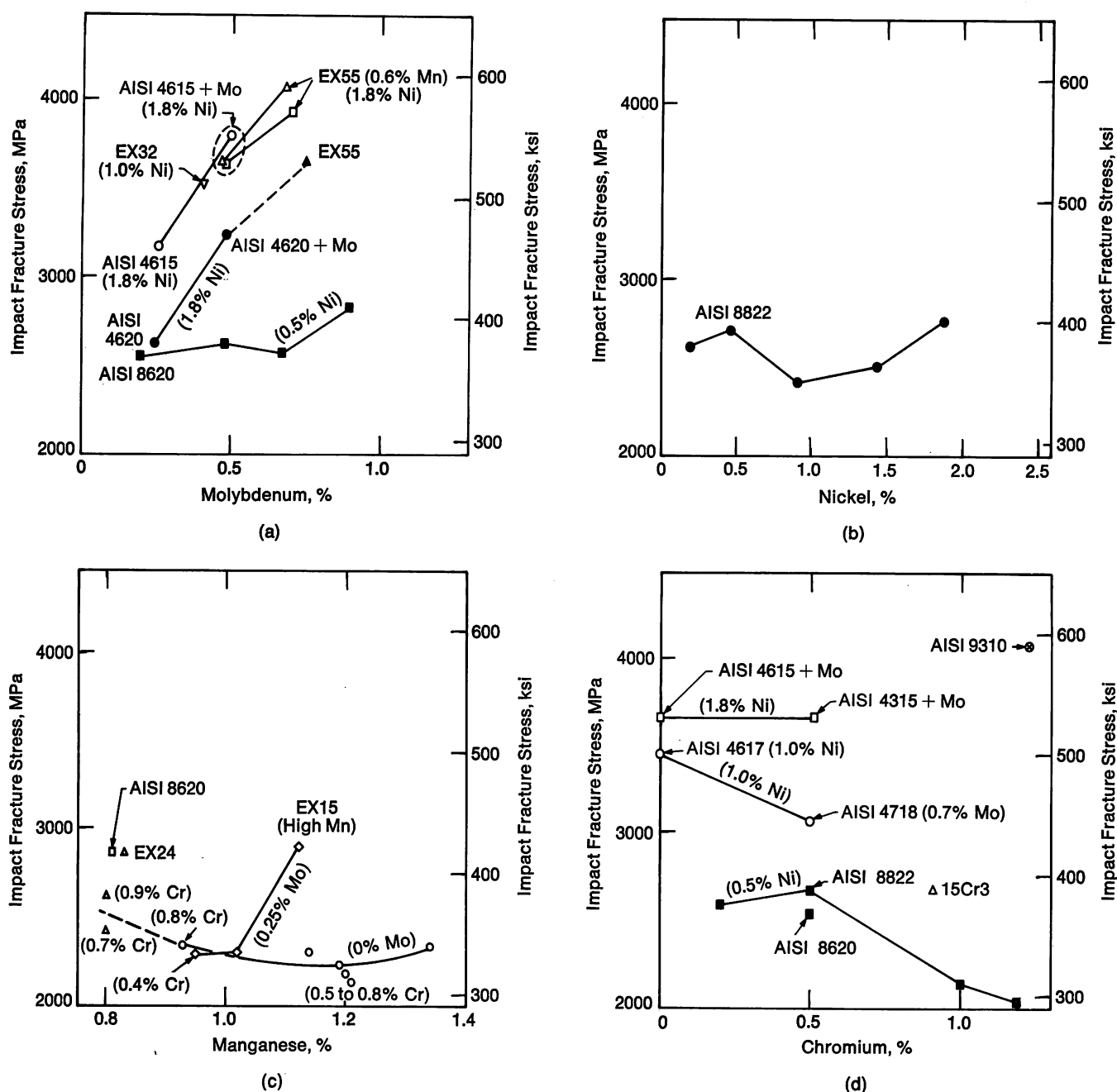
FIGURE 15—*Impact fracture stress of carburized steels (a) containing various combinations of molybdenum and nickel, (b) showing the effect of high and low nickel modifications of AISI 8620, (c) containing various combinations of manganese and molybdenum and (d) containing various combinations of chromium and nickel. (Open data points are for vacuum melted heats; solid data points are for air melted heats.)*

## References

1. A. F. de Retana and D. V. Doane, *Metal Progress*, **100** (3), 1971, 65.

2. D. E. Diesburg, *ASTM STP 672*, 1979, 207.

3. D. E. Diesburg and Y. E. Smith, *Metal Progress*, **115** (6), 1979, 35.

4. Y. E. Smith and D. E. Diesburg, *Metal Progress*, **115** (5), 1979, 67.

# Steels for the Gas and Oil Industry

by S. A. Golovanenko
Chnitchermet Institute

The need for energy gives impetus to increasing the effectiveness of processes for the obtaining, refining, conversion and transportation of oil and gas. At this time in the USSR, energy related processes are the most demanding for the utilization of steels, particularly so because of the adverse climatic environments associated with gas and oil deposits. The need for improved materials that would serve under the adverse conditions of temperature and environment poses a challenge for the next decade to develop economic steels with improved strength and reliability.

## Steels for Gas and Oil Pipe Lines

At this time, there are four classes of steels for U-O and spiral welded pipes of large diameter operating at pressures of 5.6-7.6 MPa (55-75 atm).

1. Hot-rolled plain carbon and low alloy Mn-Si steels for pipes up to 1020 mm (40 in.).

2. Normalized Mn-Si and Mn-V steels with nitrogen strengthening for pipes of 1020-1220 mm (40-48 in.) diameter.

3. Controlled rolled Mn-V-Nb steels for pipes of 1420 mm (56 in.) diameter and 7.6 MPa (75 atm) pressure operating in Arctic regions.

4. Heat treated Mn-V-B steels for pipes of 1020-1420 mm (40-56 in.) diameter.

Table I lists the chemical compositions and typical properties of the four classes of pipe steels.

By optimization of composition and use of new technology in melting, rolling and thermal treatment, it is anticipated that the toughness and strength of these steels can be improved. In the melting of these steels, improved cleanliness will be achieved by lowering sulfur, phosphorus and other impurities, the shape of non-metallic inclusions will be improved, and the gas content of the steels will be lowered.

Improvements of properties through controlled rolling will be achieved primarily by development of optimum schedules which will include low finishing temperatures. The desired low finishing temperatures cannot be implemented on some of the older conventional rolling mills.

Heat treatment of gas transmission pipe is not widely used and awaits further developments. These developments will include intercritical heat treatment yielding a two-phase (ferrite/martensite) microstructure. Experiments which were conducted showed that, for heavier plate (up to 14 mm, 0.55 in.) after increasing hardenability by selective alloying, it was possible to obtain properties characteristic of two-phase steels, i.e., a low yield strength and a high elongation (25%) (Figure 1); these values are not attained for conventionally quenched-and-tempered steels of comparable tensile strength. In any event, for the commercial exploitation of heavy section two-phase steels, it is necessary to have special production schedules for pipes and other parts.

## Steels for the Transportation of Gas at Cryogenic Temperatures

In the 1980s, we should see the development of gas transmission at low temperature. Gas transmission at −70 C (−95 F) or of liquified gas at −120 C (−185 F) increases the gas throughput 1.5-2 and 3-4 times, respectively, in comparison to conventional gas transmission parameters. Correspondingly with low temperature gas transmission, the diameter of the pipe line can be decreased; however, the number of compressors and refrigeration stations are increased. The overall effectiveness of cryogenic gas transmission still requires serious cost effectiveness studies.[1]

Studies conducted in the USSR on gas linepipe showed that increased low temperature properties of reduced pearlite steels with carbide strengthening can be achieved not just with controlled rolling. Additional alloying of reduced pearlite steel with up to 1% Ni and up to 0.15% Nb increases the toughness of the solid solution, and gives rise to a finer substructure which insures the use of the steel to −100 C (−150 F). The composition and properties of this type of steel, Grade 06G2NAB, are given in Table II.

Steel 06G2NAB has good weldability under various conditions, manual or automatic; the hardness in the weld metal zone does not exceed HV 280 which is evidence that no low temperature transformation products are present. Studies have shown that, to insure high values of impact strength in the weld zone metal at tem-

**Table I**—Composition and Mechanical Properties of Typical Plate Steels Used for Gas Transmission Linepipe

| Grade | Desig-nation | Element, % | | | | | | | | Tensile Strength, MPa (ksi) | 0.2% Yield Strength, MPa (ksi) | Elon-gation, % | Impact Properties | | | | Pipe Diameter, mm, (in.) |
|---|---|---|---|---|---|---|---|---|---|---|---|---|---|---|---|---|---|
| | | | | | | | | | | | | | Charpy V-Notch Energy, J (ft-lb) | | | DWTT, % Shear | |
| | | C | Mn | Si | V | Nb | N | S max | P max | | | | −60 C (−76 F) | −40 C (−40 F) | −15 C (5 F) | | |
| 1 | 17GS[a] | 0.15 0.25 | 1.2 | 0.5 | — | — | — | 0.035 | 0.035 | 490 (71.1) | 353 (51.2) | 24 | — | 39 (29) | — | — | 530- 820 (21-32)[e] |
| 2 | 17G1S-U[b] | 0.15 0.20 | 1.35 | 0.5 | — | — | — | 0.02 | 0.025 | 510 (73.9) | 363 (52.6) | 23 | — | 39 (29) | — | — | 1020-1220 (40-48)[e] |
| | 17G2AF[b] | 0.17 0.19 | 1.5 | 0.4 | 0.1 | — | 0.015 0.025 | 0.012 | 0.02 | 588 (85.3) | 432 (62.6) | 22 | — | 47 (35) | 72 (53)[g] | — | 1020-1420 (40-56)[e] |
| 3 | 09G2FB[c] | 0.13 | 1.7 | 0.35 | 0.1 | 0.05 | — | 0.010 | 0.02 | 549 (79.6) | 451 (65.4) | 22 | 47 (35) | — | 72 (53) | 85 | 1220-1420 (48-56)[e] |
| 4 | 16GFR[d] | 0.14 0.18 | 1.35 | 0.3 | 0.07 | — | — | 0.010 | 0.022 | 686 (99.5) | 539 (78.2) | 16 | 47 (35) | — | 64 (47) | 80 | 1220-1420 (48-56)[f] |

a — Hot controlled rolled.
b — Normalized.
c — Controlled rolled.
d — Heat treated pipe.

e — U-O pipe.
f — Spiral welded pipe.
g — At 0 C (32 F).

peratures of −100 C (−150 F), it is necessary to normalize the weld area after welding; this treatment is in harmony with the processing schedule of pipes at the Kharchez Pipe Plant producing pipe of 1020 mm (40 in.) diameter by 12 mm (0.47 in.) wall. The toughness of mid thickness specimens subjected to the Battelle DWTT is ≥ 80% shear fracture appearance down to −80 C (−110 F).
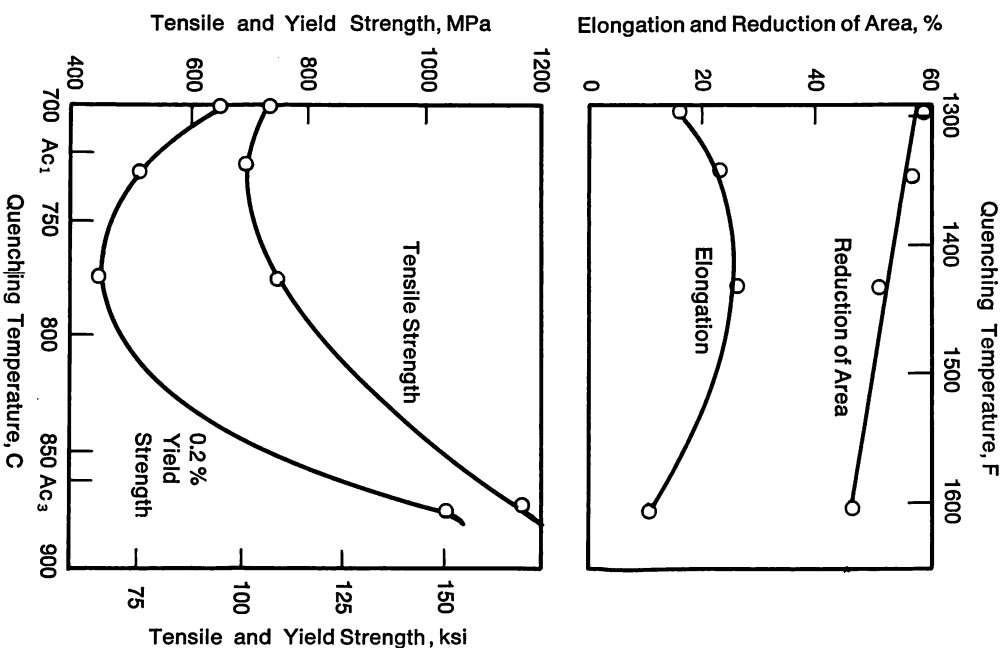
*FIGURE 1—Properties of Steel 16GFR air cooled from inter-critical temperature range.*

## Studies of Hydrogen-Induced Cracking of Steel Linepipe

In addition to the problems of increasing the volume of product that can be carried in pipe lines, there is also the problem that will need solution in the 80s, one of increasing the resistance to hydrogen-induced cracking (HIC). In almost all of the new oil and gas wells, we are encountering $H_2S$ which causes embrittlement from sulfide stress cracking (SSC).

In addition to the $H_2S$ present in the wells, hydrogen-induced cracking can be caused by the welding process, cathodic protection, corrosion from the soil,

**Table II**—Composition and Mechanical Properties of Hot-Rolled Pipe for Transmission of Low Temperature (Liquified) Gas

| Grade | Element, % | | | | | | | Tensile Strength, MPa (ksi) | | 0.2% Yield Strength, MPa (ksi) | | Elon-gation, % | Impact Properties | | | | DWTT at −80 C (−112 F), % Shear |
|---|---|---|---|---|---|---|---|---|---|---|---|---|---|---|---|---|---|
| | | | | | | | | | | | | | Charpy V-Notch Energy, J (ft-lb) | | | | |
| | C | Mn | Ni | Nb | N | S max | P max | | | | | | −70 C (−94 F) | | −120 C (−184 F) | | |
| 06G2NAB | ≤0.08 | 1.6 | 0.85 | 0.15 | 0.020 | 0.01 | 0.01 | 539 | (78) | 353 | (51) | 21 | 80 | (59) | 64 | (47) | ≥80 |

products from active sulfate reducing bacteria, and others. For this reason, inspite of the successful role of inhibitors in decreasing HIC, it is necessary to develop steels with a high resistance to HIC for sour oil and gas wells.

We studied resistance to HIC in commercial steels having a ferrite-pearlite microstructure, widely used in current linepipes. The studies were conducted under laboratory conditions in which the specimens were charged with hydrogen in a 0.1N solution of $H_2SO_4$ containing 0.5 gms/1 of $NH_2CSNH_2$. The current density was 50 ma/cm². The specimens were cut from sheet so that the longitudinal axis was perpendicular to the direction of rolling. HIC was measured by the following criteria:

1. Time to fracture under conditions of continuous hydrogen charging and stress of cylindrical specimens of 6 mm (0.24 in.) diameter with 1 mm (0.04 in.) deep notch of 0.25 mm (0.01 in.) radius. The tensile stress on the specimens was 0.3 to 0.8 of the yield strength.

2. The loss of ductility, $\Delta\psi$, brought about by a two-hour exposure of smooth specimens to hydrogen charging as compared to unexposed specimens[2] was defined by:

$$\Delta\psi = 100 \frac{\% \text{ RA unexposed-}\% \text{ RA hydrogen charged}}{\% \text{ RA unexposed}}$$

3. The degree of segregation of hydrogen, $\alpha$, on the fracture surface of the specimen was determined. The specimen was sectioned into pieces 5-6 mm (0.20-0.24 in.) long, and the amount of hydrogen in each section was determined. The degree of segregation was calculated as the ratio of the hydrogen content in the section containing the fracture surface to the hydrogen content of pieces 10 mm (0.39 in.) from the fracture. Calculation of the residual hydrogen was conducted realizing that diffused hydrogen was lost very rapidly as a result of the creation of the new fracture surface. It was assumed that the change in the concentration of hydrogen reflects the change in its overall content. It has been shown[3] that for steels of medium strength, (e.g., TS = 780 MPa, 114 ksi) for which the fracture is ductile even though the steel contains hydrogen, the degree of segregation of hydrogen at the fracture is a measure of the criti-

cal concentration of hydrogen in a zone of maximum triaxial stress.

The amount of absorbed diffusion-increased hydrogen was determined at room temperature with an inertia-free gas analyzer built by Chnitchum.[4] The residual hydrogen was analyzed by the method of reduction melting in a Leco apparatus. From the kinetic curves of the emission of hydrogen, the rate of emission was calculated. It was found that the emission of hydrogen from specimens that had been previously charged can be described by the second order differential equation; $dc/dt = kC^2$. In conjunction with data for hydrogen permeability rate constants, it characterized that there is an interaction of hydrogen with structural defects, i.e., hydrogen traps.

Hydrogen permeability was investigated by use of a two-section apparatus having a volumetric measurement capability for the hydrogen that had diffused through the steel membrance, Figure 2.
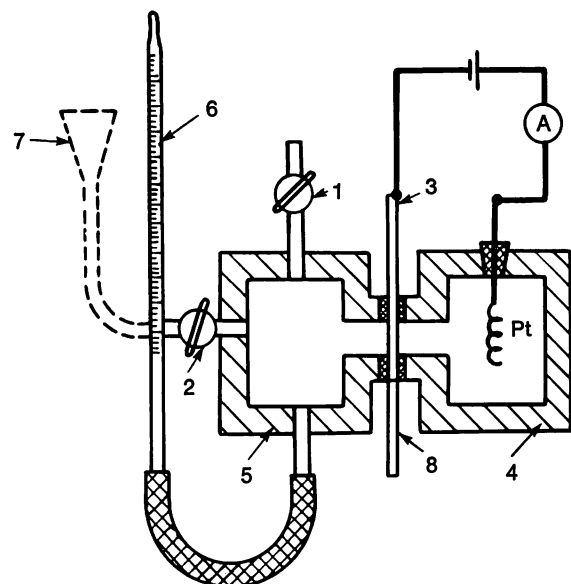


1 and 2 — two-way valves.
3 — test specimen membrane.
4 — working section (volume being hydrogenerated).
5 — measuring section.
6 — microburette.
7 — funnel.

*FIGURE 2—Schematic of the apparatus for determining hydrogen permeability through steel.*

**Table III**—Chemical Composition of Investigated Steels

| No. | Grade | Element, % | | | | | | | | | |
| --- | --- | --- | --- | --- | --- | --- | --- | --- | --- | --- | --- |
| | | C | Mn | Si | S | P | Cr | V | Al | Nb | Mo |
| 1 | 17G1S-U | 0.19 | 1.47 | 0.43 | 0.021 | 0.012 | — | — | 0.03 | — | — |
| 2 | 17G2AF | 0.18 | 1.43 | 0.35 | 0.009 | 0.012 | — | 0.11 | 0.02 | — | — |
| 3 | 09G2FB | 0.11 | 1.67 | 0.29 | 0.005 | 0.011 | — | 0.075 | 0.05 | 0.036 | — |
| 4 | 10G2MFB | 0.10 | 1.50 | 0.40 | 0.005 | 0.015 | — | 0.06 | 0.03 | 0.03 | 0.15 |
| 5 | 08G2MFB | 0.09 | 1.50 | 0.33 | 0.005 | 0.011 | — | 0.07 | 0.02 | 0.046 | 0.15 |
| 6 | 10Kh2GMAU | 0.10 | 1.00 | 0.50 | 0.020 | 0.015 | 2.0 | — | 0.06 | — | 0.30 |

**Table IV**—Mechanical Properties, Thermal Treatment and Microstructure of Investigated Steels

| No. | Grade | Thermal Treatment | Tensile Strength, MPa (ksi) | 0.2% Yield Strength, MPa (ksi) | El, % | RA, % | Impact Strength at −15 C (5 F), J (ft-lb) | Micro-structure | MnS, cm/cm² |
| --- | --- | --- | --- | --- | --- | --- | --- | --- | --- |
| 1 | 17G1S-U | normalized | 554 (80.3) | 402 (58.3) | 27 | 57 | 57 (42) | Banded Ferrite + Pearlite | 12.5 |
| 2 | 17G2AF | normalized | 588 (85.3) | 461 (66.8) | 24 | 63.6 | 80- 87 (59- 64) | — do — | 4.5 |
| 3 | 09G2FB | controlled rolled | 618 (89.6) | 481 (69.7) | 22.5 | 63.3 | 56- 57 (41- 42) | — do — | 2.0 |
| 4 | 10G2MFB | controlled rolled | 612 (88.7) | 510 (73.9) | 20.0 | 64.0 | 88-145 (65-107) | — do — | 2.7 |
| 5 | 08G2MFB | controlled rolled | 628 (91.0) | 412 (59.7) | 22.2 | 71.0 | 71 (52) | Quasi-homog-enous Ferrite + Pearlite (Bainite) | 0.2 |
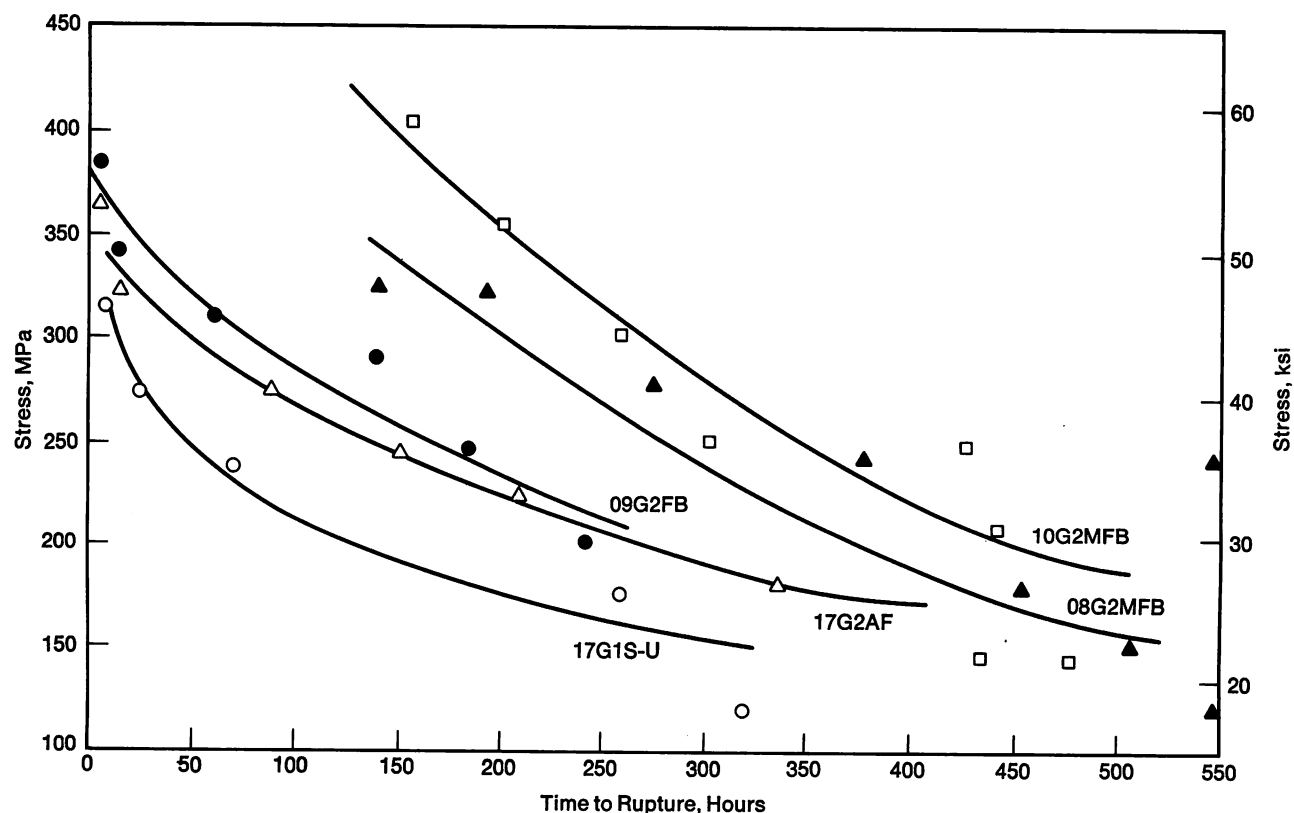


*FIGURE 3—Time to rupture as a function of applied stress. Specimens charged with hydrogen in 0.1N $H_2SO_4$ + 0.5 g/l $NH_2CSNH_2$; current density 50 ma/cm$_2$.*

**Table V**—Parameters Resulting from Addition of Hydrogen to Investigated Steels

| No. | Grade | Decrease in Ductility (Percent Loss in RA), $\Delta\psi$ | Amount of Absorbed Hydrogen, V, $cm^3/100\ g$ | Hydrogen Segregation Ratio |
|---|---|---|---|---|
| 1 | 17G1S-U | 58.0 | 6.0 | 1.35 |
| 2 | 17G2AF | 58.5 | 3.45 | 2.58 |
| 3 | 09G2FB | 56.0 | 3.9 | 2.93 |
| 4 | 10G2MFB | 45.5 | 3.5 | — |
| 5 | 08G2MFB | 72.0 | 6.7 | — |
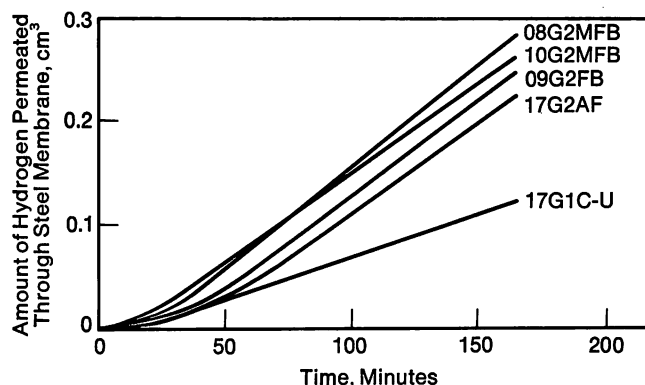


*FIGURE 4—Hydrogen permeability of investigated steels.*



*FIGURE 5—Effect of sulfide inclusion length on hydrogen evolution and rupture time.*

The character of the sulfide inclusions was determined by viewing 100 areas of a surface of 9.4 mm² (0.015 in.²) with the aide of a Quantimet 720. The chemical composition, mechanical properties and thermal treatments of the steels are presented in Tables III and IV. Steels 1-4 are normal products of the NLMZ and Azovstal plants, whereas Steel 5 is from the Nippon Steel Corporation.

Figure 3 relates time to rupture as a function of applied stress. It is noted that at all stress levels, the time to fracture for Steel 17G1S-U is relatively short. The resistance to HIC of Steels 17G2AF and 09G2FB is about the same. The longest times to fracture are demonstrated by Steels 08G2MFB and 10G2MFB.

Data on the percent loss in reduction in area, $\Delta\psi$, Table V, show that the most significant decrease in toughness occurs in Steel 08G2MFB (72%), the least affected is Steel 10G2MFB (45.5%), and Steels 17G1S-U, 17G2AF and 09G2FB decreased about the same amount (56-58%).

With respect to hydrogen permeability, the data indicated that hydrogen most readily permeates Steels 10G2MFB, 09G2FB and 08G2MFB, and permeability through Steel 17G1S-U is most difficult, Figure 4.

In the two-hour charging with hydrogen, Steels 17G1S-U and 08G2MFB absorbed about twice as much hydrogen as the other steels under investigation. MnS increased the amount of absorbed hydrogen, Table V. The sulfides are also the most effective traps for hydrogen, which cause the initiation and propagation of hydrogen-caused defects. As a consequence, at equal decrease of ductility and rupture stress, Steel 17G1S-U exhibits a two-fold reduction in degree of segregation of hydrogen in the fracture zone over Steels 17G2AF and 09G2FB, Table V.

It is possible to judge the comparable effectiveness of traps and the interaction of hydrogen with the steel by the characteristic permeability, Figure 4, and by the liberation of the hydrogen, Figure 5a. It is observed that Steel 17G1S-U exhibits the lowest hydrogen permeability and desorbs hydrogen at the fastest rate. This suggests that hydrogen interacts rather strongly with this steel, aided by the greater amount of initial and emerging (as
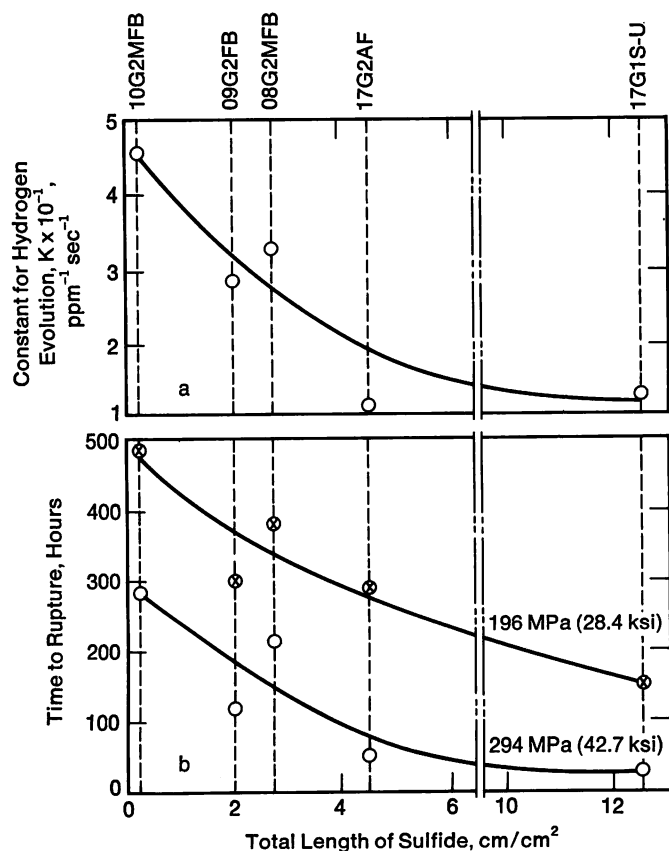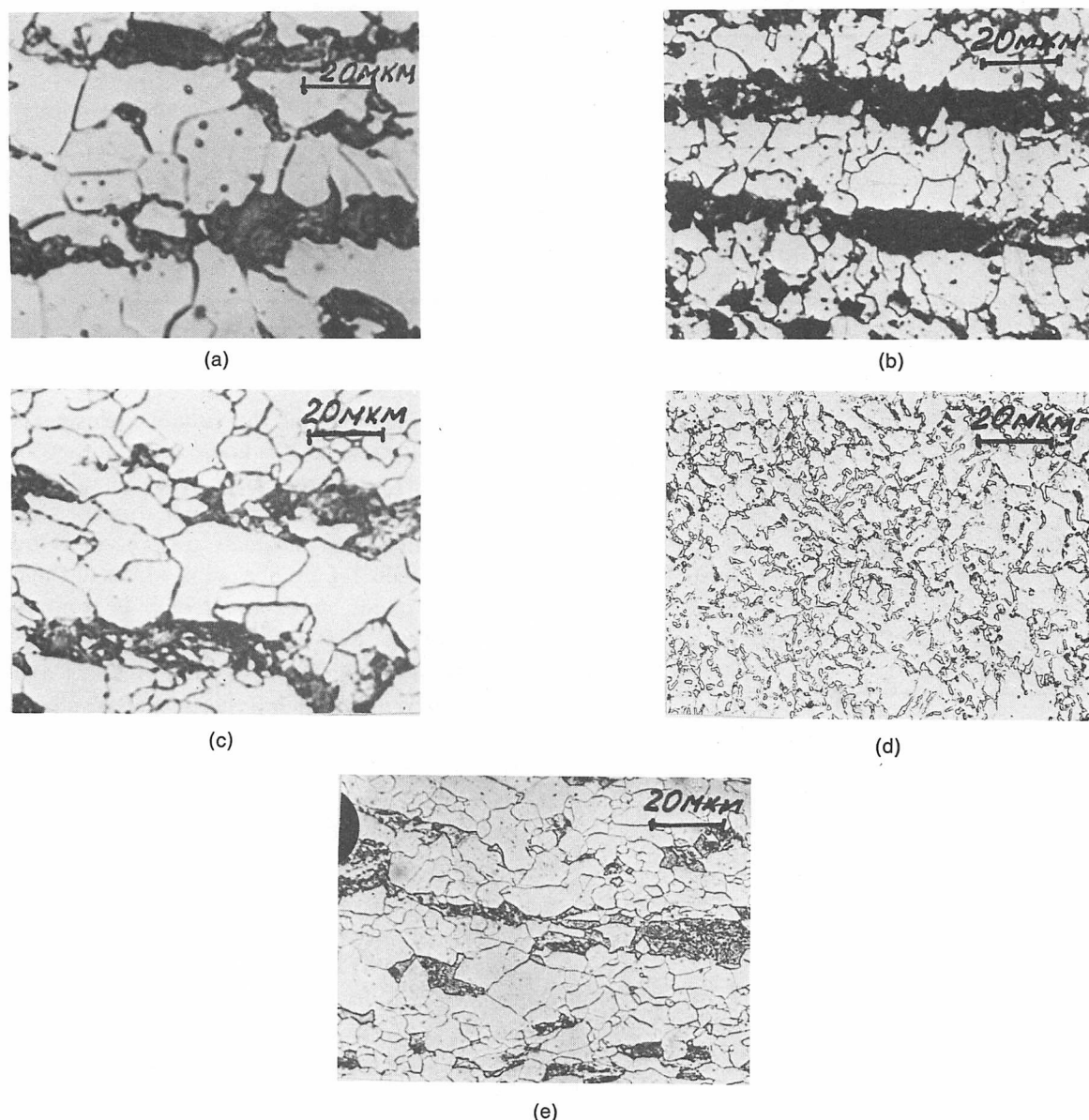
FIGURE 6—Microstructures of Steels (a) 17G1S-U, (b) 17G2AF, (c) 09G2FB, (d) 08G2MFB and (e) 10G2MFB.

result of the hydrogenizing process) structural defects (traps for hydrogen).

Steel 17G2AF and 09G2FB are very similar on the basis of occlusion, diffusion and stability characteristics with respect to HIC, even though controlled rolled Steel 09G2FB has a more appropriate chemical composition, i.e., lower carbon and sulfur contents. Apparently it had not developed its more detrimental form due to the lower finishing temperature. As can be seen from Figure 5, at all stresses, steels with large total sulfide inclusion lengths show lower times to rupture, and the evolution of hydrogen is slower.

The kinetics of hydrogen evolution and the consequent interaction of hydrogen with traps is determined not only by the amount of inclusions but as well by their shape. At more than double the sulfur content (and the resultant sulfide inclusions), the hydrogen in the nor-

malized Steels 17G1S-U and 17G2AF evolved with equal speed, and the value of K was practically the same (Figure 5). In controlled rolled steels having approximately a similar sulfur concentration, the shape of the sulfides is the dominant factor; the evolution of hydrogen is enhanced with the decreasing total length of the sulfide inclusions. Steel 10G2MFB has the maximum K value as well as the highest resistance to HIC.

Thus the lowering of sulfur below 0.005% is not an adequate condition to insure high resistance to hydrogen embrittlement. It is also necessary to have good processing technology to yield a desirable inclusion shape. Desirable results have been obtained in this direction with the addition of rare earths, calcium and other materials.

In addition to the nonmetallic inclusions, HIC resistance is dependent upon morphology of the microstructure, particularly the banding (striations), grain
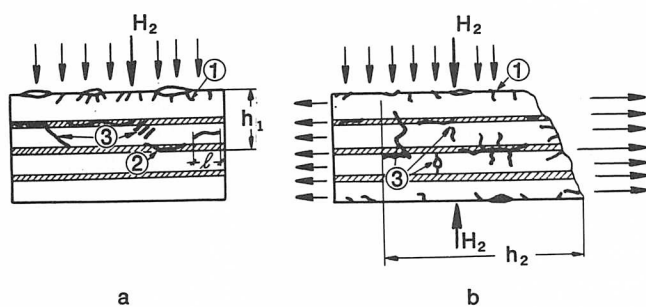
FIGURE 7—Schematic representation of blistering and cracking during: (a) stationary one-sided charging of membrane by hydrogen (static blistering); (b) during stressing to fracture of specimen charged with hydrogen (dynamic blistering). 1, 2, 3—crack type; $h_1$,—depth of charged layer; l—length of crack; cross-hatched bands represent pearlite.
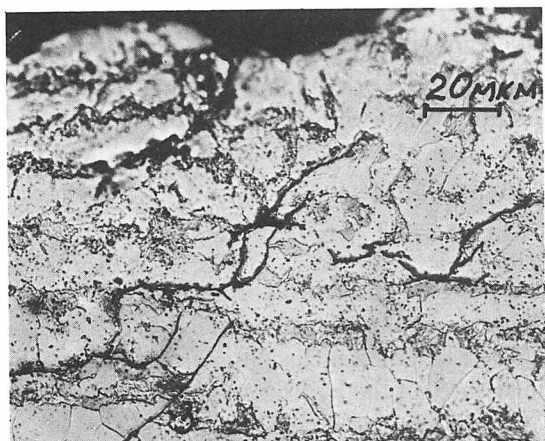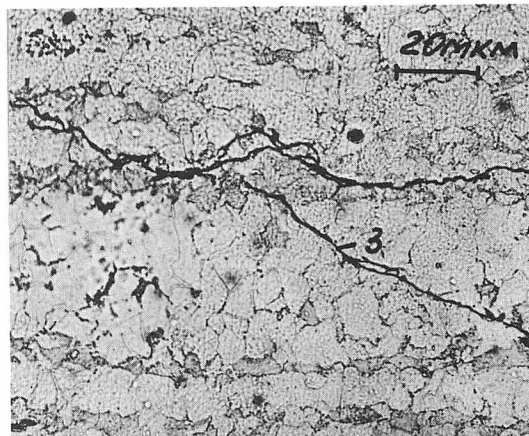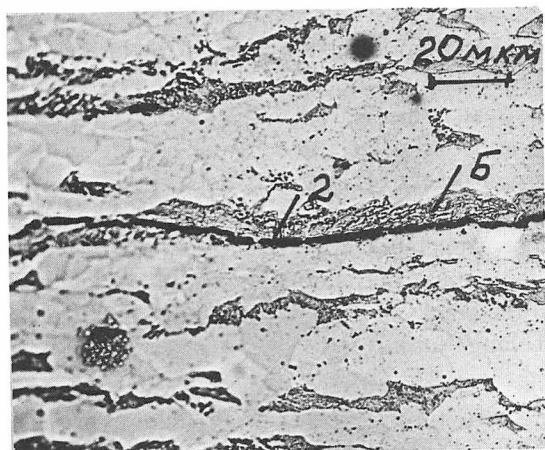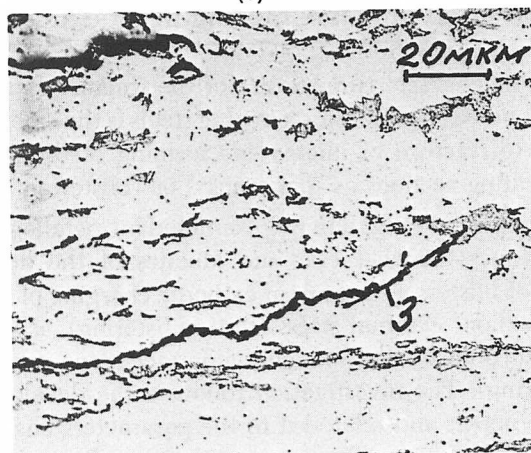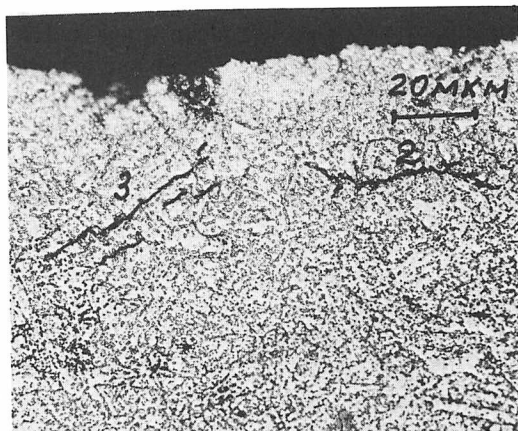


FIGURE 8—Static blistering in (a) Steel 1, (b) Steel 2, (c) Steel 3, (d) Steel 4 and (e) Steel 6.

size and the dispersivity of the structural components. Comparing the microstructures of the investigated steels, Figure 6, it is noted that the least desirable structure is in the normalized Steels 17G1S-U and 17G2AF which had the poorest resistance to HIC. These steels contained well-defined banding. The ferrite in Steel 17G1S-U is coarse grained and not fragmented in comparison to the other steels.

The microstructure of the steel most resistant to HIC (10G2MFB) is characterized by desirable morphology, i.e., fine grained ferrite, and the pearlite is well distributed. Steel 08G2MFB also has good resistance to HIC, and its microstructure consists of a fine dispersion of ferrite and pearlite and essentially no banding.

Studies conducted to ascertain the susceptibility of gas linepipe steels to hydrogen embrittlement showed that it is necessary to develop the proper microstructure to increase resistance to the development of defects which allow the penetration of the hydrogen into the steel.[5-7] The mechanism and kinetics of defect development require basic studies in conjunction with actual microstructures of the steels.

## Microstructural Features Occurring as a Result of Hydrogen Cracking in Pipe Steels

The characteristic feature of the fracture stemming from hydrogen penetration in pipe steels is the emergence prior to fracture of microvoids forming in the steel in alternating sections as "flat cracks" or "blistering."

In this investigation, we examined by metallographic techniques the character and kinetics of the development of blisters as a result of cathodic charging of hydrogen without external stress (static blistering), as well as during deformation of charged specimens (dynamic blistering). The investigation followed the development of the defect and related it to the parameters characterizing the behavior of hydrogen with the traditional results for HIC.

The investigated steels listed in Tables III and IV have microstructures of two types: Steels 1-4 are banded ferrite-pearlite structures, and Steels 5-6 have a semi-homogeneous structure. Steel 6 of Type 10Kh2GMAU, after laboratory remelting and casting, had a structure of quasi-homogeneous sorbite after tempering (tempered bainite).

To determine the character of the cracking under static blistering conditions, metallographic analysis was conducted of the surface and cross section after 3 and 30 hours of hydrogen charging (Figure 2). The depth of hydrogen penetration was measured as evident by the depth of the cracks, the amount of cracks and their length. The length of a crack per area of the affected zone was taken as the defect density.

The character of the defects is shown schematically in Figure 7 which shows the surface blisters and the extent of cracking. The diameter of the blisters varied from 0.02 to 1.2 mm (0.0008 to 0.05 in.). The distribution of the blisters was difficult to relate to a specific microstructure. The blisters developed during dynamic testing were smaller in diameter and depth than those developed during static conditions. In the membranes, the internal cracking was localized on the surfaces at the points of hydrogen penetration (Figure 7a), whereas in the fracture specimens, the entire specimen was permeated with cracks, some of which extended to the surface (Figure 7b).

The cracks can be divided into three groups:

1. Surface cracks randomly oriented or radial to the bottom of the blister.
2. Parallel to the surface of the specimen but not related to the surface.
3. Cracks which serve to combine cracks of Type 2.

The paths of the cracks of all types are associated with the nonmetallic inclusions such as sulfides, silicates and oxides. Elongated inclusions concentrated nearer the surface of entry of the hydrogen are the centers of initiation of the cracks.

The degree of growth and morphology of cracks of Type 2 and 3 are determined by the microstructure of the matrix and the nonmetallic inclusions as well as the presence or absence of stress. The influence of external stress is associated with the distribution during testing and basically is tied to the change in the morphology of cracks of Type 3. Under conditions of static blistering, they are at an angle of 45° to the surface as would be expected. Under dynamic conditions of blistering, they appear perpendicular to the axis of the stress and to the cracks of Type 2 (which always lie along the axis of elongation).

The Type 2 cracks in steels with banded ferrite-pearlite structures (Steel 1-4), lie along or near the pearlite band (Figures 8a and b) or along a bainite component, Figure 8c. During dynamic blistering, there is a clear unity between the nonmetallic inclusions, Figures 9b and c. In the quasi-homogeneous structure, cracks of this type are very short and propagate primarily through prior martensitic islands (Figure 8d) or through sections of anomolous structure where the number of carbides has increased. During dynamic blistering in Steels 5 and 6, cracks of this type were not observed.

Type 3 cracks in ferrite-pearlite steels under static blistering conditions propagate between F-P and F-F grain boundaries or through ferrite grains at locations of cementite precipitates (Figures 8a, b and d). In the controlled rolled steels with poorly defined banding, the cracks tend toward branching (Figures 8b and d). The branching can occur in the ferrite as well as in the pearlite areas (Figure 8d).
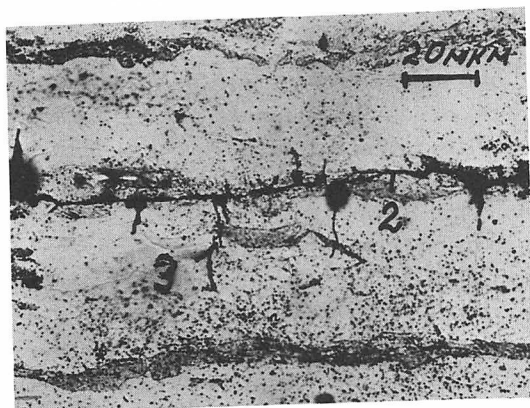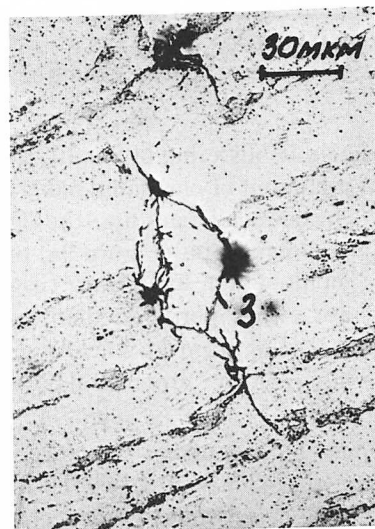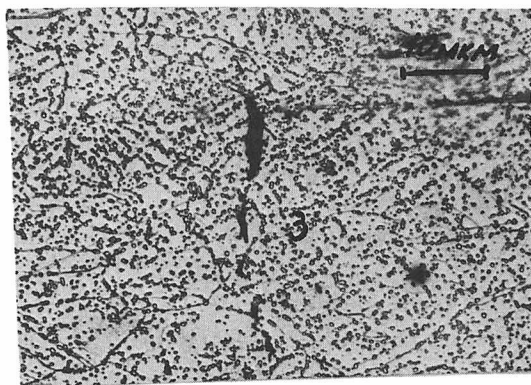
FIGURE 9—Dynamic blistering in (a, b) Steel 1; (c, d) Steel 3 and (e) Steel 6.

**Table VI**—Microstructural Parameters for Blistering and Resistance to Hydrogen-Induced Cracking

| Steel No. and Grade | 1 17G1S | 2 17G2AF | 3 09G2FB | 4 10G2MFB | 5 08G2MFB | 6 10Kh2GMAU |
|---|---|---|---|---|---|---|
| Hydrogen permeability, $cm^3/cm^2$ min $10^3$ | 0.83 | 1.8 | 1.6 | 1.65 | 2.15 | — |
| Time to rupture, h (294 MPa, 42.7 ksi) | 15 | 60 | 140 | 290 | 230 | 280 |
| Static Blistering[a] | | | | | | |
| Depth of affected zone, $h_1$, mm | 0.36 | 0.20/ 0.24 | 0.24/ 0.36 | 0.6 | — | 0.24/ 0.32 |
| Number of cracks | 55 | 44/80 | 12/35 | —/60 | — | 6/104 |
| Defect density, $mm/mm^2$ | 1.68 | 1.24/ 3.12 | 0.46/ 1.64 | 0.98 | — | 0.094/ 1.03 |
| Dynamic Blistering[b] | | | | | | |
| Depth of affected zone, $h_2$, mm | 0.48 | 0.8 | 3.6 | — | 1.05 | 0.66 |
| Number of cracks | 8 | 12 | 25 | — | 40 | 30 |
| Defect density, $mm/mm^2$ | 1.72 | 1.32 | 0.79 | 0.30 | 0.42 | 0.27 |

[a] Charging of membrane for 3/30 hours.
[b] Elongation to rupture approximately same as for hydrogen charged specimens.

During dynamic blistering of Steel 1, the steel which had the greatest amount of elongated manganese sulfides and the most pronounced banding, the Type 3 cracks have a steplike configuration (Figure 9a) or form a network around nonmetallic inclusions (Figure 9b). In Steel 3, they are either perpendicular to the pearlite patches (Figure 9c), or form an enclosing contour, the long axis of which is also perpendicular to the pearlite island (Figure 9d).

In the quasi-homogeneous structure, the Type 3 cracks are somewhat shorter than in the ferrite-pearlite steels. In Steel No. 6, as would be expected, the cracks propagate in the direction of prior martensite needles (Figure 8d) perpendicular to the axis of stress and associated with the sulfides under conditions of dynamic blistering (Figure 9d).

The aggregate of the cracks gives rise to an affected zone the depth of which varies with the composition and the microstructure of the steel and from the total time of hydrogen charging under static conditions and the stress during dynamic conditions.

The microstructure, the parameters of hydrogen charging and the time to fracture affect the elongation (Table VI).

The amount of cracking in the affected zone can only approximate the susceptibility to hydrogen embrittlement, as the lengths of the cracks are not the same for the various steels and structural variables in Steels 1-4. The depth of the affected zone can serve as an indicator only in steels having a single structure (Steels 1, 2 and 3). Increasing the time of hydrogen exposure gives rise to an increase of these characteristics, so that in the time

period of 3 to 30 hours, the created defects in all of the steels have essentially the same character, Table VI. Relative to the susceptibility to HIC and defect density for both types of blistering, the resistance increases with increasing number of the steel in Table VI. The same rating was obtained using the time to rupture values. Steel No. 1 is the most susceptible and has the greatest defect density. This is related to the presence of traps (the voids from manganese sulfide inclusions, Table IV), the ferrite-pearlite bands and the lower ductility of the matrix. The development of defects is explained by the low hydrogen permeation, by high ability to occlude and a low ductility of this steel.

The lower defect density of Steel 2 is associated with the lower aspect ratio of the sulfides. The appearance of fracture surfaces on Steels 1 and 2 is similar.

The cracks in controlled rolled Steels 3 and 4 are characterized by a larger amount of branching (Figure 8e) due to the fragmentation of the ferrite (Figure 8d) and a smaller density of defects due to lower carbon content and less banding. The lesser banding and the shorter length of the sulfides (Table IV) in Steels 3 and 4 result in a decrease of defect density.

Comparing the defect density and yield strength of Steels 3 and 5, which have the manganese sulfides of the same length (Tables IV, V), it is evident that the increase in the ferrite-pearlite anisotropy (lamination) gives rise to a decrease in the HIC. The lowest defect densities are in Steels 5 and 6 which have the quasi-homogeneous structures, in which the cracks are of Types 1 and 3 and are only 0.05 mm (0.002 in.) in length (Figures 8e and 9e).
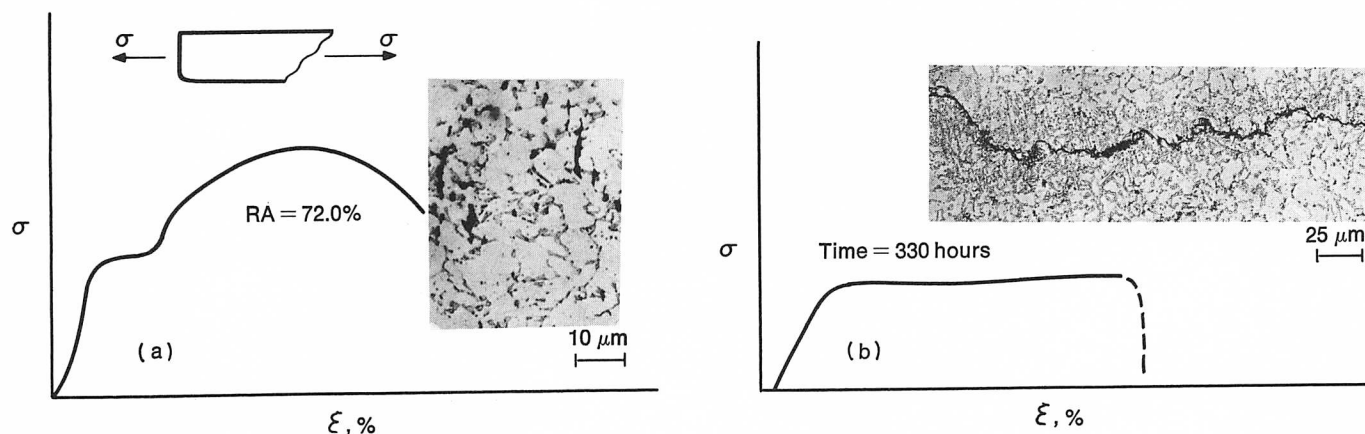
FIGURE 10—Character of the cracks in Steel 5 (a) during elongation to rupture of a hydrogen-charged specimen and (b) after holding for 330 hours in a hydrogen atmosphere under a stress of 294 MPa (42.7 ksi). This stress is 70% of the 0.2% offset yield strength.
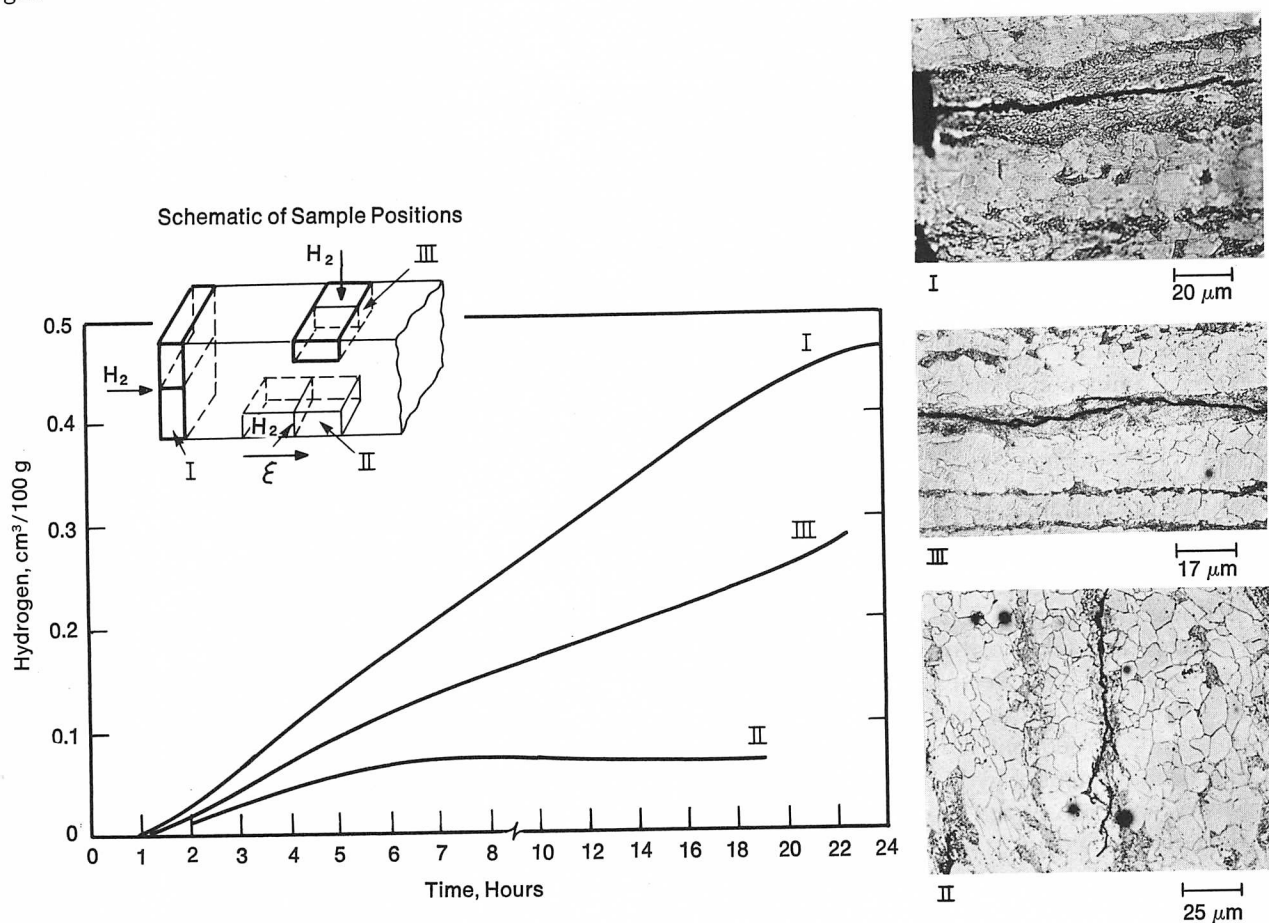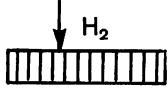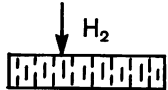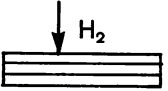


FIGURE 11—Influence of ferrite-pearlite banding on the hydrogen permeability and cracking of Steel no. 3.

It is interesting that the sulfur contents of Steels 1 and 6 are the same and that the sulfides in Steel 6 are also elongated. Consequently, the sorbite matrix reduces the deleterious influence of the elongated sulfides on the susceptibility to HIC.

The morphology of dynamic blistering which evolves under the conditions of the tests to determine the elongation during yielding had signs of static and dynamic blistering (Figure 10). The cracks occurred predomi-nantly in areas of anomolous structure in sites of elon-gated carbides in pearlite striations. In these areas, by methods of microprobe analysis, it was determined that the manganese content was higher; it had increased two-fold over the base manganese content to about 3%. Thus it was shown that, in the development of both the static and dynamic blistering in pipe line steels, blistering is assisted by inclusions in the microstructure which are only a few thousands of a millimeter in size, e.g., the

**Table VII**—Hydrogen Permeability and Cracking in Steel No. 3 Under Various Orientations of the Ferrite-Pearlite Striations Relative to Hydrogen Direction

| Specimen No. | Orientation of Striations of the Test Membrane | Depth of Hydrogen Affected Zone, h, mm | No. of Cracks | Amount of Hydrogen Introduced Into the Membrane in 24 hours, $cm^3$ | Defect Density, $mm/mm^2$ |
|---|---|---|---|---|---|
| 1 | ↓ $H_2$ | 0.72 | 6 | 0.5 | 0.17 |
| 2 | ↓ $H_2$ | 1.08 | 27 | 0.07 | 0.24 |
| 3 | ↓ $H_2$ | 0.21 | 31 | 0.35 | 1.66 |

elongated nonmetallic inclusions, the ferrite-pearlite banding and the bainitic areas in the ferrite-pearlite matrix.

The banded ferrite-pearlite microstructure is characteristic of many pipe line steels. In various processing steps, including welding, an interesting problem exists to define the role of the ferrite-pearlite banding on crack propagation as a function of direction of hydrogen permeation. Steel 3, with a relatively small elongation of the manganese sulfides (Table V), was evaluated. Hydrogen permeation and the character of the static blistering was measured on the membranes cut from plates in three mutually perpendicular directions (Table VII). Metallographic analysis of cross sections of the membranes revealed that cracks occurred predominently along pearlite patches regardless of the direction of hydrogen charging (Figure 11). Transverse orientation of the pearlite patch did result in the greatest resistance to hydrogen permeation and, consequently, the greatest amount of cracking. The movement of hydrogen along the length of the pearlite islands causes the least amount of cracking. It was thus determined that the permeation and the degree of cracking is dependent not only on the extent of banding, but also on the location of the pearlite islands with respect to the hydrogen flow direction. Characteristic of pipe line steels, the surface of cracking is determined primarily by the location of the microconstituents as a result of rolling. Their relationship with respect to hydrogen flow is important during preparation and welding of the pipe.

This investigation resulted in the development of a processing schedule for welded and seamless pipe for optimum resistance to hydrogen-induced cracking, as well as thick steel plate used for the original processing of natural gas. The increased resistance to HIC of low alloy steels can be achieved by alloying with carbide-nitride forming elements (V, Nb, Mo), lowering the carbon content and the associated banding, lowering the sulfur content, introducing shape control for the nonmetallic inclusions, and decreasing all segregating nonuniformities.

# References

1. L. C. Livshitch, et al., "Processing and Technology of Producing Natural Gas Pipe Line Steels for Transport of Gas in the Refrigerated and Pressurized Conditions." Part of collection of papers in *Design and Construction of Gas Pipe Line and Oil and Gas Installations*, NIPIESU Neftostroi, M., 1977, No. 9.

2. T. K. Sergeeva, G. G. Irzhov and A. G. Zakurgdaev, *FKhMM*, 1978 (Soviet Materials Science), Kiev, 29.

3. G. G. Irzhov, T. K. Sergeeva and E. G. Feldgander, in collection of *Quality Steels*, M, 1978, 9.

4. T. K. Sergeeva, G. G. Irzhov and V. V. Pokidyshev, *Zavodskaia Laboratorie, (Industrial Laboratory)*, 1978, M, 1979, 405.

5. P. Bastien, Int. Congress, *L'Hydrogene dans les Metaux, 1*, 1972, 11.

6. S. A. Golovanenko, B. N. Zikeev, E. B. Serebranaja and L. V. Popova, *MiTOM, Metal Science and Heat Treatment of Metals*, 1978, No. 1, 2.

7. S. A. Golovanenko, I. U. Konnova and T. K. Sergeeva, *MiTOM, Metal Science and Heat Treatment of Metals*, 1976, No. 8, 30.

# A Beta Type Ti-15Mo-5Zr-3Al Alloy for Sour Well Service

by S. Ohtani, T. Nishimura and Y. Moriguchi
Kobe Steel Ltd.

Titanium and its alloys are generally less sensitive to stress corrosion cracking and therefore are considered to be candidate materials for deep sour gas well service. The beta type titanium alloy, Ti-15Mo-5Zr-3Al, with better corrosion resistance in nonoxidizing environments than commercially pure titanium and with a higher strength-to-weight ratio was developed by Kobe Steel Ltd. This alloy's sulfide stress corrosion fracture toughness, $K_{ISSC}$, determined by J. A. Straatmann and E. P. Whelan of Climax Molybdenum Company, confirmed its applicability to deep sour well service.

## Sulfide Stress Corrosion Testing

The composition of the tested alloy is shown in Table I. This material was prepared from an ingot of about 100 kg (220 lb). Plate was rolled to a thickness of 10 mm (0.44 in.). The plate was solution treated at 735 C (1355 F) for one hour and water quenched. Machined double cantilever beam and tensile test specimens were aged at 500 C (930 F) in a vacuum furnace, and specimens were helium-gas quenched within the furnace chamber.

Room temperature tensile properties are shown in Table II. The yield and tensile strengths in the transverse direction were slightly greater than those in the longitu-

dinal direction with an associated decrease in ductility.

The procedure for performing DCB tests to determine SSC resistance has been described in detail by Heady.[1] Using the DCB specimens shown in Figure 1, tests were conducted in the standard $H_2O$—5% sodium chloride—0.5% acetic acid solution saturated with $H_2S$. Specimens were exposed in this solution for a total period of four weeks, with an intermediate inspection for crack length estimation after two weeks.
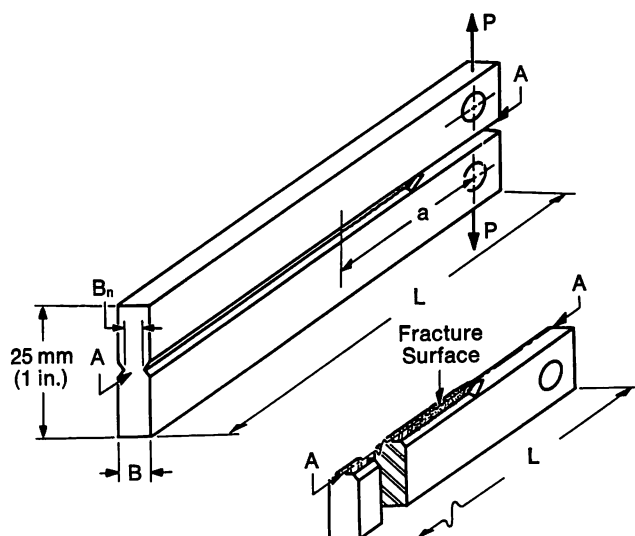


L = 102 mm (4 in.)
B = 6.35 mm (0.25 in.)
$B_n$ = 4.32 mm (0.17 in.)
a = Crack Length (from Plane of Loading)
P = Equilibrium Wedge Load at Which Crack Stops Growing

FIGURE 1—Double cantilever beam (DCB) specimen used to determine $K_{ISSC}$ values.

**Table I—Composition of Ti-15Mo-5Zr-3Al Alloy**

| | | | Element, % | | | | |
|---|---|---|---|---|---|---|---|
| Mo | Zr | Al | Fe | O | H | N | Ti |
| 14.79 | 5.16 | 2.90 | 0.0386 | 0.132 | 0.0028 | 0.0033 | Bal |

**Table II—Room Temperature Tensile Properties of Ti-15Mo-5Zr-3Al Alloy**

| Plate Direction | 0.2% Offset Yield Strength, MPa (ksi) | Tensile Strength, MPa (ksi) | Elonga-tion, % | Reduction in Area, % |
|---|---|---|---|---|
| Longitudinal | 1254 (182) | 1333 (193) | 11.0 | 11.0 |
| | 1251 (181) | 1325 (192) | 11.0 | 11.9 |
| Transverse | 1302 (189) | 1373 (199) | 5.0 | 3.1 |
| | 1296 (188) | 1376 (200) | 5.0 | 2.4 |
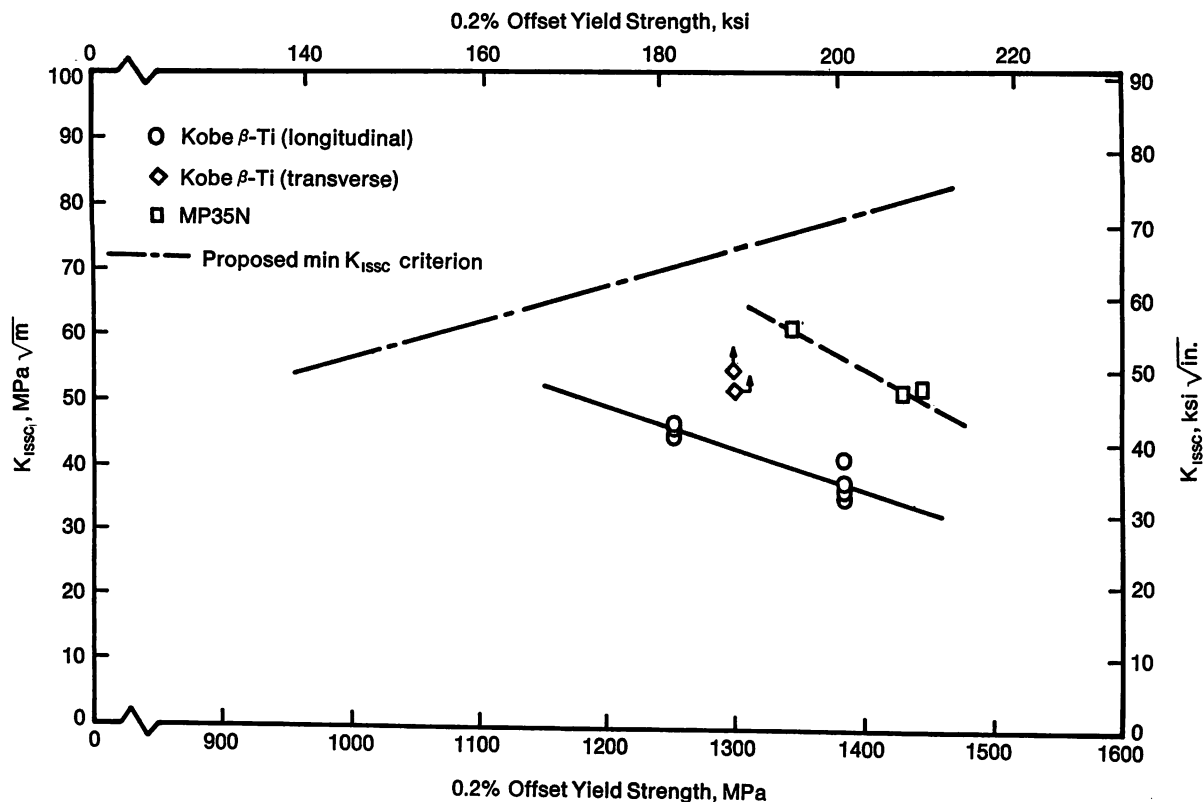
FIGURE 2—Relationship between yield strength and $K_{ISSC}$ for beta titanium alloy and MP35N.

Fracture toughness, $K_{ISSC}$, was calculated for all specimens exhibiting adequate crack development, using the procedure proposed by Heady.[1] The $K_{ISSC}$ values for the specimens are plotted in Figure 2 as a function of yield strength. Data obtained in the Climax Laboratory for MP35N (35Co, 35Ni, 20Cr, 10Mo) are also included in this figure, together with a plot of a proposed criterion for the minimum acceptable fracture toughness level for steels. The beta titanium alloy has $K_{ISSC}$ levels below the proposed criterion. However, the applicability of this extension of the criterion to these high strength levels has not yet been established, and, therefore, no undue significance should be attached to the location of the beta titanium data points with respect to this criterion plot.

When presented as in Figure 2, the beta titanium alloy appears to be less resistant to sulfide stress cracking than MP35N. Since there is a marked difference in the densities of the two alloys, however, a comparison between these two alloys may possibly be more valuable using the yield strength/density ratio as a variable instead of the yield strength alone. Figure 3 shows a plot of fracture toughness against this ratio for the beta titanium alloy and for MP35N. It is evident from this plot that, if the line for the beta titanium alloy can be extraporated to higher $K_{ISSC}$ values, reductions in the yield strength of the beta titanium alloy with associated increase in fracture toughness up to at least that of MP35N are possible without losing the strength/density advantage that the beta titanium alloy possesses over MP35N.

Although the sulfide stress corrosion resistance of the beta titanium alloy should be determined over a larger range of yield strengths, it is considered applicable to deep sour well service.

## Melting Technique

It is very difficult to produce a homogeneous titanium alloy ingot when elements having considerably higher melting points and densities than titanium are added (molybdenum, tantalum, niobium, etc.).

In our research laboratory, when the Ti-5%Ta alloy was found to have superior corrosion resistance in concentrated nitric acid solutions at higher temperatures, a satisfactory melting method was developed.[2] The consumable electrode for vacuum arc melting consists of briquettes with mixed powders of titanium and molybdenum. The effect of Mo/Ti ratio on the homogeneity of Mo distribution in the Ti-15Mo-5Zr alloy was studied. The minimum weight percent of Ti powder was found to be 31% in the case of nonconsumable electrode vacuum arc melting as shown in Table III. However, in industrial-size ingots prepared by consumable electrode melting, more than 40% of the mixed powder had to be Ti to avoid macrosegregation. An example of chemical analysis of the Ti-15Mo-5Zr-3Al alloy produced as a 300 kg (660 lb) ingot with a diameter of 300 mm (12 in.) is shown in Table IV. This ingot's briquette was added

with a mixed powder of Mo (2.49 $\mu$m) and Ti (under 100 mesh) at the weight ratio of Mo/Ti = 3/2. Another example of the chemical analysis of a Ti-5% Ta alloy ingot with a diameter of 480 mm (19 in.) is shown in Table V.

The beta titanium alloy should be melted by consumable electrode, vacuum arc melting using briquettes made by adding Mo as a mixed powder to Ti at the weight ratio of Mo/Ti = 3/2.
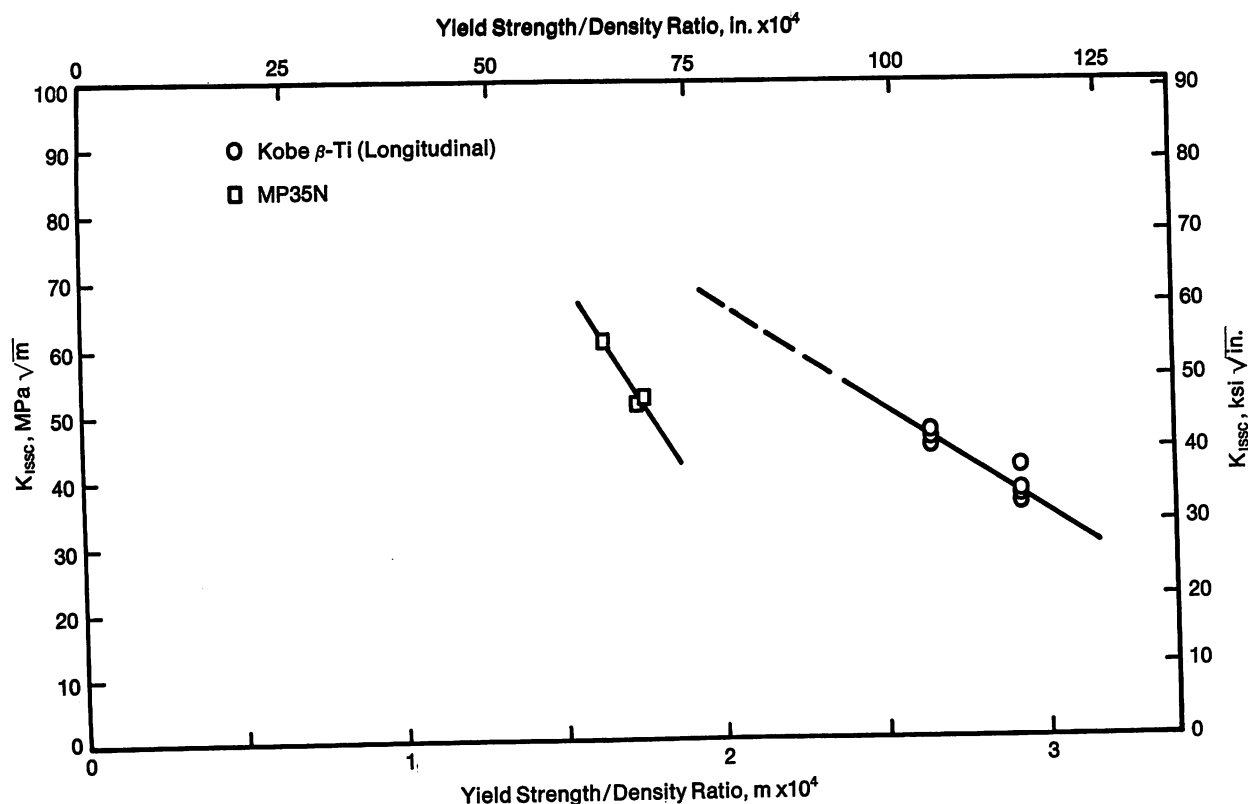


FIGURE 3—Relationship between yield strength/density ratio and $K_{ISSC}$ for beta titanium alloy and MP35N.

**Table III**—Effect of Mo/Ti Ratio in Mixed Powder on the Homogeneity of Mo in the Ti-15Mo-5Zr Alloy Produced by Tungsten Arc Melting

| Mo Powder, % | | Ti Powder, % | | Solidus of Mixed Powder,* | | Unmelted Mo |
|---|---|---|---|---|---|---|
| Vol. | Wt. | Vol. | Wt. | C | (F) | |
| 20 | 36 | 80 | 64 | 1940 | (3525) | Not Observed |
| 30 | 49 | 70 | 51 | 2050 | (3720) | Not Observed |
| 40 | 60 | 60 | 40 | 2170 | (3940) | Not Observed |
| 50 | 69 | 50 | 31 | 2250 | (4080) | Not Observed |
| 70 | 84 | 30 | 16 | 2430 | (4405) | Observed |
| 100 | 100 | 0 | 0 | 2650 | (4800) | Observed |

* Estimated from the Ti-Mo equilibrium diagram.

**Table IV**—Chemical Analysis of a 300 mm (12 in.) Diameter Ingot of a Ti-15Mo-5Zr-3Al Alloy

| Identification | | Element, % | | |
|---|---|---|---|---|
| | | Mo | Zr | Al |
| | Top | 15.05 | 5.17 | 3.00 |
| | | 14.98 | 5.09 | 2.98 |
| Ingot | Middle | 15.16 | 5.07 | 2.84 |
| | | 14.93 | 5.15 | 3.05 |
| | Bottom | 15.06 | 4.98 | 3.02 |

**Table V**—Chemical Analysis of a 480 mm (19 in.) Diameter Ingot of a Ti-5Ta Alloy

| Identification | Tantalum, % | | Center |
|---|---|---|---|
| | Edge | | |
| Top | 4.90 | 4.94 | 4.61 |
| Middle-T | 5.00 | 5.10 | 4.80 |
| Middle-B | 5.11 | 5.07 | 4.88 |
| Bottom | 4.96 | 5.02 | 5.01 |

## Heat Treatment

It is necessary to solution treat and age the titanium alloy to produce a high strength level. The strength depends on solution and aging temperature and time. Although solution treated and aged Ti-15Mo-5Zr alloy has a rather high strength level at an aging temperature below 525 C (975 F), the alloy was embrittled because of $\omega$ precipitation. To improve ductility, 3% Al is added to precipitate $\alpha$ phase instead of $\omega$ phase.
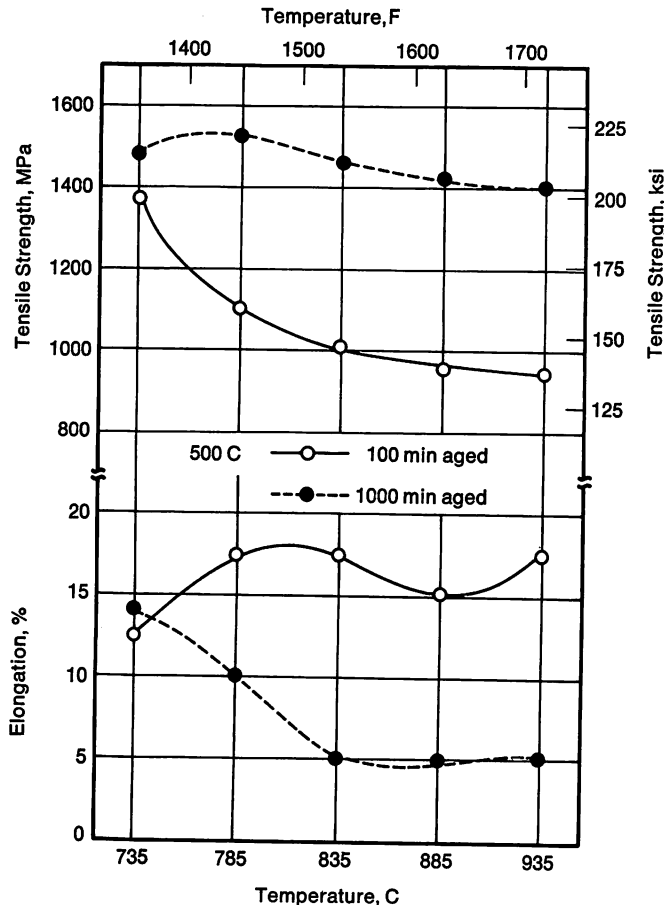


FIGURE 4—Effect of solution temperature on the tensile properties of aged Ti-15Mo-5Zr-3Al alloy.



FIGURE 5—Isochronal curves of tensile properties at various aging temperatures for Ti-15Mo-5Zr-3Al alloy.

**Table VI**—Mechanical Properties of Ti-15Mo-5Zr-3Al Alloy Solution Treated at 735 C (1355 F) and Aged at 500 C (930 F) for 1000 Minutes

| | | |
|---|---|---|
| Tensile Strength, MPa (ksi) | 1476 | (214) |
| Elongation, % | 13.8 | |
| Reduction of Area, % | 58.7 | |
| HV10 | 412 | |
| Ratio, Notched to Unnotched Tensile Strength | 1.06 | |
| Fatigue Strength, MPa (ksi) | 686 | (99) |

The effect of solution temperature on the tensile properties of an aged Ti-15Mo-5Zr-3Al alloy is shown in Figure 4, and the effect of aging temperature and time are shown in Figure 5. Considering these results, the desirable treatment and aging condition was determined as shown in Table VI. Mechanical properties of the Ti-15Mo-5Zr-3Al alloy heat treated at these conditions are shown in Table VI. The beta titanium alloy had a tensile strength of 1471 MPa (213 ksi) and an elongation of 13%. This suggests that a high strength/weight ratio can be expected for the beta titanium alloy. The alloy's specific gravity is about 5.0.

The alloy's aging transformation diagram is shown in Figure 6. At an aging temperature of 500 C (930 F), the phases are $\beta$ and $\alpha$. The $\omega$ phase, which causes embrittlement is not present. Considering the atmospheric conditions in deep sour wells, the beta titanium alloy solution treated at 735 C (1355 F), water quenched and aged at 500 C (930 F) for 1000 minutes was examined after exposure at 200 and 300 C (390 and 570 F) for up to 10,000 minutes. No $\omega$ phase could be observed by x-ray analysis.
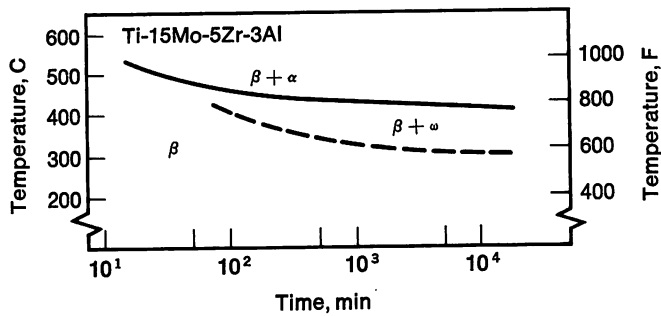
*FIGURE 6—Aging transformation diagram for Ti-15Mo-5Zr-3Al alloy.*

## Conclusions

1. The beta titanium alloy, Ti-15Mo-5Zr-3Al, is considered applicable to deep sour well service.
2. Sulfide stress corrosion fracture toughness can be expected to be superior to that of MP35N on the basis of yield strength/density ratio.

3. This alloy solution treated at 735 C (1355 F), water quenched and aged at 500 C (930 F) for 1000 minutes has a maximum tensile strength of about 1471 MPa (213 ksi) and an elongation of 13%.
4. After exposure at 200 and 300 C (390 and 370 F) for 10,000 minutes in the solution treated and aged condition, $\omega$ phase could not be observed.

## Acknowledgment

## References

1.  R. B. Heady, *Corrosion*, 33 (3), March 1977, 98.
2.  T. Noda and M. Teragaki, *U. S. Patent 3,565,602*.

# High Corrosion Resistant Nitrogen-Containing Stainless Steels for Use by the Chemical Industry

by T. Sakamoto, H. Abo, T. Okazaki, T. Ogawa, H. Ogawa and T. Zaizen
Nippon Steel Corporation

The demand for stainless steel as a corrosion resistant material has been accelerating with the development of the petrochemical industry. Ni-Cr austenitic stainless steel is the main material used in this field because of its superior workability, toughness, weldability and high temperature strength. With the recent increase in pollution control installations, the demand has risen for high quality stainless steel which can operate in highly corrosive environments. In particular, resistance to pitting corrosion in the presence of chloride ion is required. Since molybdenum and chromium are known to impart resistance to this type of corrosion, they have high potential for this use. However, both elements are ferrite formers and must be used with a high nickel content to obtain a corrosion resistant austenitic stainless steel. This is not desirable from the view point of economy and conservation of resources.

To reduce the quantity of nickel needed, an austenitic-ferritic stainless steel has been developed with high Cr and low Ni contents. Unfortunately, using this type of steel in great quantities is not promising because of difficulties in weldability and because of the strict process control needed.

To maintain the austenitic structure while reducing the Ni content, some austenite-forming element must be substituted. Carbon, nitrogen and manganese are common elements which might be utilized for this purpose, but carbon combines with chromium to form a stable carbide which degrades corrosion resistance in general and especially intergranular corrosion. Manganese is also not acceptable as a substitute because it lowers corrosion resistance and because it is an ineffective austenite former when Cr exceeds 16%.[1]

Nitrogen has a fairly high solubility in high Cr steel, is less harmful to the corrosion resistance than carbon, and is effective in increasing pitting corrosion resistance. Accordingly, its possibility as a nickel substitute has been examined. In a survey, nitrogen was found to enhance resistance to both pitting and general corrosion in acids while increasing strength even at high temperatures.[2]

Based on these data, we developed a new austenitic stainless steel (designated Steel A) maximizing the use of nitrogen as a nickel substitute. We have now succeeded in producing this steel on a large scale.[3]

Beyond this, another new steel (Steel B) having more resistance to crevice corrosion than Steel A, is being developed using copper and an increased amount of molybdenum.

This paper covers the research development, characteristics and remaining problems in utilizing these high nitrogen austenitic stainless steels.

## Nitrogen in High Chromium Stainless Steels

Resistance to pitting corrosion increases markedly when the chromium content exceeds 20%, and no pitting occurs when it is over 30%.[4] High chromium content is a prerequisite to a pitting corrosion resistant stainless steel. Therefore, the behavior of nitrogen was examined with steels containing more than 20% chromium.

### Solubility and Austenite Forming Capability of Nitrogen

The solubility of nitrogen in a molten Fe-Cr-Ni alloy is high and increases with increasing chromium.[5] The relationship between chromium content and the solubility of nitrogen is shown in Figure 1. About 0.35% N can be dissolved in a steel containing 25% Cr.

In ferritic steels, the solubility of nitrogen decreases as the temperature drops during solidification, creating blow holes as the nitrogen gas is discharged. In austenitic steels, the solubility does not decrease, and nitrogen remains in interstitial solid solution.

The nitrogen thus dissolved in high chromium steels works as an austenite former, and the data on this effect are shown in Figure 2. The relationship between the cast structure of a 10 kg (22 lb) ingot and the nickel equivalent is plotted in this figure. The equation for the Ni equivalent is based on the derivation by DeLong.[6] Austenite can be formed in 25% Cr steel with a Ni equivalent of
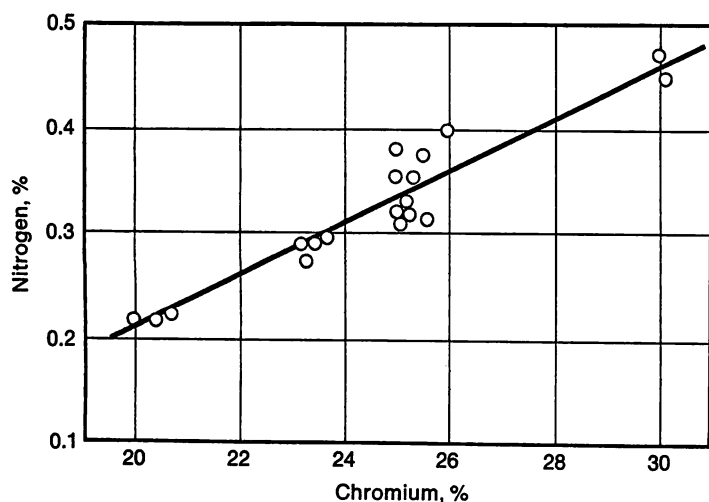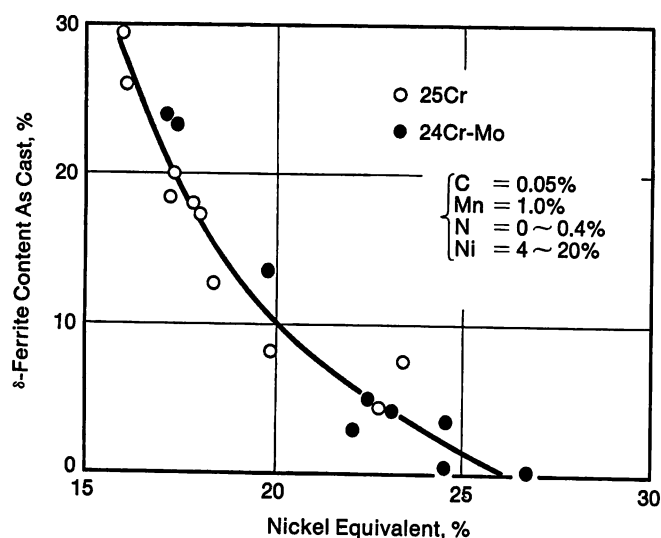
FIGURE 1—Solubility of N in Cr-Ni austenitic steels.



FIGURE 2—Relationship between nickel equivalent and δ-ferrite content.

$$Ni_{eq} = Ni + 0.5Mn + 30C + 30N$$

25%. If the solubility limit of nitrogen (0.35%) is used as a substitute for nickel, austenite is obtained with as low as 13% Ni.

Thus, the addition of 0.35% N is equivalent to the saving of 10% Ni, as the ratio of austenitic forming capability of N to Ni is estimated to be about 30:1.

### Resistance to Pitting Corrosion

Two methods were used to evaluate pitting corrosion. The first involves the measurement of pitting potential using the anodic polarization curve in an atmosphere of 5% $H_2SO_4$ + 3% NaCl at 35 C (95 F). The second was the measurement of actual pitting corrosion rates in an environment of 50 g/l $FeCl_3$ + 0.05N HCl at 50 C (120 F). The first evaluates resistance to the initiation of pitting and the second evaluates the corrosion rate after initiation. The results of these tests are shown in Figure 3.

Nitrogen not only retards the initiation of pitting
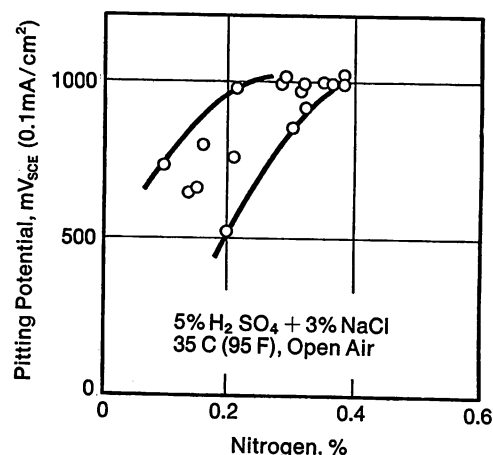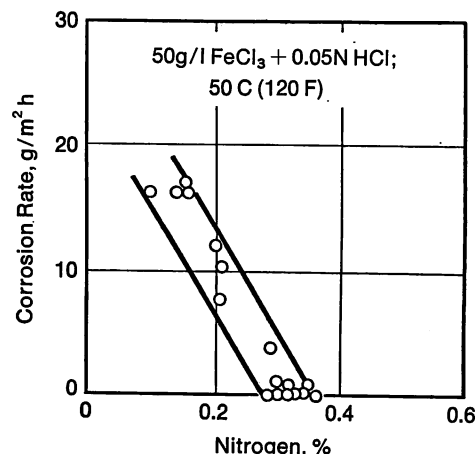




FIGURE 3—Effect of nitrogen on pitting corrosion.

$$Cr = 23 \sim 28\%$$
$$Ni = 9 \sim 16\%$$
$$Mo = 0.4 \sim 0.9\%$$

but decreases pitting corrosion rate. The addition of 0.3% N or more makes 25Cr-Ni austenitic steel essentially immune to pitting corrosion in $FeCl_3$.

### Corrosion Resistance in Acids

Nitrogen was found effective in corrosion resistance in both hydrochloric and sulfuric acids. The relationship between corrosion rate and nitrogen content for each acid is shown in Figures 4 and 5.

The addition of between 0.3 and 0.35% N is most effective in both cases.

### Mechanical Properties

Nitrogen enhances strength because it forms an interstitial solid solution with the base metal. Types 304 and 316 steels containing high nitrogen have already been produced for structural use.

The effects of nitrogen on the mechanical properties of high Cr-Ni steels are shown in Figure 6. Proof stress and tensile strength increase markedly with increasing nitrogen content, and elongation decreases slightly. Since the strengthening effect of nitrogen is maintained at fairly high temperatures, N-containing steels have better
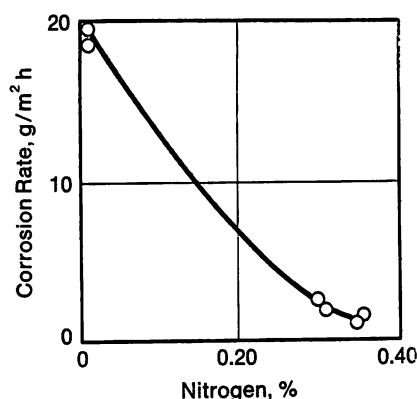
FIGURE 4—Effect of nitrogen on corrosion in 10% hydrochloric acid at 25 C (77 F).
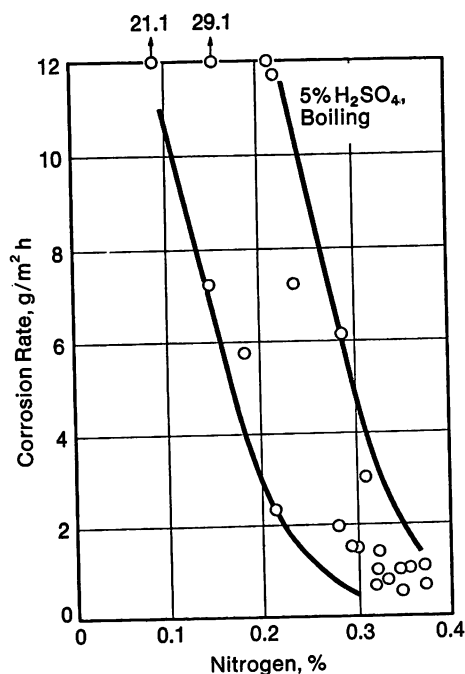


FIGURE 5—Effect of nitrogen on corrosion in sulfuric acid.

Cr = 23 ~ 25%
Ni = 7 ~ 14%
Mo = 0.5 ~ 1.5%

creep rupture and high temperature strengths than commercial stainless steels. Therefore, it also has promise as a heat resistant material.

**Weldability and Weld Metal Properties**

Although weldability is not directly affected by nitrogen, the welds of a single phase austenitic structure are susceptible to hot cracking. A filler metal having a stable austenitic structure should not be used.

An evaluation of pitting corrosion resistance of the welds was made as a function of nitrogen content with 25Cr-13Ni steel.[7] Gas tungsten arc welding (GTAW) was used, and the corrosion rate was measured in FeCl₃–HCl at 50 C (120 F). The results are shown in Figure 7. The effect of nitrogen on pitting corrosion is noticeable for both the welds and the base metal.
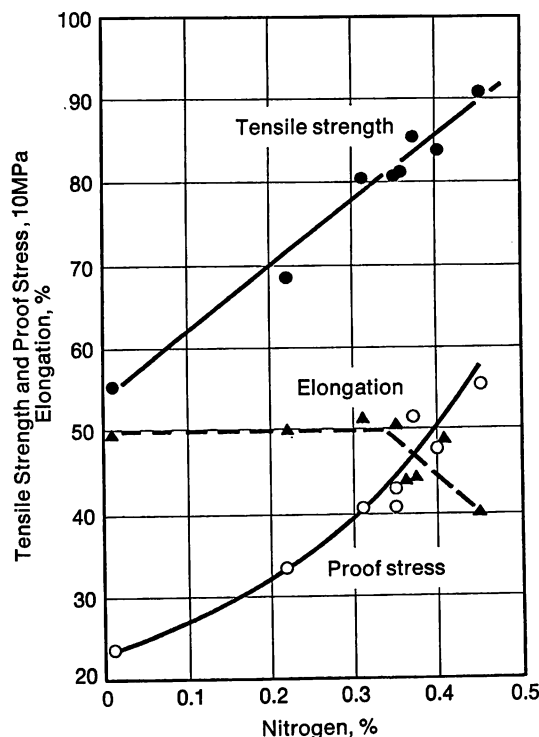


FIGURE 6—Effect of nitrogen on mechanical properties of Cr-Ni austenitic steels.

Cr = 20 ~ 30%
Ni = 17 ~ 18%

# Development of Pitting Corrosion Resistant Steel A

## Alloy Design

Some studies were carried out to define the alloy content of the pitting corrosion resistant steel (Steel A) by making use of the positive characteristics of nitrogen which were described above.

The effect of chromium on pitting corrosion resistance was examined using stainless steel containing nitrogen. The test results are shown in Figure 8. Pitting corrosion resistance increases markedly when chromium exceeds 20%, and no pitting occurs with 25% Cr or more. The discrepancy of corrosion rate values at 25% Cr shown in Figure 8 is the result of the difference in nickel content. Nickel is also an element which improves pitting corrosion resistance, but its effect is much weaker than chromium, molybdenum and nitrogen. Therefore, for the new steel, the minimum nickel content required to form an austenitic structure, assuming a nitrogen content of 0.3%, was about 13%.

The effect of molybdenum on pitting corrosion resistance is shown in Figure 9. The 24% Cr steel needed as little as 0.8% Mo for sufficient pitting resistance.

Thus, the alloy design of Steel A was determined to be 25Cr-13Ni-0.3N-0.8Mo.
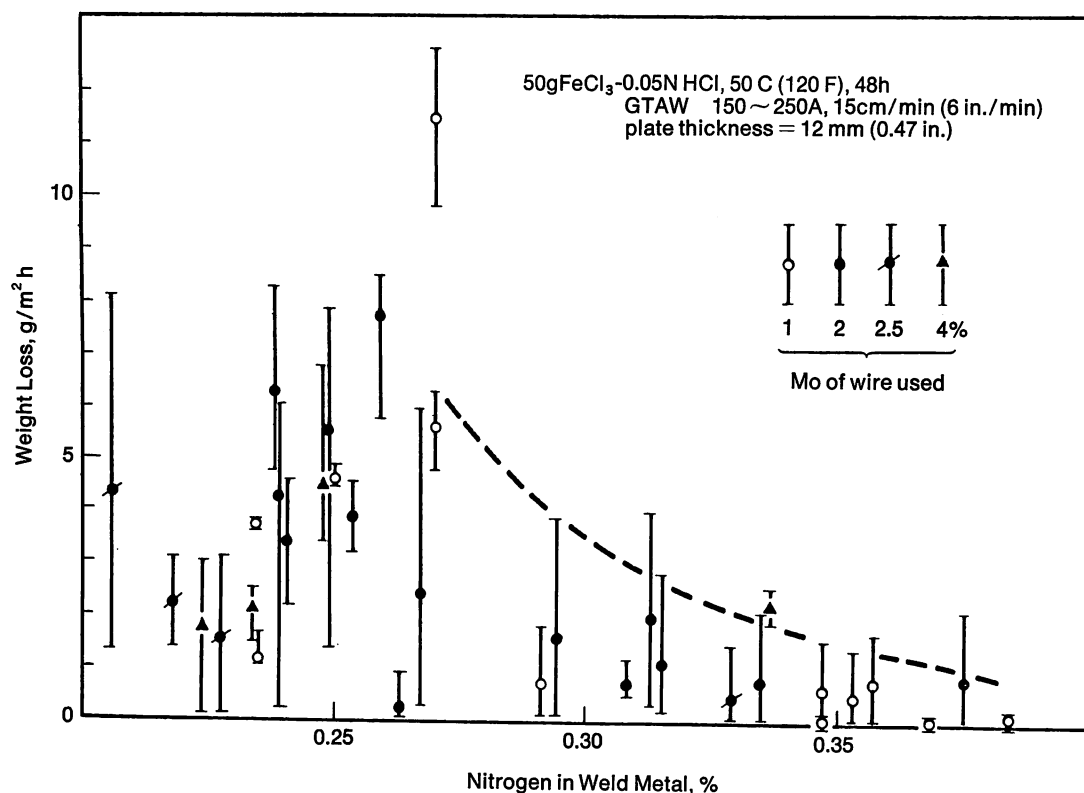
FIGURE 7—*Pitting corrosion of welded joints in high nitrogen austenitic stainless steel (Steel A).*

## Improvement of Hot Workability

High alloy austenitic steel generally has poor hot workability, and cracks are apt to initiate during hot rolling. Steel A is more susceptible to cracking than ordinary alloys because its high nitrogen content causes a higher resistance to deformation.

Additions of elements having strong affinity for oxygen or nitrogen were evaluated, and it was found that the combined addition of aluminum and calcium is effective for the improvement of hot workability without reducing corrosion resistance.

## Characteristics of Steel A

Based on the above research, Steel A was developed and has been produced commercially under the name of YUS170. It has been possible to produce this steel in large 10 ton ingots because of improvements in the steel-making method.

The typical chemical composition of Steel A is shown in Table I.

A comparison of the pitting corrosion resistance of Steel A and other commercial stainless steels is shown in Table II. Steel A has a greatly improved pitting corrosion
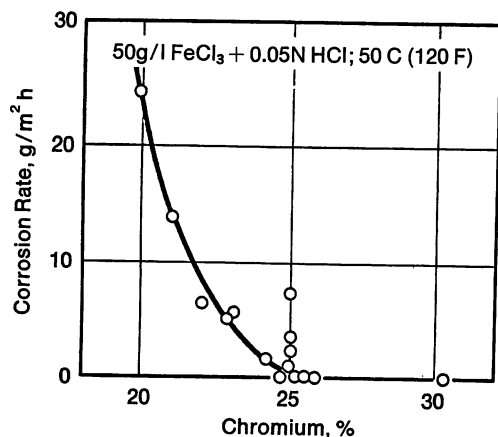


FIGURE 8—*Effect of chromium on pitting corrosion.*

Ni = 5 ～ 18%
N = 0.20 ～ 0.40%
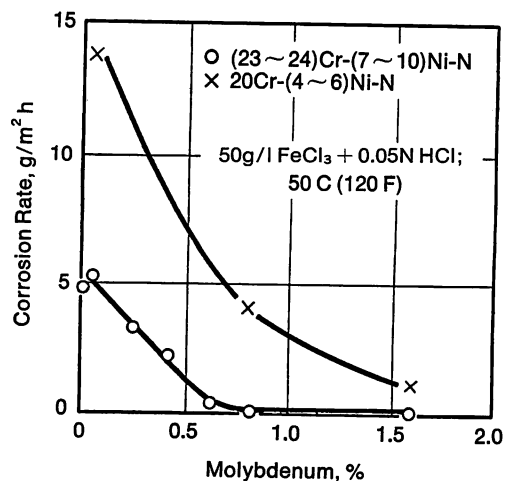


FIGURE 9—*Effect of molybdenum on pitting corrosion.*

**Table I**—Typical Chemical Composition of Steel A

| Element, % | | | | | | |
|---|---|---|---|---|---|---|
| C | Si | Mn | Ni | Cr | Mo | N |
| 0.031 | 0.82 | 1.59 | 13.45 | 24.70 | 0.93 | 0.360 |

**Table II**—Pitting Corrosion Resistance of Typical Austenitic Stainless Steels

| Steel | Corrosion Rate,[a] g/m² h | Pitting Potential,[b] mV vs SCE |
|---|---|---|
| Steel A | 0 ~ 1 | 960 |
| SUS 304 | 16 ~ 18 | 170 |
| SUS 316 | 10 ~ 15 | 440 |
| SUS 310 S | 6.8 | 400 |
| SUS 3291 J₁ | 2 ~ 6 | 640 |

[a] 5 g/l $FeCl_3$ + 0.05N HCl, 50 C (120 F), 48h.
[b] 0.1 mA/cm², 3% NaCl + 5% $H_2SO_4$, 35 C (95 F).
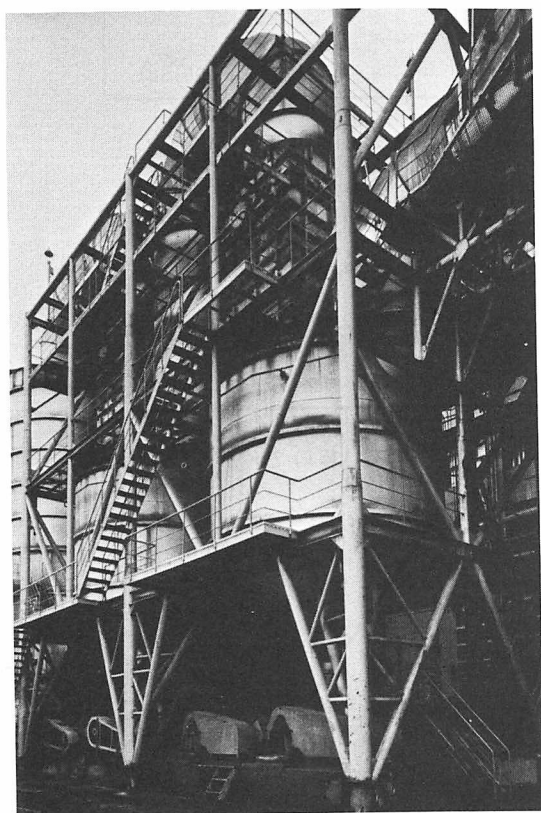


*FIGURE 10—A pollution control and purification apparatus fabricated using Steel A.*

**Table III**—Mechanical Properties of Steel A

| Shape | Proof Stress, MPa (ksi) | Tensile Strength, MPa (ksi) | Total Elongation, % |
|---|---|---|---|
| Plate | 432 (62.7) | 785 (113.9) | 49.7 |
| Sheet | 497 (72.1) | 829 (120.2) | 45.0 |
| Tube | 466 (67.6) | 790 (114.6) | 56.6 |

resistance. Another merit of this steel owing to its Cr and N contents is its resistance to strong acids such as sulfuric and hydrochloric.

The use of Steel A is most appropriate in the environment of pollution control and purification equipment. The environment within this equipment is very corrosive because of the combination of chloride ions concentrated in the water and sulfuric acid formed from $SO_2$ gas. An $SO_3$ scrubber fabricated from this steel is shown in Figure 10.

Typical mechanical properties of Steel A are shown in Table III. Its proof stress is about two times as high as that of common austenitic stainless steel, and the tensile strength is 1.5 times as large. Total elongation is nearly 50%, which is a little low for a stainless steel but still higher than that of commercial steels. The characteristics of the welds will be reviewed below with those of Steel B.

## Development of Crevice Corrosion Resistant Steel B

### Resistance to Crevice Corrosion

As described above, Steel A has superior pitting corrosion resistance, but it is not sufficiently immune to crevice corrosion.

Research with the elements that might improve crevice corrosion resistance showed molybdenum and copper were the most effective. The crevice corrosion potentials for these elements in 5% NaCl at 60 C (140 F) are shown in Figure 11. Crevice corrosion resistance increases markedly with the addition of 3% Mo and 1-2% Cu. Chromium is effective for the retardation of crevice corrosion initiation but, unfortunately, it increases the corrosion rate once the pit has formed.

The effect of nitrogen was evaluated by immersing specimens of Cu- and Mo-modified high Cr steel in $FeCl_3$-0.05N HCl solution. The test was performed at 45 C (115 F) using two 30 by 30 by 4 mm (1.2 by 1.2 x 0.16 in.) test pieces placed face to face to form the crevice. Surfaces not in contact were coated to prevent corrosion.

The results of this test are shown in Figure 12. Nitrogen was found useful also for this purpose, but its effect did not change with an addition beyond 0.3%.

The chemical composition of crevice corrosion resistant Steel B was determined to be 25Cr-16Ni-3Mo-2Cu-0.3N after studying the above research data. To compensate for the molybdenum addition, nickel was increased to 16%.

### Hot Workability and Ductility of the Welds

As Steel B has higher alloy content than Steel A, careful investigation is necessary concerning its hot workability. As in Steel A, calcium and aluminum are effective in increasing hot workability, but more careful
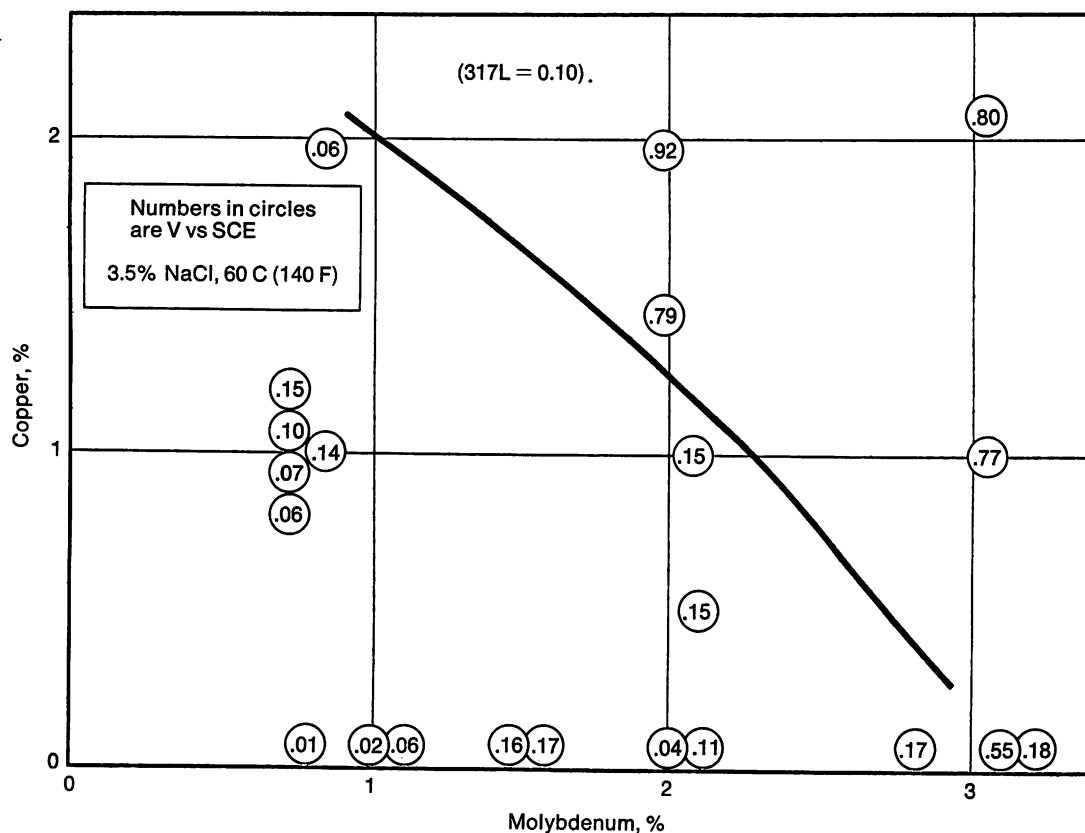
FIGURE 11—*Effects of Mo and Cu on crevice corrosion potential (sweep speed-17mV/mm).*

quantity control is needed.

The result of a hot workability evaluation as a function of S, Ca and Al contents is shown in Figure 13. This was evaluated by heating the specimen to 1270 C (2320 F) followed by rapid cooling to 1100 C (2010 F) at which temperature the Gleeble test measuring the reduction of area was performed. The good deformability region where reduction of area exceeds 60% is essentially independent of test temperature.

The most harmful element from the standpoint of hot workability is sulfur, but considerable improvement can be obtained by an appropriate addition of calcium (atomic weight ratio Ca/S = 1.25). The aluminum content must be carefully controlled. Good deformability is obtained between 0.10% and 0.02% Al. When the aluminum content is too low, the oxygen content increases, and the metal becomes brittle; when aluminum exceeds 0.10%, brittleness again occurs as a result of AlN formation. After considering the above, good hot workability was obtained in Steel B when S < 0.005%, Ca > 1.25 × S, and Al = 0.02 ~ 0.10%.

Our research showed that phosphorus in the range of 0.007 to 0.037% did not affect the hot workability.

As weld ductility has a tendency to deteriorate in a high alloy steel, the effect of molybdenum was evaluated by measuring the reduction in area after tensile testing. The ductility of welds decreased rapidly with the addition of 3.5% Mo or more, as shown in Figure 14.
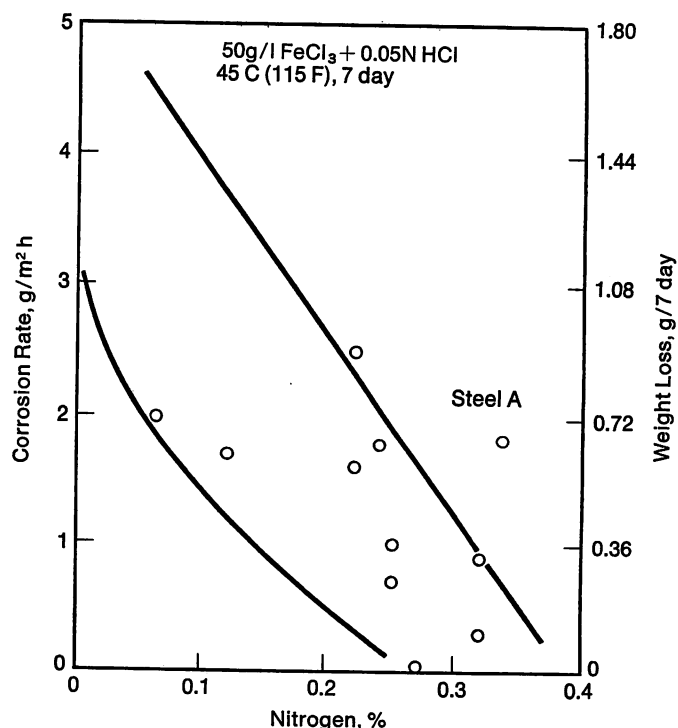


FIGURE 12—*Effect of nitrogen on crevice corrosion (25Cr-16Ni-3Mo-2Cu).*
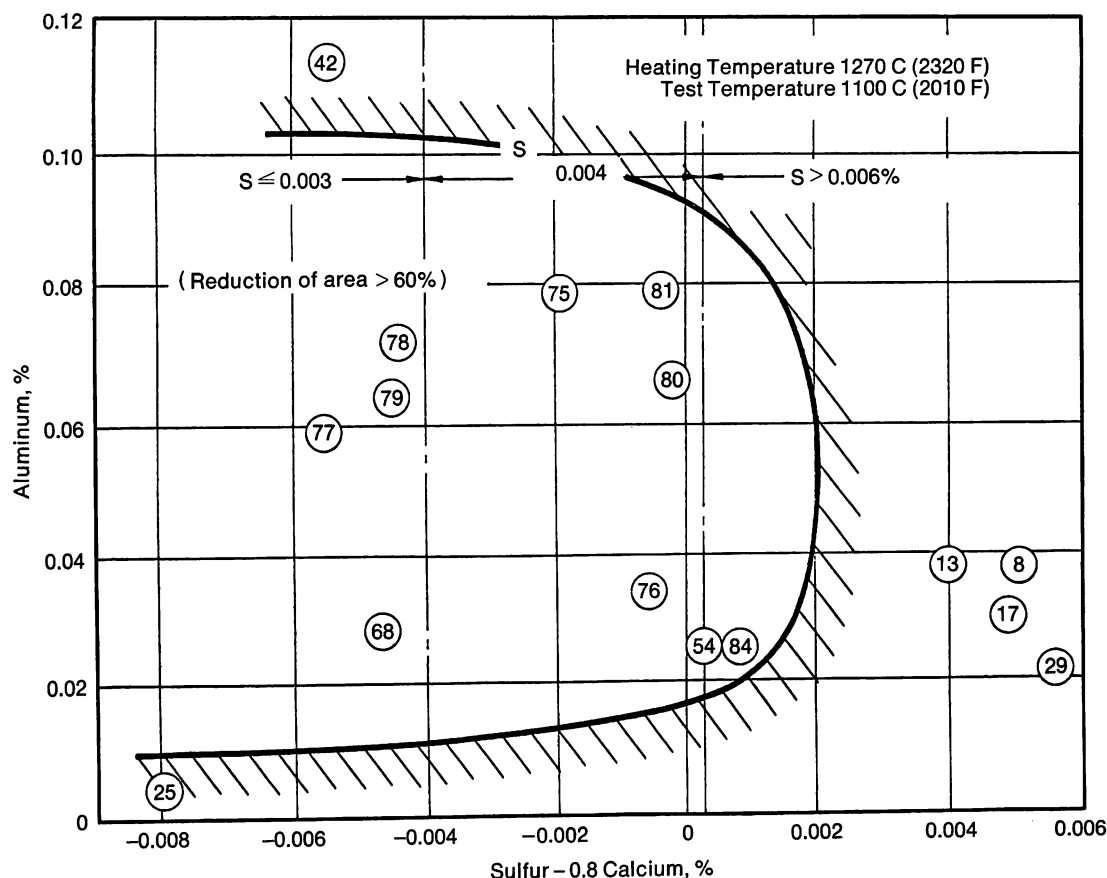
*FIGURE 13—Effects of S, Al and Ca on hot workability (numbers in circles indicate reduction in area from Gleeble test).*
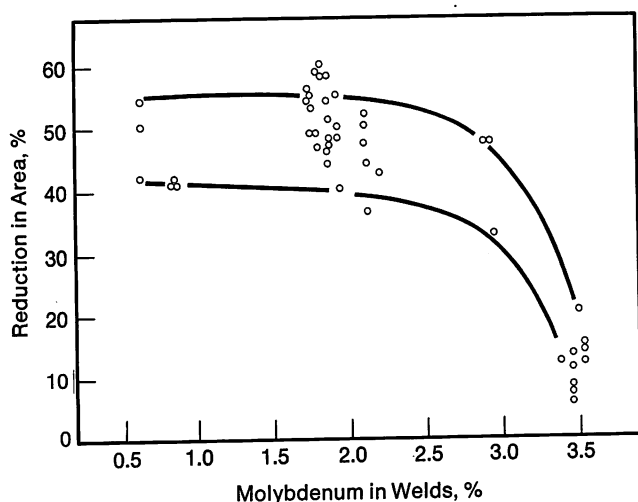


*FIGURE 14—Relationship between Mo content of welds and reduction in area in tensile tests.*

**Table IV**—Typical Chemical Composition of Steel B

| | Element, % | | | | |
|---|---|---|---|---|---|
| C | Ni | Cr | Cu | Mo | N |
| 0.02 | 16.0 | 25.0 | 2.0 | 3.0 | 0.34 |

## Characteristics of Steel B

The final chemical composition of Steel B is shown in Table IV. Passivation current, an important factor in determining the initiation period of crevice corrosion, is shown in Figure 15 for Steels A and B and for Type 304. The retardation of crevice corrosion initiation is apparent in Steel B. Resistance to intergranular corrosion in Steel B was a concern since it contains high nitrogen and more nickel than Steel A. Fortunately, the results of both the copper sulfate-sulfuric acid test and the 65% nitric acid test showed Steel B and Steel A to have about equal resistance.

It was confirmed that resistance to stress corrosion cracking in Steel B is superior to SUS 304 and SUS 316 in boiling 42% $MgCl_2$.

Mechanical properties of Steel B are listed in Table V. It has a fairly high proof stress and tensile strength and, as in Steel A, the drop in elongation is small.

To determine the characteristics of the welds, Steel B was welded by GTAW in a V-groove with WEL-50M (25Cr-50Ni-6Mo) as the filler. No problem was found concerning the toughness of the welds since the Charpy V-notch test showed an absorbing energy value at −20 C (−4 F) as high as 98 J (72 ft-lb).

Resistance of the welds to pitting corrosion was compared with that of the base metal by testing in a 50g/l
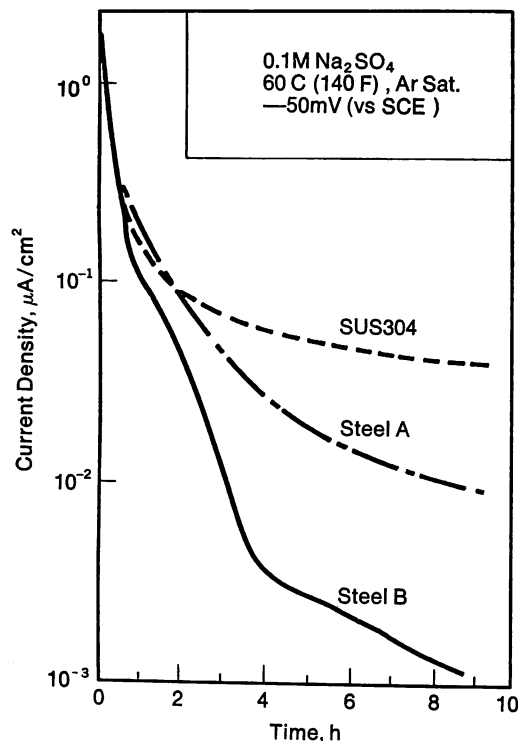
FIGURE 15—Anodic current density in passive state.

**Table V**—Mechanical Properties of Steel B

| Proof Stress, MPa (ksi) | Tensile Strength, MPa (ksi) | Elongation, % | Hardness, HV |
|---|---|---|---|
| 374 (54.2) | 755 (109.5) | 46.2 | 200–215 |
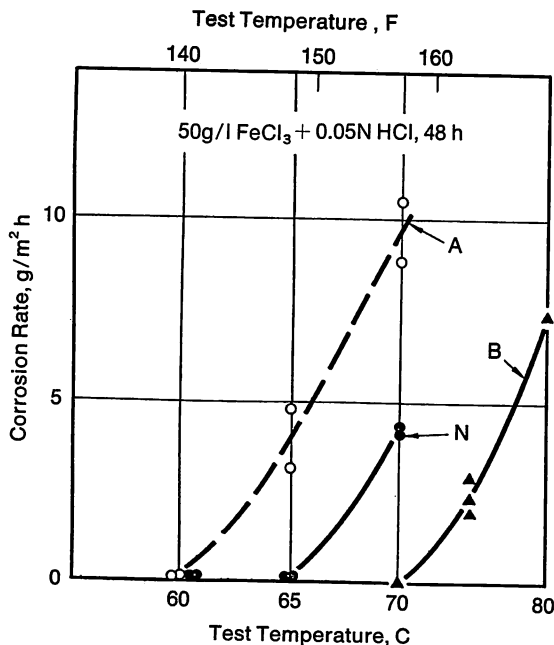


FIGURE 16—Pitting corrosion rate of Steel B.

A = Welds, TGAW autogenous (100%Ar)
N = Welds, TGAW autogenous (5%$N_2$ + 95%Ar)
B = Base metal

$FeCl_3$+0.05N HCl solution for 48 hours. Pits were formed exclusively at the bond. In the base metal, pit formation did not occur even at 70 C (160 F). The same test was performed with GTAW without a filler. The results are shown in Figure 16. The temperature of pitting initiation was 60 C (140 F). By changing the shielding gas from pure argon to 95%A-5%$N_2$, this temperature increased and became close to that of the base metal. The drop in resistance to pitting corrosion in the welds is considered the result of the loss of nitrogen during welding, and some modification of the filler metal is needed to make it similar in characteristics to the base metal.

## Remaining Research Problems

Research and development on high nitrogen austenitic stainless steels to be used in corrosive environments has been reviewed in the previous sections. However, two problems remain for which further research is needed.

The first is that pitting corrosion resistance of the welds is inferior to that of the base metal where the matching metal is used.

Since it is believed that some nitrogen is lost during welding, nitrogen has been added to the shield gas, and some recovery was achieved as described in Figure 16. Nitrogen addition to the shield gas is actually impracticable as it lowers working efficiency significantly. An alternative of using a filler metal higher in nitrogen or with more resistance to pitting corrosion is anticipated. Changing the chemical composition seems necessary to obtain a filler with higher nitrogen content than the base metals since Steels A and B are nearly saturated with nitrogen.

Although the solubility of nitrogen increases with the addition of chromium and manganese, careful consideration of the resulting structure and lowering of corrosion resistance is needed. If an increase in manganese is used, welds with a stable austenitic structure are formed, and a marked tendency for hot cracking is seen. Chromium additions favor ferrite formation and result in a loss of toughness.

To obtain a more corrosion resistant filler, molybdenum might be an effective addition to Steel A, but it is not suitable for Steel B since the base metal already contains 3% Mo. Moreover, the addition of more than 2% Mo to the filler is not effective in pitting corrosion resistance of welds tested in $FeCl_3$ (Figure 17). Garner[8] obtained similar results by measuring the pitting potential of the welds. Microsegregation of molybdenum in the dendritic structure seems to decrease its effectiveness; merely increasing molybdenum is not the solution. A remedy for this problem has not yet been obtained, but we are working toward it.
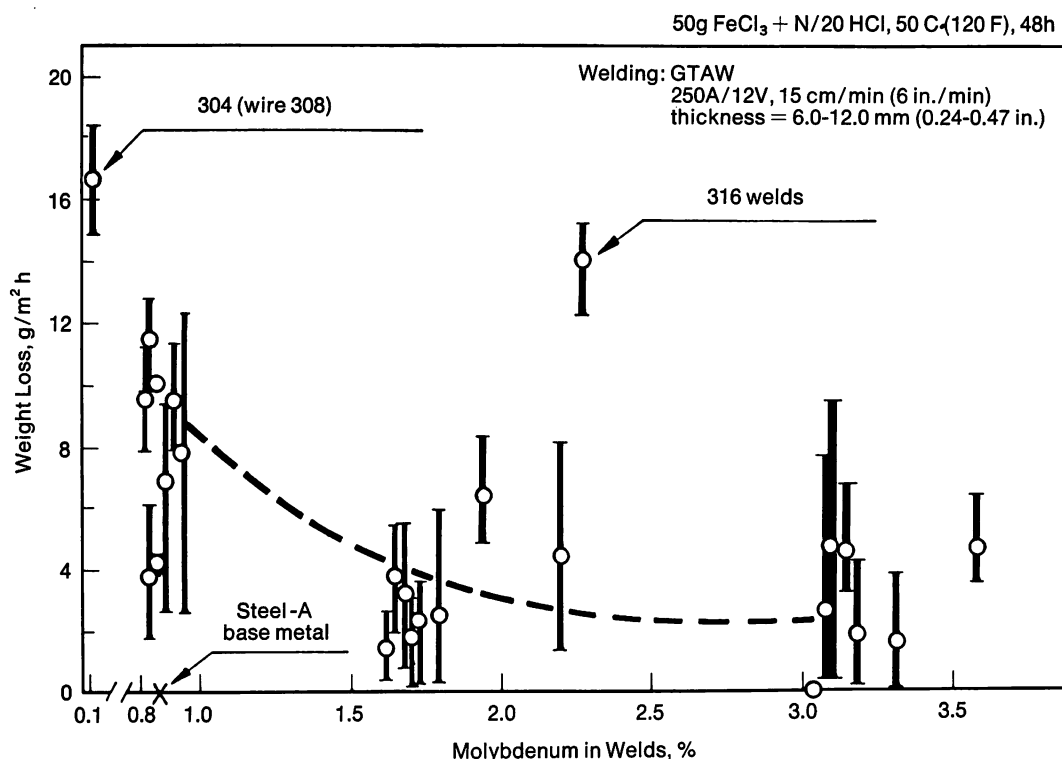
50g FeCl₃ + N/20 HCl, 50 C-(120 F), 48h



FIGURE 17—*Effect of molybdenum on pitting corrosion in Steel A welds.*
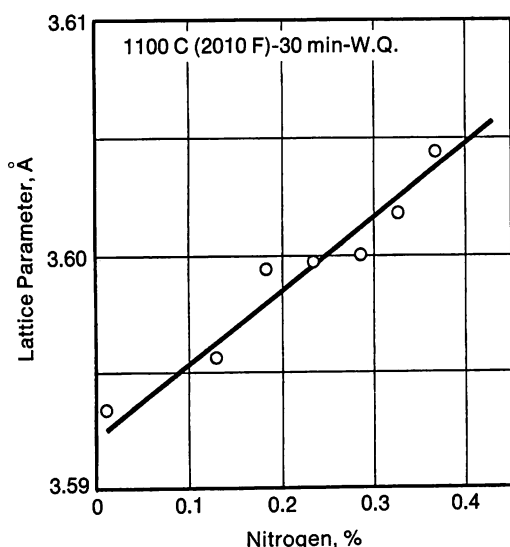


FIGURE 18—*Effect of N on lattice parameter of 25Cr-Ni austenitic steel.*

The second problem is the metallurgical state of nitrogen in the steel after various heat treatments.

Improvement in pitting corrosion resistance by adding nitrogen has been studied by Osozawa, et al.[9] who concluded that nitrogen consumes protons when it dissolves in the pitting solution, thus preventing the lowering of pH in the early stage of pit formation and helping passivate the pit before it becomes larger. This explanation is based on the assumption that nitrogen always exists in solid solution. In reality, nitrogen exists as a solid solution in Steel A after quenching from 1100 C

(2010 F) (30 min). This was verified by the measurement of lattice parameters which varied linearly with nitrogen content as shown in Figure 18.

However, nitrogen easily combines with elements such as Cr, Mo and Mn to form nitrides. In addition, the complex nitride named Z phase is known to exist and is believed to have the composition of $(Fe, Mn, Cr)_4$ $(Nb, Mo)_3N_3$. Hughes[10] has observed its precipitation in the matrix of an 18Cr-12Ni-1Nb-3Mo-0.2N steel heated at 1050 C (1920 F) for 1 hour.

This precipitation of nitrides causes a loss of nitrogen in solid solution and consequently influences metal characteristics including corrosion resistance, mechanical properties and austenitic structure formation.

In Steel B, the deterioration of corrosion resistance has been observed after a sensitizing heat treatment. The precipitation behavior of nitrogen, common to all nitrogen-containing austenitic stainless steels, should be studied further. Particular care is necessary when using nitrogen in stabilized steels containing titanium, niobium or zirconium since their strong affinity for nitrogen makes a solid solution difficult to maintain.

High nitrogen austenitic steel shows a prominent high temperature strength and can be used as a heat resistant material too. Again the state of nitrogen is a matter of concern because the precipitates after long exposure at high temperature might cause brittleness and might reduce corrosion resistance.

## Summary

In trying to develop an economical corrosion resistant austenitic steel, the effects of nitrogen as a substitute for nickel were investigated, with the following conclusions:

As much as 0.35% nitrogen is soluble in 25%Cr steel and works as an austenitic structure former about 30 times as strong as nickel.

Nitrogen in austenitic stainless steel improves the resistance to pitting corrosion as well as to strong acids.

Nitrogen is also effective in strengthening the material even at high temperature without significant reduction in ductility.

A pitting corrosion resistant austenitic steel (Steel A, 25Cr-13Ni-0.8Mo-0.3N) fully utilizing the merits of nitrogen has been developed and is being produced commercially.

A new type of steel more resistant to crevice corrosion (Steel B, 25Cr-16Ni-2Cu-3Mo-0.3N) is under development, and the problems related to corrosion resistance and hot workability have essentially been solved.

Improvement in corrosion resistance of the welds and metallurgical research concerning the behavior of nitrogen in metals are the two most important problems left for high nitrogen austenitic stainless steels.

## References

1. R. Franks, W. O. Binder and J. Thompson, *Trans. ASM, 47*, 1955, 231.
2. H. Abo, S. Noguchi, N. Hayashi and M. Ueda, *Bôshoku Gijutsu, 23*, 1974, 303.
3. H. Abo, et al., *Seitetsu-kenkyu, 292*, 1977, 38.
4. R. F. Steigerwald, *Corrosion, 22* (4), 1966, 107.
5. J. C. Humbert and J. F. Eliott, *Trans. AIME, 218*, 1960, 1076.
6. W. T. DeLong, *Met. Prog., 77* (2), 1960, 98.
7. T. Ogawa, K. Murata, S. Aoki and E. Tsunetomi, to be published in J. Japan Welding Society.
8. A. Garner, *Corrosion, 35* (3), 1979, 108.
9. K. Osozawa and N. Okamoto, *Passivity and its Breakdown on Iron and Iron Base Alloys*, U.S.A.-JAPAN seminar, 1976, 135.
10. H. Hughes, *J. I. S. I. 205*, 1967, 775.

## Discussion

H. KOHL, *Vereinigte Edelstahlwerke AG.* VEW has produced high nitrogen austenitic stainless steels since about 1965.[1-3] Table I shows chemical compositions and 0.2% proof stresses for some of these steels that were developed for special applications.[3] From steel AM53 (now P505), more than 2,000 tons were delivered.

Concerning the solubility of N in Cr-Ni austenitic stainless steels, we obtained the results shown in Figure 1.[2,3] Solubility means no formation of blowholes during solidification and no shrinkage. In Figure 1 herewith, the borderline from your Figure 1 and the area for steel AM53 are also plotted. The location of the area for AM53 confirms the applicability of high N-contents in large-scale production.

H. DIEKMANN, *Bayer AG.* Do the austenitic stainless steels with lower nickel content and high nitrogen have the same resistance to stress corrosion cracking as a steel with a nickel content of 22-25%?

T. SAKAMOTO. The nitrogen-containing steel is about equal or somewhat better in resistance to stress corrosion cracking than higher nickel steels.

M. WEISZ, *Centre d'Etudes Nucleaires.* You mentioned the possibility of using high nitrogen austenitic steels in high temperature applications. Do you have any creep rupture or low cycle fatigue data for these steels?

T. SAKAMOTO. I mentioned high temperature applications as a possible future development. We have not done any testing as yet.

D. L. SPONSELLER, *Climax Molybdenum Company.* Work done here at the University of Michigan by J. W. Free-

---

1. H. Kohl and H. Souresny, *Berg- u. Hüttenm. Mh. 111*, 1966, 501.
2. H. Kohl, *Berg- u. Hüttenm. Mh. 113*, 1968, 377.
3. H. Kohl, Proceedings *Molybdenum 1973*, Noranda, 43.

**Table I**—Chemical Analyses and Yield Strengths of Cr-Ni-Mo-N Grades

| Steel Type | Element, % | | | | | | | Minimum 0.2% Yield Strength, MPa (ksi) |
|---|---|---|---|---|---|---|---|---|
| | C (max.) | Si | Mn | Cr | Ni | Mo | N | |
| X5 CrNiMo 18 12 (MASOY) | 0.05 | 0.4 | 1 | 18 | 12 | 2.6 | — | 205 (29.7) |
| X4 CrNiMoN 22 12 (MASON 2) | 0.04 | 0.5 | 1 | 22.5 | 12.5 | 2.7 | 0.30 | 390 (56.6) |
| X4 CrNiMo 22 15 (AM53) | 0.03 | 1.5 | 1 | 23 | 15 | 1.5 | 0.35 | 400 (58.0) |
| X2 CrNiMnMoN 22 14 (AM55) | 0.03 | 1.5 | 7 | 23 | 13.5 | 1.5 | 0.47 | 440 (63.8) |
| X2 CrNiMnMoN 24 15 (AM57) | 0.03 | 0.5 | 4 | 24 | 15 | 2.2 | 0.45 + Nb | 540 (78.3) |
| X2 CrNiMoN 24 15 3 (AMO3) | 0.03 | 0.5 | 1 | 24.5 | 15.5 | 3.0 | 0.42 | 450 (65.3) |

man and coworkers showed a strong beneficial effect of nitrogen on creep strength and a very good interaction between nitrogen and molybdenum as well.

E. J. Dulis, *Crucible Inc.* What are the microstructural changes that occur when the high nitrogen steels are exposed

for long times at elevated temperatures? Does the nitrogen come out as a precipitate?

T. Sakamoto. We have not yet observed a precipitate. We are still working in this area, and the possibility of embrittlement from precipitation has not been resolved.
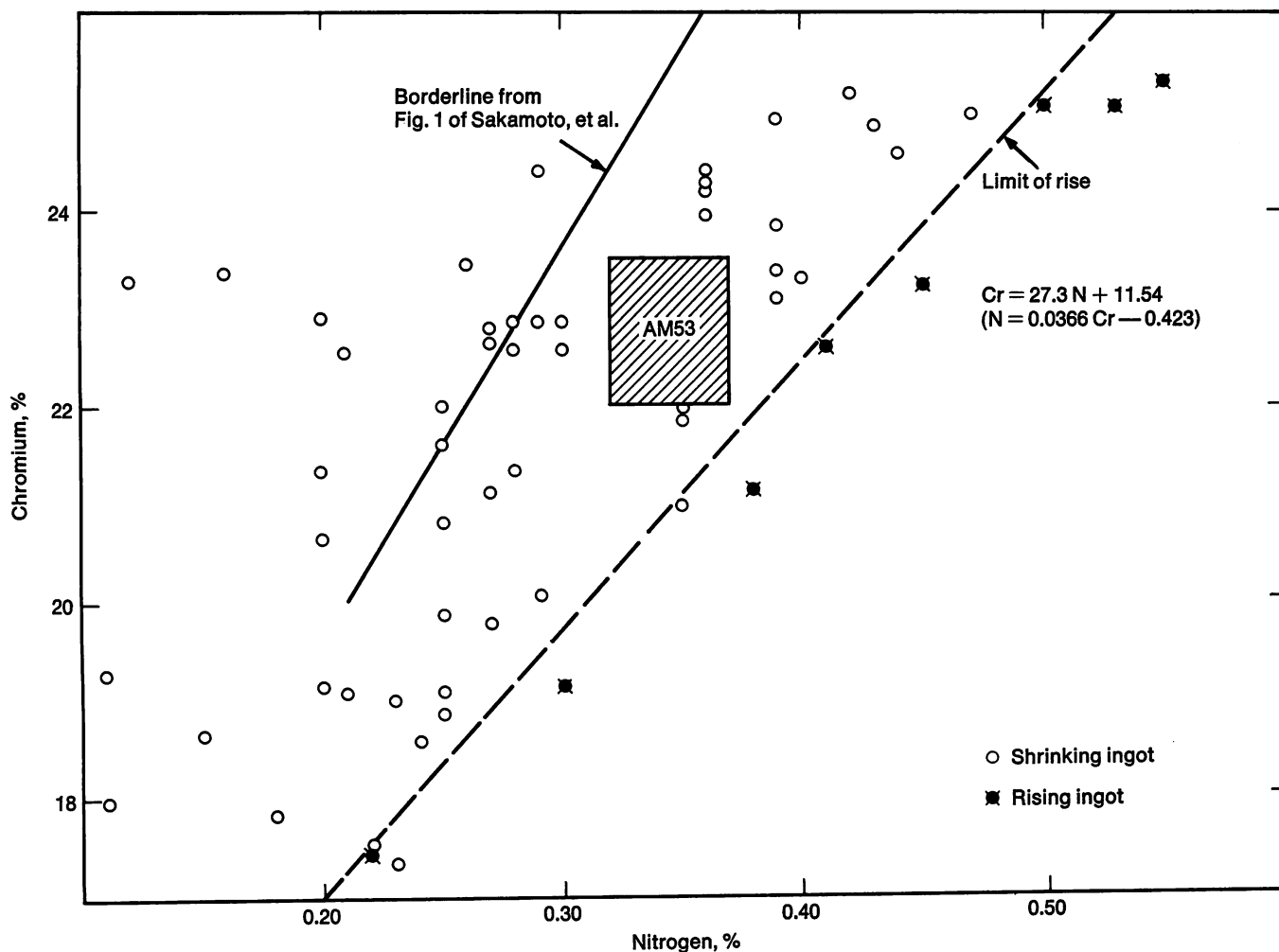


FIGURE 1—*Variation of Solubility of N with Cr Content (Cr-Ni Steel with 11% Ni).*

# On the Corrosion Behavior of a Ferritic 18 Cr-2 Mo Steel

by K. Fässler and H. Spähn
BASF Aktiengesellschaft

Some interesting new developments have taken place in recent years in the field of ferritic stainless steels.[1-16] As a material for chemical apparatus, the common highly alloyed chromium steels as listed in national standards (e.g. in the German Standard DIN 17 440) have found only limited applications. The reasons are sensitivity of several of these chromium alloyed stainless steels to intergranular corrosion (especially after welding), lower corrosion resistance compared to austenitic stainless steels, and difficulties in fabrication (especially welding). It has been shown[1-16] that the intrinsic drawbacks of customary ferritics can be overcome by metallurgical measures, primarily keeping the amount of carbon and nitrogen extremely low. The solubility in the ferrite of these two elements is rather low, both occupying interstitial sites. Stainless steels of the type dealt with in this paper are therefore sometimes termed "extra low interstitial" (ELI) ferritic stainless steels. At sufficiently low concentrations of carbon and nitrogen (and some other elements), the sensitivity of ferritic stainless steels to intergranular corrosion is definitely lowered, and their ductility at ambient temperature is increased, i.e. the transition temperature is lowered. An advantage of these steels is their resistance to stress corrosion cracking. They have, so far, shown no sensitivity to chloride stress corrosion cracking under realistic operating conditions. For this reason, cooling water systems using river water with a high chloride content represent a suitable field of application for these steels. They can be welded up to a wall thickness of 3 mm (0.12 in.) without sensitization and undue loss of impact strength so that tubes for heat exchangers can be made of these steels. Their development has lead to alloys ranging from 18 Cr-2 Mo-0 Ni to about 28 Cr-2 Mo-4 Ni. The present paper will only deal with the 18 Cr-2 Mo steel because this material can be compared in price and properties with the standard 18 Cr-9 Ni austenitic steels. In addition, the material in question has now become available in the form of pipe and sheet.

The investigations carried out with 18 Cr-2 Mo steel were aimed at its behavior under pitting corrosion, crevice corrosion and stress corrosion cracking conditions. This was done in autoclave laboratory experiments and under experimental heat exchanger conditions. To this end, model heat exchangers were fabricated and operated to investigate the influence of filler materials and weld joints between 18 Cr-2 Mo and a standard austenitic steel. The possibility of fabricating tube sheets by applying a weld overlay using explosive bonding was explored.

## Chemical Composition, Mechanical Properties and Microstructure of Welded Specimens

### Chemical Composition

The 18 Cr-2 Mo steel, furnished by Gränges Nyby AB and used for subsequent investigations, had the composition indicated in Table I.

### Welding Combinations

The following two combinations were fabricated from 2 mm (0.08 in.) thick plates:

1. 18 Cr-2 Mo steel/weld seam/18 Cr-2 Mo steel.

2. 18 Cr-2 Mo steel/weld seam/austenitic stainless steel Type 321 (steel X 10 CrNiTi 18 9, DIN 17 440).

Welding was carried out as follows:

1. Using welding rods according to Table I (i.e., 18 Cr-2 Mo base material type).

2. Using an austenitic-ferritic welding rod with

**Table I**—Chemical Composition

| | Element, % | | | | | | | | | | |
|---|---|---|---|---|---|---|---|---|---|---|---|
| | C | N | Si | Mn | P | S | Cr | Ni | Mo | Ti | Cu |
| Base Steel | 0.029 | 0.0041 | 0.38 | 0.55 | 0.014 | 0.006 | 17.0 | 0.31 | 2.3 | 0.66 | 0.17 |
| Welding Rods | 0.028 | 0.0037 | 0.51 | 0.28 | 0.015 | 0.011 | 18.7 | 0.24 | 2.4 | 0.18 | 0.17 |

**Table II**—Mechanical Characteristics

| Specimen Desig- nation | Specimen Type | Yield Strength, MPa (ksi) | | Ultimate Tensile Strength, MPa (ksi) | | Elon- gation, % | Reduction of Area, % | Micro- structure, Figure |
|---|---|---|---|---|---|---|---|---|
| OL | Base material Parallel | 359.5 | (52.1) | 528 | (76.6) | 40.0 | 70.8 | 1 and 2 |
| OQ | Transverse | 399.5 | (57.9) | 552 | (80.0) | 41.3 | 71.6 | — |
| A | 18 Cr-2 Mo/18 Cr-2 Mo welded without filler metal | 333 | (48.3) | 546.5 | (79.3) | 12.2 | 46.9 | 3a |
| B | 18 Cr-2 Mo/18 Cr-2 Mo welded with base material rod | 303 | (43.9) | 520 | (75.4) | 32.5 | 63.5 | 3b |
| C | 18 Cr-2 Mo/18 Cr-2 Mo welded with 29-9 rod (Oerlikon®) | 303 | (43.9) | 520 | (75.4) | 34.5 | 74.0 | 4a |
| D | 18 Cr-2 Mo/18 Cr-2 Mo welded with Thermanit® LMS rod | 303 | (43.9) | 520 | (75.4) | 34.0 | 74.0 | 4b |
| E | 18 Cr-2 Mo/AISI 321 welded without filler metal | 263 | (38.1) | 522 | (75.7) | 34.6 | 74.8 | 5a |
| F | 18 Cr-2 Mo/AISI 321 welded with 29-9 rod (Oerlikon®) | 263 | (38.1) | 524 | (76.0) | 34.8 | 74.1 | 5b |
| G | 18 Cr-2 Mo/AISI 321 welded with Thermanit® LMS rod | 263 | (38.1) | 524 | (76.0) | 32.9 | 67.1 | 5c |

**Table III**—Results of 180° Bend Tests

| Desig- nation of Specimen | Specimen Type | Bending Perpendicular to Weld Seam* | Bending Parallel to Weld Seam* |
|---|---|---|---|
| A | 18 Cr-2 Mo/18 Cr-2 Mo welded without filler metal | not cracked | not cracked |
| B | 18 Cr-2 Mo/18 Cr-2 Mo welded with base material rod | not cracked | not cracked |
| C | 18 Cr-2 Mo/18 Cr-2 Mo welded with 29-9 rod (Oerlikon®) | not cracked | fissure after bending 90°. Fine fissure found on 2nd specimen |
| D | 18 Cr-2 Mo/18 Cr-2 Mo welded with Thermanit® LMS rod | not cracked | not cracked |
| E | 18 Cr-2 Mo/AISI 321 without filler metal | not cracked | Fine cracks (< 1 mm, 0.04 in.) on the 18 Cr-2 Mo side |
| F | 18 Cr-2 Mo/AISI 321 welded with 29-9 rod | not cracked | not cracked |
| G | 18 Cr-2 Mo/AISI 321 welded with Thermanit® LMS rod | not cracked | Fine incipient crack, 2 mm (0.08 in.) long, at the 18 Cr-2 Mo side |

\* Duplicate tests.

0.10% C, 30% Cr and 9% Ni (Oerlikon® 29-9).

3. Austenitic-ferritic welding rod with 0.07% C, 25% Cr, 8% Ni, 1.5% Mo with an addition of Nb for stabilization (Thermanit® LMS).

The TIG welding process was employed throughout using argon as the inert gas (8 l/min), a current of 70 A and a velocity of 9-10 cm/min (3.5-4 in./min).

**Mechancial Properties**

The mechanical characteristics determined using the flat tensile specimens specified in DIN 50 140 are compiled in Table II.

The figures given in Table II are mean values for two specimens. The direction of texture and the direction of applied force were parallel for all welded specimens.
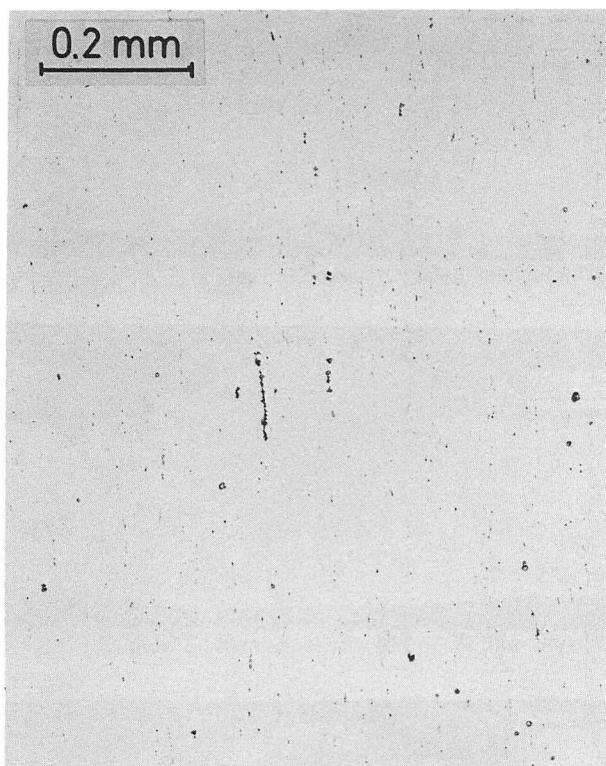
FIGURE 1—Microstructure of 18 Cr-2 Mo (furnished in 1974). Longitudinal section showing numerous slag inclusions and carbides parallel to rolling direction. Polished, unetched.



a. ASTM grain size 6-7.                    (100 X)



b.                    (500 X)

FIGURE 2—Etched micrographs of 18 Cr-2 Mo.
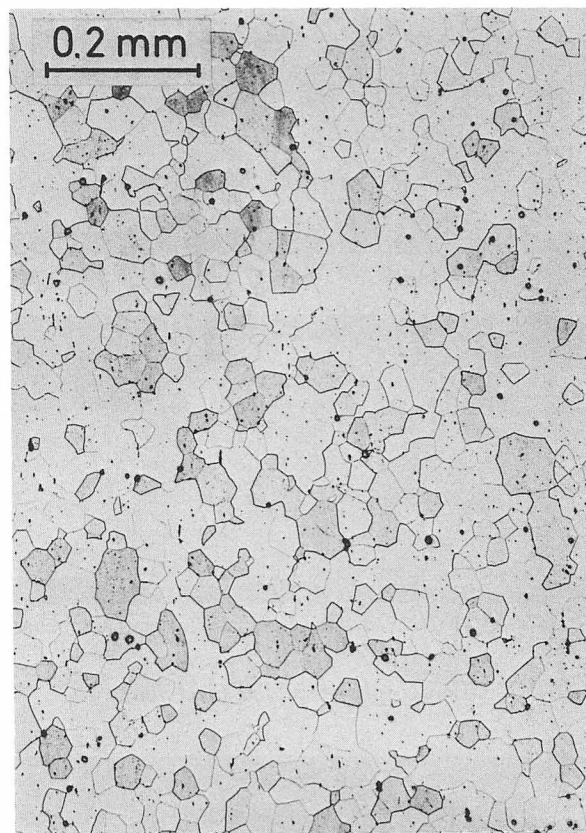
Fracture occurred within the weld seam for specimens A and B. With specimens C and D, fracturing was about 20 mm (0.8 in.) from the weld seam as it was for specimens E, F and G (always in the 18 Cr-2 Mo base material).

### Bending Tests

Specimens 70 by 70 by 2 mm (2.8 by 2.8 by 0.08 in.) containing a weld seam were bend tested parallel and normal to the weld seam. In the first instance, the bend angle was set to 90°, then the specimens were examined, and bending was continued to 180°. There was only one specimen which showed a crack immediately adjacent to the weld seam at a bend angle of 90° (bending parallel to the weld seam). This was a type C specimen (18 Cr-2 Mo/29-9 CrNi welding rod/18 Cr-2 Mo). Table III shows the results for a bend angle of 180°.

It is very probable that the fissure observed on one specimen of type C was caused by a penetration notch due to undercutting. In the heat affected zone of the 18 Cr-2 Mo steel, an orange peel structure was observed on the surface after bending due to grain coarsening.

### Microstructure

Figures 1 and 2 show the microstructure of the plate material as delivered. Numerous slag inclusions and carbides, longitudinally orientated, are present. The ASTM grain size is between 6 and 7.

a. 18 Cr-2 Mo/18 Cr-2 Mo without filler metal (specimen A, Table 2).
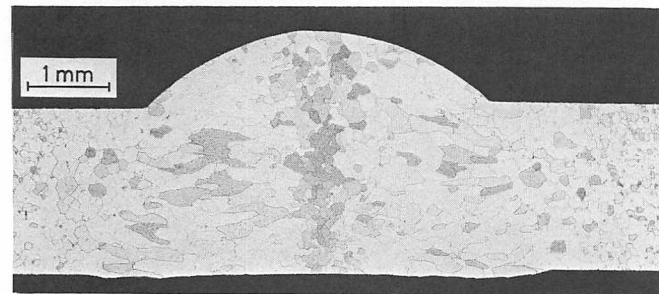


b. 18 Cr-2 Mo/18 Cr-2 Mo with identical filler metal (specimen B, Table 2).

FIGURE 3—*Micrographs of welded specimens.*
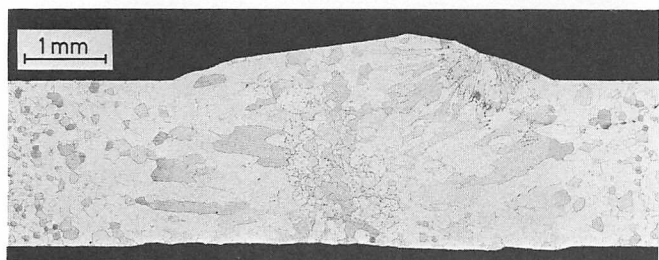


a. 18 Cr-2 Mo/18 Cr-2 Mo with 29 Cr-9 Ni filler metal (specimen C, Table 2).
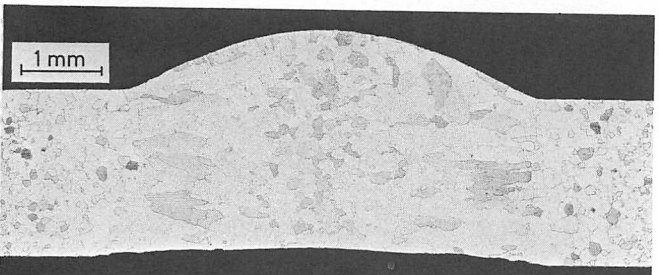


b. 18 Cr-2 Mo/18 Cr-2 Mo with Thermanit® LMS (specimen D, Table 2).

FIGURE 4—*Micrographs of welded specimens.*



a. Without filler metal (specimen E, Table 2).
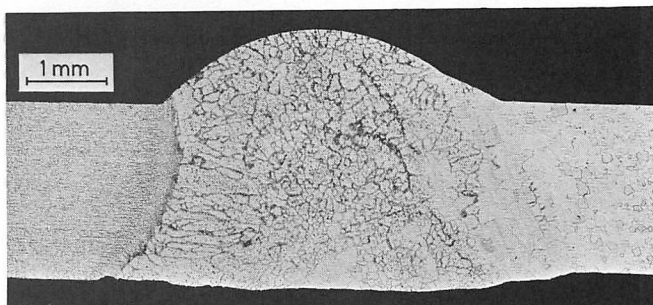


b. Welded with 29 Cr-9 Ni wire (specimen F, Table 2).
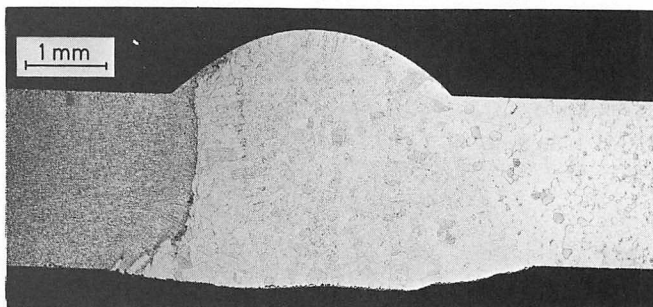


c. Welded with Thermanit® LMS (specimen G, Table 2).

FIGURE 5—*Ferritic steel 18 Cr-2 Mo welded to stainless steel AISI Type 321.*

The results of a metallographic examination transverse to the weld seam are shown in Figures 3 to 5.

Figures 6 to 8 show the results of a metallographic investigation of cross seam welds (see Figure 9 for position of specimens). Grain coarsening in the weld seams and heat affected zones of the 18 Cr-2 Mo steel can be clearly recognized in Figures 6 to 8.

All welded specimens showed lower strength and ductility than the base material. This effect is the result of grain coarsening during welding. Nevertheless, the specimens could be easily bent to an angle of 90° and, with one exception, to 180°. Despite the loss of ductility induced by welding, there is sufficient toughness both in the weld metal and the heat affected zone.

## Corrosion Behavior

### Intergranular Corrosion Testing

Welded specimens 70 by 70 mm (2.8 by 2.8 in.) were tested according to DIN 50 914 (Euro-Norm 144-72) in the sulfuric acid/copper sulfate solution (Monypenny-Strauss). After the test, the specimens were bent 90° longitudinal and perpendicular to the weld seam.

No specimens (A to G, Tables II and III) showed intergranular attack in the heat affected zones of the welds. Also all cross seam welds made of 4 plates and welded according to A to G of Table II showed no intergranular attack after test.
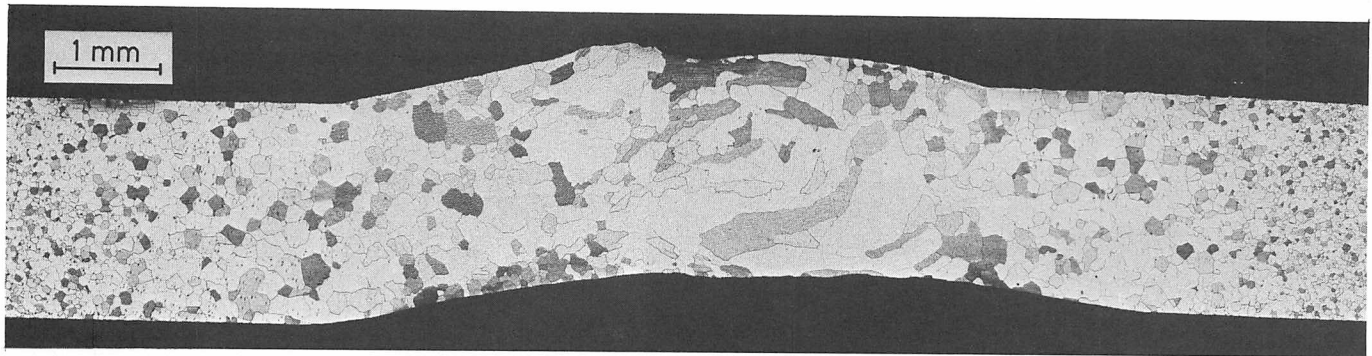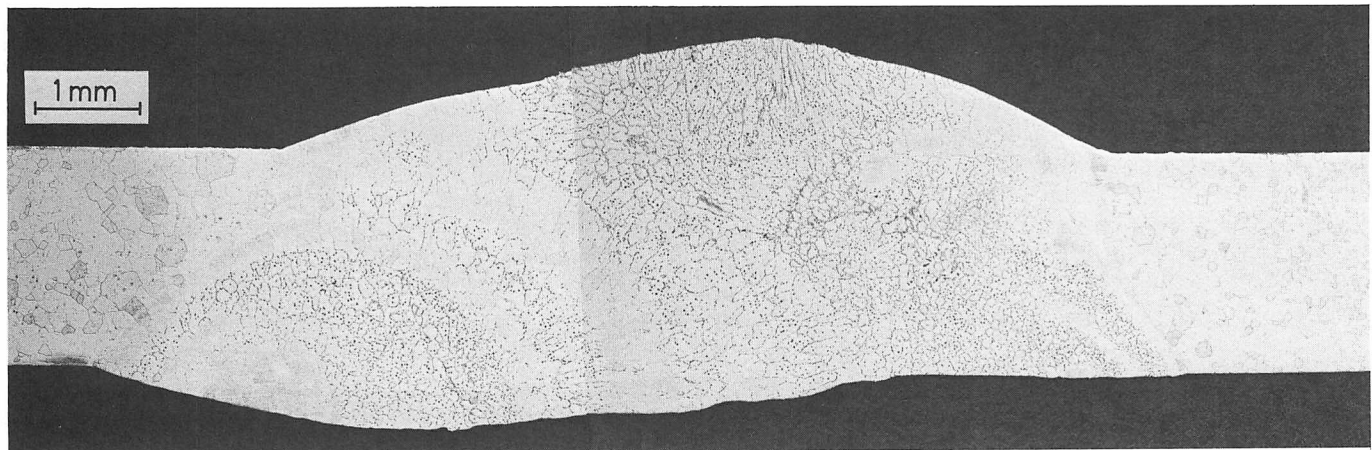
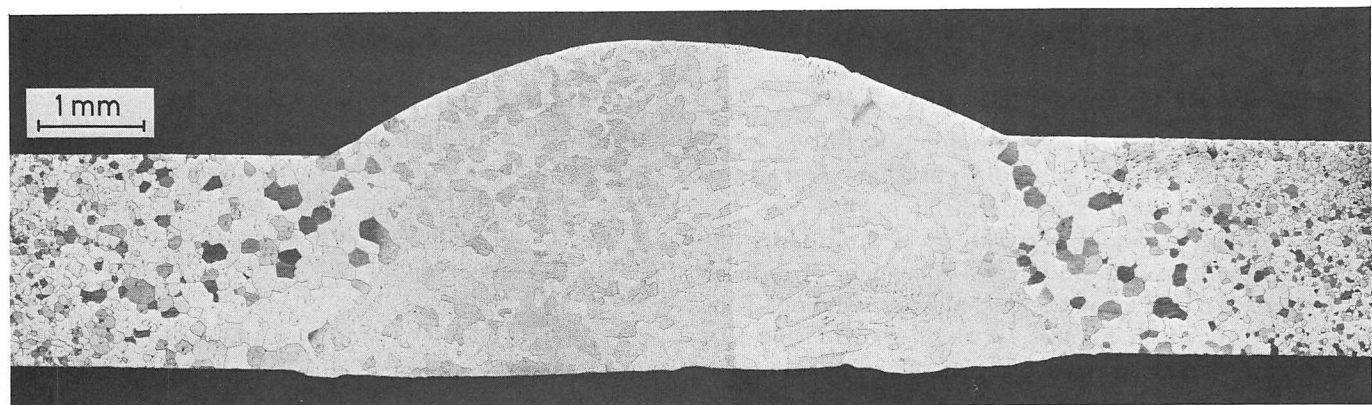a. 18 Cr-2 Mo/18 Cr-2 Mo without filler metal.
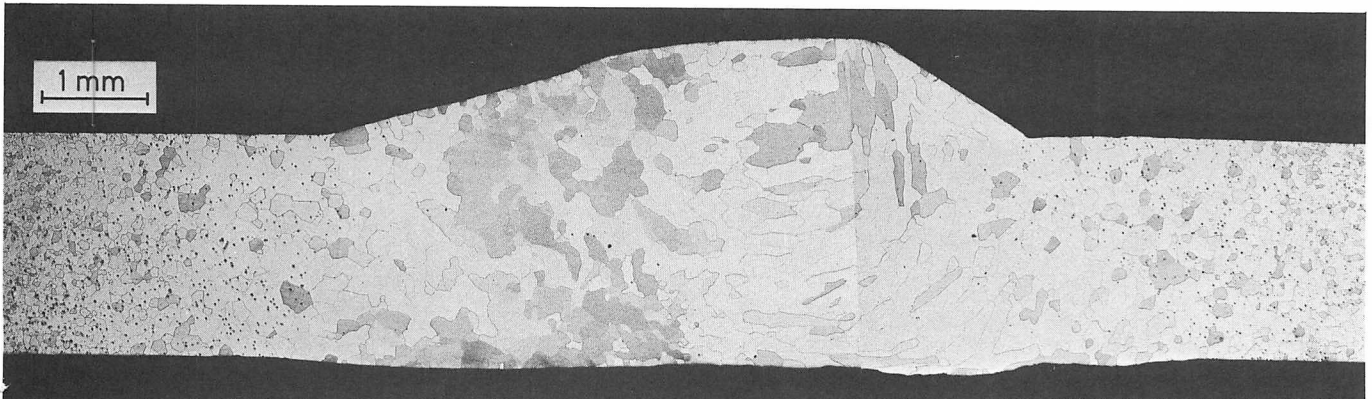


b. 18 Cr-2 Mo/18 Cr-2 Mo welded with identical filler metal.
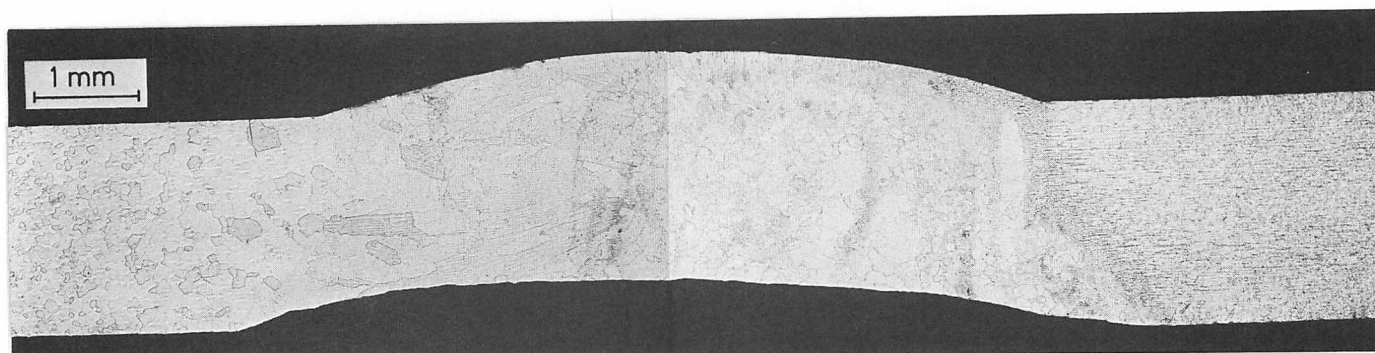
FIGURE 6—Cross seam welds.



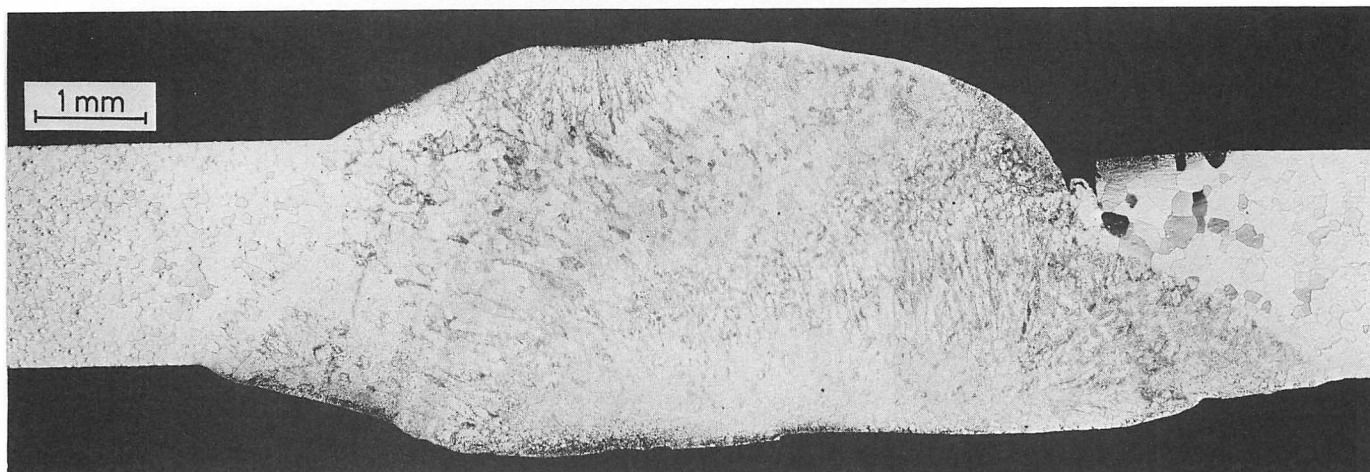a. 18 Cr-2 Mo/18 Cr-2 Mo welded with 29 Cr-9 Ni filler metal.



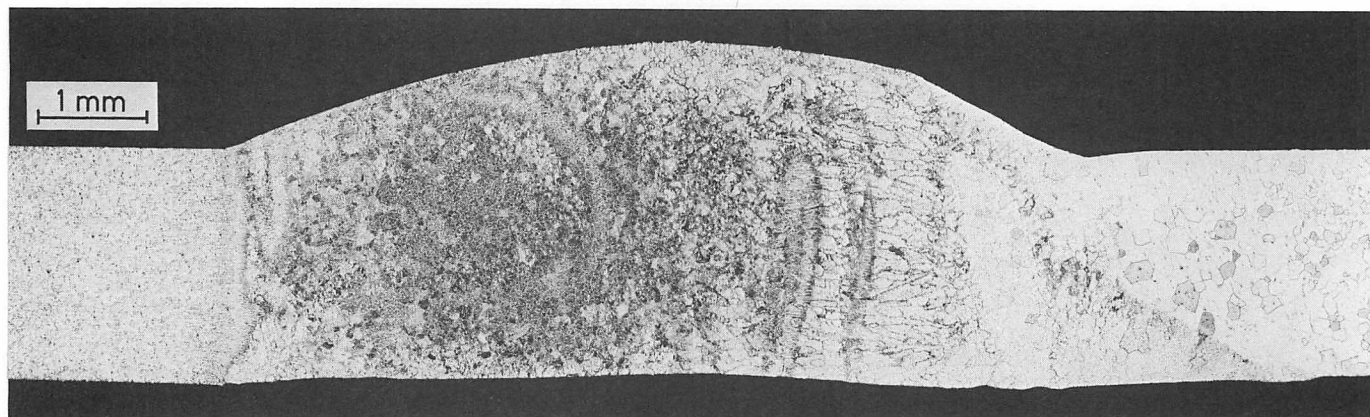b. 18 Cr-2 Mo/18 Cr-2 Mo welded with Thermanit® LMS wire.

FIGURE 7—Cross seam welds.

a. 18 Cr-2 Mo/AISI 321 without filler metal.



b. 18 Cr-2 Mo/AISI 321 welded with 29 Cr-9 Ni filler metal.



c. 18 Cr-2 Mo/AISI 321 welded with Thermanit® LMS wire.

FIGURE 8—Cross seam welds.

## Pitting Behavior in a Standardized River Water

Potentiostatic potential/current density curves were taken at 20 and 80 C (68 and 176 F) in Rhine river water with a chloride content standardized to 400 ppm by adding sodium chloride. The water was saturated with oxygen. Again, cross seam welded specimens of type A to G were used. They were pickled after welding. The results are shown in Figures 10 to 13. At 20 C (68 F), there is a pronounced passive region. The initiation potentials for pitting lie between 550 and 650 mV against the standard hydrogen electrode for the 18 Cr-2 Mo/18 Cr-2 Mo combination. They are somewhat lower for

the combination 18 Cr-2 Mo/stainless steel 321 (Figures 10 and 11), ranging between 500 and 600 mV. There is no clear influence of the weld materials investigated. As can be concluded from the difference between the initiation potential of pitting and the open-circuit potential, there is practically no danger for pitting at this temperature.

At 80 C (176 F), the pitting initiation potentials are more negative, and the influence of different weld metals is more pronounced. As Figure 12 demonstrates, the passive range of the combination 18 Cr-2 Mo/18 Cr-2 Mo welded with 29-9 or Thermanit® LMS wire is definitely
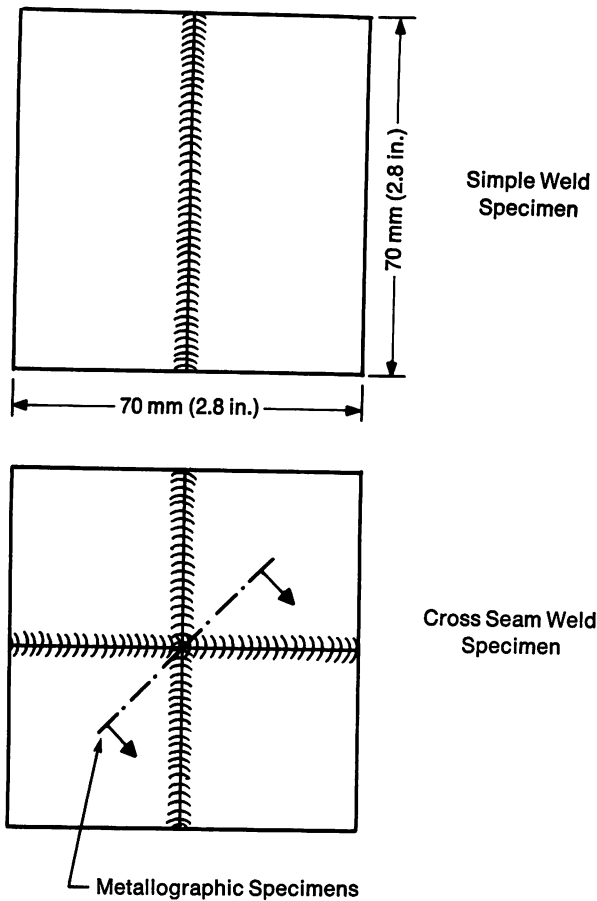
FIGURE 9—Weld specimens.

narrowed; in other words, pitting corrosion becomes more likely. In both cases, the welded 18 Cr-2 Mo combination is close to the border of pitting. In contrast to this, Figure 13 indicates no danger of pitting corrosion and no influence of the weld metals investigated in the case of the 18 Cr-2 Mo/AISI 321 combination.

### Behavior Under Stress Corrosion Cracking Conditions

Stress corrosion tests were carried out in boiling 42% magnesium chloride solutions using single and cross beam specimens (test duration 28 days). Under the conditions of this test, the 18 Cr-2 Mo steel actively corrodes at a measureable rate. It is for this reason that stress corrosion cracking cannot occur.

As extensively described in the literature, austenitic 18 Cr-8 Ni steels such as Type 321 crack within few hours in the magnesium chloride solution. Before this, it was an important observation that the welded 18 Cr-2 Mo/Type 321 combination showed no stress corrosion cracking after 28 days. It is evident that the 18 Cr-2 Mo steel undergoing active corrosion exerts a cathodic protection for the austenitic stainless steels thus suppressing stress corrosion cracking.

Autoclave corrosion tests were carried out in the river water standardized to a chloride content of 400 ppm. The test temperatures were 80, 100 and 130 C (176, 210 and 265 F). The specimens investigated were welded and roughly ground plates 50 by 20 by 2 mm (2 by 0.8 by 0.08 in.) with high internal tensile stresses and U-bend specimens. Some of the specimens were pickled after
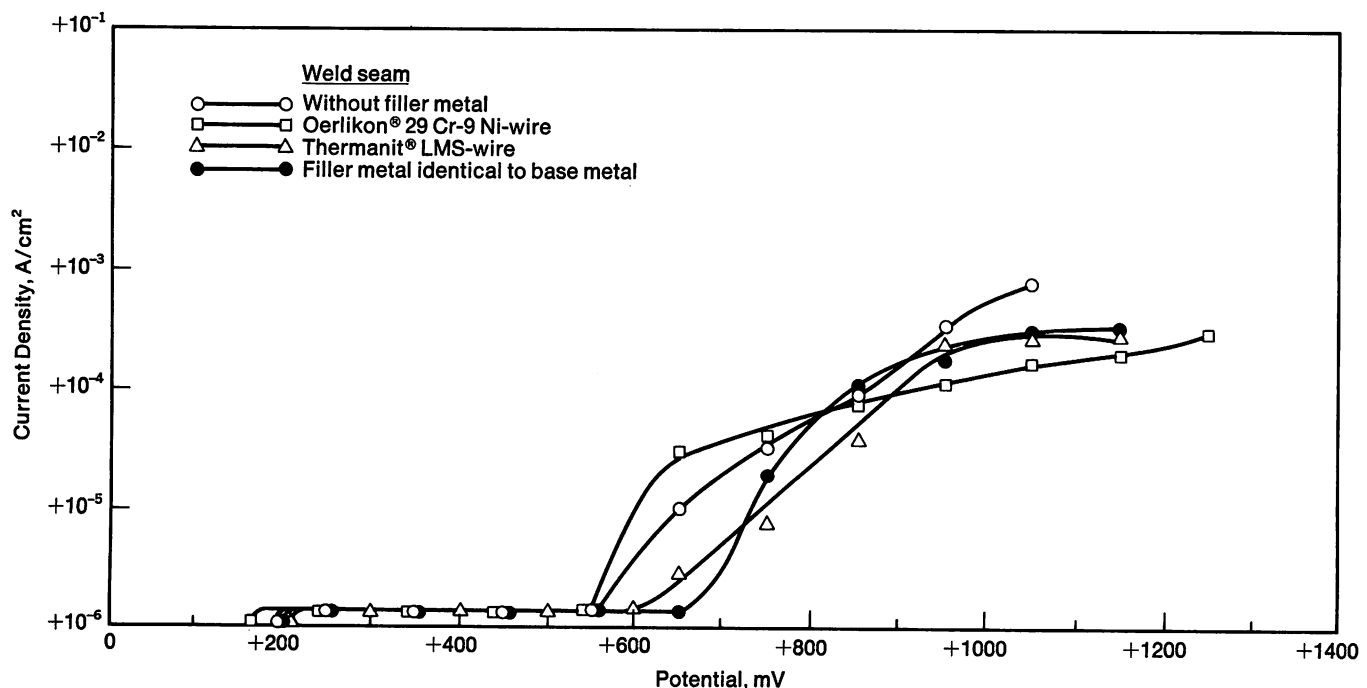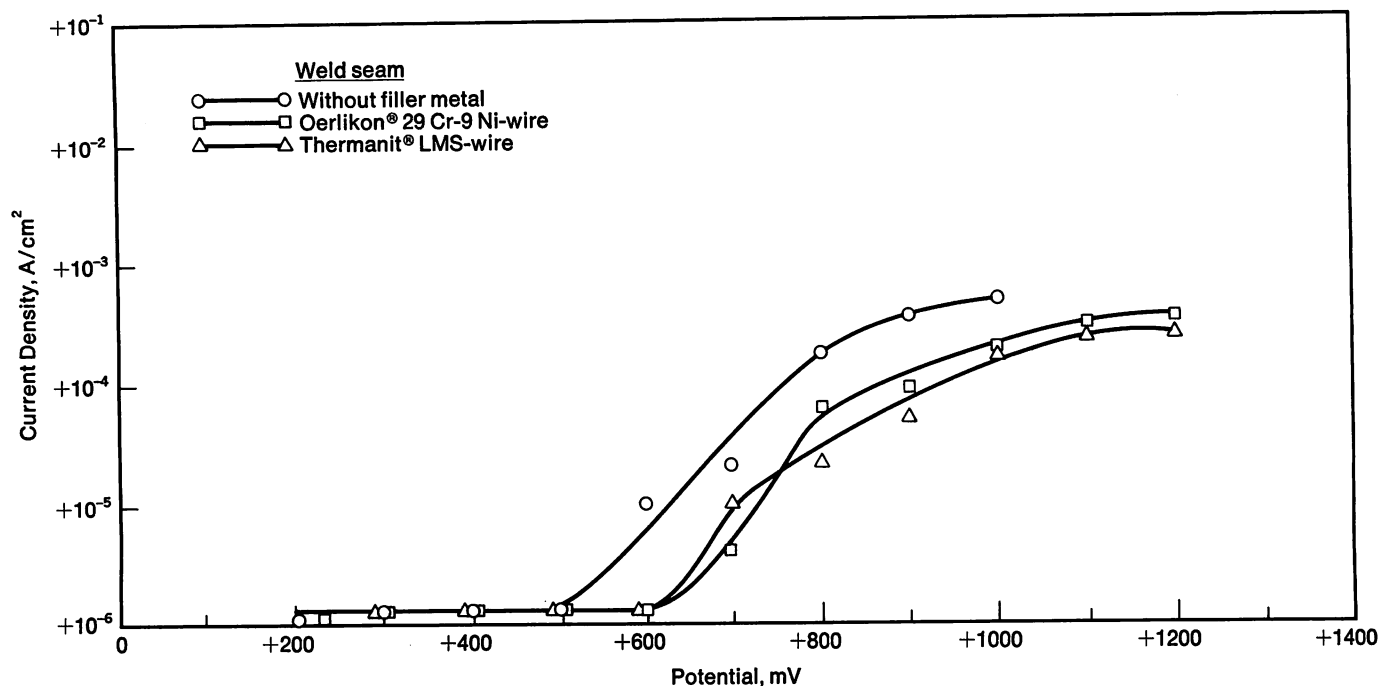


FIGURE 10—Potentiostatic curves in Rhine river water standardized to a chloride content of 400 ppm and saturated with oxygen. Test temperature 20 C (68 F). Weld combination, 18 Cr-2 Mo/18 Cr-2 Mo.

welding; others were tested in the as welded (ground) condition. The solution was changed every week during the first five weeks of testing. Thereafter, an uninterrupted test period of three weeks followed for the 100 and 130 C (210 and 265 F) tests. The specimens were not cleaned after the change of test solutions.

In 1978, new weld materials became available. Therefore, specimens were welded with weld metal identical with the base material, with Type 316L welding wire and with a 309 MoL welding rod, again in each case with the TIG welding process using argon as the inert gas.



FIGURE 11—Potentiostatic curves in Rhine river water standardized to a chloride content of 400 ppm and saturated with oxygen. Test temperature 20 C (68 F). Weld combination, AISI Type 321/18 Cr-2 Mo.
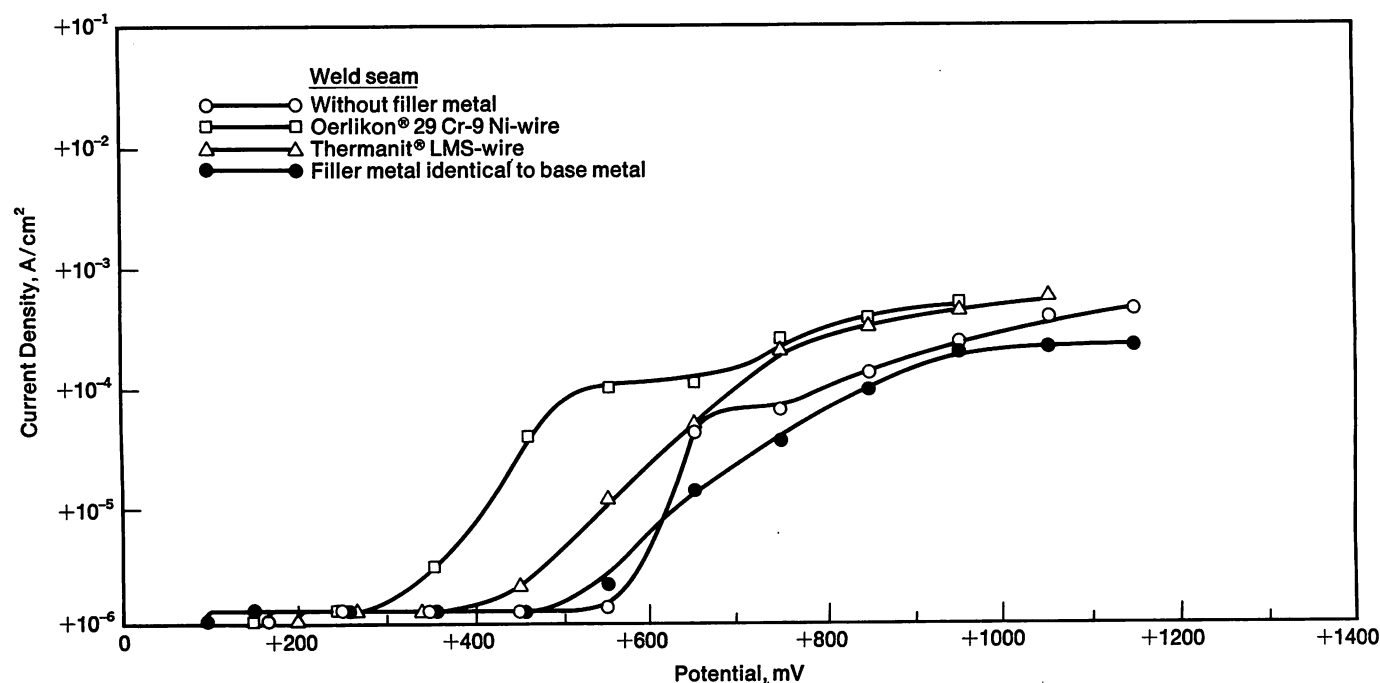


FIGURE 12—Potentiostatic curves in Rhine river water standardized to a chloride content of 400 ppm and saturated with oxygen. Test temperature 80 C (176 F). Weld combination, 18 Cr-2 Mo/18 Cr-2 Mo.
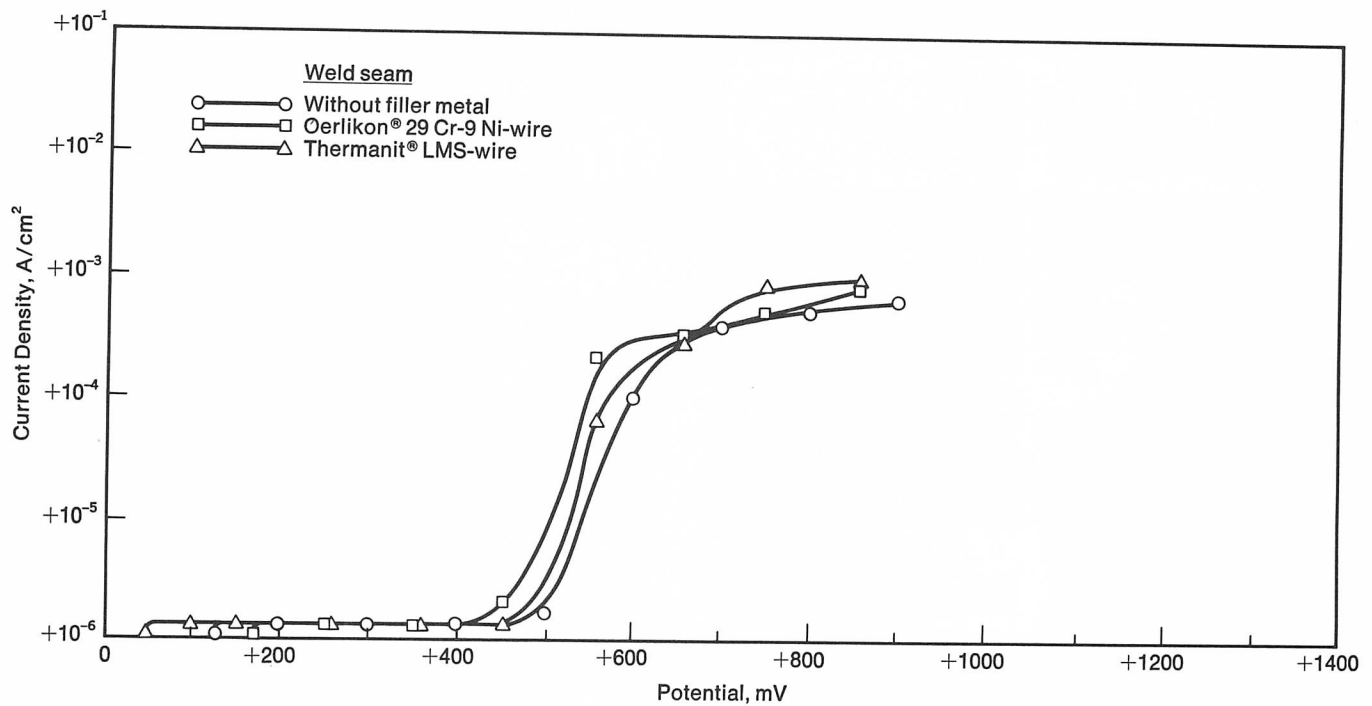
FIGURE 13—*Potentiostatic curves in Rhine river water standardized to a chloride content of 400 ppm and saturated with oxygen. Test temperature 80 C (176 F). Weld combination, AISI Type 321/18 Cr-2 Mo.*

**Table IV**—Chemical Composition of Base Material Used for the Second Series of Stress Corrosion Cracking Experiments

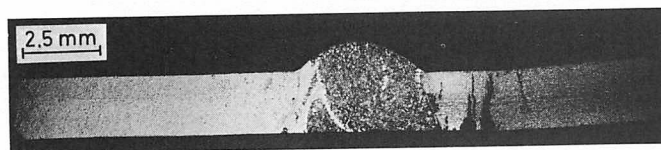| Element, % | | | | | | | | | | |
|---|---|---|---|---|---|---|---|---|---|---|
| C | N | Si | Mn | P | S | Cr | Ni | Mo | Ti | Cu |
| 0.027 | 0.0082 | 0.56 | 0.53 | 0.025 | 0.002 | 17.6 | 0.31 | 2.23 | 0.62 | 0.066 |



a. Numerous pits in the base material.
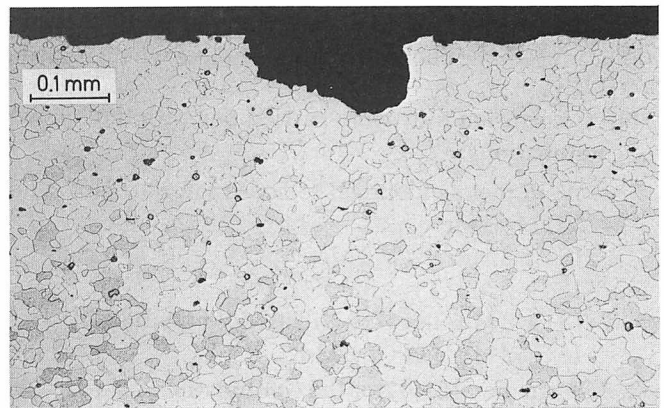


b. Pits in the base material at higher magnification (cross section).

FIGURE 14—*Surface appearance in the transition region between weld metal Type 316L and base material 18 Cr-2 Mo (not pickled after welding).*
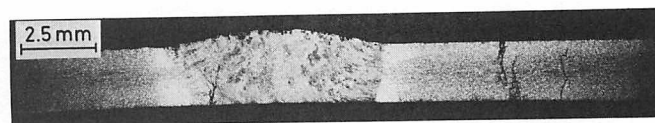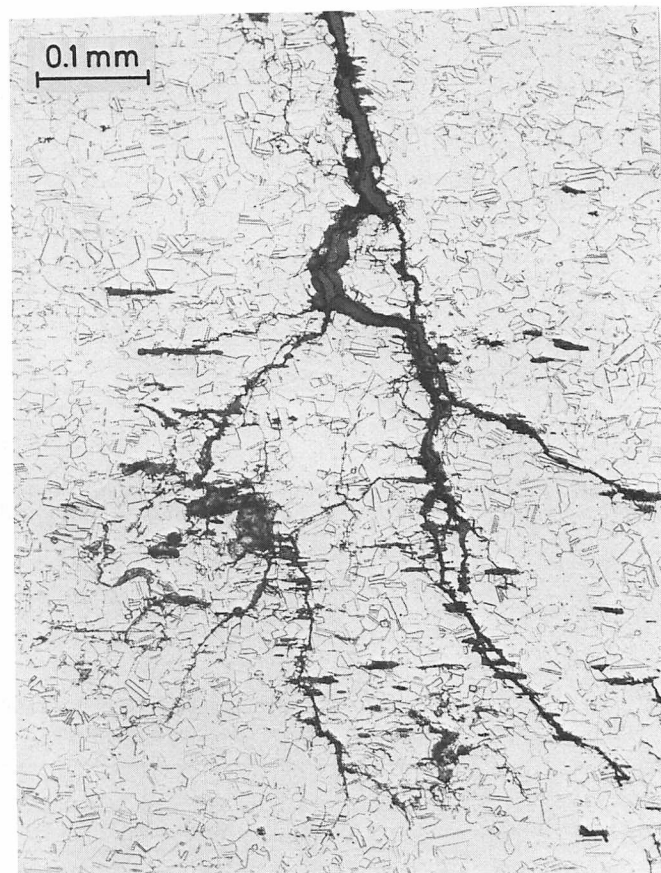
a. Macrograph (18 Cr-2 Mo at left).



a. Many cracks in the base material (Type 321 on both sides).



b. Micrograph (Type 321).



b. Transgranular cracking.

FIGURE 15—Stress corrosion cracking in Type 321. 18 Cr-2 Mo remained crack free.

FIGURE 16—Weld combination Type 321/Type 321.

Also new 18 Cr-2 Mo plate material of 1978 origin was now used, the chemical composition of which is given in Table IV.

Stress corrosion tests were carried out with the following combinations:

1. Weld metals identical to base material, 316L and 309 MoL for:
   18 Cr-2 Mo/18 Cr-2 Mo
   18 Cr-2 Mo/Type 321
   18 Cr-2 Mo/18 Cr-10 Ni-2.5 Mo, Ti stabilized
   18 Cr-2 Mo*/18 Cr-2 Mo*
2. Weld metal 316L for the combination:
   25 Cr-25 Ni-2.5 Mo/18 Cr-10 Ni-2.5 Mo, Ti stabilized (comparable designation ASTM A 371, ER 308 L).

3. Weld metal 1.4316 (X 2 CrNi 19 9) for the combination Type 321/ Type 321.
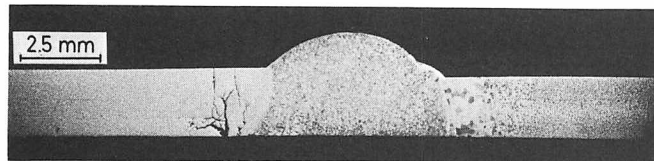
**Experiments at 80 C (176 F), air at 1 bar.** The specimens for this investigation were not pickled after welding so that oxide layers were present in the heat affected zones. In these areas, pitting was observed on the 18 Cr-2 Mo steel as shown in Figures 14a and 14b. In contrast to this, Type 321 stainless steel, 18 Cr-10 Ni-2.5 Mo and 25 Cr-25 Ni-2.5 Mo steels showed no pitting corrosion in these areas.

In a test period of a few weeks, in which the corrosive medium was changed every week, no stress corrosion cracking could be detected.
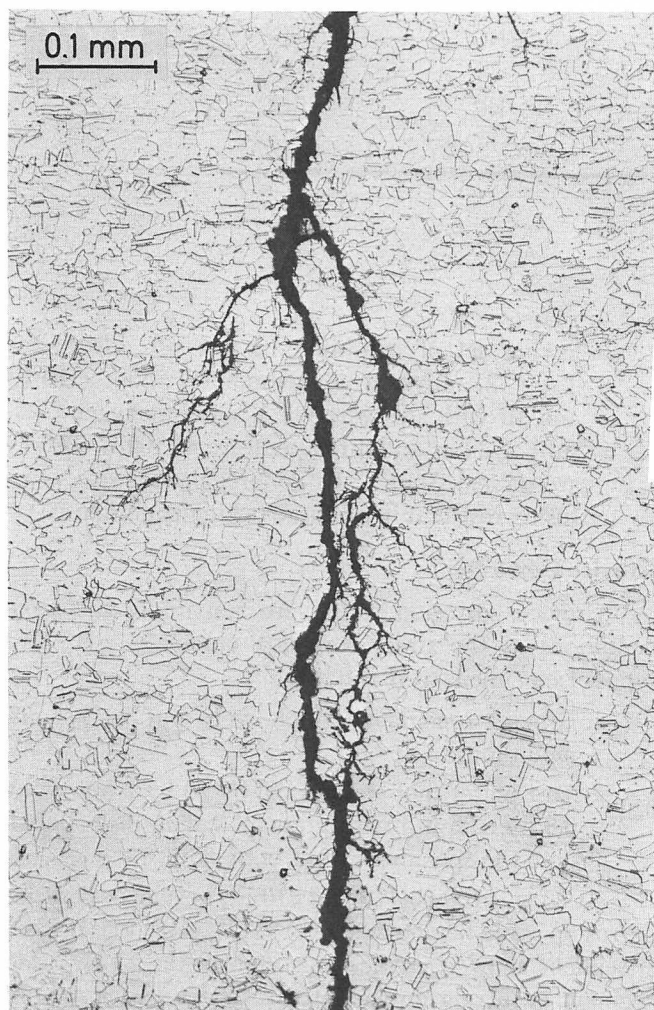
**Tests at 100 C (210 F), oxygen at 2 bar.** Again, very fine pitting occurred on 18 Cr-2 Mo specimens which had not been pickled after welding. Pickled specimens were completely free of pitting. Specimens with coarse ground

* Base material as per earlier series.
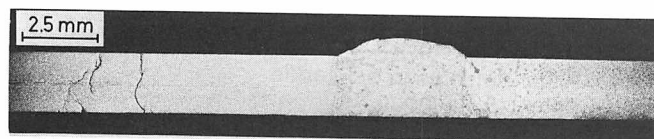
a. Many cracks in Type 321.
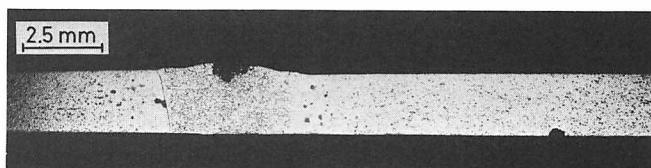


b. Many cracks in the 18 Cr-10 Ni-2.5 Mo.



a. Combination 25 Cr-25 Ni-2.5 Mo/AISI Type 321; many stress corrosion cracks in T 321, no cracks in 25 Cr-25 Ni-2.5 Mo.
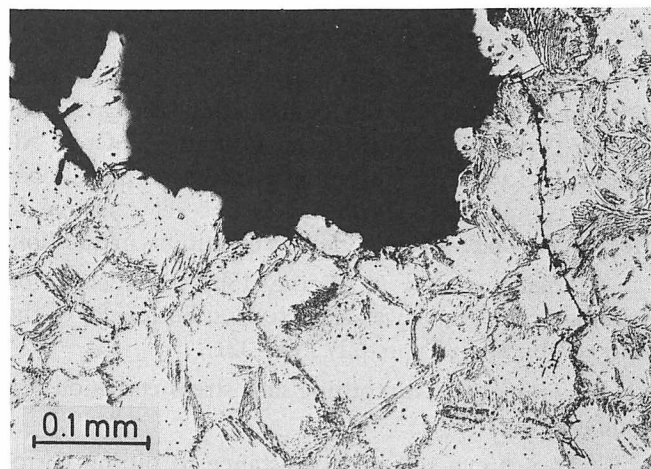


b. Cracking in base materials on both sides of weld seam (base material Type 321).

FIGURE 18—Stress corrosion cracking as a function of alloy chemistry in the austenitic stainless steels.



c. Transgranular cracking at higher magnification.

FIGURE 17—18 Cr-2 Mo welded to AISI Type 321 and to 18 Cr-10 Ni-2.5 Mo.



a. Macrograph of 18 Cr-2 Mo/T 316 weld metal/18 Cr-2 Mo.



b. Micrograph showing transgranular cracking starting from a pit in the T 316L filler metal.

FIGURE 19—Stress corrosion cracking in the weld seam (weld metal T 316L).

surfaces which had not been pickled showed fine pitting. However, there was no sign of stress corrosion cracking when the coarse grinding procedure had been applied.

The coarsely ground specimens welded to Type 321 stainless steel showed pronounced transgranular stress corrosion cracking in the austenite after a test time of 8 weeks (Figures 15a and 15b). The 18 Cr-2 Mo steel remained uncracked and so did the austenitic steels 18 Cr-10 Ni-2.5 Mo and 25 Cr-25 Ni-2.5 Mo.

In the Type 321/Type 321 combination, stress cor-

rosion occurred on both sides of the weld (Figures 16a and 16b). All U-bend specimens remained uncracked.

**Tests at 130 C (265 F), oxygen at 2 bar.** The 18 Cr-2 Mo steel showed no stress corrosion cracking. This held true for the old analysis (Table I) as well as for the new one (Table IV). Pitting corrosion on the unpickled, coarsely ground specimens was definitely more pronounced than under the foregoing conditions.

In the 18 Cr-2 Mo/Type 321 and 18 Cr-2 Mo/18 Cr-10 Ni-2.5 Mo combinations, stress corrosion occurred in

**Table V**—Stress Corrosion Cracking in Rhine River Water

| Material Combinations (Weld Metals 18 Cr-2 Mo, 316 L and 309 MoL) | Rhine River Water Adjusted to a Chloride Content of 400 ppm | | |
|---|---|---|---|
| | 80 C (176 F) Air (1 Bar) Testing Time: 5 Weeks | 100 C (210 F) $O_2$ (2 Bar) Testing Time: 8 Weeks | 130 C (265 F) $O_2$ (2 Bar) Testing Time: 8 Weeks |
| 18 Cr-2 Mo/18 Cr-2 Mo | NC/NC | NC/NC | NC/NC |
| 18 Cr-2 Mo/Type 321 | NC/NC | NC/SCC | NC/SCC |
| 18 Cr-2 Mo/18 Cr-10 Ni-2.5 Mo | NC/NC | NC/NC | NC/SCC |
| 18 Cr-2 Mo (old)/ 18 Cr-2 Mo (old) | NC/NC | NC/NC | NC/NC |
| 25 Cr-25 Ni-2.5 Mo/ 18 Cr-10 Ni-2.5 Mo | NC/NC | NC/NC | NC/SCC |
| Type 321/Type 321 | NC/NC | SCC/SCC | SCC/SCC |

NC  = No Cracking.
SCC = Stress Corrosion Cracking (transgranular).

the austenite. Cracking was not just confined to the coarsely ground area, but occurred on finely ground and and on U-bend specimens as well. In all cases, the 18 Cr-2 Mo remained crack free. These results are compiled in Figures 17a, 17b and 17c. It is clearly recognized that it is only the austenite which undergoes stress corrosion cracking.

Figure 18a shows that Type 321 undergoes stress corrosion cracking in the combination 25 Cr-25 Ni-2.5 Mo/Type 321. Evidently, the austenitic 25 Cr-25 Ni-2.5 Mo steel with its substantially increased nickel content as compared to Type 321 is not yet sensitive to stress corrosion cracking under the conditions in question.

As demonstrated in Figure 18b, stress corrosion cracking occurred, as was expected, on both sides of the weld combination Type 321/Type 321.

In summary of the pitting and stress corrosion test results:

1. To achieve sufficient resistance to pitting corrosion under given corrosion conditions, it is mandatory to pickle the 18 Cr-2 Mo steel after welding.

2. None of the weld metals, 18 Cr-2 Mo, 316L or 309 MoL, underwent stress corrosion cracking in combination with 18 Cr-2 Mo. There was only one case in which SCC could be observed in the welding seam, viz. in the combination 18 Cr-2 Mo (old)/18 Cr-2 Mo (old) welded with 316L, temperature 130 C (265 F), 2 bar $O_2$. This is shown in Figures 19a and 19b.

3. Both the "old" 18 Cr-2 Mo steel and the new one were resistant to SCC under all testing conditions applied.

4. The results in river water with a chloride content of 400 ppm are summarized in Table V. The fol-

lowing set of conditions is not yet critical for Type 321: River water temperature 80 C (176 F) and air with a pressure of 1 bar. An oxygen pressure of 2 bar and a temperature of 100 C (210 F) are critical. Steel 25 Cr-25 Ni-2.5 Mo is stress corrosion resistant in all three testing conditions.

### Crevice Corrosion

Crevice corrosion tests were run under the same conditions as the stress corrosion cracking tests. Two types of specimens were used:

1. U-bend specimens which were put in Teflon® mountings.

2. Test plates (not welded) 50 by 20 by 2 mm (2 by 0.8 by 0.08 in.) with grooved Teflon disks bolted onto the specimens from both sides.

At 80 and 100 C (176 and 210 F), no signs of crevice corrosion could be detected. At 130 C (265 F), the U-bend specimens showed crevice corrosion in the 18 Cr-2 Mo segment occurring on the lateral surface in the area of the Teflon mounting. Crevice corrosion occurred also on the Type 321 segment but was less pronounced than on the ferritic side.

In contrast to the results obtained with the U-bend specimens, no crevice corrosion attack could be detected under the grooved Teflon disks after 8 weeks of testing at 130 C (265 F). Only a discoloration of the surface could be seen.

### Heat Exchanger Experiments

To study the performance of 18 Cr-2 Mo under actual heat exchanger conditions, large scale model heat exchangers were fabricated. After experiments to fabri-

**Table VI**—Stretch-Forming Experiments for Fabricating Heat Exchanger Plates from 18 Cr-2 Mo

| Experiment | Stretch Forming Conditions | State |
|---|---|---|
| 1 | Foil between plate and die on both sides; full pressure 20,000 N (4500 lb) | Many cracks, including center of plate |
| 2 | Plate oiled on both sides with deep drawing oil; half pressure 10,000 N (2250 lb) | Cracks in jacked area |
| 3a | Plate oiled with deep drawing oil on both sides; prestretch formed up to half depth with 5000 N (1120 lb) | Crack free |
| 3b | Final stretch forming to finished size with 10,000 N (2250 lb) | Cracks in jacked area |
| 4a | Both sides covered with foil and oiled with deep drawing oil; preliminary stretch forming up to 50% of final depth with 5000 N (1120 lb) | Crack free |
| 4b | Final stretch forming to finished size with 7500 N (1690 lb) | Cracks in jacked area |
| 5 | Plate preheated to about 100 C (210 F); oiled with deep drawing oil on both sides; half pressure 10,000 N (2250 lb) | Cracks in jacked area |

cate heat exchanger plates under standard stretch-forming conditions, the investigations were confined to heat exchangers of the tubular type.

**Stretch-Forming Experiments with 18 Cr-2 Mo**

Plates 400 by 1300 mm (15.7 by 50 in.) and 0.8 mm (0.03 in.) thick, were stretch-formed under the conditions given in Table VI.

As these results showed, the fabrication of heat exchanger plates under standard conditions is virtually impossible; despite its excellent deep drawing properties, 18 Cr-2 Mo has limited stretch-forming capability.

**Tubular Heat Exchanger Experiments**

Because of the difficulties in fabricating heat exchanger plates, corrosion studies under heat exchanger conditions were confined to tubular units.

As tubesheets cannot be made of 18 Cr-2 Mo (the minimum toughness cannot be reached in the required plate thickness), boiler plate H II (DIN 17 155) was used. It was protected from corrosion by explosive bonding of 2.5 mm (0.1 in.) 18 Cr-2 Mo plate to boiler plate or by an 18 Cr-2 Mo weld overlay.

**Explosive bonding and weld overlay results.** Chemical analyses of plate and base material used for explosive bonding are given in Table VII.

Explosive bonding was followed by a heat treatment at 850 C (1560 F). Figures 20a and 20b show details of the bonding zones in cross and longitudinal sections. The photomicrographs demonstrate the satisfactory bonding between 18 Cr-2 Mo cladding and the boiler plate base material. Figure 21 illustrates the typical cold worked microstructure with the saw-toothed pattern caused by explosive bonding.

Weld overlaying was done by the AGA* process, a gas metal plasma arc process described in the literature. [17,18] The chemical composition of the weld metal is given in Table VIII.

The first layer was a little less than 8 mm (0.31 in.) thick. The total two-layer weld deposit thickness was about 14 mm (0.55 in.). Both layers showed considerable grain coarsening as demonstrated by the cross section in the micrographs of Figures 22a and 22b.

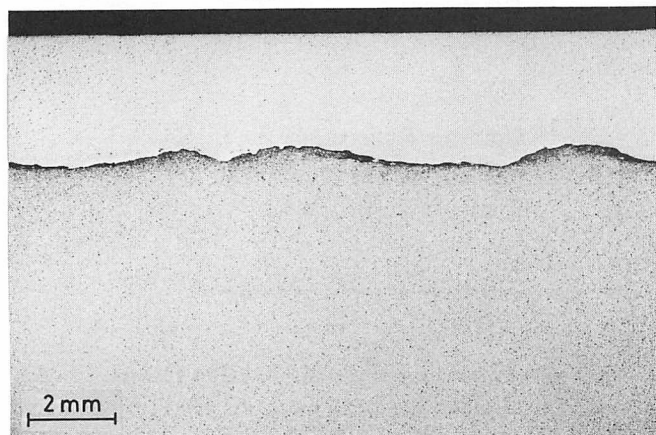The carbon and nitrogen contents of the 18 Cr-2 Mo

---

\* AGA Arc Weld AB, Sweden.

**Table VII**—Chemical Composition of 18 Cr-2 Mo Plate and Boiler Plate

| | Element, % | | | | | | | | | | | |
|---|---|---|---|---|---|---|---|---|---|---|---|---|
| | C | Si | Mn | P | S | Cr | Ni | Mo | Ti | N | Cu | Co |
| 18-2 Plate | 0.023 | 0.38 | 0.58 | 0.028 | 0.002 | 17.98 | 0.41 | 2.38 | 0.52 | 0.010 | 0.038 | 0.050 |
| Boiler Plate | 0.12 | 0.25 | 0.4 0.7 | 0.08 max | 0.06 max | — | — | — | — | — | — | — |
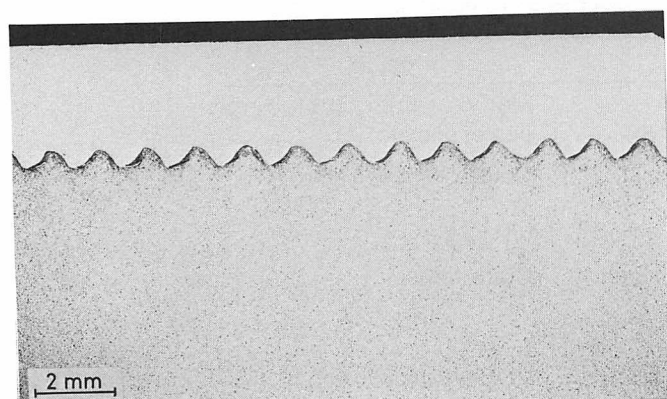
a. Parallel to cladding direction.



b. Transverse to cladding direction.

FIGURE 20—Explosive bonding of 18 Cr-2 Mo sheet to mild steel tubesheet.



FIGURE 21—Cold work caused by explosive bonding.

weld was analyzed; the results are shown in Figures 23 and 24. The carbon content in the single-layer weld deposit was slightly higher than in the weld metal proper (Figure 23). The maximum tolerable carbon content of 250 ppm was, however, not exceeded. The carbon content was constant over a broad range. It increased steeply just about 2 mm (0.08 in.) above the interface between the base material and the weld deposit.

The first layer of the two-layer deposit showed exactly the same pattern (Figure 24). In the second layer, the carbon content was identical with that of the weld metal proper.

The nitrogen content was, to about 1 mm (0.04 in.) above the interface, higher than specified for the as-deposited welded metal. Except for two measuring points, it was, however, below the maximum allowable value of 250 ppm (note the scale change in Figures 23 and 24). In the region up to 2 mm (0.08 in.) above the base material, the sum of carbon plus nitrogen ranged
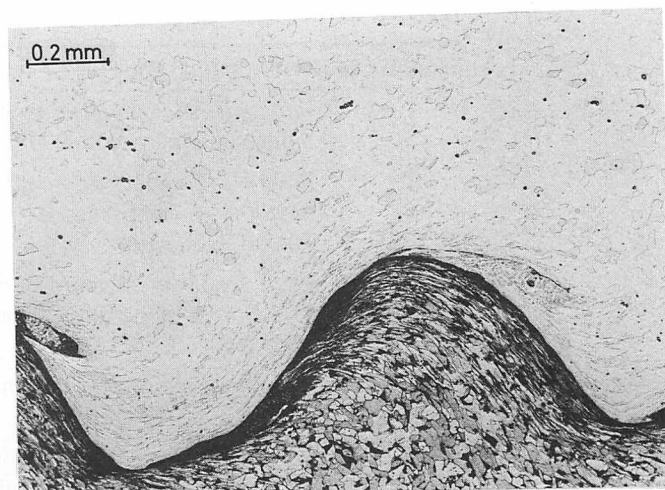
beyond the maximum allowable value of 400 ppm. This was to be expected. It is of no importance for the corrosion behavior of the weld overlay as a whole. It was found that, above this zone, the limiting value for both the single- and double-pass weld overlay was exceeded in only two cases. For the single-pass deposit, the sum of carbon and nitrogen was 480 ppm at 2 mm (0.08 in.) below the outer surface. For the double-pass deposit, a value of 450 ppm was reached within 1 mm (0.04 in.) of the weld overlay above the base material surface. In all other parts of the overlay, the maximum allowable value of 400 ppm was not exceeded.

From these results, it can be concluded that explosive bonding and weld overlaying of 18 Cr-2 Mo is a means of protecting tubesheets against corrosion in a sufficiently reliable manner. It should be added, however, that the mechanical properties of the weld metal deposited in the one- or two-pass weld overlay process have not been measured.

**Design and materials selection for experimental heat exchangers.** Three tubular heat exchangers were fabricated each with 19 tubes 500 mm (19.7 in.) in length, an external diameter of 25 mm (1 in.) and a wall thickness of 2 mm (0.08 in.). AISI Type 321 stainless steel served as a reference material as did its molybdenum-bearing 18 Cr-10 Ni-2.5 Mo (Ti stabilized) counterpart. Also included were tubes made of the ferritic-austenitic stainless steel, AFNOR Z5CNDU 21-08* (20-22 Cr, 5.5-8.5 Ni, 2-3 Mo and 1-2 Cu) and tubes of a highly alloyed austenitic stainless steel SIS 2343** (17 Cr, 12 Ni, 2.8 Mo
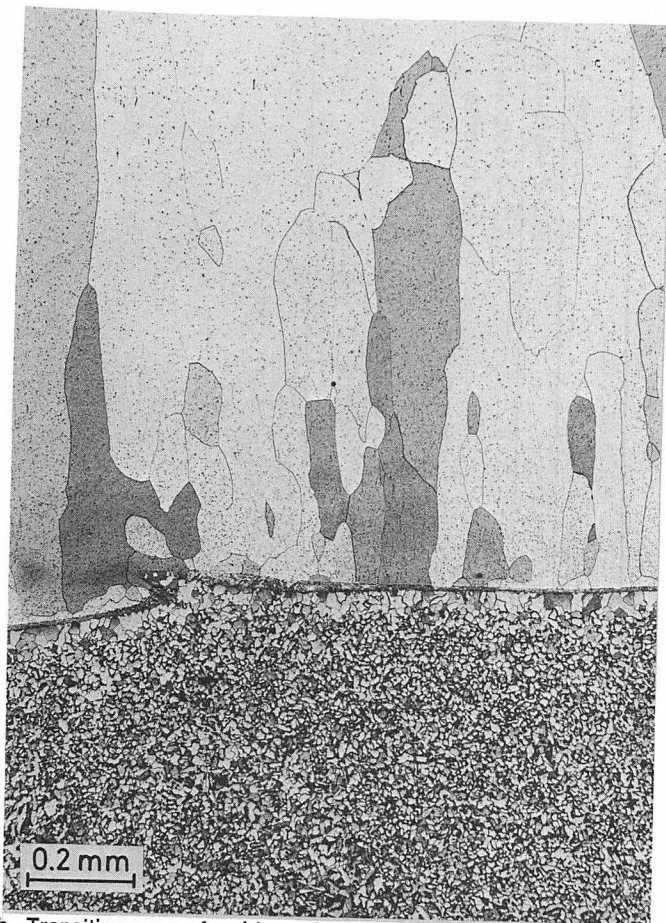
* Uranus 50® supplied by Creusot-Loire, France.
** Steel R 442 supplied by Fagersta A.B., Sweden.

Table VIII—Chemical Composition of Weld Metal for Weld Overlay

| Element, % | | | | | | | | | | | |
|---|---|---|---|---|---|---|---|---|---|---|---|
| C | Si | Mn | P | S | Cr | Ni | Mo | Ti | N | Cu | Co |
| 0.018 | 0.32 | 0.29 | 0.014 | 0.009 | 17.28 | 0.20 | 2.30 | 0.58 | 0.014 | 0 | 0.046 |
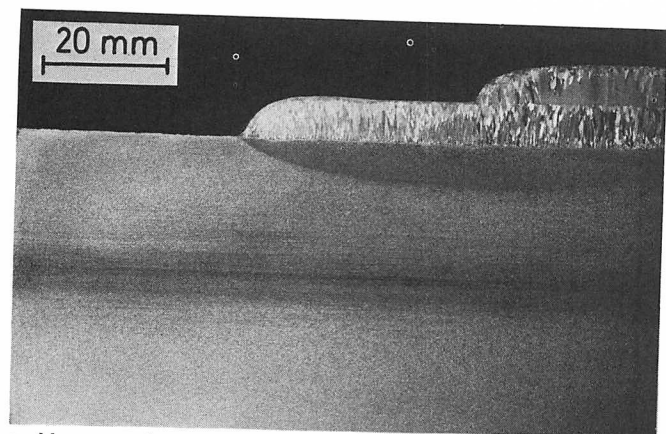
a. Macrograph.



b. Transition area of weld overlay/base material with consider-able grain coarsening.

FIGURE 22—*Two-pass weld overlay.*



FIGURE 23—*Carbon and nitrogen content in a one-pass weld overlay as a function of distance from base material.*

In 192 isotope camera was developed to detect weld defects in tube-to-tubesheet weldments. The method is illustrated in Figures 26 and 27. In principal the γ-ray emitting isotope, Ir 192, is inserted into the tube by means of a centering device. The γ-rays pass through the weld seam, and the exposed film shows the image of the weld seam projected as a circular ring. All tube-to-tubesheet welds of the three experimental heat exchangers were tested by this method. Only a few tolerable weld defects could be found.

**Experimental procedure and results of corrosion tests.** The experimental heat exchangers have been operated over a period of 14 months. They were heated by low pressure steam (400 kPa, 58 psi) on the shell side and cooled by natural Rhine river water on the tube side.

The average chloride content during this operating period was 150 ppm, the lowest value being 50 and the highest 270 ppm.

The streaming velocity of the cooling water was chosen such that the exit temperature corresponded to the highest temperature in the previous autoclave experi-

and 0.3 Mn, max).

The welding procedure applied throughout was TIG using pure argon as the inert gas.

Table IX lists the materials used in the three heat exchangers. Details of design can be taken from Figure 25.

Tube-to-tubesheet welds may contain defects, like pores, slag inclusions, etc., which can lead to leaks. Leakage has been comparatively frequent, and no NDT method was available to detect even large defects. An
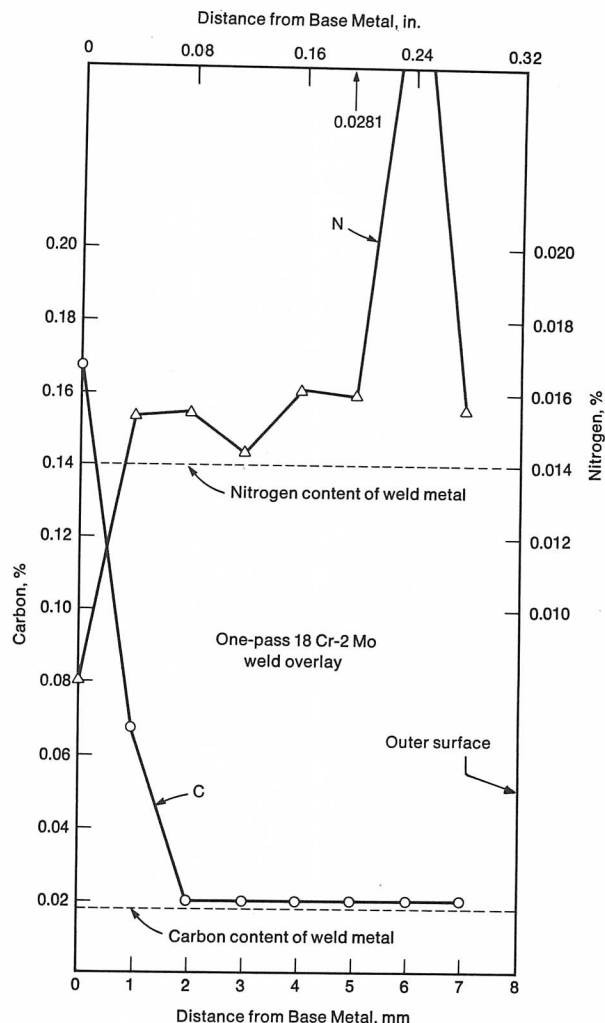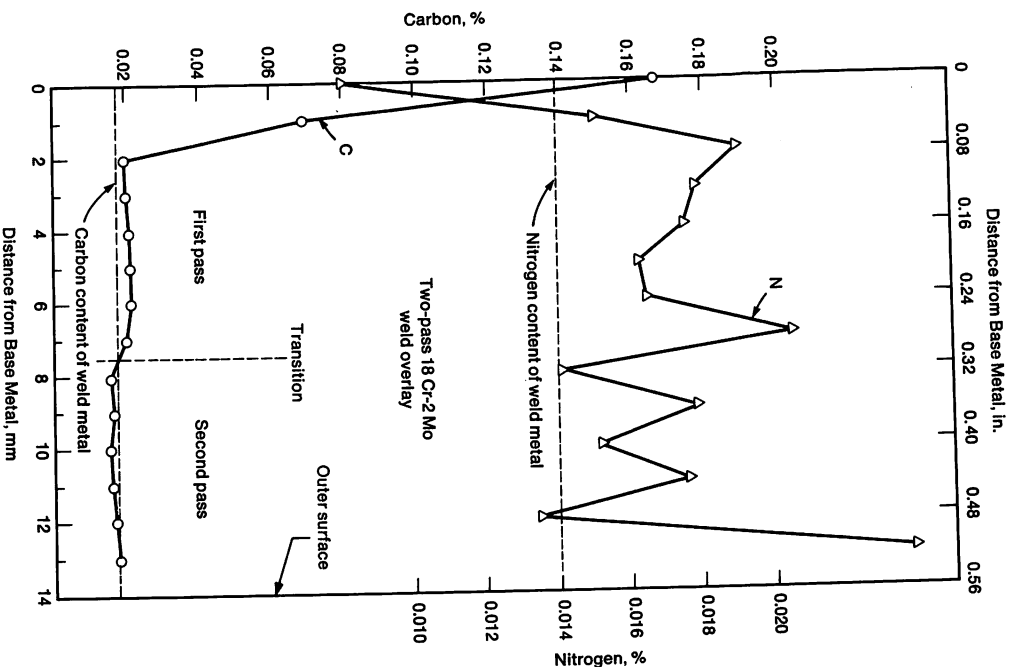
FIGURE 24—Carbon and nitrogen content in a two-pass weld overlay as a function of distance from base material.

ments (130 C, 265 F). The Rhine river water flowed continuously through the tubes, and the water exit temperature was continuously recorded. Figure 28 is a schematic of the test stand and the flow media. Heat exchanger 2 is in series with heat exchanger 1 so that the tube plates on the hot side (130 C, 265 F) have the same corrosion conditions, and a comparison of the corrosion behavior of the two different tubesheet materials is possible.

No damage had occurred after four months and eleven months operating time. A careful die penetrant test in the tubesheet area showed neither SCC nor pitting corrosion.

After 14 months, the tubesheet, 1R, of heat exchanger 1 (18 Cr-2 Mo) showed slight pitting corrosion in the 6 o'clock position which was caused by a deposit of algea and other substances. This finding is documented in Figure 29. The second tubesheet, 1L, of heat exchanger 1 showed no corrosion attack whatsoever. The tubesheet, 2L (Type 321), showed stress corrosion cracking in the 6 o'clock position. The tubes (Type 321 and 18 Cr-10 Ni-2.5 Mo, Ti stabilized) and the tube-to-tubesheet welds showed no cracking after 14 months. On the

**Table IX**—Base Materials and Weld Metals Used in Experimental Heat Exchangers

| Exchanger No. | Tube Material | Weld Metal | Tube Sheet Material | Shell Material |
|---|---|---|---|---|
| 1 | 18 Cr-2 Mo | 18 Cr-2 Mo; 316L; 309 MoL | 18 Cr-2 Mo explosively clad | 18 Cr-2 Mo |
| | 18 Cr-2 Mo | 18 Cr-2 Mo; 316L; 309 MoL | 18 Cr-2 Mo boiler plate + weld overlay | |
| 2 | AISI Type 321 | 19 Cr-9 Ni (ELC) (X 2 CrNi 19 9) | AISI Type 321 | 18 Cr-2 Mo/ AISI Type 321 |
| | 18 Cr-10 Ni-2.5 Mo, Ti stabilized (X 10 CrNiMoTi 18 10) | 19 Cr-12 Ni-2.7 Mo, Nb stabilized (X 5 CrNiMoNb 19 12) | | |
| 3 | 18 Cr-2 Mo | 18 Cr-2 Mo; 316L; 309 MoL 20 Cr-8 Ni-2.5 Mo-1.6 Cu (ELC) | 20-22 Cr-5.5-8.5 Ni-2-3 Mo-1-2 Cu (AFNOR Z5CNDU 21-08) | 20-22 Cr-5.5-8.5 Ni-2-3 Mo-1-2 Cu (AFNOR Z5CNDU 21-08)/ AISI Type 316 |
| | 17 Cr-12 Ni-2.8 Mo-0.3 Mn (SIS 2343) | 20 Cr-25 Ni-4.3 Mo-1.5 Cu (ELC) (X 2 NiCrMoCu 25 20 5) | | |
| | 20-22 Cr-5.5-8.5 Ni-2-3 Mo-1-2 Cu (AFNOR Z5CNDU 21-08) | 20 Cr-8 Ni-2.5 Mo-1.6 Cu (ELC) | | |
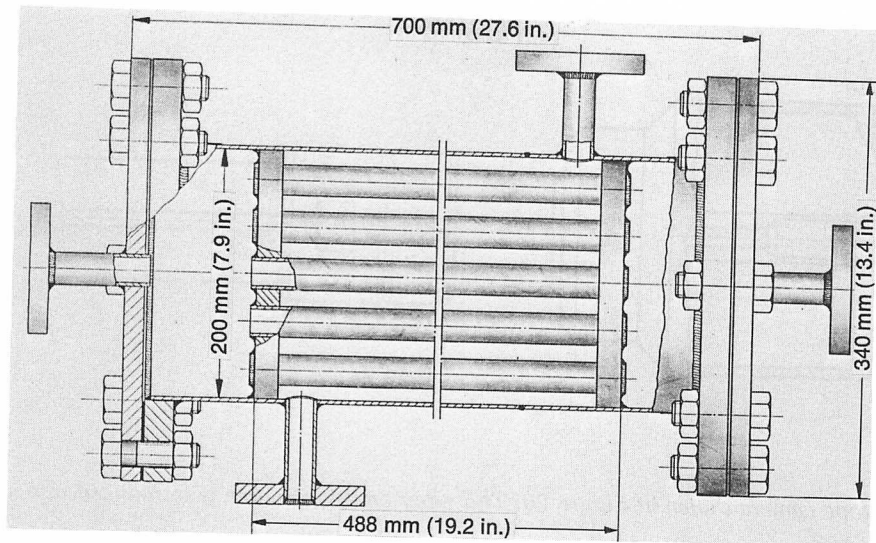
Corrosive agent { around tubes: steam through
tubes: Rhine river water
130 C (265 F) (110-150 ppm Cl⁻)

Operating time: 1 year, continuous flow of cooling
water

Tube-to-tubesheet welds:
TIG with filler metal (3 filler
metals: identical with base
metal, T 316 L, T 309 MoL)
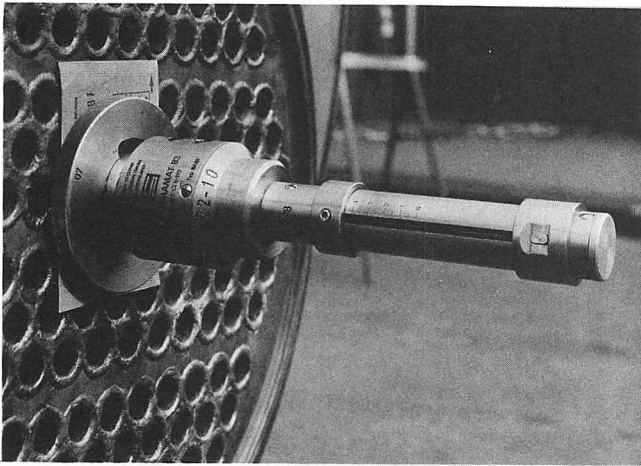
FIGURE 25—Design of heat exchanger No. 1.



FIGURE 26—Radiography of tube-to-tubesheet welds by
means of isotope, Ir 192, by which welding defects (especially
pores) can be detected during manufacture.

other hand, SCC had occurred in all flanges made of
Type 321 in the packing area. The second tubesheet,
2R, of heat exchanger 2 (18 Cr-2 Mo) showed no corrosion
damage. This held true for heat exchanger 3, the tube-
sheets of which were made of the ferritic-austenitic steel
AFNOR Z5CNDU 21-08.

Then a discontinuous operation followed in which
the flow of cooling water is interrupted daily for 30 min-
utes without throttling the steam supply. During this
period the river water is evaporated and a high chloride
concentration is reached. After 30 minutes, the normal
cooling water flow is reestablished and the water exit
temperature of 130 C (265 F) adjusted.
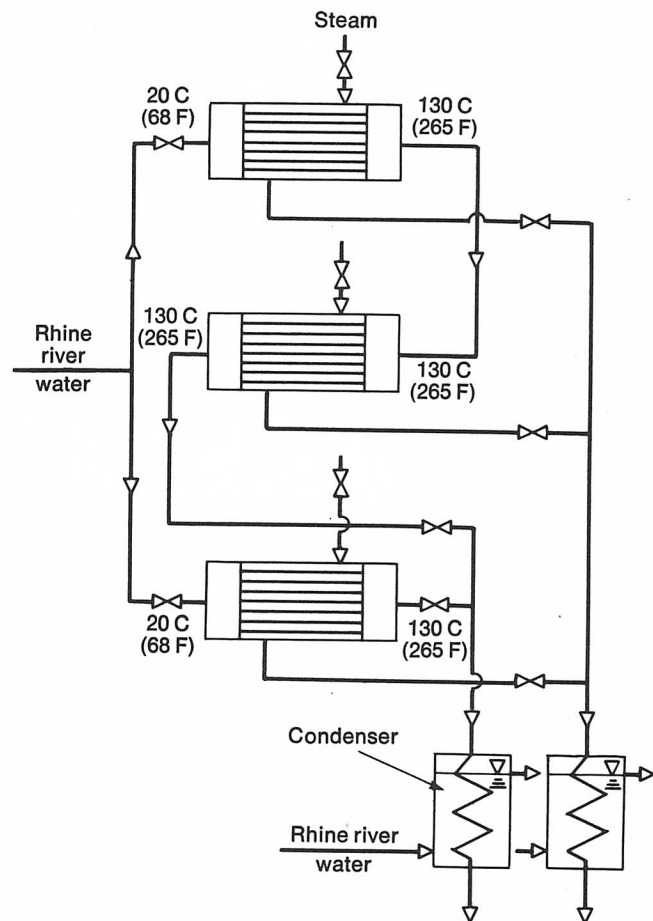


FIGURE 28—Model experimental heat exchanger circuit.

Gammamat B3
— Type BASF —
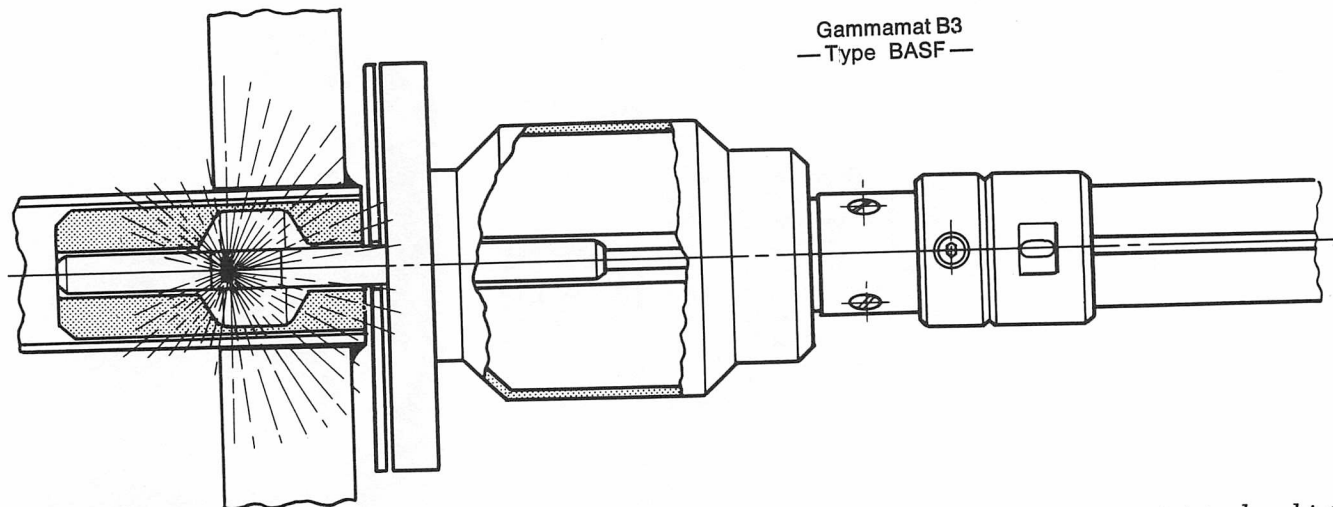
FIGURE 27—*Principal of the radiographic isotope camera shown in Figure 26. The γ-ray emitting source is introduced into a tube by means of a centering device.*



30 mm
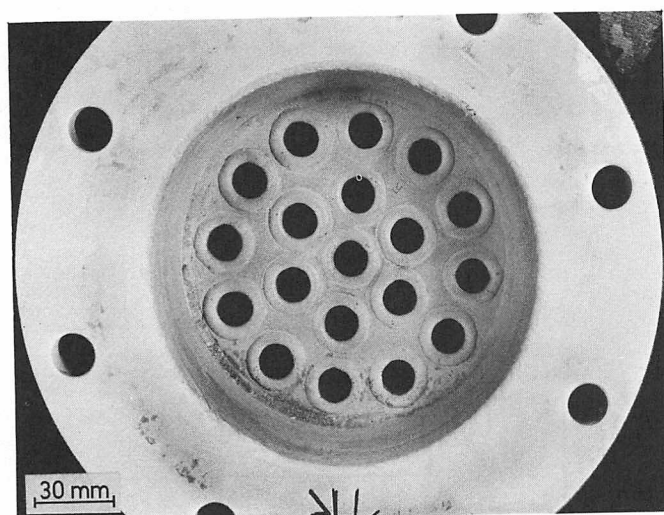
FIGURE 29—*Tubesheet 1R (mild steel boiler plate H II) explosively clad with 18 Cr-2 Mo sheet with slight pitting in the lower area (6 o'clock position).*



2 mm

a. Macrograph.



0.2 mm
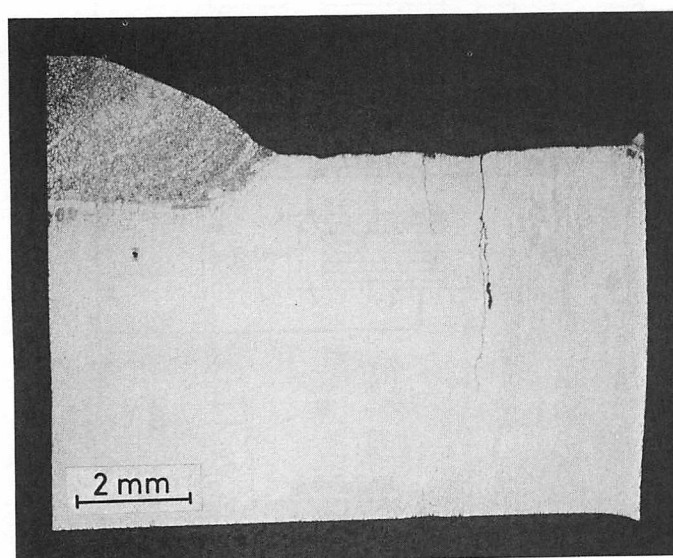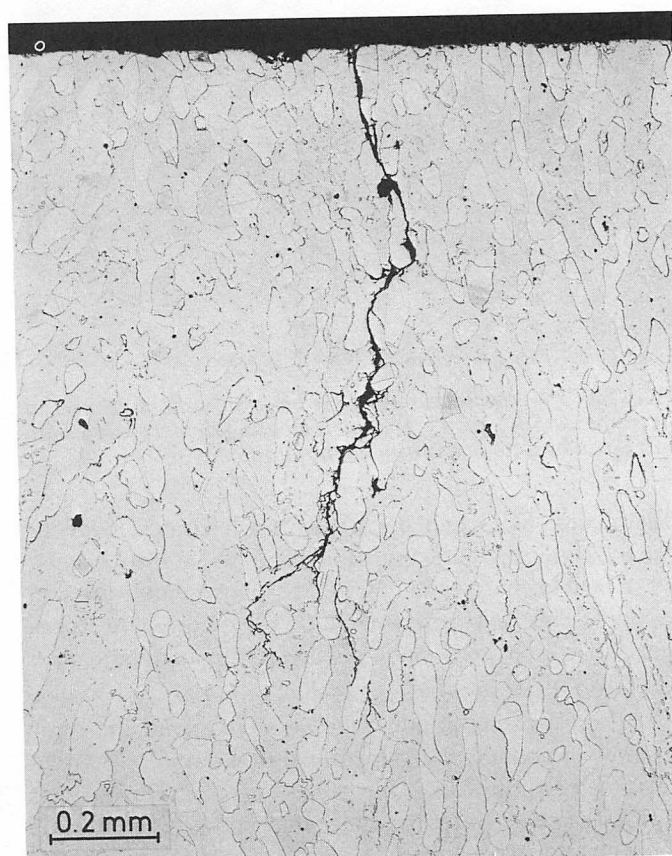
b. Micrograph showing transgranular cracking.

FIGURE 30—*Stress corrosion cracking in the tubesheet made of ferritic-austenitic stainless steel AFNOR Z5CNDU 21-08.*

a. Macrograph.



b. Transgranular cracking at higher magnification.

*FIGURE 31—Stress corrosion cracking of tube of austenitic stainless steel SIS 2343.*

After four months of discontinuous operation, no indication of stress corrosion cracking of heat exchanger 1 could be found. In addition to the cracks observed on the Type 321 tubesheet of heat exchanger 2, stress corrosion cracks were found in the austenitic stainless steels Type 321 and 18 Cr-10 Ni-2.5 Mo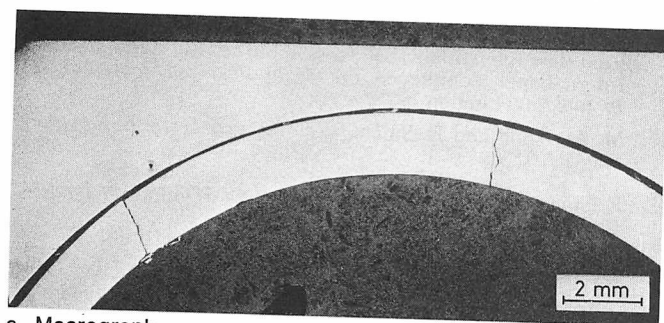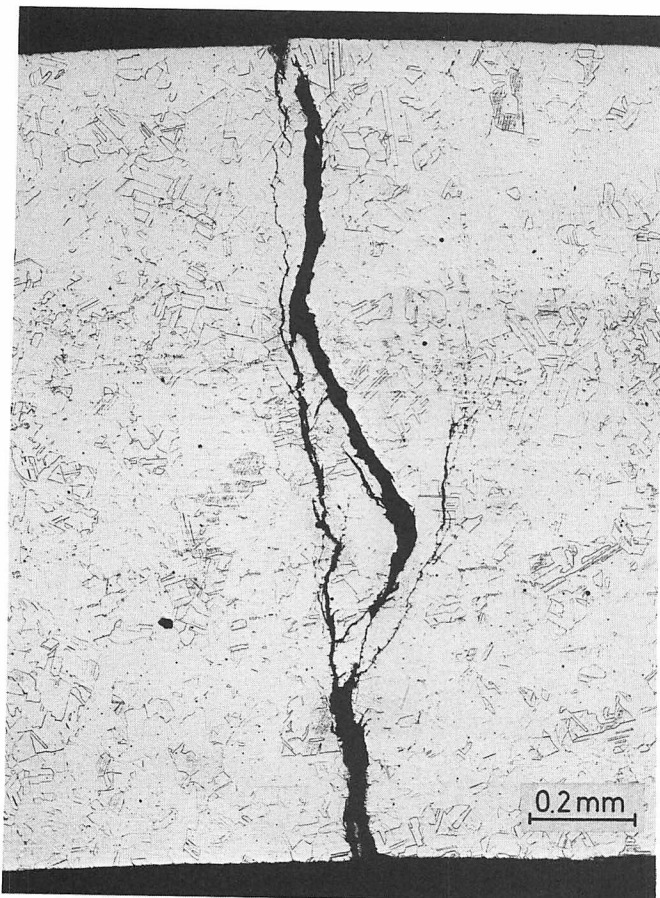 (titanium stabilized). The 18 Cr-2 Mo tubes and the second tubesheet of this heat exchanger (fabricated by applying an 18 Cr-2 Mo weld overlay) were crack free. Heat exchanger 3 showed stress corrosion cracking of the ferritic-austenitic AFNOR Z5CNDU 21-08 tubesheet (Figures 30a and b). The same held true for the austenitic SIS 2343 tubes (Figures 31a and b) as well as for the Type 316 shell plates (Figures 32a and b). The 18 Cr-2 Mo tubes remained crack free.

## Conclusions

The ferritic stainless steel 18 Cr-2 Mo has been shown to be suited for applications in cooling water systems which have a chloride content of 400 ppm. No stress corrosion cracking and no pitting corrosion occurs under such conditions at the temperature investigated in autoclave and heat exchanger experiments (130 C, 265 F). Provided this steel is sufficiently resistant to the product to be cooled, it is an alternative to austenitic steels when stress corrosion cracking is likely to occur. Tubes with a wall thickness up to 3 mm (0.12 in.) have sufficient toughness. Tubesheets can be made of boiler plate protected by an explosive cladding or a weld overlay of 18 Cr-2 Mo. A combination of Type 304 stainless steel and 18 Cr-2 Mo is possible. This means in practice that Type 304 tubes that failed by stress corrosion cracking, can be replaced by 18 Cr-2 Mo tubes.

## Acknowledgment

## References

1. A. P. Bond and E. A. Lizlovs, *Werkstoffe und Korrosion, 21* (5), 1970, 336.

2. A. P. Bond, H. P. Dundas, O. Jarleborg and W. Schmidt, *DFBO-Mitteil, 24* (5), 1973, 86.

3. W. A. Matejka and R. J. Knoth, "E-Brite 26-1-The High-Purity Approach to High-Chromium Ferritic Stainless Steels." ASTM Symposium, 1973, Bal Harbour, Florida.

4. R. J. Knoth and W. A. Matejka, "E-Brite 26-1, A New Stainless Steel for Chemical Process Equipment," Corrosion 74 (NACE), 1974, Chicago, Illinois.

5. N. Pesall and J. I. Nurminen, *Corrosion, 30* (11), 1974, 381.

6. L. Troselius, *Br. Corr. J., 10* (4), 1975, 174.

7. Ch. Åslund and K.-E. Jonsson, "Die neuen titanstabilisierten ferritischen Chromstähle." Gränges Nyby Stahl GmbH, 1976.

8. Ch. Åslund and W. Schmidt, *Ingenieur Digest, 15* (5), 1976, 57.

9. L. Rademacher, J. Baurmann and J. Kubisch, *TEW-Technische Berichte, 2* (1), 1976, 19.

10. O. H. Jarleborg, J. M. Sawhill and R. F. Steigerwald, *Stahl u. Eisen, 97* (1), 1977, 29.

11. R. F. Steigerwald, A. P. Bond, H. J. Dundas and E. A. Lizlovs, *Corrosion, 33* (8), 1977, 279.

12. O. H. Jarleborg, "Ein neuer rostfreier Stahl mit Zukunft 18 Cr-2 Mo." Climax Molybdenum GmbH, 1977.

13. *Stainless Steel '77,* Climax Molybdenum Company, 1977.

14. Anon., "X 1 CrNiMoNb 28 4 2—als Superferrit ein neuer Sonderstahl mit hoher allgemeiner Korrosionbeständigkeit, insbesondere für Beanspruchungen in chloridreichen Lösungen." *Thyssen Edelstahl, Techn. Berichte, 5* (1), 1979.

15. Anon., "Schweißen von Nyby ELI-T-Stählen." Gränges Nyby Stahl GmbH, Düsseldorf.

16. J. Hammond and R A. E. Hooper, "The Weldability of stabilized (low interstitial) 18% Cr-2% Mo ferritic stainless steel," International Conference *Trends in steels and consumables for welding*, London 1978.

17. M. Areskong and E. Smårs, *Welding and Metal Fabrication,* May 1976.

18. E. Smårs and G. Bachström, *Exploiting Welding in Production Technology, 1,* London, 1975.
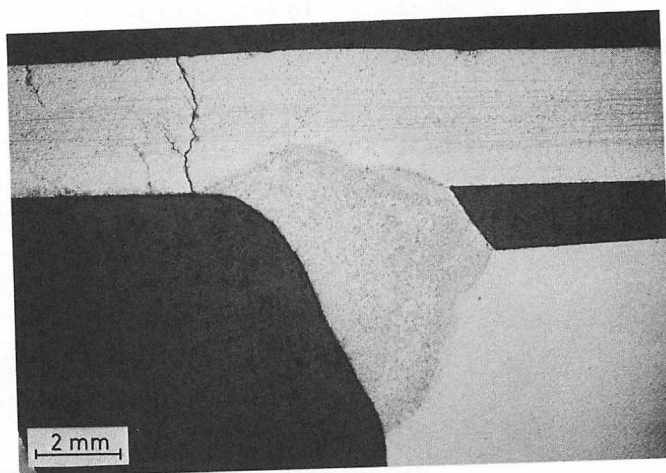
a. Macrograph.
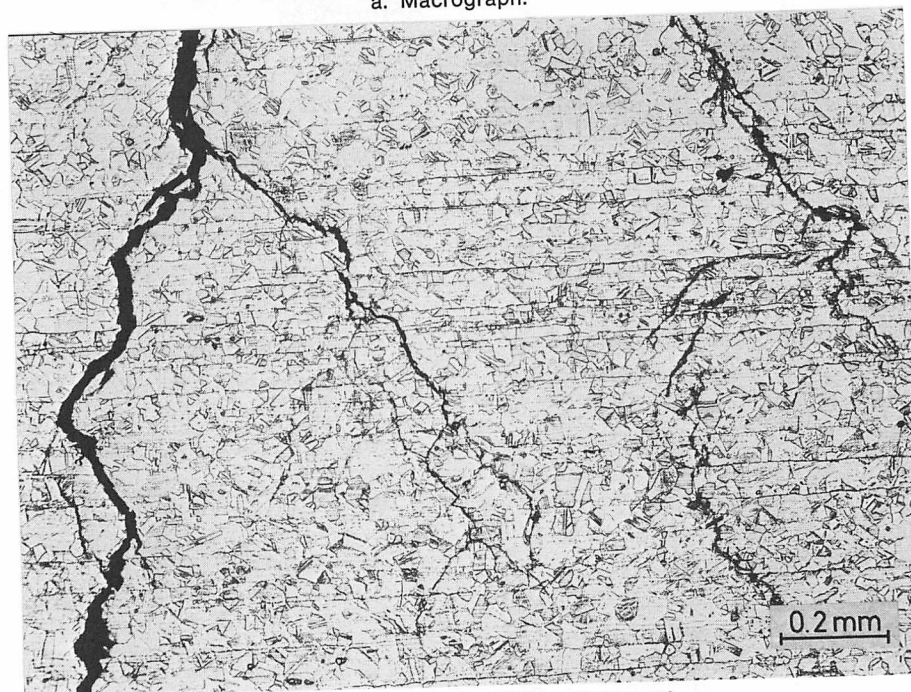


b. Micrograph showing transgranular cracking.

FIGURE 32—*Stress corrosion cracking of shell plate of austenitic stainless steel AISI Type 316.*

# Discussion

G. R. PRESCOTT, *C. F. Braun & Company.* A cooling water temperature of 130 C (265 F) is rather high. Why was this temperature selected?

H. SPÄHN. It is an operational range that we encounter. Also, for the purpose of alloy evaluation, if the temperature is low, say 60 C (140 F) there is no stress corrosion cracking on any austenitic stainless steel.

M. WEISZ, *Centre d'Etudes Nucleaires.* In the stress corrosion evaluation in heat exchangers, what is the nature of the stresses? Also, you stated that there was no stress corrosion of Type 321 stainless in combination with the ferritic stainless steels, but your Figures 15 and 16 appear to contradict that.

H. SPÄHN. The stresses were residual from welding and fabrication. Regarding stress corrosion, the two cases represent different conditions, one in magnesium chloride and the other in Rhine River water. In the former, the pH at the boiling temperature of 146 C (295 F) is about 1.5. Under these aggressive conditions, the 18% Cr-2% Mo ferritic steel corrodes at a measurable rate and cathodically protects the austenitic steel. This does not happen in the Rhine River water which has a pH of 7 to 7.5.

# Material Problems in the Hydrocarbon Processing Industries

by G. R. Prescott
C. F. Braun & Co.

Problems associated with the interaction of hydrogen and metals are generally well known to metallurgists and corrosion experts. The literature on this subject is extensive and reflects a continuing effort to gain more insight into the many ways that hydrogen can cause problems. In spite of this, hydrogen-related failures continue to occur in the hydrocarbon processing industry.

In recent years, the temper embrittlement of 2¼ Cr-1 Mo and 3 Cr-1 Mo has become a metallurgical phenomenon of considerable concern to users of high pressure, thick wall vessels. It has long been known that some change in mechanical properties invariably occurred as a result of operating for long periods in the 260 to 540 C (500 to 1000 F) range. While the overall effect was believed to be within acceptable limits, the results of recent research prove otherwise.

## Hydrogen Attack

Hydrogen attack is generally defined as an internal chemical reaction between hydrogen and metal carbides to form methane gas. Methane cannot diffuse out of the steel, and the accumulated gas eventually produces fissures or blisters. The combined action of decarburization and fissuring results in severe loss of strength and ductility. This irreversible damage was first observed during the development of the Haber synthetic ammonia process in 1908 in Germany. Bosch[1] described
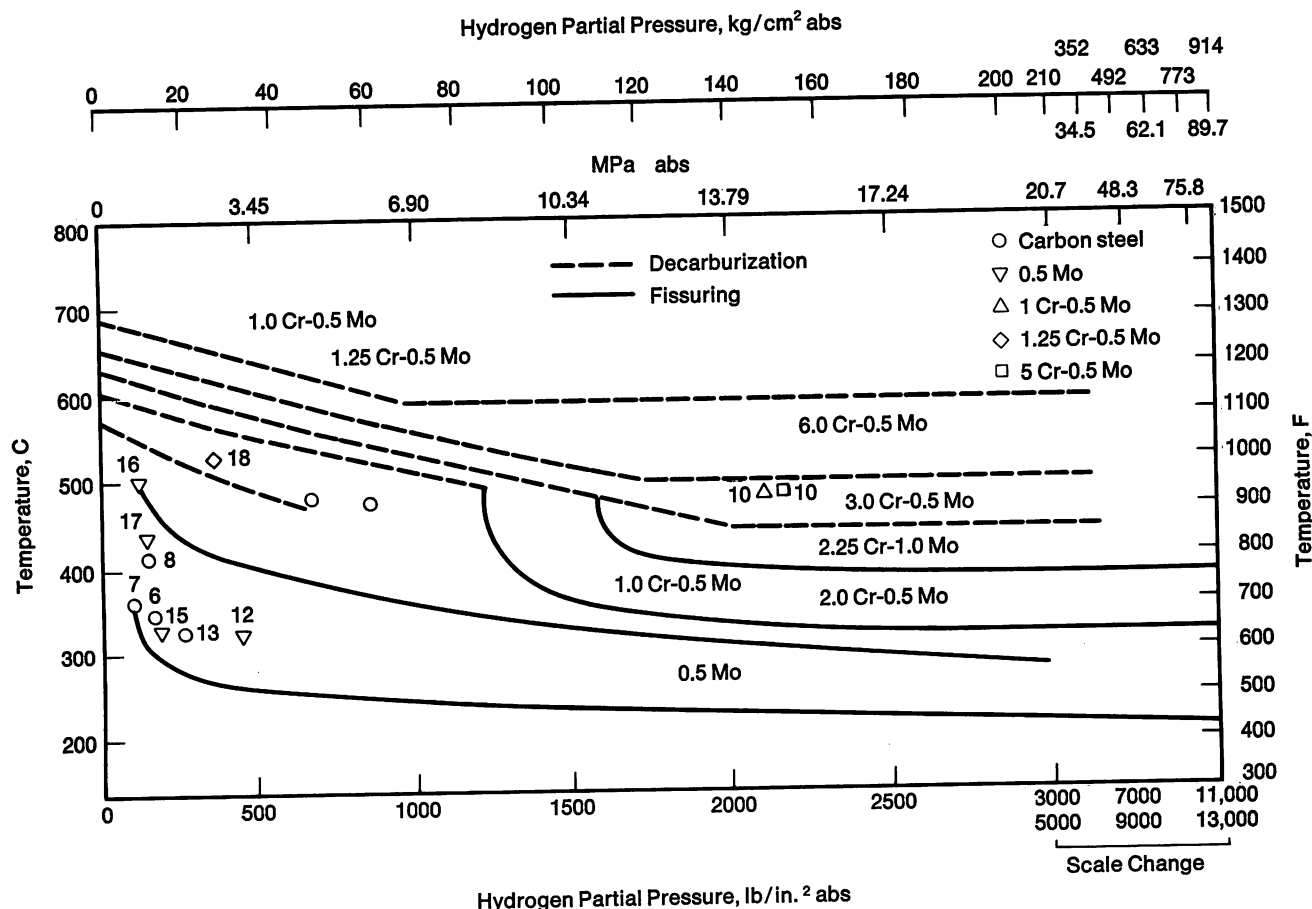


FIGURE 1—Nelson curve defining safe upper limits for steels in hydrogen service.

in detail the various forms of attack in 1933.

Since these early days, a tremendous amount of work has been done to define the safe limits of application for carbon and alloy steels. George Nelson assembled and correlated this information into the well-known and widely used Nelson curves reproduced in Figure 1. The curves define the safe upper limit for carbon and low alloy steels in hydrogen service in terms of hyrogen partial pressure and temperature. These curves provide a fairly reliable basis for selecting steels for hydrogen service. Today, these curves are revised as needed by the American Petroleum Institute and issued as API Publication 941.

Our major problem with hydrogen attack is the inadvertent use of the wrong alloy or weld rod which results in a component or weld susceptible to hydrogen attack and subsequent failure. This type of metal deterioration is very insidious, since no outward change in appearance occurs, and it cannot be detected by conventional inspection tools. For these reasons, most companies have resorted to the relatively new portable spectrographic metal analyzers during the fabrication stage to make sure each weld and component has the proper alloy content. Based on experience to date, this precaution has prevented many unexpected and dangerous failures.

A less serious problem is the present temperature limitations on 2¼ Cr-1 Mo and 3 Cr-1 Mo alloys. In ammonia plants and hydrocrackers, we are operating at hydrogen partial pressures in the range of 10 MPa (1500 psi) to 17 MPa (2500 psi). Vessels currently designed and fabricated from these alloys weigh 500 to 1000 metric tons with wall thicknesses up to 300 mm (12 in.) or more. It would be useful to have more supporting data establishing the upper temperature limit of these alloys. It would also be useful to investigate the possible extension of the upper temperature limit by the addition of minor amounts of strong carbide forming elements such as titanium, tantalum or tungsten.

## Hydrogen Embrittlement

Our current practice is to limit the strength of alloy steels to 690 MPa (100 ksi) in vessels for high pressure, high temperature hydrogen service. This is a costly restraint, and it is imposed as a result of the interaction of hydrogen with the steel to produce embrittlement and subsequently a delayed fracture. From a mechanical and metallurgical standpoint, it would be a simple matter to design and fabricate vessels based on 827 MPa (120 ksi) minimum tensile strength, or even 896 MPa (130 ksi) minimum. No new technology would be required, and the vessel wall thickness would decrease by about one-third. This represents a substantial savings in resources and effort when considering vessels with wall thicknesses in

the range of 250 to 380 mm (10 to 15 in.). The sole reason for this limitation is hydrogen and its deleterious effect on the higher strength steels.

High pressure, high temperature hydrogen is only one source of hydrogen that must be considered. Another common and potent source is from wet hydrogen sulfide. This acid solution produces hydrogen atoms on the metal surface, and the sulfides somehow promote the entry of atomic hydrogen into the steel, rather than the combination of these atoms to form harmless molecular hydrogen gas. The petroleum industry has considerable experience with broken valve and pump components made from high strength alloys, broken bolts and cracked welds in pipe and pressure vessels.

The weld cracking problem occurs mostly on carbon steel where alloy electrodes were inadvertently used, or in multipass submerged-arc welds made with fluxes designed for single-pass welds. These fluxes, when improperly used, build up excessive manganese and silicon contents and produce relatively hard, high strength welds susceptible to cracking in wet sulfides. It is common practice to limit the hardness of weld deposits to HB 200. Based on the rule of thumb that the tensile strength is equal to the Brinell hardness times 500, we are back again to the same 685 MPa (100 ksi) tensile strength upper limit for aqueous sulfides as we have for high pressure, high temperature hydrogen.

The effect of hydrogen on high strength steel is demonstrated in Figure 2. This set of curves appears in many publications[2] because it demonstrates the essential features of delayed fracture caused by hydrogen. The reduction in notched strength is severe, from 2068 MPa (300 ksi) to 517 MPa (75 ksi), and the fractures occur with nil ductility. It further demonstrates that complete reversibility occurs if the steel is sufficiently outgassed.

Figure 3 is another well-known set of curves[3] that shows the effect of hydrogen embrittlement and delayed
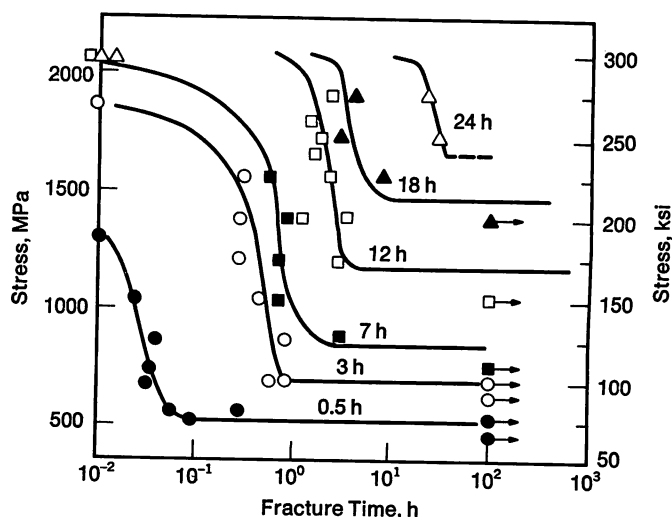
FIGURE 2—Static fatigue curves for various concentrations corresponding to different baking times at 150 C (300 F).
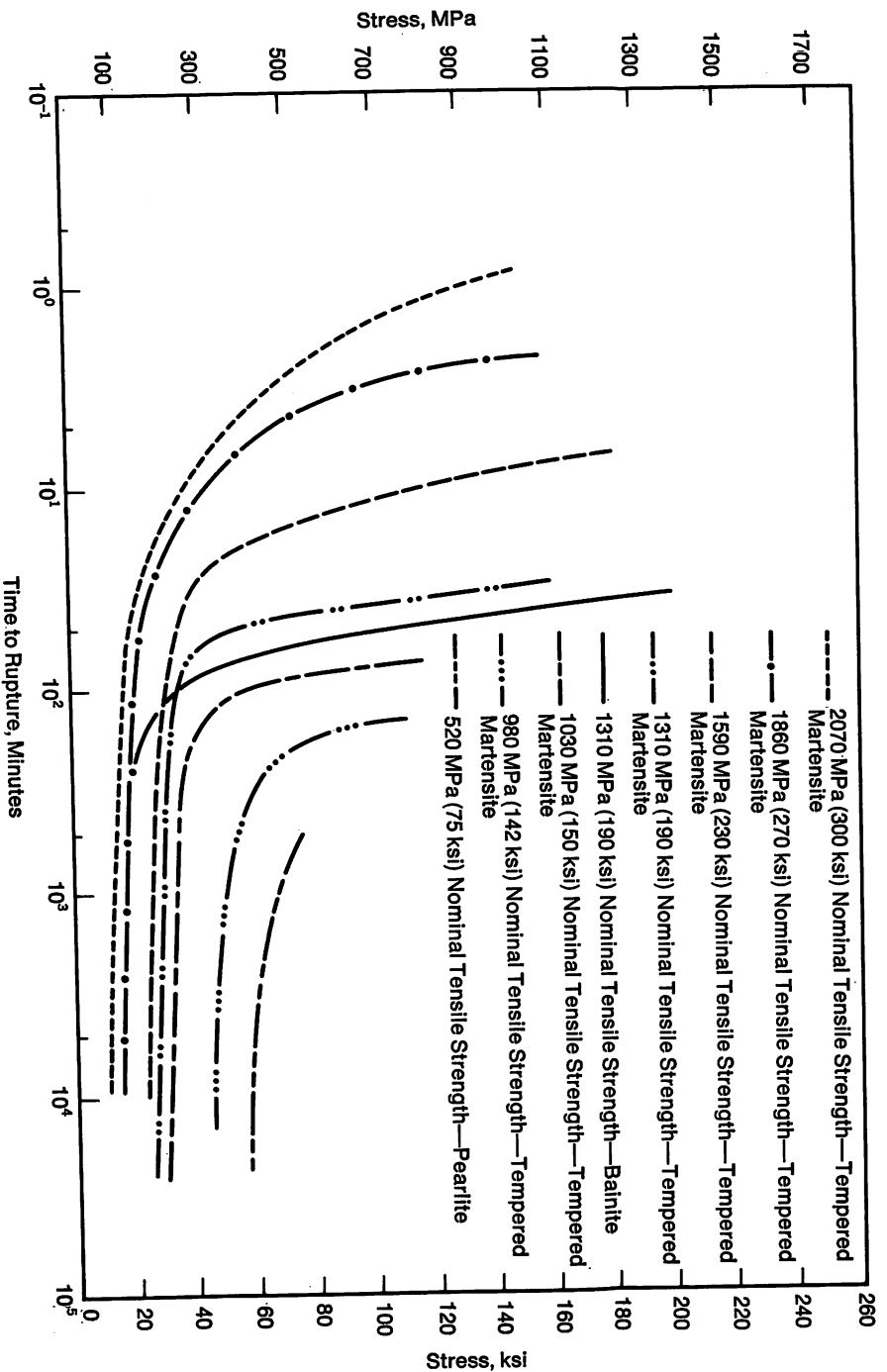
FIGURE 3—*Delayed failure characteristics of unnotched specimens of an SAE 4340 steel during cathodic charging with hydrogen under standardized conditions.*

BATTELLE CHARGING CONDITION A:

Electrolyte:  4% $H_2SO_4$ in water

Poison:  5 drops per liter of cathodic poison composed of 2 g phosphorus dissolved in 40 ml $CS_2$

Current density:  1.2 mA/cm² (8 mA/in.²)

Legend:
- 2070 MPa (300 ksi) Nominal Tensile Strength—Tempered Martensite
- 1860 MPa (270 ksi) Nominal Tensile Strength—Tempered Martensite
- 1590 MPa (230 ksi) Nominal Tensile Strength—Tempered Martensite
- 1310 MPa (190 ksi) Nominal Tensile Strength—Tempered Martensite
- 1310 MPa (190 ksi) Nominal Tensile Strength—Bainite
- 1030 MPa (150 ksi) Nominal Tensile Strength—Tempered Martensite
- 980 MPa (142 ksi) Nominal Tensile Strength—Tempered Martensite
- 520 MPa (75 ksi) Nominal Tensile Strength—Pearlite

fracture on an alloy steel heat treated to strength levels from 517 MPa (75 ksi) to 2068 MPa (300 ksi). At 979 MPa (142 ksi), the effect of hydrogen induced by cathodic charging on unnotched specimens is still severe. Even at 517 MPa (75 ksi), some reduction in tensile strength is evident.

The foregoing data utilized the common laboratory practice of cathodically charging specimens with hydrogen. This technique is quick and effective, but it does not represent exposure conditions encountered in operating plants. Rocketdyne[4] changed the test environment and reported the results of tests in 69 MPa (10,000 psi) helium and 69 MPa (10,000 psi) hydrogen on pressure vessels steels, all at ambient temperature. Steels such as A-302 in unnotched specimens showed little change in properties. Notched specimens showed a significant decrease in reduction of area and a slight decrease in tensile strength. High strength steels were severely embrittled. The machined notch used in these experiments was not particularly sharp.

In 1974, U.S. Steel[5] tested a number of steels in high pressure hydrogen, including several pressure vessel steels. Wedge opening loading (WOL) specimens were used with precracks induced by fatigue. The test environment was hydrogen at ambient temperature, ranging in pressure from 20 MPa (3000 psi) to 96 MPa (14,000 psi). Applying the rules of fracture mechanics, the results showed that steels up to 690 MPa (100 ksi) were resistant to the effects of hydrogen (see Table I). Over that strength level, the critical flaw depth decreased with strength from 33% to 2% of thickness in 41 MPa (6000 psi) hydrogen. The results of this work tend to substantiate the 690 MPa (100 ksi) upper limit applied to pressure vessels in high pressure hydrogen.

Several years ago, extensive cracking developed in the closing girth seam of an ammonia converter. The converter developed a leak in this 125 mm (5 in.) thick weld after three years of operation. The plant was shut down without any undue damage or problem.

Examination of this weld disclosed that the crack continued around the full 360 degrees of the inside surface (see Figure 4a for typical appearance). The crack

**Table I**—Values of $K_H$ for Steels Exposed to Hydrogen at Various Pressures

| Grade | Tensile Strength, MPa | (ksi) | Yield Strength, MPa | (ksi) | Critical Flaw Depth, Percent of Member Thickness 21 MPa (3 ksi) | 41 MPa (6 ksi) | 69 MPa (10 ksi) |
|---|---|---|---|---|---|---|---|
| Resistant Steels | | | | | | | |
| A516 | 572 | (83) | 290 | (42) | — | — | (50)* |
| A106 | 558 | (81) | 345 | (50) | — | — | — |
| HY-80 | 690 | (100) | 586 | (85) | — | — | (50)* |
| Steels with Moderate Susceptibility | | | | | | | |
| A372, N&T | 814 | (118) | 586 | (85) | 41 | 33 | 31 |
| A372, Q&T-1100 | 807 | (117) | 600 | (87) | 34 | 25 | — |
| 4130, Q&T-1175 | 820 | (119) | 634 | (92) | 43 | 32 | 9 |
| 4145, Q&T-1100 | 896 | (130) | 669 | (97) | 31 | 28 | 24 |
| 4147, Q&T-1235 | 903 | (131) | 724 | (105) | 43 | 41 | — |
| A517 Grade F | 834 | (121) | 758 | (110) | 41 | 31 | 33 |
| 4147, Q&T-1200 | 958 | (139) | 779 | (113) | 50 | 12 | |
| Steels with Appreciable Susceptibility | | | | | | | |
| 4147, Q&T-1170 | 1007 | (146) | 869 | (126) | 8 | 5 | — |
| HY-130 | 986 | (143) | 938 | (136) | 8 | 6 | 3 |
| 4145, Q&T-1050 | 1130 | (164) | 1055 | (153) | 2 | 2 | — |

\* Crack propagation did not occur. The values in parentheses are based on the highest initial stress intensity, $K_o$.

on the inside surface did not show any evidence of ductility. The crack penetrated through the weld metal for a distance of 460 mm (18 in.) on the outside surface. The crack on the outside surface exhibited a limited amount of ductility, as shown in Figure 4b.

The brief investigation strongly indicated that the crack occurred in the closing seam because of inadequate postweld heat treatment. The scheduled heat treatment was 565-595 C (1050-1100 F) for five hours. The other weld seams received this heat treatment in a furnace, and no cracks were found in these welds. The closing weld was locally postweld heat treated, using a technique that did not effectively penetrate the full wall thickness. The outside surface reached 595 C (1100 F), but subsequent tests indicated that the inside surface reached only about 510 C (950 F).

These circumstances produced a relatively high strength weld at the inside surface, estimated at about 965 MPa (140 ksi), exposed to high pressure hydrogen at moderate temperatures of less than 150 C (300 F). The exposure of this high strength weld to hydrogen produced extensive cracking. It is not known whether the



a. Typical brittle appearance of crack on inside surface.
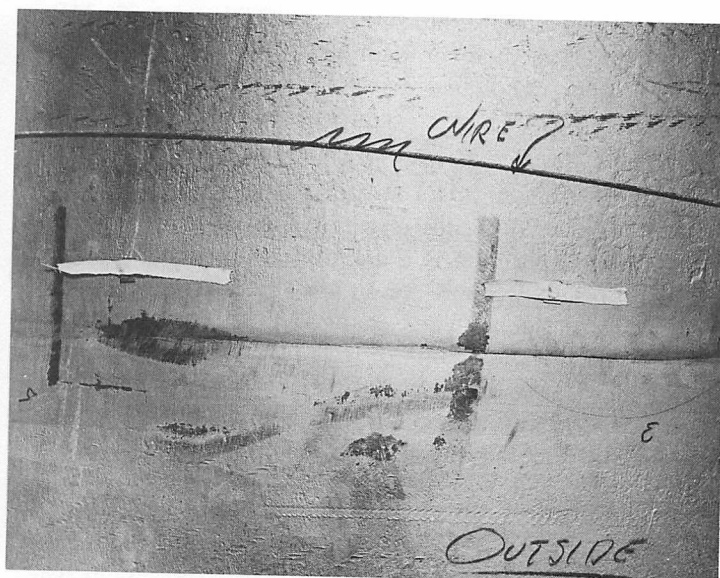


b. Crack shows some ductility on outside surface.

*FIGURE 4—Cracks in ammonia converter.*

weld started with a significant crack not revealed by radiography at the fabrication stage, or whether a crack was initiated and subsequently grew to the final size. The object lesson from this case history is to establish the effectiveness of the proposed local postweld heat treat procedure, especially on thick wall vessels.

## Temper Embrittlement

In the petroleum industry, Cr-Mo alloys are used in high pressure, high temperature hydrocrackers, hydro-sulfurizers and catalytic reforming vessels. In the fertilizer industry, critical ammonia plant equipment is also constructed of Cr-Mo alloys. The hydrogen conditions of temperature and partial pressure generally require the use of 2¼ Cr-1 Mo or 3 Cr-1 Mo. In addition to their resistance to hydrogen, these alloys exhibit good high temperature mechanical strength. It has been demonstrated by various fabricators that plate or forgings up to 375 mm (15 in.) thick can be successfully heat treated to the appropriate strength level, currently 517 MPa (75 ksi) to 690 MPa (100 ksi), and fabricated into pressure vessels weighing up to 1200 metric tons.

The many years of successful experience on literally hundreds of 2¼ Cr-1 Mo vessels give both the designer and user of these vessels a high degree of confidence. Until about 1965, all 2¼ Cr-1 Mo vessels built to ASME Code were based on the annealed condition of 414 MPa (60 ksi) minimum tensile. After that, the Code established the so-called normalized-and-tempered condition with a tensile strength in the range of 517 MPa (75 ksi) to 690 MPa (100 ksi).

Temper embrittlement of alloy steels is manifested by an upward shift in transition temperature, and the problem has been around for more than 50 years. Most of the early work on temper embrittlement was related to Ni-Cr and Ni-Cr-Mo steels used for steam turbine rotor forgings. McMahon[6] summarized the state-of-research in 1968 as follows:

1. Only alloy steels are susceptible. Carbon steels do not embrittle.

2. The temperature range for embrittlement is from 345 to 565 C (650 to 1050 F). Embrittlement is reversible by heating for short times above 565 C (1050 F).

3. Temper embrittlement is manifested by an upward shift in the ductile-brittle transition temperature.

4. The cause of embrittlement is segregation of Mn, Si, P, Sn, Sb and As in the grain boundaries.

In the early seventies, articles began to appear dealing with the susceptibility of 2¼ Cr-1 Mo steel to temper embrittlement. Bruscato[7] demonstrated the effect of weld metal chemistry (see Figure 5) on Charpy V-notch
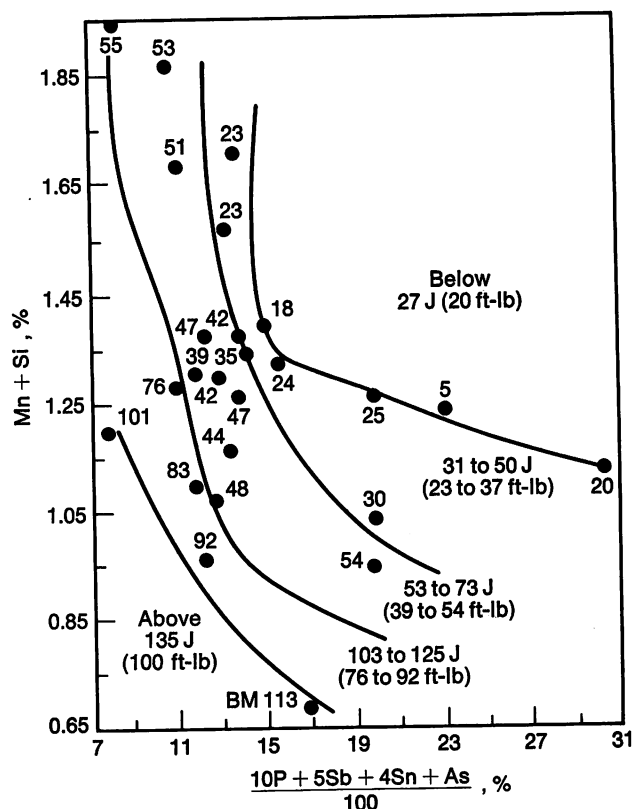
FIGURE 5—Effect of chemistry on 10 C (50 F) Charpy V-notch impact energy of step cooled 2¼ Cr-1 Mo manual weld metal.
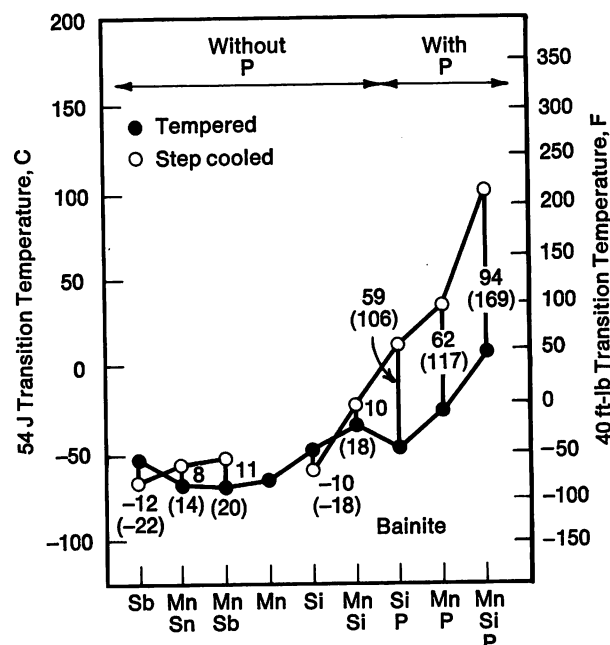
FIGURE 6—Effect of various elements on temper embrittlement of 2¼ Cr-1 Mo.

impact strength at 10 C (50 F). With low tramp elements and low Mn plus Si, high toughness was achieved. The step cooling treatment is a time-temperature treatment designed to promote embrittlement.

McMahon[8] demonstrated the potent influence of phosphorus by using high purity 2¼ Cr-1 Mo vacuum

melts doped with Mn, Si, P, Sn and Sb. The results are shown in Figure 6.

A very disturbing paper was presented in 1974 by investigators at Japan Steel Works.[9] A desulfurizer reactor, after 30,000 hours of service at temperatures between 330 and 430 C (630 and 810 F), developed cracks at the base of a Type 347 stainless weld joining a 321 support bar to the Type 347 overlay. The cracks, which propagated from the overlay into the base metal, were removed and repaired. While attempting a local stress relief on the repairs, three major brittle fractures propagated about halfway around the vessel circumference, accompanied by loud noises.

Subsequent examination of this vessel proved that the 54 J (40 ft-lb) transition temperature of metal near the inside surface was 40 C (105 F). By deembrittling and

testing, it was concluded that the 54 J (40 ft-lb) transition temperature had shifted upward by about 100 C (180 F). In this same paper, thirty-eight heats of $2\frac{1}{4}$ Cr-1 Mo were correlated with a J factor parameter equal to $(Si + Mn) (P + Sn) \times 10^4$. Figure 7a shows an excellent correlation between the 54 J (40 ft-lb) transition temperature and the parameter. Figure 7b shows another correlation between the shift in FATT and 54 J (40 ft-lb) transition temperature with the parameter.

The Japanese steelmakers immediately applied the necessary controls to their steelmaking process, and offered steels with a maximum J factor of 200. For this reason, Japan has been the primary source of steel and pressure vessels where temper embrittlement control was desired. In actual production heats, the J factor normally is 100 or less. During the last couple of years, another control option has been negotiated with European steelmakers. They will guarantee a 54 J (40 ft-lb) transition temperature of −40 C (−40 F) on plates and forgings after the step cooling treatment shown in Figure 8.

Control of residual elements and manganese plus silicon is only part of the problem in achieving a vessel with good toughness. Figure 9 shows the effect of aus-
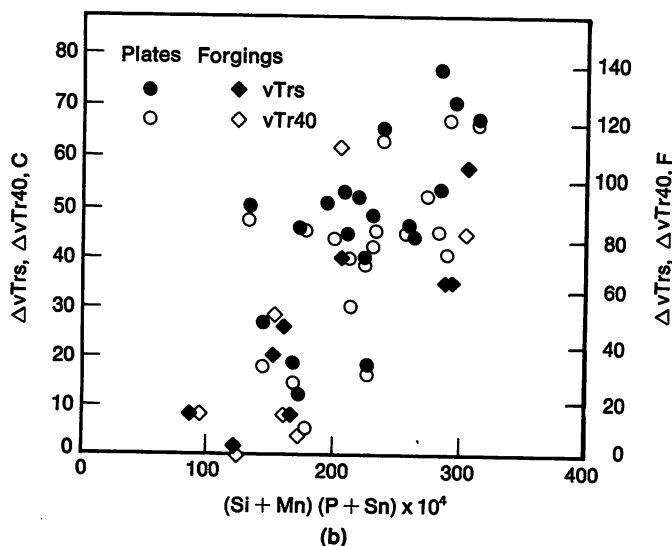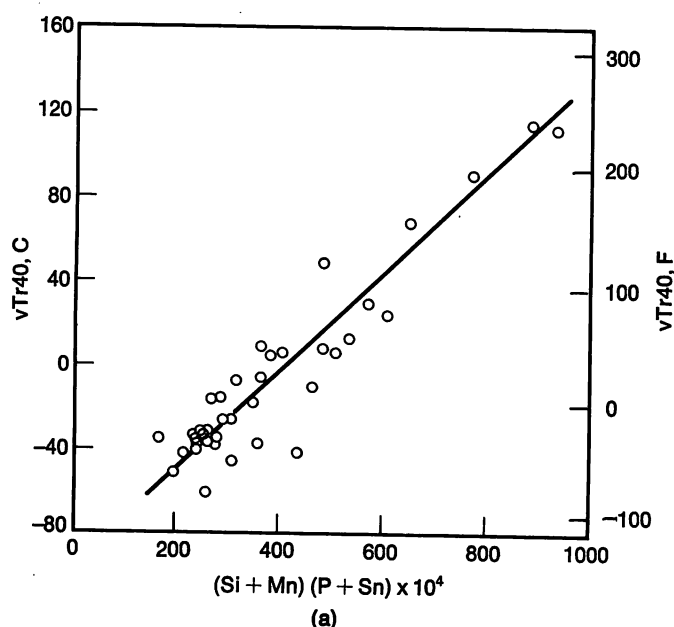


FIGURE 7—Relationship between transition temperature shifts by step cooling and embrittlement factor (J-factor) on $2\frac{1}{4}$ Cr-1 Mo steel.
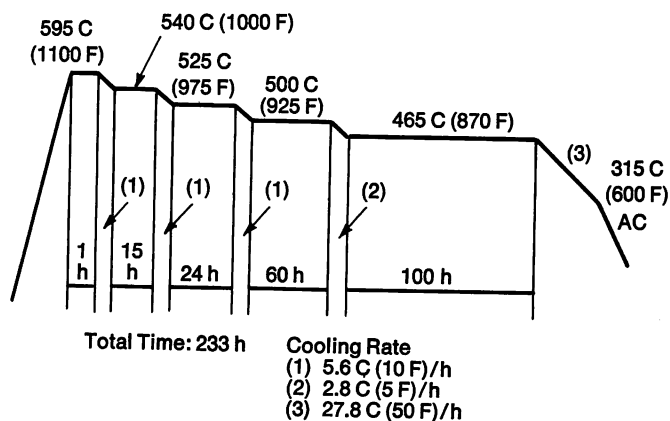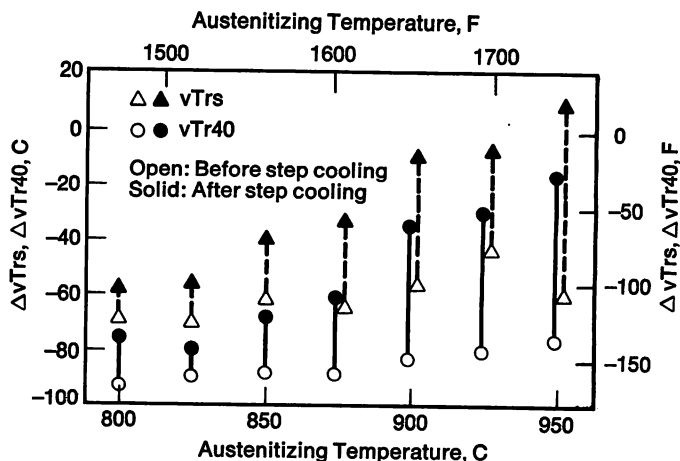


FIGURE 8—Step cooling treatment.



FIGURE 9—Variation of transition temperatures before and after step cooling with austenitizing temperatur on $2\frac{1}{4}$ Cr-1 Mo steel.

tenitizing temperature on shift in transition temperature. As might be expected, the larger the austenite grain size, the greater the upward shift in transition temperature.[10] Also the cooling rate, which determines transformation products, influences the initial transition temperature and change in transition temperature,[11] as shown in Figure 10.

Takahashi[12] showed that proper selection of tempering parameters for both tempering and postweld heat treatment is very important as shown in Figure 11. If the proper combination of time and temperature is not used, the shift in the transition temperature can be excessive.

The final correlation[13] in this series (see Figure 12) shows the strong influence of molybdenum content on the initial FATT. Figure 13 also shows the effect of molybdenum.[14] At 2% Cr, 0.5% Mo produces the smallest shift, but 1% Mo yields the lowest initial transition temperatures. Possibly this alloy could benefit from some optimization studies in alloy content.

## Combined Effects of Hydrogen and Temper Embrittlement

Very little work has been done on the combined effects of hydrogen and temper embrittlement. Some work is beginning to appear in unpublished internal reports of Japanese fabricating companies, such as Figure 14 by Kobe investigators.[15] The advantages gained by carefully selecting the tempering parameter are completely lost when the steel is charged with 4 ppm of hydrogen.

Mitsubishi also field tested a submerged arc weld for one year in a reforming unit. The results (Table II)[16] show that the postweld heat treated 54 J (40 ft-lb) transition temperature of −34 C (−30 F) is raised to 78 C



FIGURE 10—*Variation of transition temperature before and after step cooling with cooling rate from austenitizing temperature on 2¼ Cr-1 Mo steel.*



$$P = T (\log t + 20)$$
$$T = \text{Temp (K)}$$
$$t = \text{Time (h)}$$
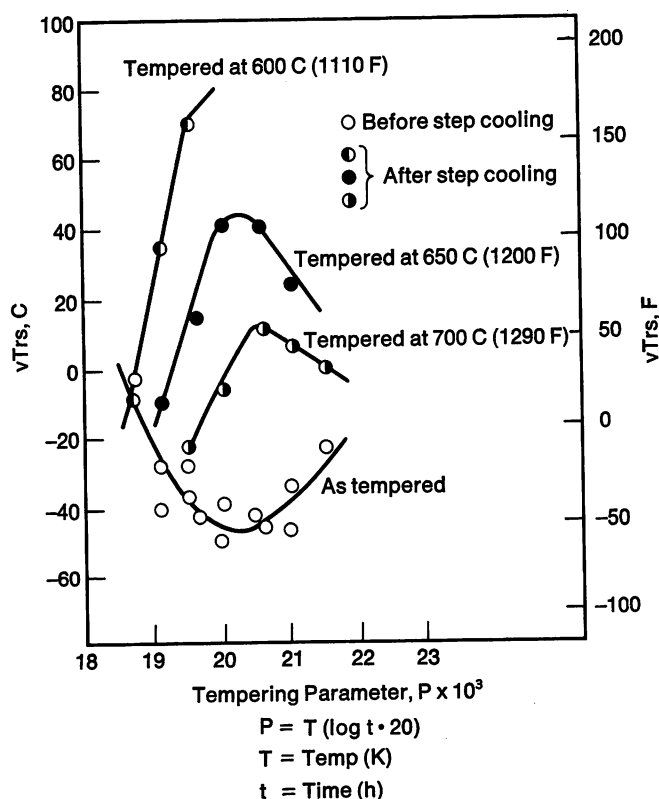
FIGURE 11—*Effect of tempering temperature on fracture appearance transition temperature before and after step cooling on 2¼ Cr-1 Mo steel.*



FIGURE 12—*Effect of Mo content on temper embrittlement susceptibility of 2¼ Cr steel (0.32-0.42% Si, 0.60-0.72% Mn, 0.019-0.022% P, 0.006-0.010% Sn, 0.1-0.16% C, 0.18-0.19% Mo, 2.25-2.32% Cr, <0.021% As, <0.0035% Sb).*

FIGURE 13—Effects of alloying element and austenitizing temperature on fracture appearance transition temperature before and after isothermal embrittlement treatment at 500 C (930 F) for 100 hours.
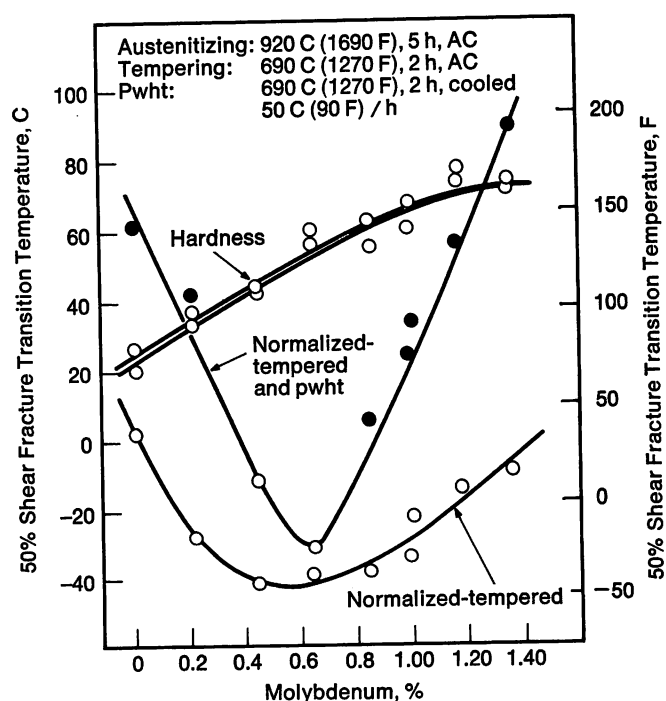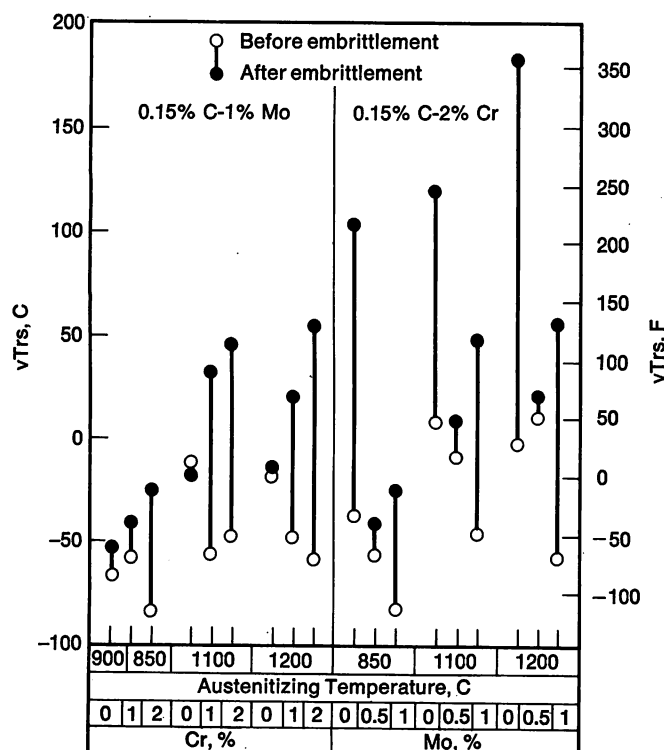


FIGURE 14—Effect of 4 ppm hydrogen and tempering treatment on FATT.

$$P = T\,(\log t \bullet 20)$$
$$T = Temp\,(K)$$
$$t = Time\,(h)$$

(172 F) after the test. Step cooling raised the transition temperature to 26 C (79 F). Thus, the exposure to hydrogen plus reforming temperatures of 450 C (840 F) added 50 C (90 F) to the transition temperature resulting from step cooling only.

## Cyclic Effects in Hydrogen Service

Hydrocarbon processing plants are subjected to a thermal cycle with each shutdown and start-up. Many shutdowns are planned, and the plants come down at a slow controlled rate so that the effect of the thermal cycle is minimized from a mechanical and metallurgical standpoint. Other shutdowns are unplanned, and some plants tend to come down rather hurriedly. This can create problems in thick wall vessels operating in high temperature, high pressure service.

Cooling a thick wall vessel in hydrogen service from the operating temperature supersaturates the metal with respect to hydrogen. The excess hydrogen is trapped in

the metal and tends to collect in discontinuities, such as small cracks or nonmetallic inclusions, and exerts pressures high enough to initiate cracks. In the steel industry, this cracking process is called flaking, and it generally happens during cooling. Steel billets or forgings absorb hydrogen in the furnaces created by the decomposition of water. These billets or forgings develop internal cracks if they are not cooled slowly enough to permit the hydrogen to diffuse out of the metal.

Two papers[17, 18] in recent years have addressed the problem of hydrogen-induced flaking in thick walled vessels as a result of cool-down procedures. The gist of these two papers is summarized in Figure 15, which shows the conditions of hydrogen concentration in the vessel wall from hydrogen diffusing through the wall under normal operating conditions. Note that the hydrogen in solid solution is relatively high at the inside surface, very low at the outside surface, and a straight line relationship is assumed between the two boundary con-

**Table II**—Combined Effect of Temper Embrittlement and Hydrogen Embrittlement on 54 J (40 ft-lb) Transition Temperature

| Welding Process | As PWHT, v Tr 40 | After Step Cooling, v Tr 40 | After One Year in Reformer, v Tr 40 |
|---|---|---|---|
| Submerged Arc Weld Metal | −34 C (−30 F) | 26 C (79 F) | 78 C (172 F) |
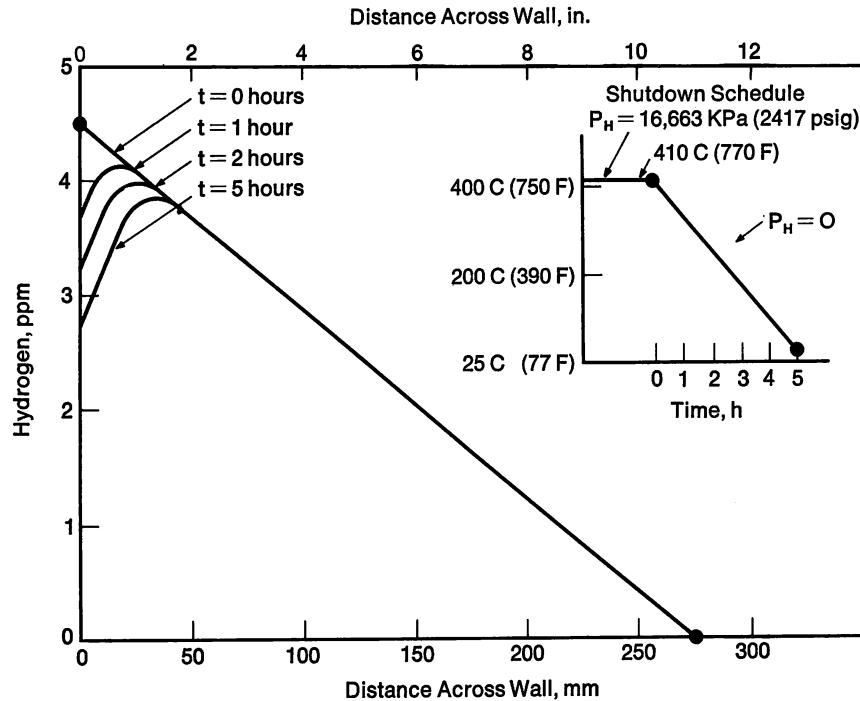
FIGURE 15—Transient hydrogen distribution in the wall during shutdown at a cooling rate of 77 C (138 F)/hour.
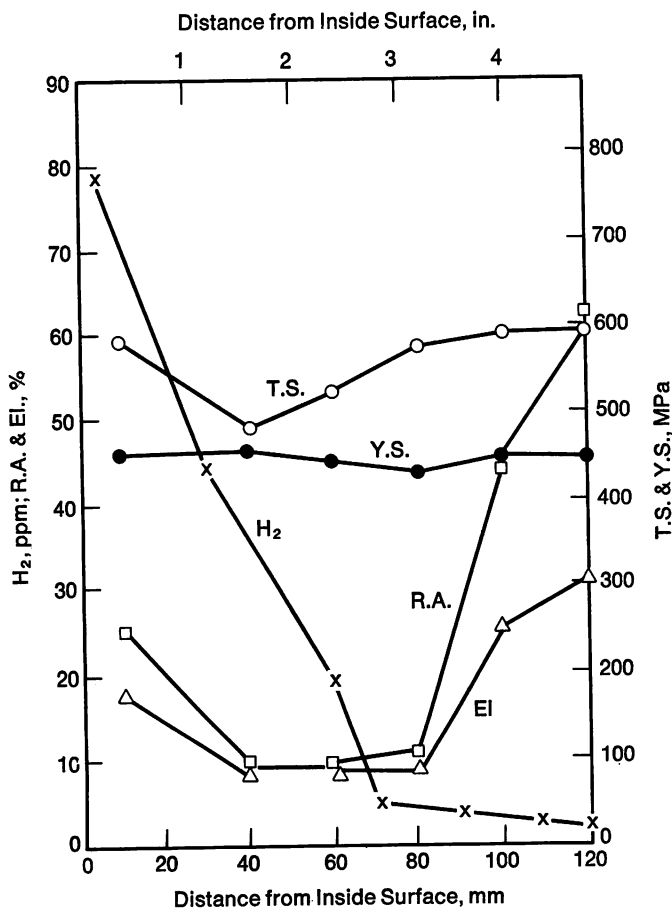


FIGURE 16—Hydrogen content and mechanical properties of ammonia converter used for 10 years. Material: 1 Ni-0.85 Cr, Thickness: 120 mm (4.7 in.), Pressure: 300 kg/cm², Temperature: 400-580 C (750-1075 F).
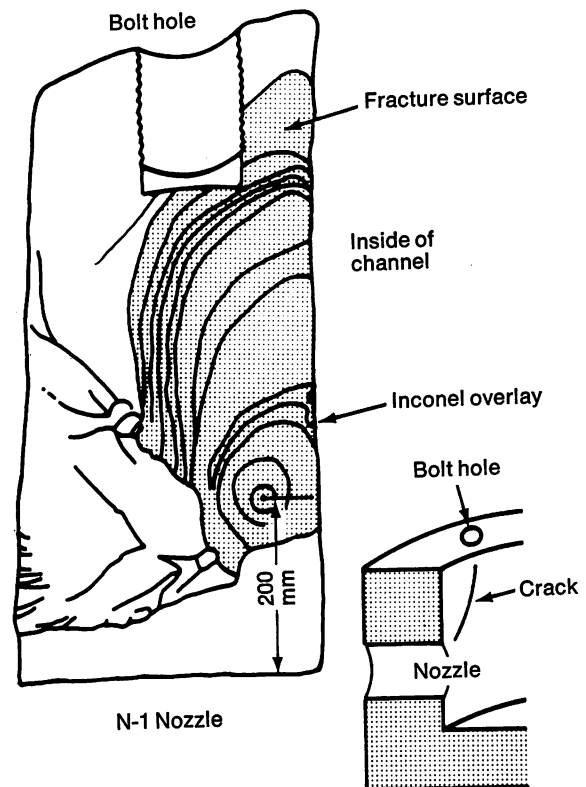


FIGURE 17—Sketch showing location of major cracks in the channel forging of Synloop waste heat boiler.

ditions. A Japan Steel Works report[19] showing hydrogen contents across the 100 mm (4 in.) wall of a 10-year-old ammonia converter tends to support this assumption (Figure 16). When a shutdown occurs, the situation changes in accordance with the changes in temperature and hydrogen partial pressure. For the shutdown schedule shown in Figure 15, the partial pressure of hydrogen

is reduced to zero, and the vessel is cooled at a rate of 77 C/hour (139 F/hour). Note the degree of supersaturation that forms in the time interval of one to five hours. The maximum supersaturation is located about 25 to 50 mm (1 to 2 in.) below the surface, and this is where cracks would tend to originate.

An example of this type of cracking in a heat exchanger channel was reported recently by Asahi Chemical.[20] Figure 17 is a sketch that clearly shows the internal origin and propagation pattern of an internal crack that ultimately reached a bolt hole after three years of service. The 3 Cr-1 Mo forged channel is 375 mm (15 in.) thick. It was ultrasonically tested once by the steel mill supplying the forging, and twice by the fabricator. It is unlikely that original defects of any significant size were missed by these inspections.

The heat exchanger was subjected to a comparatively severe thermal shock during an unscheduled shut-

down. The average cooling rate of the effluent gas is 97 C (175 F) per hour during the first hour, and the channel cracked to the extent shown in Figure 17 after 20 shutdowns.

Another contributing factor to the cracking susceptibility of this forging is temper embrittlement. The investigation established that the 54 J (40 ft-lb) transition temperature was 120 C (250 F) after three years of service at 480 C (895 F). The overall failure appears to be the result of the combined action of hydrogen-induced flaking and temper embrittlement.

Another recent paper[21] describes cracks. that occurred in the outlet forgings of two ammonia converters operating in series. The general configuration and arrangement of the converters is shown in Figure 18. Ammonia synthesis gas enters the inlet nozzle at 400 C (750 F), travels up the annular space between the catalyst container and the shell, then enters the catalyst bed



FIGURE 18—Ammonia converters.

at the top and travels down the catalyst bed to the outlet nozzle. On .Converter A, the outlet gas temperature is 510 C (950 F), and Converter B has an outlet temperature of 480 C (900 F). The hydrogen partial pressure is 12 MPa (1750 psig). The materials of construction are shown in Figure 18.

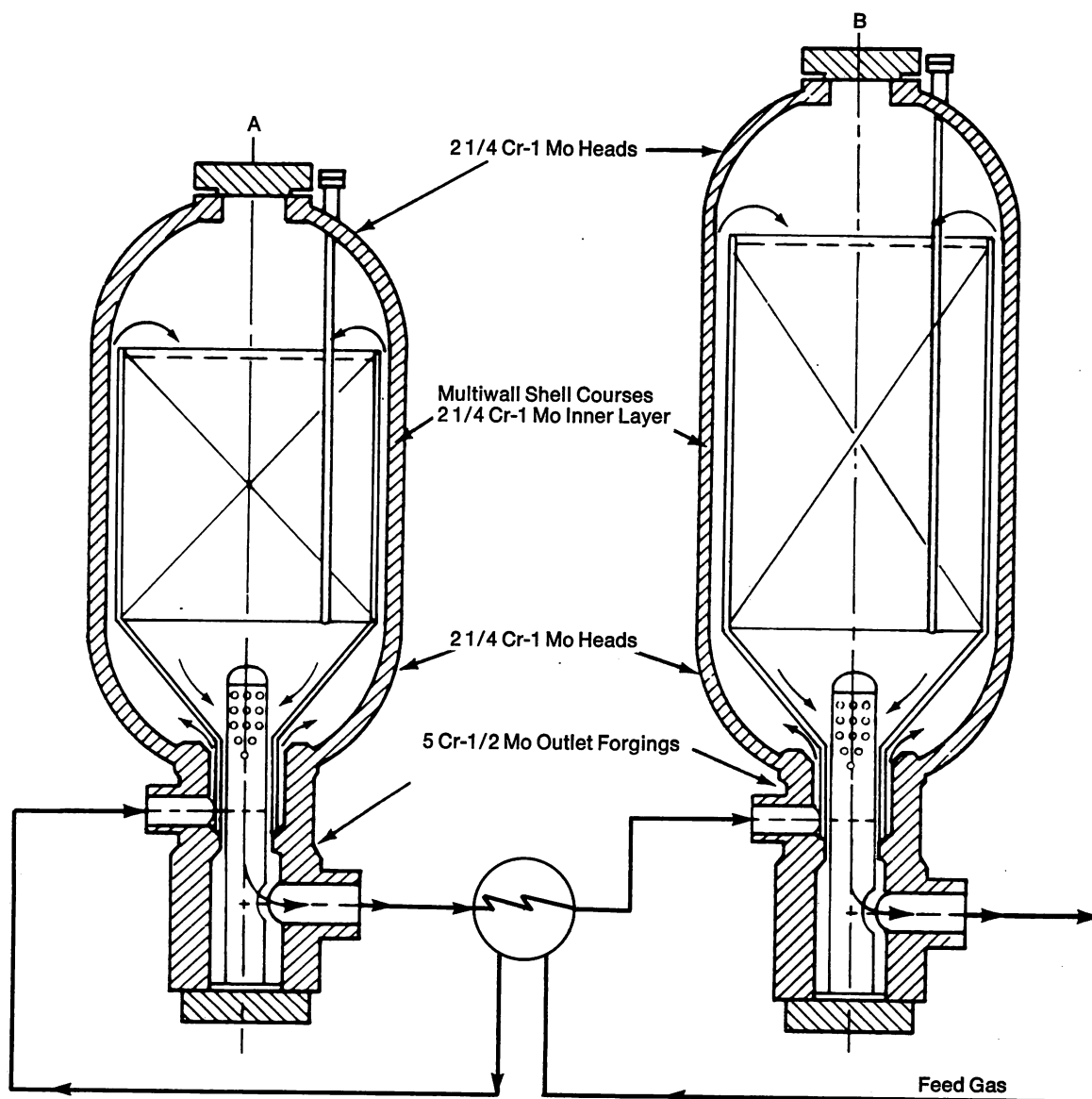A crack was observed in the 5 Cr-½ Mo outlet forging of the A converter after a service life of eight years. The crack was located near the bore which forms the outlet nozzle. Further examination by ultrasonic methods revealed the presence of additional subsurface cracks. The location of the cracks is shown in Figure 19, as the outlet nozzle is viewed from inside the forging. The largest crack, designated A, surfaced at the nozzle bore. The remaining cracks, 75 to 150 mm (3 to 6 in.) in length, were 25 to 50 mm (1 to 2 in.) below the surface. The dimensions shown in Figure 19 indicate the distances from the inside surface to the far side of the cracks. The cracks were ground out and the forging was weld repaired and stress relieved.

The almost identical forging on Converter B was carefully inspected at this time, and no cracks were detected. However, approximately one year later, cracks were found in the B converter during a surveillance check by ultrasonic examination. Again the cracks were below the surface. Figure 20 shows the location of two large cracks, one 200 mm (8 in.) long and the other 150 mm (6 in.) long. The cracks were gouged out, and the forging was repaired.

The nature of cracks found in the outlet forgings strongly indicates that some form of cumulative damage occurs on thick wall vessels in ammonia plants. The most probable explanation is the combined effect of thermal stresses and hydrogen-induced cracking resulting from supersaturation of hydrogen during cooling. The rate of decrease in temperature appears to determine the number of shutdowns that can be sustained before cracks are initiated. The cool down rate on these forgings was relatively mild, about 28 C (50 F) per hour, which probably accounts for the fact that the equipment sustained over 200 shutdowns before trouble developed. Every effort should be made to cool thick wall process equipment at the slowest rate possible. The cumulative effect emphasizes the need for close inspection and surveillance at every opportunity. This is especially true for older plants that have been subjected to a large number of shutdowns.

## Conclusions and Comments

Hydrogen attack of carbon and alloy steels has been reasonably well handled in the past by the Nelson curve. It is a useful and widely used guide based on service experience. Occasionally the curves undergo significant revision, such as the recent downward shift of the C-½ Mo curve by 56 C (100 F). Several years ago, the 2¼ Cr-1 Mo curve underwent a similar downward shift. A considerable amount of equipment already in service, and thought to be safe, suddenly became suspect as a result of revisions in the curves. This situation is very dangerous if the operators do not respond by proper surveillance and action.
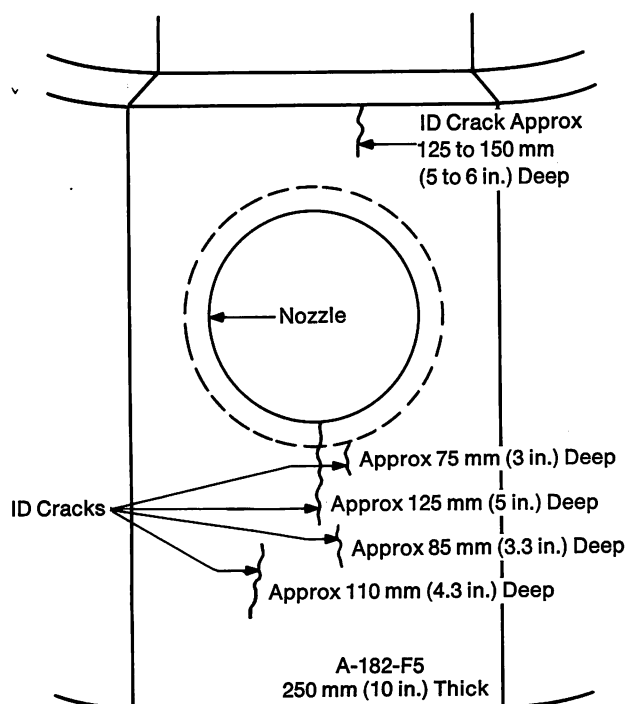
FIGURE 19—Crack locations in converter. Dimensions are measured from inside diameter.
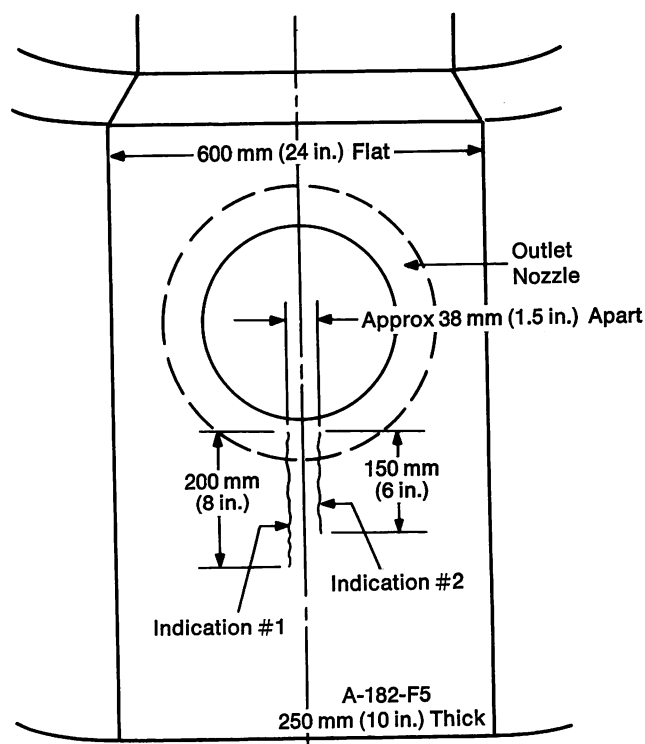
FIGURE 20—Location and size of cracks in converter. View is from inside of bottom forging.

It would be far better if these limits could be more accurately defined by planned programs of testing in laboratories and operating equipment. Microstructural effects have not been properly assessed. For example, Yamazaki[22] reports that the postweld heat treating temperature of 2¼ Cr-1 Mo weldments is related to resistance to hydrogen attack. At the extreme of no postweld heat treatment, the heat affected zone is attacked about 100 C (180 F) below the Nelson curve. Our piping code, ANSI B31.3, allows 2¼ Cr-1 Mo to be used in the as-welded condition up to 13 mm (0.5 in.) thickness. This appears to be an unsafe situation in hydrogen service not only from the standpoint of hydrogen attack, but from the standpoint of hydrogen embrittlement and delayed fracture.

Hydrogen embrittlement of moderately high strength alloys, 690 MPa (100 ksi) to 1034 MPa (150 ksi), is a costly restraint imposed on pressure vessel design. A modification of existing Cr-Mo alloys might conceivably extend the upper limit of susceptibility. One Japanese steelmaker[23] is testing 2¼ Cr-1 Mo with low silicon, phosphorus and sulfur. The alloy is further modified by the addition of vanadium, titanium and boron. Preliminary tests have demonstrated its greater hardenability, improved creep rupture properties, and lower susceptibility to notch effects in a hydrogen atmosphere. This alloy should also have improved resistance to hydrogen attack.

In the future, controls will continue to be imposed on Cr-Mo alloys that are susceptible to temper embrittlement. The tramp elements, Sn, Sb, P and As, must be controlled at acceptably low values. A number of investigators have demonstrated the beneficial effects of low silicon, although its importance seems to diminish when the tramp elements are held at low levels. The results of a tremendous amount of excellent research have been published on this subject, and this has been reflected in improved steels and welds. Again, it seems possible that further modifications can be made to inhibit temper embrittlement. Takaishi[24] reported that aluminum minimizes embrittlement, and Kanazawa[25] showed that additions of rare earth metals and titanium reduced susceptibility.

The cyclic effects of hydrogen seem to merit some additional work. The models created by the authors of the cited references[17, 18] appear to fit the pattern of cracking found in the two case histories described in this paper.

We know the solubility of hydrogen as a function of temperature and hydrogen partial pressures. We also know the rate of diffusion and the distribution of hydrogen across the wall of the vessel. The model predicts,

probably with a fair degree of accuracy, the situation as a function of time after the hydrogen pressure is reduced and cooling begins. The missing information is how many cycles can be tolerated under a given set of operating and shutdown conditions. This type of information must come from controlled laboratory tests.

# References

1. C. Bosch, *Chem Fabrik, 6*, 1933, 127; *Z VDJ 77*, 1933, 305; C. F. Stahly, *Eisen, 53*, 1938, 1187.

2. H. H. Johnson, J. G. Morlet and A. R. Troiano, *WADC-TR-262*, May 1957.

3. E. R. Slaughter, E. E. Fletcher, A. R. Elsea and G. K. Manning, *WADC-TR-56-83*, June 1955.

4. R. J. Walter and W. T. Chandler, *NASA Report CR-124410*, October 1973.

5. A. W. Loginow and E. H. Philps, *ASME Paper No. 74-PET-4*.

6. C. J. McMahon, Jr., *Temper Embrittlement of Steel*, ASTM STP 407, 1968, 127.

7. R. Bruscato, *Welding Research Supplement, 49*, April 1970, 148-S.

8. C. J. McMahon, Jr., J. C. Murza, J. Yu and R. A. Swift, *API Proceedings, Refining*, 1977.

9. J. Watanabe, et al., information presented at the ASME 29th Petroleum Mechanical Engineering Conference, September 15-18, Dallas, Texas, 1974.

10. Y. Yoshino, J. Watanabe and R. Chiba, Proceedings of Int. Conf. on the *Effect of Hydrogen on Behavior of Metals*, September 7-11, Jackson, Wyoming, 1975.

11. J. Watanabe and R. Chiba, *Japan Steel Works Tech. Review, 38*, 1978, 79.

12. E. Takahashi, et al., Preprints for National Meeting of J. W. S. No. 18, 1976.

13. Information presented to API Task Group in Chicago, February 20, 1974, Japan Steel Works.

14. T. Funakoshi and A. Kamada, *Reports of Materials Research Committee, Iron and Steel Inst., Japan*, 1976, 85.

15. E. Takahashi, et al., Preprints for National Meeting of J. W. S. No. 26, 1980.

16. Mitsubishi Heavy Industries, Ltd., Unpublished results.

17. T. Sakai and H. Kaji, presented at ISIJ Fall Meeting, Sapporo, October 1975.

18. G. H. Gieger and D. F. Angeles, presented at 35th Meeting of API, May 1970.

19. Japan Steel Works, *Muroran Tech. Rep.*, March 1962, 37.

20. I. Setoyama, E. Wada and Funakoshi, *AIChE Symposium on Ammonia Plants*, November 1978.

21. G. R. Prescott and Fred W. Badger, presented at *Symposium on Safety in Ammonia Plants*, AIChE, San Francisco, November 1979.

22. D. Yamazaki, T. Shinkawa, H. Makimoto and T. Oe, *Mitsubishi Juko Giho, 13* (1), 1976, 63.

23. Japan Steel Works, Unpublished results.

24. S. Takaishi, H. Nakao and R. Yamaba, *Tetso-to-Hagane, yl.*, 1975, S 294.

25. S. Kanazawa, Y. Otoguto, K. Hashimoto, M. Satoh, T. Takeda and T. Horiya, *Tetso-to-Hagane 63*, 1977, S 761.

# Discussion

W. C. HAGEL, *Climax Molybdenum Company.* You state that temper embrittlement of 2¼ Cr-1 Mo and 3 Cr-1 Mo steels is of considerable concern. Do you have a specific example of temper embrittlement in 3 Cr-1 Mo? Does not an increase in chromium content reduce the tendencies toward temper embrittlement?

G. R. PRESCOTT. The failure of a 3 Cr-1 Mo heat exchanger channel resulted from an increase in transition temperature of 140 C (250 F). The work of several major fabrica-tors and steel companies indicates that the 2¼ Cr and the 3 Cr steels are about the same from the standpoint of temper embrittlement.

D. L. SPONSELLER, *Climax Molybdenum Company.* The author expressed interest in trying to boost the Nelson curve for 2¼ Cr-1 Mo by additions of titanium, tantalum or tungsten. Work at the Climax laboratory showed that the addition of niobium, as little as 0.03%, increased the resistance of a manganese-molybdenum steel to hydrogen attack.

# Stainless Steels for Environmental Control Systems and Special Process Streams

by R. K. Pitler
Allegheny Ludlum Industries, Inc.

The 1970s was a period of significant change in the way society viewed the costs and benefits of much of our industrial technology. There developed over the decade a great public awareness of the environmental effects of our manufacturing and transportation methods. There now exists a demand that these effects be modified in regard to present technology, and that they be anticipated and controlled before any new technology is introduced. This awareness has resulted in the establishment of legal requirements governing permissible emission or effluent levels for vehicles, power plants, industrial processes and waste treatment facilities. This trend will only continue in the 1980s. It presents a challenge and an opportunity for those of us who develop and supply new materials.

There are two approaches to solving environmental control problems. One is to put something at the end of the process to control or modify the emission or effluent. The second is to redesign the process so that harmful emissions are not generated; for example, removing sulfur before burning by using solvent-refined coal in a power plant instead of cleaning up the sulfur in the combustion products after burning the coal. These redesigned processes offer opportunities for new materials in addition to those opportunities available in environmental control hardware used to clean up current processes. While some of the newer processes are interesting as applications for new materials, they will not be treated in this paper.

This paper will describe some of the materials problems associated with several current or proposed environmental control systems. It will discuss the alloys selected to solve these problems and some of the newer materials now available which are capable of improved performance in the increasingly severe environments we expect to see in the 1980s. The chemical compositions of the alloys discussed are given in Table I.

## Automotive Catalytic Converters

The largest single application for stainless steel in the United States is for the automotive catalytic converter. This market is estimated to use approximately 115,000 tons per year or about 10% of total stainless steel production. These converters are of two types: the pellet bed (Figure 1) and the ceramic monolith (Figure 2). In the converter, the ceramic pellet or the ceramic monolith is coated with a catalyst (platinum, palladium) which serves to complete the oxidation of CO and hydrocar-



Basic Converter Assembly

Insulation
Upper Cover
Washer
Upper Shell
Upper Retainer
Stud
Catalyst
Lower Retainer
Lower Shell
Support Channels
Insulation
Fill Plug
Washer
Lower Cover
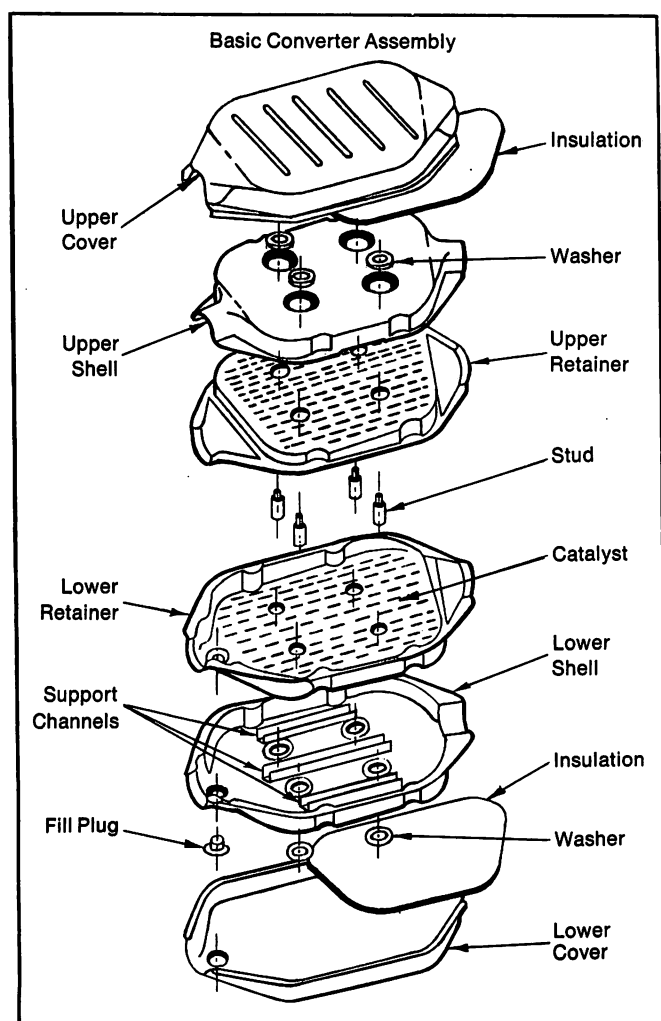
FIGURE 1—Pellet bed catalytic converter.

**Table I**—Chemical Composition of Alloys

| Alloy | Element, % | | | | | | | |
|---|---|---|---|---|---|---|---|---|
| | Cr | Ni | Mo | Cu | C | Ti | Nb | Other |
| AISI 1010 | — | — | — | — | 0.04 | — | — | — |
| HSLA Steel | 0.7 | 0.3 | — | — | 0.08 | — | — | — |
| 409 | 11.5 | — | — | — | 0.05 | 0.5 | — | — |
| 408 | 12.0 | — | — | — | 0.025 | 0.4 | 0.70 | 1 Al |
| 406 | 12.0 | — | — | — | 0.05 | — | — | 3.5 Al |
| Fecralloy | 16.5 | — | — | — | 0.02 | — | — | 5 Al, 0.25 Y |
| 430 | 16.5 | — | — | — | 0.05 | — | — | — |
| 439 | 18.0 | — | — | — | 0.05 | 12 x C | — | — |
| 18-0 | 18.0 | — | — | — | 0.02 | 0.15 | 0.45 | — |
| 18-2 | 18.0 | — | 2.0 | — | 0.02 | 0.15 | 0.45 | — |
| 18-SR | 18.0 | — | — | — | 0.04 | 0.55 | — | 2 Al, 1 Si |
| Kanthal DSD | 23.0 | — | — | — | — | — | — | 5 Al |
| 304 | 18.5 | 9.0 | — | — | 0.05 | — | — | — |
| 316 | 17.0 | 11.0 | 2.5 | — | 0.05 | — | — | — |
| 317 | 19.0 | 12.0 | 3.5 | — | 0.05 | — | — | — |
| 309 | 23.0 | 13.5 | — | — | 0.05 | — | — | — |
| 310 | 25.0 | 21.0 | — | — | 0.05 | — | — | — |
| E-Brite 26-1 | 26.0 | — | 1.0 | — | 0.002 | — | 0.10 | — |
| 29-4 | 29.0 | — | 4.0 | — | 0.005 | — | — | — |
| 29-4-2 | 29.0 | 2.0 | 4.0 | — | 0.005 | — | — | — |
| AL 4X (JS777, 904L) | 21.0 | 25.0 | 4.5 | 1.5 | 0.05 | — | — | — |
| 20 Cb-3 | 20.0 | 35.0 | 2.5 | 3.5 | 0.04 | — | 0.8 | — |
| AL-6X | 20.0 | 24.0 | 6.0 | — | 0.03 | — | — | — |
| Inconel 625 | 22.0 | Bal | 9.0 | — | 0.04 | — | 3.5 | 3 Fe |
| Hastelloy C-276 | 15.0 | Bal | 15.0 | — | 0.02 | — | — | 6 Fe, 3 W |
| Hastelloy G | 22.0 | Bal | 6.5 | 2.0 | 0.05 | — | 2.0 | 20 Fe |
| Hastelloy C-4 | 16.0 | Bal | 16.0 | — | 0.01 | 0.7 | — | 3 Fe, 2 Co |
| CD 4 MCu | 26.0 | 5 | 2.0 | 3.0 | 0.03 | — | — | — |

Balance Fe unless otherwise noted.
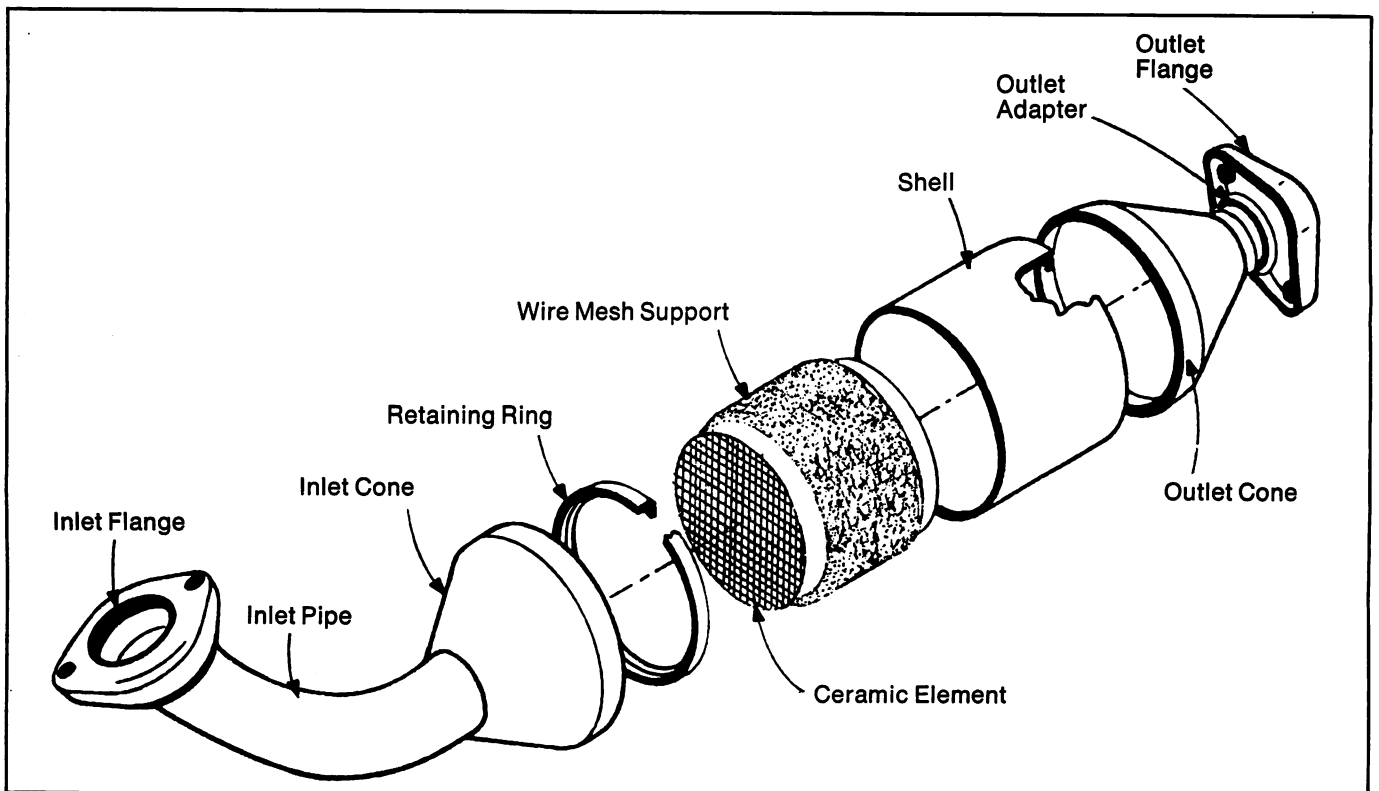


*FIGURE 2—Ceramic monolith catalytic converter.*

bons. More recent models have employed in addition a reducing catalyst, rhodium, to lower $NO_x$ levels.

The alloy used in these converters is Type 409 (Table I), an 11% Cr, Ti stabilized ferritic material. It was selected on the basis of a satisfactory service experience in conventional mufflers for which it was originally developed. It combines oxidation resistance, corrosion resistance to exhaust condensates and under-car road environments, good formability, weldability, low cost and the low thermal expansion coefficient of a ferritic steel which minimizes thermal stresses. Type 409 has allowed the converter to meet the 80,000 km (50,000 mile) or 5-year design life requirement. Recently, the more severe duty cycles found in light trucks, which now require an emission control system, have dictated a material change in the pellet bed converter. Operating temperature increases from 600-650 C to 800-850 C (1110-1200 F to 1470-1560 F) required a more oxidation resistant and creep resistant alloy. The 18% Cr-2% Mo alloy stabilized with Nb and Ti, developed by Climax Molybdenum, was selected. This alloy is now being replaced by a similar molybdenum-free alloy (18-0, Table I) to provide the same required properties at lower alloy content. Additional work is being done on lower chromium versions of Nb- and Ti-containing ferritic steels. One of them, Type 408, looks like a probable candidate for catalytic converter service. The composition of Type 408 is given in Table I, and a comparison of its strength properties with other alloys is given in Table II. As more vehicles like the light truck are required to have emission control devices, we can expect increased use of stainless steels like 409 and 18-2, as well as the continued development of newer alloys specifically for these applications.

**Table II**—Relative Hot Strength of Converter Alloys

| Alloy | Time to 1% Total Strain at 870 C (1600 F) and 8.27 MPa (1.2 ksi), h |
|---|---|
| 409 | 25 |
| 18-2 | 285 |
| 18-0 | 255 |
| 408 | 280 |

There is also an application for Type 304 wire mesh in the ceramic monolith converter. This mesh, as shown in Figure 2, placed around the ceramic monolith, provides a cushioning effect and prevents failure of the ceramic from vibration and road shock. A development, also aimed at increasing the reliability of the monolithic converter, is to replace the ceramic monolith with a metallic cellular catalyst support structure. The metal substrate has potential advantages in thermal properties for rapid heat up, high surface area, good gas flow, and durability in manufacture, assembly and service.
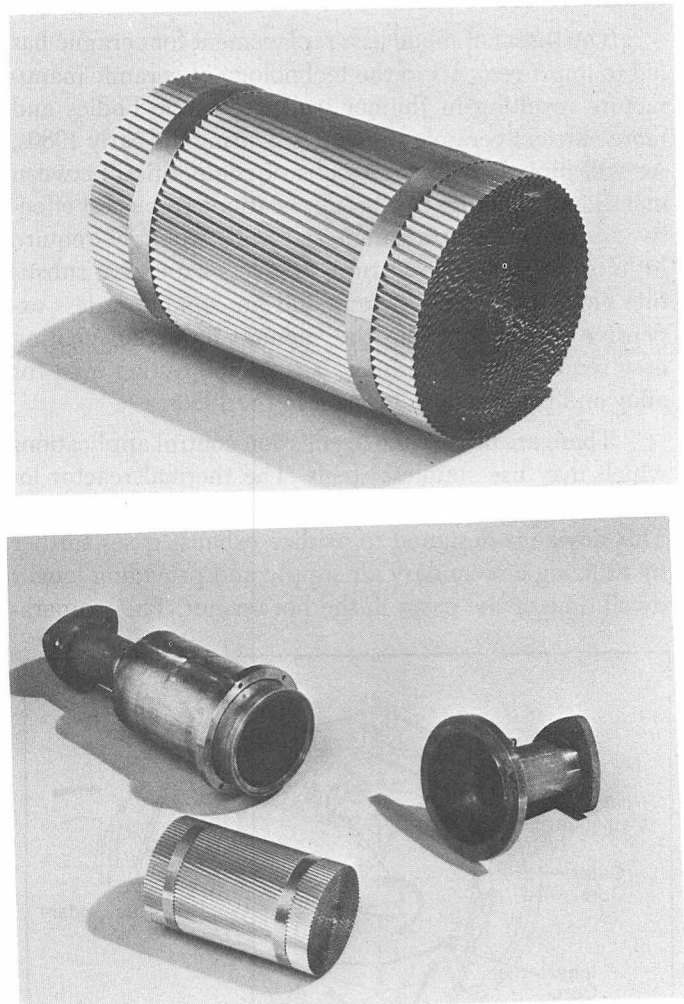




FIGURE 3—Wrapped corrugated Fecralloy core.

**Table III**—Engine Exhaust Corrosion Tests on 0.05 mm (0.002 in.) Sheet

| Exposure Temperature, C (F) | Alloy | | | |
|---|---|---|---|---|
| | 18-SR | Type 310 | Kanthal DSD | Fecralloy |
| 950 (1740) | Failed at 390 Hours | Failed at 625 Hours | OK at 615 Hours | OK at 625 Hours |
| 1000 (1830) | Failed at 215 Hours | Highly Oxidized at 420 Hours | OK at 420 Hours | OK at 420 Hours |
| 1050 (1920) | Failed at 30 Hours | Deformed at 30 Hours | OK at 30 Hours | OK at 30 Hours |
| 1085 (1985) | Failed | Failed | Failed | OK at 185 Hours |

The alloy described by Dulieu and coworkers[1] for this application is a Cr-Al-Fe alloy containing yttrium which was originally developed by G. E.[2] and produced for development purposes by Harwell. This alloy, called Fecralloy, has the strength and oxidation resistance to replace the ceramic substrate as a support for the catalyst. Some properties taken from Dulieu's paper are shown in Table III.[1] Fecralloy is superior in engine corrosion tests to 18-SR, Type 310 or Kanthal DSD according to these results. Figure 3 shows a wrapped corrugated Fecralloy core used to replace a ceramic substrate in a monolithic converter.

The threat of metal as a replacement for ceramic has led to improvements in the technology of ceramic manufacture resulting in thinner walled ceramic bodies and more efficient ceramic substrates. During the early 1980s, we will probably see the results of competition between metals and ceramics for this application. To be cost effective, a metal substrate material will probably require little or no expensive yttrium or a less expensive substitute element for the yttrium, and be capable of less expensive processing than the vacuum induction melting now required for Fecralloy. It is an interesting area for alloy and process development in the 1980s.

There are other vehicle emission control applications which may use stainless steels. The thermal reactor located near the exhaust manifold is shown in Figure 4.[3] This device is designed to oxidize exhaust gases further by utilizing a secondary air supply and providing longer dwell time of the gases in the hot reactor. The temperatures involved require good oxidation resistant materials such as Types 309, 310 and possibly Inconel in the core and Type 430 in the thicker or cooler portions.[3]

A second potential control device is the particulate trap. This will probably consist of a container holding a metallic filter similar to steel wool. It must be capable of removing the particulate matter in diesel exhaust, probably operating at temperatures up to about 1090 C (2000 F) in a highly oxidizing atmosphere. Some of the stainless austenitic or ferritic alloys may be suitable, but more likely a high nickel alloy or a special ferritic alloy like Type 406 or even Fecralloy may be required. Emission standards for particulates have not been set. The design and eventual use of particulate traps will probably be delayed until there is definition of the conditions which must be met by diesel exhaust systems.

Vehicle emission control devices are expected to be with us through the 1980s. Materials used will be conventional stainless steels as well as some alloys developed specifically for these applications. The cost effectiveness of these devices is going to depend on the ingenuity of the designer of the device, the alloy designer and the



FIGURE 4—Thermal reactor.

EPA Revised New Source Performance Standards

| Coal Equiv. SO₂ Content, lb per 10⁶ Btu | SO₂ Removal | Max. SO₂ Emission |
|---|---|---|
| Up to 2 | 70% | 0.6 lb/10⁶ Btu |
| 2-6 | 70%-90% | 1.2 lb/10⁶ Btu |
| 6-12 | 90% | |
| 12 & up | 90% Plus | |



FIGURE 5—SO₂ control standards for new utility power plants.

ability of the alloy supplier to devise lower cost processing methods.

## Flue Gas Desulfurizing (FGD)

A major market developing for specialty steels and alloys is that for flue gas desulfurizing systems. As with the automotive catalytic converter, the driving f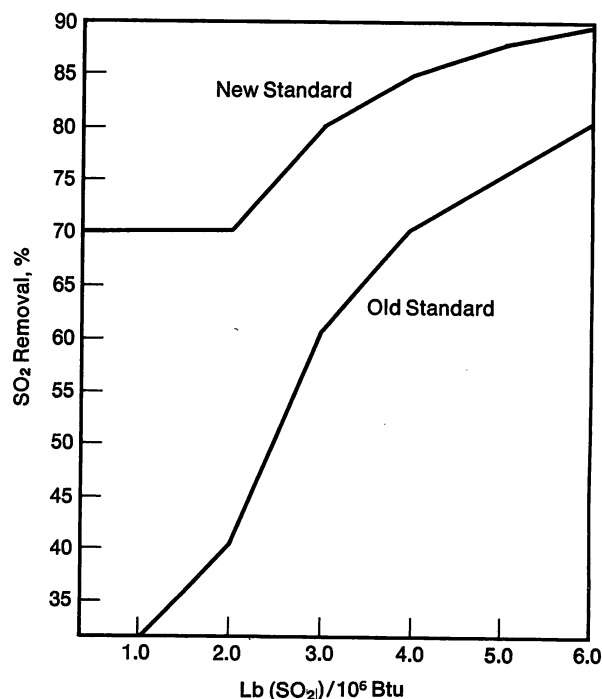orce for this new market in the U.S. is the government-mandated environmental standard. Figure 5 shows the new source EPA $SO_2$ control standard for utility power plants. This new standard demands at least a 70% $SO_2$ removal from the combustion product regardless of the sulfur content of the coal. No longer can the burning of a low sulfur coal permit the power plant to avoid installing an $SO_2$ scrubbing system. The result of this standard is that, by the year 1986, approximately 65,000 megawatts of generating capacity in the United States will have a FGD system (Figure 6).[4] This estimate is based on units now under construction or on order as of November 1978. This is about 24% of the coal fired generating capacity and about 12% of the total generating capacity in the

U.S. One estimate on worldwide needs indicates that the purchase of scrubbers will grow into a $6.8 billion market by 1985.[5]

Figure 7 shows a schematic view of a scrubber system.[6] Flue gas at about 150 C (300 F) enters the quench section. This gas contains $SO_2$, $H_2SO_3$, $H_2SO_4$, chlorides and particulate matter. Materials in the quench section are subject to general corrosion, localized corrosion and erosion attack. In the absorber tower and mist eliminator, the temperature drops to about 50 C (120 F), and most of the particulate matter has been removed. The slurry usually is controlled to a pH of 5.5-6. Pitting and crevice corrosion from chlorides are the major problems in this section. If a heat exchanger is placed in the reheat area, the heat exchanger itself can see temperatures above 100 C (210 F), and stress corrosion becomes a problem in addition to pitting and crevice corrosion. At the reheat section, the temperature has increased to about 70 C (160 F). If the gas stays dry, corrosion problems are minimal. However, the gas temperature drops slowly through this section and through the ducting, fan and stack causing condensation and dew point corrosion from $H_2SO_3$, $H_2SO_4$ and chlorides in the condensate. It should be pointed out that deposits which are likely to form provide many crevices at which localized attack can occur. Table IV summarizes these corrosive environments for the various sections of the scrubber. There are various
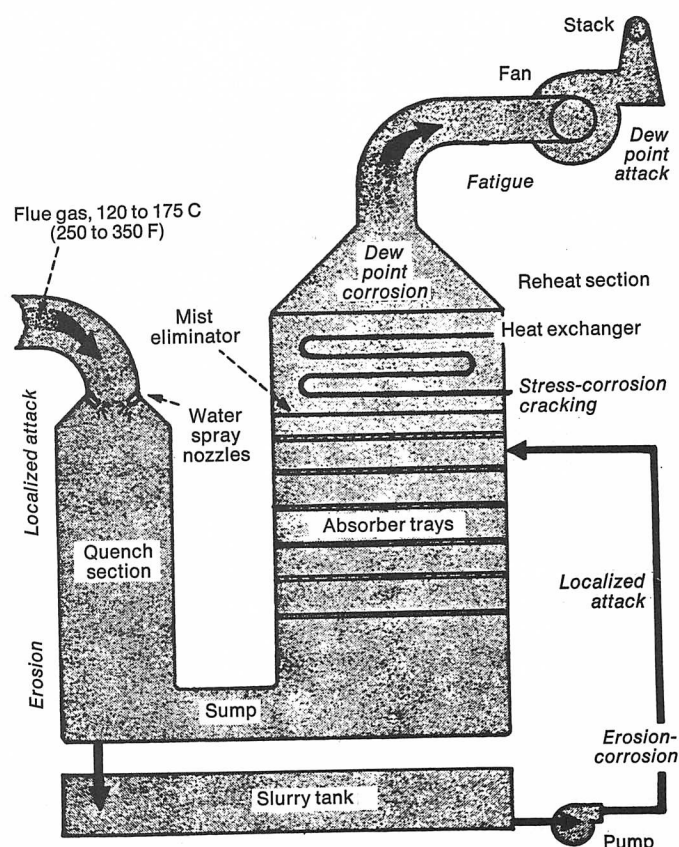
FIGURE 6—Flue gas desulfurizing operating capacity for new and retrofit installations through 1986.

FIGURE 7—Schematic view of a flue gas desulfurizing system. Type of attack sustained by the scrubber system depends on component location.

**Table IV**—Typical Scrubber Environments

| Section | Temperature, C | Temperature, (F) | Corrosive Media | Type of Attack |
|---|---|---|---|---|
| Quench | 150 | (300) | $SO_2$, $H_2SO_3$, $H_2SO_4$, $Cl^-$, particulates | general, pitting, crevice, erosion |
| Absorber Tower | 50 | (120) | $SO_2$, $H_2SO_3$, $H_2SO_4$, $Cl^-$ | pitting, crevice |
| Heat Exchanger | >100 | (210) | $SO_2$, $H_2SO_3$, $H_2SO_4$, $Cl^-$ | pitting, crevice, stress corrosion |
| Reheat | 70 | (160) | $SO_2$, $H_2SO_3$, $H_2SO_4$, $Cl^-$ | general, pitting, crevice (dew point attack) |
| Ducting/Fan/Stack | 60-70 | (140-160) | $SO_2$, $H_2SO_3$, $H_2SO_4$, $Cl^-$ | general, pitting, crevice (dew point attack) |

**Table V**—Corrosion Test in Power Plant Flue Gas Scrubber Using Once-Through Scrubbing Water[a]

| Material | Average Corrosion Rate, mm/yr | Average Corrosion Rate, (mpy) | Maximum Depth of Pit or Crevice Corrosion for Test Period, mm | Maximum Depth of Pit or Crevice Corrosion for Test Period, (in.) |
|---|---|---|---|---|
| Hastelloy C-276 | 0.028 | (1.1) | 0.03[b] | (0.001) |
| Inconel 625 | 0.030 | (1.2) | 0.13 | (0.005) |
| AL-6X | 0.036 | (1.4) | 0.05 | (0.002) |
| Hastelloy G | 0.038 | (1.5) | 0.13 | (0.005) |
| Incoloy 825 | 0.066 | (2.6) | 0.18 | (0.007) |
| Type 317 | 0.089 | (3.5) | 0.18 | (0.007) |
| Carpenter 20 Cb-3 | 0.226 | (8.9) | 0.15 | (0.006) |
| Type 316 | 0.782 | (30.8) | 0.23 | (0.009) |
| Type 304 | 4.587 | (180.6) | 0.79 | (0.031) |
| AISI Type 1010 Steel | >8.222 | (>323.7) | Corroded away | |
| HSLA Steel | >12.078 | (>475.5) | Corroded away | |

[a] Exposed in outlet gas stream of scrubber at Weirton Steel Division at 60 C (140 F) for 19 days. Gas believed to contain entrained droplets and an extremely aggressive acid condensate with unknown chloride content. pH of water in scrubber reported as low as 2.6 with 100 ppm chloride.

[b] Indicates one sample that showed no localized attack, and on the duplicate sample it was difficult to determine if surface was mechanically damaged or pitted to depth of 0.03 mm (0.001 inch).

designs of FGD systems, and the comments made above about the corrosion conditions to be found would apply generally to all of these designs.

A comparison of a broad range of alloys for service in flue gas scrubbing processes was made by Hoxie and Tuffnell in 1976.[7] They exposed these alloys on spools in a scrubber using once-through water as a scrubbing medium. Table V contains data from their paper. These data were plotted by them to show the effect of molybdenum content in the alloy on the pitting or crevice corrosion behavior in the scrubber environment (Figure 8).[7] Molybdenum content shows a strong influence on resistance to pitting corrosion in scrubber environments. Michaels and Hoxie developed similar data on samples exposed in the upper sections of the absorber tower at

a temperature of about 55 C (130 F).[6] However, they analyzed their data on corrosion resistance by plotting the sum of general corrosion rate plus the maximum localized attack against the percent molybdenum plus chromium. A similar trend, as shown in Figure 9, exists.[6] Alloys having the highest molybdenum plus chromium levels such as Hastelloy C-276 and Inconel 625 are almost untouched while some of the stainless steels (316 and 317) and even 20 Cb-3 are inadequate for this environment. Clearly, for the severe high chloride, acid conditions in the wet scrubber, alloys better than the conventional stainless steels are required. In the less severe corrosion environments, austenitic stainless steels like 316 and 317 with molybdenum can be considered. Alloys with intermediate molybdenum plus chromium contents such as Incoloy 826 or 904L (AL-4X) may be a
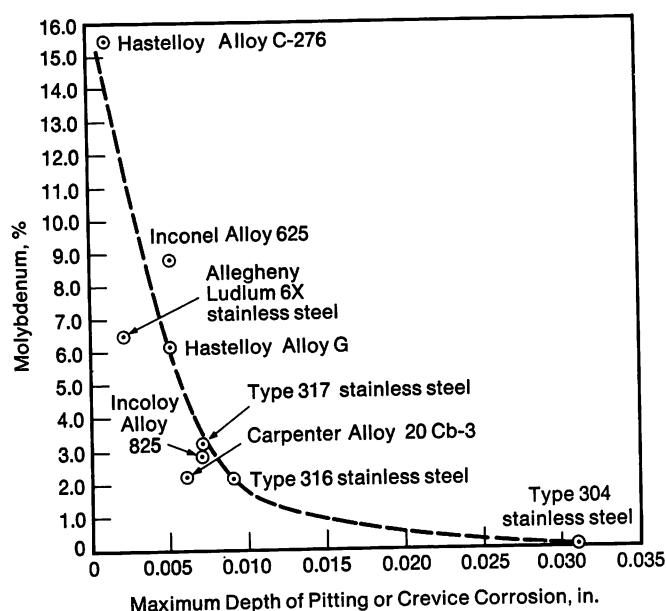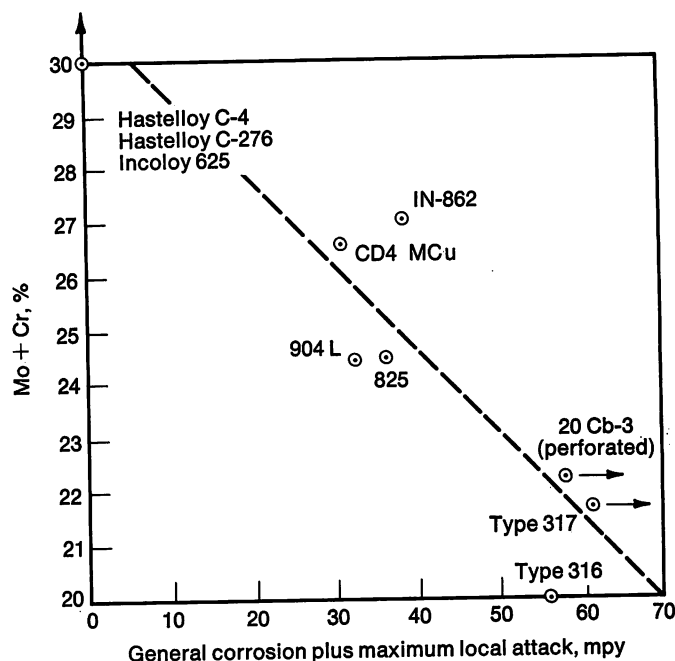
FIGURE 8—Effect of molybdenum on corrosion.



FIGURE 9—Effect of % (Mo + Cr) on corrosion.

more economical choice than the more highly alloyed materials, while giving better performance than the stainless steels.

It may be possible to rate alloys accurately for flue gas desulfurizing systems in the laboratory without the need to install them in actual operating systems. A rubber band crevice corrosion test in a simulated scrubber environment, made up of 7 volume % $H_2SO_4$, 3 volume % HCl to which is added 1 weight % $CuCl_2$ and 1 weight % $FeCl_3$, has been used to test Type 316 stainless steel, AL-6X, Inconel 625, and AL 29-4-2; a 29% Cr, 4% Mo, 2% Ni ferritic alloy. Data on weight loss at three different temperatures after 96-hour exposures are shown in Table VI and plotted in Figure 10. Type 316, AL-6X and Inconel 625 are rated about as might be expected. Hoxie and Tuffnell showed AL-6X to be slightly better than Inconel 625 in maximum depth of pitting while these data in a simulated environment show the Inconel 625 alloy to be slightly better on the basis of weight loss. The alloy with the best performance is the ferritic alloy AL 29-4-2.



FIGURE 10—Crevice corrosion in a simulated scrubber environment.

These corrosion data have been plotted against weight % (Mo + Cr) in Figure 11 following the technique of Michaels and Hoxie. The effect of combined molybdenum plus chromium content is consistent with previous findings.[6] The alloy with the lowest corrosion rate is the one with the highest level of molybdenum plus chromium, 29-4-2.

There is a large and growing market for materials suitable for service in the flue gas desulfurizing systems being used by power generating plants and industrial

**Table VI**—Crevice Corrosion in a Simulated Scrubber Environment*

| Alloy | Wt. Loss, g/cm² | | |
| --- | --- | --- | --- |
| | 24 C (75 F) | 50 C (120 F) | 70 C (160 F) |
| Type 316 | 0.0002 | 0.0081 | 0.0206 |
| AL-6X | 0.0000 | 0.0001 | 0.0087 |
| Inconel | 0.0000 | 0.0001 | 0.0042 |
| AL 29-4-2 | 0.0000 | 0.0000 | 0.0002 |

* 7 Vol. % $H_2SO_4$
  3 Vol. % HCl
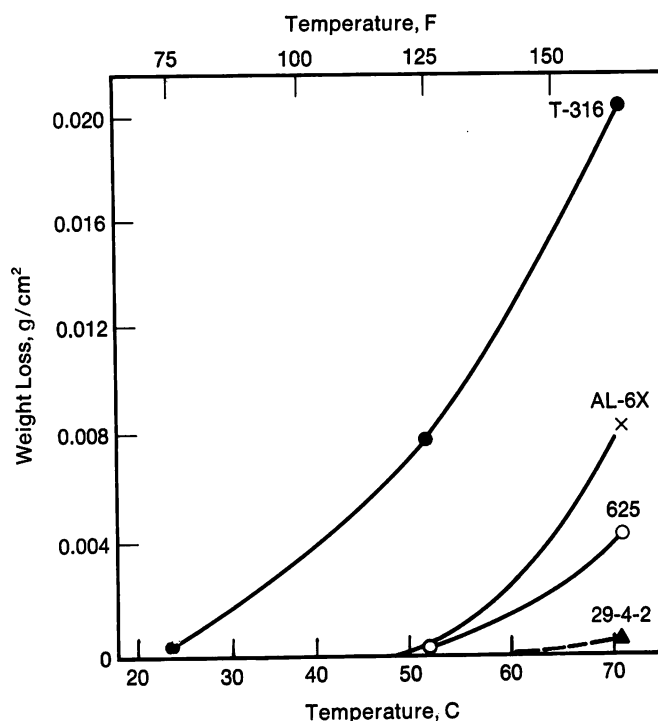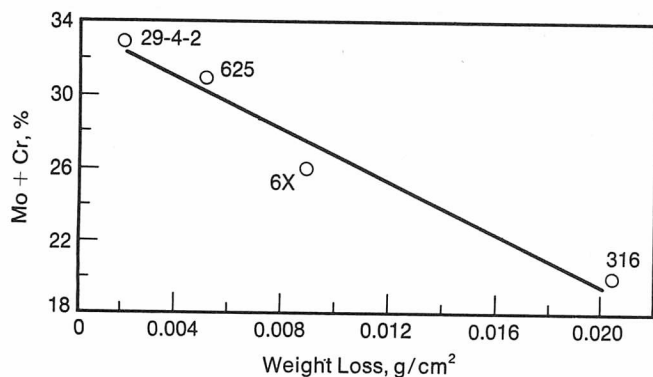  1 Wt. % $CuCl_2$
  1 Wt. % $FeCl_3$

FIGURE 11—Corrosion performance in a simulated scrubber environment at 70 C (160 F).

plants. In the 1980s, this market will utilize a variety of alloys from the molybdenum-containing stainless steels to high molybdenum, nickel-base alloys. The economics of selecting alloys for the variety of corrosive environments within a system will mean that a range of materials will be selected. It is likely that the new family of superferritic stainless steels such as 29-4-2 will find a place in this market based on outstanding resistance to high chloride, acid environments. These alloys will also be useful in the heat exchanger sections where stress corrosion cracking can be a problem. High levels of chromium and molybdenum will be required in any of the alloys used.

## Sewage Treatment

The increasingly stringent pollution control regulations have also had an effect on sewage treatment plants. Kopecki has described the increasing complexity of these plants which are beginning to resemble chemical plants.[8] It is much more difficult to quantify the size of the market for materials for sewage treatment plants than for catalytic converters or power plant flue gas desulfurizers. The size of the local population and the type of industrial waste which may be connected to the system will influence the size and complexity of the installation. For example, some plants digest sludge, some dry the sludge, others incinerate it and some pipe it to remote sites and spread it over the ground. However, this market is expected to grow through the 1980s as the trend toward improved waste treatment facilities continues.

Sewage treatment plants handle chlorine, chlorides, sulfuric acid, sulfates, carbon dioxide, oxygen and some polymers.[8] The conventional stainless steels like Types 430, 304 and 316 have been satisfactory for most wastewater treatment requirements. These materials are used in process tanks, storage tanks, piping and in some architectural areas such as louvers, doors, windows and safety railing. Stainless steel piping competes with anodically protected carbon steel based on an analysis of overall life cycle costs which include initial costs, maintenance costs
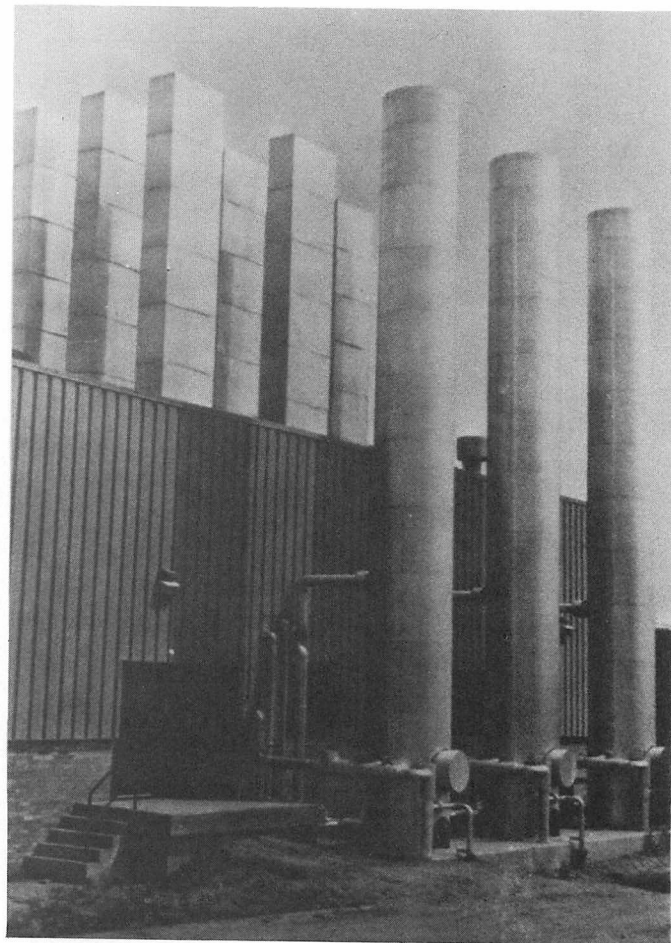


FIGURE 12—Wet oxidation sewage treatment plant.

and downtime costs. Some experience with the 11% Cr Type 409 alloy in sewage plant service indicates that it is not sufficiently corrosion resistant in these process streams, although it may be suitable as an aerator material.

An interesting application for conventional stainless steels is in sludge oxidation and incineration. Wet oxidation of sludges to render them sterile and inoffensive and prepare them for efficient vacuum dewatering can be done at pressures up to 6.9 MPa (1000 psi) and temperatures up to 260 C (500 F). In a plant such as the one shown in Figure 12, Type 304 stainless has been used for heat exchangers, reactors, valves and piping.[9]

In sludge incinerators, operating conditions are hot, wet and abrasive. Operating temperatures can approach 800 C (1470 F), and creep strength, corrosion resistance and erosion resistance can be important. Scrubbers, fans and ducting of Types 304, 316 and 316L have been used successfully in these incinerators.[9]

The austenitic stainless steels have found a place in the growing market for sewage treatment plants. Their combination of corrosion resistance, erosion resistance and creep strength make them cost-competitive with other materials when maintenance costs are considered. Upgraded materials may be required in some parts as fans or because of special effluent streams being treated.

However, for the 1980s, the conventional stainless steels will be the workhorse alloys.

## Pulp and Paper Industry

Environmental controls on effluents have impacted many industries. In some industries, this impact has required new environmental control equipment which can be constructed of conventional materials and has not significantly affected the industrial process itself. However, the pulp and paper industry is an example of an industry where process changes have occurred. The closing of the process system and the recycling of process water, especially in the paper bleaching stages, has resulted in a demand for materials superior to the Type 304, 316 and 317 stainless steels that up to now have been adequate. The principal corrosion problem is pitting and crevice corrosion resulting from a build-up of chloride ion concentrations, lowered pH and some increase in temperatures.[10]

Hill and Johnson have described the properties of a variety of new austenitic and ferritic stainless alloys in comparison to the Type 304, 316 and 317 stainless steels used in the pulp and paper industry.[11] Their comparisons were made on the basis of laboratory tests for general corrosion resistance and on crevice corrosion tests in ferric chloride, saturated sodium chloride and anodic polarization tests. The newer alloys tested include the ferritic alloys 18-2, E-Brite 26-1* alloy, 29-4 and 29-4-2 and the austenitic alloy AL-6X. As was found with these same alloys under flue gas desulfurizing conditions, the alloys having higher contents of chromium plus molybdenum were the most resistant to crevice and pitting attack. Hill and Johnson suggest that where stress corrosion cracking is a problem, ferritic Type 439 or 18-2 could be considered as replacements for Type 304. The higher chromium plus molybdenum alloys AL-6X, AL 29-4 and AL 29-4-2 are suggested where chloride pitting environments are extremely severe.

The performance in actual bleach plants has confirmed the laboratory work of Hill and Johnson. A study of 114 test spools of various materials placed in the operating environments of the bleach plants in 23 different paper mills was conducted by the Metals Subcommittee of the Corrosion and Materials Engineering Committee of the Technical Association of the Pulp and Paper Industry (TAPPI).[12] Figure 13 shows the alloys tested in this study as described by Tuthill, Rushton, Geisler, Heasley and Edwards and their relative pitting and crevice corrosion resistance based on a "severe, moderate and slight or no" corrosion type of rating system.[12] The only alloys given "slight or no" corrosion ratings for all conditions are AL 29-4, AL 29-4-2 and Titanium. Hastelloy G, Hastelloy C-276 and AL-6X are the next best. Other alloys intermediate between Type 317 and the Titanium, AL 29-4,

* E-Brite 26-1 is a Registered Trademark of Allegheny Ludlum Steel Corporation.
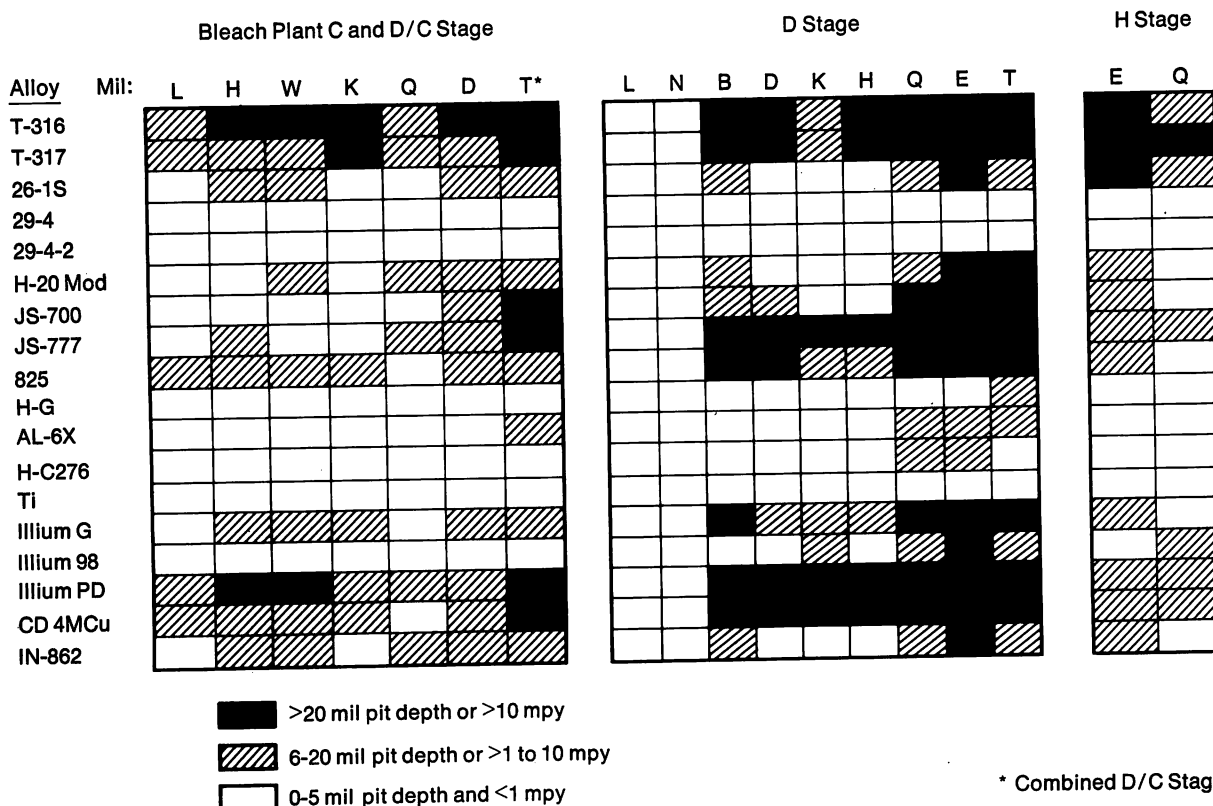


FIGURE 13—Corrosion in bleach plant operating environments.

>20 mil pit depth or >10 mpy

6-20 mil pit depth or >1 to 10 mpy

0-5 mil pit depth and <1 mpy

* Combined D/C Stage

AL 29-4-2 class may give adequate service and might be selected on economic grounds. The 21% Cr, 4.5% Mo, 1.5% Cu, 25% Ni alloy (904L, AL-4X, JS-777) is one such alloy that is finding increasing usage in the pulp and paper industry.

The bleach plant in the pulp and paper industry is one example where the demands of environmental control have created a need for better materials. Many of the newer high chromium, high molybdenum stainless steels will find application in this industry which has historically used carbon steel and Types 304, 316 and 317 stainless steels.

## Steelmaking Techniques

The later half of the 1970s saw the introduction of new techniques for making stainless steels. The argon-oxygen decarburization process and the vacuum decarburization process reduced the cost of raw materials for making stainless steel and permitted the attainment of lower carbon and sulfur levels. It is now possible to supply lower levels of carbon in the conventional grades and in some of the newer grades like 6X, 439 and 18-2. This improves fabricability of these grades and, in the case of the unstabilized austenitic alloys, their resistance to intergranular corrosion. Vacuum induction melting has been used to obtain the very low carbon and nitrogen levels attained in E-Brite 26-1 alloy, AL 29-4 and AL 29-4-2. Some work published by Kawasaki has indicated that very low carbon and nitrogen levels are obtainable in the large tonnage batches associated with more conventional steelmaking practices.[13]

The demand for better alloys to stand up to the conditions imposed by environmental control systems will also demand a continuation of process innovation in the stainless steel producing industry. The 1980s present a challenge to both the alloy developer and the process developer. To the need for controlling the environmental effects of our industrial processes is added the need to make efficient use of our energy and of our material re-sources. Long lasting, maintenance-free equipment is required to meet both those needs. It appears that some of the newer materials now available put us well on our way toward meeting the requirements of the 1980s.

## Acknowledgment

## References

1. C. A. Dulieu, W. D. J. Evans, R. J. Larbey, A. M. Verrall, A. J. J. Wilkins and J. H. Povey, *S.A.E. Paper 770299*, Detroit, Michigan, February 28-March 4, 1977.

2. C. S. Wukusick, *U. S. A. E. C. Contract No. AT(40-1)-2847*, General Electric Company, NMPO Report No. GEMP-414.

3. D. J. Bologna, *ASM Technical Report System No. 76-58*, Cleveland, Ohio, October 28, 1976.

4. B. A. Laseke and T. W. Devitt, *Fifth Symposium on Flue Gas Desulfurization*, Las Vegas, Nevada, March 4-8, 1979.

5. Anon., *Nickel Topics, 32* (4), 1979, 14.

6. H. T. Michaels and E. C. Hoxie, *Chemical Engineering, 85* (13), June 5, 1978, 161.

7. E. C. Hoxie and G. W. Tuffnell, *Resolving Corrosion Problems in Air Pollution Control Equipment*, NACE, Houston, Texas, 1976, 65-71.

8. E. S. Kopecki, *American Metal Market* (Nickel Stainless Supplement), November 9, 1979, 18A.

9. Committee of Stainless Steel Producers, *Stainless Steel for Sludge Incineration*, AISI, April 1973.

10. L, H. Laliberte, *Pulp and Paper Industry Corrosion Problems*, NACE, Houston, Texas, 1974, 51.

11. J. B. Hill and M. J. Johnson, *TAPPI Publication*, Proceedings, 1978 TAPPI Engineering Conference, 493.

12. A. H. Tuthill, J. D. Rushton, J. J. Geisler, R. H. Heasley and L. L. Edwards, *TAPPI, 62* (11), November 1979, 49.

13. S. Iwaoka, H. Kaito, T. Ohtani, N. Ohashi, M. Takedo and N. Kinoshita, *Stainless Steel '77*, Climax Molybdenum Company, London, England, September, 1977, 139.

## Discussion

J. D. REDMOND, *Climax Molybdenum Company*. To evaluate the influence of Mo on the creep properties of ferritic stainless steels used for catalytic converters, the Climax laboratory studied some low interstitial 18 Cr stainless steels with nominal Mo contents of 0, 1 and 2%. The chemical analyses are listed in Table I. The steels were stabilized with a combination of titanium plus niobium. The niobium content was higher than that needed to prevent sensitization because previous work by General Motors had indicated a beneficial effect on creep strength at the higher niobium level.

**Table I**—Chemical Compositions of Experimental Steels

| Heat No. | Element, % | | | | | | | | | | | | | |
|---|---|---|---|---|---|---|---|---|---|---|---|---|---|---|
| | Cr | Mo | C | N | O | Mn | Si | Ni | Cu | S | P | Ti | Nb | Al |
| 1947A | 18.22 | <0.005 | 0.021 | 0.233 | 0.0201 | 0.44 | 0.40 | 0.22 | 0.092 | 0.011 | 0.017 | 0.14 | 0.54 | 0.030 |
| B | —* | 0.88 | — | — | — | — | — | — | — | — | — | — | — | — |
| C | —* | 1.77 | — | — | — | — | — | — | — | — | — | — | — | — |

* Not analyzed but assumed to be approximately the same for all steels in the series.

**Table II**—Room Temperature Mechanical Properties

| Heat No. | Mo, % | 0.2% Yield Stress, MPa (ksi) | Ultimate Tensile Strength, MPa (ksi) | Reduction In Area % | Elongation, % | ASTM Grain Size | HRB |
|---|---|---|---|---|---|---|---|
| 1947A | 0 | 287 (41.6) | 430 (62.4) | 52.1 | 28.1 | 4.7 | 76.2 ± 2.8 |
| B | 1 | 296 (42.9) | 445 (64.6) | 63.7 | 26.6 | 5.1 | 76.9 ± 1.3 |
| C | 2 | 322 (46.7) | 476 (69.0) | 58.8 | 25.5 | 4.9 | 81.2 ± 1.4 |

Tensile results are the average of duplicate specimens; hardness value is the mean of five measurements + the 99% confidence interval about the mean.

The room temperature mechanical properties are listed in Table II. The Mo additons had the predictable effect of increasing yield stress and tensile strength and lowering ductility slightly.

The creep rupture life at 870 C (1600 F) was determined for each steel in the recrystallized condition, and the results are depicted in Figure 1. Each had been annealed at 1095 C (2000 F) for five minutes and water quenched. Increasing the Mo content improved the rupture life at all stress levels tested.

The creep rupture life at 870 C and 8.3 MPa (1600 F, 1.2 ksi) was determined for each steel in the following conditions:

a. Annealed at 1095 C (2000 F) for 5 minutes, water quenched
b. Annealed as in (a) + prestrained 5%
c. Annealed as in (a) + aged at 760 C (1400 F) for 200 hours, water quenched

The 5% prestrain was chosen to simulate the plastic deformation which occurs in the fabrication of the catalyst bead support plate. The 760 C (1400 F) aging treatment corresponds to the normal operating conditions of a catalytic converter; this heat treatment produced extensive precipitation of Laves phase.

The creep rupture life at 8.3 MPa (1.2 ksi) for each condition is shown in Figure 2. In all cases, increasing the Mo



FIGURE 1—*Creep rupture life of low interstitial 18Cr ferritic stainless steels with 0, 1 and 2% Mo. Prior to creep testing at 870 C (1600 F), each steel was recrystallized at 1095 C (2000 F) for 5 minutes and water quenched.*

content improved the creep properties. Figure 3 evaluates another aspect of the molybdenum effect. Total creep strain after 100 hours at 870 C, 8.3 MPa (1600 F, 1.2 ksi) is shown for each steel in all three conditions. The Mo-free steel after the 200 hour aging treatment exhibited a strain of more than 16% whereas the 18 Cr-2 Mo steel had less than 1% creep.

Exposure at 870 C (1600 F) resulted in the precipitation of Laves phase in all three steels. In the Mo-free steel, the Laves was $Fe_2Nb$ while in the 1 and 2% Mo steels, the Laves
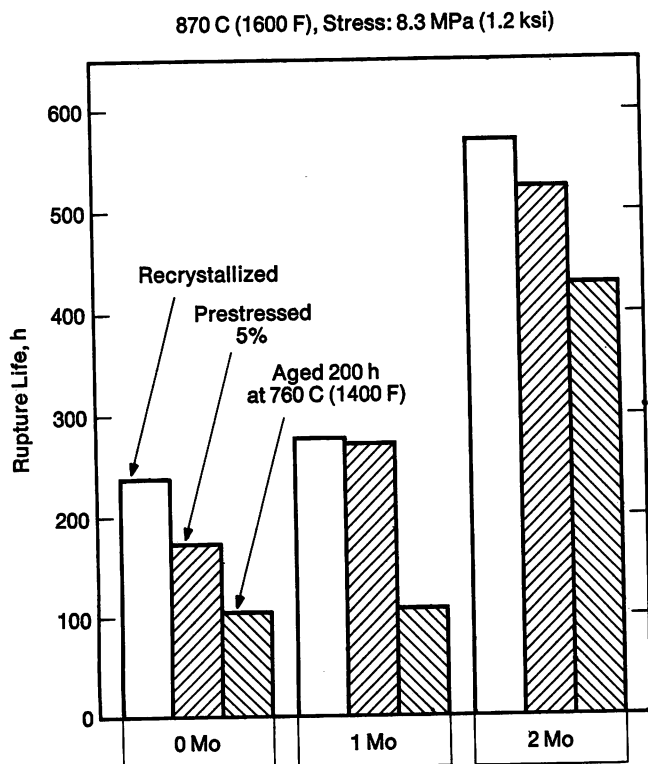


FIGURE 2—*Creep rupture life of low interstitial 18Cr ferritic stainless steels with 0, 1 and 2% Mo at 870 C (1600 F) and 8.3 MPa (1.2 ksi).*
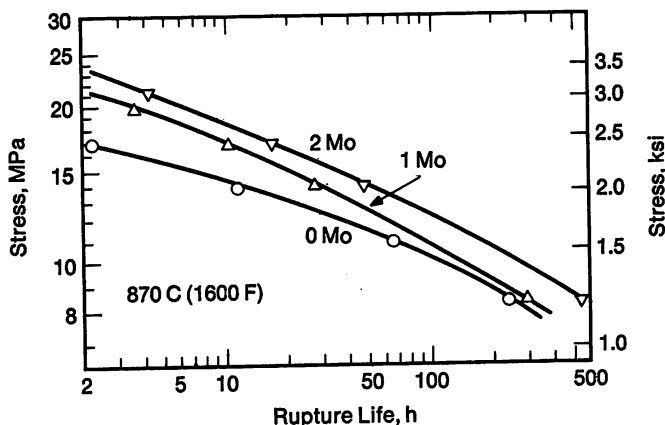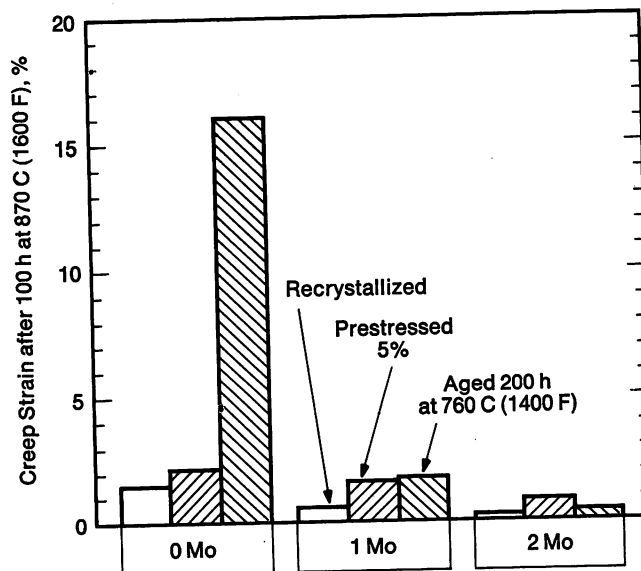


FIGURE 3—*Total creep strain after 100 hours at 870 C (1600 F) and 8.3 MPa (1.2 ksi) for low interstitial 18Cr ferritic stainless steels with 0, 1 and 2% Mo.*

**Table III**—Microprobe Analyses of Laves Phase Particles Extracted after Aging at 870 C (1600 F) for 384 Hours

| Element | 18Cr-0Mo | | 18Cr-1Mo | | 18Cr-2Mo | |
| --- | --- | --- | --- | --- | --- | --- |
| | Wt. Pct. | At. Pct. | Wt. Pct. | At. Pct. | Wt. Pct. | At. Pct. |
| Fe | 54.69 | 60.25 | 48.27 | 54.52 | 49.27 | 54.98 |
| Nb | 32.66 | 21.62 | 29.90 | 20.30 | 20.12 | 13.50 |
| Mo | $\ll 1$ | $\ll 1$ | 10.02 | 6.59 | 17.00 | 11.04 |
| Cr | 7.07 | 8.37 | 6.88 | 8.34 | 8.31 | 9.96 |
| Si | 3.74 | 8.19 | 4.06 | 9.12 | 3.99 | 8.86 |
| Ti | 1.22 | 1.57 | 0.86 | 1.14 | 1.28 | 1.66 |

was $Fe_2(Nb, Mo)$. As the bulk Mo content increased, the Mo in the Laves phase increased while the niobium content decreased. A detailed microprobe analysis for Laves phase particles extracted after aging at 870 C (1600 F) for 384 hours is listed in Table III. Apparently, molybdenum plays a dual role in improving the creep strength of the 18 Cr low interstitial ferritic stainless steels. First, it acts as a solid solution strengthener. Second, Mo enhances the role of the Nb by substituting for it in the lattice of the Laves phase which inevitably forms at these temperatures. This in turn allows more of the Nb to remain in the matrix to strengthen by carbide formation or some other undetermined mechanism.

C. T. SIMS, *General Electric Company*. The effect of molybdenum in improving the effect of chromium on corrosion resistance is dramatic, particularly in view of the fact that both elements are in the same group of the periodic system. Do you have any information on why this is occurring?

R. K. PITLER. I do not have a theoretical explanation for this synergistic effect. It has been observed before, particularly in some early work on ferritic stainless steels.

J. B. GUERNSEY, *Jessop Steel Company*. The role of copper in nickel-chromium-molybdenum alloys is not straightforward. Copper is definitely beneficial under very acidic conditions, but in more borderline environments where localized, pitting and crevice corrosion are encountered, copper has a detrimental effect. In your Figure 13, for example, H-20 Mod and JS-700 significantly outperform JS-777 which is the same alloy except for the addition of 2% Cu.

R. K. PITLER. One additional point is that the 2% Ni addition to the 29% Cr-4% Mo ferritic steel results in a dramatic improvement in the general corrosion resistance in sulfuric acid. It does not appear to influence pitting or crevice corrosion, but it does slightly degrade the resistance to stress corrosion cracking.

W. E. NUTTALL, *Armco, Inc.* Is the material that you designated Type 408 available commercially, and if so, how does its weldability compare with Type 409?

R. K. PITLER. I would say that it is not truly available commercially, and we have only limited information on its weldability.

# Nickel-Base Molybdenum-Containing Alloys for the Chemical Process Industry

by A. I. Asphanani and F. G. Hodge
Cabot Corporation

The term High Performance Alloys is used to describe a wide variety of nickel-base alloys that contain chromium and/or relatively high molybdenum contents. Included are the alloys called "Superalloys" in the gas turbine industry since they were destined for use in aircraft and aerospace applications and those alloys described as "Corrosion Resistant Alloys" that find application in the CPI. The emphasis of this paper will be on the latter group and specifically on those alloys described in Table I. With respect to a usage time frame, some of these alloys are relative newcomers but are assuming important roles in the chemical process industry. The austenitic stainless steels were developed and utilized early in the 1900s, while the development of the nickel-base alloys did not begin until about 1930. Initially, some of the alloys were produced only as castings, and the wrought versions were developed later. Since that time, there has been a steady progression of different or improved alloys emerging from the laboratories of the nickel-base alloy producers, and this trend is expected to continue.

Historically, while the stainless steels became the workhorses of the CPI, the use of these alloys was typically reserved for applications where it was adjudged that nothing else would work. At one time, the primary factor in the selection of construction materials was initial cost, and very little thought was given to the possible maintenance and downtime costs associated with the equipment. Today, the increasing costs of maintenance and downtime have placed a greater emphasis on the reliable performance of the process equipment. Data recently published[1] demonstrate that these costs have reached significant proportions. The annual amortized cost of equipment over the expected life is now important in the material selection.

Nickel has some unique electrochemical properties which make it important on its own as an alloying base. In reducing acid systems, nickel quite often assumes an open-circuit potential almost equal to the platinum potential. It does not, however, readily liberate hydrogen, and some oxidizing ion species are, therefore, required to promote the corrosion of pure nickel. Under certain circumstances, nickel has the ability to form a passive film and thereby show good corrosion resistance to many aerated aqueous environments. Unfortunately, the passive film formed is not very stable, and nickel pits when exposed to oxidizing chloride environments such as, for example, seawater.

One of the most important attributes of nickel, with respect to the formation of corrosion resistant alloys, is its metallurgical compatibility with a number of other metals such as copper, chromium, molybdenum and iron. A survey of the binary phase diagrams for nickel and these other elements shows a considerable solid solubility for them, and thus one can design alloys with wide ranges in composition. Nickel alloys are, in general, all austenitic; however, they can be subject to precipitation of intermetallic and carbide phases when aged. In some alloys designed for high temperature service, intermetallic and carbide precipitation reactions are encouraged

**Table I**—Composition of Hastelloy Nickel-Base Alloys

| Alloy | Element, % | | | | |
|---|---|---|---|---|---|
| | Cr | Mo | W | Fe | C |
| B-2 | 1.0[a] | 26.0-30.0 | — | 2.0 | 0.02[a] |
| C-276 | 14.5-16.5 | 15.0-17.0 | 3.0-4.5 | 4.0-7.0 | 0.02[a] |
| C-4 | 14.0-16.0 | 14.0-17.0 | — | 3.0[a] | 0.015[a] |
| G[b] | 21.0-23.5 | 5.5-7.5 | 1.0[a] | 18.0-21.0 | 0.05[a] |

[a] Maximum.
[b] Also contains 1.5-2.5 Cu, 1.75-2.5 Nb + Ta.

**Table II**—Mechanical Properties and Design Strengths of Sheet Materials at Room Temperature

| Alloy | Density, kg/m³ (lb/in.³) | Ultimate Tensile Strength, MPa (ksi) | 2% Offset Yield Strength, MPa (ksi) | Elongation in 51 mm (2 in.), % | HRB |
|---|---|---|---|---|---|
| B-2 | 9217 (0.333) | 955 (139) | 526 (76) | 53 | 95 |
| C-276 | 8885 (0.321) | 792 (115) | 356 (52) | 61 | 90 |
| C-4 | 8638 (0.312) | 801 (116) | 421 (61) | 54 | 90 |
| G | 8304 (0.300) | 703 (102) | 319 (46) | 61 | 84 |

to increase properties; however, for corrosion applications, the precipitation of second phases usually promotes corrosion attack. The problem is rarely encountered, however, because the alloys are supplied in the annealed condition, and the service temperatures rarely approach the level required for sensitization. In the iron-chromium-nickel austenitic stainless steels, the minimization of carbide precipitation can be achieved by lowering the carbon content to a maximum of about 0.03%. As the nickel content is increased from the nominal 8% in these alloys to that of the majority element, i.e., more than 50%, the nature of the carbide changes from a predominantly $M_{23}C_6$ to a $M_6C$, and the carbon solubility decreases by a factor of 10. It was, therefore, very difficult in the past to produce "L" grade material because of the state-of-the-art of melting. Many alloys attempted to circumvent this problem by adding carbide stabilizers to tie up the carbon with varying degrees of success. Some of the most recent developments in the nickel alloy field involve changes in melting technique. The transfer of alloys from air induction or vacuum induction melting to air arc plus argon-oxygen decarburization has provided a means for producing nickel alloys comparable in HAZ performance to the "L" grades of stainless steels but with carbon contents of 0.01% or less.

Mechanically, these alloys are viable materials of construction, and all have ASME design strengths above that for Type 316L stainless steel. Table II compares the average mechanical properties and the design values. A higher design strength can be important in the utilization of one of these alloys since it may be possible to use a thinner section and thereby reduce the relative material cost.

## Characteristics of Individual Alloys

### Hastelloy Alloy B-2

Within the nickel-molybdenum series, there is one major alloy: Hastelloy alloy B-2. Alloy B-2 is a low carbon and low silicon (0.02%, 0.08% maximum) version of Hastelloy alloy B. The alloy is uniquely different from other corrosion alloys because it does not contain chromium. Molybdenum, the primary alloying element, provides significant corrosion resistance to reducing environments. The presumed mechanism for the improved

resistance is the rendering of the Ni-Mo alloy similar to pure molybdenum in its resistance to hydration.

Alloy B-2 was developed to be resistant to hydrochloric acid and is used in many applications in the distillation, condensation and handling of this acid. Alloy B-2 is recommended for service in handling all concentrations of hydrochloric acid in the temperature range 70 to 100 C (160 to 210 F) and for handling wet hydrogen chloride gas as shown in Figure 1.

Alloy B-2 has excellent resistance to pure sulfuric acid at all concentrations and temperatures below 60% acid and good resistance to 100 C (210 F) above 60% acid as shown in Figure 2. The alloy is resistant to a number of other environments such as hydrofluoric and phosphoric acids and numerous organic acids such as acetic, formic and cresylic. It is also resistant to many chloride-bearing salts (nonoxidizing) such as aluminum chloride, magnesium chloride and antimony chloride.

Since alloy B-2 is nickel-rich ($\sim$ 70%), it is resistant to chloride-induced stress corrosion cracking (SCC). Alloy B, for example, is used as spray nozzles for a magnesium chloride dryer. By virtue of the high molybdenum content, it is highly resistant to pitting attack in acid
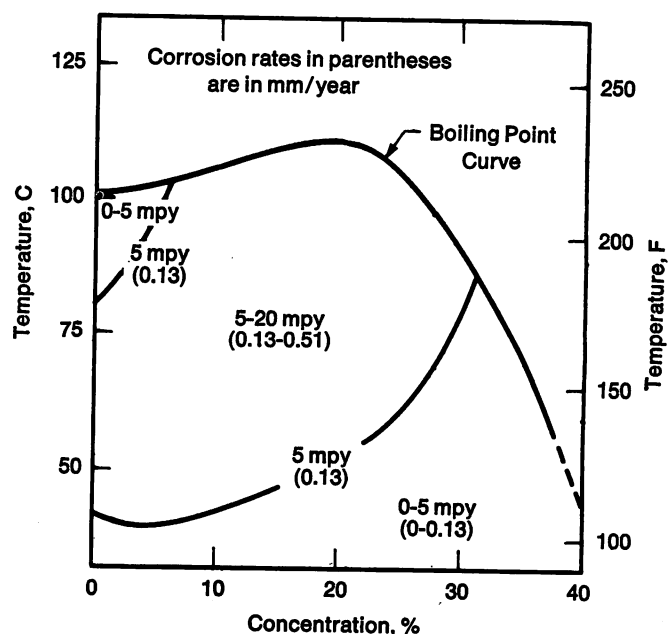


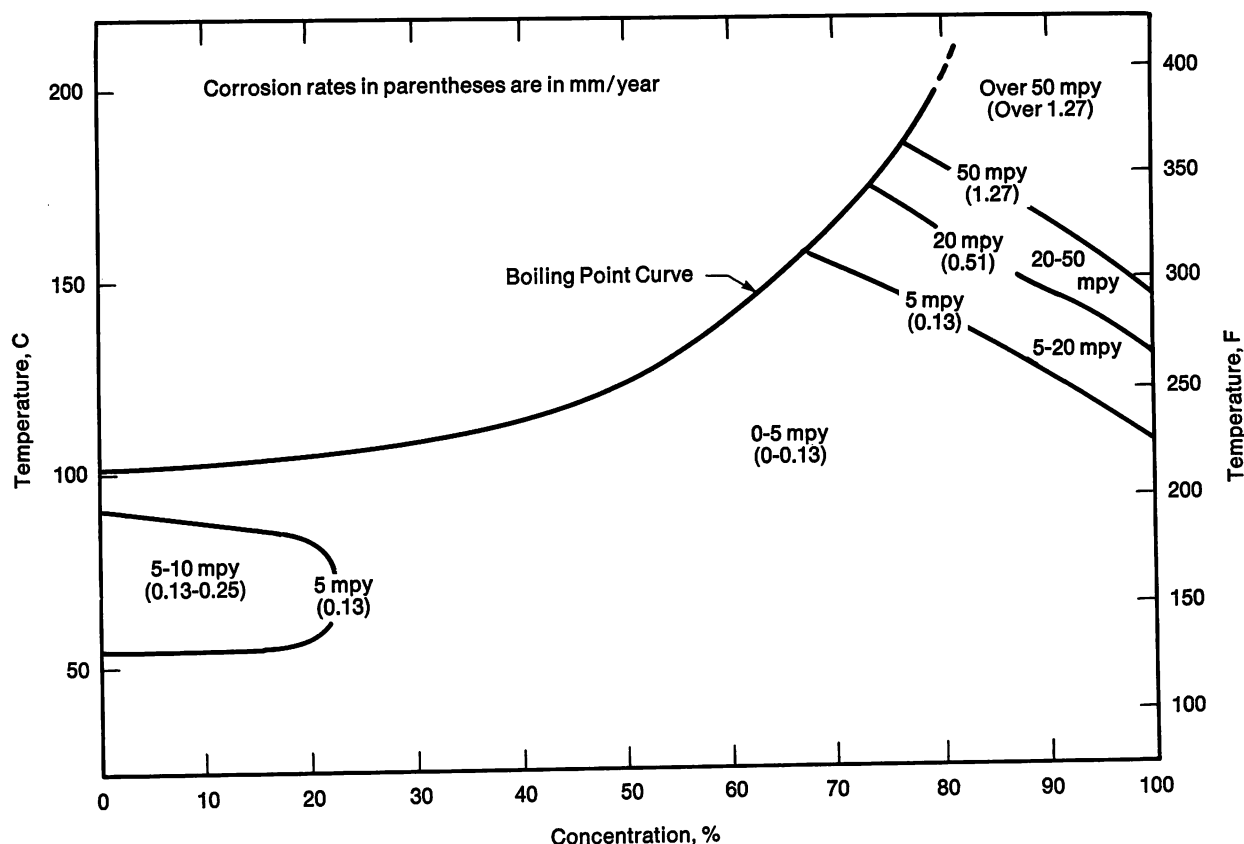FIGURE 1—Resistance of Hastelloy alloy B-2 to hydrochloric acid.

FIGURE 2—Resistance of Hastelloy alloy B-2 to sulfuric acid.

chloride environments.

Alloy B-2 is not recommended for elevated temperature service except in very specific circumstances. There is no chromium in the alloy and, therefore, the alloy scales heavily at temperatures above 760 C (1400 F) in air. A nonprotective layer of molybdenum trioxide (MoO₃) forms and results in a heavy, green oxidation scale. In a dry chlorine environment, however, alloy B-2 has demonstrated good resistance. Alloy B-2 has excellent elevated temperature (> 900 C, 1650 F) mechanical properties because of the high molybdenum content and has been used for mechanical components in reducing environments and vacuum furnaces. Because of the formation of the intermetallic phases Ni₃Mo and Ni₄Mo after long time aging, the use of alloy B-2 in the temperature range of 600-850 C (1110-1560 F) is not recommended regardless of environment.

The major factor which limits the use of alloy B-2 is poor corrosion resistance in oxidizing environments. It has virtually no corrosion resistance to oxidizing acids such as nitric and chromic or to oxidizing salts such as ferric chloride or cupric chloride. The presence of oxidizing salts in reducing acids must also be given attention. Oxidizing salts such as ferric chloride, ferric sulfate or cupric chloride, even when present in the ppm range, can significantly accelerate attack in hydrochloric or sulfuric acids. Even dissolved oxygen has sufficient oxidizing power to affect the corrosion rates for

alloy B-2 in hydrochloric acid.

Alloy B-2 also shows excellent resistance to pure phosphoric acid. Alloy B-2 has found wide acceptance in a number of key chemical processes by virtue of its resistance to corrosive catalysts. The application typically involves the halogens (Cl, F and Br) with or without the presence of reducing type acids, such as hydrochloric, hydrofluoric, bromic or sulfuric. The alloy has unique resistance to the aluminum chloride catalysts used in the alkylation of benzene to ethyl benzene (Friedel-Crafts type processes). The ethyl benzene is used for production of styrene and cumene. Alloy B-2 is also used in the isomerization of paraffin hydrocarbons such as butane to isobutane with antimony chloride-aluminum chloride catalysts.

The halide catalyst systems used in the newer processes for acetic acid and ethylene glycol have demonstrated significant cost reductions for producing these chemicals. Alloy B-2 is demonstrating excellent corrosion resistance in this equipment and is considered to be a prime factor in making these both viable chemical processes.

Castings for use in conjunction with alloy B-2 equipment are available in two compositions, both of which are listed in ASTM A494. The N-12M-2 version corresponds to Chlorimet 2. For good, consistent corrosion resistance, the carbon range for N-12M-1 is too broad, and some castings are encountered that have poor inter-

granular corrosion resistance but are within specification.

The corrosion resistance of Alloy B castings, in general, is not, even with the identical composition, the same as the wrought version. This is the result of significant interdendritic segregation and carbides that exist in the as-cast structure. It is less of a problem with the N-12M-2 composition because of the lower carbon content and the higher molybdenum content. A comparison of the isocorrosion diagram in hydrochloric acid[2] shows that there is still a minor difference.

### Hastelloy Alloy C-276

Hastelloy alloy C-276 is a low carbon (0.02% maximum) and low silicon (0.08% maximum) version of Hastelloy alloy C. Alloy C-276 was developed to overcome the corrosion problems associated with welding of alloy C. When used in the as-welded condition, alloy C was often susceptible to serious intergranular corrosion attack in many oxidizing and chloride-containing environments. The low C and Si content of alloy C-276 prevents continuous grain boundary precipitates in the weld heat affected zone. Thus alloy C-276 can be used in most applications in the as-welded condition without severe intergranular attack.

The descriptions of the applications for alloy C-276 in the process industries are extensive and diverse. The alloy is extremely versatile because of its equal levels of chromium and molybdenum which provide it with good

resistance in both oxidizing and reducing media including conditions with halogen ion contamination. The pitting and crevice corrosion resistance of alloy C-276 makes it an excellent choice when dealing with acid chloride salts whether in the process or merely handling hot seawater in heat exchangers.

Isocorrosion diagrams for alloy C-276 have been developed for a number or inorganic acids[3]; for example, sulfuric acid in Figure 3. Rather than having one or two acid systems where the corrosion resistance is exceptional, as was the case with alloy B-2, alloy C-276 is a good compromise material for a number of systems. For example, in sulfuric acid coolers handling 98% acid from the absorption tower, alloy C-276 is not the optimum alloy for the process side corrosion but it is excellent for the water side corrosion permitting the use of brackish water or seawater. Concentrated sulfuric acid is used to dry chlorine gas. The dissolved chlorine accelerates the corrosion of alloy B-2, but alloy C-276 has performed quite satisfactorily in a number of chlorine drying installations.

Other examples are the spray applications of alloy C-276 powder to steam plant boiler tubes to prevent liquid phase corrosion. A complex alkali iron sulfate that forms a liquid slag in the range of 570-700 C (1060-1290 F) was attributed with causing the rapid attack experienced on the chrome-moly steel tubes. A spray application, without removal of the tubes, of a thin coating of alloy C-276 was instrumental in reducing the rate of attack
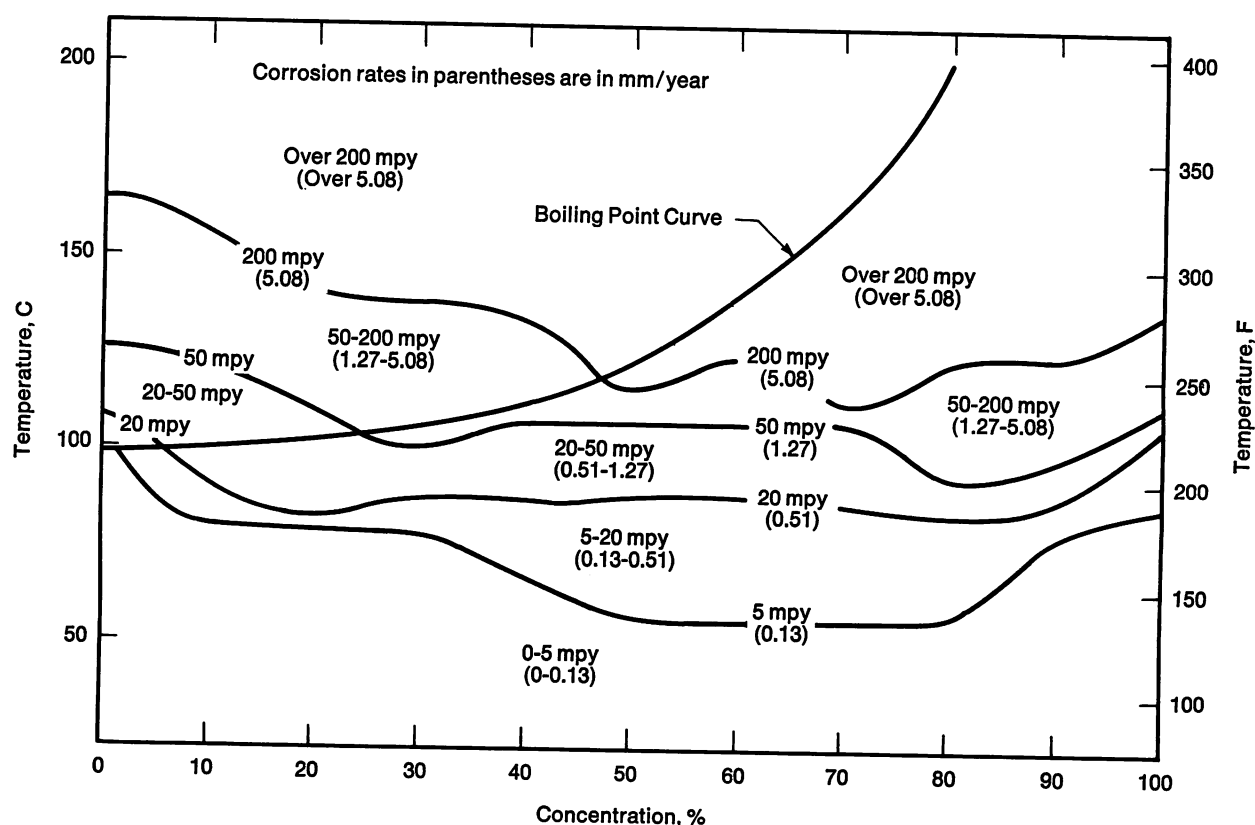


FIGURE 3—Resistance of Hastelloy alloy C-276 to sulfuric acid.

from 41 mpy to 3 mpy.

Many new applications for alloy C-276 have evolved as a result of increased activity in scrubbers for the pollution control industry. Induced draft fans operate in a particularly aggressive environment because they are exposed to wet/dry conditions. Alloy C-276 has functioned very satisfactorily for years in an induced draft fan for a municipal incinerator in Grosse Point, Michigan. Alloy C-276 has been indicated as a satisfactory material for scrubber construction where problems of localized attack have occurred with Ni-Cr-Mo-Fe-Cu alloys because of pH, temperature or chloride content.

### Hastelloy Alloy C-4

To achieve improved stability with regard to precipitation of both carbides and intermetallic phases, a new Ni-Cr-Mo alloy known as Hastelloy alloy C-4 has been developed. The control of these secondary phases results in excellent high temperature stability, such that the corrosion resistance and mechanical properties in the thermally aged condition are similar to the annealed condition.

Within the broad scope of chemical processing, numerous examples exist where oxidizing and reducing conditions can cause serious intergranular corrosion of a sensitized (precipitated) microstructure. The sensitized structure can result from several sources such as: (1) improper anneal, (2) welding, (3) thermomechanical processing such as hot forming or rolling operations, (4) stress relief or normalizing treatments required for carbon steel backing of clad materials, or (5) operation of process equipment in the sensitizing range. Alloy C-4 represents a significant improvement since the alloy can be subjected to temperatures in the normal sensitizing range 550 to 1090 C (1020 to 1995 F) for extended periods without experiencing the severe corrosion attack that plagues the common austenitic alloys.

As shown in Table I, the compositions of alloys C-4 and C-276 are, with the exception of iron and tungsten, approximately the same. Likewise, the general corrosion resistance of the two alloys is generally the same. In strongly reducing media like hydrochloric acid, alloy C-4 has slightly higher rates than alloy C-276, but in oxidizing media the results are reversed. It would appear that these differences relate to the effects of iron and tungsten. Alloy C-4 offers good corrosion resistance to a wide variety of media including organic acids and acid chloride solutions. Isocorrosion diagrams for alloy C-4 have also been developed for a series of inorganic acids.[3]

Castings for use in conjunction with alloys C-276 or C-4 are currently available in two compositions that are listed in ASTM A494. The CW-12M-1 version corresponds to cast alloy C while the CW-12M-2 version corresponds to Chlorimet 3. For good, consistent corrosion resistance, the carbon range for the CW-12M-1 is too

broad, and some castings are encountered that have poor intergranular corrosion resistance but are within the specification.

A further problem associated with the corrosion resistance of cast alloy C is the precipitated intermetallic phases in the interdendritic areas. These phases are not homogenized with a solution heat treatment and promote localized attack in some media. Severe interdendritic attack was observed on cast alloy C bolts in a pulp and paper chlorine-containing environment. Bolts made from wrought bar stock had corrosion rates less than 1 mpy. Similar experiences have been encountered with cast pipe fittings and valves.

Modification of the composition of Alloy C to produce alloy C-4 has eliminated the presence of the intermetallic phases in the wrought alloy and minimized its presence in the cast alloy. The CW-12M-2 composition is closer to being stable by virtue of the absence of the tungsten, however, the chromium, molybdenum and iron levels can also produce the metallurgical instability.

Hastelloy alloy C-4C has been developed to couple low carbon with a balanced composition to avoid the intermetallic phases. Corrosion resistance of castings made from this alloy approaches that of wrought alloys C-276 and C-4 in the accelerated corrosion test normally applied (ASTM G-28) to these alloys. Coverage for this alloy under ASTM A494 has been requested.

### Hastelloy Alloy G

Hastelloy alloy G has a nickel base with additions of 22% chromium, 19% iron, 6.5% molybdenum and 2% copper and stabilized with 2% niobium plus tantalum. Although some competitive materials use only 8 or 10 times the carbon content, a larger amount of niobium is used in alloy G to promote more satisfactory stabilization. It is the intent to have alloy G used in the as-welded condition, even under circumstance of multipass welding. The niobium addition has also been noted to provide better resistance than titanium in highly oxidizing environments. Because of the nickel base, the alloy is resistant to chloride-induced stress corrosion cracking.

The 2% copper addition is effective in enhancing the corrosion resistance of the alloy in reducing acids such as sulfuric and phosphoric. The copper addition appears to alter the cathodic process by changing the over voltage for the reaction. This effectively reduces the corrosion rate of the alloy. The isocorrosion diagram for alloy G in sulfuric acid (Figure 4) compares very favorably with that of alloy C-276 at the dilute end (< 50%). Other less expensive alloys also resist pure sulfuric acid; however, alloy G also resists combinations of sulfuric and halides. Alloy G has excellent resistance to phosphoric acid and has been used in wet process acid evaporators, agitator shafts, pumps and super phosphoric acid evaporators.
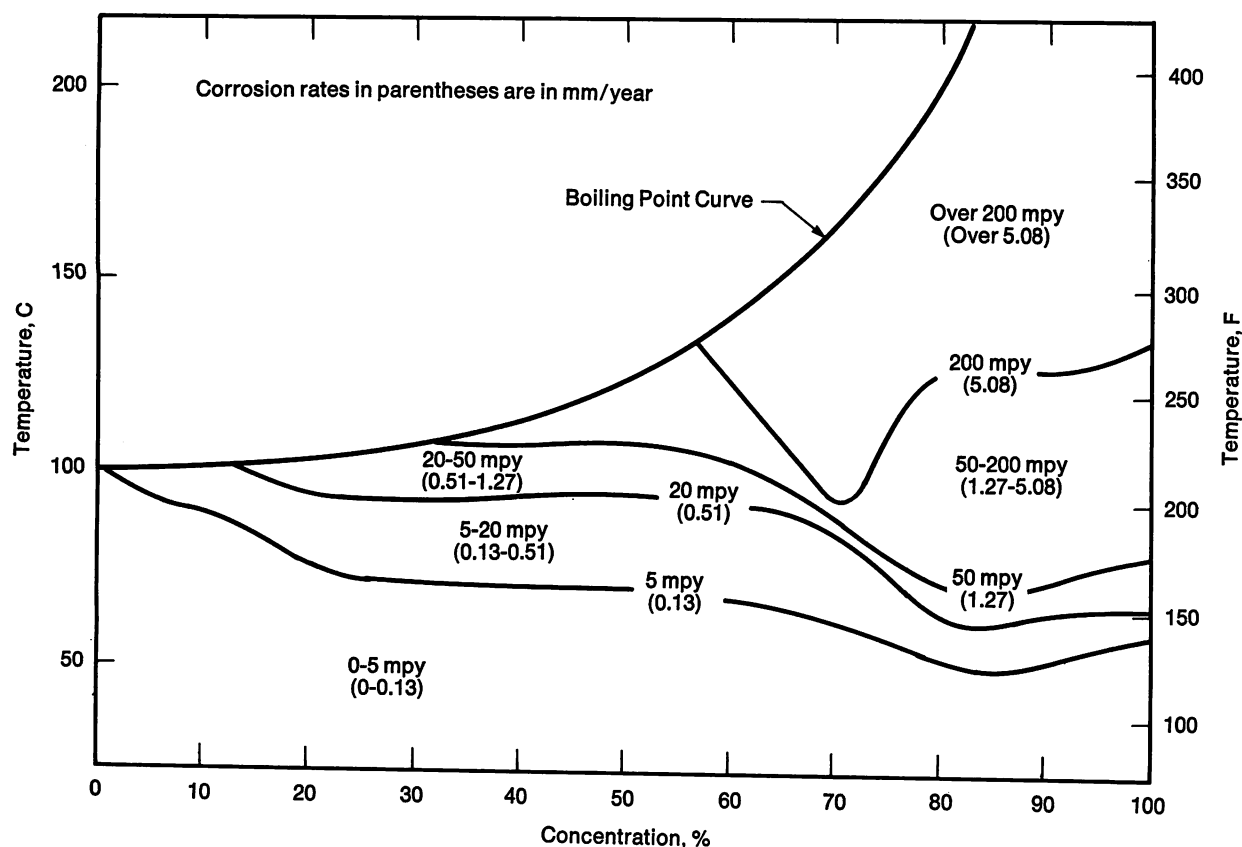
FIGURE 4—Resistance of Hastelloy alloy G to sulfuric acid.

Applications for alloy G have had a rapid increase in the past few years. In addition to traditional applications in sulfuric and phosphoric acids, alloy G has found wide acceptance in other types of chemical applications such as HF manufacture and processing of organic chemicals, particularly those with chlorides present. However, the largest growth has been in pollution control equipment. Alloy G has demonstrated excellent performance in municipal garbage incinerator systems, including fans, ducts and scrubber equipment. The $SO_2$ scrubbing systems for power plants using water or alkaline quench have been incorporating alloy G as a major material of construction because of its resistance to sulfuric acid and conditions where the chloride ion can concentrate. Two recent publications[4,5] summarize the results of corrosion tests run in a number of scrubber environments and in actual plant experience. These data show the diverse nature of attack that can occur depending on the chemistry of the system. One scrubber environment has been encountered where, because of low pH, high chloride levels and oxidizing ions, pitting attack has occurred wherever fly ash deposits. In areas where the surface is kept clean, much less attack occurred. As discussed earlier, there are some scrubber conditions where only alloy C-276 is resistant.

Cast components for use with alloy G wrought equipment can be obtained from material of the same composition. No coverage is presently available within the ASTM; however, it has been requested and should be available in the future. Castings in alloy G suffer from similar problems encountered in other cast nickel-base alloys, i.e., lower corrosion resistance than the equivalent wrought alloys. Fewer intermetallic phases form, but carbides have been observed on grain boundaries, and a solution anneal following casting is suggested.

An improved version of alloy G, Hastelloy alloy G-3, has been introduced during 1979 and offers some improvement in the areas of carbide precipitation in the wrought and cast versions. No coverage is yet available in ASTM or ASME; however, ASME code case 1860 has been granted. The significant compositional differences include lower carbon (0.015% max. vs. 0.05% max.), lower Nb + Ta (0.3% typical vs. 2.0%) and increased molybdenum (7.0% nominal vs. 6.5% nominal).

## Corrosion Properties

### Uniform Corrosion

Generally, the high performance alloys offer much better resistance to uniform corrosion than do the austenitic stainless steels. The data presented in Table III clearly depict the superior performance of the nickel-base alloys over that of Type 316L stainless steel in various organic and inorganic acids (formic, acetic, phosphoric, hydrochloric and sulfuric). The excellent resistance of

**Table III**—Corrosion of Nickel-Base Alloys and Type 316L in Indicated Acids (Duplicate Specimens)

| Alloy | Boiling: 24-Hour Period | | | Boiling: Four 24-Hour Periods | | | | |
| | 10% HCL | 10% H$_2$SO$_4$ | 10% HNO$_3$ | 99% CH$_3$COOH | 40% HCOOH | 88% HCOOH | 55% H$_3$PO$_4$ | 85% H$_3$PO$_4$ |
|---|---|---|---|---|---|---|---|---|
| B-2 | 7 mpy[a] | 1.8 mpy | 19,309 mpy | 1.2 mpy | 0.4 mpy | 0.6 mpy | 3.6 mpy | 4 mpy |
| C-276 | 228 | 23 | 17 | 0.4 | 2.9 | 1.8 | 2.8 | 20 |
| C-4 | 250 | 22 | 5.9 | 0.4 | 2.9 | 2.0 | 2.5 | 61 |
| G | 1154 | 25 | 0.8 | 1.6 | 5.1 | 4.3 | 3.9 | 27 |
| 316L | 17,986[b] | 2397 | 2.1 | 3.8 | 42 | 19 | 7.9 | 645 |

[a] Multiply by 0.0254 to obtain millimeters per year.
[b] Specimens dissolved.

**Table IV**—Corrosion of Nickel-Base Alloys and Type 316L in Chloride Solutions (Duplicate Specimens)

| Alloy | 10% FeCl$_3$; Specimens with Artificial Crevice | | Smooth Specimens; 24 h Period | |
| | 25 C (77 F)— 240 h | 50 C (122 F)— 100 h | 7 Vol. % H$_2$SO$_4$ + 3 Vol. % HCl + 1% FeCl$_3$ + 1% CuCl$_2$ | |
| | | | 25 C (77 F) | 102 C (215 F) |
|---|---|---|---|---|
| C-276 | 0.2 mpy | 0.2 mpy | 0.3 mpy | 24 mpy |
| C-4 | 0.3 | 0.5 | 0.3 | 1477 (pitting) |
| 625 | 1.5 | 124 (crevice) | 0.3 | 1892 (pitting) |
| G | 16 | 23 (crevice) | 0.4 | 1758 (pitting) |
| 316L | 312 (crevice) | 460 (crevice) | 101 (pitting) | 3909 (pitting) |

**Table V**—Stress Corrosion Cracking Test Results (U-Bend Specimens)

| Alloy | 200 h Exposure; Boiling 45% MgCl$_2$ | 30-Day Exposure; 4% NaCl + 1% H$_3$PO$_4$ | |
| | | Boiling at ~101 C (214 F) | Autoclave at ~141 C (285 F) |
|---|---|---|---|
| B-2 | no cracking | * | * |
| C-276 | no cracking | no cracking | no cracking |
| C-4 | no cracking | * | * |
| G | no cracking | no cracking | no cracking |
| 316L | cracking | cracking | cracking |

* Not tested; however, as this chloride environment is not as severe as the boiling 45% MgCl$_2$, it can be assumed that no cracking would occur.

the high performance alloys is expected from their high chromium and/or molybdenum contents. The addition of chromium imparts resistance to oxidizing environments[6] while the addition of molybdenum, especially to nickel, provides an improved resistance to reducing environments, specifically in hydrochloric acid.

**Localized Corrosion**

Localized forms of corrosive attack (pits, crevices and "underdeposit" corrosion) are usually induced on stainless steels from the presence of chloride ions and occur frequently under oxidizing conditions. With chromium additions, corrosion resistance to oxidizing environments improves. The addition of both chromium and molybdenum (and tungsten to some extent) appears effective in reducing the localized corrosive attack in oxidizing chloride solutions. Type 316L stainless steel pits and suffers crevice corrosion attack at room temperature.

Chromium and molybdenum (or tungsten) also contribute significantly to the excellent resistance of the high performance nickel-base alloys to pitting/crevice corrosion. No attack on the nickel alloys is observed in room temperature tests (Table IV). However, at temperatures above ambient, i.e., 50 and 100 C (120 and 210 F), only alloy C-276 with its 16% molybdenum and 4% tungsten shows no pitting attack. Even alloy C-4, with nominally 16% molybdenum, suffers a small amount of localized attack presumably because of the lack of tungsten. Alloy 625 with 9% molybdenum suffers localized attack whether at 50 or 100 C (120 or 210 F) (Table IV). The effect of molybdenum (and tungsten) on the resistance of nickel-base alloys to localized corrosion has previously

been discussed.[8]

**Stress Corrosion Cracking**

While austenitic stainless steels, typically the 300 series, are highly susceptible to chloride stress cracking, the high performance alloys, especially the nickel-base alloys, offer much improved resistance to SCC in a wide variety of chloride environments. The data presented in Table V confirm the excellent resistance of alloys with more than 40% nickel. No cracking of these alloys is observed in boiling $MgCl_2$ in accordance with data established earlier on the beneficial effect of increasing nickel content.[9]

# Applications

Applications of Hastelloy alloys have expanded with the greater degree of sophistication achieved in chemical engineering. Today's continuous processing plants, often large single-train units, demand dependable performance. The malfunction of a single component can shut down several processes that are interdependent for feedstocks. Also, the chemical industry is constantly developing new processes operating at higher temperatures and pressures, both of which tend to create new corrosion problems.

It also is important to note that some major breakthroughs in chemical processing have been the result of new catalyst systems. The new catalyst systems, particularly those based on the halogen series, can be extremely aggressive requiring the use of corrosion resistant alloys.

**Chemical Industry**

Alfa-Laval AB, Lund, Sweden, was faced with the problem of finding a material that would withstand both sulfuric acid and brackish seawater. The solution was to use Hastelloy alloy C-276 in the company's unique, compact plate heat exchangers. The heat exchangers are used to cool concentrated sulfuric acid with seawater as the cooling medium (Figure 5).

The plate exchanger consists of a variable number of gasketed alloy C-276 channel plates clamped between a stationary frame plate and a movable pressure plate. The channel plates and pressure plate are hung on a central carrying bar. Standard platage for the $H_2SO_4$ cooling consists of parallel channels with all inlets and outlets at the same end.

Typically, a 998 Mg (1100 t) per day pyrite plant uses four plate coolers for absorption acid cooling and three for drying tower cooling. Each of these seven units has a heat transfer surface of about 40 m² (430 ft²) and cools 250 m³/h (8800 ft³/h) of 98.5% sulfuric acid from 90 to 70 C (195 to 160 F) and 96% $H_2SO_4$ from 70 to 55 C (195 to 130 F).

Although Hastelloy alloy C-276 is used primarily where seawater is the cooling media, it is also used for 90 to 96% acid and fresh-water cooling because stainless steel can corrode at these concentrations.

In an organic acid application in the United Kingdom, a Hastelloy alloy C-276 heat exchanger is used as a reboiler in the esterification of ethyl acrylate plastic. The reboiler supplies heat to speed the reaction between ethyl alcohol and acrylic acid in an extremely corrosive process (Figure 6).

Steam at 276 kPa (40 psi) heats the mixture to 140 C (285 F). The exchanger contains 787 seamless tubes of alloy C-276 which are 39 mm (1.5 in.) in diameter by 2.7 mm (0.11 in.) wall. The tubes are contained in a shell which is 3 m (9.8 ft) long by 160 mm (6.3 in.) in diameter. Alloy C-276 gives about 18 months service and has been determined to be the most economical material of construction to withstand the extremely corrosive conditions.
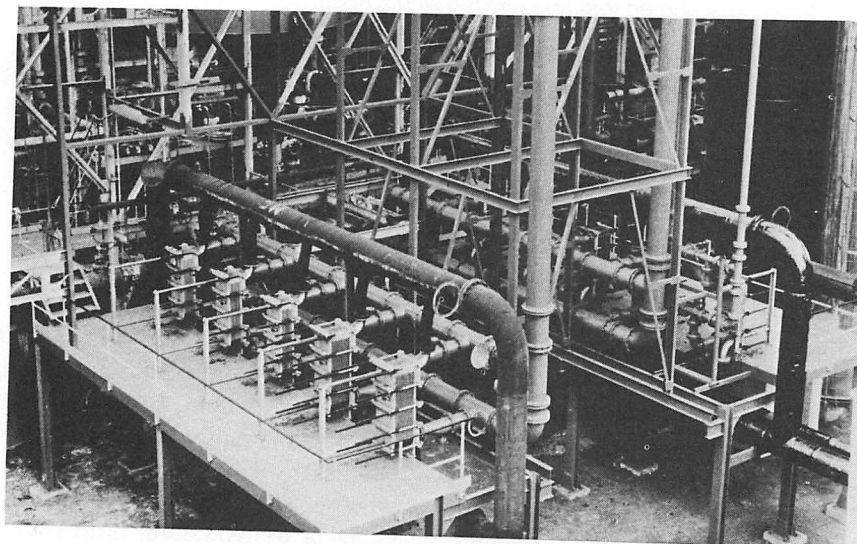


*FIGURE 5—Sulfuric acid/seawater heat exchanger using Hastelloy alloy C-276.*
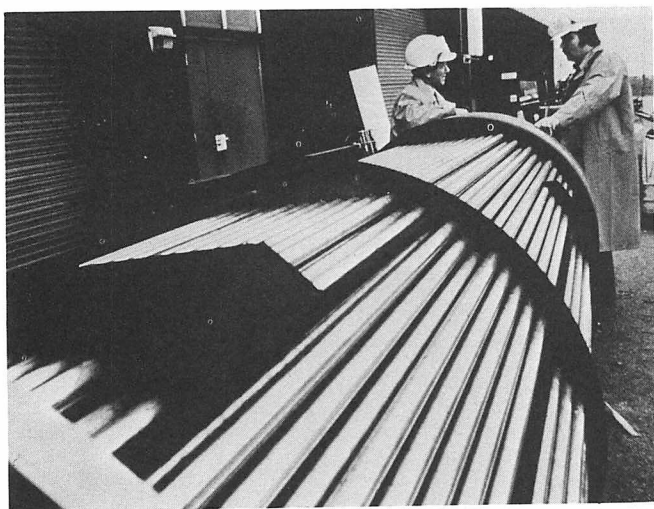
FIGURE 6—*Hastelloy alloy C-276 tubing in a heat exchanger used in the esterification of ethyl acrylate plastic.*

At the same plant, Hastelloy alloy B-2 heat exchangers are used in the methyl methacrylate plant because of its resistance to hot 98% sulfuric acid in the esterification process (Figure 7).

## Petrochemicals

In the Phillips Petroleum catalytic isomerization process for the production of high purity isobutane, Hastelloy alloy B is extensively used to protect reactor vessels and other components from the severe pitting attack to which steels are subject. In many instances, steel reactor shells are lined with 1.5 mm (16 gauge) alloy B sheet.

One typical plant processes 700 m³ (4400 barrels) per day of normal butane, 40% of which is converted to isobutane in the vapor phase, using aluminum chloride as the catalyst. Feed Stock is heated to 115 C (240 F). It is then passed, consecutively, through the preheaters and reactors lined with Hastelloy alloy B. Both of the bed-type vessels are filled with bauxite particles on which
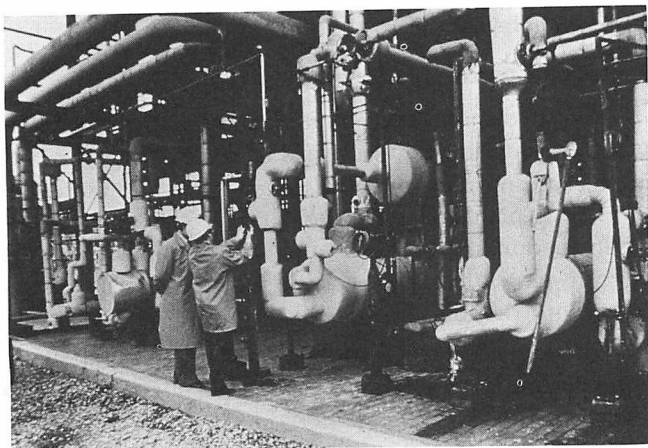


FIGURE 7—*A heat exchanger fabricated from Hastelloy alloy B-2 in a methyl methacrylate plant.*
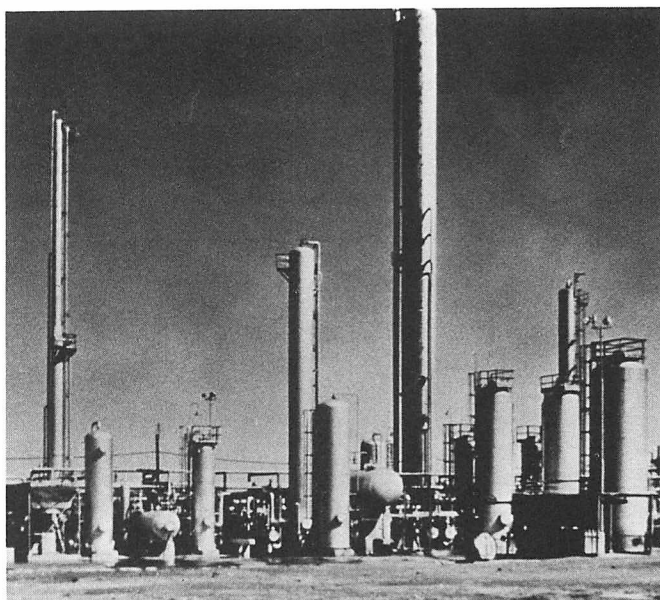


FIGURE 8—*Preheaters and reactors in this petrochemical plant processing normal butane are lined with Hastelloy alloy B.*

aluminum chloride has been sublimed at 150 C (300 F). Up to 10% hydrogen chloride is used to promote the catalytic reaction (Figure 8).

There are two preheaters and two reactors in the plant. Processing is done in two parallel streams up to the reaction stage. From the reactor, the effluent passes through a bauxite-filled guard chamber and an HCl feed tank that is lined, on the bottom half, with alloy B. From here, the effluent passes through an HCl stripper and a deisobutanizer. Isobutane is the final overhead product of this vessel.

## Agrichemicals

As the world demand for food increases, so does the need for fertilizers, herbicides, fungicides and insecticides. Many aggressive chemicals are involved in the manufacturing processes, and they attack ordinary engineering materials during processing as readily as they attack the weeds, insects and fungi when in use.

Hastelloy alloy G is seeing considerably increased use in the production of phosphate fertilizers, where phophorus pentoxide is the prime corrodant. At the same time, Hastelloy alloy C-276 is specified to handle sodium hypochlorite, carbonates and sulfuric acid in the control chemicals.

One of the largest applications of alloy G is in the Bartow, Florida plant of Farmland Industries. Farmland supplies phophorus pentoxide extensively throughout the midwestern United States.

A major component in this plant is a huge alloy G draft tube in an isothermal reactor used in the early stages of the phosphate conversion process (Figure 9). Alloy G also is used in the system's evaporator where the
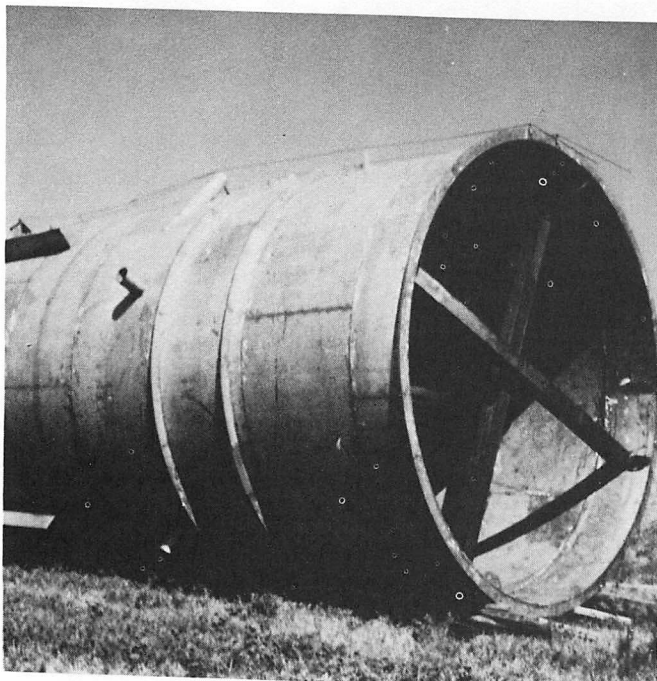
FIGURE 9—*Hastelloy alloy G draft tube in an agrichemical plant reactor.*



FIGURE 10—*High performance alloy vessel used in the production of carbomate nematicides.*

$P_2O_5$ concentration, and corrosive attack, is greatest.

The draft tube fits into a 10.7 m (35 ft) diameter reactor. The tube is 4.1 m (13.5 ft) in diameter and 6.8 m (22.3 ft) long. It operates 24 hours a day, seven days a week. The process at this point is carried out under a vacuum of 241 to 267 mm (9.5 to 10.5 in.) of mercury, absolute, and at temperatures bewteen 77 and 82 C (170 and 180 F). Here the solution is about 30% $P_2O_5$ and 40% solids. Its specific gravity is 1.65. Slurry is pumped through the draft tube at a rate of 12.6 m³/second (445 ft³/second).

Nearly 8 km (5 mi) of Hastelloy alloy G tubing is used in the tube bundle of the final evaporator which brings the acid content of the solution to its shipping concentration. In tests conducted before a final material selection was made, Hastelloy alloy G showed more than double the corrosion resistance of the nearest competitive alloy.

Operating temperature of the bundle ranges from 175 to 205 C (350 to 400 F). The solution is 68% $P_2O_5$, 0.25% fluorine and 0.5% solids.

Farmland Industries also use a 910 mm (36 in.) diameter Hastelloy alloy G centrifugal pump. The pump and tube bundle have been operating since 1973. Finally, in another reactor at Farmland, agitator blades are made of alloy G. Here the material withstands an abrasive-corrosive environment consisting of 28 to 30% $P_2O_5$ and 40 to 50% gypsum at 82 C (180 F). Upon inspection after 2½ years of service, the blades were still in excellent condition.
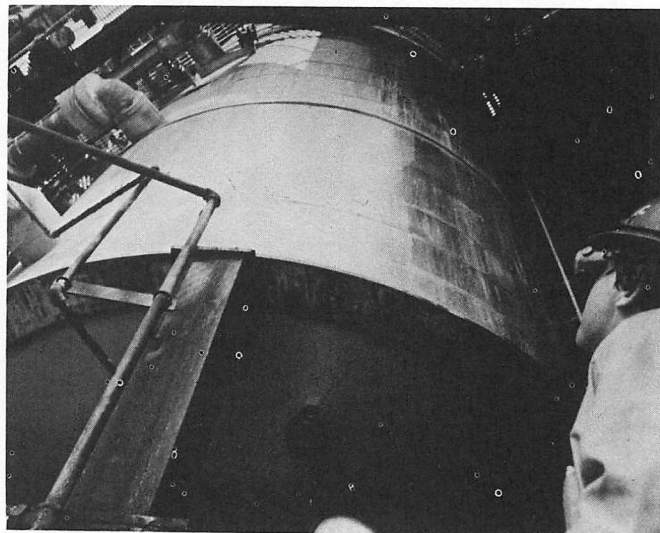
The use of Hastelloy alloy C-276, and its earlier version, alloy C, in the production of carbamate nematicides has developed extensively during the past 10 to 15 years. Recently FMC Corporation, Baltimore, Maryland, used alloy C-276 to replace a glass-lined vessel in this process. Previously, a set of glass-lined vessels required inspection every four to five weeks and often had to be patched because of the corrosive and erosive action of the solutions. Each maintenance shutdown lasted about 36 hours. Now maintenance is limited to only two periods a year. As a bonus, it is no longer necessary to keep a stand-by vessel in reserve (Figure 10).

The first step in production of the nematicide involves mixing a phenolic compound with abrasive soda ash. The reaction is exothermic, so the vessel is cooled by pumping water through a coil which encircles it. Chemicals are mixed with an alloy C-276 agitator for about eight hours. A chlorinated compound is then charged into the reactor, and the reaction mass is heated with steam.

Since being put into service, the alloy C-276 vessel has eliminated as many as eleven 36-hour maintenance periods each year.

### Pollution Control

Waste disposal and pollution control often are linked when considering the problems of removing particulate matter and noxious chemicals from fumes generated by processing plants, electrical generating plants or municipal incinerators. In many instances, there is a combination of corrosion and erosion which tends to attack any material of construction.

In the earliest wet scrubbers used in waste and pollution control, the most favored material was 316L stainless steel. However, this material failed quite rapidly in the more corrosive areas of the scrubbers. In those areas of severe attack, Hastelloy alloy C-276 has emerged as the most satisfactory material, although there are many
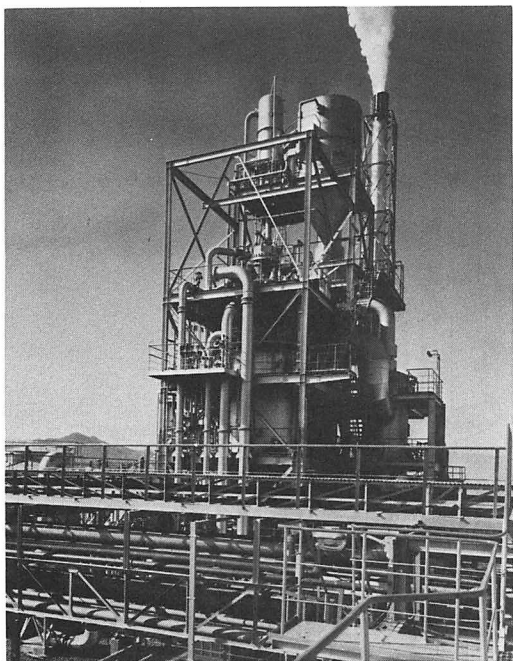
FIGURE 11—High performance nickel-base alloys are used for piping, valves, etc. in this liquid incinerator.

conditions where Hastelloy allow G is the preferred material.

Erosion can be caused by fly ash and other solids, and corrosion can result from sulfur dioxide, chlorine and chlorinated wastes, hydrochloric acid, sulfur, calcium and magnesium. It is not uncommon to encounter pH levels as low as 2.

Those chemical processing plants which must dispose of chlorinated wastes, such as those resulting from the manufacture of pesticides, herbicides and plastics such as polyvinyl chloride, now utilize incineration. Temperatures of gases after incineration range from 1000 to 1600 C (1830 to 2910 F) depending on the quantity and type of solvent.

Trane Thermal Company, Conshohocken, Pennsylvania makes liquid incinerators for chemical disposal and now uses Hastelloy alloys B and C-276 for components such as piping, nozzles, valves, switches, pumps and downcomer tubes (Figure 11).

Many of Trane's nozzles feeding waste materials into combustion chambers are made of Hastelloy alloys, depending upon the temperature range and chemicals involved. Chemical reactions occur at the face of the nozzle between the hot gases and the cooler liquid being injected.
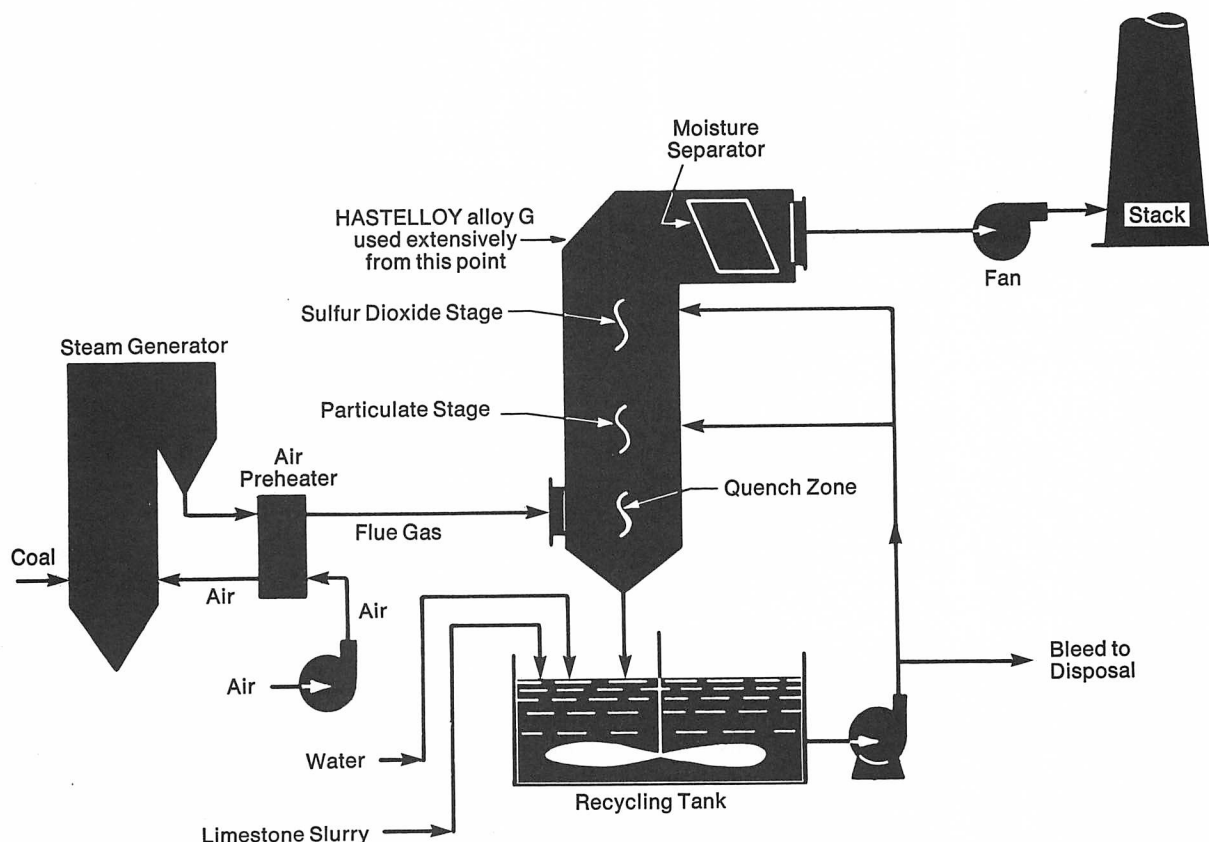


FIGURE 12—Design of coal fired power plant is based on materials that will last for 20 years.
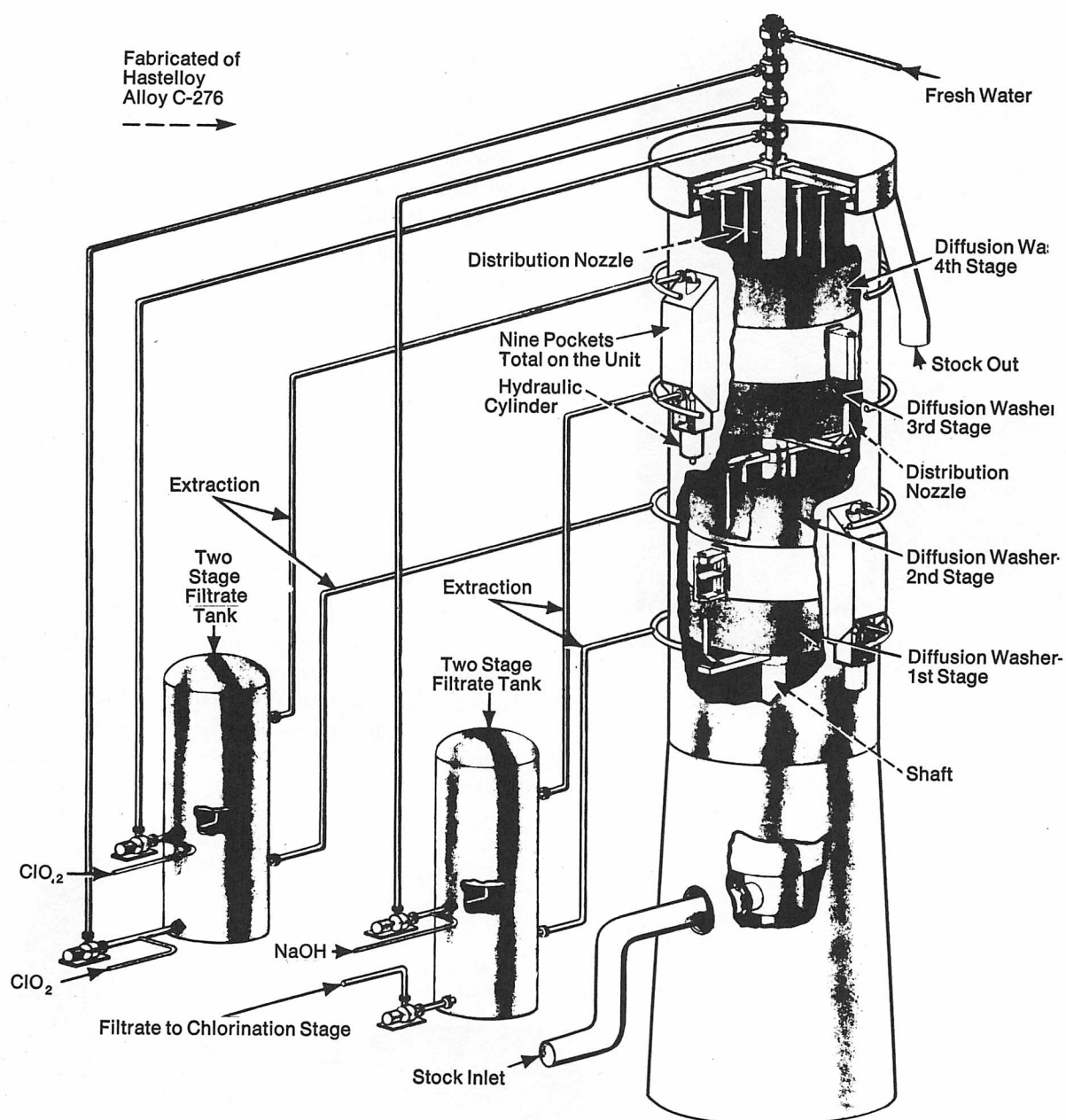
Fabricated of
Hastelloy
Alloy C-276
– – – –→

Fresh Water

Distribution Nozzle

Diffusion Wa:
4th Stage

Nine Pockets
Total on the Unit

Stock Out

Hydraulic
Cylinder

Diffusion Washel
3rd Stage

Extraction

Distribution
Nozzle

Two
Stage
Filtrate
Tank

Diffusion Washer·
2nd Stage

Extraction

Two Stage
Filtrate Tank

Diffusion Washer-
1st Stage

Shaft

ClO₂

NaOH

ClO₂

Filtrate to Chlorination Stage

Stock Inlet

FIGURE 13—*Typical displacement bleaching installation with four bleach stages in one tower.*

In the company's exclusive quench system, high temperature combustion products containing HCl, SO₂ O₂, N₂, CO₂ and water are cooled by radiation and direct contact with the cooling liquid. The downcomer tube must be able to withstand corrosion in this environment at metal temperatures up to 120 C (250 F). This is one section which must not fail during operation. If failure should occur, downstream equipment would be exposed to high temperature gases in a few seconds.

A 400 MW coal fired electric power plant at Duck Creek (Canton), Illinois makes extensive use of Hastelloy alloy G in its scrubber system. The plant produces about 196 Mg (216,000 t) of fly ash and 735 Mg (800,000 t) of SO₂ sludge annually. In designing the plant, engineers sought materials that could withstand erosive and corrosive conditions for a minimum of 20 years (Figure 12).

Because of the variety of coals to be used, a range of chemical and physical properties are needed in the materials of construction. Total ash content of coal can be as high as 18 to 20%. Fly ash is likely to contain chlorides (0.04%), sulfur (5%), calcium and magnesium. All of these contaminants can affect the behavior of engineering materials in the system.

At the heart of the plant's flue gas cleaning system is a two-stage wet limestone scrubber which eliminates sulfur dioxide and particulate emissions. Combustion gases pass through a final heat exchanger and then enter the gas cleaning areas through a manifold system, supplying four centrifugal draft fans. Any of the fans can be isolated into or out of the system, supplying gas flow to the four quarter-size scrubber modules. As with the fans, any scrubber module can be isolated for service. Gas

volume entering the system is about 61,170,000 m³/day (22 x 10⁸ ft³/ day). Each scrubber module is 3.35 m (11 ft) wide by 12.7 m (42 ft) long by 13.7 m (45 ft) high.

Hastelloy alloy G was used in scrubber modules from the point where the hot gases emerge from the limestone slurry, in the ductwork conveying gases through the demister and on to the stack, and in the demister chevrons. This material has been in service for four years.

## Pulp and Paper Industry

Hastelloy alloy C-276 is widely used in the pulp and paper industry at points where chlorides and sulfides are being handled in high concentrations. More recently, there has been an increase in the use of Hastelloy alloy G in waste disposal and pollution control equipment used at pulp and paper mills.

A new pulp bleaching process, developed in Finland, uses many Hastelloy alloy C-276 components. Known as displacement bleaching, the process is faster and requires less investment in equipment and reduces demands for water and energy. Displacement bleaching units process as much pulp in 1½ hours as conventional bleaching systems can handle in 12 to 14 hours (Figure 13).
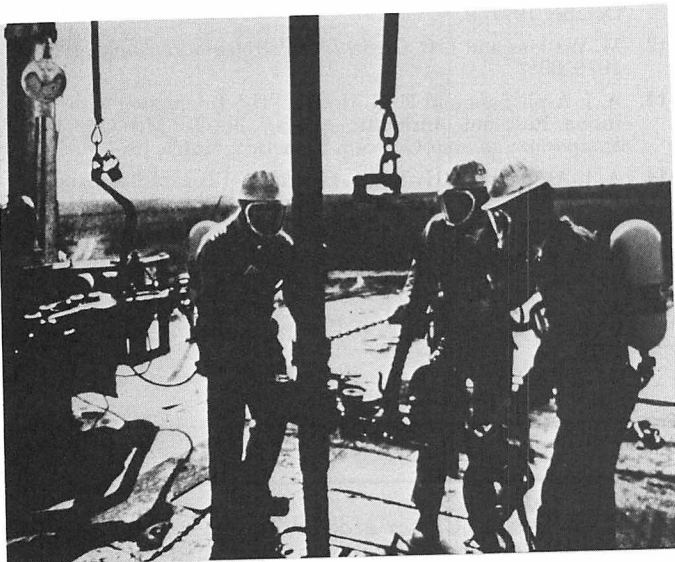


FIGURE 14—Hastelloy alloy C-276 has found use in deep sour wells.

Three distinct materials systems are involved in the design of a tower which is 26 m (85 ft) high and 4.6 m (15 ft) in diameter. The outer shell is brick-lined steel. Diffusers and the upper section of the central shaft are made of unalloyed titanium. Distribution nozzles, the lower section of the central shaft and nine tower pockets are fabricated from Hastelloy alloy C-276. The pockets house hydraulic equipment which moves diffuser assemblies through a 2.5 mm/second (0.1 in./second) upstroke for 60 to 70 seconds and a rapid downstroke of less than 0.5 seconds.

Pockets are from 3.0 to 3.7 m (9.8 to 12 ft) high, 760 mm (30 in.) wide and 760 mm (30 in.) deep. The pockets are bolted to the steel shell.

The materials must withstand the destructive attack of chlorine and chlorine dioxide during the 90-minute processing cycle required to remove lignin from cellulose. Hastelloy alloy C-276 was selected because, in addition to its outstanding corrosion resistance and high strength, it is readily weldable in the field, offers good galling resistance and provides a high degree of rigidity.

## Oil and Gas Industry

With the continuous increase in the price of energy and the dwindling of conventional energy sources, there is a rush to exploit unconventional energy reserves and energy recovery systems. "Deep drilling" (e.g., deep sour gas wells) and more efficient "enhanced recovery" methods (e.g., forced $CO_2$ and fireflooding) are among the feasible methods being considered in search of new sources of fossil fuels. However, the corrosiveness of the environments involved with these unconventional energy sources restricts the materials selection to the high performance alloys, since inhibitors were already proven cumbersome and almost totally ineffective.

In deep sour gas applications, the elevated temperatures (reaching 200 C, 390 F), the pressures (approaching 150 MPa, 22 ksi), and the high hydrogen sulfide contents (up to about 35% $H_2S$) are challenging problems.[10-11] The selected material for such applications must not stress crack in hydrogen sulfide (or under cathodic hydrogen charging) and must resist corrosion and SCC in hot chloride brines containing sulfur/hydrogen sulfide.

**Table VI**—Chloride/Sulfide Stress Cracking and Localized Corrosion Test Results

| Alloy | Condition | Yield Strength, MPa (ksi) | NACE Solution,[a] Room Temperature | NACE Solution,[a] 200 C (390 F) (Autoclave) | 10% FeCl₃,[b] 70 C (158 F) |
|---|---|---|---|---|---|
| 316L | 40% cold work | >827 (>120) | cracking | cracking | pitting |
| 20-MOD | 48% cold work | 827 (120) | no cracking | cracking | pitting |
| G | 59% cold work | 1054 (153) | no cracking | cracking | pitting |
| C-276 | 37% cold work | 1076 (156) | no cracking | no cracking | no pitting |
| C-276 | 48% cold work | 1248 (181) | no cracking | no cracking | no pitting |

[a] NaCl + 0.5% CH₃COOH saturated with H₂S; C-shape specimens, σ ~100% Y, 1000-hour exposure.

[b] 24-hour exposure.

Such resistance to all of these environmental degradations must be maintained at strength levels of about 1034 MPa (150 ksi) to handle the high pressures encountered in the deep wells. Various research programs have identified several high performance alloys as potential candidates for production tubes/pipes[12,13] and have contributed to the understanding of the environmental stress cracking of these alloys.[14-16] Hastelloy alloy C-276 appears the most suitable material among the alloys (Figure 14) which show the best resistance to all forms of corrosion in the simulated deep sour gas well environment. Pertinent data are presented in Table VI. They show the excellent resistance of alloy C-276 to hydrogen cracking, to chloride/sulfide stress cracking at 200 C (390 F) and to localized corrosive attack.

The results of laboratory and field tests should be confirmed by service performances in more than two wells in the Central Mississippi region, where a large amount of seamless Hastelloy alloy C-276 tubular products is scheduled to be used. This alloy is also being used in some $CO_2$ wells contaminated with hydrogen sulfide.

Finally, it should be added that more and more data are showing the inability of "conventional" materials to handle some critical areas of enhanced recovery systems involving severe corrosion problems. The apparent success of high performance alloys in handling such problems, such as alloys G and C-276 in corrosive $CO_2$ wells and C-276 in fireflooding, is opening the door for a "high alloy technology" in oil and gas production, where the inconvenience (in offshore applications) or the ineffectiveness (in sour gas applications) of inhibitors could be totally eliminated.

These are just a few of the hundreds of applications of Hastelloy alloys in chemical process, petrochemical and other industries where corrosion, alone, or in combination with erosion, is a major problem. As the use of larger units increases and the utilization of more aggressive catalysts becomes more widespread, the need for these alloys will become even more universal.

# References

1. Anon., Chemical Week, 119, July 7, 1976.
2. Chlorimet 2; Bulletin A/3C; The Duriron Company Inc., Dayton, Ohio.
3. T. S. Lee III and F. G. Hodge, Materials Performance, 15, September 1976, 29.
4. E. C. Hoxie and G. W. Tuffnell, Resolving Corrosion Problems in Air Pollution Control Equipment, (NACE), 1976, 65.
5. C. Velzy, Ibid. 35.
6. H. H. Uhlig, Corrosion and Corrosion Control, Second Edition, John Wiley and Sons, Inc., 1971, 355.
7. H. H. Uhlig and A. I. Asphahani, Corrosion Behavior of Cobalt-Base Alloys in Aqueous Media. Submitted for publication, 1978.
8. A. I. Asphahani, Localized Corrosion of High Performance Alloys, Paper No. 248, NACE T-3L Symposium, Atlanta, March 1979.
9. H. R. Copson, Physical Metallurgy of Stress Corrosion Cracking, T. N. Rhodin, Editor, Interscience, New York, 1959, 247.
10. R. N. Tuttle, Materials Performance, 13, February 1974, 42.
11. R. N. Tuttle and T. W. Hamby, Materials Performance, 16, October 1977, 9.
12. M. Watkins and J. B. Greer, J. of Petroleum Technology, June 1976, 698.
13. A. I. Asphahani and F. G. Hodge, "H₂S Interaction with Corrosion Resistant Austenitic Alloys," NACE Meeting, T-1F Symposium on Sour Gas, San Francisco, March 1977.
14. A. I. Asphahani, "Hydrogen Cracking of Nickel-Base Alloys." Paper No. 3C-2, Second Int. Cong., Hydrogen in Metals. Paris, June 1977.
15. R. D. Kane, M. Watkins, D. F. Jacobs, and G. L. Hancock, Corrosion, 33, September 1977, 309.
16. A. I. Asphahani, "High Performance Alloys for Deep Sour Gas Wells," Paper No. 42, NACE-Corrosion 78, Houston, March 1978.

# Discussion

H. SPÄHN, BASF AG. I was interested in your potentiostatic method. Were some of the potentials cathodic to the open-circuit potential, or did this solution ever cause pitting by itself in the highly alloyed materials?

F. G. HODGE. In several instances, the tests were actually run cathodic to the open-circuit potential in ferric chloride. We have run a variety of environments in ferric chloride with concentrations from 0.4 to 7%. At times, pitting occurs in the open-circuit condition if the temperature is high enough. Temperature is one of the critical parameters, and we have seen underestimations of temperature in pollution control devices.

D. V. DOANE, Climax Molybdenum Company. In your corrosion rate equations, there was a plus sign for the chromium contribution. Is this just a progression analysis problem?

F. G. HODGE. I think it is. We have been evaluating that equation for the past five years, and it appears to fit very well. The sign of the chromium coefficient has never changed. Only molybdenum has had a negative sign as far as corrosion rate in HCl is concerned.

# Stainless Steels with High Strength and High Corrosion Resistance

by H. Kohl, G. Rabensteiner and G. Hochörtler
Vereinigte Edelstahlwerke

The wide variety of stainless steel grades has come to be regarded as materials essential to today's technology and civilization.

As the range of applications widens, requirements tend to become more and more stringent, calling for new grades to be developed for special purposes.

In general these steels may be divided into three groups:

- Low interstitial ferritic stainless steels,
- Austenitic steels with very high alloy contents, and
- Improved austenitic-ferritic stainless steels.

This paper deals with the development of a high alloy austenitic stainless steel and of an austenitic-ferritic stainless steel. The most important a priori requirements are large scale production capability and weldability. At the same time, a suitable filler metal had to be developed.

## Austenitic Chromium-Nickel Steel with 6.3% Molybdenum

The use of conventional austenitic stainless steel grades often is limited because of the risk of pitting, crevice corrosion and stress corrosion cracking.

Additions of up to 4.5% molybdenum have definitely improved resistance to these forms of corrosion, but until quite recently, higher additions of molybdenum raised problems in production and workability of these steels.[1-4]

Now, steels containing about 6% molybdenum have

been reported, and grades AL-6X, 254 SMO and NSCD have been produced on an industrial scale.[4, 5]

In Austria, Vereinigte Edelstahlwerke (VEW) has succeeded in producing a steel with 17% chromium, 16% nickel and 6.3% molybdenum with copper and nitrogen additions in the form of bar, sheet and seamless tube, all on an industrial scale. Table I shows the chemistry and mechanical properties of this steel (A 963). Minimum yield strength at 0.2% offset in the solution annealed condition is 300 MPa (43.5 ksi), higher than for conventional austenitic chromium-nickel steels.

Of greatest interest in a steel termed corrosion resistant is its behavior in environments that lead to pitting, crevice corrosion and stress corrosion cracking.

Corrosion resistance of high molybdenum steels is essentially determined by microstructure and will be satisfactory even under extreme conditions (e.g. in chlorinated seawater) if precipitates are nonexistent or very low. Therefore, the alloying constituents of the steel under consideration were chosen to ensure that the steel, even if sensitized for a short time (as during welding), is not depleted in alloying elements locally so that it retains its full resistance.

This effect is brought about in particular by the addition of about 0.15% nitrogen which results in mechanical properties that—in an austenitic stainless steel—are excellent, and, on the other hand, delays the rate of precipitation.

Time to formation of visible pits in a steel exposed to an aqueous solution containing 10% $FeCl_3$ + 5% NaCl can be regarded as a measure of resistance to this form of

**Table I**—Chemical Composition and Mechanical Properties of Steel A 963

| | Element, % | | | | | |
|---|---|---|---|---|---|---|
| | C | Cr | Mo | Ni | Cu | N |
| A 963 | 0.03 max. | 17.0 | 6.3 | 16.0 | 1.6 | 0.15 |

| 0.2% Yield Strength, MPa (ksi) | Tensile Strength, MPa (ksi) | Elongation (5d), % | Reduction in Area, % | ISO-V Impact Energy, J (ft-lb) |
|---|---|---|---|---|
| ≥ 300 (43.5) | ≥ 600 (87.0) | ≥ 30 | ≥ 30 | ≥ 80 (108) |

**Table II**—Nominal Chemical Composition of Indicated Steels

| Grade | Designation | Element, % | | | | | |
| --- | --- | --- | --- | --- | --- | --- | --- |
| | | C | Cr | Mo | Ni | N | Other |
| VEW A 500 | X5 CrNi 18 9 | < 0.05 | 18.5 | — | 9.5 | — | — |
| VEW A 200 | X2 CrNiMo 18 10 | < 0.03 | 17 | 2.2 | 11.5 | — | — |
| VEW A 100 | X5 CrNiMo 18 12 | < 0.05 | 17.5 | 2.7 | 13 | — | — |
| VEW A 400 | X3 CrNiMoN 17 13 5 | < 0.04 | 17 | 4.3 | 13.5 | 0.15 | — |
| VEW A 963 | X2 CrNiMoCuN 17 16 | < 0.03 | 17 | 6.3 | 16 | 0.15 | 1.6% Cu |
| VEW A 901 | X2 CrNiMoSi 19 5 | < 0.03 | 18.5 | 2.7 | 4.7 | — | 1.7% Si |
| VEW A 905 | X3 CrMnNiMoN 25 6 4 | < 0.04 | 25.5 | 2.3 | 3.7 | 0.37 | 5.8% Mn |

**Table III**—Formation of Visible Pits in Indicated Steels

| | A 500 X5 CrNi 18 9 | A 200 X2 CrNiMo 18 10 | A 100 X5 CrNiMo 18 12 | A 400 X3 CrNiMoN 17 13 5 | A 963 X2 CrNiMo CuN 17 16 |
| --- | --- | --- | --- | --- | --- |
| | Time to Formation, h | | | | |
| Temp.   % Mo | < 0.5 | 2.2 | 2.7 | 4.3 | 6.3 |
| 22 C  (72 F) | < 0.5 | ≤ 5 | ≤ 100 | > 1000 | > 2000 |
| 35 C  (95 F) | ≤ 0.5 | ≤ 0.5 | < 5 | < 70 | > 2000 |

Test solution: 10% $FeCl_3$ + 5% NaCl

corrosion. Other steels tested for comparison purposes were X5 CrNi 18 9 (VEW A 500), X2 CrNiMo 18 10 (VEW A 200), X5 CrNiMo 18 12 (VEW A 100) and X3 CrNiMoN 17 13 5 (VEW A 400) (Table II). Table III shows results of visual examination of specimen surfaces after exposure. The results clearly illustrate the superiority of grade VEW A 963, particularly at the high temperature range.

Another criterion of resistance to pitting in a steel is the pitting potential. Figure 1 shows pitting potentials of VEW A 963 and four other grades determined by the potentiodynamic method in synthetic seawater. Figure 2 compares the variation of pitting potential with temperature for steel VEW A 963 and for steel X3 CrNiMoN 17 13 5 (VEW A 400) which is suitable for cooling circuit applications provided that heat treatment and processing operations are conducted correctly. Pitting can be a problem in this type of application.

Some applications require resistance to crevice corrosion. This form of corrosion may occur underneath joints, washers and coatings.

Tests were conducted in accordance with ASTM G 48-76 in a solution containing $FeCl_3$ to determine susceptibility of certain austenitic stainless steels to crevice corrosion. Figure 3 shows results of these tests. The conditions specified in the standard did not produce crevice corrosion in VEW A 963, therefore the test was repeated at higher temperatures using test specimens with a pickled surface as well (Figure 4).

Testing the resistance to stress corrosion cracking poses problems. A test method frequently used in the past consists of exposing specimens to a solution containing 45% $MgCl_2$ at 155 C (310 F). Specimens of 5 mm (0.2 in.) diameter from all conventional austenitic stainless steels, i.e. chromium-nickel and chromium-nickel-molybdenum steels under a load corresponding to 70% of tensile strength gave times to failure from one to two hours. Under these extreme conditions, from 8 to 13 hours passed before specimens from VEW A 963 failed.

VEW has developed a test method permitting better differentiation among austenitic grades. The test is conducted in a solution containing 3% NaCl under condi-
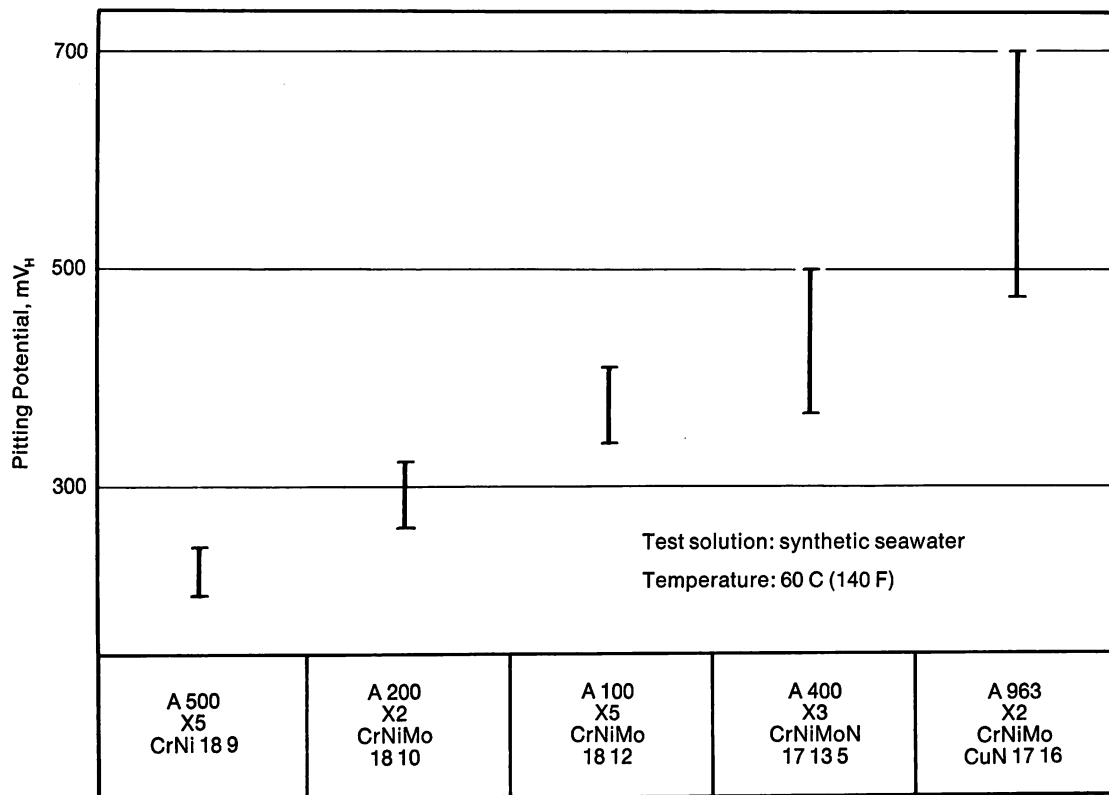
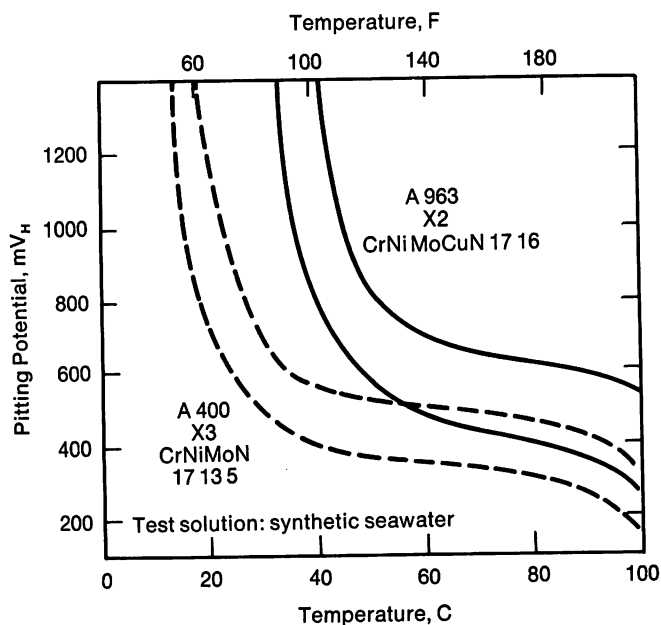*FIGURE 1—Pitting potential of different steel grades.*



*FIGURE 2—Variation of pitting potential with temperature.*



*FIGURE 3—Crevice corrosion test in ferric chloride (ASTM G48-76).*

tions that lead to crust formation. A tensile test specimen under uniaxial load is heated electrically so that a crust forms at the "water line" of the specimen immersed (Figure 5) in the solution. According to unpublished test results obtained by W. Wedl, time to failure under the conditions chosen for a conventional chromium-nickel steel (VEW A 500) varies with the tensile load from 10 to 100 hours, for an austenitic-ferrite steel (X2 CrNiMoSi 19 5, VEW A 901, Table II) from 100 to 1000 hours, and
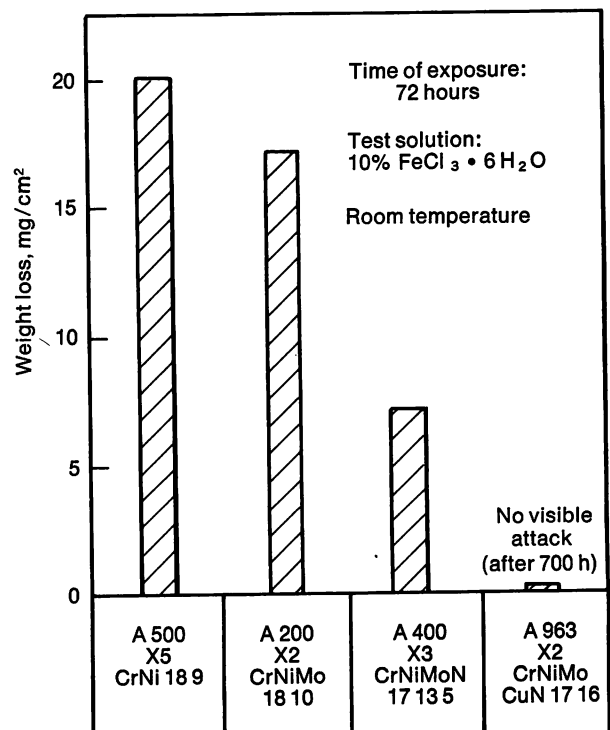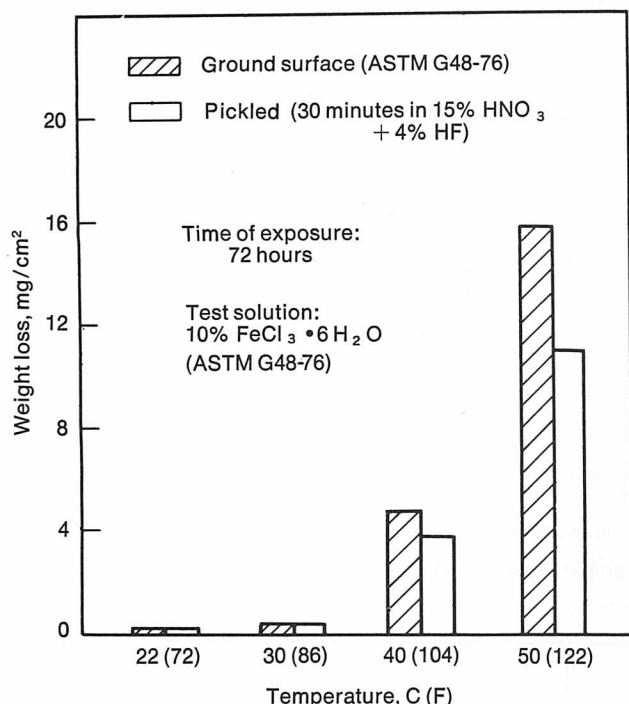
FIGURE 4—*Crevice corrosion of steel grade A 963, influence of temperature and surface finish.*
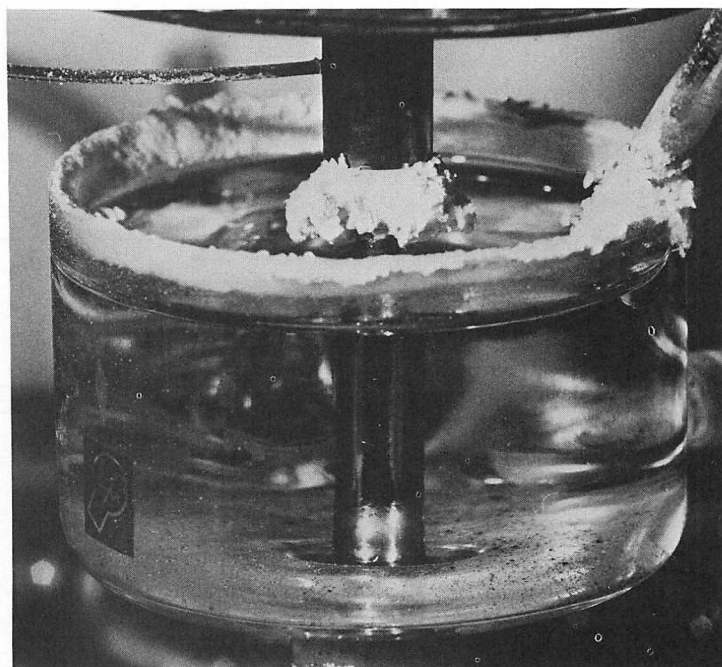


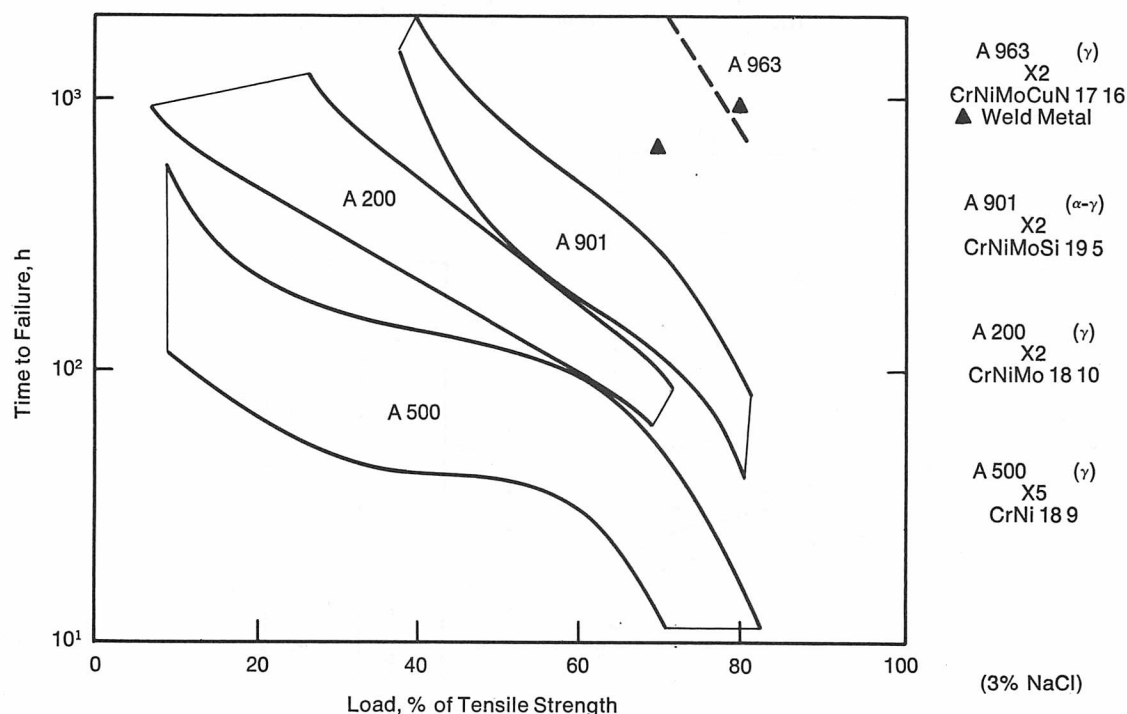FIGURE 5—*SCC testing with crust formation.*



FIGURE 6—*SCC of steel grade A 963 tested with crust formation.*

lies between these two for chromium-nickel-molybdenum steel X2 CrNiMo 18 10 (VEW A 200) (Figure 6).

Specimens from VEW A 963 failed only under very high loads of 70 and 80% of tensile strength. Time to failure averaged from 1000 to 2000 hours which is 10 times better than for the two-phase steel X2 CrNiMoSi 19 5 and 100 times better than for X5 CrNi 18 9 under the same load conditions.

The weldability of steels containing 6% Mo had been a problem until now as no analogous austenitic filler metals containing more than 5% molybdenum were available. Systematic efforts led to the development of austenitic welding electrodes containing 6.5% molybdenum giving a deposit which is highly resistant to weld decay.[6] Table IV shows test results and chemical analysis of Böhler FOX CN 20/25 M developed

**Table IV**—Chemical Composition and Mechanical Properties of Fox CN 20/25M

| Diameter, mm (in.) | Weld Metal Composition, % | | | | | | | |
|---|---|---|---|---|---|---|---|---|
| | C | Si | Mn | Cr | Mo | Ni | Cu | N |
| 2.5 (0.1) | 0.039 | 0.42 | 3.88 | 19.71 | 6.62 | 25.15 | 2.44 | 0.14 |
| 3.25 (0.13) | 0.032 | 0.42 | 3.95 | 19.87 | 6.36 | 25.10 | 2.23 | 0.13 |
| 4.0 (0.15) | 0.029 | 0.41 | 4.53 | 20.27 | 6.29 | 24.72 | 2.38 | 0.12 |

| | | |
|---|---|---|
| 0.2% Proof stress, MPa (ksi) | 448 | (65.0) |
| 0.1% Proof stress, MPa (ksi) | 478 | (69.3) |
| Tensile strength, MPa (ksi) | 675 | (97.9) |
| Elongation, % | 39 | |
| Reduction of area, % | 55 | |

Room temperature impact strength, J (ft-lb)*

| | | |
|---|---|---|
| 2.5 mm (0.1 in.) dia. | 77 | (57) |
| 3.25 mm (0.13 in.) dia. | 89 | (66) |
| 4.0 mm (0.15 in.) dia. | 87 | (64) |

* Average of five values.

Ground | Pickled

Weld metal X3  NiCrMoCuN 25 20 6 (FOX CN 20 25 M)

Weld metal X4  CrNiMoN 18 16 5 (FOX AS N5)



FIGURE 7—Resistance in 10% FeCl₃ + 5% NaCl at ambient temperature. Appearance of samples after 500 hours.

by VEW. The deposit has very similar corrosion resistance to steel VEW A 963 and is superior by far to deposits obtained with the 18% chromium, 4.5% molybdenum electrodes used until now with respect to pitting and crevice corrosion resistance (Figure 7). Böhler FOX CN 20/25 M deposits fully austenitic weld metal which, because of the high manganese and molybdenum contents, is highly resistant to hot cracking as demonstrated in a number of tests.

Resistance of a deposit to stress corrosion cracking was also tested by immersion of all-weld-metal test specimens in a solution containing 3% NaCl under crust formation. Excellent results, which can be compared with those of VEW A 963, were obtained (Figure 6).

## Austenitic-Ferritic Chromium-Nickel-Molybdenum Steel with Manganese and Nitrogen Additions

Austenitic-ferritic stainless steels are used for an ever increasing number of applications requiring corrosion resistance.[7-10] Compared to conventional austenitic steels, the two-phase steels possess considerably better mechanical properties and improved resistance to stress corrosion cracking. On the other hand, they may pose problems with regard to weldability, intergranular corrosion and susceptibility to embrittlement. Alloying additions must, therefore, be balanced with particular care. Steel A 905, developed by VEW, combines high tensile strength, high impact strength, good weldability and excellent corrosion resistance in a highly satisfactory way. Table V gives the chemical analysis and mechanical properties. The addition of about 6% manganese allows a nitrogen content of 0.37% which results in particularly good mechanical properties.
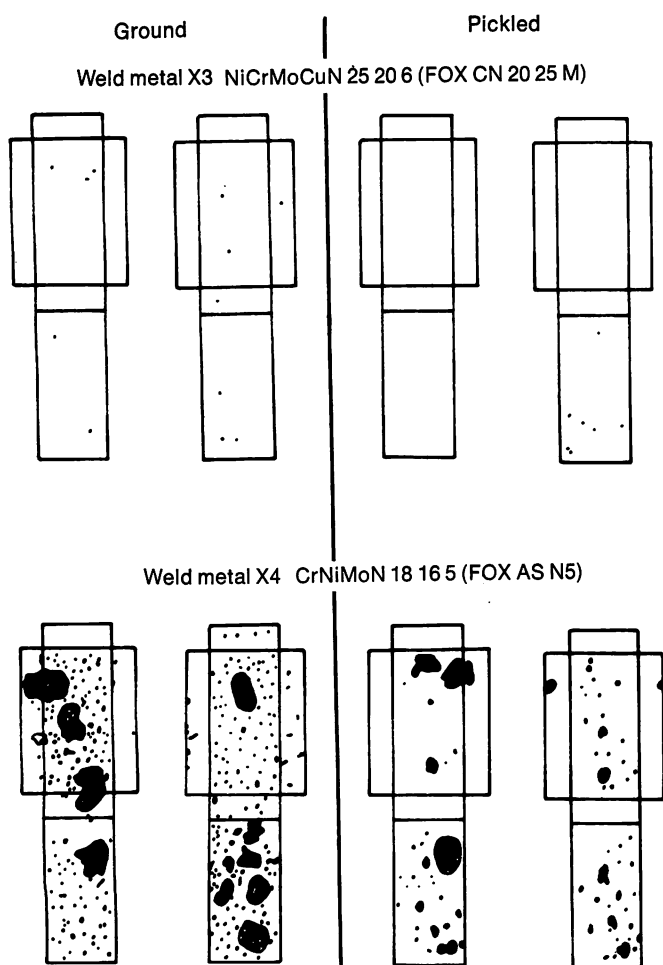
**Table V**—Chemical Composition and Mechanical Properties of Steel A 905

| | Element, % | | | | | |
|---|---|---|---|---|---|---|
| | C | Mn | Cr | Mo | Ni | N |
| A 905 | 0.04 max. | 5.8 | 25.5 | 2.3 | 3.7 | 0.37 |

| 0.2% Yield Strength, MPa (ksi) | Tensile Strength, MPa (ksi) | Elongation (5d), % | Reduction in Area, % | ISO-V Impact Energy, J (ft-lb) |
|---|---|---|---|---|
| ≧ 590 (85.6) | > 750 (108.8) | > 30 | > 50 | > 63 (46) |

If a two-phase steel is required to compete with purely austenitic steels in terms of resistance to chloride-containing media (e.g. seawater), its alloy content must be increased to counteract the unavoidable chromium and molybdenum partitioning between austenite and ferrite. As regards pitting resistance, two-phase VEW A 905 can be compared to grade X3 CrNiMoN 17 13 5 (VEW A 400). Figure 8 shows pitting potentials of these two grades at different temperatures. VEW A 400, a grade specifically developed for use in the presence of chloride-containing media, is superior to VEW A 905 only in the higher temperature ranges, which is also demonstrated by a pitting test conducted in a solution containing 10% FeCl₃ + 5% NaCl.

In the quenched condition, VEW A 905 resists attack by boiling nitric acid (65%; Huey test). Corrosion rates are in the order of 0.1 g/m²h. Corrosion rates are higher after sensitizing for one hour at 650 C (1200 F) (Figure 9).

Resistance to stress corrosion cracking was tested in the same manner as for grade VEW A 963 (solution with 3% NaCl with crust formation) (Figure 10). For VEW A 905, time to failure is even longer than for the two-phase VEW A 901 which has proven resistant to stress corrosion cracking in many cases. In Figure 10, load is expressed in percentages of tensile strength. Superiority of the two-phase steels is even more conspicuous when time to failure is plotted as a function of absolute load (Figure 11).

Weldability of VEW A 905 is good. Results of metallographic and mechanical tests confirm the absence of grain coarsening in the heat affected zone (Figure 12) so that the steel retains its properties in this area.

VEW has developed a similar electrode possessing adequate mechanical properties and good corrosion resistance. Table VI shows the chemistry, mechanical properties and corrosion resistance of the deposit obtained with this electrode (Böhler FOX CN 26/7 N). Results of stress corrosion cracking tests with crust formation are given in Figure 11.
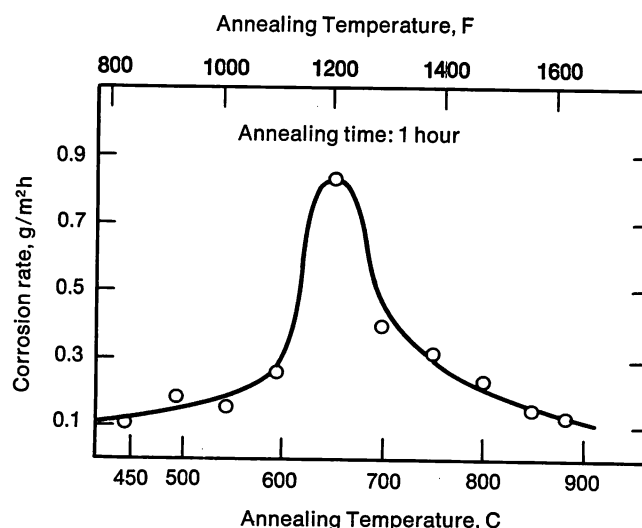
## Conclusions

VEW A 963, an austenitic stainless steel containing 17% chromium, 16% nickel and 6.3% molybdenum
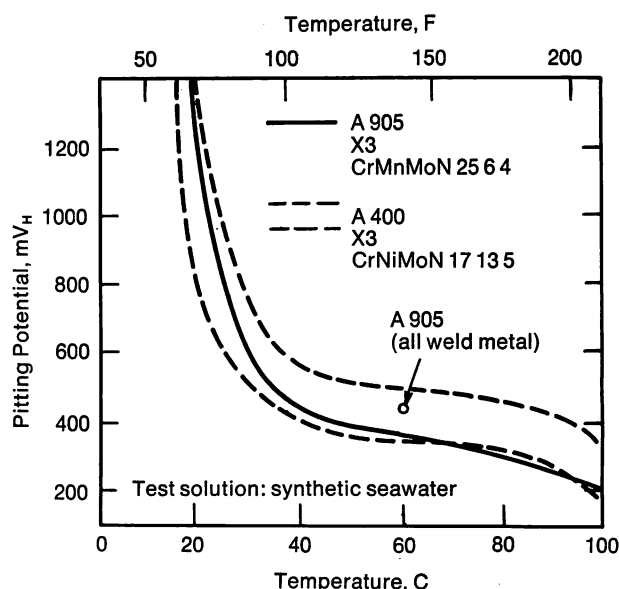
| Time to formation of visible pits in 10% FeCl₃ + 5% NaCl, h | Temp. C (F) | A 905 | A 400 |
|---|---|---|---|
| | 22 (72) | >1000 | >1000 |
| | 35 (95) | >5 <8 | <70 |

*FIGURE 8—Pitting corrosion of steel A 905.*

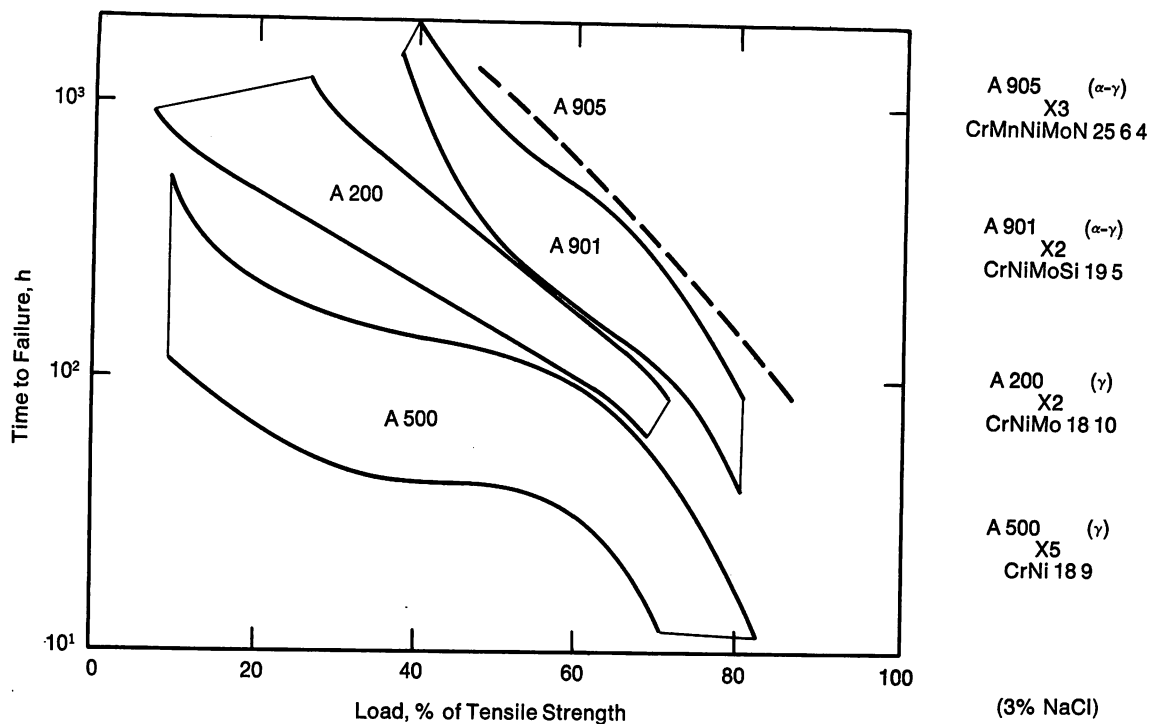*FIGURE 9—Huey test of sensitized specimens of grade A 905.*

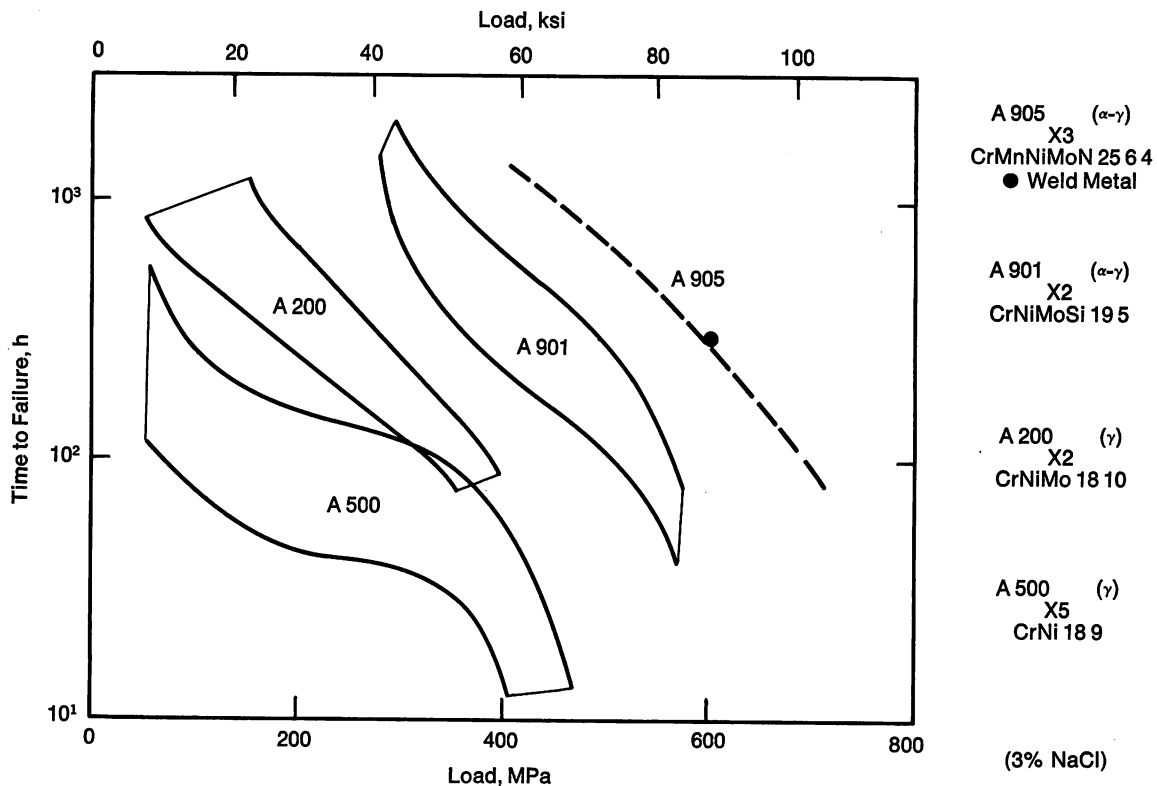FIGURE 10—SCC of steel grade A 905 tested with crust formation.

A 905 (α-γ)
X3
CrMnNiMoN 25 6 4

A 901 (α-γ)
X2
CrNiMoSi 19 5

A 200 (γ)
X2
CrNiMo 18 10

A 500 (γ)
X5
CrNi 18 9

(3% NaCl)



FIGURE 11—SCC of steel A 905 tested with crust formation.

A 905 (α-γ)
X3
CrMnNiMoN 25 6 4
● Weld Metal

A 901 (α-γ)
X2
CrNiMoSi 19 5

A 200 (γ)
X2
CrNiMo 18 10
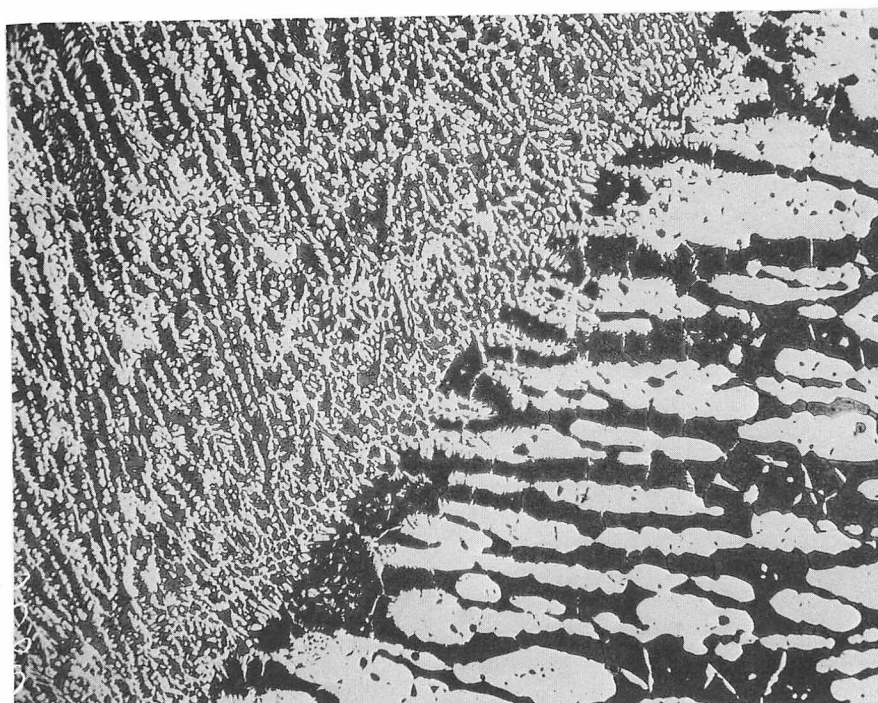
A 500 (γ)
X5
CrNi 18 9

(3% NaCl)

*FIGURE 12—HAZ microstructure (base metal-A 905, weld metal-Fox CN 26/7 N). Etchant-Beraha.*

**Table VI**—Chemical Composition and Mechanical Properties of Fox CN 26/7 N

| | | Weld Metal Composition, % | | | | |
|------|------|------|------|------|------|------|
| C | Si | Mn | Cr | Mo | Ni | N |
| 0.04 | 0.70 | 4.50 | 26.00 | 2.00 | 7.50 | 0.35 |

| | | |
|---|---|---|
| 0.2% Proof stress, MPa (ksi) | 720 | (104.4) |
| Tensile strength, MPa (ksi) | 910 | (132.0) |
| Elongation, % | 34 | |
| Reduction of area, % | 51 | |
| | | |
| Impact energy (DVM), J (ft-lb) | 47 | (35) |
| (ISO-V), J (ft-lb) | 49 | (36) |
| | | |
| Weld metal corrosion resistance | | |
| Huey test, g/m²h | 0.11 | |
| Pitting potential, mV$_H$[a] | 450 | |
| Intercrystalline corrosion[b] | *resistant* | |

[a] In seawater at 60 C (140 F).
[b] DIN 50 914.

VEW A 905, an austenitic-ferritic grade containing 25.5% chromium, 3.7% nickel, 2.3% molybdenum, 5.8% manganese and 0.37% nitrogen, combines high strength, high impact strength, good weldability and high corrosion resistance. FOX CN 26/7 N is a welding electrode of similar composition that has been developed recently for this steel.

Both VEW A 963 and A 905 are grades possessing outstanding properties that permit their use for a wide range of applications in chemical engineering involving particularly stringent requirements.

## References

1. H. Thier, A. Bäumel and E. Schmidtmann, *Arch Eisenhütten-wesen, 40* (4), 1969, 333.
2. A. Bäumel, E. M. Horn and G. Siebers, *Werkstoffe und Korro-sion, 23,* 1972, 973.
3. A. Kügler, *Berg- u. Hüttenm. Mh., 122* (11), 1977, 507.
4. H. E. Deverell and J. R. Maurer, *Materials Performance, 17* (3), 1978, 15.
5. K. O. Nordin, *Stainless Steel '77,* Climax Molybdenum Co., London, 1977, 205.
6. G. Rabensteiner and H. Schabereiter, *Schweißtechnik/Sou-dure, 69* (2), 1979, 26.
7. W. Wessling, H. E. Bock and W. Fuchs, *Z. f. Werkstofftechnik, 4* (4), 1973, 186.
8. J. Hochmann, et al., *Metaux, 49,* 1974, 390.
9. J. P. Desolneux, *Werkstoffe und Korrosion, 28,* 1977, 325.
10. Ch. Schuster and H.-J. Eckstein, *Neue Hütte, 22* (5), 1977, 266.

with copper and nitrogen additions, due to the high molybdenum content, possesses excellent resistance to pitting and crevice corrosion. Tests conducted to assess resistance to stress corrosion cracking with crust formation also yielded highly satisfactory results. Weldability of the steel is good. The electrode FOX CN 20/25 M yields deposits of equal corrosion resistance and satisfactory resistance to embrittlement.

# Discussion

M. R. GALLER, *Lukens Steel Company*. Please comment on the temperature range of hot workability and any difficulties you have encountered with steel A 963 (Cr-Ni-6Mo).

H. KOHL. The temperature range is that normally used with austenitic stainless steels. However, special care is taken in furnace times (to avoid recrystallization and grain growth) and in forming rates.